

Asymmetric Chiral-at-Rhodium Catalysis Driven by Visible Light or Electricity

A DISSERTATION

In

Chemistry

Presented to the Faculties of Philipps-Universität Marburg in Partial Fulfillment
of the Requirements for the Degree of Doctor of Science

(Dr. rer. nat.)

Xiaoqiang Huang

Fujian, P. R. China

Marburg/Lahn 2019

Die vorliegende Dissertation entstand in der Zeit von Oktober 2015 bis November 2018 am Fachbereich Chemie der Philipps-Universität Marburg unter der Betreuung von Herrn Prof. Dr. Eric Meggers.

Vom Fachbereich Chemie der Philipps-Universität Marburg (Hochschulkennziffer: 1180) als Dissertation am _____ angenommen.

Erstgutachter: Prof. Dr. Eric Meggers

Zweitgutachter: Prof. Dr. Armin Geyer

weitere Mitglieder Prüfungskommission: Prof. Dr. Jörg Sundermeyer

Tag der mündlichen Prüfung: _____

Acknowledgements

First and foremost, any words is not enough to express my sincere gratitude to my supervisor, Prof. Meggers. I learned a lot from you, from your attitude toward academic research, your enthusiastic motivation, and your ways to think and solve problems. The point touched me most is your endless passion to fearlessly challenge the real difficulty in science. I really enjoyed the highly efficient research mode during past three years with your directions. Your advice and support on me have been priceless. Without you, I can not be as good as now. Many Thanks!

A very special gratitude to my master supervisor, Prof. Jiao, for introducing me into the academic research, and for your constant support and encouragement.

I am really grateful to Prof. Geyer and Prof. Sundermeyer for referring my thesis and being the defense committee.

Next, I would like to appreciate all the contributors of my publications from the department and other institutes. Your contributions are indispensable and it is really pleasant to work with you. Special thanks to Dr. Haohua Huo who led me to the chiral-at-metal catalysis and always gives me sparking inspirations, Dr. Chuanyong Wang for your pioneering contribution on developing rhodium catalyst and also your useful suggestions, Dr. Jiajia Ma for your synthesis of **RhS** catalyst and I really like the discussions with you, Dr. Shipeng Luo for your invaluable help in the Chem. Sci. paper, and Jiahui Lin, Tianqi Shen, Lifang Zhao, Wenjian Zhou, Xiaoqing Ma, Dr. Qi Zhang and Dr. Xiaodong Shen for your help with substrate and catalyst synthesis. Thanks a lot to Dr. Lili Zhang not only for your help with single crystals but also for your daily help in the lab, Dr. Klaus Harm and all colleges in the X-ray crystallography department, Dr. Xiulan Xie for assistant in NMR issues, Dr. Olaf Burghaus for your kind help with EPR, and all the other facility member of the university whose support is very important for my research. Also collaborators from other institutes are greatly appreciated. Thanks Prof. Webster for the cyclic voltammetry studies, Taylor R. Quinn and Prof. Olaf Wiest for calculations on the [2+2] chemistry, my former lab mate Dr. Xinyao Lin for calculations on the [2+3] photocycloaddition, Marianna Marchini and Prof. Paola Ceroni for photophysical measurements, Shuming Chen and Prof. K. N. Houk for your calculations on enolate chemistry.

A special mention to Ina Pinnschmidt, Marcel Hemming, Andrea Tschirch and Dr. Sabrina Höbenreich, for your kind help. Thanks a lot to Yvonne Grell for translating the abstract into German.

Thanks a lot to all the other former and current group members, Dr. Xiao Zhang, Dr. Yu Zheng, Dr. Nathalie Nett, Dr. Francisco F. de Assis, Dr. Wei Zuo, Dr. Thomas Cruchter, Dr. Lucie Jarrige, Dr. Naifu Hu, Thomas Mietke, Tabea-Melanie Faber, Sabine Duewel, Jie Qin, Yuqi Tan, Zijun Zhou, Yubiao Hong, Chenhao Zhang, Erik Winterling, Xiang Shen, Tianjiao Cui, Yuanze Tang, Xingwen Zheng, Xin Nie, Philipp Steinlandt, Dr. Midori Akiyama, Takuya Mochizuki and Kenichi Endo. I really appreciate your kind help and company.

At last but not least, I would like to thank my parents and sister who have supported me along the way.

Thanks for all your support!

Publications and Poster Presentations

Publications presented in this thesis:

1. X. Huang, R. D. Webster, K. Harms, E. Meggers, Asymmetric Catalysis with Organic Azides and Diazo Compounds Initiated by Photoinduced Electron Transfer, *J. Am. Chem. Soc.* **2016**, *138*, 12636-12642.
2. X. Huang, T. R. Quinn, K. Harms, R. D. Webster, L. Zhang, O. Wiest, E. Meggers, Direct Visible-Light-Excited Asymmetric Lewis Acid Catalysis of Intermolecular [2+2] Photocycloadditions, *J. Am. Chem. Soc.* **2017**, *139*, 9120-9123.
3. X. Huang, S. Luo, O. Burghaus, R. D. Webster, K. Harms, E. Meggers, Combining the Catalytic Enantioselective Reaction of Visible-Light-Generated Radicals with a By-Product Utilization System, *Chem. Sci.* **2017**, *8*, 7126-7131.
4. X. Huang, X. Li, X. Xie, K. Harms, R. Riedel, E. Meggers, Catalytic Asymmetric Synthesis of a Nitrogen Heterocycle through Stereocontrolled Direct Photoreaction from Electronically Excited State, *Nat. Commun.* **2017**, *8*, 2245.
5. X. Huang, J. Lin, T. Shen, K. Harms, M. Marchini, P. Ceroni, E. Meggers, Asymmetric [3+2] Photocycloadditions of Cyclopropanes with Alkenes or Alkynes through Visible-Light Excitation of Catalyst-Bound Substrates, *Angew. Chem. Int. Ed.* **2018**, *57*, 5454-5458.
6. X. Huang, Q. Zhang, J. Lin, K. Harms, E. Meggers, Electricity Driven Asymmetric Lewis Acid Catalysis, *Nat. Catal.* **2019**, *2*, 34-40.

Poster Presentations:

1. “20th European Symposium on Organic Chemistry (ESOC 2017)”, Poster: *Direct Visible-Light-Excited Asymmetric Lewis Acid Catalysis of Intermolecular [2+2] Photocycloadditions*, 2nd-6th July **2017**, Cologne, Germany.
2. “ORCHEM 2018”, Poster: *Asymmetric Photocycloadditions Catalyzed by a Single Chiral-at-Metal Rhodium Complex*, 10th-12th September **2018**, Berlin, Germany.

Abstract

Driving asymmetric catalysis with visible light or electricity is of significant value because they represent ‘green’ and sustainable methods to synthesize non-racemic chiral molecules and in addition offer ample opportunities for chemists to discover new mechanistic scenarios and invent previously unknown transformations. However, steering the reaction course of photo- and/or electrochemically generated reactive intermediates in a stereocontrolled and catalytic fashion is very challenging. This thesis presents novel applications of previously in the Meggers group developed chiral-at-metal rhodium complexes to the areas of asymmetric photocatalysis and asymmetric electrosynthesis.

1) A bis-cyclometalated chiral-at-metal rhodium complex (designated as **RhS**) in combination with the photoredox catalyst [Ru(bpy)₃](PF₆)₂ enables visible-light-activated asymmetric α -amination and α -alkylation of 2-acyl imidazoles with aryl azides or α -diazo carboxylic esters as radical precursors, respectively (Chapter 3.1). As the first utilization of these reagents for photoinduced asymmetric catalysis, this novel proton- and redox-neutral transformations feature the advantage of leaving molecular N₂ as the sole by-product and provide yields of up to 99% as well as excellent enantioselectivities of up to >99% ee with broad functional group compatibility.

2) A bis-cyclometalated chiral-at-metal rhodium complex (designated as **RhO**) is demonstrated to catalyze stereocontrolled chemistry of photo-generated radicals and at the same time an enantioselective sulfonyl radical addition to alkenes (Chapter 3.2). Specifically, employing Hantzsch ester as photoredox mediator, rhodium bound β -enolate carbon-centered radicals are generated by a selective photoinduced single electron reduction and then trapped by allyl sulfones in a highly stereocontrolled fashion, providing radical allylation products with up to 97% ee. The hereby formed sulfonyl radicals are utilized through an enantioselective radical addition to form enantioenriched sulfones, which minimizes waste generation.

3) A simple and robust catalysis scheme that only relies on a single bis-cyclometalated rhodium catalyst (**RhS**) is introduced to achieve the stereocontrol of bond forming reactions directly from an electronically excited state. This is showcased by an intermolecular [2+2] photocycloaddition of enones with alkenes, which provides a wide range of cyclobutanes with up to >99% ee and up to >20:1 d.r. (Chapter 3.3). The catalyst/substrate complexation enhances visible-light-absorption,

achieves selective direct photoexcitation, and enables stereocontrolled direct bond formation from the photoexcited state. All reactive intermediates remain bound to the chiral catalyst thereby providing a robust catalytic scheme (no exclusion of air necessary) with excellent stereinduction. This strategy is further applied to a previously elusive visible-light-induced [2+3] photocycloaddition of acceptor-substituted alkenes with vinyl azides (Chapter 3.4). A wide range of complex 1-pyrrolines are obtained as single diastereoisomers and with up to >99% ee using a simple reaction setup and mild reaction conditions. This work expands the scope of stereocontrolled direct bond formation from photoexcited states which was previously limited to [2+2] photocycloadditions.

4) The chiral-at-metal complex **RhS** is shown to catalyze visible-light-activated catalytic asymmetric [3+2] photocycloadditions between acyl cyclopropanes and alkenes or alkynes, which provide access to cyclopentanes and cyclopentenones, respectively, in 63-99% yields and with excellent enantioselectivities of up to >99% ee (Chapter 3.5). Coordination of the cyclopropane with the chiral catalyst generates the visible-light-absorbing complex, lowers the reduction potential of the cyclopropane, and provides the asymmetric induction and overall stereocontrol. Enabled by a mild single electron transfer reduction of directly photoexcited catalyst/substrate complexes, the scope of asymmetric photocycloadditions is extended to simple mono-acceptor-substituted cyclopropanes with the synthesis of previously inaccessible enantioenriched cyclopentane and cyclopentenone derivatives.

5) A versatile electricity driven chiral-at-rhodium Lewis acid catalysis is disclosed (Chapter 3.6). Powered by an electric current, the oxidative cross coupling of 2-acyl imidazoles with silyl enol ethers provides a sustainable avenue to synthetically useful non-racemic 1,4-dicarbonyls, including products bearing all-carbon quaternary stereocenters. A chiral-at-rhodium complex (**RhS** or a sterically more demanding derivative) activates a substrate towards facile anodic oxidation by raising the highest occupied molecular orbital upon enolate formation, which enables mild redox conditions, high chemo- and enantioselectivities (up to >99% ee), and a broad substrate scope.

This thesis demonstrates the robustness and versatility of bis-cyclometalated rhodium-based Lewis acids by developing several mechanistically diverse and synthetically attractive asymmetric catalysis schemes. These chiral-at-rhodium Lewis acids are among the most powerful catalysts to address the long-standing challenge of stereocontrol in photochemical and electrochemical reactions.

Zusammenfassung

Asymmetrische Katalyse mit sichtbarem Licht oder mit elektrischer Energie zu betreiben, ist von erheblichem Wert, da dies eine „grüne“ und nachhaltige Methode zur Synthese von chiralen Molekülen darstellt. Darüber hinaus bietet sie Chemikern die Gelegenheit, neue mechanistische Szenarien zu entdecken und bisher unbekannte Transformationen zu entwickeln. Es ist jedoch eine große Herausforderung, den Reaktionsverlauf von photo- und/ oder elektrochemisch erzeugten reaktiven Zwischenstufen stereokontrolliert und katalytisch zu steuern. Diese Arbeit präsentiert neuartige Anwendungen von zuvor in der Meggers-Gruppe entwickelten *chiral-at-metal* Rhodium-Komplexen auf den Gebieten der asymmetrischen Photokatalyse und der asymmetrischen Elektrosynthese.

1) Ein biscyclometallierter *chiral-at-metal* Rhodium-Komplex (als **RhS** bezeichnet) in Kombination mit dem Photoredoxkatalysator $[\text{Ru}(\text{bpy})_3](\text{PF}_6)_2$ ermöglicht eine durch sichtbares Licht aktivierte asymmetrische α -Aminierung und α -Alkylierung von 2-Acylimidazolen mit Arylaziden bzw. von α -Diazocarbonyl-estern als Radikalvorläufer (Kapitel 3.1). Als erste Verwendung dieser Reagenzien für die photoinduzierte asymmetrische Katalyse weisen diese neuen protonen- und redoxneutralen Umwandlungen den Vorteil auf, dass molekularer Stickstoff als einziges Nebenprodukt entsteht und Ausbeuten von bis zu 99% sowie ausgezeichnete Enantioselektivitäten von bis zu > 99% ee erreicht werden können. Darüber hinaus wird eine breite funktionelle Gruppenkompatibilität gewährleistet.

2) Es konnte zudem gezeigt werden, dass ein biscyclometallierter *chiral-at-metal* Rhodium-Komplex (als **RhO** bezeichnet) zugleich eine stereokontrollierte Chemie von photo-generierten Radikalen als auch eine enantioselektive Sulfonyl-Radikaladdition an Alkene ermöglichen kann (Kapitel 3.2). Insbesondere unter Verwendung von Hantzsch-Estern als Photoredox-Mediatoren werden Rh-gebundene β -Enolat Radikale durch eine selektive photoinduzierte Einelektronenreduktion erzeugt und dann durch Allylsulfone hochstereokontrolliert abgefangen, wodurch radikalische Allylierungsprodukte mit bis zu 97% ee erhalten werden. Die dabei gebildeten Sulfonylradikale werden durch eine enantioselektive Radikaladdition zur Bildung enantiomerenreiner Sulfone verwendet, wodurch die Abfallerzeugung minimiert wird.

3) Ein einfaches und robustes Katalyseverfahren, das nur einen einzigen biscyclometallierten Rhodiumkatalysator (**RhS**) verwendet, wird eingeführt, um die Stereokontrolle von Bindungsbildungsreaktionen direkt aus einem elektronisch angeregten Zustand zu erreichen. Dies zeigt eine intermolekulare [2+2]-Photocycloaddition von Enonen mit Alkenen, die ein breites Spektrum an Cyclobutanen mit bis zu 99% ee und bis zu >20:1 d.r. liefert (Kapitel 3.3). Die Katalysator-/ Substrat-Komplexierung verbessert die Absorption von sichtbarem Licht, erreicht eine selektive direkte Photoanregung und ermöglicht die stereokontrollierte direkte Bindungsbildung aus dem photoangeregten Zustand. Alle reaktiven Zwischenprodukte bleiben an den chiralen Katalysator gebunden, wodurch ein robustes katalytisches System (kein Luftausschluss erforderlich) mit hervorragender Stereoinduktion bereitgestellt wird. Diese Strategie wird auch auf eine bisher schwer umsetzbare, durch sichtbares Licht induzierte [2+3]-Photocycloaddition von Akzeptor-substituierten Alkenen mit Vinylaziden angewendet (Kapitel 3.4). Eine Vielzahl an komplexen 1-Pyrrolinen kann jeweils als einfache Diastereoisomere mit bis zu >99% ee erhalten werden, unter Verwendung eines einfachen Reaktionsaufbaus und unter milden Reaktionsbedingungen. Diese Arbeit erweitert den Bereich der stereokontrollierten direkten Bindungsbildung aus photoangeregten Zuständen, der zuvor auf [2+2]-Photocycloadditionen beschränkt war.

4) Der *chiral-at-metal*-Komplex **RhS** ermöglicht eine durch sichtbares Licht aktivierte katalytische asymmetrische [3+2]-Photocycloaddition zwischen Acylcyclopropanen und Alkenen bzw. Alkinen, wodurch Cyclopentane bzw. Cyclopentene zugänglich sind. Hierbei werden Ausbeuten von 63-99% sowie ausgezeichnete Enantioselektivitäten von bis zu >99% ee (Kapitel 3.5) erreicht. Die Koordination des Cyclopropanes an den chiralen Katalysator erzeugt den sichtbares Licht absorbierenden Komplex, senkt das Reduktionspotential des Cyclopropanes und sorgt für die asymmetrische Induktion und die gesamte Stereokontrolle. Mittels einer milden Enelektronentransfer-Reduktion der direkt photoangeregten Katalysator-/ Substrat-Komplexe kann der Anwendungsbereich asymmetrischer Photocycloadditionen auf einfache Monoakzeptor-substituierte Cyclopropane ausgeweitet werden, wodurch bisher nicht zugängliche enantiomerenreine Cyclopentan- und Cyclopentenderivate synthetisiert werden können.

5) Eine vielseitige, durch Elektrizität betriebene *chiral-at-Rhodium* Lewis-Säure-Katalyse wird beschrieben (Kapitel 3.6). Durch elektrischen Strom angetrieben, bietet die oxidative Kreuzkupplung von 2-Acylimidazolen mit Silylenolethern einen nachhaltigen Weg zu synthetisch nützlichen

nicht-racemischen 1,4-Dicarbonylen, einschließlich Produkten, die quartäre Stereozentren enthalten. Ein *chiral-at*-Rhodiumkomplex (**RhS** oder ein sterisch anspruchsvolleres Derivat) aktiviert ein Substrat in Bezug auf eine einfachen leichten anodische Oxidation, indem das höchstes besetztes Molekülorbital bei der Enolatbildung angehoben wird. Dies ermöglicht milde Redoxbedingungen, hohe Chemo- und Enantioselektivitäten (bis zu >99% ee) und ein breites Substratspektrum.

Diese Arbeit demonstriert die Robustheit und Vielseitigkeit von biscyclometallierten auf Rhodium-basierenden Lewis-Säuren, indem sie mehrere mechanistisch unterschiedliche und synthetisch attraktive asymmetrische Katalyseverfahren entwickelt. Diese *chiral-at*-Rhodium Lewis-Säuren gehören zu den leistungsfähigsten Katalysatoren, welche die langjährige Herausforderung der Stereokontrolle in photochemischen und elektrochemischen Reaktionen in Angriff nehmen können.

Table of Content

Acknowledgements.....	I
Publications and Poster Presentations	III
Abstract	V
Zusammenfassung.....	VII
Table of Content	XI
Chapter 1. Theoretical Part.....	1
1.1 Introduction.....	1
1.2 Asymmetric Catalysis via Photoinduced SET	4
1.2.1 α -Functionalization of Carbonyls by Radical Addition to Enamines	4
1.2.2 α -Functionalization of Carbonyls through α -Iminyl/Carbonyl Radicals	7
1.2.3 Radical (Conjugate) Addition to Electron Deficient C=X Bonds	10
1.2.4 Radical-Radical Cross Coupling	15
1.2.5 Transition Metal Catalyzed Cross Coupling.....	17
1.2.6 Asymmetric Photocycloaddition Initiated by SET	21
1.3 Asymmetric Photocatalysis via Direct Bond Formation from Excited State	23
1.3.1 Lewis/Brønsted Acid Mediated Bathochromic Shift.....	23
1.3.2 H-Bonding Catalyst Mediated Intramolecular Energy Transfer	25
1.3.3 Dual-Catalyst for Selective Intermolecular Energy Transfer	26
1.3.4 Photooxygenation with Singlet Oxygen	27
1.4 Catalytic Asymmetric Electrosynthesis.....	29
1.4.1 Separated Electrochemical Process and Asymmetric Catalysis	29
1.4.2 Generation of Active Chiral Catalyst by Electrochemistry	31
1.4.3 Redox Activation upon Catalyst/Substrate Complexation	35
1.5 Asymmetric Photoredox Catalysis with Chiral-at-Metal Lewis Acids.....	37
1.5.1 α -Functionalization of Carbonyls through Enolate Intermediate	37
1.5.2 β -Functionalization of Enones by Radical Conjugate Addition	39
1.5.3 Radical-Radical Recombination of Ketones.....	41
1.6 Conclusions.....	43
Chapter 2. Aim of the Work.....	50
Chapter 3. Results and Discussion	53
3.1 Photoinduced Asymmetric Amination with Organic Azides and Alkylation with Diazo Compounds	53
3.1.1 Research Background and Reaction Design.....	53

3.1.2 Reaction Development of α -Amination.....	54
3.1.3 Further Extension to α -Alkylation.....	58
3.1.4 Substrate Scope	60
3.1.5 Mechanistic Studies.....	63
3.1.6 Conclusions	74
3.2 Combining the Catalytic Enantioselective Reaction of Visible-Light-Generated Radicals with a By-Product Utilization System	77
3.2.1 Research Background and Reaction Design.....	77
3.2.2 Reaction Development	79
3.2.3 Substrate Scope and Conversions of Products	83
3.2.4 Robustness Screening.....	86
3.2.5 Mechanistic Studies.....	87
3.2.6 Conclusions	93
3.3 Direct Visible-Light-Excited Asymmetric Lewis Acid Catalysis of Intermolecular [2+2] Photocycloaddition	97
3.3.1 Side Product Inspired Reaction Design and Research Background	97
3.3.2 Reaction Development	99
3.3.3 Substrate Scope	102
3.3.4 Mechanistic Studies.....	105
3.3.5 Conclusions	114
3.4 Catalytic Asymmetric Synthesis of 1-Pyrroline through Stereocontrolled Direct [2+3] Photocycloaddition from Excited State.....	117
3.4.1 Research Background and Reaction Design.....	117
3.4.2 Reaction Development	120
3.4.3 Mechanistic Studies.....	123
3.4.4 Substrate Scope and Synthetic Applications	128
3.4.5 Conclusions	132
3.5 Asymmetric [3+2] Photocycloaddition Enabled by Visible Light Excitation of Catalyst Bound Cyclopropanes.....	135
3.5.1 Research Background and Reaction Design.....	135
3.5.2 Development of [3+2] Photocycloaddition with Alkenes	137
3.5.3 Extension to [3+2] Photocycloaddition with Alkynes	142
3.5.4 Substrate Scope	143
3.5.5 Mechanistic Studies.....	147
3.5.6 Conclusions	151
3.6 Electricity Driven Asymmetric Lewis Acid Catalysis	154
3.6.1 Reaction Design and Research Background.....	154
3.6.2 Reaction Development	157
3.6.3 Substrate Scope	161
3.6.4 Mechanistic Studies.....	166
3.6.5 Extensions to Other Transformations	168
3.6.6 Conclusions	173

Chapter 4. Summary and Outlook	177
4.1 Summary	177
4.2 Outlook	185
Chapter 5. Experimental Part.....	187
5.1 General Materials and Methods.....	187
5.2 Photoinduced Asymmetric α-Amination and α-Alkylation.....	191
5.2.1 General Procedure	191
5.2.2 Synthesis of Substrates	191
5.2.3 Experimental and Characterization Data of Novel Products	195
5.2.4 Removal of 2-Aryl Imidazolyl Group	228
5.2.5 Single-Crystal X-Ray Diffraction Studies	229
5.3 Photoinduced Asymmetric β-Alkylation and β-Sulfonylation	232
5.3.1 General Procedure	232
5.3.2 Modifications for the Synthesis of Λ/Δ -RhO	232
5.3.3 Synthesis of Substrates	234
5.3.4 Experimental and Characterization Data of Novel Products	242
5.3.5 Single-Crystal X-Ray Diffraction Studies	260
5.4 Asymmetric [2+2] Photocycloaddition	264
5.4.1 General Procedure	264
5.4.2 Synthesis of Substrates	264
5.4.3 Experimental and Characterization Data of Novel Products	269
5.4.4 Single-Crystal X-Ray Diffraction Studies	288
5.5 Asymmetric [2+3] Photocycloaddition	293
5.5.1 General Procedure	293
5.5.2 Synthesis of Substrates	293
5.5.3 Experimental and Characterization Data of Novel Products	303
5.5.4 Synthetic Applications	326
5.5.5 Single-Crystal X-Ray Diffraction Studies	333
5.6 Asymmetric [3+2] Photocycloaddition	337
5.6.1 General Procedure	337
5.6.2 Synthesis of Substrates	337
5.6.3 Experimental and Characterization Data of Novel Products	344
5.6.4 Quantum Yield Measurement Using Powermeter as the Detector	385
5.6.5 Single-Crystal X-Ray Diffraction Studies	387
5.7 Asymmetric Electrosynthesis	389
5.7.1 General Procedure	389
5.7.2 Synthesis of Substrates	390
5.7.3 Experimental and Characterization Data of Novel Products	398
5.7.4 Single-Crystal X-Ray Diffraction Studies	425

Chapter 6. Appendices.....	432
6.1 List of Figures.....	432
6.2 List of Tables	437
6.3 List of Organometallic Complexes	438
6.4 List of Novel Organic Compounds	440
Statement.....	452
Curriculum Vitae.....	453

Chapter 1. Theoretical Part

1.1 Introduction

As the fundamental feature of organic compounds, chirality greatly influences the properties of molecules, and its implications are enormous in many areas including biology, medicine and material science.¹ For example, the diverse stereochemistry of organic molecules not only significantly enhances the richness of biological world, but also plays a profound role in many biological activities such as molecular communication. As for medicinal chemistry, the pharmaceutical effects of a drug can differ completely between enantiomers and/or diastereomers. In addition, many properties of materials derive from their chirality, and very often, reinforced properties are obtained from stereodefined polymers rather than the stereorandom ones.

Considering this importance, the synthesis of homochiral molecules is a long-standing goal in organic chemistry. To meet the growing need of chiral molecules, many methods have been developed, among which asymmetric catalysis is among the most economic and sustainable strategies. Recently, the invention of new techniques as well as the renaissance of traditional ones stimulate the development of asymmetric catalysis, which provides new opportunities, but also challenges for the generation of novel enantioenriched compounds.

Visible-light-activated catalysis has emerged as a powerful and green tool for synthetic chemistry during the last decade.² On one hand, photoredox catalysis provides accesses to a variety of reactive radicals and/or radical ions under mild and catalytic conditions.³ Taking the commonly used ruthenium-based polypyridyl photocatalyst $[\text{Ru}(\text{bpy})_3]^{2+}$ as an example (**Figure 1**, left), driven by visible light, an electron in one of the Ru-centered t_{2g} orbitals (HOMO) can be excited to a bpy-centered π^* orbital (LUMO), which is defined as metal to ligand charge transfer (MLCT). After intersystem crossing (ISC), the long-lived excited triplet photocatalyst, which consists of a Ru^{III} oxidizing center and a highly reducing ligand framework, is a remarkably better oxidant and at the same time a stronger reductant compared with the ground state. As a result, this excited species is able to initiate single electron transfer (SET) via oxidative quenching or reductive quenching pathways, generating highly reactive open-shell radicals and/or radical ions for follow-up bond formations. On

the other hand, electronically excited states of organic molecules can be accessed via photochemical activation which is hardly achieved by thermal activation, and possess distinctive reactivity, such as direct photocycloaddition and energy transfer process (EnT).⁴

In addition to photochemistry, the organic electrosynthesis is extremely attractive from the viewpoint of green chemistry and sustainable development (**Figure 1**, right).⁵ Since only the electrons serve as reagents, the electrochemistry avoids the use of stoichiometric amount of redox reagents (usually environmentally unfriendly), reduces the amount of waste generation, and allows simple and mild ways to access reactive open-shell radicals and radical ions. Thus it provides a robust and economic fashion to create diverse structurally different compounds. Recently, the combination of novel concepts in modern organic synthesis promotes a renaissance of synthetic electrochemistry. However, catalytic asymmetric electrosynthesis remains underdeveloped with limited number of general and highly stereoselective examples reported.

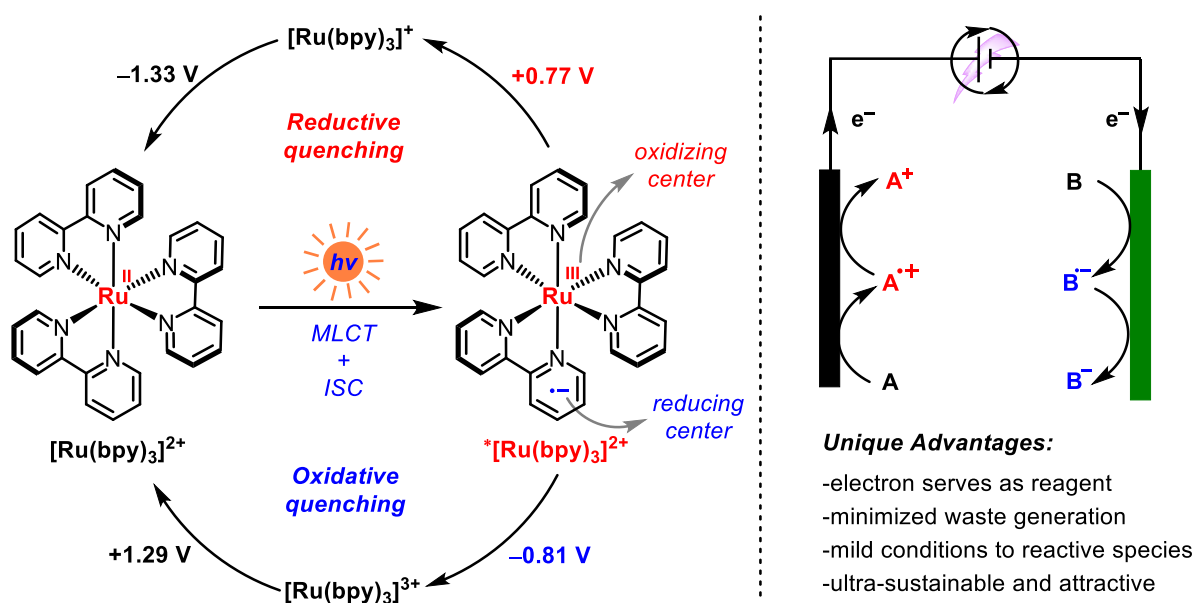


Figure 1. Visible light and electricity driven chemistry providing new opportunities for asymmetric catalysis. Potentials refer to SCE in MeCN.

To combine these appealing techniques with asymmetric catalysis, several challenges should be addressed (**Figure 2**). Fundamentally, the binding of a chiral catalyst to a substrate could decrease the activation barrier, thus achieving an enantioselective reaction. Indeed, many thermal reactions can not proceed without a suitable catalyst owing to the high energy barrier. However, the highly reactive

nature of the excited state renders the uncatalyzed background feasible. In addition, the photoinduced or electrochemically-generated intermediate radicals, radical ions, and/or ions are also high-energy, which makes it difficult to suppress the non-catalyzed side reactions that could affect asymmetric induction and overall yields. Besides, stabilities of the chiral catalysts under a photoreaction set-up or an electrochemical cell need to be considered.

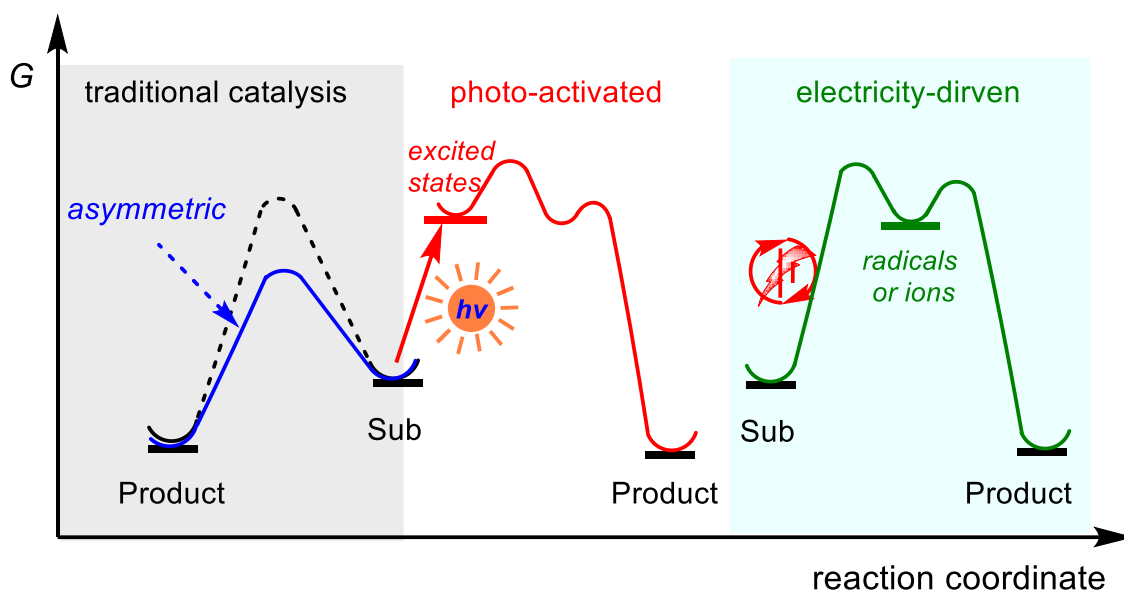


Figure 2. Enthalpy diagrams of a thermal, a photo-activated, and an electricity-driven reaction.

Novel strategies have been developed to solve these challenges and prompt the booming of asymmetric catalysis.⁶ This chapter summarizes the representative advances in these areas. According to the difference in mechanisms, it is divided into asymmetric catalysis with photoinduced SET, with direct bond formations from excited states, and driven by electricity. At the end of this chapter, the emerging concept of chiral-at-metal catalysis will be highlighted.

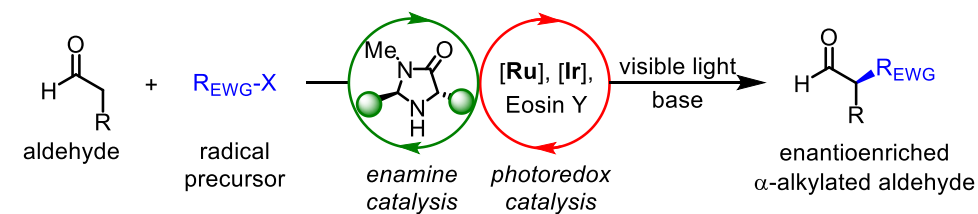
1.2 Asymmetric Catalysis via Photoinduced SET

Photoinduced single electron transfer (SET) has recently attracted much attention not only because of the mild and simple conditions provided by photoredox catalysis, but also owing to the versatile and useful reactivity of radicals and radical ions generated via SET processes.⁷ These reactive species offer a fertile test ground for chemists to develop new mechanistic pathways and to discover novel transformations, especially in stereocontrolled fashions.

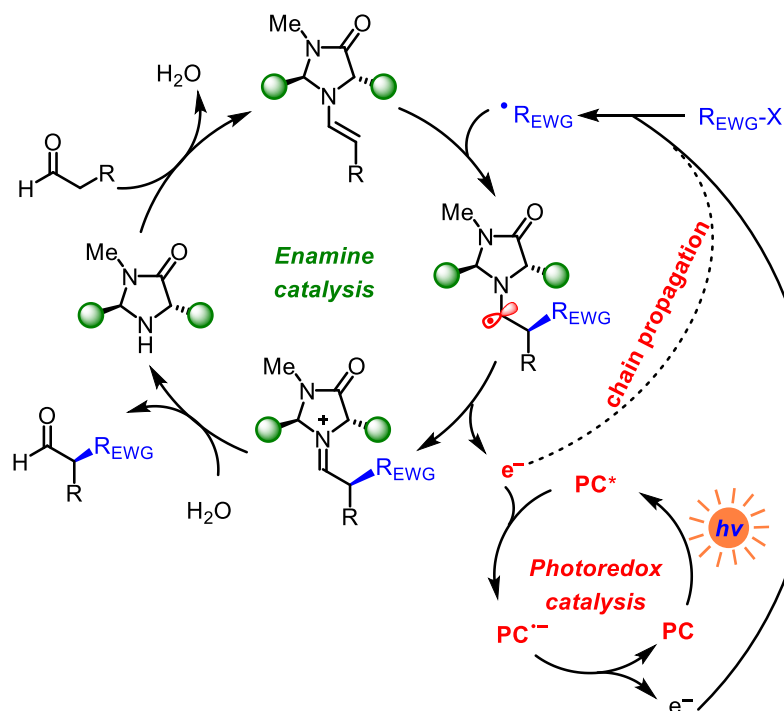
1.2.1 α -Functionalization of Carbonyls by Radical Addition to Enamines

In 2008, for the first time, Nicewicz and MacMillan merged photoredox catalysis with chiral enamine catalysis achieving the direct asymmetric alkylation of aldehyde (**Figure 3**).⁸ By the employment of acceptor-substituted alkyl bromides as radical precursors, $[\text{Ru}(\text{bpy})_3]^{2+}$ as photoredox catalyst and a chiral imidazolidinone as enamine catalyst, the challenging stereoselective C-C bond formation could be achieved under the illumination with a household compact fluorescent lamp (CFL) at room temperature, which is otherwise hard to make by ionic $\text{S}_{\text{N}}2$ pathway.

Mechanistically, the photoredox cycle produces alkyl radical via SET reduction of the alkyl bromide by the reduced PC^- species, which is initially generated by the reductive quenching of photoexcited PC^* by a sacrificial amount of enamine species. And at the same time, in the organocatalysis cycle, an enamine intermediate is formed by the condensation of the chiral imidazolidinone with an aldehyde. Then, the electron deficient alkyl radical stereoselectively adds to the electron rich enamine generating an α -amino radical intermediate. In the seminal report, it was proposed that the highly reducing α -amino radical transfers an electron to the excited photocatalyst (PC^*), thereby closing the photoredox cycle and generating iminium cation intermediate. Finally, hydrolysis of the iminium ion regenerates the chiral amine with the release of α -alkylated aldehyde. Notably, further mechanistic studies including the determination of quantum yield, elucidate that a radical chain manifold is the main reaction pathway.⁹ That is, SET from the intermediate α -amino radical to the alkyl bromide could directly furnish alkyl radical, hence enabling a self-propagating radical chain process.



Dual catalysis & radical chain mechanism:



Selected examples:

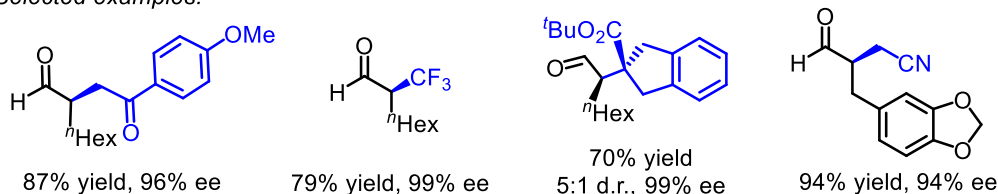


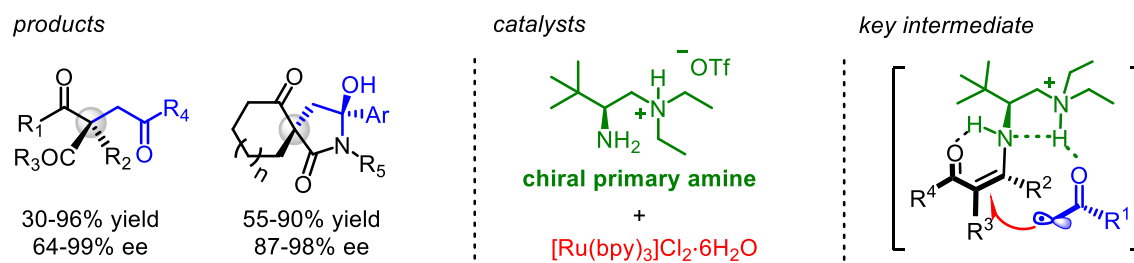
Figure 3. Merging photoredox and enamine catalysis for α -functionalization of aldehydes reported by MacMillan. Radical chain mechanism revised by Yoon.

This pioneering work has had many profound implications. The dual-catalyst system has been expanded to yield a variety of methodologies, such as asymmetric α -trifluoromethylation^{10a}, α -benzylation^{10b}, and α -cyanoalkylation^{10c}. Moreover, using *N*-2,4-dinitrophenylsulfonyloxy functionalized carbamates as nitrogen radical source, an enantioselective α -amidation of aldehydes was accomplished with a single enamine catalyst without the need for any external photoredox catalyst, in which a radical chain mechanism plays a vital role.^{10d} Besides, organic dyes, inorganic semiconductor, and other metal-based octahedral complexes were demonstrated to be suitable

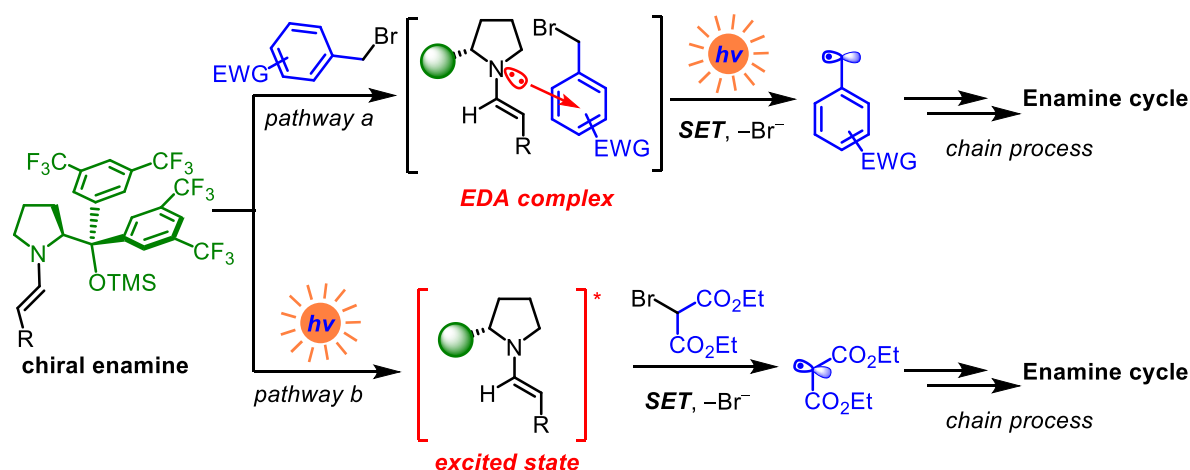
photoredox catalysts intertwining with asymmetric enamine catalysis.¹¹ But the most important impact of this work was the showcase of the integration of radical reactivity provided by photoredox catalysis with asymmetric organocatalysis, which laid a solid foundation for the development of modern photoredox catalysis.

As a very related example, Luo's group reported an enantioselective α -alkylation of 1,3-dicarbonyls using dual photoredox and chiral primary amine catalysis for the construction of a series of all-carbon quaternary stereocenters which are otherwise difficult to build by thermal activation (**Figure 4a**).¹² Hydrogen bonding between the intermediate enamine and the phenacyl radical species is proposed to explain the high asymmetric induction.

a) Luo, Approach to quaternary centers by dual primary amine/[Ru] catalysis



b) Melchiorre, A single chiral amine catalyst



c) Alemán, Bifunctional photoaminocatalyst

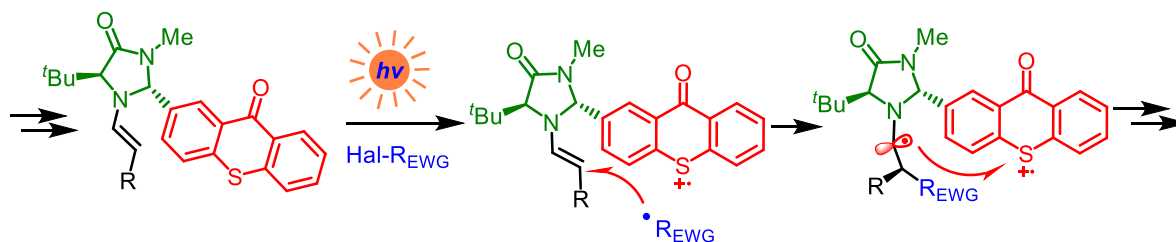


Figure 4. Selected other strategies for asymmetric photoredox α -functionalization of aldehydes.

While the dual-catalyst strategy relies on an additional photoredox catalyst together with a chiral catalyst to separate the photochemical process from stereodetermining bond formation, an attractive alternative is to combine stereoinduction and photoactivation in a single chiral catalyst. In this context, Melchiorre and co-workers disclosed a unique reaction scheme that a single chiral amine catalyst triggers the photochemical generation of alkyl radicals without usage of any external photoredox catalyst (**Figure 4b**).¹³ Two different pathways for the radical initiation are demonstrated depending on the substrate. Electron deficient benzyl bromides, which upon association with the electron-rich enamine species, can form colored electron donor-acceptor (EDA) complexes.^{13a} The EDA complex is capable of absorbing visible light and inducing SET event, thereby leading to the generation of a benzyl radical. A second radical formation pathway involves the direct photoexcitation of an enamine intermediate by near-UV light and the following SET between excited state enamine with bromomalonate, enabling access to an alkyl radical.^{13b} In analogy to the reaction scheme described in **Figure 3**, these radicals later engage in the enamine catalysis proceeding with a self-propagating radical chain mechanism. It is noteworthy that a related EDA complex which is formed with deprotonated cyclic β -ketoester and cinchonine-based phase-transfer catalyst has also been proved to participate in a similar asymmetric photoreaction.^{13c}

Another interesting strategy is to use a bifunctional photoaminocatalyst that constitutes of a photoactive thioxanthone group and an imidazolidinone moiety, as developed by Alemán *et al.* (**Figure 4c**).¹⁴ Excellent enantioselectivities and yields could be obtained for the alkylations of aldehydes by using this newly-developed photocatalyst, while the combination of enamine cat and thioxanthone gave similar results. Detailed mechanistic investigations were presented as well.

1.2.2 α -Functionalization of Carbonyls through α -Iminyl/Carbonyl Radicals

In 2017, the MacMillan group reported an elegant reaction which was interpreted as a combination of triple catalytic activation—photoredox catalysis, singly-occupied molecular orbital (SOMO) activation, and hydrogen atom transfer (HAT)—for the direct enantioselective α -alkylation of aldehydes (**Figure 5**).¹⁵ The combination of a bis-cyclometalated iridium-based photocatalyst, a chiral imidazolidinone or prolinol, and a thiophenol successfully enables both intra- and intermolecular coupling of aldehyde α -methylene with simple olefins. The reaction is proposed to proceed through an

interesting hydrogen and electron-borrowing mechanism. Accordingly, the enamine cycle starts with the condensation of the chiral amine with an aldehyde, generating an enamine intermediate. Concurrently, excited photocatalyst forms upon the irradiation by visible light. Then, SET between enamine and excited iridium species generates a reduced Ir(II) species and the key $3\pi e^-$ enaminy radical (also called α -iminyl radical cation). The radical species can be trapped reversibly by an olefin to generate a secondary nucleophilic radical intermediate. Subsequent HAT with a thiol catalyst leads to the iminium ion, the hydrolysis of which furnishes the enantioenriched product with the regeneration of the chiral amine catalyst. Finally, reduction of the thiyl radical by the reduced Ir(II) species regenerates the Ir(III) catalyst and thiol catalyst, thereby completing the photoredox and HAT catalysis.

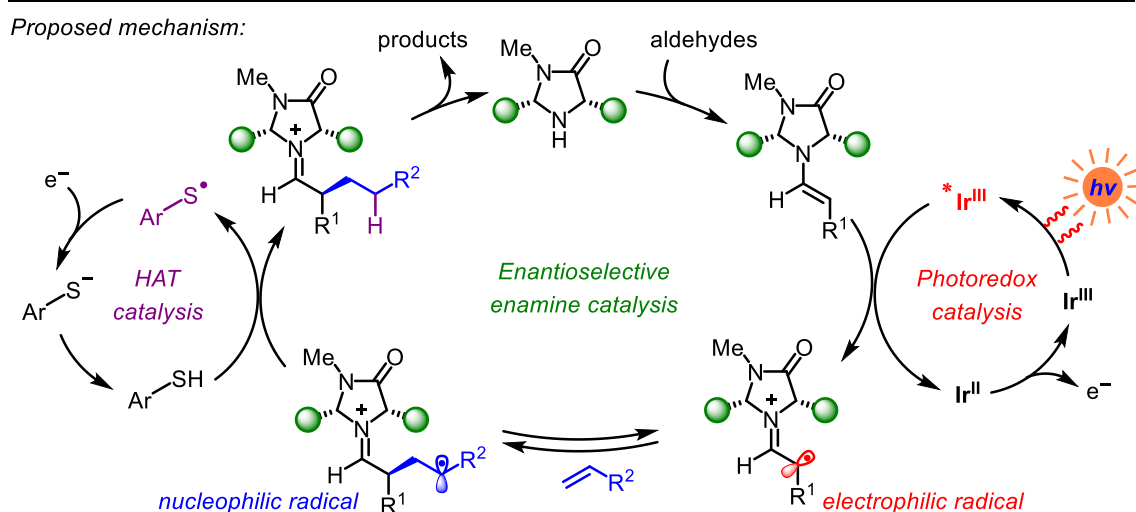
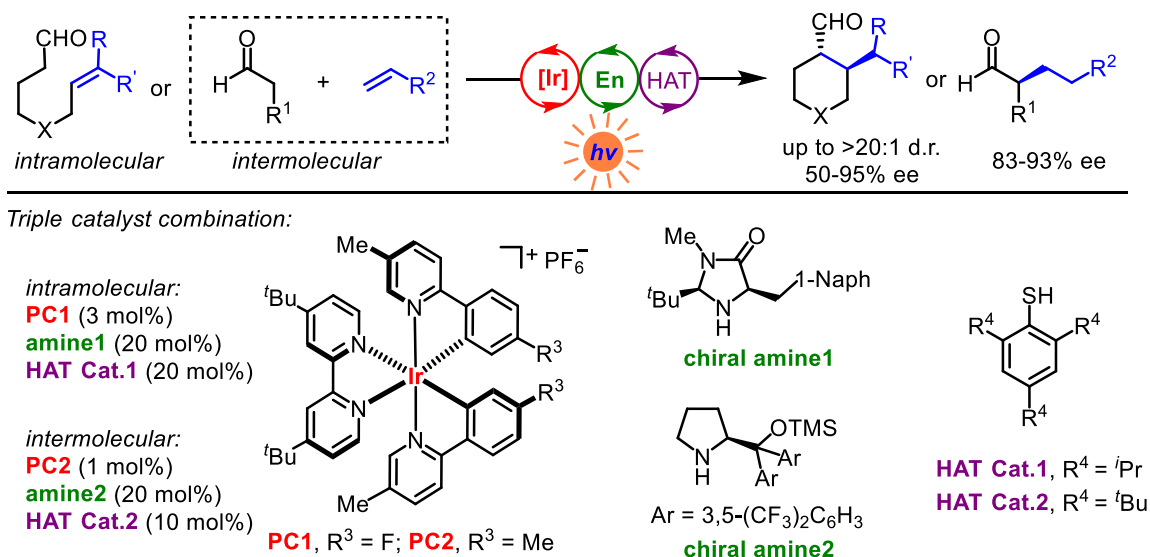


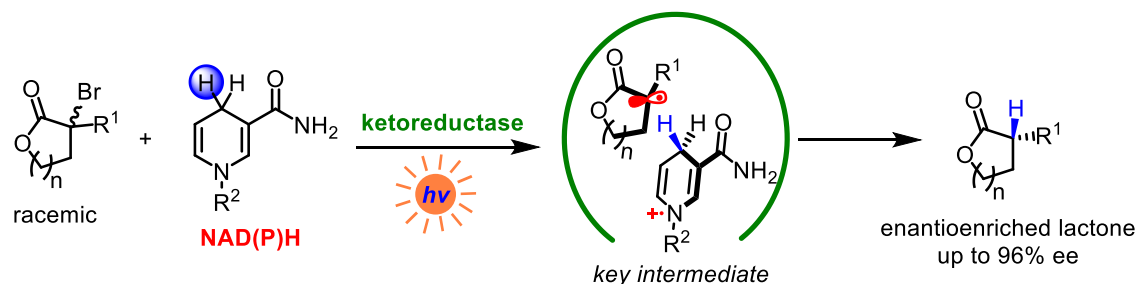
Figure 5. Enantioselective α -alkylation of aldehydes with olefins via triple catalytic activation.

This reaction avoids the use of stoichiometric oxidant and organic halides, allowing the construction of high-value molecules in an atom- and step-economic way. Noteworthy is that this work illustrates how the merger of photoredox catalysis with established activation modes could result in an unconventional transformation. Interestingly, this α -iminyl radical cation could also undergo a β -deprotonation to generate a β -enaminy radical intermediate, thereby enabling the direct β -arylation of carbonyl compounds.¹⁶

On the other hand, the related α -carbonyl carbon-centered radicals could be formed reductively (**Figure 6**). In 2016, the Hyster group reported a nicotinamide-dependent enzyme-catalyzed enantioselective radical dehalogenation of α -bromolactones (**Figure 6a**).^{17a} Under irradiation with visible light, the photoexcited cofactor NADH (the reduced form of nicotinamide adenine nucleotide) or NADPH (the reduced form of nicotinamide adenine dinucleotide phosphate) acts as a reductant to induce SET reduction of the enzyme bound lactone bromide, generating the key α -carbonyl radical intermediate. Subsequently, HAT between the radical intermediate and NAD(P)H radical cation produces the enantioenriched product with the stereochemistry controlled by the enzyme. Later, the same group expanded the scope to an enantioselective deacetoxylation by the integration of xanthene-based photocatalysis with enzyme catalysis.^{17b} These reports highlight the great potential of applying photoredox catalysis for the access of non-natural reactivity of enzymes.¹⁸

Very recently, Jiang and co-workers demonstrated an asymmetric radical cross coupling of a prochiral α -acyl carbon-centered radical, generated by SET reductive debromination of racemic α -bromoketone, with an α -amino radical derived from oxidative decarboxylation of *N*-aryl amino acid (**Figure 6b**).¹⁹ A chiral phosphoric acid catalyst provides good asymmetric induction and chemoselectivity, while the dicyanopyrazine-derived chromophore (DPZ) enables the photoredox process. Notably, various fluoro-hetero-quaternary and all-carbon quaternary stereocenters could be successfully constructed, which is otherwise difficult to achieve.

a) Hyster's work on visible-light-activated enzymatic radical dehalogenation



b) Jiang's work on radical cross coupling

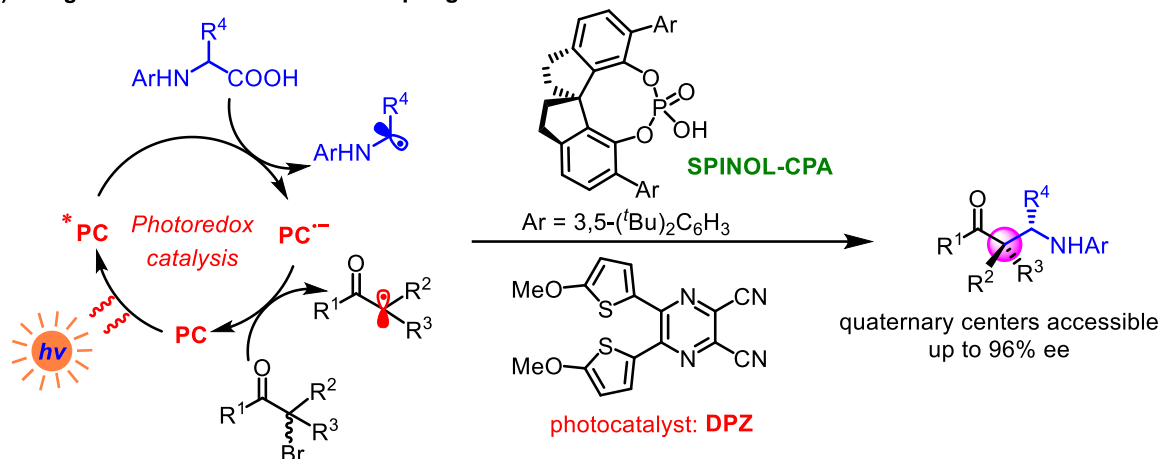


Figure 6. Reductive generations of α -carbonyl carbon-centered radicals and their asymmetric transformations.

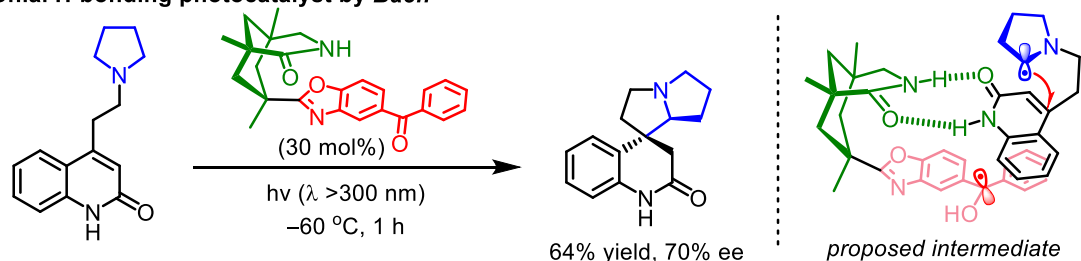
1.2.3 Radical (Conjugate) Addition to Electron Deficient C=X Bonds

Catalytic enantioselective conjugate addition of electron rich radicals to electron deficient C=C bonds is more challenging owing to the uncatalyzed background reaction. With respect to the area of stereocontrolled reactions initiated by photoinduced photoreactions, in 2005 Bach's group presented an asymmetric hydrogen-bonding photocatalysis, in which an intramolecular addition of α -amino alkyl radical to a quinolone scaffold mechanism is proposed (**Figure 7a**).²⁰ Significant enantiomeric excess of up to 70% could be obtained under irradiation of UV-light at low temperature.

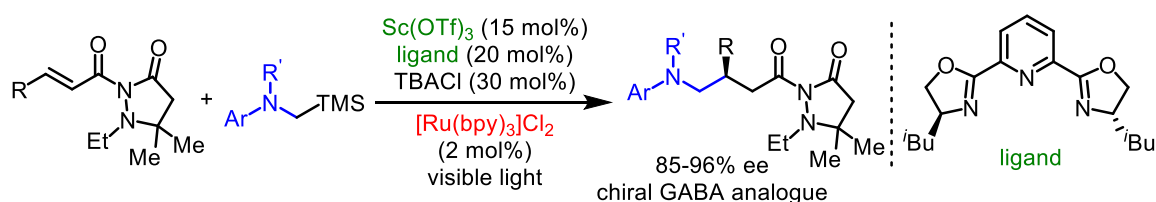
Later in 2015, Yoon and co-workers demonstrated a more general and highly enantioselective intermolecular addition of α -amino radicals to Michael acceptors by using the dual photoredox/chiral Lewis acid strategy (**Figure 7b**).²¹ [Ru(bpy)₃]²⁺ photoredox catalyst is used for the oxidative generation of electron rich radical species from α -silylalkyl amine, which then adds to the chiral Lewis acid bound α,β -unsaturated carbonyl substrate in a stereoselective fashion to produce a secondary

α -carbonyl radical. SET reduction of this electrophilic radical species by the reduced $[\text{Ru}]^-$ species furnishes an enolate intermediate which undergoes sequential protonation and ligand exchange to generate β -functionalized product and complete the Lewis acid cycle. Alternatively, SET between α -silylalkyl amine and α -carbonyl radical results in a radical chain mechanism. The scandium(III)/chiral PyBOX ligand based Lewis acid catalysis is independent of the photoinduced SET and more importantly, it can accelerate the rate of radical addition so significantly that the racemic background reaction is suppressed. To be mentioned, the ability of chiral Lewis acid to control the stereochemistry of radical conjugate addition can be traced back to Sibi's report on magnesium bisoxazoline complex catalyzed enantioselective radical conjugate additions.²²

a) Chiral H-bonding photocatalyst by Bach



b) Dual photoredox/chiral Lewis acid catalysis, reported by Yoon



Possible mechanism:

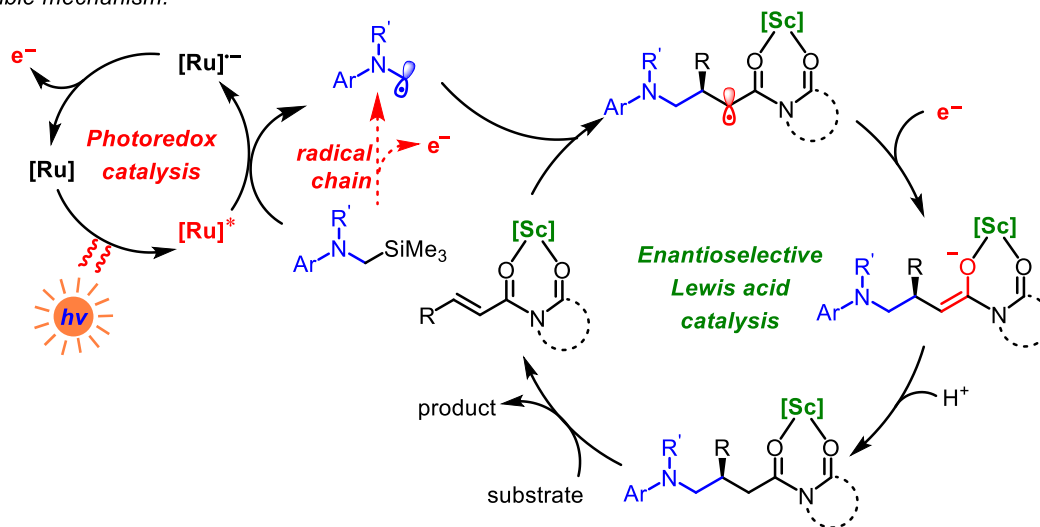


Figure 7. Enantioselective conjugate addition of α -amino radicals.

2-vinylpyridine & 2-vinylquinoline + ArHNCH₂COOH
SPINOL-CPA (15 mol%), DPZ (0.2 mol%), 3 W blue LEDs, -35 °C
ArHNCH₂CH(R)CH₂Py/Q
67 - >99% ee

Ar = 2-CF₃C₆H₄ or 2-naphthyl

The reaction scheme illustrates the asymmetric synthesis of 1,2-disubstituted cyclohexanones. The starting material is a cyclohexanone with a substituent R^1 and a chain length $n = 0-3$. It reacts with a chiral amine (20 mol%) and a photocatalyst under UV or visible light in the presence of benzoic acid to yield the product in 64-98% ee. The reaction proceeds via two pathways: a HAT or SET pathway and a SET pathway. The HAT or SET pathway involves the formation of an iminium ion, which is then attacked by a radical R^\bullet to form an unstable radical cation. This intermediate undergoes intramolecular SET and tautomerization to form an imine. The SET pathway involves the formation of an imine, which is then attacked by a radical R^\bullet to form an unstable radical cation. This intermediate undergoes intramolecular SET and tautomerization to form an imine. The reaction is catalyzed by a chiral amine (20 mol%) and a photocatalyst under UV or visible light in the presence of benzoic acid. The reaction is catalyzed by a chiral amine (20 mol%) and a photocatalyst under UV or visible light in the presence of benzoic acid.

Reaction Conditions:

- chiral amine (20 mol%)
- photocatalyst
- UV or visible light
- benzoic acid

Reaction Pathways:

- HAT or SET:** The reaction proceeds via a HAT or SET pathway, involving the formation of an iminium ion, which is then attacked by a radical R^\bullet to form an unstable radical cation. This intermediate undergoes intramolecular SET and tautomerization to form an imine.
- SET:** The reaction proceeds via a SET pathway, involving the formation of an imine, which is then attacked by a radical R^\bullet to form an unstable radical cation. This intermediate undergoes intramolecular SET and tautomerization to form an imine.

Key Intermediates and Reagents:

- iminium ion**
- unstable radical cation**
- imine**
- SET** (Single Electron Transfer)
- HAT** (Hydrogen Atom Transfer)
- intramolecular SET**
- tautomerization**
- (S,S)-amine** (e.g., TBADT)
- (R,R)-amine** (e.g., Ir[dF(CF₃)ppy]₂(dtbbpy)⁺)

12

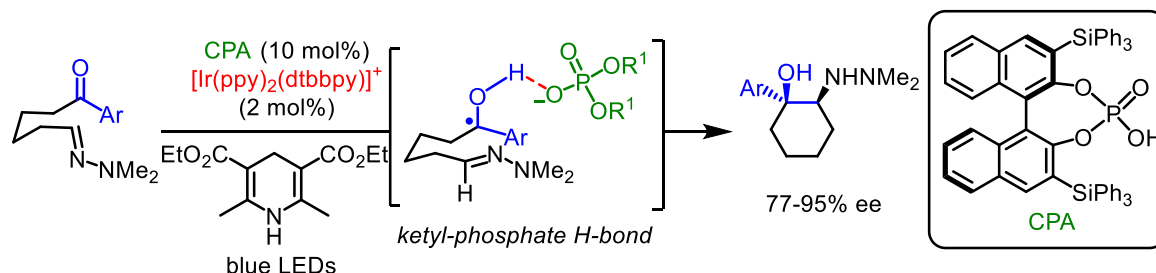
The Jiang group disclosed a cooperative photoredox and chiral phosphoric acid catalysis scenario for the visible-light-induced asymmetric conjugate addition of *N*-aryl glycine derived radicals to α -branched 2-vinylazaarenes (**Figure 8b**).²⁴

Another elegant strategy revealed by Melchiorre and co-workers is the merger of a well-designed chiral organic amine catalyst with photoredox catalysts, which was applied to the enantioselective radical conjugate addition to β,β -disubstituted cyclic enones leading to the building of quaternary stereocenters with high fidelity (**Figure 8c**).^{25a} Particularly, the chiral amine catalyst contains a redox-active carbazole motif at a strategic position that is crucial to facilitate a rapid intramolecular SET reduction of the unstable α -iminyl radical cation. This SET event and the subsequent tautomerization prevent the potential back-electron transfer and trigger the reversible radical addition/ β -scission processes toward the desirable iminium ion trapping direction, resulting in a more stable imine intermediate. Finally, the SET reduction of the carbazole motif and the following hydrolysis afford the product. Overall, by this way of electron-relay mechanism, previously limited construction of quaternary carbon stereocenter was successfully accomplished.

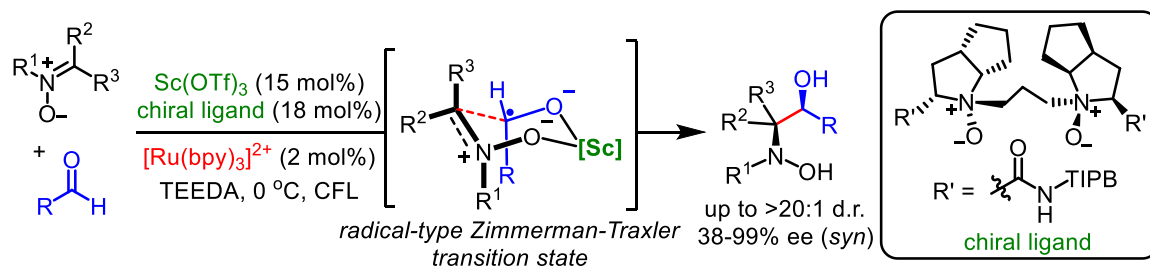
Besides acceptor-substituted C=C bonds, C=N bonds could also be used as acceptors for photoinduced asymmetric radical additions (**Figure 9**). In 2013, the Knowles group disclosed a dual photoredox/Brønsted acid catalysis to enable an asymmetric aza-pinacol cyclization (**Figure 9a**).²⁶ A concerted proton-coupled electron transfer (PCET) process collectively mediated by an iridium-based photoredox catalyst and a chiral phosphoric acid is proposed to produce the key neutral ketyl radical intermediate. The following intramolecular radical addition generates a new C-C bond and after follow-up SET forms an enantioenriched *syn*-1,2-amino alcohol derivative with excellent stereoselectivity. During the stereodetermining radical addition step the ketyl radical remains hydrogen bonded with the conjugate base of the chiral Brønsted acid.

In 2018, Huang's group reported an elegant intermolecular reductive coupling of aldehydes with nitrones catalyzed by dual photoredox/Lewis acid catalysis with a chiral *N,N'*-dioxide ligand (**Figure 9b**).²⁷ The proposed key radical addition step goes through a radical-type Zimmerman-Traxler transition state, thus providing excellent stereoselectivity for the synthesis of enantioenriched vicinal amino alcohols. Further applications of this protocol for the concise synthesis of pharmaceutically related molecules were demonstrated.

a) Knowles, PCET enabled asymmetric aza-pinacol cyclization



b) Huang, Reductive cross-coupling of nitron with aldehyde



c) Phipps, Enantioselective Minisci-type addition

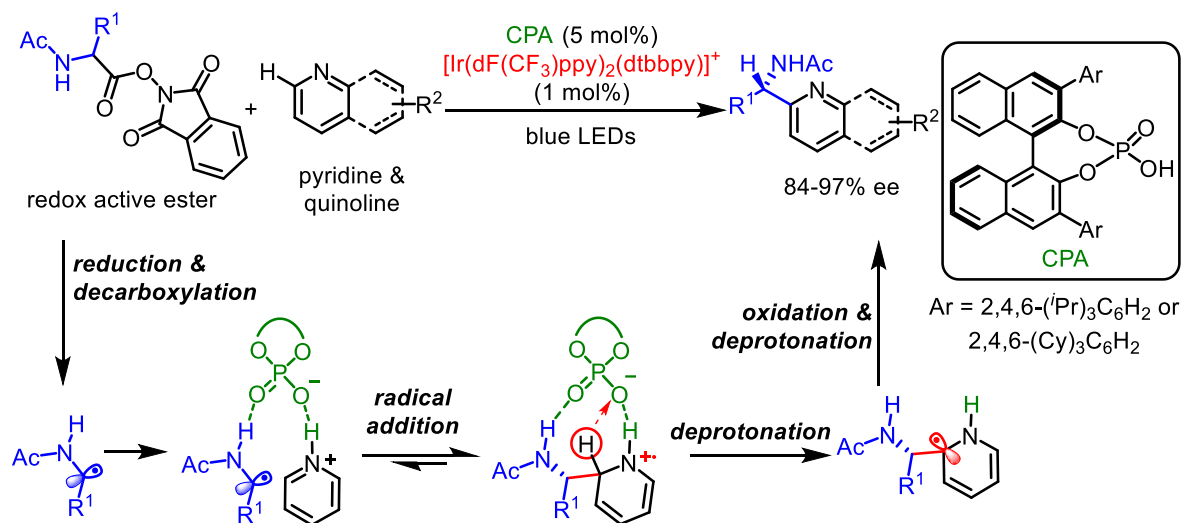


Figure 9. Dual photoredox/acid catalysis enabled enantioselective radical additions.

Very recently, Phipps and co-workers expanded the dual-catalyst system to a photoinduced enantioselective Minisci-type radical addition to heteroarenes (**Figure 9c**).²⁸ Amino acid derived redox active ester was used as the precursor of nucleophilic *N*-acyl α -amino radical. Noteworthy is the multiple-role of the chiral phosphoric acid, the conjugate anion of which is supposed to not only engage in the H-bonding with both *N*-acyl α -amino radical and protonated *N*-heteroarene, but also facilitate the key intra- and/or intermolecular deprotonation step which is supposed to be the

irreversible product-determining step. Under the CPA provided chiral environment, sequence reversible radical addition and irreversible deprotonation steps could lead to the differentiation of diastereomers, thus explaining the asymmetric induction of this reaction.

1.2.4 Radical-Radical Cross Coupling

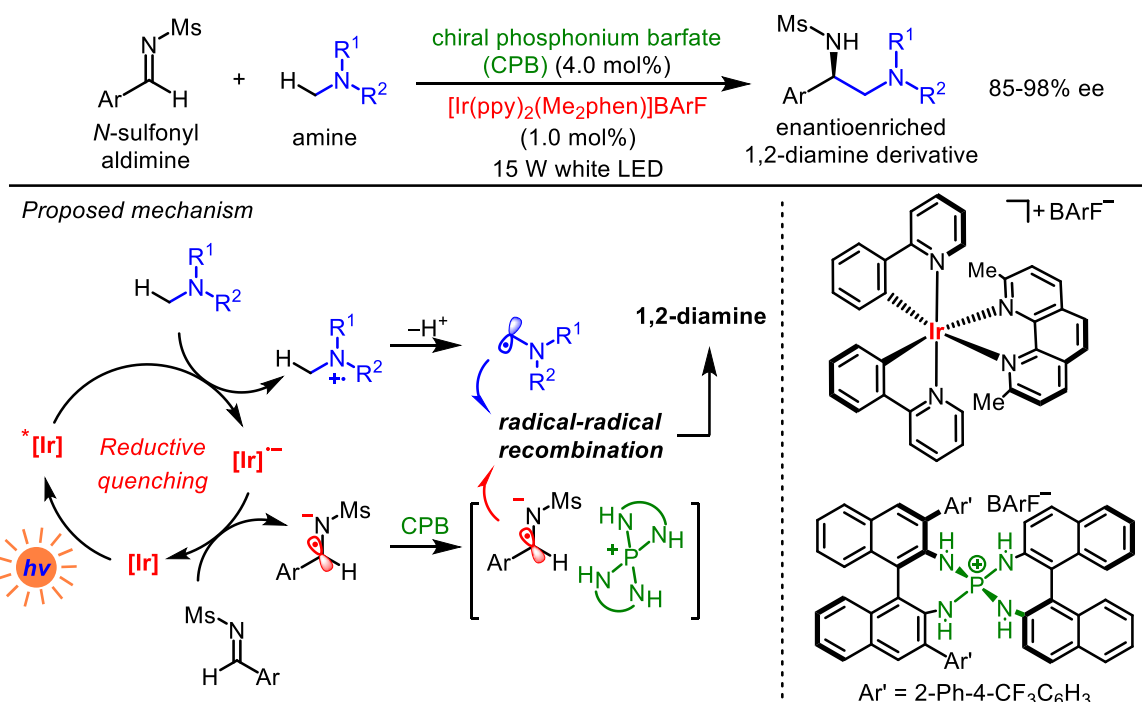


Figure 10. Ooi's work on synergistic catalysis of photoredox catalyst and chiral arylaminophosphonium barfate for a photoinduced asymmetric radical-radical cross coupling.

In some cases, radical-radical recombination mechanism rather than radical conjugate addition is proposed for the cross coupling of nucleophilic radicals with electrophilic unsaturated C=X bonds. For instance, Ooi's group reported an asymmetric radical-radical cross coupling event enabled by synergistic catalysis of iridium-based photoredox catalyst and chiral arylaminophosphonium barfate (**Figure 10**).^{29a} In the proposed mechanism, reductive quenching of photoexcited iridium species generates an amino radical cation, which after deprotonation gives an α-amino carbon-centered radical. And the resulting reduced iridium species can transfer a single electron to the imine, generating the corresponding prochiral radical anion intermediate. The interaction of this radical anion with the chiral aminophosphonium ion affords the key chiral ion pair. Finally, radical coupling of two radical species furnishes the 1,2-diamine product with the stereochemistry being controlled by the chiral ionic

Brønsted acid. Later, they expanded the scope of amino radical precursors to silylamines, where an oxidative quenching pathway of the photoexcited $^*\text{Ir}(\text{ppy})_3$ might be operative.^{29b} These reports show the insensitivity of the redox-neutral bond formation to the sequence of the photoredox events, and more importantly, this radical-radical cross coupling mechanism shed light on new reaction pathways of photogenerated radicals.³⁰

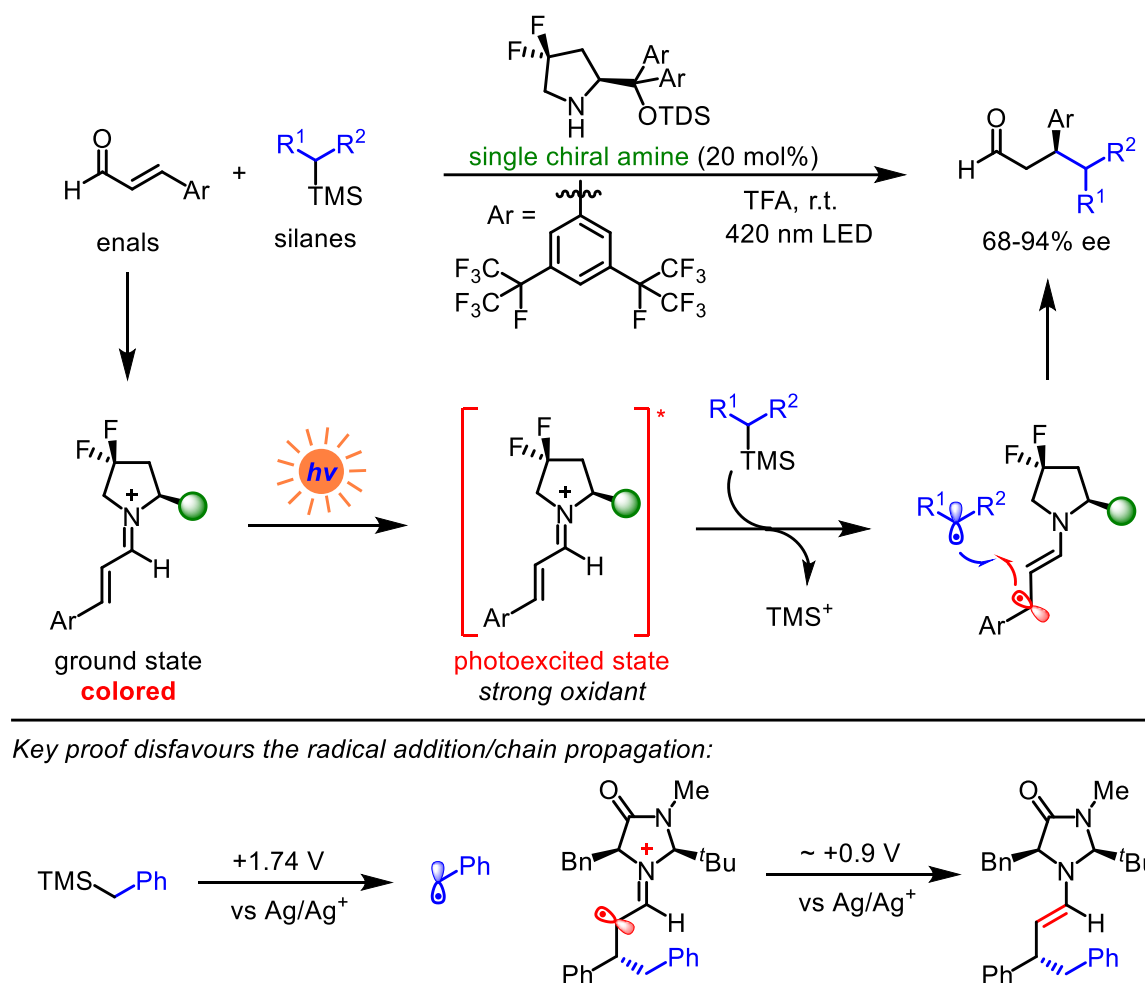


Figure 11. Melchiorre's work on stereocontrolled β -alkylation of enals enabled by direct photoexcitation of iminium ion and radical-radical recombination.

As for β -functionalization of enones, a radical-radical recombination pathway is also feasible. As an elegant demonstration, Melchiorre and co-workers developed a single chiral amine catalyzed enantioselective β -alkylation of enals with benzylic silanes (**Figure 11**).^{31a} Accordingly, selective photoexcitation of colored iminium ion intermediate forms an electronically excited state, which acts as a strong oxidant to oxidize silane to generate the key β -enaminy radical intermediate and

concurrently gives a benzyl radical upon irreversible desilylation. Recombination of these two radicals in a stereocontrolled way furnishes the β -functionalized product. This radical-radical cross coupling mechanism is supported by several observations. The poor nucleophilicity of benzyl radical and low tendency of radical trapping using iminium ion render a radical conjugate addition unlikely, which is in consistent with a determined quantum yield of 0.05. Importantly, redox potentials indicate that SET oxidation of the benzyl silane by the α -iminyl radical cation is endergonic, which suggests the radical conjugate addition/chain propagation mechanism is unfavorable.

It is worth noting that back in 1980th, Mariano has reported transformations of iminium salts with UV-light excitations.³² Melchiorre's work inspires chemists to unlock untraditional transformations by exploiting the reactivity of visible-light-excited iminium ions. Later, they further applied this strategy to achieve the expansion of radical precursors to readily available 4-alkyl-1,4-dihydropyridine^{31b}, unactivated olefin^{31c}, and even toluene derivatives^{31d}. Furthermore, a radical-polar cascade through excited iminium ion and ground state enamine sequence allowed the stereoselective cyclization of enal with racemic cyclopropanol, affording stereochemically dense cyclopentanol.^{31e}

1.2.5 Transition Metal Catalyzed Cross Coupling

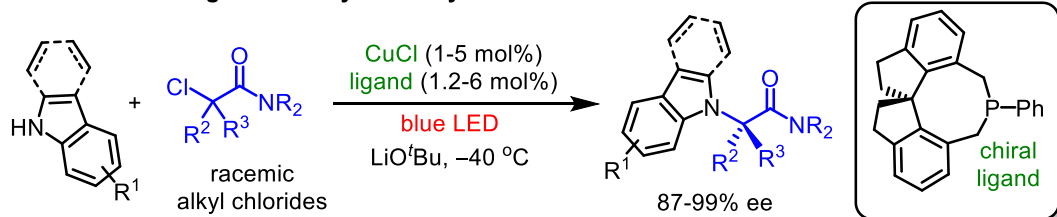
Merger of photoredox catalysis with nickel chemistry opens a conceptually new single-electron transmetalation framework to overcome the otherwise challenging Csp³-Csp²/sp³ cross coupling, and provides ample opportunities for developing novel asymmetric catalytic photoreactions. Pioneering work in dual photoredox/nickel catalysis was reported in 2014 by Molander³³, Doyle and MacMillan,³⁴ respectively. The first enantioselective example was presented in Molander's paper, where 50% ee was obtained for the cross coupling of an aryl bromide with a benzyl trifluoroborate employing a chiral bisoxazoline ligand (**Figure 12a**). The initially proposed mechanistic scheme starts with the oxidative addition of the aryl bromide to the Ni(0) catalyst with the formation of arylnickel(II) complex (**Figure 12b**, blue solid). Concurrently, SET oxidation of trifluoroborate by photoexcited [Ir]* forms a C-centered benzylic radical, which is trapped by the arylnickel(II) complex delivering a Ni(III) species. Reductive elimination of this Ni(III) intermediate furnishes the cross coupling product and Ni(I) complex, the latter of which is reduced by the iridium-based reducing species to regenerate the Ni(0) complex, thus closing the nickel catalysis and photoredox catalysis. Later, computational studies by

Based on this work, highly enantioselective photoinduced nickel catalyzed cross couplings were developed. In 2016, Fu and MacMillan achieved an enantioselective decarboxylative arylation of naturally abundant α -amino acids, approaching to valuable chiral benzylic amines in up to 93% ee (**Figure 12c**).³⁶ More recently, Rovis and Doyle reported an enantioselective desymmetrization of cyclic *meso*-anhydrides with benzyl trifluoroborates as radical precursor, which provides access to *trans* keto-acids with high stereoselectivity (up to >20:1 d.r., up to 94% ee, **Figure 12d**).³⁷ Interestingly, based on a UV/Vis study, the authors proposed that a Ni^{0/II/III} cycle is more likely for this desymmetrization reaction.

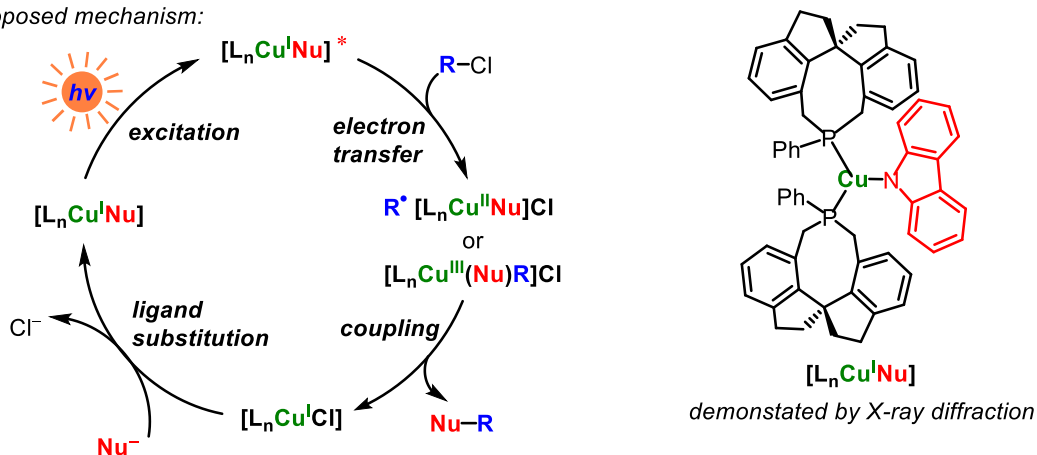
With respect to photoinduced asymmetric copper catalysis, Fu pioneered this area. In 2016, the Fu group disclosed a single Cu-based photocatalytic scheme for the enantioconvergent C-N cross coupling of amines with racemic tertiary alkyl chlorides to yield fully substituted stereocenters with good yields and excellent enantioselectivities (up to 99% ee) (**Figure 13a**).³⁸ Notably, a single and earth-abundant copper based complex not only provides asymmetric induction but also serves as photoredox catalyst initiating an electron transfer process. A possible catalytic cycle initiates with the irradiation of a Cu-nucleophile complex, which leads to the excited state copper complex. Then, electron transfer with alkyl chloride forms an electrophilic alkyl radical and a Cu(II) complex. Subsequently, bond forming coupling could occur through an outer- or inner-sphere mechanism, generating Cu(I) species with the formation of product. A copper(I) complex that contains two chiral phosphine and a carbazolidine motif was characterized and proved to be a plausible intermediate for this catalysis. Significance of this work is that it represents the seminal advance in the field of based metal catalyzed asymmetric cross coupling of alkyl halides driven by visible light.

Based on their earlier work on copper catalyzed radical C-H cyanation,^{39a} the Liu group integrated asymmetric copper catalysis with photoinduced radical generation, achieving an enantioselective decarboxylative cyanation of *N*-hydroxy-phthalimide ester (**Figure 13b**).^{39b} An oxidative quenching cycle of *fac*-Ir(ppy)₃ generates benzylic radical and concurrently forms the oxidizing PC⁺, the latter of which can oxidize LCu(I)-CN species to generate a Cu(II) intermediate. Further reaction with the nucleophile TMS-CN, followed by combining with the prochiral benzylic radical furnishes the coupling product and regenerates a Cu(I) complex. Notably, both of the alkyl radical intermediate and the active Cu(II) species are generated through mild photoredox catalysis. This is distinctive from their previous non-photo catalysis^{39a} where a strong F⁺ oxidant is needed.

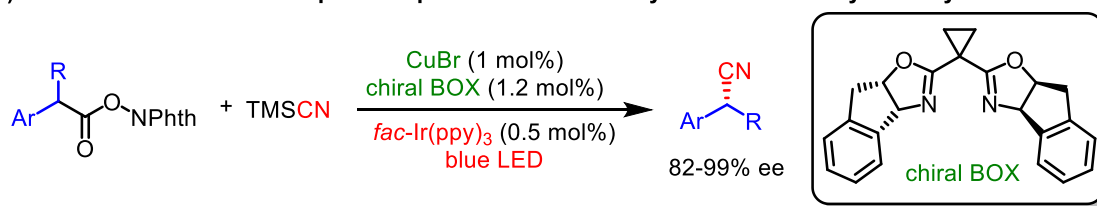
a) Fu's work on a single Cu catalyst for asymmetric C-N formation



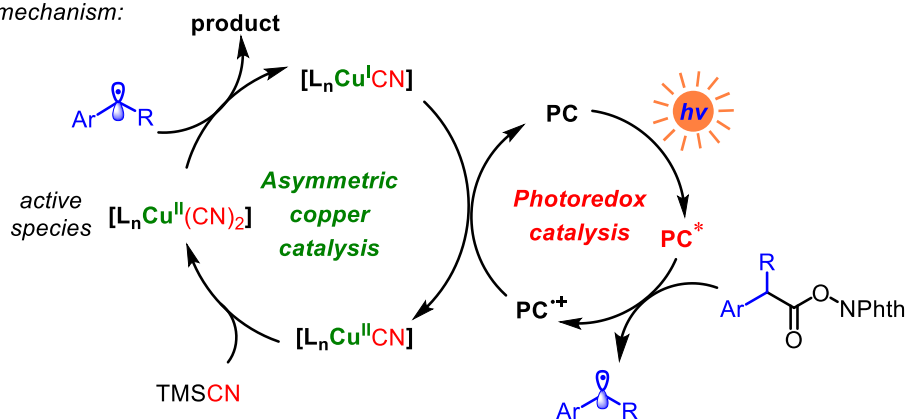
Proposed mechanism:



b) Lin and Liu's work on cooperative photoredox/Cu catalysis for decarboxylative cyanation



Proposed mechanism:



c) Mei and Han's work on dual photoredox/Cu catalysis for cyanoalkylation of styrenes

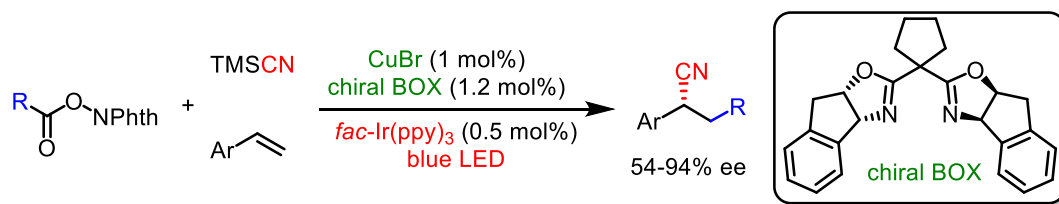


Figure 13. Photoinduced asymmetric copper catalysis.

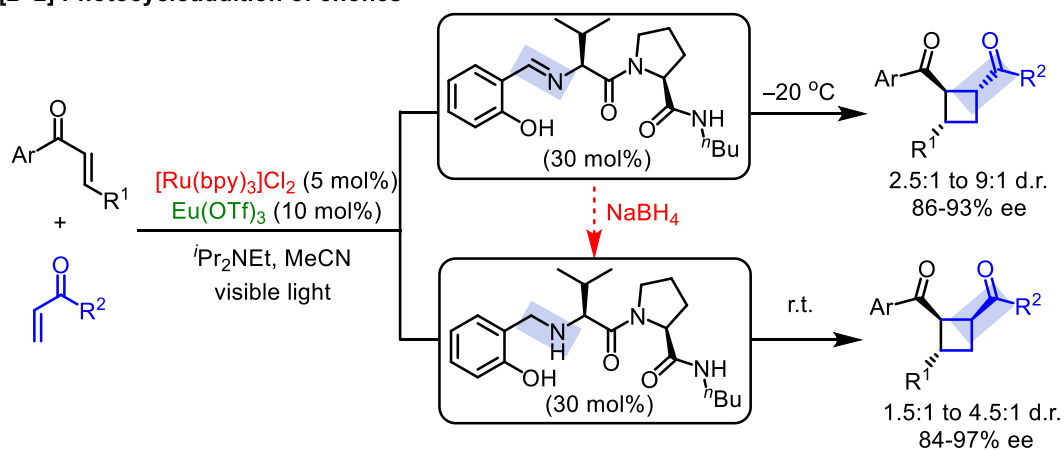
Very recently, an enantioselective three-component radical cyanoalkylation of alkenes was reported by Mei, Han and co-workers by the employment of a dual chiral copper/photocatalyst strategy (**Figure 13c**).⁴⁰ A photogenerated alkyl radical adds to a styrene to afford the benzylic radical, the trapping of which by the active Cu(II) intermediate furnishes the radical difunctionalization product in up to 94% ee. It is impressive that in all these three reactions the loading of chiral catalyst could be as low as 1 mol%, showcasing the high catalytic efficiency of the copper catalyst.

1.2.6 Asymmetric Photocycloaddition Initiated by SET

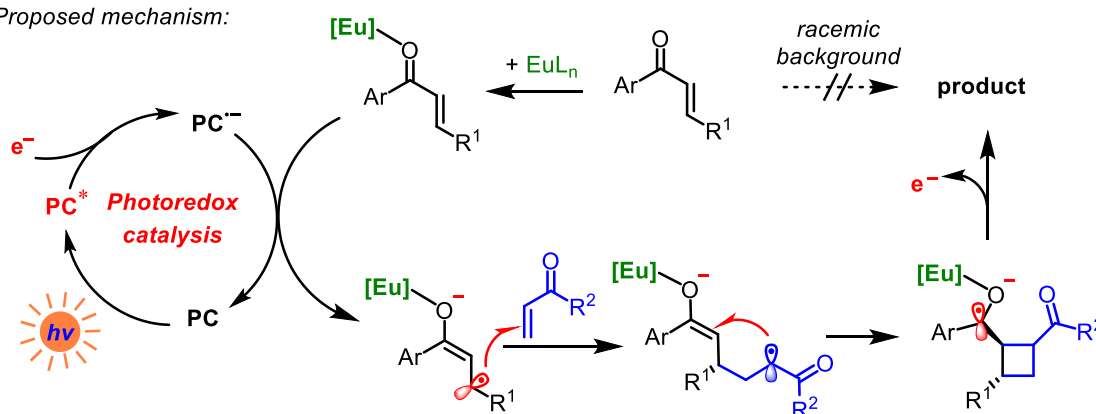
Photocycloaddition is undoubtedly among the most efficient methods to construct cyclic structural motifs. However, because of the uncatalyzed background reaction, achieving catalytic asymmetric photocycloaddition is extremely difficult. In 2014, Yoon developed a dual-catalyst system for the intermolecular asymmetric [2+2] photocycloaddition of enones yielding a series of enantioenriched cyclobutanes (**Figure 14a**).^{41 a} This system includes a visible light absorbing ruthenium-based photoredox catalyst and a chiral Lewis acid co-catalyst, the latter of which is capable of both controlling stereochemistry and activating one of the substrates toward facile SET reduction. Specifically, the photoexcited [Ru]* accepts an electron to form the highly reducing [Ru]⁻. Selectively reduction of the Lewis acid bound substrate, rather than the free substrate, results in the key metallo enolate radical intermediate which is then trapped by another electron deficient enone, thus producing a secondary electrophilic radical intermediate. Subsequently, intramolecular radical cyclization forms the ketyl radical. Finally, the release of a single electron generates final cyclobutanes product.

The key to the success of this reaction is that only the chiral Lewis acid coordinated substrate could undergo the selective SET event while the resultant reactive radical intermediates remain bound to the chiral catalyst, therefore avoiding the complications arising from uncatalyzed racemic background reaction and ensuring high asymmetric induction. Interestingly, altering the chiral Schiff base ligand to the corresponding reduced secondary amine ligand leads to the complementary diastereoselectivity, highlighting the flexibility of this dual-catalyst system.

a) [2+2] Photocycloaddition of enones



Proposed mechanism:



b) [3+2] Photocycloaddition of cyclopropyl ketone with alkene

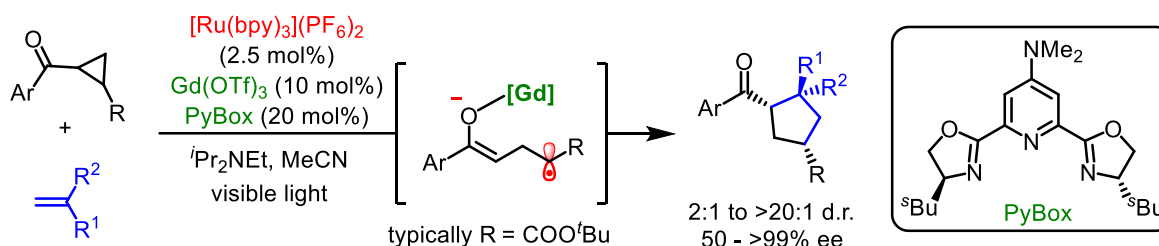


Figure 14. Yoon's reports on dual photoredox/chiral Lewis acid catalysis enabled asymmetric photocycloadditions which involve SET processes.

Later, they extended the scope of asymmetric photocycloaddition to a previously unfeasible [3+2] photocycloaddition of aryl cyclopropyl ketones with alkenes (**Figure 14b**).^{41b} Accordingly, sequential SET reduction and ring opening of the Lewis acid coordinated cyclopropane gives the key remote enolate radical intermediate, which engages in stepwise radical cycloaddition with an alkene to give the cyclopentane product. Again, this work demonstrates the robustness of dual photoredox/Lewis acid catalyst strategy and is anticipated to promote the development of stereocontrolled photochemical transformations.

1.3 Asymmetric Photocatalysis via Direct Bond Formation from Excited State

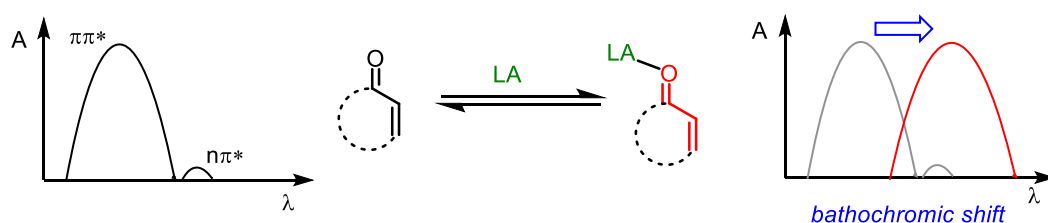
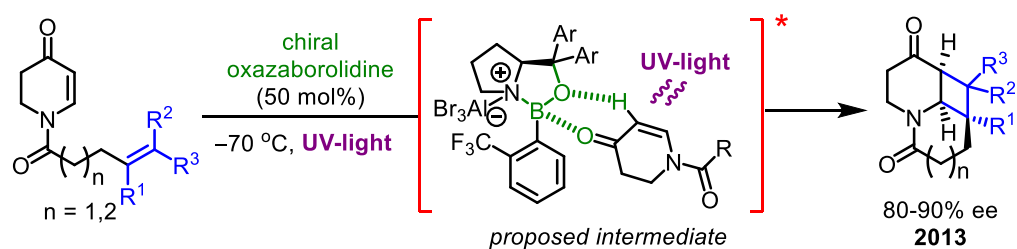
Direct bond formation from electronically excited state, without any charge separation, is an appealing alternative to photoinduced SET. While an excited state can be uniquely accessed by photochemical techniques, its reactivity toward [2+2] photocycloaddition is the most frequently used photochemical reaction.⁴² Typically, the stereodetermining step of this photocycloaddition occurs directly on the excited states without the involvement of free radicals or radical ions, which is mechanistically distinguish from the above-mentioned SET induced cycloadditions (**Figure 14**). Consequently, the problems arising from free radical intermediates, such as undesirable side reactions and limited substrate scope, could be avoided. However, performing such reaction in a catalytic asymmetric way remains underexplored, which is mainly due to the difficulty in suppressing the background racemic reaction of the excited substrate that is not associated with a chiral catalyst.

1.3.1 Lewis/Brønsted Acid Mediated Bathochromic Shift

One of the strategies to address this challenge is based on the bathochromic shift provided by Lewis/Brønsted acid catalysis. As illustrated in **Figure 15a**, upon coordination of a Lewis acid, the $\pi\pi^*$ absorption of a α,β -unsaturated carbonyl compound significantly shifts to the longer wavelength. Hence, selective photoexcitation of the chiral Lewis acid bound substrate over the free substrate can be achieved by using a light source with the selected emission wavelength.

The application of this effect in catalytic asymmetric photoreaction can be traced back to 2010, when Bach's group⁴³ reported the first example of enantioselective intramolecular [2+2] photocycloaddition of coumarins^{43a,b} (**Figure 15b**). A chiral oxazaborolidine was identified as the ideal catalyst to facilitate the reaction, providing the cycloadduct in 82% ee. Later, dihydropyridones^{43c} and 3-alkenyloxy-2-cycloalkenones^{43d} were successfully applied to the asymmetric intramolecular photocycloadditions. Furthermore, chiral Lewis acid catalyzed intermolecular [2+2] photocycloadditions of cyclic enones^{43f} and phenanthrene-9-carboxaldehydes^{43g} have been achieved. Although these reactions often require high catalyst loading, UV-light irradiation, and low temperature, the concept of bathochromic shift paves a way for the development of novel enantioselective photochemical reactions.

a) Chromophore activation of enone by Lewis Acid

b) *Bach*, Lewis acid catalysis

other cyclic structures:

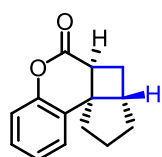
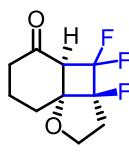
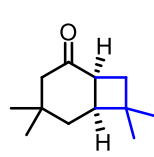
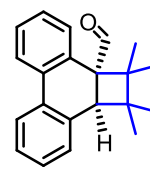
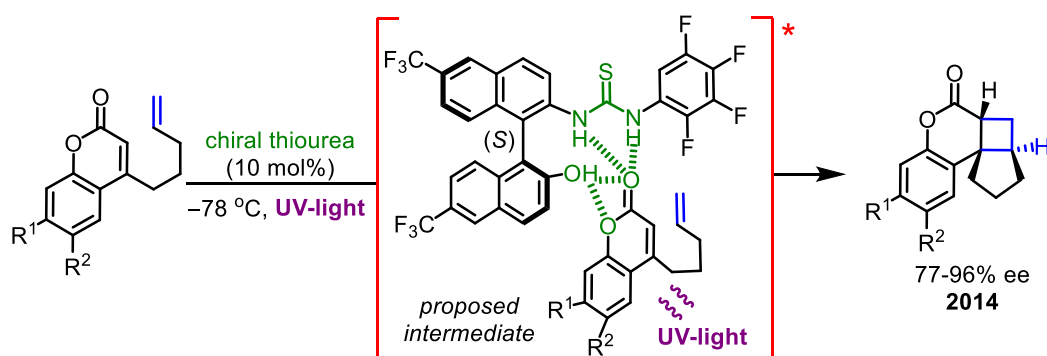
82% ee
from *coumarin*
2010 & 201276% ee
from *3-alkenyloxy-2-cycloalkenone*
201493% ee
from *cyclic enones*
201894% ee
from *phenanthrene-9-carboxaldehyde*
2018 (visible light)c) *Sibi and Sivaguru*, Brønsted acid catalysis

Figure 15. Asymmetric [2+2] photocycloadditions enabled by chromophore activation and direct excitation.

In 2014, a chiral thiourea based Brønsted acid was introduced to catalyze an enantioselective [2+2] photocycloaddition of coumarins (**Figure 15c**).⁴⁴ Sibi, Sivaguru *et al.* proposed a three-point bonding mode between the chiral thiourea and coumarin substrate, which explains the bathochromic shift, prolonged lifetime of the excited state, and also increased ISC rate. All of these effects contribute to the catalytic efficiency and asymmetric induction of the overall photocycloaddition.

1.3.2 H-Bonding Catalyst Mediated Intramolecular Energy Transfer

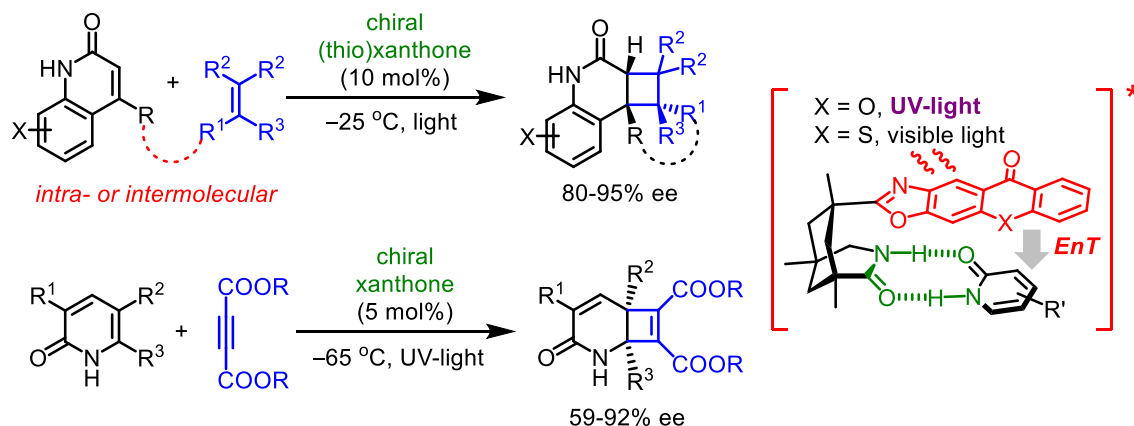
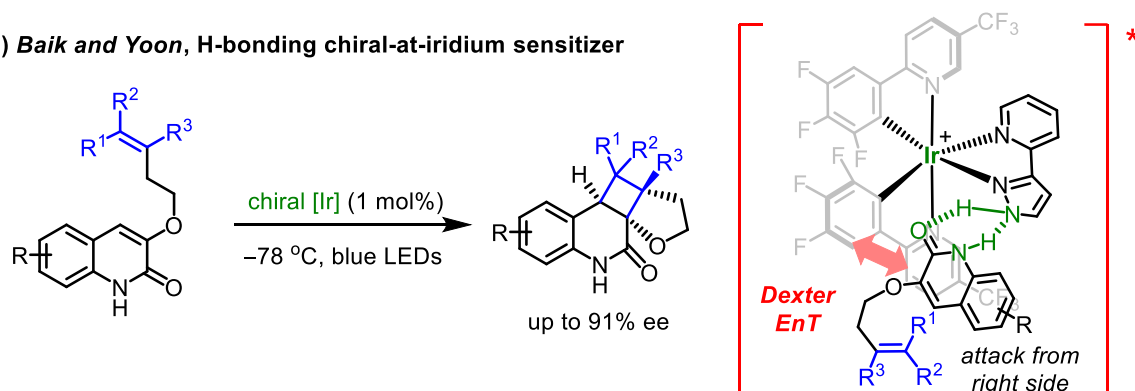
a) *Bach*, H-bonding organocatalysisb) *Baik and Yoon*, H-bonding chiral-at-iridium sensitizer

Figure 16. Asymmetric [2+2] photocycloadditions enabled by H-bonding catalysis through intramolecular energy transfer (EnT).

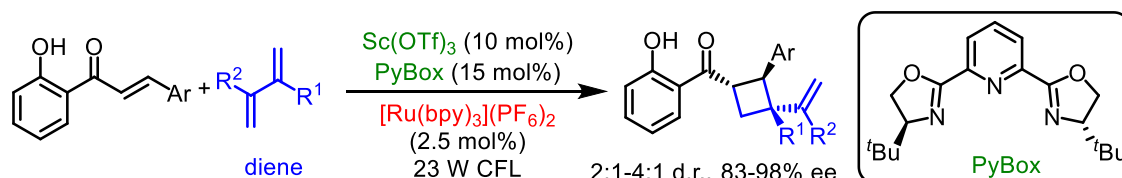
As pioneering work, in 2009, Bach developed a chiral xanthone photosensitizer for the enantioselective intramolecular [2+2] photocycloaddition of 2(1*H*)-quinolones under the irradiation of UV-light (**Figure 16a**).^{45a} Later, they expanded to intermolecular cycloaddition of 2-pyridone with acetylenedicarboxylate.^{45c} By using a related thioxanthone catalyst, visible light activation could be achieved.^{45d,e} This type of catalyst consists of a (thio)xanthone moiety that after photoexcitation is responsible for energy transfer (EnT), and an amide group at the chiral backbone which is supposed to engage in H-bonding interactions with the substrate. The formed H-bonding complex not only provides enantioface differentiation but also allows a selective intramolecular EnT, both of which play vital roles for obtaining high asymmetric induction.

Inspired by this work and the chiral-at-metal H-bonding catalyst developed by Meggers⁴⁶, Baik and Yoon recently developed an interesting chiral-at-metal iridium-based photosensitizer for a related

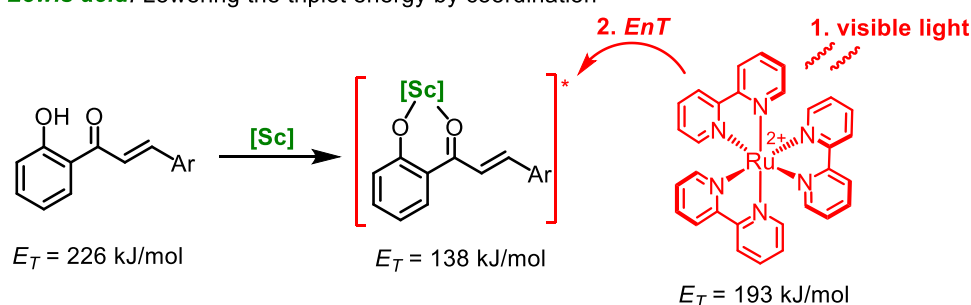
enantioselective [2+2] photocycloaddition (**Figure 16b**).⁴⁷ Mechanistic studies elucidate that a series of H-bonding between the coordinated pyrazole ligand and substrate quinolone, as well as π - π interactions organize this prochiral substrate in an appropriate position within the metal-centered chiral environment. Only the intermediate that is competent for the effective (intramolecular) Dexter type energy transfer event can participate in the photocycloaddition, which is supposed to guarantee the effective asymmetric induction.

1.3.3 Dual-Catalyst for Selective Intermolecular Energy Transfer

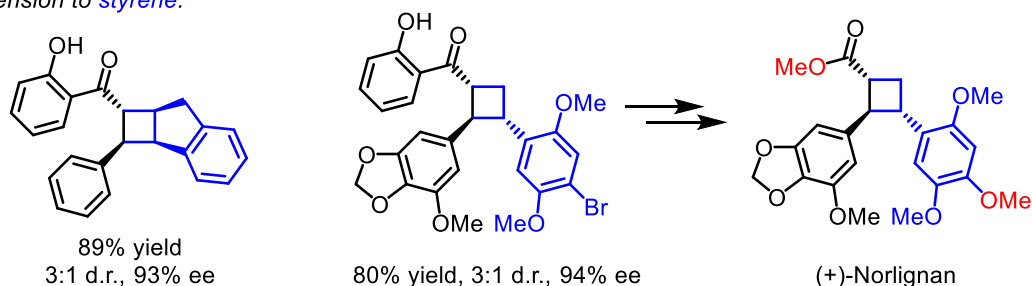
a) Yoon, Dual chiral Lewis acid/photosensitizer



Role of **Lewis acid**: Lowering the triplet energy by coordination



Extension to *styrene*:



b) Bach, Proof of the principle for E_T activation upon iminium ion formation

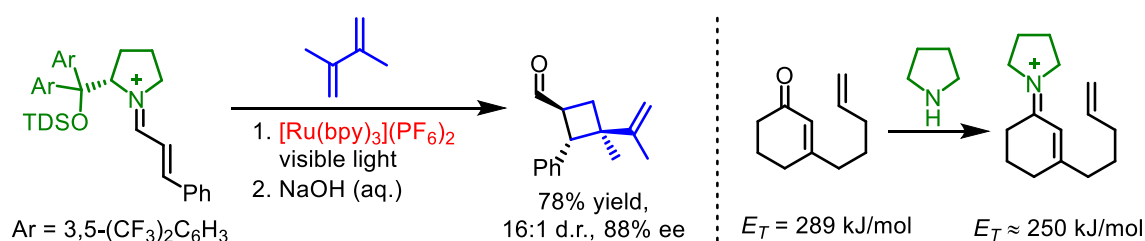


Figure 17. Enantioselective [2+2] photocycloadditions via triplet chromophore activation.

In 2016, Yoon *et al.* for the first time applied triplet chromophore activation for the dual Lewis acid/photosensitizer catalyzed asymmetric [2+2] photocycloaddition of 2'-hydroxychalcone with diene (**Figure 17a**).^{48a} They discovered that Lewis acid coordination can significantly decrease the triplet energy of the chalcone substrate, thereby enabling the selective intermolecular EnT from an additional excited photosensitizer to the chiral catalyst bound substrate rather than the free substrate. As the result, stereocontrolled cycloadditions occur on the electronically excited states to yield enantioenriched cyclobutanes in good yields and enantioselectivities, albeit with unsatisfactory d.r. values. Later, they utilized this strategy to expand the scope of alkene to different styrene generating 1,2-diary cyclobutanes in high level of enantioselectivities.^{48b} And a natural product was synthesized from one of the cycloadducts, demonstrating the utility of this reaction.

Recently, Bach's group showed that iminium ion formation can also lower the triplet energy of the corresponding α,β -unsaturated carbonyl compound (**Figure 17b**).⁴⁹ As a proof of the principle study, the photocycloaddition of a chiral iminium ion with a diene catalyzed by the triplet sensitizer $[\text{Ru}(\text{bpy})_3]^{2+}$ furnished the cyclobutane upon hydrolysis in 88% ee with an excellent d.r. value of 16:1.

1.3.4 Photooxygenation with Singlet Oxygen

As the lowest excited state of the dioxygen molecule, singlet oxygen is easily accessible through visible light sensitization and its reaction toward aerobic oxidation has been well established.⁵⁰ It is worth mentioning that in 2017 the Xiao group devised a novel bifunctional chiral photocatalyst for the enantioselective hydroxylation of β -ketoesters with singlet oxygen under visible light conditions (**Figure 18**).^{50c} The in situ formed photocatalyst is a nickel based enolate complex with a newly designed chiral bisoxazoline ligand containing a thioxanthone chromophore. Upon visible light excitation, this complex enables the formation singlet oxygen via triplet energy transfer. The following oxygenation with enolate furnishes the α -hydroxy- β -dicarbonyl compounds in good to excellent enantiopurities. Notably, besides serving as visible-light-absorbing antenna, the thioxanthone-containing sidearm benefits the asymmetric induction and efficiency of the photoreaction through the dynamic steric effect.⁵¹ Both yield and ee of the product dropped significantly when the combination of a chiral BOX ligand and an additional photosensitizer was used instead. This elegant design is anticipated to inspire the development of new photocatalyst for

asymmetric photoreactions.

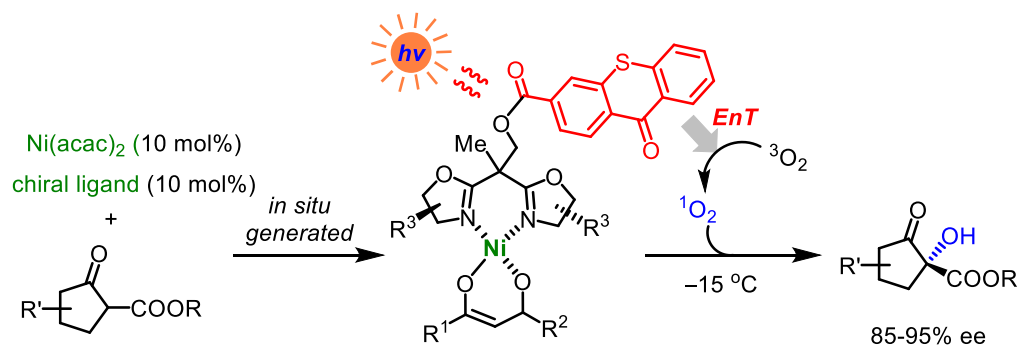


Figure 18. Xiao's work on enantioselective hydroxylation catalyzed by a bifunctional photocatalyst.

1.4 Catalytic Asymmetric Electrosynthesis

Although organic electrosynthesis is currently experiencing a renaissance with plenty of new electrochemical methodologies established recently,⁵² catalytic asymmetric electrochemistry is still in its infancy. Owing to the above-mentioned challenges (**Figure 2**), only limited examples of electrochemical asymmetric catalysis were reported, which usually suffer with modest enantioselectivity. According to different roles of the chiral catalyst in electrochemical processes, the examples can be classified into three strategies (**Figure 19**): a) the asymmetric catalysis is separated from the electrochemical process, where the substrate is converted electrochemically into a reactive intermediate which is then interfaced with asymmetric catalysis; b) the active chiral catalyst is generated electrochemically—either by direct electrolysis or through indirect electrolysis with a redox mediator; c) Redox activation upon catalyst/substrate complex formation, in which a single chiral catalyst is typically enough to facilitate the electrochemical process and at the same time provide stereochemical control.

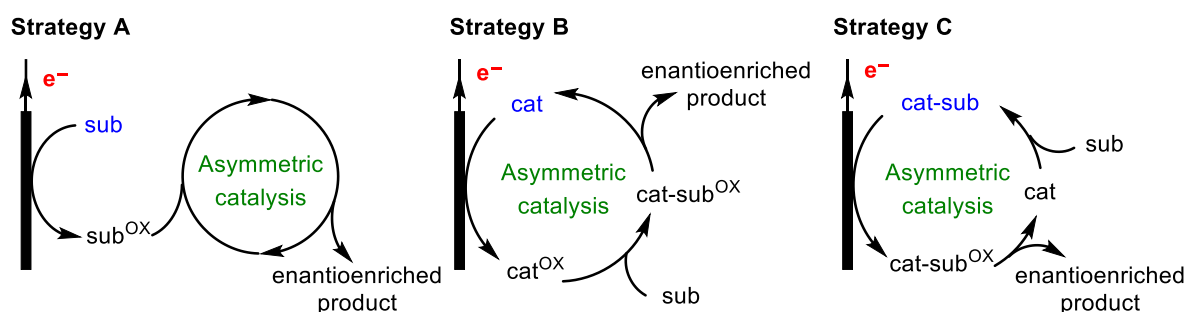


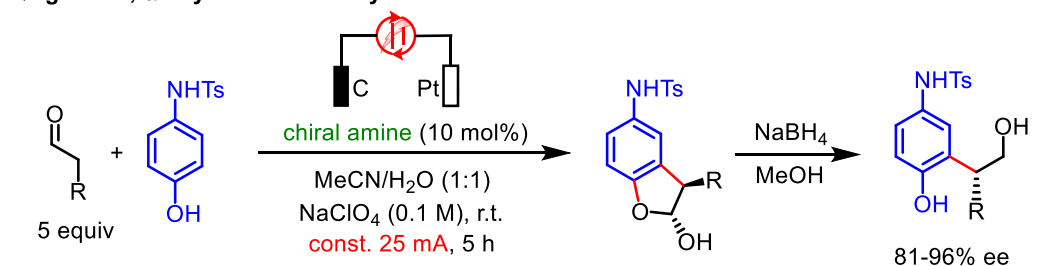
Figure 19. Strategies for catalytic asymmetric organic electrosynthesis (taking anodic oxidations as examples).

1.4.1 Separated Electrochemical Process and Asymmetric Catalysis

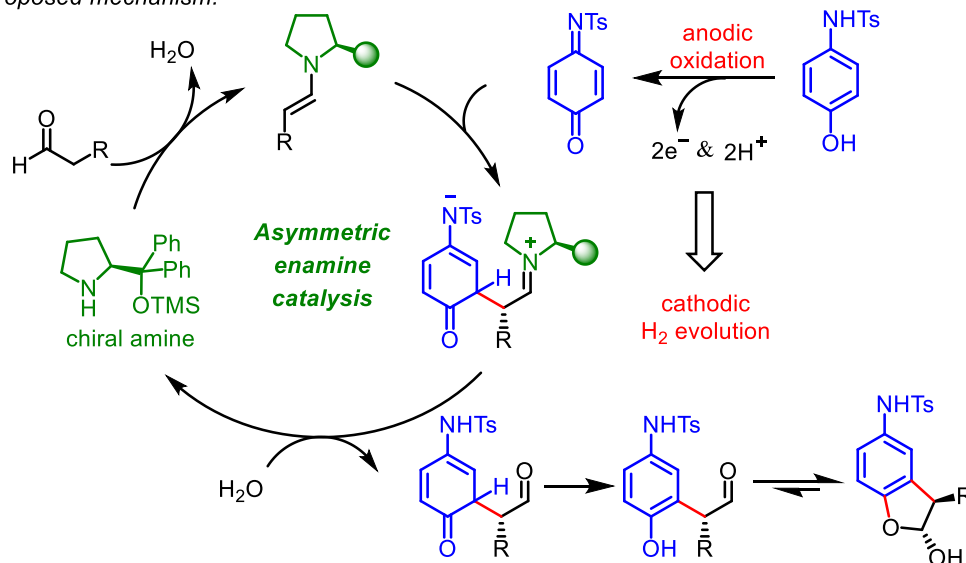
The combination of anodic oxidation with chiral enamine catalysis leads to two examples of highly enantioselective electrochemical transformations (**Figure 20**).⁵³ In 2010, Jørgensen and co-workers demonstrated a regio- and stereoselective anodic oxidation/organocatalysis sequence for the α -arylation of aldehydes with electron-rich aminophenols (**Figure 20a**).^{53a} The reaction works smoothly under simple conditions with an undivided cell and provides *meta*-alkylated aniline in good

to excellent enantioselectivities (up to 96% ee) which is impossible by Friedel-Crafts reaction of aniline. Mechanistically, the electrochemical oxidation of aminophenol delivers the electrophilic intermediate, which is subsequently trapped by the electron rich chiral enamine to form the iminium ion intermediate. The following hydrolysis, several proton transfers and work-up procedure finally give the product formation. This work represents a new concept merging asymmetric organocatalysis with organic electrosynthesis.

a) Jørgensen, α -Arylation of aldehyde



Proposed mechanism:



b) Luo, CDC of amine with ketone

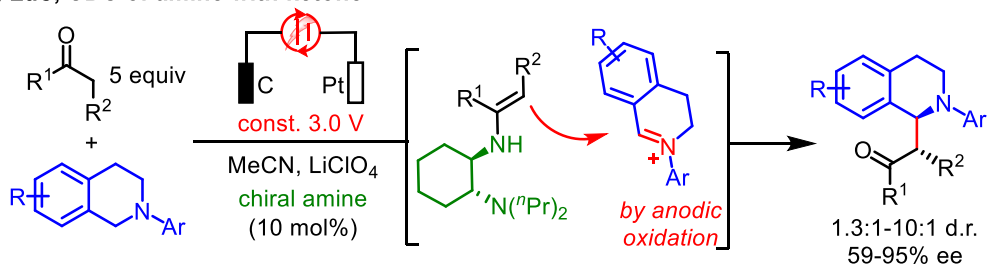


Figure 20. Separating asymmetric enamine catalysis from anodic oxidation.

In 2017, Luo's group reported an asymmetric oxidative coupling of simple ketones with tetrahydroisoquinolines by the combination of anodic oxidation and chiral primary amine catalysis (**Figure 20b**).^{53b} Within an undivided cell, diverse C1-alkylated tetrahydroisoquinolines could be formed in good yields with high stereoselectivities (up to 10:1 d.r. and up to 95% ee). Electrochemical analysis suggests that the tertiary amine is the species to be oxidized forming the corresponding iminium ion intermediate, the interception of which by the catalytic amount of chiral enamine results in the stereoselective C-C bond formation.

In general, these reactions employ easily oxidizable substrates to generate the reactive electrophiles which are then involved in the independent asymmetric catalysis. In principle, these anodic processes could be replaced by other oxidation methods, but electrosynthesis is featured as the more economic and environmentally friendly protocol. In related to the dual-catalyst strategy in asymmetric photocatalysis, the separation of electrochemical process from stereodetermining bond formation step avoids the interference of electrolysis on asymmetric catalysis and improves the compatibility of chiral catalyst in the electrochemical cell, thereby ensuring high asymmetric induction.

1.4.2 Generation of Active Chiral Catalyst by Electrochemistry

For asymmetric redox catalysis, electrochemistry offers a sustainable tool for the generation of active catalyst by direct electrolysis or facilitated by a substoichiometric amount of redox mediator. Selected examples in **Figure 21** show how the direct electrolysis can interact with asymmetric catalysis. In 1999, the Kashiwagi group demonstrated an asymmetric electrocatalytic kinetic resolution of amines by a chiral 1-azaspiro[5.5]undecane *N*-oxyl radical (**Figure 21a**).^{54a} This TEMPO analogue can be easily oxidized to the corresponding chiral oxoammonium ion ($E_{1/2} = +0.62$ V vs Ag/AgCl) which then enables the selective oxidation of amine. And the thereby remaining amine is found to be enantioenriched in the (*R*)-enantiomer with *S* factors ranging from 4.7 to 5.8. Later, the same group modified a graphite felt electrode with this type of chiral *N*-oxyl radical, achieving one elegant example of desymmetric oxidation of a diol, yielding a chiral lactone in 98% ee with the a TON number of 459.^{54b}

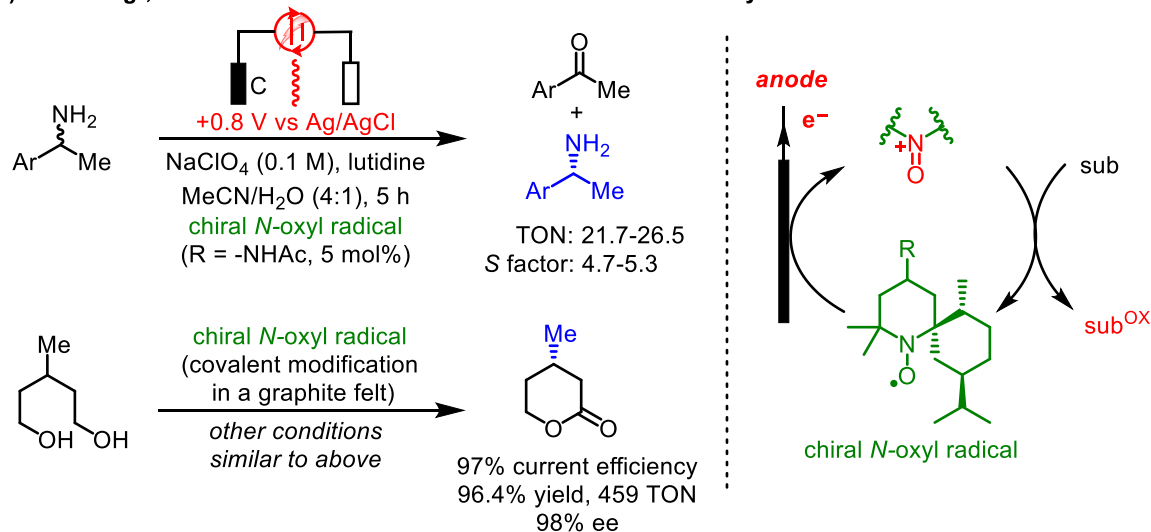
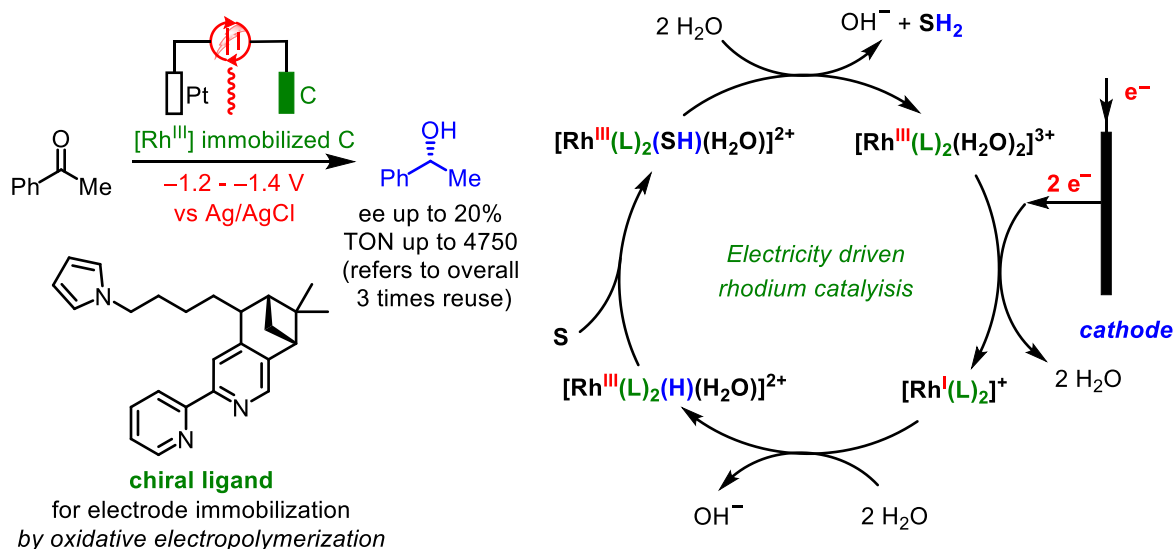
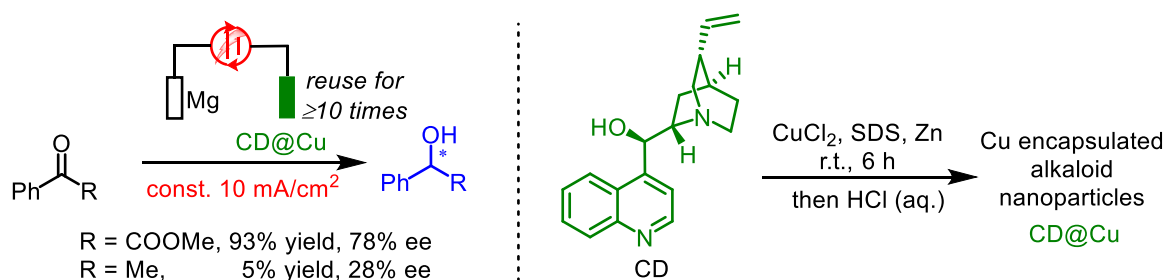
a) *Kashiwagi*, Enantioselective anodic oxidation with chiral *N*-oxyl radicalb) *Moutet*, Asymmetric electrocatalytic hydrogenation with chiral Rh(III) complexc) *Wang and Lu*, Asymmetric electrocatalytic hydrogenation with alkaloid@Cu

Figure 21. Selected examples of asymmetric catalysis with direct electrochemical generation of active catalyst.

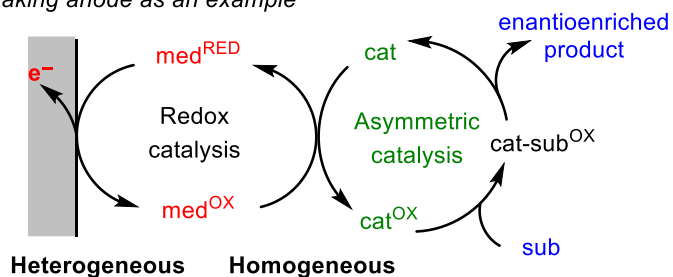
With respect to cathodic reduction, an electricity driven rhodium catalysis was developed by Moutet *et al.* in 1999 for the enantioselective hydrogenation of aromatic ketones (**Figure 21b**).^{55a,b} The rhodium complex containing a pyrrole-substituted chiral bipyridyl ligand was immobilized to a carbon

electrode by oxidative electropolymerization. The resultant active material served as the cathode in a divided cell for the heterogeneous electroreduction of ketone. From the viewpoint of mechanism, it was proposed that the key rhodium hydride intermediate is formed from the electrochemically generated Rh(I) species. However, the enantiomeric excess remained low (up to 20% ee) in these studies. In 2016, Wang and Lu introduced another heterogeneous chiral electrode that enables electrocatalytic ketone reduction in up to 71% ee (**Figure 21c**).^{55c} The entrapment of a chiral alkaloid CD within metallic copper nanoparticles afforded a copper encapsulated alkaloid composite, which was compacted into a coin and used as the cathode directly. Interestingly, the enantioselectivity dramatically decreased when using the non-entrapped CD system that consists of a metallic Cu cathode and the chiral alkaloid solution. Furthermore, the CD@Cu electrode could be reused for 10 times without a significant deactivation, highlighting the potential for practical applications.

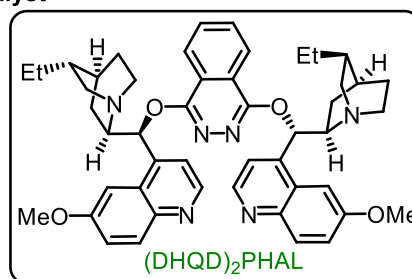
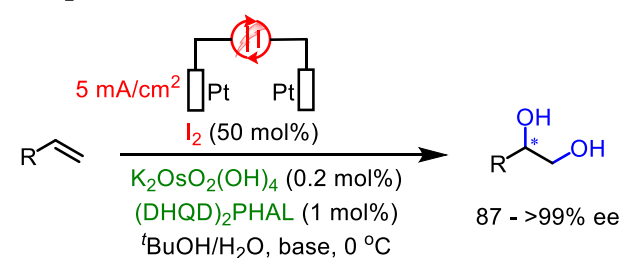
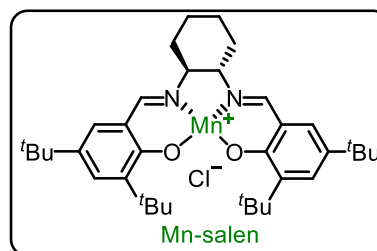
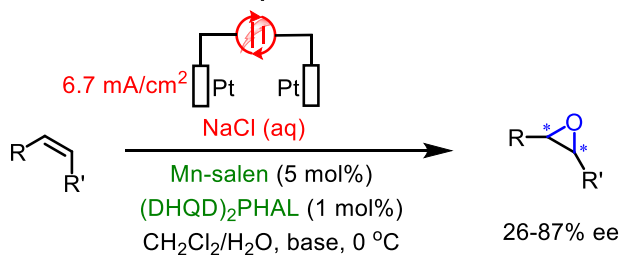
On the other hand, indirect electrolysis using a mediator, where a homogenous redox process instead of the heterogeneous electron transfer is in charge of the generation of active catalyst, allows lower potential and offers higher chemoselectivity, thereby circumventing the issue of poor tolerance of catalyst in a direct electrolysis (**Figure 22a**).⁵⁶ By this strategy, many elegant asymmetric electrocatalysis have been reported.⁵⁷ In 1996, Torii *et al.* developed an electricity-driven iodine-assisted Sharpless asymmetric dihydroxylation of various alkenes, affording diols in high yields with excellent enantioselectivities (up to >99% ee, **Figure 22b**).^{57a} It was proposed that an electrochemically generated active iodine-oxidizing species is responsible for the two-electron oxidation of the initial Os-catalyst $\text{Os(VI)O}_2(\text{OH})_4^{2-}$ to form the active $\text{Os(VIII)O}_6(\text{OH})_2^{2-}$ species which then enables the follow-up oxidative process. Besides, Tanaka and co-workers successfully employed an optically active Mn-salen complex and a CH_2Cl_2 /aqueous NaCl two-phase system for the asymmetric epoxidation of olefins (**Figure 22c**).^{57c} In an undivided cell, the electrochemically formed active chlorine species $[\text{Cl}^+]$, moves from aqueous phase to the organic phase and assists the oxidation of Mn(III)-salen precatalyst, thereby furnishing the catalytic active chiral Mn-oxo intermediate. Furthermore, enzyme catalysis has been proved to be compatible with indirect electrolysis.^{57b,d,e} For example, Schmid's group developed a monooxygenase catalyzed electrochemical epoxidation of alkenes, delivering chiral epoxides in excellent enantioselectivities (97 to >99% ee). Cathodic reductive regeneration of co-factor FADH_2 replaces the native regeneration cycle which involves enzyme StyB and requires the usage of stoichiometric amount of NADH (**Figure 22d**).^{57d}

a) General principle of mediated generation of chiral catalyst

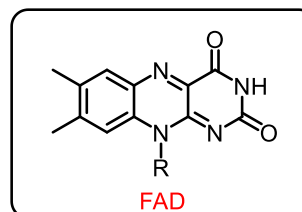
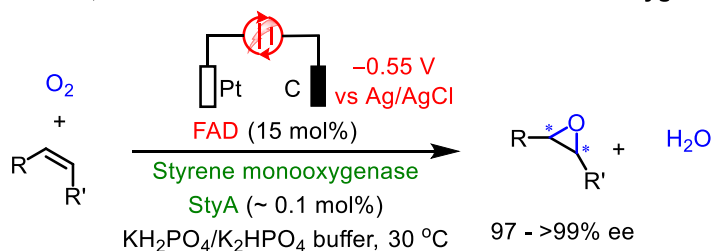
taking anode as an example

**Advantages:**

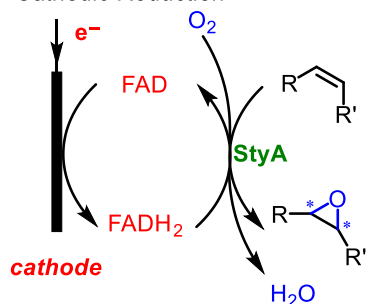
- eliminate kinetic inhibition
- allow mild conditions
- reduce side-reaction
- avoid electrode passivation

b) Torii, I_2 -Mediated dihydroxylation with the Sharpless' catalystc) Tanaka, Cl^- -Mediated epoxidation with a chiral Mn-salen complex

d) Schmid, FAD-Mediated ketone reduction with a monooxygenase



Cathodic Reduction



Native cycle

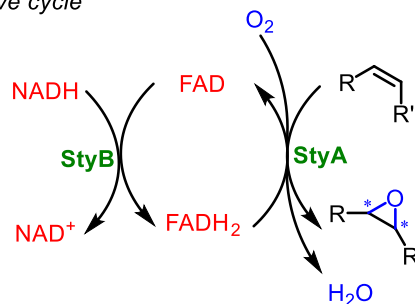


Figure 22. Generation of chiral catalyst through indirect electrolysis with a redox mediator.

1.4.3 Redox Activation upon Catalyst/Substrate Complexation

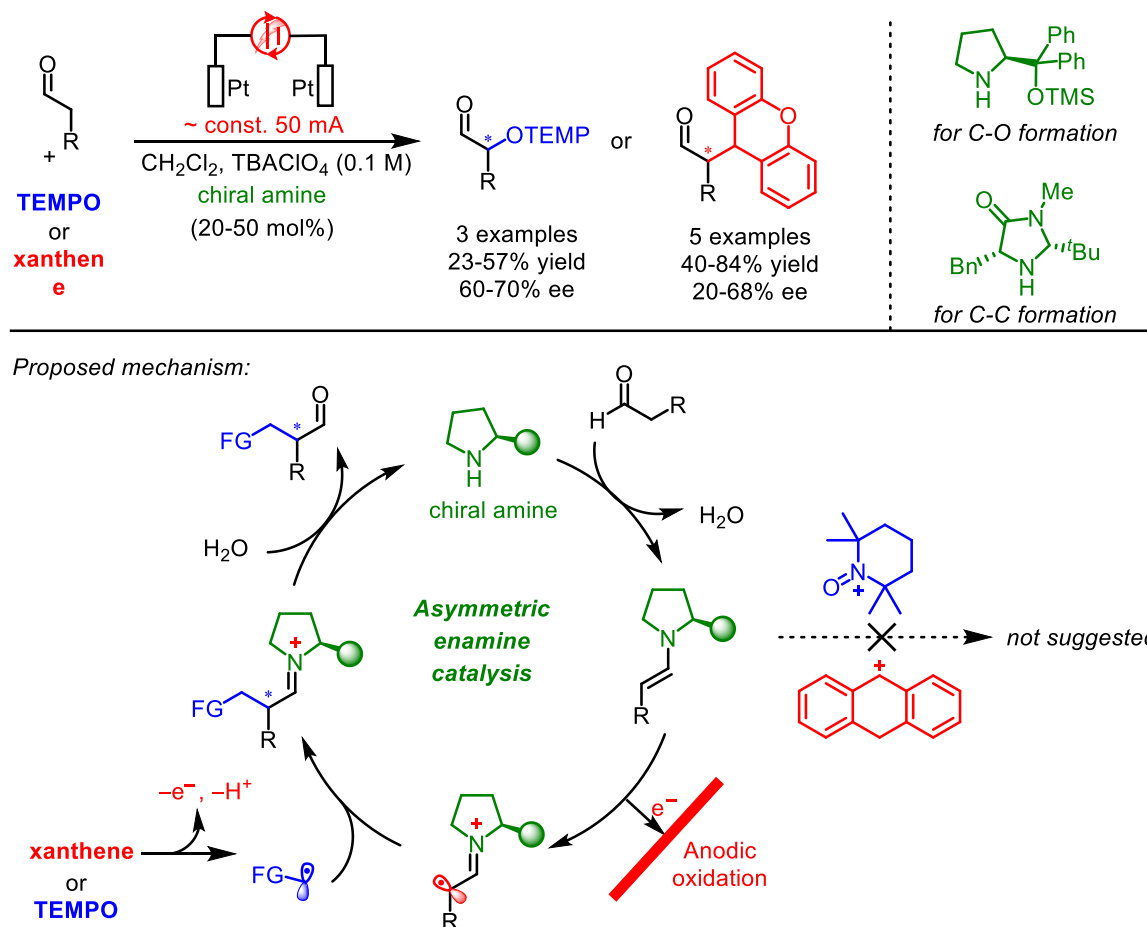


Figure 23. Enamine formation facilitated anodic oxidation, as reported by Jang.

Another simple but appealing strategy is to utilize the change of redox potential upon catalyst/substrate complexation. If the chiral catalyst bound substrate features decreased oxidation/reduction potentials compared with the free substrate, selective electrochemical oxidation/reduction under relatively milder conditions would be possible, thus paving way to interesting catalytic asymmetric electrosynthesis. For instance, enamines are well-known to be easier oxidized than the parent amines and carbonyl compounds, and combining this property with anodic oxidation, the Jang group demonstrated the elegant enantioselective α -oxyamination^{58a} and α -alkylation^{58b} of aldehydes with TEMPO or xanthene, respectively (**Figure 23**). Mechanistic investigations suggest that rather than the formation of TEMPO/xanthene-derived electrophilic cation intermediate, the selective anodic oxidation of chiral enamine species is operative under the electrochemical conditions. The resultant $3\pi\text{e}^-$ enaminy radical can be trapped by the free radical TEMPO, or the electrochemically generated

benzylic carbon center radical, thereby furnishing α -functionalizations of aldehydes. Although these transformations are limited with respect to substrate scope and enantioselectivity, they showcase different reactivity of an enamine species under electrochemical conditions (compared with examples in **Figure 20**) and this redox activation strategy is believed to inspire further development of synthetically valuable asymmetric electrocatalysis.

1.5 Asymmetric Photoredox Catalysis with Chiral-at-Metal Lewis Acids

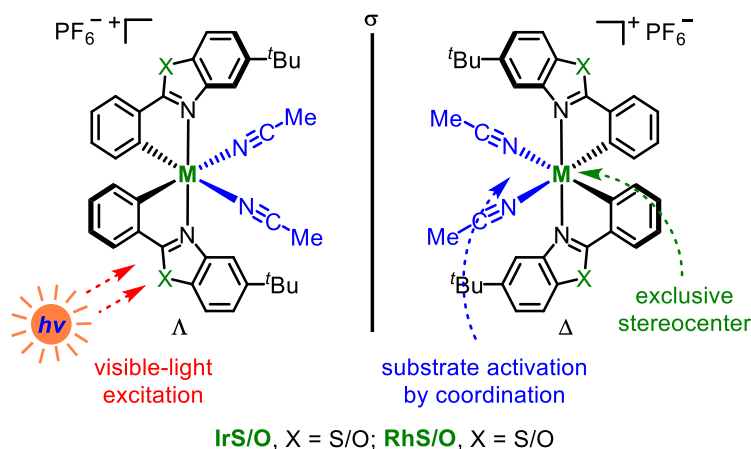


Figure 24. Overview of the chiral-at-metal Lewis acid catalysts developed by Meggers.

Before the author of this thesis started PhD research, the Meggers group had already developed a class of chiral-at-metal iridium and rhodium based Lewis acid catalysts (**Figure 24**).⁵⁹ This type of catalyst is based on an octahedral iridium(III) or rhodium(III) center that is cyclometalated by two 5-(*tert*-butyl)-2-phenylbenzo[*d*]oxazole or 5-(*tert*-butyl)-2-phenylbenzo[*d*] thiazole ligands together with two labile acetonitriles and one hexafluorophosphate counter anion. The assembly of achiral ligands leads to the exclusive metal-centered chirality. These compounds feature inert octahedral configuration, fast ligand (acetonitriles) exchange kinetics, intimate contact between bound substrates and the stereogenic metal center, as well as unique photophysical and redox properties. All of these characteristics together render the chiral-at-metal complexes robust and promising chiral catalysts, especially for catalyzing visible-light-activated asymmetric reactions.⁶⁰ The beautiful photochemistry enabled by these catalysts are highlighted in this part, which are the foundation stones of this thesis.

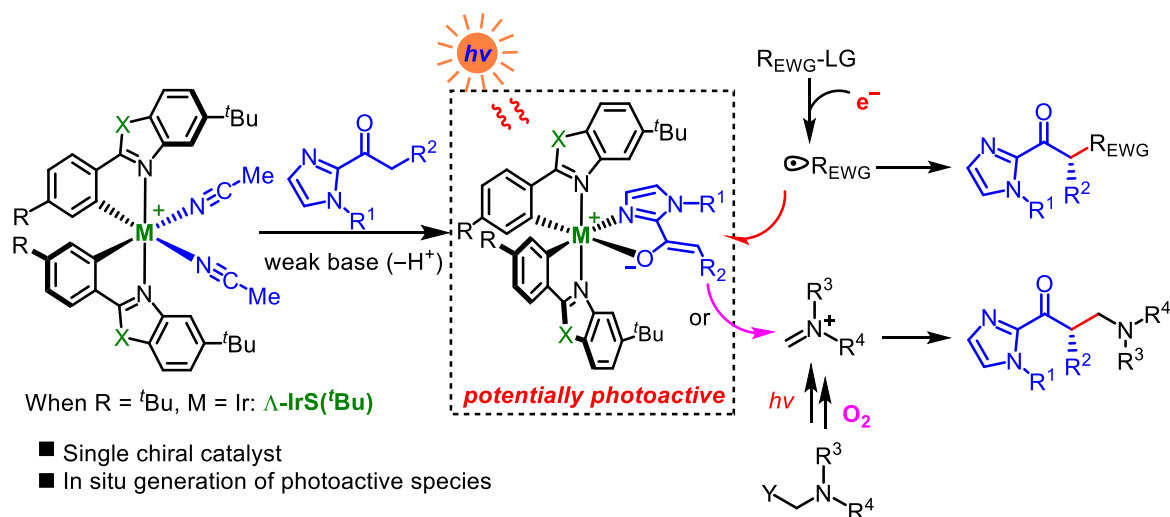
1.5.1 α -Functionalization of Carbonyls through Enolate Intermediate

In 2014, Haohua Huo for the first time demonstrated the photoreactivity of the chiral-at-iridium catalyst by developing a visible-light-induced enantioselective alkylation of 2-acyl imidazole.^{61a} As illustrated in **Figure 25**, a key iridium enolate intermediate that is formed upon coordination/deprotonation sequence, acts as a photoactivated reductant for the generation of a radical

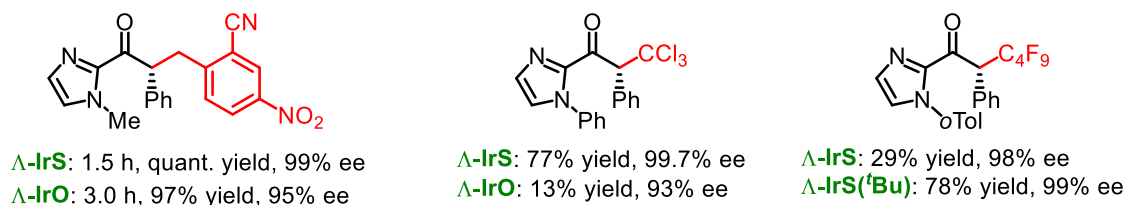
intermediate from an electron deficient alkyl halide. At the same time this enolate species could trap the electrophilic radical in a highly stereocontrolled fashion, leading to the C-C bond formation product in excellent yield and enantioselectivity. This unique catalysis only relies on a single chiral-at-iridium catalyst that features a combination of exclusive metal-centered-chirality, the catalytically active Lewis acidity, and simultaneously the ability to initiate a photoredox process after visible-light-excitation. This work opened a new world for the synthesis of chiral compounds by inducing versatile chiral-at-metal catalysis with visible light as renewable energy source.

Based on the mechanistic scheme, Haohua Huo later expanded the scope of radical precursors, achieving enantioselective α -trichloromethylation^{61b} and α -perfluoroalkylation^{61c} with a single chiral-at-iridium catalyst. Furthermore, a chiral-at-rhodium complex was demonstrated by Xiaodong Shen to be capable of catalyzing a visible-light-activated asymmetric amidation with (ODN)-*N*-functionalized carbamates as amino radical source, whereas the iridium catalysts failed to enable this transformation.^{61d} This difference can be rationalized by the much faster ligand-exchange kinetics of the rhodium complex, which makes it match the high reactivity of the short-lived nitrogen-centered radical intermediate. Notably, the benzothiazole derived complexes (**RhS** or **IrS**) gave better stereocontrol, and in some cases higher yields, than the corresponding benzoxazole based congeners (**RhO** or **IrO**), which can be attributed to a higher steric congestion around the coordination sites of the **RhS/IrS** complexes.

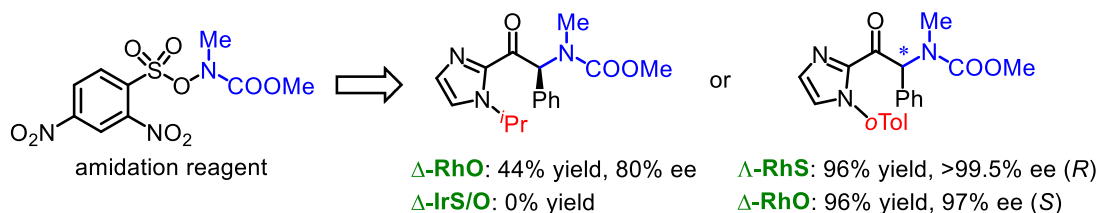
Besides the above-mentioned redox neutral catalysis, Chuanyong Wang discovered that a single chiral-at-iridium complex **IrO** was able to catalyze the asymmetric photoinduced oxidative coupling of 2-acyl imidazole with *N,N*-diaryl-*N*-(trimethylsilyl)methylamine using air as terminal oxidant.^{61e} Mechanistically, a visible-light-activated substrate bound iridium complex is supposed to facilitate the aerobic oxidative generation of an iminium ion intermediate. Subsequent nucleophilic trapping by the iridium enolate species furnishes the aminomethylation product. Interestingly, a rhodium analogue **RhO** alone can hardly give any product indicating poor photoactivity of the Rh-based complex, but this could be overcome by the combination with an additional photoredox catalyst. Later, the synthetically more attractive *N*-methyl aniline was introduced for the similar Mannich-type reaction by Yuqi Tan and Wei Yuan.^{61f} In this study, **IrO** failed to catalyze the photoinduced alkylation with *N,N*-dialkyl aryl amine, while the related **RhO** showed excellent efficiency.



[Ir]-catalyzed radical addition with *R*-Hal:



[Rh]-catalyzed radical amidation:



Mannich-type aminomethylation with a photogenerated electrophile:

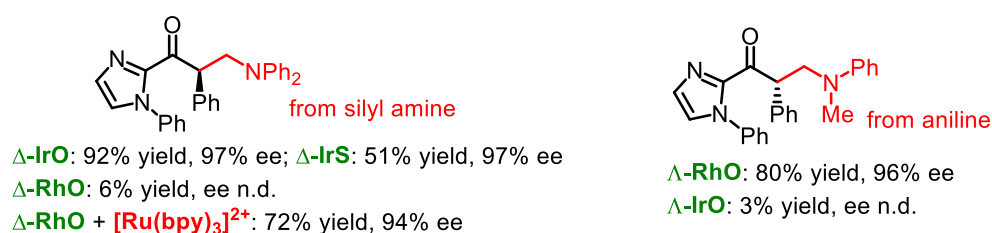


Figure 25. Enantioselective α -functionalization of carbonyls by a single chiral-at-metal catalyst.

1.5.2 β -Functionalization of Enones by Radical Conjugate Addition

As mentioned above, performing conjugate addition of nucleophilic radicals to electron-deficient alkenes in a catalytic and asymmetric way is a formidable challenge caused by the uncatalyzed racemic background reaction. Remarkably, the unique properties of the chiral-at-rhodium complex

pave new way to circumvent this issue (**Figure 26**). In 2016, Haohua Huo for the first time demonstrated that the combination of 4 mol% of Λ -**RhS** with a photoredox catalyst (2.0 mol%) enabled the enantioselective alkyl radical addition to acceptor-substituted alkene, providing β -alkylated carbonyl compounds with excellent enantioselectivity (up to 99% ee).^{62a} The additional photoredox catalyst is responsible for the SET oxidation of the organotrifluoroborate to generate the nucleophilic alkyl radical, which is then trapped by the rhodium bound enone to form the C-C bond with the stereochemistry controlled by the rhodium-centered chirality. Noteworthy is the high enantioselectivities achieved by usage of only 4 mol% Λ -**RhS**, especially considering the uncatalyzed background competition could erode the enantiopurities of products.

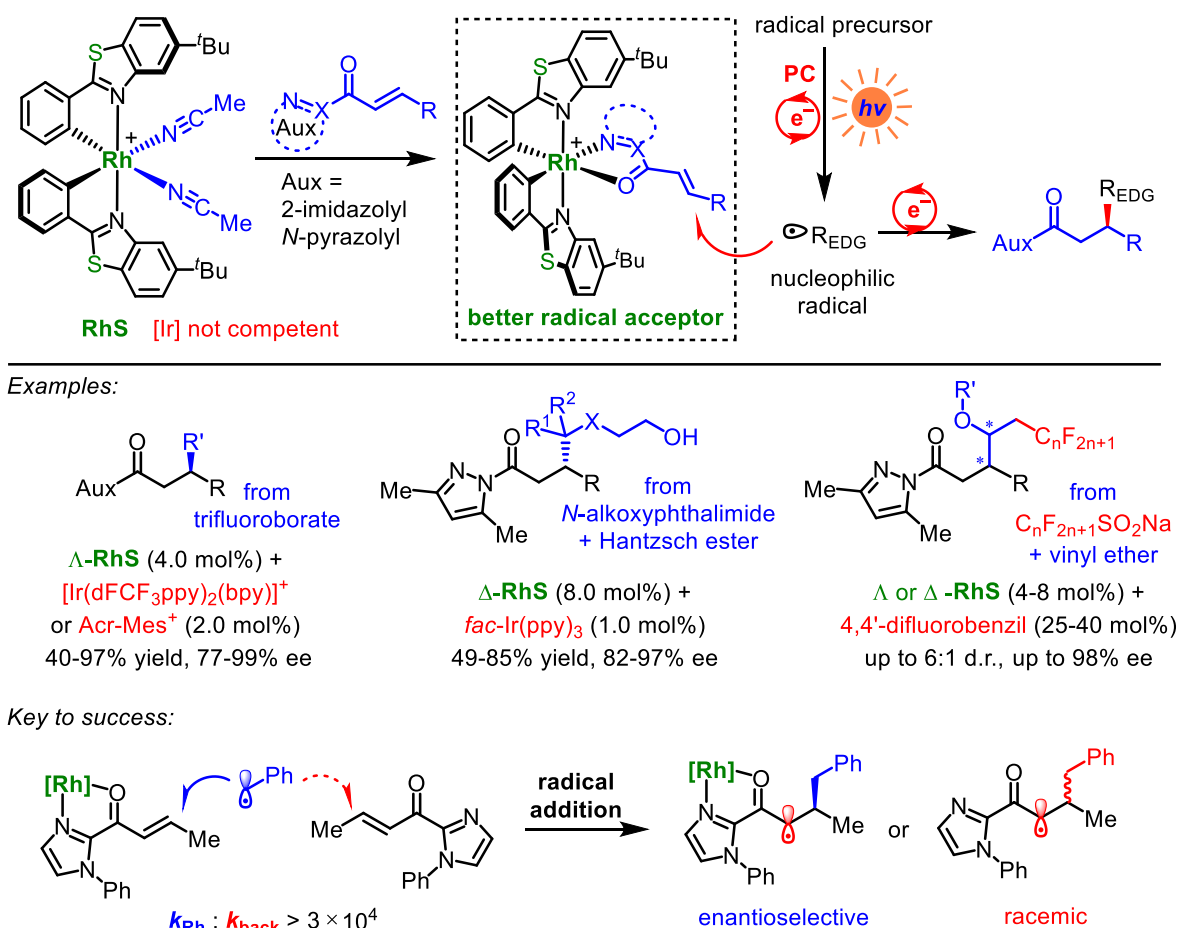


Figure 26. Enantioselective radical conjugate addition by dual chiral-at-Rh/photoredox catalysis.

Inspired by this pioneering work, Chuanyong Wang creatively combined radical translocation (1,5-HAT) with dual chiral rhodium/photoredox catalysis to achieve an catalytic asymmetric Csp³-H bond alkylation.^{62b} Specifically, oxygen-centered radicals are initially generated through $\text{fac-Ir}(\text{ppy})_3$

mediated photoredox SET reduction of *N*-alkoxyphthalimides with Hantzsch ester as terminal reductant. Subsequent 1,5-HAT of the oxygen-centered radicals afford nucleophilic C-centered radicals, which engage in the following stereocontrolled radical conjugate addition. Interestingly, a significant amount of product (33% yield, 92% ee for the standard compound) could form when only a single chiral **RhS** was employed in the absence any additional photoredox catalyst.⁶³

Later, Jiajia Ma expanded the scope of this chemistry by developing a visible-light-activated asymmetric three-component fluoroalkylation with perfluoroalkyl sulfinate, electron-rich vinyl ether, and α,β -unsaturated *N*-acyl pyrazole.^{62c} The visible-light-excited organic photoredox mediator, 4,4'-difluorobenzil, induces SET oxidation for the generation of an electrophilic perfluoroalkyl radical, which is then trapped by a vinyl ether to form a nucleophilic α -oxy carbon-centered radical. Finally, stereocontrolled radical addition delivers dual C-C bond formation products with good to excellent enantioselectivity (up to 98% ee).

Indeed, the racemic background reaction also works. For example, full conversion with the formation of racemic product in 75% yield was observed when the Csp³-H bond alkylation reaction was performed under the same conditions without chiral **RhS**.^{62b} On sharp contrast, 70% yield with 92% ee could be obtained by adding 8.0 mol% Δ -**RhS**. This surprising effect is mainly attributed to the strong acceleration of the radical conjugate addition reaction by the chiral-at-rhodium Lewis acid. Alternatively, the competitive visible-light-absorption of Rh-based species (inner filter effect) could also slow down the rate of the photoredox catalyst mediated radical generation step.

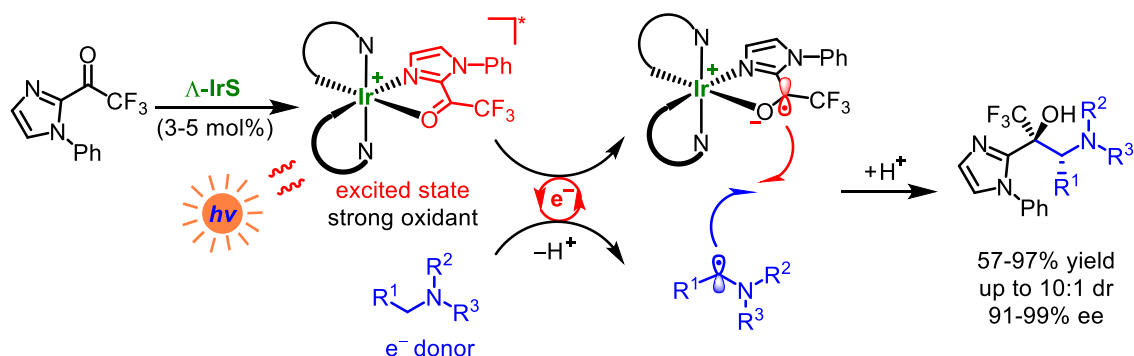
1.5.3 Radical-Radical Recombination of Ketones

With respect to a radical-radical recombination pathway, chiral-at-metal complexes have also shown great potential to steering the reaction course in a stereocontrolled fashion. In 2016, Chuanyong Wang demonstrated that a single chiral iridium complex could catalyze the cross coupling of trifluoromethyl ketones with tertiary amines, generating chiral 1,2-amino alcohols with excellent stereoselectivity (up to 10:1 d.r. and 99% ee).^{64a} In this mechanistic scenario, **IrS** serves as both a photoredox catalyst and as Lewis acid, which induces SET between photoexcited iridium bound carbonyl complex and electron donor amine, while at the same time controlling the stereochemistry of the subsequent radical-radical recombination. This method provides an efficient, sustainable and

atom-economic method to synthesize enantiopure trifluoromethyl-containing compounds with one or two stereocenters constructed. This elegant example expands the reactivity of the chiral-at-metal catalysts and provides an attractive mechanistic alternative for developing novel synthetic transformations.

Short after that, Jiajia Ma extended the scope of ketones to more general 2-acyl imidazoles by employing dual photoredox/chiral-at-rhodium catalysis.^{64b} In this case, an electron exchange between the rhodium bound ketone and α -silyl amine was mediated by an additional $[\text{Ru}(\text{bpy})_3]^{2+}$ based photoredox catalysis, which was important to compensate for the apparent lack of photoredox activity of the rhodium catalyst in this context. Interestingly, substituting the chiral **RhS** with the iridium congener **IrO** resulted in the formation of almost racemic product (<5% ee), both in the absence and presence of the $[\text{Ru}(\text{bpy})_3]^{2+}$ catalyst, which could be ascribed to the significant differences in ligand-exchange kinetic between the Rh- and Ir- complexes.

a) A visible-light-activated single chiral-at-iridium catalyst



b) Dual photoredox/chiral-at-rhodium catalyst

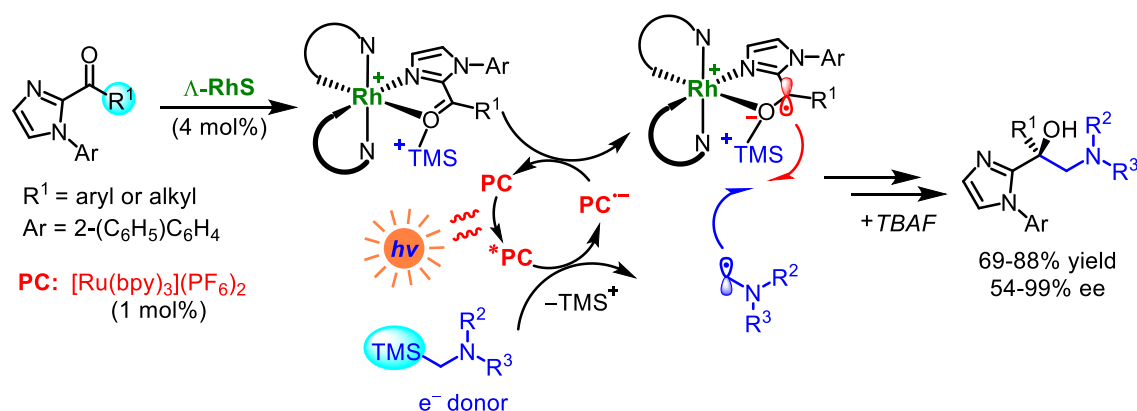


Figure 27. Enantioselective radical-radical recombination catalyzed by chiral-at-metal complexes.

1.6 Conclusions

Catalytic, asymmetric synthesis of enantiomerically pure molecules using visible light and/or electricity as energy source is of high significance both from an economical and sustainable perspective. High reactivity of the photo- and electrochemically formed intermediates provides fertile testing ground for chemists to discover new mechanistic scenarios and invent previously unknown transformations, although with formidable challenges in achieving stereocontrol. During the past decades, powered by the combination with photoredox catalysis, the synthetic potentials of many traditional and newly-developed asymmetric catalysts, such as chiral amines, Lewis/Brønsted acids, transition metals (Ni/Cu), and H-bonding catalysts, have been greatly expanded. Besides photoinduced SET catalysis, elegant strategies have been developed to control the stereochemistry of direct bond formation from the electronically excited state, including chiral catalyst induced bathochromic shift and triplet chromophore activation. However, stereocontrolled direct bond formation of an electronically excited state is mainly limited to [2+2] photocycloadditions. With respect to electrochemistry, catalytic asymmetric electrosynthesis has been studied for decades. But given the recently booming of organic electrosynthesis, it is notable to consider that its implication in asymmetric catalysis remains largely underexplored.

Very recently, Meggers and co-workers discovered a class of unique bis-cyclometalated chiral-at-metal iridium and rhodium based Lewis acids. The chirality of these catalysts exclusively originate from the stereogenic metal centers, which at the same time act as catalytically active Lewis acid center, and part of visible-light-absorbing chromophore. This novel structural architecture exhibits attractive potential as asymmetric catalyst across mechanistically distinct photoinduced reactions and is anticipated to provide ample opportunities for achieving stereocontrol in photochemical and even electrochemical synthesis.

Reference

- 1 B. M. Trost, *Proc. Natl. Acad. Sci. USA* **2004**, *101*, 5348-5355.
- 2 D. M. Schultz, T. P. Yoon, *Science* **2014**, *343*, 1239176.

- 3 C. K. Prier, D. A. Rankic, D. W. C. MacMillan, *Chem. Rev.* **2013**, *113*, 5322-5363.
- 4 F. Strieth-Kalthoff, M. J. James, M. Teders, L. Pitzer, F. Glorius, *Chem. Soc. Rev.* **2018**, *47*, 7190-7202.
- 5 M. Yan, Y. Kawamata, P. S. Baran, *Chem. Rev.* **2017**, *117*, 13230-13319.
- 6 For selected reviews on catalytic asymmetric photoreactions, see: a) R. Brimiouille, D. Lenhart, M. M. Maturi, T. Bach, *Angew. Chem. Int. Ed.* **2015**, *54*, 3872-3890; b) A. F. Garrido-Castro, M. C. Maestro, J. Alemán, *Tetrahedron Lett.* **2018**, *59*, 1286-1294; c) M. Silvi, P. Melchiorre, *Nature* **2018**, *554*, 41-49; for a review on asymmetric electrosynthesis, see: d) Z.-Y. Cao, J. Zhou, in *Multicatalyst System in Asymmetric Catalysis*, John Wiley & Sons, Inc., **2014**, pp. 475-500.
- 7 G. Pandey, in *Photoinduced Electron Transfer V* (Ed.: J. Mattay), Springer Berlin Heidelberg, Berlin, Heidelberg, **1993**, pp. 175-221.
- 8 D. A. Nicewicz, D. W. C. MacMillan, *Science* **2008**, *322*, 77-80.
- 9 M. A. Cismesia, T. P. Yoon, *Chem. Sci.* **2015**, *6*, 5426-5434.
- 10 a) D. A. Nagib, M. E. Scott, D. W. C. MacMillan, *J. Am. Chem. Soc.* **2009**, *131*, 10875-10877; b) H.-W. Shih, M. N. Vander Wal, R. L. Grange, D. W. C. MacMillan, *J. Am. Chem. Soc.* **2010**, *132*, 13600-13603; c) E. R. Welin, A. A. Warkentin, J. C. Conrad, D. W. C. MacMillan, *Angew. Chem. Int. Ed.* **2015**, *54*, 9668-9672; d) G. Cecere, C. M. König, J. L. Alleva, D. W. C. MacMillan, *J. Am. Chem. Soc.* **2013**, *135*, 11521-11524.
- 11 For selected examples, see: a) M. Neumann, S. Földner, B. König, K. Zeitler, *Angew. Chem. Int. Ed.* **2010**, *50*, 951-954; b) M. Cherevatskaya, M. Neumann, S. Földner, C. Harlander, S. Kümmel, S. Dankesreiter, A. Pfitzner, K. Zeitler, B. König, *Angew. Chem. Int. Ed.* **2012**, *51*, 4062-4066; c) A. Gualandi, M. Marchini, L. Mengozzi, M. Natali, M. Lucarini, P. Ceroni, P. G. Cozzi, *ACS Catal.* **2015**, *5*, 5927-5931.
- 12 Y. Zhu, L. Zhang, S. Luo, *J. Am. Chem. Soc.* **2014**, *136*, 14642-14645.
- 13 a) E. Arceo, I. D. Jurberg, A. Álvarez-Fernández, P. Melchiorre, *Nat. Chem.* **2013**, *5*, 750-756; b) M. Silvi, E. Arceo, I. D. Jurberg, C. Cassani, P. Melchiorre, *J. Am. Chem. Soc.* **2015**, *137*, 6120-6123; c) Ł. Woźniak, J. J. Murphy, P. Melchiorre, *J. Am. Chem. Soc.* **2015**, *137*, 5678-5681; d) A. Bahamonde, P. Melchiorre, *J. Am. Chem. Soc.* **2016**, *138*, 8019-8030.
- 14 T. Rigotti, A. Casado-Sánchez, S. Cabrera, R. Pérez-Ruiz, M. Liras, V. A. de la Peña O'Shea, J.

- Alemán, *ACS Catal.* **2018**, 8, 5928-5940.
- 15 A. G. Capacci, J. T. Malinowski, N. J. McAlpine, J. Kuhne, D. W. C. MacMillan, *Nat. Chem.* **2017**, 9, 1073-1077.
- 16 M. T. Pirnot, D. A. Rankic, D. B. C. Martin, D. W. C. MacMillan, *Science* **2013**, 339, 1593-1596.
- 17 a) M. A. Emmanuel, N. R. Greenberg, D. G. Oblinsky, T. K. Hyster, *Nature* **2016**, 540, 414-417; b) K. F. Biegasiewicz, S. J. Cooper, M. A. Emmanuel, D. C. Miller, T. K. Hyster, *Nat. Chem.* **2018**, 10, 770-775.
- 18 For more applications of enzyme catalysis in photochemistry, see: a) Z. C. Litman, Y. Wang, H. Zhao, J. F. Hartwig, *Nature* **2018**, 560, 355-359; b) K. Lauder, A. Toscani, Y. Qi, J. Lim, S. J. Charnock, K. Korah, D. Castagnolo, *Angew. Chem. Int. Ed.* **2018**, 57, 5803-5807; c) X. Guo, Y. Okamoto, M. R. Schreier, T. R. Ward, O. S. Wenger, *Chem. Sci.* **2018**, 9, 5052-5056.
- 19 J. Li, M. Kong, B. Qiao, R. Lee, X. Zhao, Z. Jiang, *Nat. Commun.* **2018**, 9, 2445.
- 20 A. Bauer, F. Westkämper, S. Grimme, T. Bach, *Nature* **2005**, 436, 1139-1140.
- 21 L. Ruiz Espelt, I. S. McPherson, E. M. Wiensch, T. P. Yoon, *J. Am. Chem. Soc.* **2015**, 137, 2452-2455.
- 22 a) M. P. Sibi, J. Ji, J. H. Wu, S. Gürtler, N. A. Porter, *J. Am. Chem. Soc.* **1996**, 118, 9200-9201; b) M. P. Sibi, J. Ji, *J. Org. Chem.* **1997**, 62, 3800-3801.
- 23 a) X. Shen, Y. Li, Z. Wen, S. Cao, X. Hou, L. Gong, *Chem. Sci.* **2018**, 9, 4562-4568; b) Y. Li, K. Zhou, Z. Wen, S. Cao, X. Shen, M. Lei, L. Gong, *J. Am. Chem. Soc.* **2018**, 140, 15850-15858.
- 24 Y. Yin, Y. Dai, H. Jia, J. Li, L. Bu, B. Qiao, X. Zhao, Z. Jiang, *J. Am. Chem. Soc.* **2018**, 140, 6083-6087.
- 25 a) J. J. Murphy, D. Bastida, S. Paria, M. Fagnoni, P. Melchiorre, *Nature* **2016**, 532, 218-222; b) for recent extension to a single chiral amine system, see: Z.-Y. Cao, T. Ghosh, P. Melchiorre, *Nat. Commun.* **2018**, 9, 3274.
- 26 L. J. Rono, H. G. Yayla, D. Y. Wang, M. F. Armstrong, R. R. Knowles, *J. Am. Chem. Soc.* **2013**, 135, 17735-17738.
- 27 C.-X. Ye, Y. Y. Melcamu, H.-H. Li, J.-T. Cheng, T.-T. Zhang, Y.-P. Ruan, X. Zheng, X. Lu, P.-Q. Huang, *Nat. Commun.* **2018**, 9, 410.
- 28 R. S. J. Proctor, H. J. Davis, R. J. Phipps, *Science* **2018**, 360, 419-422.

- 29 a) D. Uraguchi, N. Kinoshita, T. Kizu, T. Ooi, *J. Am. Chem. Soc.* **2015**, *137*, 13768-13771; b) T. Kizu, D. Uraguchi, T. Ooi, *J. Org. Chem.* **2016**, *81*, 6953-6958.
- 30 For another asymmetric example not discussed in this thesis, see: Y. Liu, X. Liu, J. Li, X. Zhao, B. Qiao, Z. Jiang, *Chem. Sci.* **2018**, *9*, 8094-8098.
- 31 a) M. Silvi, C. Verrier, Y. P. Rey, L. Buzzetti, P. Melchiorre, *Nat. Chem.* **2017**, *9*, 868-873; b) C. Verrier, N. Alandini, C. Pezzetta, M. Moliterno, L. Buzzetti, H. B. Hepburn, A. Vega-Peñaloza, M. Silvi, P. Melchiorre, *ACS Catal.* **2018**, *8*, 1062-1066; c) P. Bonilla, Y. P. Rey, C. M. Holden, P. Melchiorre, *Angew. Chem. Int. Ed.* **2018**, *57*, 12819-12823; d) D. Mazzarella, G. E. M. Crisenza, P. Melchiorre, *J. Am. Chem. Soc.* **2018**, *140*, 8439-8443; e) Ł. Woźniak, G. Magagnano, P. Melchiorre, *Angew. Chem. Int. Ed.* **2017**, *57*, 1068-1072.
- 32 a) P. S. Mariano, *Acc. Chem. Res.* **1983**, *16*, 130-137; b) P. S. Mariano, *Tetrahedron* **1983**, *39*, 3845-3879; c) R. M. Borg, R. O. Heuckeroth, A. J. Y. Lan, S. L. Quillen, P. S. Mariano, *J. Am. Chem. Soc.* **1987**, *109*, 2728-2737.
- 33 J. C. Tellis, D. N. Primer, G. A. Molander, *Science* **2014**, *345*, 433-436.
- 34 Z. Zuo, D. T. Ahneman, L. Chu, J. A. Terrett, A. G. Doyle, D. W. C. MacMillan, *Science* **2014**, *345*, 437-440.
- 35 O. Gutierrez, J. C. Tellis, D. N. Primer, G. A. Molander, M. C. Kozlowski, *J. Am. Chem. Soc.* **2015**, *137*, 4896-4899.
- 36 Z. Zuo, H. Cong, W. Li, J. Choi, G. C. Fu, D. W. C. MacMillan, *J. Am. Chem. Soc.* **2016**, *138*, 1832-1835.
- 37 E. E. Stache, T. Rovis, A. G. Doyle, *Angew. Chem. Int. Ed.* **2017**, *56*, 3679-3683.
- 38 Q. M. Kainz, C. D. Matier, A. Bartoszewicz, S. L. Zultanski, J. C. Peters, G. C. Fu, *Science* **2016**, *351*, 681-684.
- 39 a) W. Zhang, F. Wang, S. D. McCann, D. Wang, P. Chen, S. S. Stahl, G. Liu, *Science* **2016**, *353*, 1014-1018; b) D. Wang, N. Zhu, P. Chen, Z. Lin, G. Liu, *J. Am. Chem. Soc.* **2017**, *139*, 15632-15635.
- 40 W. Sha, L. Deng, S. Ni, H. Mei, J. Han, Y. Pan, *ACS Catal.* **2018**, *8*, 7489-7494.
- 41 a) J. Du, K. L. Skubi, D. M. Schultz, T. P. Yoon, *Science* **2014**, *344*, 392-396; b) A. G. Amador, E. M. Sherbrook, T. P. Yoon, *J. Am. Chem. Soc.* **2016**, *138*, 4722-4725.

- 42 S. Poplata, A. Tröster, Y.-Q. Zou, T. Bach, *Chem. Rev.* **2016**, *116*, 9748-9815.
- 43 a) H. Guo, E. Herdtweck, T. Bach, *Angew. Chem. Int. Ed.* **2010**, *49*, 7782-7785; b) R. Brimiouille, H. Guo, T. Bach, *Chem. Eur. J.* **2012**, *18*, 7552-7560; c) R. Brimiouille, T. Bach, *Science* **2013**, *342*, 840-843; d) R. Brimiouille, T. Bach, *Angew. Chem. Int. Ed.* **2014**, *53*, 12921-12924; e) R. Brimiouille, A. Bauer, T. Bach, *J. Am. Chem. Soc.* **2015**, *137*, 5170-5176; f) S. Poplata, T. Bach, *J. Am. Chem. Soc.* **2018**, *140*, 3228-3231; g) S. Stegbauer, C. Jandl, T. Bach, *Angew. Chem. Int. Ed.* **2018**, *57*, 14593-14596.
- 44 N. Vallavoju, S. Selvakumar, S. Jockusch, M. P. Sibi, J. Sivaguru, *Angew. Chem. Int. Ed.* **2014**, *53*, 5604-5608.
- 45 a) C. Müller, A. Bauer, T. Bach, *Angew. Chem. Int. Ed.* **2009**, *48*, 6640-6642; b) C. Müller, A. Bauer, M. M. Maturi, M. C. Cuquerella, M. A. Miranda, T. Bach, *J. Am. Chem. Soc.* **2011**, *133*, 16689-16697; c) M. M. Maturi, T. Bach, *Angew. Chem. Int. Ed.* **2014**, *53*, 7661-7664; d) R. Alonso, T. Bach, *Angew. Chem. Int. Ed.* **2014**, *53*, 4368-4371; e) A. Tröster, R. Alonso, A. Bauer, T. Bach, *J. Am. Chem. Soc.* **2016**, *138*, 7808-7811.
- 46 a) L.-A. Chen, W. Xu, B. Huang, J. Ma, L. Wang, J. Xi, K. Harms, L. Gong, E. Meggers, *J. Am. Chem. Soc.* **2013**, *135*, 10598-10601; b) L.-A. Chen, X. Tang, J. Xi, W. Xu, L. Gong, E. Meggers, *Angew. Chem. Int. Ed.* **2013**, *52*, 14021-14025; c) W. Xu, M. Arieno, H. Löw, K. Huang, X. Xie, T. Cruchter, Q. Ma, J. Xi, B. Huang, O. Wiest, L. Gong, E. Meggers, *J. Am. Chem. Soc.* **2016**, *138*, 8774-8780.
- 47 K. L. Skubi, J. B. Kidd, H. Jung, I. A. Guzei, M.-H. Baik, T. P. Yoon, *J. Am. Chem. Soc.* **2017**, *139*, 17186-17192.
- 48 a) T. R. Blum, Z. D. Miller, D. M. Bates, I. A. Guzei, T. P. Yoon, *Science* **2016**, *354*, 1391-1395; b) Z. D. Miller, B. J. Lee, T. P. Yoon, *Angew. Chem. Int. Ed.* **2017**, *56*, 11891-11895.
- 49 F. M. Hörmann, T. S. Chung, E. Rodriguez, M. Jakob, T. Bach, *Angew. Chem. Int. Ed.* **2017**, *57*, 827-831.
- 50 For selected examples, see: a) A. Córdova, H. Sundén, M. Engqvist, I. Ibrahim, J. Casas, *J. Am. Chem. Soc.* **2004**, *126*, 8914-8915; b) H. Sundén, M. Engqvist, J. Casas, I. Ibrahim, A. Córdova, *Angew. Chem. Int. Ed.* **2004**, *43*, 6532-6535; c) W. Ding, L.-Q. Lu, Q.-Q. Zhou, Y. Wei, J.-R. Chen, W.-J. Xiao, *J. Am. Chem. Soc.* **2017**, *139*, 63-66.

- 51 S. Liao, X.-L. Sun, Y. Tang, *Acc. Chem. Res.* **2014**, *47*, 2260-2272.
- 52 For selected examples, see: a) E. J. Horn, B. R. Rosen, Y. Chen, J. Tang, K. Chen, M. D. Eastgate, P. S. Baran, *Nature* **2016**, *533*, 77-81; b) A. Badalyan, S. S. Stahl, *Nature* **2016**, *535*, 406; c) N. Fu, G. S. Sauer, A. Saha, A. Loo, S. Lin, *Science* **2017**, *357*, 575-579.
- 53 a) K. L. Jensen, P. T. Franke, L. T. Nielsen, K. Daasbjerg, K. A. Jørgensen, *Angew. Chem. Int. Ed.* **2010**, *49*, 129-133; b) N. Fu, L. Li, Q. Yang, S. Luo, *Org. Lett.* **2017**, *19*, 2122-2125.
- 54 a) Y. Kashiwagi, F. Kurashima, C. Kikuchi, J.-i. Anzai, T. Osa, J. M. Bobbitt, *Chem. Commun.* **1999**, 1983-1984; b) Y. Kashiwagi, F. Kurashima, S. Chiba, J.-i. Anzai, T. Osa, J. M. Bobbitt, *Chem. Commun.* **2003**, 114-115.
- 55 a) J.-C. Moutet, C. Duboc-Toia, S. M énage, S. Tingry, *Adv. Mater.* **1999**, *10*, 665-667; b) J.-C. Moutet, L. Y. Cho, C. Duboc-Toia, S. p. M énage, E. C. Riesgo, R. P. Thummel, *New J. Chem.* **1999**, *23*, 939-944; c) H.-P. Yang, Q. Fen, H. Wang, J.-X. Lu, *Electrochem. Commun.* **2016**, *71*, 38-42.
- 56 For a recent review, see: R. Francke, R. D. Little, *Chem. Soc. Rev.* **2014**, *43*, 2492-2521.
- 57 a) S. Torii, P. Liu, N. Bhuvaneswari, C. Amatore, A. Jutand, *J. Org. Chem.* **1996**, *61*, 3055-3060; b) R. Yuan, S. Watanabe, S. Kuwabata, H. Yoneyama, *J. Org. Chem.* **1997**, *62*, 2494-2499; c) H. Tanaka, M. Kuroboshi, H. Takeda, H. Kanda, S. Torii, *J. Electroanal. Chem.* **2001**, *507*, 75-81; d) F. Hollmann, K. Hofstetter, T. Habicher, B. Hauer, A. Schmid, *J. Am. Chem. Soc.* **2005**, *127*, 6540-6541; e) V. Höllrigl, K. Otto, A. Schmid, *Adv. Synth. Catal.* **2007**, *349*, 1337-1340; f) B.-L. Chen, H.-W. Zhu, Y. Xiao, Q.-L. Sun, H. Wang, J.-X. Lu, *Electrochem. Commun.* **2014**, *42*, 55-59.
- 58 a) N. N. Bui, X. H. Ho, S. i. Mho, H. Y. Jang, *Eur. J. Org. Chem.* **2009**, 5309-5312; b) X. H. Ho, S. i. Mho, H. Kang, H. Y. Jang, *Eur. J. Org. Chem.* **2010**, 4436-4441.
- 59 For a detailed protocol, see: a) J. Ma, X. Zhang, X. Huang, S. Luo, E. Meggers, *Nat. Protoc.* **2018**, *13*, 605-632; For initial publications of: **IrO** by Haohua, see b) H. Huo, C. Fu, K. Harms, E. Meggers, *J. Am. Chem. Soc.* **2014**, *136*, 2990-2993; **IrS** by Xiaodong Shen, see: c) X. Shen, H. Huo, C. Wang, B. Zhang, K. Harms, E. Meggers, *Chem. Eur. J.* **2015**, *21*, 9720-9726; **RhO** by Chuanyong Wang, see: d) C. Wang, L.-A. Chen, H. Huo, X. Shen, K. Harms, L. Gong, E. Meggers, *Chem. Sci.* **2015**, *6*, 1094-1100; **RhS** by Jiajia Ma, see: e) J. Ma, X. Shen, K. Harms, E. Meggers, *Dalton Trans.* **2016**, *45*, 8320-8323.
- 60 For an review, see: L. Zhang, E. Meggers, *Acc. Chem. Res.* **2017**, *50*, 320-330.

- 61 a) H. Huo, X. Shen, C. Wang, L. Zhang, P. Röse, L.-A. Chen, K. Harms, M. Marsch, G. Hilt, E. Meggers, *Nature* **2014**, *515*, 100-103; b) H. Huo, C. Wang, K. Harms, E. Meggers, *J. Am. Chem. Soc.* **2015**, *137*, 9551-9554; c) H. Huo, X. Huang, X. Shen, K. Harms, E. Meggers, *Synlett* **2016**, *27*, 749-753; d) X. Shen, K. Harms, M. Marsch, E. Meggers, *Chem. Eur. J.* **2016**, *22*, 9102-9105; e) C. Wang, Y. Zheng, H. Huo, P. Röse, L. Zhang, K. Harms, G. Hilt, E. Meggers, *Chem. Eur. J.* **2015**, *21*, 7355-7359; f) Y. Tan, W. Yuan, L. Gong, E. Meggers, *Angew. Chem. Int. Ed.* **2015**, *54*, 13045-13048.
- 62 a) H. Huo, K. Harms, E. Meggers, *J. Am. Chem. Soc.* **2016**, *138*, 6936-6939; b) C. Wang, K. Harms, E. Meggers, *Angew. Chem. Int. Ed.* **2016**, *55*, 13495-13498; c) J. Ma, X. Xie, E. Meggers, *Chem. Eur. J.* **2018**, *24*, 259-265; d) B. Tutkowski, E. Meggers, O. Wiest, *J. Am. Chem. Soc.* **2017**, *139*, 8062-8065.
- 63 Later some elegant Giese-type radical conjugate additions using a single chiral-at-rhodium catalyst were developed, see: a) S.-X. Lin, G.-J. Sun, Q. Kang, *Chem. Commun.* **2017**, *53*, 7665-7668; b) F. F. de Assis, X. Huang, M. Akiyama, R. A. Pilli, E. Meggers, *J. Org. Chem.* **2018**, *83*, 10922-10932; c) J. Ma, J. Lin, L. Zhao, K. Harms, M. Marsch, X. Xie, E. Meggers, *Angew. Chem. Int. Ed.* **2018**, *57*, 11193-11197.
- 64 a) C. Wang, J. Qin, X. Shen, R. Riedel, K. Harms, E. Meggers, *Angew. Chem. Int. Ed.* **2016**, *55*, 685-688; b) J. Ma, K. Harms, E. Meggers, *Chem. Commun.* **2016**, *52*, 10183-10186.

Chapter 2. Aim of the Work

Chiral-at-metal complexes developed previously in the Meggers group show attractive potential to realize diverse asymmetric photocatalysis for the synthesis of enantioenriched compounds. The former members Haohua Huo, Xiaodong Shen, Chuanyong Wang, and Jiajia Ma have demonstrated three types of appealing photoreactions based on intermediate Ir/Rh-bound enolates (**Int. A**), Ir/Rh-bound ketyl radicals (**Int. B**), and Rh-bound enones (**Int. C**), whereas other intermediates (**Int. D-G**) remain to be explored and the applications of these catalysts in electronically excited state chemistry or modern electrosynthesis were still untouched (**Figure 28**).

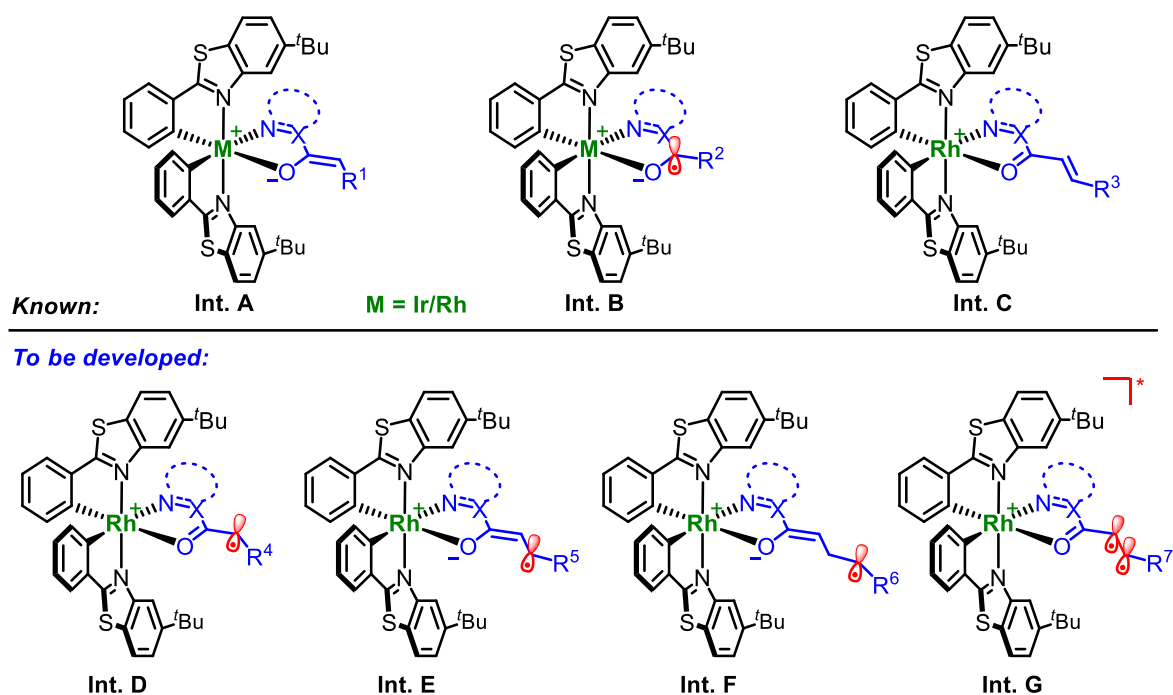


Figure 28. Diverse reactive intermediates based on the chiral-at-metal complexes.

Aim of this work is to exploit new reactivity of this type of chiral-at-metal catalysts in order to develop and discover novel catalytic asymmetric transformations which are interfaced either with photochemistry or electrochemistry. In particular, this thesis will concentrate on chiral-at-rhodium catalysts, as opposed to the more investigated chiral-at-iridium congeners, considering its apparently superior properties for chiral Lewis acid catalysis involving highly reactive intermediates such as free radicals. Built on the fantastic contributions by former group members, rhodium-bound carbonyl α -, β -,

γ -carbon-centered radical intermediates (**Int. D-F**) are expected to be generated by photoinduced and/or electricity-driven SET processes and engaged in further stereocontrolled transformations. Besides photoinduced redox catalysis, previously unexplored direct bond formation from the photoexcited chiral-at-rhodium complex (**Int. G**) will be another focus of this thesis. Furthermore, this thesis will apply this unique catalyst to electrochemistry with the aim of spurring the development of catalytic asymmetric electrosynthesis.

In details, this thesis will focus on the following aims:

1) Driving chiral-at-rhodium catalysis by photoinduced SET

As for electron-deficient radical addition to rhodium enolates (**Int. A**), there was only one example achieved by a single chiral-at-rhodium catalyst, which is the enantioselective amidation as reported by Xiaodong Shen (**Figure 25**). This could be explained by the inferior photoredox ability of the chiral-at-rhodium enolate intermediate. As firstly discovered by Chuanyong Wang, the combination of an additional photoredox catalyst could address this problem. Although achieving asymmetric photoreaction by a single catalyst is more attractive from the viewpoint of green chemistry, dual-catalyst strategy has the benefit of an easier optimization with separated photochemical process and stereodetermining bond formation. Therefore, the starting point of this thesis is to merger the advantage of a photoredox catalyst in generating radical species with the super asymmetric induction and ligand-exchange kinetics of the chiral **RhS** catalyst for the development of more general and broad asymmetric radical enolate chemistry.

In addition, photoinduced SET reduction of **Int. C**, which was previously used to intercept electron-rich radical species in Giese-type radical conjugate additions (**Figure 26**), would generate a new radical species **Int. E**. The trapping of **Int. E** in a stereocontrolled way could lead to an alternative access to asymmetric β -functionalized carbonyls. More importantly, a new mechanistic scheme with the stereocontrol of photogenerated prochiral radical species would be added to the reservoir of asymmetric chiral-at-metal catalysis.

Furthermore, the remote radical rhodium enolate intermediate (**Int. F**) is supposed to be created upon the SET reduction/ring expansion sequence of a photoexcited rhodium bound cyclopropyl ketone, thereby providing more possibilities for developing novel asymmetric photocatalysis and expanding the scope of substrate that could be activated by the chiral-at-rhodium complex.

2) Unprecedented chiral-at-rhodium catalysis with direct bond formation on excited state

The direct bond formation of visible-light-excited states is an appealing complimentary to photoredox catalysis and cannot be achieved by non-photochemical methods. While the direct reaction of the excited chiral-at-metal complex had never been accomplished before, the author of this thesis envisioned that upon direct visible-light-excitation of the rhodium bound enone (**Int. C**), the triplet state rhodium complex (**Int. G**) could be able to participate in a stereocontrolled [2+2] photocycloaddition with an alkene. If so, a really robust reaction scheme that only relies on a single chiral catalyst would be developed, in which, since no charge separation is involved, simple and mild conditions with broad substrate scope as well as excellent asymmetric induction could be anticipated. This chiral-at-rhodium catalysis features direct visible-light-excitation, efficient intersystem crossing (ISC) and intimate contact with prochiral diradical species. Hence, it is supposed to surpass those previously developed catalytic systems for asymmetric photocycloadditions (see Chapter 1.3). And based on these advantages, this thesis also aims to broaden the direct bond formation of excited states from [2+2] photocycloaddition to some other unprecedented asymmetric photo transformations.

3) Driving chiral-at-rhodium catalysis by electricity

Relatively limited examples of asymmetric electrosynthesis have been reported which is probably mainly caused by poor compatibility of the chiral catalysts with electrochemical conditions. In consideration of the robustness of this chiral-at-metal rhodium complex, this thesis targets to develop an electricity driven asymmetric chiral-at-rhodium catalysis. Through a redox activation strategy, a single chiral rhodium catalyst should facilitate the selective anodic SET oxidation upon enolization (**Int. A** \rightarrow **Int. D**), thereby providing mild conditions and good tolerance. Although chiral acid/base catalysts are well-demonstrated to activate the frontier molecular orbitals of substrates, their applications in asymmetric electrochemistry remains largely unexplored. If this hypothesis works, it is anticipated to inspire further applications of asymmetric catalytic strategies in modern organic electrosynthesis.

Chapter 3. Results and Discussion

3.1 Photoinduced Asymmetric Amination with Organic Azides and Alkylation with Diazo Compounds

3.1.1 Research Background and Reaction Design

Construction of C-N bond in a catalytic and enantioselective way is a constant demand in organic synthesis. Chemists have developed a variety of elegant amination reactions for the synthesis of chiral α -amino carbonyl compounds, considering their wide distribution in natural products and biologically active molecules.¹ Among these strategies, visible-light-induced electron transfer provides a mild and powerful tool to generate highly reactive radicals and radical ions, and therefore enables efficient C-N bond formations.² However, controlling the stereochemistry with such reactive intermediates,^{3,4} along with the need to prevent postreaction racemization of products, makes visible-light activated asymmetric α -amination of ketones a considerable challenge.

As a result, only two examples of visible-light-induced catalytic asymmetric α -amination of carbonyls are reported by MacMillan group⁵ and Meggers group⁶, respectively (**Figure 29a**). But these two reactions need the usage of *N*-2,4-dinitrophenylsulfonyloxy functionalized carbamates as nitrogen radical source with the addition of equivalent amounts of base and the release of a sulfonate anion as by-product. Mechanistically, the key amino radicals are formed through the photoinduced single electron reduction, and then engage in the enantioselective bond formations with enamines or enolates. Despite this significant progress, the effective asymmetric building of C-N bonds with higher atom economy and milder conditions is highly desirable, which could be achieved by exploration of new amination reagents.

Organic azides are unique and versatile building blocks that feature the advantage of N₂ as leaving group and sole by-product.⁷ In 2011, Liu and co-workers reported a visible-light-induced azide reduction, which was proposed to occur through amino radical intermediates formed via a sequential reduction/protonation/N₂ exclusion process (**Figure 29b**).⁸ Inspired by this elegant work and combined with previous work on asymmetric α -functionalization of ketones,⁹ the author of this thesis envisioned that organic azides might be applied to a redox- and proton-neutral environmentally

benign α -amination reaction (**Figure 29c**). However, the manipulation of these high-energy synthons under visible light conditions in an enantioselective manner has not been accomplished before this work. Two main reasons might be responsible for this: First, azides typically generate nitrene intermediates under photochemical activation resulting in potential side reactions and narrow functional group compatibility,¹⁰ and second, the highly negative reduction potentials of organic azido compounds render them difficult to be reduced under mild conditions.

This chapter presents how to address these challenges to achieve a mild and efficient α -amination of 2-acyl imidazoles using acceptor-substituted aryl azides. In addition, a further application of this strategy to asymmetric alkylations with diazo compounds is also demonstrated.

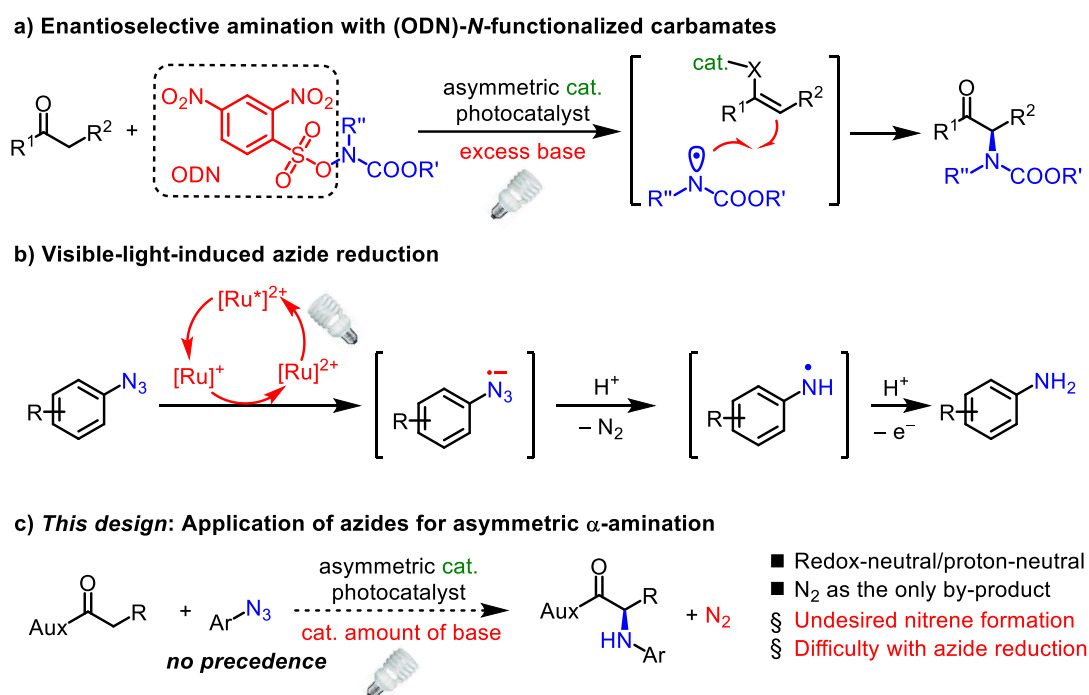


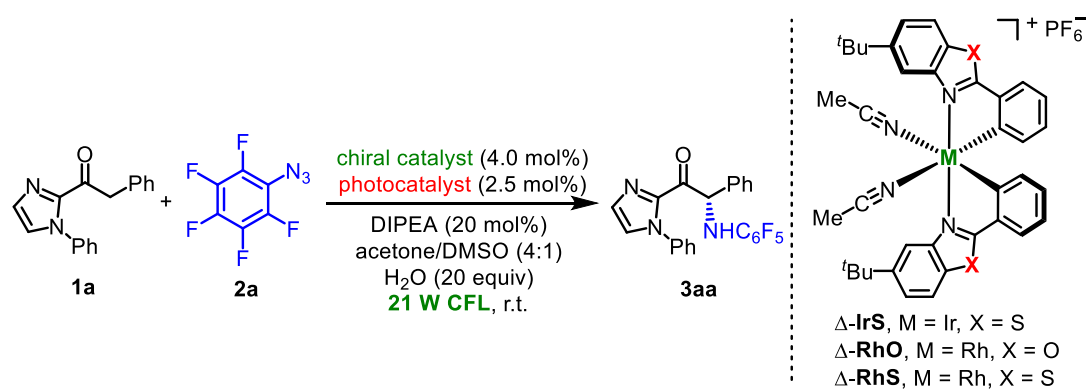
Figure 29. Previous reports and this design for visible-light-induced enantioselective α -amination.

3.1.2 Reaction Development of α -Amination

To verify the hypothesis of using azides as amination reagents, pentafluorophenyl azide **2a** was chosen as the model substrate. This is because electron-acceptor-substituted phenyl azides are easier to be reduced, and the thereby formed amino radical is regarded as an electron deficient radical species which can add to an electron rich enolate.⁹ Based on previous work on a chiral-at-metal iridium complex catalyzed perfluoroalkylation,¹¹ the author of this thesis commenced this investigation with

the reaction of 2-acyl imidazole **1a** and **2a** using Δ -**IrS** as a single dual functional catalyst in the presence of catalytic amounts of diisopropylethylamine (DIPEA) (**Table 1**, entry 1). Unfortunately, the catalyst Δ -**IrS** did not show any reactivity (entries 1,2). Inspired by Chuanyong Wang's and Haohua Huo's work on dual-catalyst strategy,¹² the author tested the reaction employing a chiral Lewis acid Δ -**RhO**¹³ (4.0 mol%) together with a photoredox catalyst [Ru(bpy)₃](PF₆)₂ (2.5 mol%). Encouragingly, the desired amination product **3aa** was obtained in a yield of 24% but with 86% ee (entry 3). Revealingly, the related catalyst Δ -**RhS**,¹⁴ in which the benzoxazole ligands are replaced by benzothiazoles, provided **3aa** in 70% yield and 98% ee (entry 4).

Table 1. The development of dual-catalyst system for α -amination.^[a]



Entry	Chiral catalyst	Photocatalyst	Yield [%]	Ee [%]
1	Δ - IrS	none	0	n.a.
2	Δ - IrS	[Ru(bpy) ₃](PF ₆) ₂	0	n.a.
3	Δ - RhO	[Ru(bpy) ₃](PF ₆) ₂	24	86
4	Δ - RhS	[Ru(bpy) ₃](PF ₆) ₂	70	98
5	Δ - RhS	[Ir(ppy) ₂ (dtbbpy)](PF ₆)	62	98
6	Δ - RhS	<i>fac</i> -Ir(ppy) ₃	37	89
7 ^[b]	Δ - RhS	none	0	n.a.
8 ^[b]	none	[Ru(bpy) ₃](PF ₆) ₂	0	n.a.
9 ^[b,c]	Δ - RhS	[Ru(bpy) ₃](PF ₆) ₂	0	n.a.

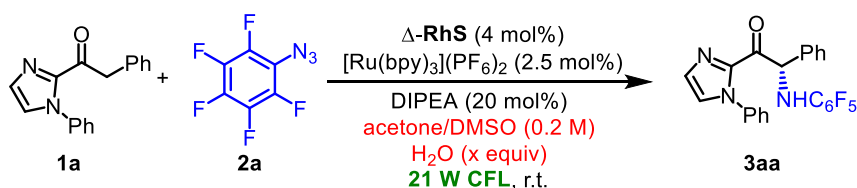
[a] Reaction conditions: **1a** (0.10 mmol), **2a** (0.30 mmol), chiral catalyst (4.0 mol%), photocatalyst (2.5 mol%), DIPEA (20 mol%) and H₂O (20 equiv) in acetone/DMSO (4:1, 0.2 M) were stirred at room temperature for 14-24 h irradiated with a 21 W CFL; isolated yield; ee was determined by HPLC on a chiral stationary phase. [b] Na₂HPO₄ instead of DIPEA in acetone/DMSO (9:1, 0.2 M). [c] Under dark conditions.

Other photoredox catalysts, such as $[\text{Ir}(\text{ppy})_2(\text{dtbbpy})](\text{PF}_6)$ and *fac*- $\text{Ir}(\text{ppy})_3$, showed lower efficiency (entries 4-6). Control experiments confirmed that the chiral Lewis acid, the photoredox catalyst, and visible light are all indispensable in this process (entries 7-9). The solvent effect was evaluated by the reaction of *N*-*o*-tolyl substituted 2-acyl imidazole **1b** with **2a** (Table 2). A series of strong polar organic solvents could deliver target product, albeit in low yields (23-27%, entries 1-3). Solvents, including CH_2Cl_2 , THF, and MeOH, could hardly give any product (entry 6), which is attributed to the poor solubility of the ruthenium-based photocatalyst in these solvents. Interestingly, the reaction in the strong coordinative solvent (MeCN) could form **3ba** with excellent enantioselectivity of 92% ee (entry 4). Overall, acetone was identified as a good solvent (entry 5) and the conditions with mixed solvents of acetone/DMSO (4:1) in the concentration of 0.2 M gave the best results in this round of screening (entry 10).

Table 2. Solvent effect on α -amination.^[a]

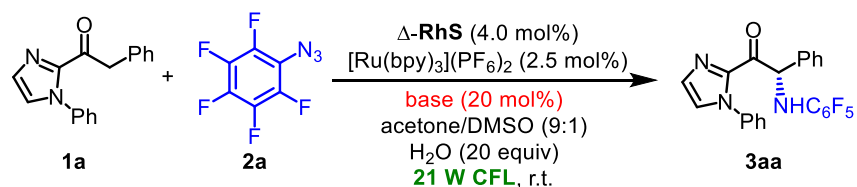
Entry	$\Delta\text{-RhS}$ [mol%]	Solvent	Yield [%]	Ee [%]
1	2.0	DMSO (0.4 M)	27	95
2	2.0	DMF (0.4 M)	25	92
3	2.0	NMP (0.4 M)	23	95
4	2.0	MeCN (0.4 M)	30	92
5	2.0	Acetone (0.4 M)	38	96
6	2.0	MeOH and the others ^[b]	<5	n.a.
7	2.0	Acetone (0.2 M)	49	n.d.
8	2.0	Acetone (0.1 M)	42	n.d.
9	4.0	Acetone (0.2 M)	58	98
10	4.0	Acetone/DMSO (4:1, 0.2 M)	64	98

[a] Reaction conditions: **1b** (0.10 mmol), **2a** (0.30 mmol), $\Delta\text{-RhS}$ (x mol%), $[\text{Ru}(\text{bpy})_3](\text{PF}_6)_2$ (2.5 mol%), DIPEA (20 mol%) in solvent were stirred at room temperature for 14-32 h irradiated with a 21 W CFL; isolated yield; ee was determined by HPLC on a chiral stationary phase. [b] Including CH_2Cl_2 , PhCH_3 , THF, and 1,4-dioxane.

Table 3. Effect of water and solvent ratio on α -amination.^[a]

Entry	Acetone/DMSO	H ₂ O [x equiv]	Yield [%]	Ee [%]
1	4:1	0	61	97
2	4:1	5	64	98
3	4:1	20	70	98
4	4:1	50	68	98
5	9:1	20	77	98
6	1:1	20	71	98

[a] Reaction conditions: **1a** (0.10 mmol), **2a** (0.30 mmol), Δ -RhS (4.0 mol%), [Ru(bpy)₃](PF₆)₂ (2.5 mol%), DIPEA (20 mol%), and H₂O (x equiv) in solvent were stirred at room temperature for 14-32 h irradiated with a 21 W CFL; isolated yield; ee was determined by HPLC on a chiral stationary phase.

Table 4. Base effect on α -amination.^[a]

Entry	Base	Conversion	Yield [%]	Ee [%]
1	DIPEA	Full	77	98
2	2,6-lutidine	Full	73	98
3	Na ₂ HPO ₄	Full	82	98
4	NaOAc	Low	<10	n.d.
5	Na ₂ CO ₃	Full	<5	n.d.
6	K ₃ PO ₄	Full	0	n.a.
7	None	Low	0	n.a.

[a] Reaction conditions: **1a** (0.10 mmol), **2a** (0.30 mmol), Δ -RhS (4.0 mol%), [Ru(bpy)₃](PF₆)₂ (2.5 mol%), Base (20 mol%) and H₂O (20 equiv) in acetone/DMSO (9:1, 0.2 M) were stirred at room temperature for 14-24 h irradiated with a 21 W CFL; isolated yield; ee was determined by HPLC on a chiral stationary phase.

Considering that an additional proton source might be beneficial for the proton transfer process, 20 equiv of water was added. And indeed, an increased yield of **3aa** by 10% was observed (Table 3, entries 1-4). Besides, a slight modification in the ratio of the mixed solvent (acetone/DMSO = 9:1) gave an improved yield of 77% for the formation of **3aa** (entry 5).

Further optimization of the reaction conditions resulted in the identification of Na₂HPO₄ as the preferred base, providing 82% yield and 98% ee for the reaction **1a** + **2a** → **3aa** (Table 4, entry 3). While a base is required (entry 7), sodium acetate gave very low conversion which was attributed to the competitive coordination of acetate with the chiral Lewis acid (entry 4). It is noteworthy that strong bases, such as Na₂CO₃ and K₃PO₄, led to product decomposition (entry 5, 6), indicating that **3aa** is very sensitive to strong basic conditions.

In summary, a mild dual-catalyst system that consists of a chiral Lewis acid, a photoredox catalyst, and catalytic amount of weak base was identified as the optimal conditions for the present α -amination (Table 4, entry 3).

3.1.3 Further Extension to α -Alkylation

A few examples of visible-light-induced catalytic asymmetric α -alkylation of ketones had been reported, which employed organic bromides/iodides¹⁵ or α -silylalkylamines^{12a} as alkylation reagents with stoichiometric amount of base or oxidant, respectively. At that time, a racemic photoredox α -alkylation of aldehydes using diazoacetates as alkylation reagents was reported by Gryko *et al.*¹⁶ Encouraged by the above-mentioned positive amination results and the literature reports, the author of this thesis became interested in investigating the dual-catalyst system with related diazo compounds. Luckily, the alkylation product **5aa** was obtained in excellent yield of 93% with 92% ee when ethyl diazo acetate (EDA) **4a** was used instead of azide **2a** under the same reaction conditions (Table 5, entry 1), thus demonstrating the versatility of this newly developed catalytic system in enolate chemistry. Lowering the loading of [Ru(bpy)₃](PF₆)₂ to 1.5 mol% did not affect the reaction efficiency (entry 4). A quantitative yield with an improve ee of 97% ee was obtained by using a more bulky *o*-tolyl group as the *N*-substituent of imidazole (entry 5). The Ru photocatalyst and visible light are necessary for this reaction (entries 2,3). Other Lewis acids including Sc(OTf)₃, Cu(OAc)₂, and FeCl₃ could not catalyzed the racemic reaction, highlighting the unique reactivity of the chiral-at-metal **RhS**

in this transformation (entries 7-9). Furthermore, the reaction employing α -bromo ethyl acetate in place of EDA in the presence of stoichiometric amounts of base resulted in a low conversion with the formation of **5ba** in 33% yield (entry 10), which showed the advantage of using EDA as alkylation reagent.

Table 5. Asymmetric α -alkylation with EDA.^[a]

Entry	Substrate	Variation	Yield [%]	Ee [%]
1	1a	None	5aa , 93	92
2	1a	Without [Ru]	5aa , 0	n.a.
3	1a	Without 21 W CFL	5aa , 0	n.a.
4	1a	1.5 mol% of [Ru]	5aa , 94	92
5	1b	1.5 mol% of [Ru]	5ba , 99	97
6 ^[b]	1b	Zn(OTf) ₂ instead of Δ -RhS	5ba , 20	0
7 ^[b]	1b	Sc(OTf) ₃ instead of Δ -RhS	5ba , 0	0
8 ^[b]	1b	Cu(OAc) ₂ instead of Δ -RhS	5ba , 0	0
9 ^[b]	1b	FeCl ₃ instead of Δ -RhS	5ba , 0	0
10 ^[c]	1b	α -Bromo ethyl acetate instead of 4a , 2.0 equiv of Na ₂ HPO ₄	5ba , 33	n.d.

[a] Reaction conditions: **1a** or **1b** (0.10 mmol), **4a** (0.30 mmol), Δ -RhS (4.0 mol%), [Ru(bpy)₃](PF₆)₂ (2.5 mol%), Na₂HPO₄ (20 mol%) and H₂O (20 equiv) in acetone/DMSO (9:1, 0.2 M) were stirred at room temperature for 6-18 h irradiated with a 21 W CFL; isolated yield; ee was determined by HPLC on a chiral stationary phase. [b] 20 mol% of Lewis acid and 1.5 mol% of [Ru(bpy)₃](PF₆)₂. [c] 1.5 mol% of [Ru(bpy)₃](PF₆)₂.

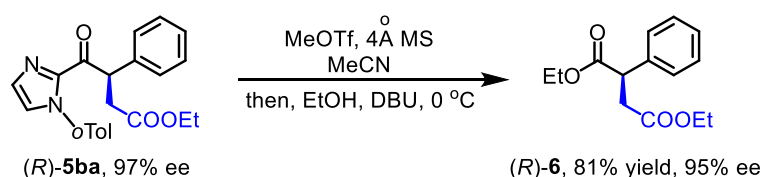


Figure 30. Removal of the imidazolyl group of compound **5ba**.

In addition, the removal of the imidazole moiety of **5ba** worked smoothly, giving 1,4-diester **6** in 81% yield with little loss in enantiomeric excess (95% ee, **Figure 30**). Unfortunately, the amination product **3aa** is more sensitive and apparently not incompatible under these conditions.

3.1.4 Substrate Scope

The substrate scope of amination with aryl azides under optimal conditions is shown in **Figure 31**. Good yields and excellent enantioselectivities were obtained in the amination of 2-acyl imidazoles with different substituents at the *N*-atom of imidazole (**3aa-da**) or different electron-rich aromatic groups at the stereogenic carbon (**3ea-ga**, **3ja**). Other functional groups, such as naphthyl (**3ha**), 2-thienyl (**3ia**), and chloride (**3ka**), were well tolerated giving moderate yields and satisfying enantioselectivities. On the other hand, a wide range of electron-deficient aromatic azides performed well both in yields and enantioselectivities (**3bb-bg**). Remarkably, bromo (**3bb**) and cyano groups (**3bf-bg**), which are vulnerable to reducing conditions, are compatible under the present mild protocol, providing the potential for further transformations. Intriguingly, chemoselective amination with an aryl azido group over an aliphatic azido group was observed (**3bh**). And the structure of **3bh** was confirmed by selective ^1H - $\{^{19}\text{F}\}$ decoupling NMR experiments with the assistant of Dr. Xiulan Xie (**Figure 32**). Notably, 8 examples of these amination products were formed with an enantioselectivity of 99% ee or even higher without any postreaction racemization.

The substrate scope with respect to enantioselective alkylation with α -diazo carboxylic esters under photoredox conditions was evaluated as well (**Figure 33**). Accordingly, the alkylation of a variety of 2-acyl imidazoles worked well, providing asymmetric 1,4-diketones in good to excellent yields (81-99%) with excellent enantioselectivities (95-98% ee), regardless of the electronic nature or position of substituents (**5ba-qa**). C=C double and C \equiv C triple bonds were found to be well tolerated (**5bc-be**, **5bh**), indicating a mechanism without the involvement of carbene intermediates. Notably, the present asymmetric alkylation was compatible with various natural alcohol derivatives (**5be-bh**), highlighting the potential utility of this protocol in further late-stage functionalization.

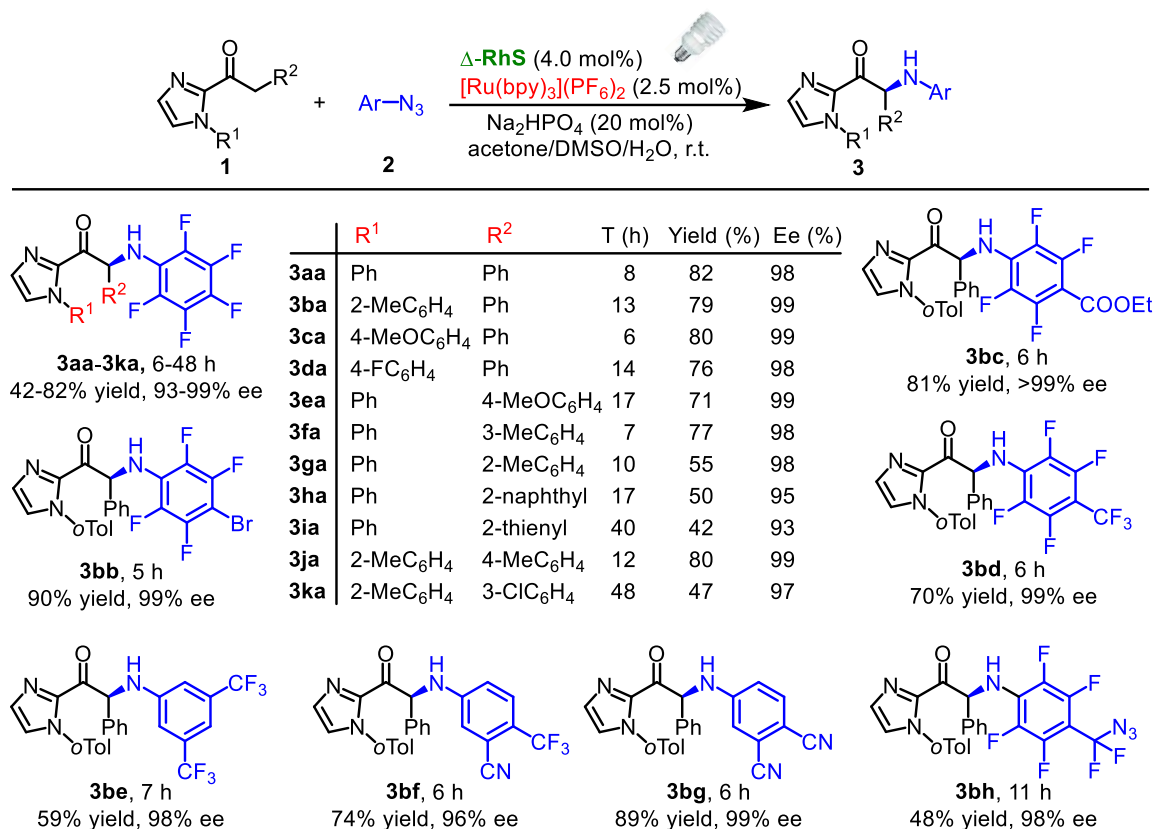


Figure 31. Substrate scope of the enantioselective α -amination with aryl azides.

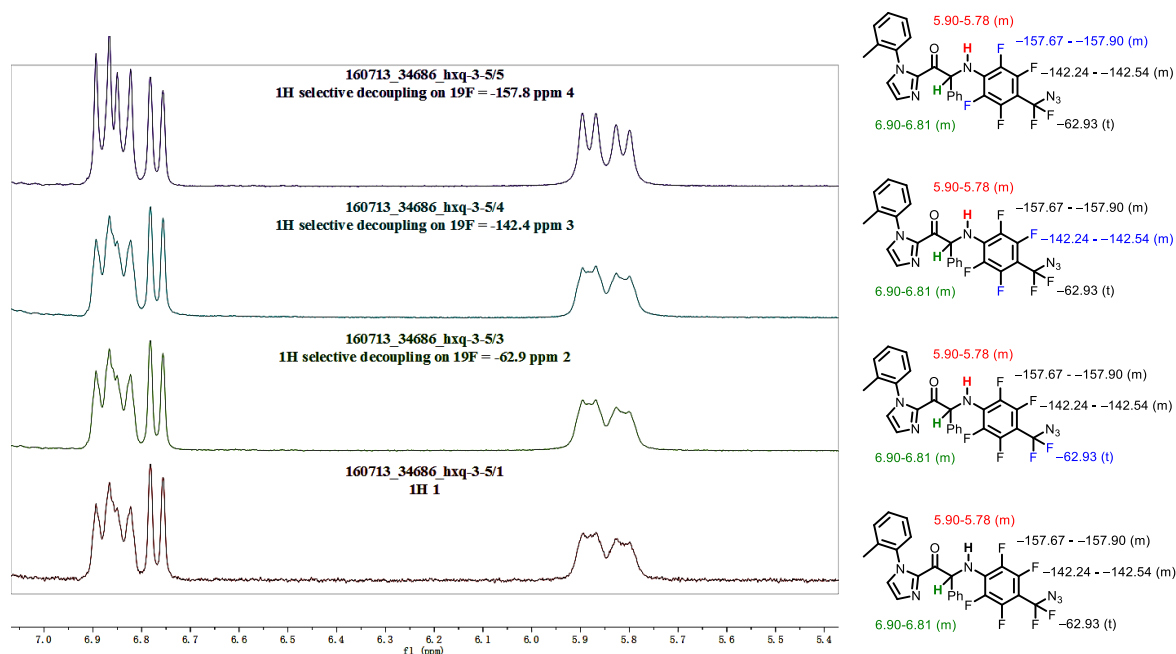


Figure 32. Selective ^1H - $\{^{19}\text{F}\}$ decoupling NMR experiments of compound **3bh**. The splitting disappeared only when selective decoupling on ^{19}F = -157.8 ppm. Mixture of two roammers.

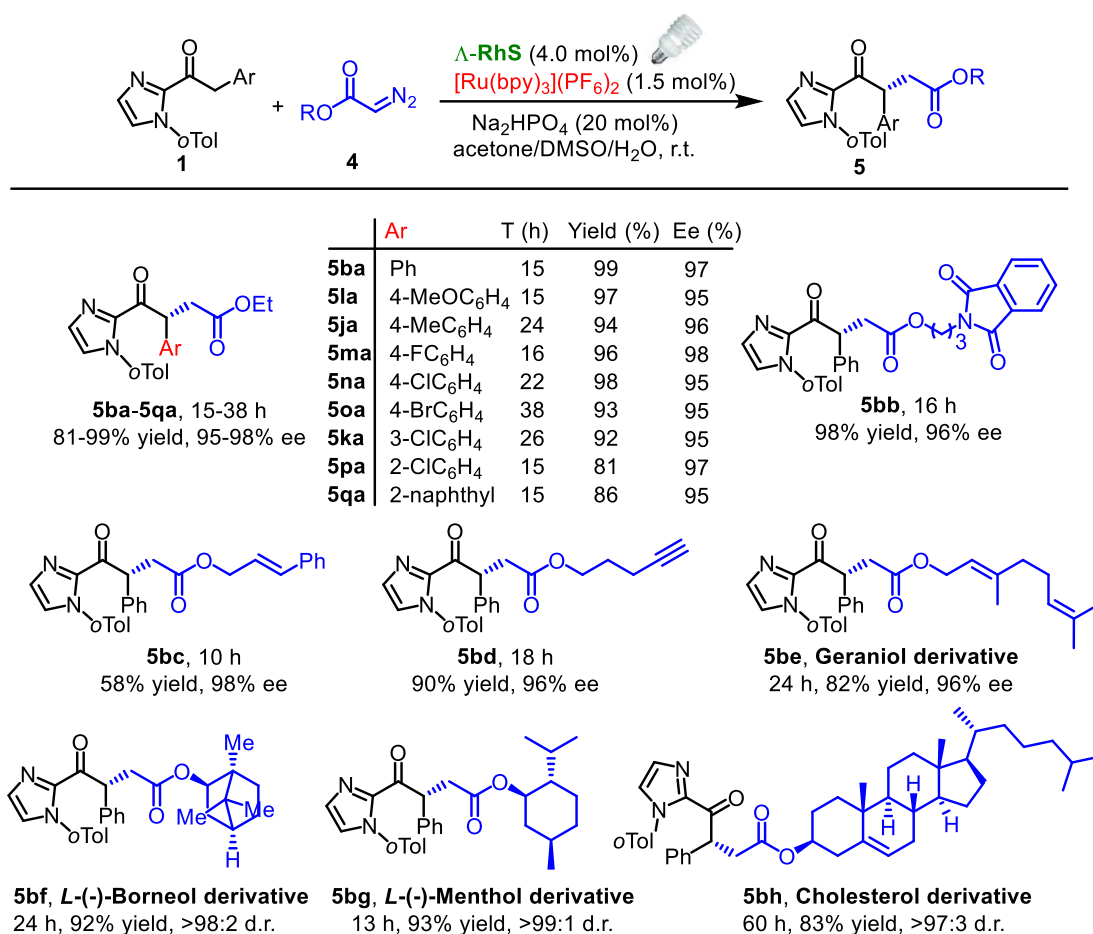
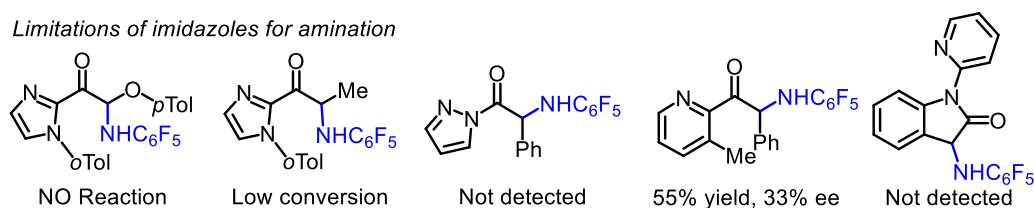


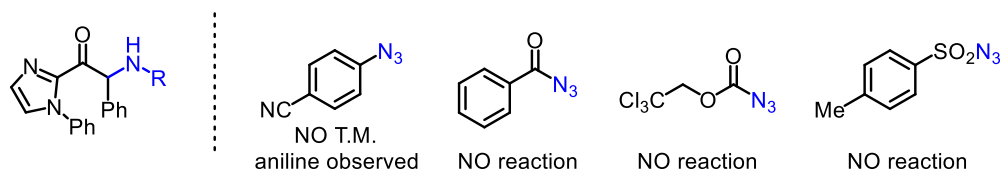
Figure 33. Substrate scope of the enantioselective α -alkylation with diazo compounds. The structure of **5oa** was determined by X-ray crystallography and all other compounds were assigned accordingly.

Although the functional group tolerance of this reaction is quite good, there are some limitations with respect to the scope (**Figure 34**). An aromatic substituent at the stereogenic carbon is needed for both amination and alkylation. Other auxiliaries, such as *N*-pyrazole, or *N*-pyridinyl indolinone failed to give any product. A 2-acyl pyridine underwent the amination with pentafluorophenyl azide **2a**, but gave low enantioselectivity (33% ee). Besides, only aryl azides bearing more than two electron deficient groups can work smoothly, as *para*-cyano phenyl azide, acyl azides and a tosyl azide were demonstrated to be unsuitable as amination reagents. In addition, diazo compound is limited to the ester-type.

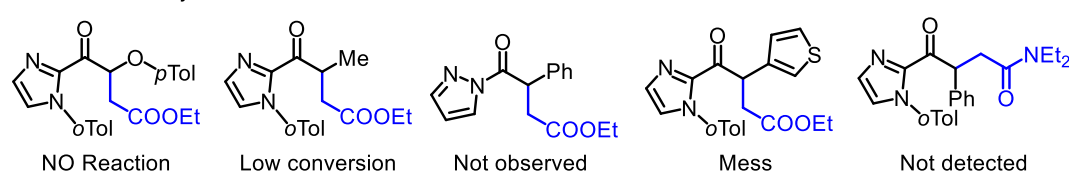
Limitations of imidazoles for amination



Limitations of azides



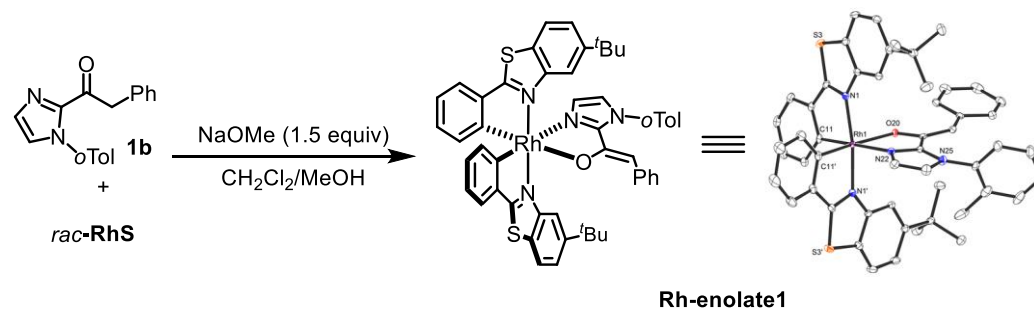
Limitations of alkylation

**Figure 34.** Limitations of the present asymmetric α -functionalization.

3.1.5 Mechanistic Studies

1) Identification of Rh-enolate1 intermediate

Based on previous studies and the requirement for a base, it is expected that the reaction proceeds through a rhodium bound enolate intermediate. To support this assumption, the **Rh-enolate1** was synthesized independently by the reaction of *rac*-**RhS** (0.1 mmol), imidazole **1b** (1.2 equiv), and NaOMe (1.5 equiv) in MeOH/CH₂Cl₂ (1/4, 0.05 M) at room temperature (**Figure 35**). This intermediate is stable and could be purified by column chromatography (silica gel, *n*-Hexane/EtOAc) followed by recrystallization (CH₂Cl₂/Et₂O). The structure was further confirmed by X-ray diffraction.

**Figure 35.** Synthesis and X-ray diffraction structure of the key **Rh-enolate1** intermediate.

Its competence as catalyst in the amination and alkylation reactions was demonstrated (**Table 6**). Indeed, comparable yields were obtained with **Rh-enolate1** as the catalyst in the absence of any base, thus providing alternative base-free conditions for these transformations. These results support that the in situ formed rhodium bound enolate serves as a key intermediate in the present transformations.

Table 6. Catalytic behavior of **Rh-enolate1**.

Entry	Substrate	Conditions ^[a]	[Rh]	Variation	Yield [%]
1	2a	Table 4 , entry 3	RhS	None	4ba , 79
2	2a	Table 4 , entry 3	Rh-enolate1	No base	4ba , 74
3	3a	Table 5 , entry 5	RhS	None	5ba , 99
4	3a	Table 5 , entry 5	Rh-enolate1	No base	5ba , 99

[a] For entries 1 and 2, **1b** (0.10 mmol); entries 3 and 4, **1b** (0.96 mmol).

2) Demonstration of a radical pathway rather than a nitrene/carbene mechanism

Five sets of experiments support that the reaction proceeds through a radical pathway rather than a nitrene/carbene process (**Figure 36**). First, both amination and alkylation were completely inhibited by air together with the generation of the oxygenation product **7**, which implies that α -carbonyl carbon radicals derived from imidazole substrate might form (**Figure 36a**). Second, when silyl enol ether **8a** was added to the reaction mixture of **1b** and **2a**, the C-C and C-N bond formation products **9ba** (42% yield) and **10** (22% yield) were isolated, respectively (**Figure 36b**), indicating the intermediate formation of α -carbonyl carbon radicals and aminyl radicals. Third, when TEMPO was added to the reaction mixture of **1b** and **4a**, the TEMPO adducts **11** (84% yield) and **12** (6% yield) were isolated (**Figure 36c**), being indicative for two types of intermediate α -carbonyl carbon radicals. Fourth, the isolation of the radical addition product **13** instead of the cyclopropanation product **14** in the reaction with ethyl diazo acetate **4a** renders a mechanism through carbene intermediates unlikely (**Figure 36d**). The intermediate formation of the cyclopropanation compound was ruled out by the independent synthesis of **14** and re-subjection to the standard photoredox conditions under which no conversion to **13** was detected. Besides, the radical trapping product **16** was detected, together with the formation of

alkylation product **5ba**, when the alkene **15** was added to the reaction mixture of **1b** with **4a** under standard conditions, which supports the generation of EDA derived carbon centered radical. Fifth, if the styrene was added to the reaction mixture of **1b** with **2a**, the amination product **3ba** was detected in 80% yield, while aziridination product was not observed at all (**Figure 36e**). This implies nitrene intermediate might not be involved in this transformation, which is different from Yoon's recent report.¹⁷

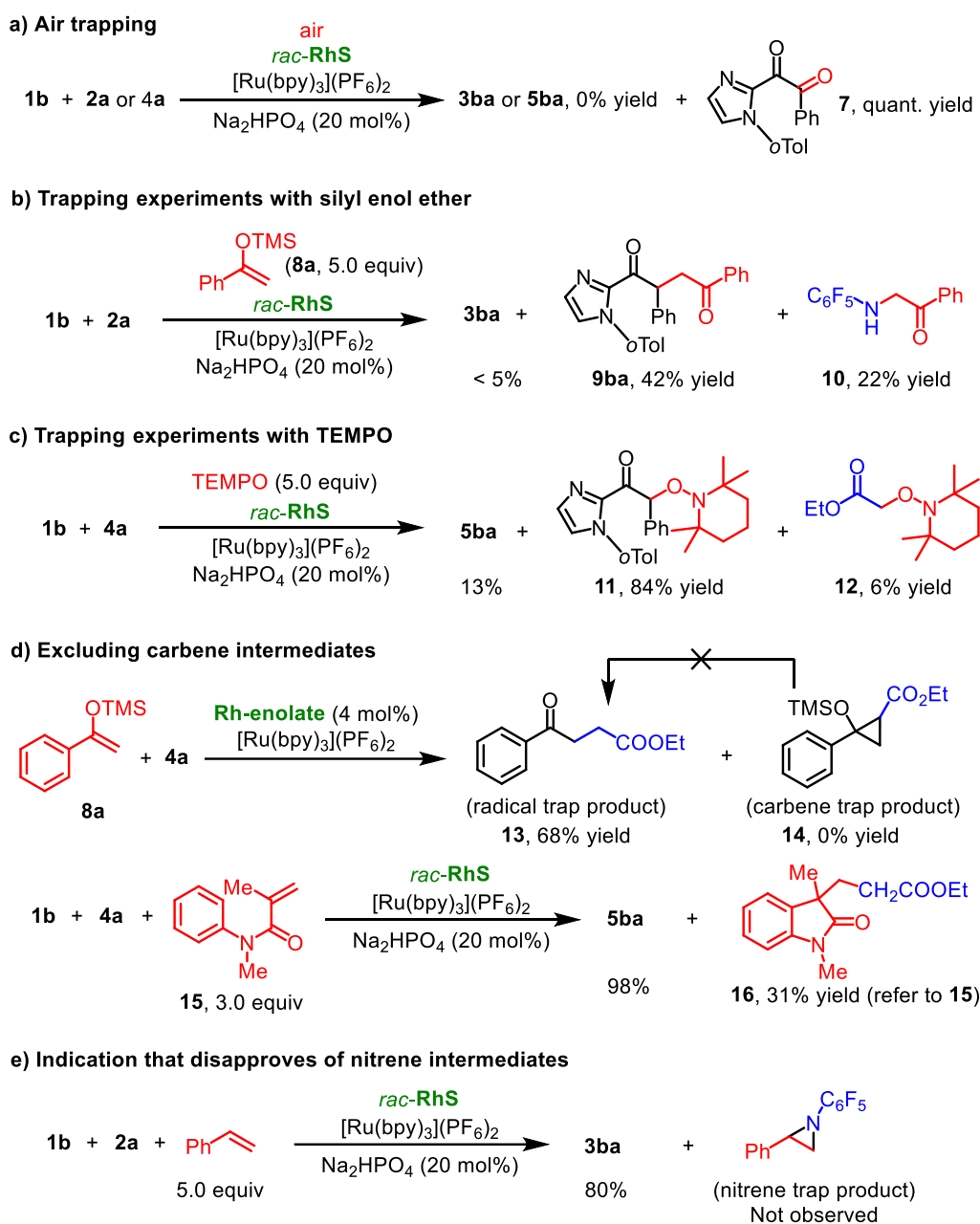


Figure 36. Control experiments supporting a radical mechanism involved in dual-catalytic system.

3) EPR experiments

In order to further confirm a radical pathway under the optimal conditions, the alkylation reaction was monitored by electron paramagnetic resonance (EPR) spectroscopy. With the addition of DMPO as free radical spin-trapping agent, signals with 6 lines ($g = 2.006$, $a_N = 15.9$ G, $a_H^\beta = 22.5$ G) were observed and identified as EPR signals of DMPO-adduct, which is in good agreement with the literature (**Figure 37**).¹⁸

All these results support the formation of an ethyl acetate α -carbon radical through single electron reduction of the diazo compound **4a**, suggesting that the mechanism is distinct from recent work¹⁶ by Gryko and coworkers in which a direct reaction between an intermediate iminyl cation radical and a diazo compound was proposed without the involvement of the carbon radical derived from the diazo compound (see below for further discussion).

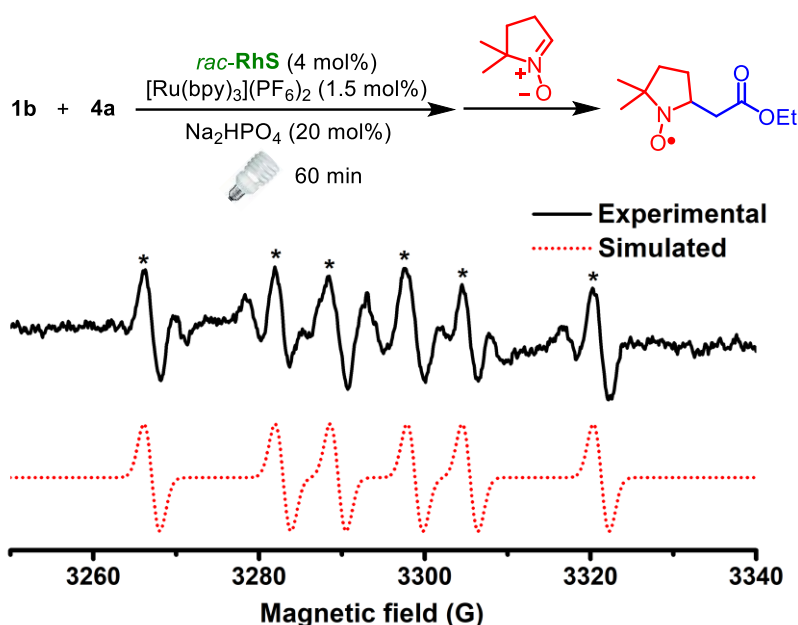


Figure 37. EPR experiments that demonstrate the involvement of the carbon centered radical derived from EDA. EPR spectra (X band, 9.7 GHz, r.t.) of the DMPO-adduct generated under conditions: **1b** (0.10 mmol), **4a** (0.30 mmol), *rac*-RhS (4.0 mol%), [Ru(bpy)₃](PF₆)₂ (1.5 mol%), Na₂HPO₄ (20 mol%) and H₂O (20 equiv) in acetone/DMSO (9:1, 0.2 M) stirring at room temperature under visible light. After 60 min stirring, DMPO solution was added and then analyzed by EPR.

5) UV/Vis absorption and Stern-Volmer quenching experiments

The current dual-catalyst system relies on [Ru(bpy)₃](PF₆)₂ as photocatalyst, which indicates that the Ru species is responsible for photoredox catalysis. To confirm this, the UV/Vis absorption spectra

were measured. As shown in **Figure 38**, the Ru species is a much better visible light absorbing antenna compared with the **Rh-enolate1**, although both of them could be photoexcited under the irradiation of the 21 W CFL. Besides, the emission of [Ru] could be detected when irradiating the reaction mixture.

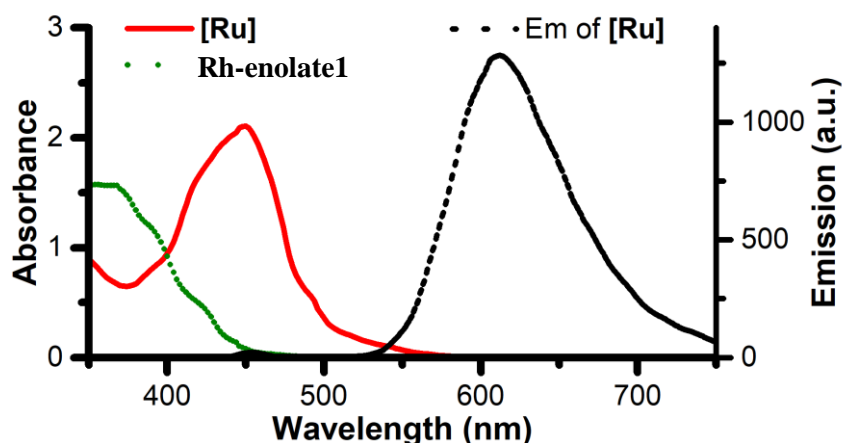


Figure 38. UV/Vis absorption spectra of [Ru] and **Rh-enolate1** and luminescence emission spectrum of [Ru]. Concentrations in solution of acetone/DMSO/H₂O (9:1:0.72): [Ru] = 0.05 mM, **Rh-enolate1** = 0.05 mM, Em of [Ru] = 0.10 mM. [Ru] = [Ru(bpy)₃](PF₆)₂.

Then, a series of Stern-Volmer quenching experiments were performed to verify the initial electron transfer step of the photoredox process. To avoid the influence of the competitive absorption of the **Rh-enolate1** (with wavelength <470 nm), quenching experiments were carried out under different conditions. First, the solutions of [Ru] were excited at $\lambda = 470$ nm and the emission was measured at 610 nm (emission maximum). As the results, imidazole **1b**, azide **2a**, diazo compound **4a**, silyl enol ether **8a** and *rac*-**RhS** could not quench the luminescence. Only **Rh-enolate1** was capable of quenching the excited state of [Ru]. Second, the solutions of [Ru] with different concentration of quencher (0, 0.5, 1.0, 2.0, 4.0 mM) were excited at $\lambda = 470$ nm, 510 nm, and 530 nm, respectively. At the same time, the absorbance of the mixture was measured too. As shown in **Figure 39**, the absorption of the mixture kept a constant with the increment of **Rh-enolate1**, indicating there is no competitive absorption by **Rh-enolate1** in 530 nm. And only the intermediate **Rh-enolate1** but not the pre-catalyst **RhS** nor the silyl enol ether, can quench the excited [Ru] species. In addition, the quenching effect of **Rh-enolate1** is similar using exciting light with different wavelengths (**Figure 40**). Third, the solutions of a mixture of [Ru] and **Rh-enolate1** (0.1 mM and 0.27 mM, respectively) were excited at $\lambda = 470$ nm and the emission was measured at 610 nm. In these cases, imidazole **1b**, azide

2a, diazo compound **4a**, and silyl enol ether **8a** could not quench the luminescence. In conclusion, all these results support that [Ru] is responsive for the photoinduced redox process and **Rh-enolate1** is the key species to quench the photoexcited [Ru]* species.

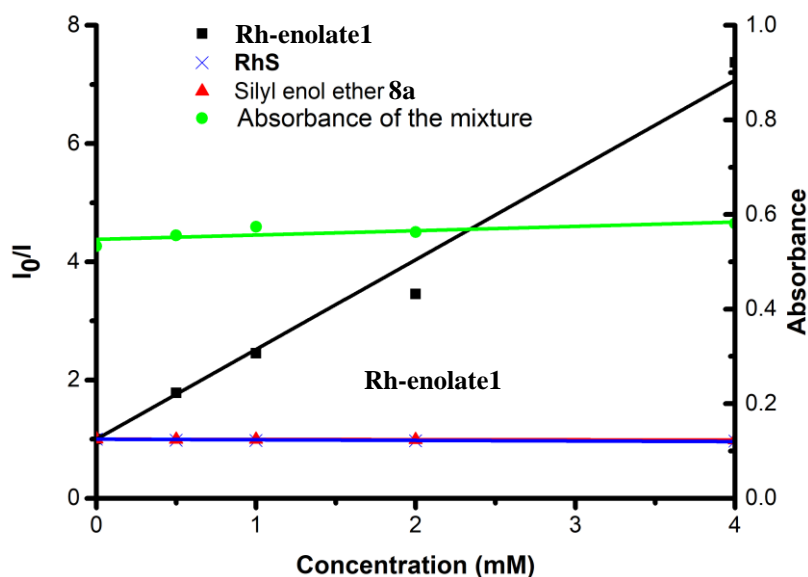


Figure 39. Stern-Volmer quenching experiments with photoexcited [Ru(bpy)₃](PF₆)₂ (0.5 mM, λ_{ex} = 530 nm, λ_{em} = 610 nm). I_0 and I are respective luminescence intensities in the absence and presence of the indicated concentrations of the corresponding quencher. Absorption refer to the absorbance of the solutions of [Ru] with different concentration of **Rh-enolate1**.

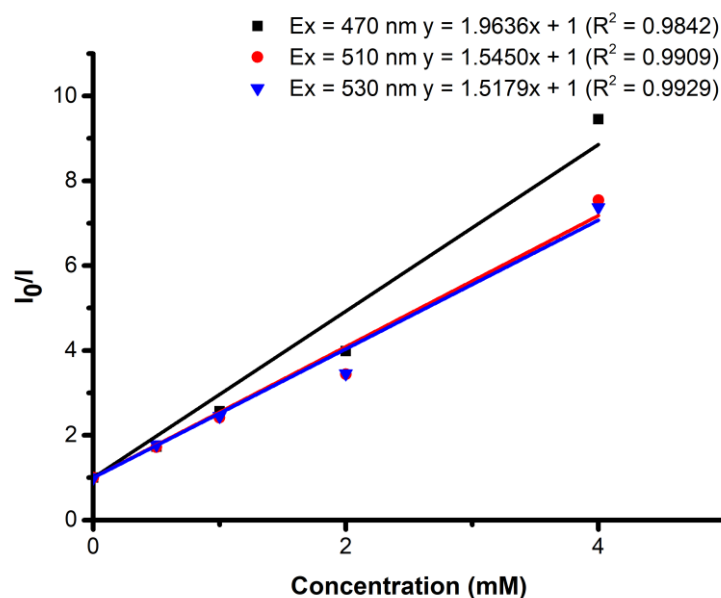


Figure 40. Quenching effect of **Rh-enolate1** on the solution of [Ru] excited by light with different wavelengths.

6) Cyclic voltammetry

Cyclic voltammetry was conducted to identify the quenching mechanism of **Rh-enolate1** on photoexcited $[\text{Ru}]^*$ (**Figure 41**). Surprisingly, **Rh-enolate1** ($E_p^{[\text{Rh-enolate1}]/[\text{Rh-enolate1}]} = +0.08 \text{ V}$, vs Fc/Fc^+ in MeCN (the same reference and solvent below)) has a significantly lower oxidation peak potential than **RhS** ($E_p^{[\text{RhS}]/[\text{RhS}]} = +1.25 \text{ V}$). Therefore, in consistent with the quenching experiments, the **Rh-enolate1** is able to transfer a single electron to the excited $[\text{Ru}]$ ($E_{1/2}^{[\text{Ru}]/[\text{Ru}]^-} = +0.37 \text{ V}$) initiating a reductive quenching cycle. Furthermore, a SET reduction of **2a** ($E_p^{2\text{a}/2\text{a}^-} = -1.82 \text{ V}$) or **4a** ($E_p^{4\text{a}/4\text{a}^-} = -1.97 \text{ V}$) by the reduced $[\text{Ru}]^-$ species ($E_{1/2}^{[\text{Ru}]/[\text{Ru}]^-} \approx -1.73 \text{ V}$) appears also feasible to regenerate the ground state $[\text{Ru}]$ and radical species when considering that the subsequent protonation and N_2 exclusion might facilitate the SET step. On the other hand, the reduction peak potential of **2a** or **4a** is too negative so that **2a** or **4a** cannot quench the excited state of $[\text{Ru}]$ ($E_{1/2}^{[\text{Ru}]/[\text{Ru}]^+} \approx -1.21 \text{ V}$) by an oxidative quenching cycle.

All these results, together with the quenching experiments, strongly suggest that SET between the rhodium enolate and the excited $[\text{Ru}]$ is a key step for the initial reductive quenching of photoredox cycle.

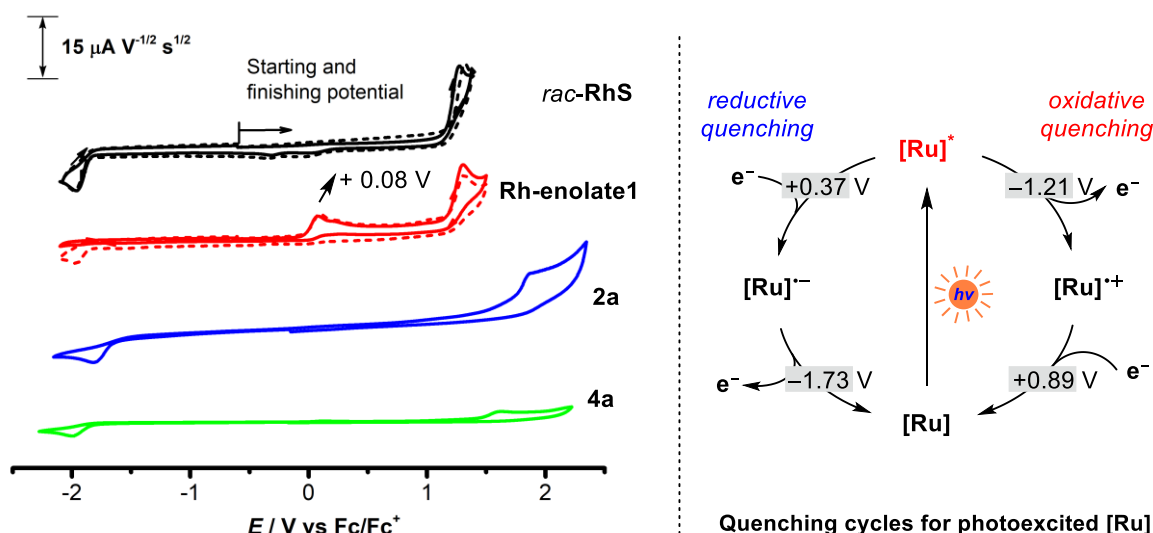


Figure 41. Cyclic voltammograms of **RhS**, **Rh-enolate1**, **2a**, **4a** and quenching mechanism for photoexcited $[\text{Ru}]$. CV were recorded in CH_3CN containing $0.1 \text{ M } n\text{Bu}_4\text{NPF}_6$ at $22 \pm 2^\circ \text{C}$ with a 1 mm diameter glass carbon electrode. (—) Scan rate = 0.1 V s^{-1} , and (---) scan rate = 1 V s^{-1} . The current data were normalised by dividing by the square root of the scan rate. All potentials refer to Fc^+/Fc .

7) Quantum yield measurement

To evaluate the possibility of a radical chain mechanism, the quantum yield of the reaction **1a** + **4a** \rightarrow **5a** was determined. Photo flux of the spectrophotometer was measured by standard ferrioxalate actinometry.¹⁹ A 150 W xenon lamp (50% of light intensity, 420 ± 5 nm bandpass filter) was used as the light source. As a result, a quantum yield of 0.1 was obtained. However, the photoredox catalyst [Ru] absorbs only a fraction of the overall light at 420 nm due to the competitive light absorption from the present rhodium bound enolate intermediates (inner filter effect, see **Figure 38**). Thus, this value represents an overall quantum yield and does not take into account that there is no chain process in this system. Nevertheless, considering competing light absorption, quenching effects, and other deactivation pathways, the contribution of a chain process is likely.

8) Mechanistic picture

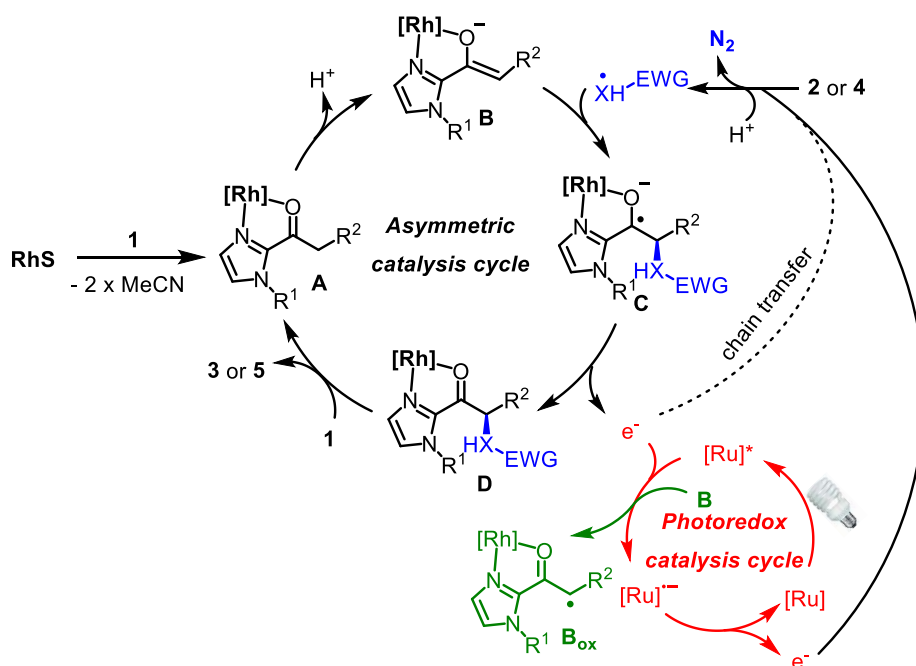


Figure 42. Proposed mechanism of dual-catalyst enabled α -functionalization.

Based on the above results, a mechanism consisting of the cooperation between a photoredox and an asymmetric catalysis cycle is given in **Figure 42**. Substrate coordination to **RhS** (intermediate **A**) and base-induced deprotonation generates the electron-rich rhodium enolate **B**, which initially serves

as the single electron donor for photoexcited $[\text{Ru}]^*$ ($\mathbf{B} \rightarrow \mathbf{B}_{\text{ox}} + e^-$), thereby generating strongly reducing $[\text{Ru}]^-$ which in turn transfers a single electron to the organic azide or diazo substrate. Sequential N_2 extrusion and protonation produces nitrogen- or carbon-centered radicals, respectively. The subsequent stereoselective addition of these electron-deficient radicals to the electron-rich double bond of the rhodium enolate \mathbf{B} constitutes the chirality generating step and provides the Rh-coordinated ketyl radical \mathbf{C} . The ketyl \mathbf{C} is a strong reducing agent and either directly reduces the azide/diazo reagent to afford chain propagation or quenches photoexcited $[\text{Ru}]^*$ to produce the reduced species $[\text{Ru}]^-$. The oxidation of ketyl \mathbf{C} leads to Rh-coordinated product (intermediate \mathbf{D}), which after product release and re-coordination of new substrate engages in a new catalytic cycle.

9) Origins of asymmetric induction: computational and experimental studies

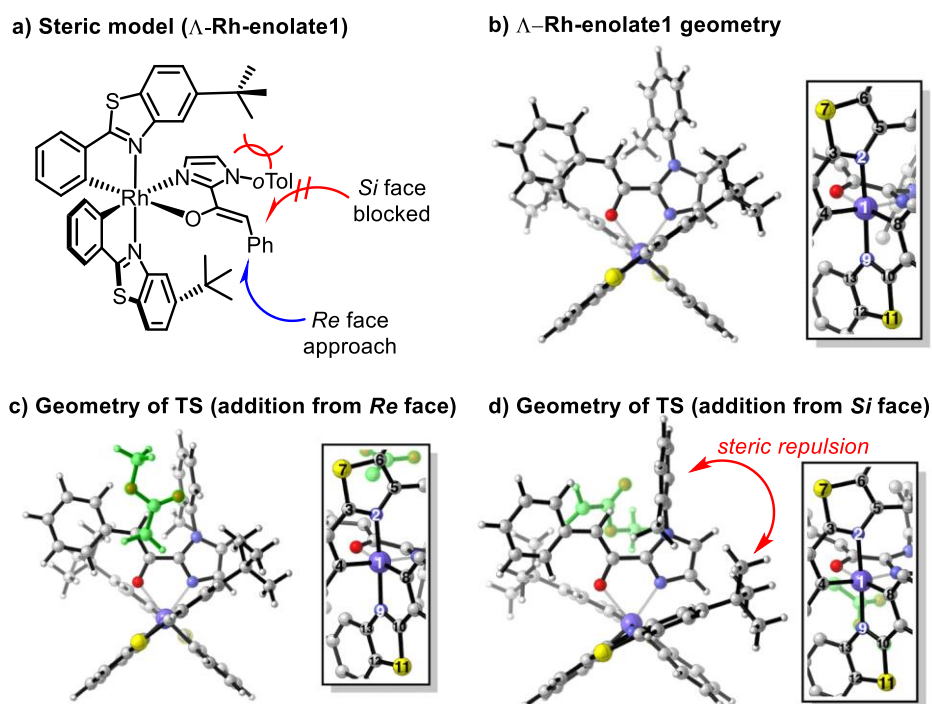


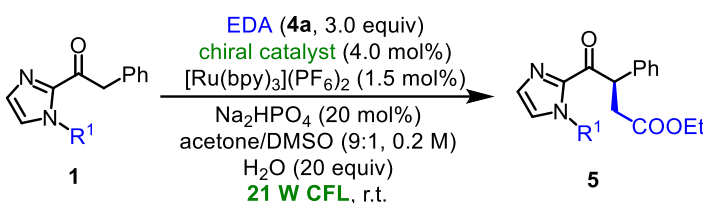
Figure 43. Steric model for the reaction and geometries of Λ -Rh-enolate1 and transition states (picture from ACS publications²⁰).

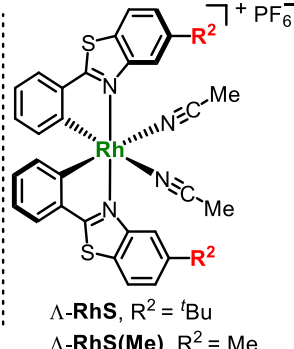
The *tert*-butyl groups in the catalyst and *N*-substituent of imidazoles play a vital role for the asymmetric induction. The enantiodetermining step of the current reaction is the radical addition to rhodium bound enolate intermediate. As observed from the crystal structure of the key Rh-enolate

species, the prochiral sp² enolate carbon is sterically shielded from one side by the *tert*-butyl group of the benzothiazole ligand (**Figure 43a**). Since the catalyst is C₂ symmetric, only the *Si* face (or *Re* face) is selectively blocked by the Λ -RhS (or Δ -RhS). This steric model can reasonably explain the asymmetric induction obtained and is in perfect agreement with the stereochemistry of products.

Indeed, a computational study by Dr. Shuming Chen and Prof. K. N. Houk supports this model.²⁰ They demonstrated that distortion of the rhodium bound enolate and benzothiazole ligand framework is the dominating factor in enforcing enantioselectivity (**Figure 43b-d**). In particular, the *N*-substituent of imidazoles contributes to stereodiscrimination by interacting sterically with the *tert*-butyl group. This interaction induces more severe distortion of the benzothiazole ligands when the radical adds to the unfavorable face (*Si* face for a Λ -catalyst, **Figure 43d**). These calculations well account for the observation that higher enantioselectivities are obtained when using *N*-*o*-tolyl substituted imidazoles as substrates (For example, see entries 4,5 in **Table 5**).

Table 7. Effect of imidazole *N*-substituents and steric groups on catalyst.^[a]





Λ -RhS, R² = *t*Bu
 Λ -RhS(Me), R² = Me

Entry	R ¹	R ²	Experimental ee	Calculated $\Delta\Delta G^\ddagger$ ^[b]
1	Me (1r)	<i>t</i> Bu	5ra , 87%	3.1
2	<i>i</i> Pr (1s)	<i>t</i> Bu	5sa , 89%	2.8
3	Ph (1a)	<i>t</i> Bu	5aa , 92%	2.9
4	<i>o</i> Tol (1b)	<i>t</i> Bu	5ba , 97%	5.6
5	Ph (1a)	Me	5aa , 88%	1.0 (68% ee) ^[c]

[a] Reaction conditions: see **Table 5** entry 4. [b] values are denoted in kcal/mol calculated by Shuming. [c] The computed 1.0 kcal/mol $\Delta\Delta G^\ddagger$ predicts 68% ee.

To further study the effect of catalyst and imidazole *N*-substituent, Shuming Chen calculated a series of transition state structures and energies for the additions of carbon centered radical to rhodium bound enolates. And the author of this thesis tested a set of 2-acyl imidazoles with different *N*-substituent, synthesized a new chiral-at-metal rhodium catalyst Λ -**RhS(Me)** bearing methyl groups on the cyclometalating ligands, and examined its reactivity. As summarized in **Table 7**, with the enlargement of the imidazole *N*-substituent from methyl to *o*-tolyl, the experimental ee values increase regularly from 87% ee to 97% ee (entries 1-4). *N*-*o*-Tolyl substituted substrate provided by far the greatest $\Delta\Delta G^\ddagger$ (5.6 kcal/mol) in good consistency with the experimental results (entry 4). Besides, the catalyst Λ -**RhS(Me)** yielded the product **5aa** in 88% ee which is somehow higher than the calculated prediction (68% ee, entry 5).

10) Discussion of other pathways

There are two other possible pathways needed to be discussed. First is the cross coupling of rhodium bound α -carbonyl carbon centered radicals (**B_{ox}** in **Figure 42**) with amino/ α -ester carbon radicals. Only the initial quenching cycles generate **B_{ox}**. After initiation, the ketyl radical intermediate (**C**, **Figure 42**) or a chain process can enable the follow-up SET events generating amino/ α -ester carbon radicals but without the generation of **B_{ox}** intermediate. Considering that the concentration of [Ru] is quite low, the amount of **B_{ox}** should be much lower than the ground state Rh bound enolate intermediate (**B**, **Figure 42**). Once the amino/ α -ester carbon radicals form, they will not recombine with intermediate **B_{ox}**, but rather add to intermediate **B**. In addition, amino/ α -ester carbon radicals are electrophilic and therefore prone to react with electron rich enolate **B** instead of electron deficient α -carbonyl radical **B_{ox}**. Overall, the radical-radical recombination pathway is very unlikely.

The second possible pathway constitutes the addition of radical intermediate **B_{ox}** to triplet carbenes/nitrenes, which is similar to the mechanism proposed by Gryko *et al.* for the related racemic α -alkylation of carbonyls catalyzed by a secondary amine in combination with a [Ru(bpy)₃](PF₆)₂ or a porphyrin photocatalyst.^{16,21} As displayed in **Figure 44**, they proposed that oxidation of enamine by the excited photocatalyst generates a radical cation intermediate, which could react with EDA or the EDA derived triplet carbene, following electron transfer and substrate/product exchange form the final product. But this is apparently not the case under the presented reaction conditions, considering 1) that the α -ester carbon radical generated from EDA is trapped by control experiments (**Figure 36d**) as well

as EPR experiments (**Figure 37**); 2) that cyclopropanation/aziridination products have never been observed either under the conditions with additional alkenes (**Figure 36d,e**) or in the reactions that start with substrates containing C=C double bonds (**Figure 33**); 3) as discussed above, the concentration of intermediate **B_{ox}** is much lower compared with rhodium bound enolate in the current catalytic system; 4) more importantly, the acceptor-substituted nitrenes and α -ester triplet carbenes¹⁷ are electrophilic and known to react with electron rich alkenes.¹⁷ In stark contrast, the coupling of these electrophilic species with another electron deficient radical (in this case, intermediate **B_{ox}**) is unreasonable.

In summary, the mechanism described in **Figure 42** is reliable and in good accord with all experimental and computational results.

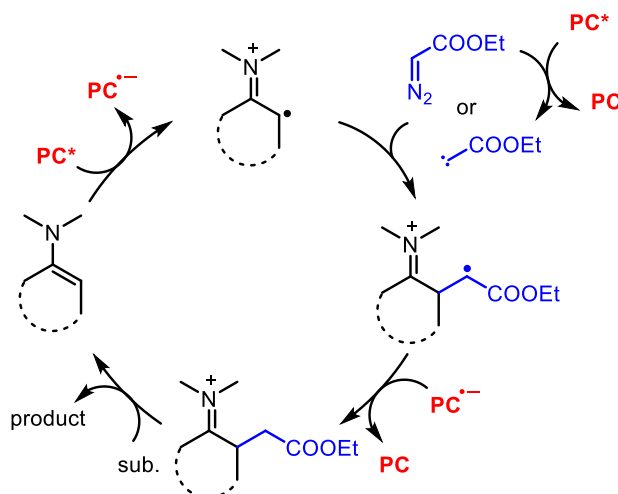


Figure 44. A radical addition to carbene mechanism proposed by Gryko *et al.*

3.1.6 Conclusions

This chapter demonstrated that acceptor-substituted aryl azides and α -diazo carboxylic esters are suitable reagents for generating intermediate radicals for asymmetric photoredox reactions.²² These were exploited for the efficient visible-light-activated enantioselective α -alkylation and amination of 2-acyl imidazoles using a combination of a chiral rhodium-based Lewis acid catalyst and a photoredox catalyst. Yields of up to 99% and enantioselectivities of up to >99% ee were achieved. Molecular nitrogen as the sole by-product, redox and proton neutral reaction conditions, as well as a broad compatibility with other functional groups render this transformation attractive. Detailed mechanistic

investigations suggest that an intermediate rhodium enolate complex acts as a reductive quencher to initiate a radical process with the aryl azides and α -diazo carboxylic esters serving as precursors for nitrogen and carbon-centered radicals, respectively. In collaboration with the Houk group, a computational study revealed the origins of the asymmetric induction, which provides new insights and directions for catalyst modifications and condition optimizations. Mechanism-inspired new reaction development is presented in the following chapters.

Reference

- 1 A. K. Mailyan, J. A. Eickhoff, A. S. Minakova, Z. Gu, P. Lu, A. Zakarian, *Chem. Rev.* **2016**, *116*, 4441-4557.
- 2 For a comprehensive review on photoinduced electron transfer in organic synthesis, see: G. Pandey, *Top. Curr. Chem.* **1993**, *168*, 175-221.
- 3 For a review on the catalysis of radical reactions, see: A. Studer, D. P. Curran, *Angew. Chem. Int. Ed.* **2015**, *55*, 58-102.
- 4 For reviews on catalytic asymmetric photoreactions, see: a) R. Brimioulle, D. Lenhart, M. M. Maturi, T. Bach, *Angew. Chem. Int. Ed.* **2015**, *54*, 3872-3890; b) E. Meggers, *Chem. Commun.* **2015**, *51*, 3290-3301; c) C. Wang, Z. Lu, *Org. Chem. Front.* **2015**, *2*, 179-190; d) A. F. Garrido-Castro, M. C. Maestro, J. Alemán, *Tetrahedron Lett.* **2018**, *59*, 1286-1294.
- 5 G. Cecere, C. M. König, J. L. Allewa, D. W. C. MacMillan, *J. Am. Chem. Soc.* **2013**, *135*, 11521-11524.
- 6 X. Shen, K. Harms, M. Marsch, E. Meggers, *Chem. Eur. J.* **2016**, *22*, 9102-9105.
- 7 S. Bräse, C. Gil, K. Knepper, V. Zimmermann, *Angew. Chem. Int. Ed.* **2005**, *44*, 5188-5240.
- 8 Y. Chen, A. S. Kamlet, J. B. Steinman, D. R. Liu, *Nat. Chem.* **2011**, *3*, 146-153.
- 9 L. Zhang, E. Meggers, *Acc. Chem. Res.* **2017**, *50*, 320-330.
- 10 S. O. Scholz, E. P. Farney, S. Kim, D. M. Bates, T. P. Yoon, *Angew. Chem. Int. Ed.* **2016**, *55*, 2239-2242.
- 11 H. Huo, X. Huang, X. Shen, K. Harms, E. Meggers, *Synlett* **2016**, *27*, 749-753. This work is accomplished by Haohua Huo and the author of this thesis. For more details, see Haohua Huo's

PhD thesis.

- 12 a) C. Wang, Y. Zheng, H. Huo, P. Röse, L. Zhang, K. Harms, G. Hilt, E. Meggers, *Chem. Eur. J.* **2015**, *21*, 7355-7359; b) H. Huo, K. Harms, E. Meggers, *J. Am. Chem. Soc.* **2016**, *138*, 6936-6939.
- 13 C. Wang, L.-A. Chen, H. Huo, X. Shen, K. Harms, L. Gong, E. Meggers, *Chem. Sci.* **2015**, *6*, 1094-1100.
- 14 J. Ma, X. Shen, K. Harms, E. Meggers, *Dalton Trans.* **2016**, *45*, 8320-8323.
- 15 For selected examples, see: a) D. A. Nicewicz, D. W. C. MacMillan, *Science* **2008**, *322*, 77-80; b) M. Neumann, S. Földner, B. König, K. Zeitler, *Angew. Chem. Int. Ed.* **2011**, *50*, 951-954; c) E. Arceo, I. D. Jurberg, A. Álvarez-Fernández, P. Melchiorre, *Nat. Chem.* **2013**, *5*, 750-756; d) H. Huo, X. Shen, C. Wang, L. Zhang, P. Röse, L.-A. Chen, K. Harms, M. Marsch, G. Hilt, E. Meggers, *Nature* **2014**, *515*, 100-103.
- 16 K. Rybicka-Jasińska, Ł. W. Ciszewski, D. Gryko, *Adv. Synth. Catal.* **2016**, *358*, 1671-1678.
- 17 S. O. Scholz, E. P. Farney, S. Kim, D. M. Bates, T. P. Yoon, *Angew. Chem. Int. Ed.* **2016**, *55*, 2239-2242.
- 18 L. Julià M. P. Bosch, S. Rodriguez, A. Guerrero, *J. Org. Chem.* **2000**, *65*, 5098-5103.
- 19 M. A. Cismesia, T. P. Yoon, *Chem. Sci.* **2015**, *6*, 5426-5434.
- 20 S. Chen, X. Huang, E. Meggers, K. N. Houk, *J. Am. Chem. Soc.* **2017**, *139*, 17902-17907.
- 21 a) K. Rybicka-Jasińska, W. Shan, K. Zawada, K. M. Kadish, D. Gryko, *J. Am. Chem. Soc.* **2016**, *138*, 15451-15458; b) K. Rybicka-Jasińska, K. Orłowska, M. Karczewski, K. Zawada, D. Gryko, *Eur. J. Org. Chem.* **2018**, *47*, 6634-6642.
- 22 X. Huang, R. D. Webster, K. Harms, E. Meggers, *J. Am. Chem. Soc.* **2016**, *138*, 12636-12642.

3.2 Combining the Catalytic Enantioselective Reaction of Visible-Light-Generated Radicals with a By-Product Utilization System

3.2.1 Research Background and Reaction Design

The recently by the Meggers group introduced bis-cyclometalated chiral-at-metal iridium- or rhodium-based Lewis acids (LA) can activate a variety of substrates through two-point binding towards many novel reactions (**Figure 45a**).¹ Upon coordination with the chiral LA and deprotonation, α -mono-substituted carbonyls with a suitable auxiliary, such as 2-imidazolyl, *N*-pyrazolyl, or 2-pyridinyl, will form the LA bound enolates that are highly nucleophilic and have been demonstrated to undergo a series of electrophilic additions (optionally radical addition) in a highly enantioselective fashion. For example, chapter 3.1 of this thesis showcases the reactivity of the chiral-at-rhodium complex, which in combination with a photoredox catalyst, enabling asymmetric α -amination and α -alkylation of 2-acyl imidazoles. In this case, the rhodium bound enolate not only serves as radical acceptor but also facilitates the initial reductive quenching of photoredox catalysis (**Figure 45a**, left).

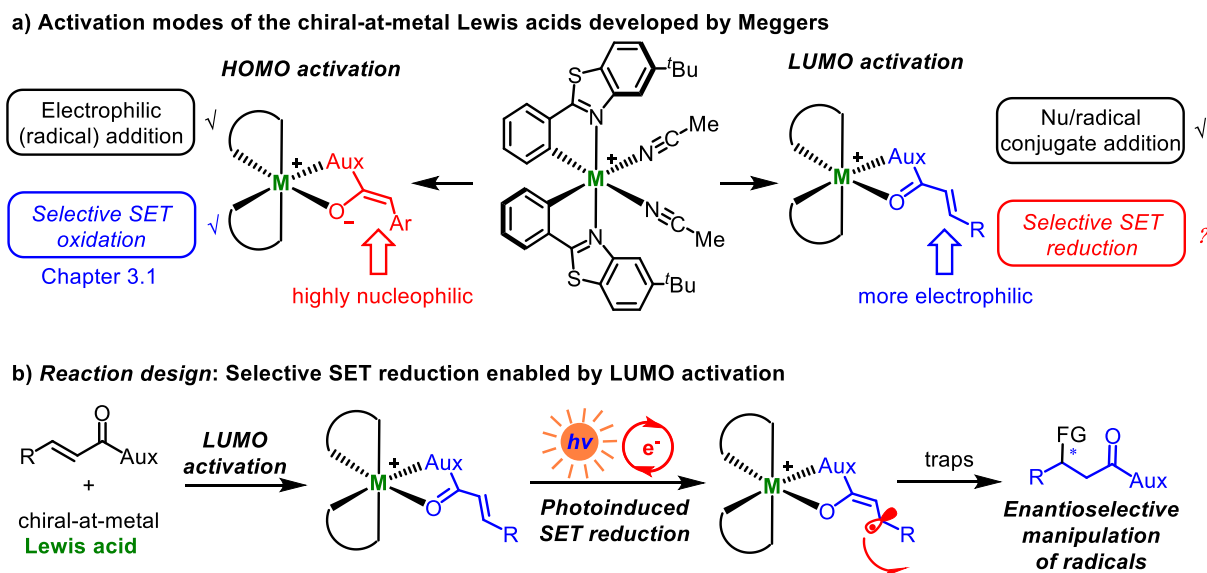


Figure 45. Reaction design to expand the reactivity of the Meggers catalysts by trapping the β -enolate radical.

On the other hand, LUMO activation of α,β -unsaturated carbonyls by the chiral-at-metal complexes have also been well investigated (**Figure 45a**, right). The β -positions of carbonyl compounds become more electrophilic after coordination, thus enabling highly stereoselective

conjugate additions of nucleophiles or nucleophilic radicals. In these cases, the prochiral carbon centers are in the neutral ground states during the key stereodetermining steps. However, the selective SET reduction of LA bound α,β -unsaturated substrates and following manipulation of the rhodium bound radicals remains elusive. The author of this thesis envisioned that the merger of LUMO activation by chiral-at-metal catalysts with photoinduced mild SET reduction might offer new opportunities for the enantioselective transformations of prochiral radicals, which would pave paths to new chemistry and expand the reactivity of the Meggers catalysts (**Figure 45b**).

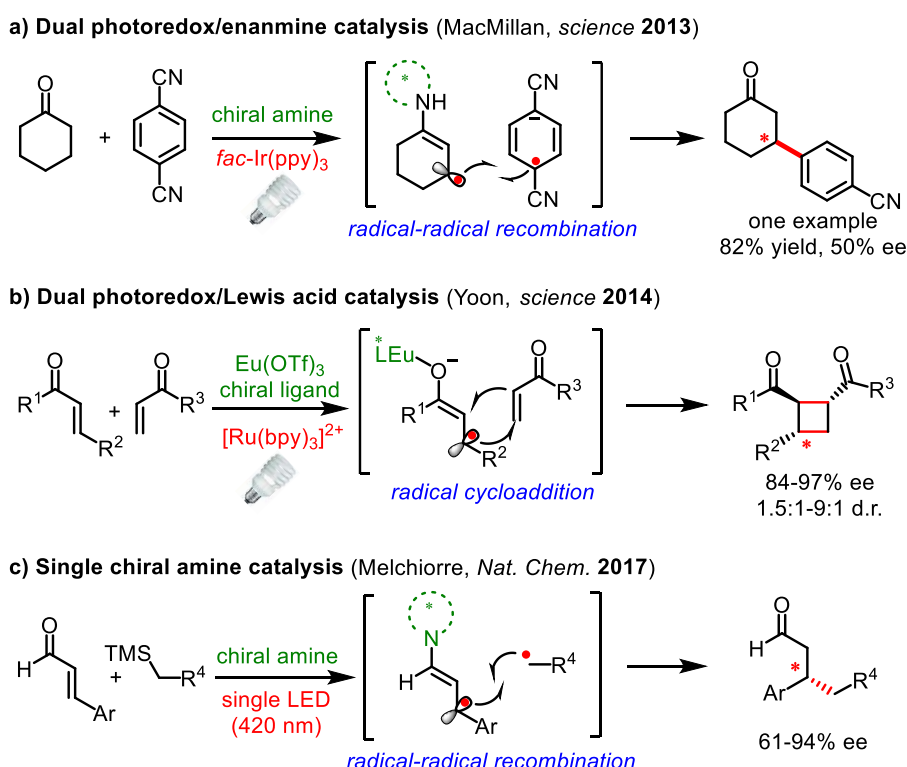


Figure 46. Previous reports on visible-light-activated asymmetric transformations with allylic C(sp²) radical intermediates.

The conversion of prochiral carbon-centered radicals into stereocenters in a catalytic and enantioselective fashion is extremely challenging owing to the inherent high reactivity and conformational flexibility of such radical species.² Over the past few years, photoinduced electron transfer (PET) has emerged as a powerful tool to access radical species in a mild and economic way,³ thus spurring the discovery of novel asymmetric catalytic systems involving radical processes.⁴ However, catalytic asymmetric PET-processes developed to date mainly deal with achiral radicals reacting with a prochiral C(sp²)-center bound to a chiral catalyst. In contrast, strategies for the direct

stereocontrol of photo-generated carbon radical centers are underdeveloped.⁵ In this respect, some elegant protocols have been disclosed in enantioselective transformations of photo-generated allylic carbon radicals. In 2013, MacMillan and co-workers introduced a radical-radical recombination process by combination of a chiral amine and photoredox catalyst in which only one example with moderate enantioselectivity was reported showing the challenge of stereocontrol over such radical intermediates (**Figure 46a**).⁶ After that, Yoon and co-workers described a dual Lewis acid and photoredox catalysis for the enantioselective radical [2+2] cycloadditions (**Figure 46b**).⁷ Later, Melchiorre and co-workers reported that a single chiral iminium ion enabled the enantioselective coupling of β -enaminyll radicals with alkyl radicals (**Figure 46c**).⁸ Despite these significant processes, novel transformations with new mechanisms are still highly desirable.

This chapter demonstrates that a rhodium-based Lewis acid bearing exclusive metal-centered chirality can effectively control the stereochemistry of visible-light-generated prochiral radicals for the asymmetric radical allylation reaction with allyl sulfones as radical traps. Notably, the leaving sulfonyl radicals can be utilized providing enantioenhanced β -sulfonyl carbonyl compounds, thus minimizing waste generation.

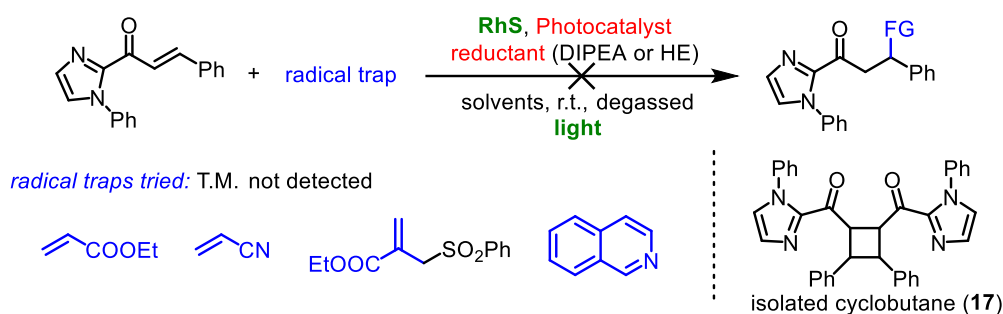
3.2.2 Reaction Development

To begin with, the bis-cyclometalated rhodium based complex **RhS** was chosen as Lewis acid considering its superior kinetic properties together with *fac*-Ir(ppy)₃ as photoredox catalyst and DIPEA or Hantzsch ester (**HE**) as reducing agent (**Figure 47**). Since the rhodium bound allylic radical is considered as an electron rich radical, Michael acceptors, allyl sulfone, and isoquinoline were selected as radical traps. However, when an α,β -unsaturated 2-acyl imidazole was employed as substrate, the desired molecule could never be detected (**Figure 47a**). Interestingly, the [2+2] homo-coupling product, a cyclobutane **17**, was isolated in some cases, which was a key inspiration for the development of the previous elusive excited state chemistry described in the following chapters.

Then, an α,β -unsaturated *N*-acyl pyrazole was used as model substrate (**Figure 47b**). A lot of radical acceptors were tested, including acrylonitrile, benzophenone, isoquinoline, DEAD, a silyl acrylate, and tosyl azides, but all failed to give the target product. Finally, a sulfonyl reagent, namely ethyl 2-((phenylsulfonyl)methyl)acrylate, gave the desired β -allylation product in 92% yield with

moderate ee of 78%, together with the formation of the C-S formation product in around 80% yield with 80% ee. This unexpected but unavoidable product is assumed to form via the conjugate addition of leaving sulfonyl radical to the rhodium bound substrate. Notably, the additional photoredox catalyst *fac*-Ir(ppy)₃ was found to be not essential which is ascribed to the ability of Hantzsch ester serving as photoredox mediator for the generation of radical species under mild conditions.⁹

a) Initial attempts with β -aryl acyl imidazole



b) Initial attempts with β -methyl *N*-acyl pyrazole

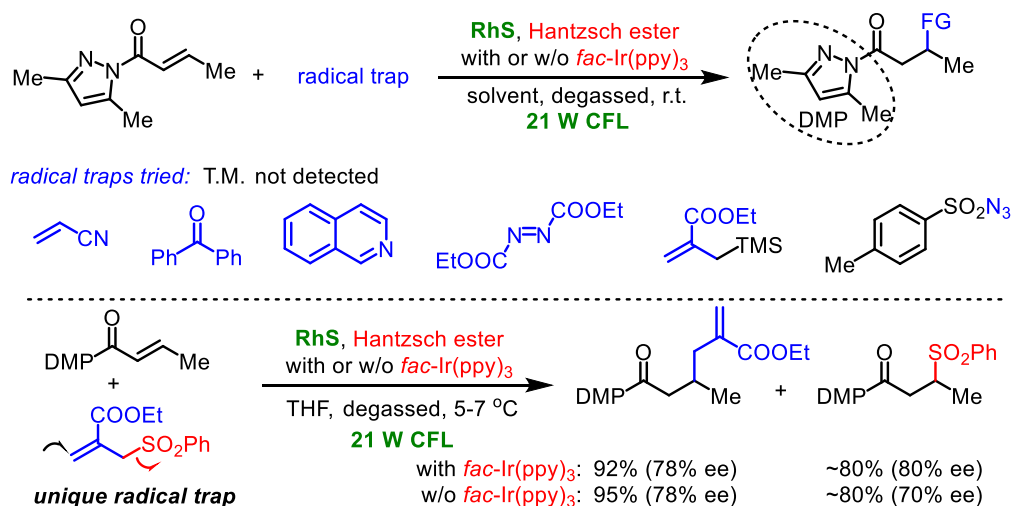


Figure 47. Initial attempts to trap the rhodium bound β -enolate radical intermediates.

These results imply that the rhodium bound allylic radical species is relatively unreactive and if the follow-up chemistry is not efficient enough, the back electron transfer toward the rhodium bound substrate could be dominated. When the sulfone reagent was used, the radical trapping and especially the subsequent fragmentation process shifted the equilibrium of electron transfer toward the desired product generation. And the formation of β -sulfonyl carbonyls is beneficial for shifting the equilibrium of a potentially reversible radical fragmentation. Furthermore, the utilization of the leaving sulfonyl radicals providing β -sulfonyl carbonyl compounds is also very attractive from the perspective of green

and sustainable chemistry, which is without precedence in the chemistry of these well-developed sulfone-based radical trapping reagents.¹⁰ Therefore, the author of this thesis decided to optimize this unusual transformation with both two products.

The cyano substituted allyl sulfone **19a** was chosen as the model radical trap for the further optimization considering the better nucleophilicity of **19a** compared with the ester analogue. Indeed, the rhodium catalyst Δ -**RhS** enabled the reaction affording the expected allylation product **20a** and C-S formation product **21a** in excellent yields with moderate enantioselectivities (Table 8, entry 2). Interestingly, the related Δ -**RhO** provided **20a** with much higher ee (96% ee, entry 3) indicating the mechanism differs from the previous reports¹¹ on Giese-type radical reactions in which **RhS** featuring a higher steric congestion, worked better than **RhO**. Inspired by the resolution method of **RhS** developed by Jiajia Ma,¹² the resolution process of **RhO** was modified by using a fluorinated chiral auxiliary, namely (*R*)-3-fluoro-2-(4-phenyl-4,5-dihydrooxazol-2-yl)phenol, instead of the chiral proline that was originally exploited by Chuanyong Wang.¹³ Both of the corresponding fluorinated auxiliary coordinated rhodium complexes are stable and can be separated by flash chromatography, thus improving the atom economy of catalyst synthesis (see experimental part).

Other types of Lewis acids were investigated as well. The well-established iridium catalyst Δ -**IrS** could not give any detectable product (entry 1). Besides, the chiral rhodium complex Δ -**RhPP** recently developed by Yu Zheng,¹⁴ which contains pinene-derived cyclometalating ligands and is supposed to be sterically more demanding, gave modest yields for both products but with low enantioselectivities (entry 4). Other none-chiral Lewis acid such as Sc(OTf)₃ gave very low efficiency while LiBF₄ could even not catalyze the process (entries 5,6) and no conversion was observed without Lewis acid (entry 7). Overall, the Meggers' chiral-at-rhodium complexes show a unique reactivity for this reaction.

HE with different substituents at 2- or 3-position also worked very well (entries 8,9) while 4-methyl substituted **HE-4**, which is a white solid, failed to facilitate the reaction. And DIPEA could not accomplish the transformation (entry 11). To be mentioned, all reactions were performed under N₂ atmosphere with regular Schlenk technique instead of the tedious freeze-pump-thaw degassing cycles, because the trace amount of dioxygen dissolved in the solvent could be consumed by the highly reducing Hantzsch ester. All these aspects highlight the multiple functions of **HE** in the current system acting as photoredox mediator as well as electron donor and proton source.⁹

Table 8. Effect of Lewis acid catalyst and Hantzsch ester on the β -functionalization.^[a]

<div style="display: flex; justify-content: space-around; align-items: flex-start;"> <div style="text-align: center;"> <p>$\Delta\text{-IrS}$, M = Ir, X = S $\Delta\text{-RhS}$, M = Rh, X = S $\Delta\text{-RhO}$, M = Rh, X = O</p> </div> <div style="text-align: center;"> <p>$\Delta\text{-RhPP}$</p> </div> <div style="text-align: center;"> <p>HE-1, R¹ = Et, R² = Et, R³ = H HE-2, R¹ = Me, R² = Et, R³ = H HE-3, R¹ = Me, R² = <i>t</i>Bu, R³ = H HE-4, R¹ = Me, R² = Et, R³ = Me</p> </div> </div>				
Entry	Lewis acid	Hantzsch ester	20a , Yield (ee)	21a , Yield (ee)
1	$\Delta\text{-IrS}$	HE-1	<5%	<5%
2	$\Delta\text{-RhS}$	HE-1	92% (83% ee)	95% (84% ee)
3	$\Delta\text{-RhO}$	HE-1	85% (96% ee)	92% (85% ee)
4	$\Delta\text{-RhPP}$	HE-1	74% (40% ee)	77% (10% ee)
5 ^[b]	Sc(OTf) ₃	HE-1	10%	10%
6 ^[c]	LiBF ₄	HE-1	0%	0%
7	None	HE-1	0%	0%
8	$\Delta\text{-RhO}$	HE-2	78% (96% ee)	82% (80% ee)
9	$\Delta\text{-RhO}$	HE-3	80% (94% ee)	85% (85% ee)
10	$\Delta\text{-RhO}$	HE-4	0%	85%
11 ^[d]	$\Delta\text{-RhO}$	None	0%	0%

[a] Reaction conditions: **18a** (0.20 mmol), **19a** (0.10 mmol), Lewis acid (8.0 mol%) and **HE** (0.15 mmol) in 1,4-dioxane (0.1 M) were stirred at room temperature for 24 h with a 21 W CFL; isolated yield; ee was determined by HPLC on a chiral stationary phase. [b] 20 mol% of Sc(OTf)₃. [c] 200 mol% of LiBF₄. [d] 0.15 mmol DIPEA was added.

Next, the effect of solvent was investigated (**Table 9**). Increasing the temperature to 35 °C could accelerate the reaction without significant erosion on yields or enantioselectivities (entries 1,2). Acetone gave a little worse ee for the product **20a** while similar results could be obtained by using solvents like CH₂Cl₂ or THF (entries 3-5). Notably, the undesired hydrogenation of **1a** is negligible. Specifically, in the reaction using CH₂Cl₂ as solvent, 1-(3,5-dimethyl-1*H*-pyrazol-1-yl)butan-1-one could only be isolated in less than 5% yield (entry 4).

Table 9. Effect of solvent and light source on the β -functionalization.^[a]

	18a , 0.1 mmol	19a , 0.05 mmol	Δ - RhO (8.0 mol%) HE-1 (1.5 equiv) solvent (0.1 M) temp., N ₂ , light	20a	21a
Entry	Solvent	Temp.	Light	20a , Yield (ee)	21a , Yield (ee)
1	1,4-Dioxane	r.t.	21 W CFL	85% (96% ee)	92% (85% ee)
2	1,4-Dioxane	35 °C	21 W CFL	82% (95% ee)	90% (86% ee)
3	Acetone	35 °C	21 W CFL	81% (89% ee)	85% (87% ee)
4 ^[b]	CH ₂ Cl ₂	35 °C	21 W CFL	81% (92% ee)	86% (87% ee)
5	THF	35 °C	21 W CFL	82% (94% ee)	90% (86% ee)
6	1,4-Dioxane	r.t.	24 W Blue LEDs	77% (92% ee)	80% (80% ee)
7	1,4-Dioxane	r.t.	Under dark	0%	0%

[a] Reaction conditions: **18a** (0.10 mmol), **19a** (0.05 mmol), Δ -**RhO** (8.0 mol%) and **HE-1** (0.075 mmol) in solvent (0.1 M) were stirred at room temperature for 24 h or 35 °C for 15 h with a 21 W CFL; isolated yield; ee was determined by HPLC on a chiral stationary phase. [b] 1-(3,5-Dimethyl-1*H*-pyrazol-1-yl)butan-1-one was detected in less than 5% yield.

Furthermore, illumination with blue LEDs, which do not emit any UV light, provided comparable results (entry 6). Together with the control experiments under dark (entry 7), this confirms that the reaction is activated by visible light.

In summary, a mild and selective reduction system, which consists of the chiral-at-rhodium complex **RhO** and the readily available Hantzsch ester as photoredox mediator and reductant, was established for the stereocontrolled chemistry of visible-light-generated radicals and at the same time for the enantioselective sulfonyl radical conjugate addition (**Table 8**, entry 3).

3.2.3 Substrate Scope and Conversions of Products

With the optimized conditions in hand, the substrate scope with respect to radical acceptors was investigated (**Table 10**). A wide range of allyl sulfones **19** with different leaving groups worked well delivering radical allylation product **20a** in good yields and excellent ee (up to 97% ee) along with the recycled C-S formation products **21a-h** in good yields and acceptable ee (up to 89% ee) (entries 1-8). Electronic property of the substituent on the sulfonyl moiety has little influence on the reaction

efficiency, while a bulky mesityl sulfonyl trap gave the best ee for the sulfonyl radical addition product **21f**, albeit in lower conversion (entry 6). As expected, lower yields and slightly lower ee were observed for radical functionalization product **20b** when allyl sulfone bearing a less electron deficient ester group was employed (compare entries 9 with 1). It is noteworthy that functional groups including a C≡C triple bond, a C=C double bond and an imide are well tolerated under these mild conditions (entries 11-13).

Table 10. Substrate scope of the β -functionalization with respect to allyl sulfones.^[a]

$\Delta\text{-RhO}$ (8.0 mol%), HE-1 (1.5 equiv), 1,4-dioxane (0.1 M), r.t., N_2 , 21 W CFL

Entry	EWG	R	20 , Yield (ee)	21 , Yield (ee)
1	CN	C ₆ H ₅	20a , 85% (96% ee)	21a , 92% (85% ee)
2	CN	4-MeC ₆ H ₄	20a , 68% (96% ee)	21b , 70% (79% ee)
3	CN	4-BrC ₆ H ₄	20a , 81% (97% ee)	21c , 88% (80% ee)
4	CN	4-CF ₃ C ₆ H ₄	20a , 78% (95% ee)	21d , 78% (76% ee)
5	CN	2-MeC ₆ H ₄	20a , 71% (95% ee)	21e , 72% (86% ee)
6 ^[b]	CN	2,4,6-Me ₃ C ₆ H ₂	20a , 57% (94% ee)	21f , 60% (89% ee)
7 ^[b]	CN	2-Naphthyl	20a , 82% (94% ee)	21g , 88% (83% ee)
8 ^[b]	CN	1-Naphthyl	20a , 78% (91% ee)	21h , 84% (80% ee)
9	COOEt	C ₆ H ₅	20b , 65% (94% ee)	21a , 68% (84% ee)
10 ^[b]	COOEt	4-MeOC ₆ H ₄	20b , 65% (92% ee)	21i , 63% (81% ee)
11 ^[b]		C ₆ H ₅	20c , 60% (92% ee)	21a , 69% (82% ee)
12 ^[b]		C ₆ H ₅	20d , 62% (92% ee)	21a , 72% (83% ee)
13 ^[b]		C ₆ H ₅	20e , 73% (92% ee)	21a , 78% (82% ee)
14	CN	CF ₃	20a , <5%	<5%
15	CN	1- ⁿ Hex	20a , <5%	<5%

[a] Reaction conditions: see **Table 8** entry 3; isolated yield; ee was determined by HPLC on a chiral stationary phase. [b] 35 °C.

N-acyl pyrazoles are recognized as a useful and reactive synthetic building block. Indeed, enantioenriched β -functionalized *N*-acyl pyrazoles obtained by this newly-developed protocol, could be easily converted into other none-racemic chiral compounds, such as an alcohol **24** (Figure 49a) or an amide **25** (Figure 49b), the latter of which could give single crystals for the determination of the absolute structure of product.

3.2.4 Robustness Screening

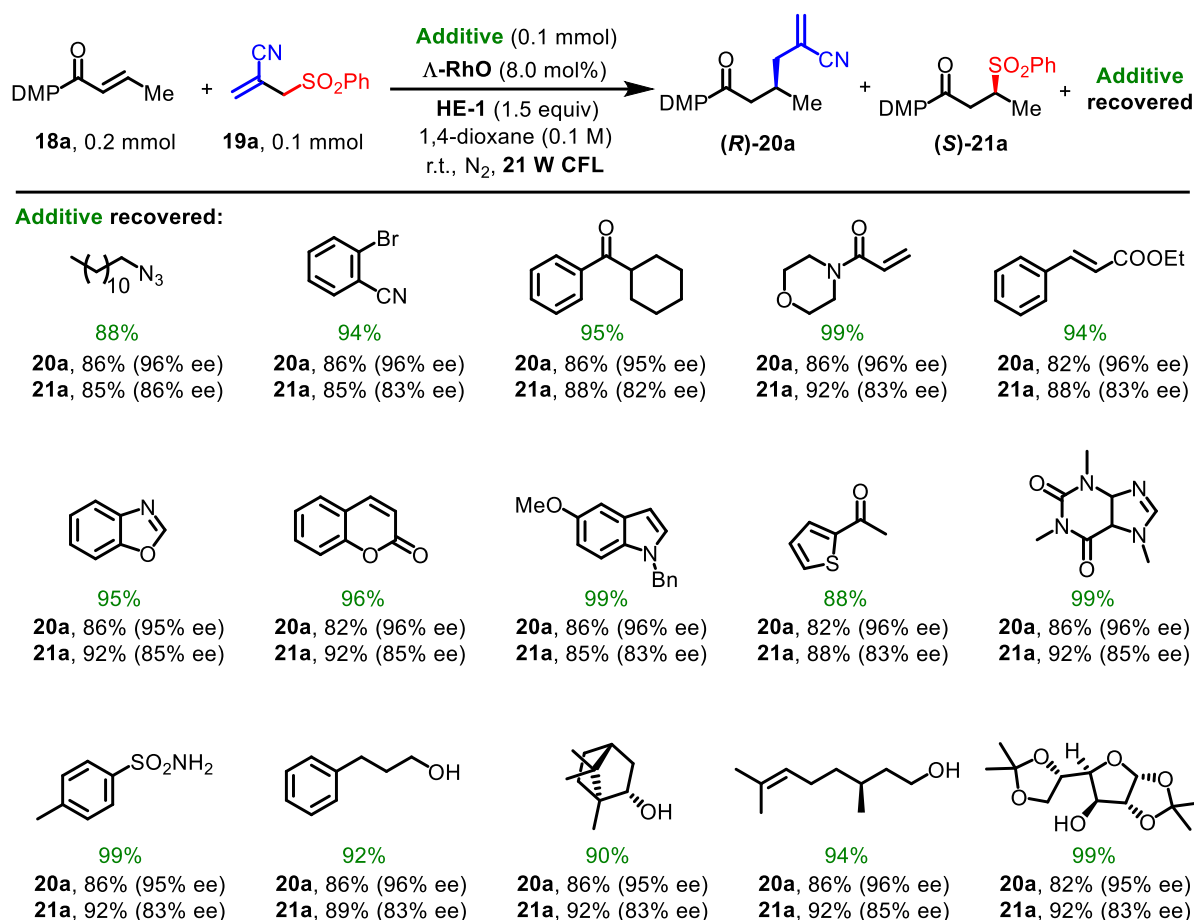


Figure 50. Robustness screening in the presence of additives. Isolated yields.

To further evaluate the functional group tolerance and robustness of this catalytic system,¹⁵ a series of common chemical functionality was added to the reaction mixture of **18a** + **19a** \rightarrow **20a** + **21a** (Figure 50). Gratifyingly, this net reduction reaction showed high chemoselectivity towards Lewis acid coordinated *N*-acyl pyrazoles, as additives containing azido, cyano, and carbonyl groups that are vulnerable to reductive conditions could be recovered in high yields. Importantly, heterocycles which

Lewis acid forms the LA/substrate complex **A**, which is a much better electron acceptor than free substrate **18**. Therefore, the selective SET reduction of **A** by visible-light-excited **HE** ($[\text{HE}]^*$)⁹ generates the key Rh-coordinated radical intermediate **B**. The trapping of intermediate **B** by an electron-deficient allyl sulfone **19** delivers secondary radical intermediate **C**. The subsequent fragmentation¹⁰ of **C** provides the sulfonyl radical **E** and enolate intermediate **D**, the latter of which yields C-C bond formation product **20** upon protonation. Meanwhile, the sulfonyl radical **E** undergoes a stereocontrolled radical addition¹⁶ to **A** in a reversible fashion and a subsequent HAT followed by ligand exchange provides the C-S bond formation product **21**.

This reaction scheme has five key features. 1) The cheap and readily available Hantzsch ester serves as photoredox mediator as well as electron donor and proton source. 2) LUMO activation of carbonyls by the powerful bis-cyclometalated Lewis acid ensures a highly chemoselective reduction. 3) Metal-centered chirality provides the effective asymmetric induction for the reaction of prochiral radicals. 4) Ally sulfone acts as dual-functional reagent that not only traps the stabilized rhodium bound radical species but also produces enantioenriched β -sulfonyl carbonyl compounds minimizing the waste generation. 5) Overall, it is a rare example in which a single chiral catalyst facilitates two mechanistically distinct processes.

2) Identification of the intermediate rhodium bound substrate

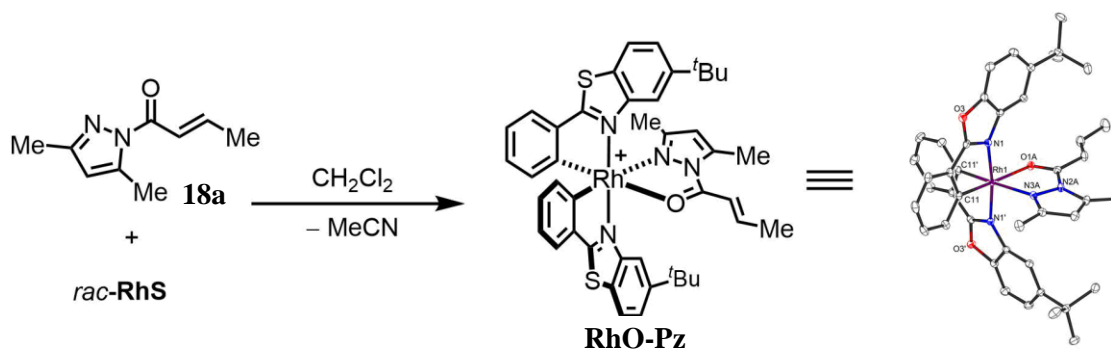


Figure 52. Preparation and identification of the key **RhO-Pz** intermediate. The counter anion (PF_6^-) is omitted.

The key rhodium bound α,β -unsaturated *N*-acyl pyrazole **RhO-Pz** (**Figure 51**, intermediate **A**) could be easily synthesized. The acetonitriles of **RhO** are very labile and could be quickly exchanged by the substrate.¹¹ Accordingly, the mixture of *rac*-**RhO** (83.1 mg, 0.1 mmol) and **18a** (16.4 mg, 0.1

mmol) was dissolved in CH_2Cl_2 (2 mL) in a flask. The solvent was removed by rotary evaporation after stirring for one minute. This dissolution/evaporation cycle was repeated for five times. Then, the resulting solid was recrystallized from $\text{CH}_2\text{Cl}_2/\text{Et}_2\text{O}$ to give pure **RhO-Pz**, which could be characterized by single crystal X-ray diffraction (**Figure 52**).

3) UV/Vis absorption and luminescence spectra

To confirm the role of **HE** as photoactive mediator, UV/Vis absorption spectra of **RhO**, **RhO-Pz** and **HE-1** were measured (**Figure 53**). Upon coordination (**RhO** \rightarrow **RhO-Pz**), the absorption spectrum of the rhodium species barely changed with little shift to the blue region. Although both **HE-1** and **RhO-1a** absorb visible light with wavelength <425 nm, considering the much higher concentration of **HE-1** (at the beginning of the reaction ~ 19 times over $[\text{Rh}]$), it is supposed that **HE** acts a visible light harvesting antenna being consistent with recent reports.⁹ In addition, the emission of **HE-1** was observed with maximum wavelength at 455 nm, while **RhO-Pz** is non-luminescent at room temperature, indicating a much longer life time of the photoexcited **HE**.

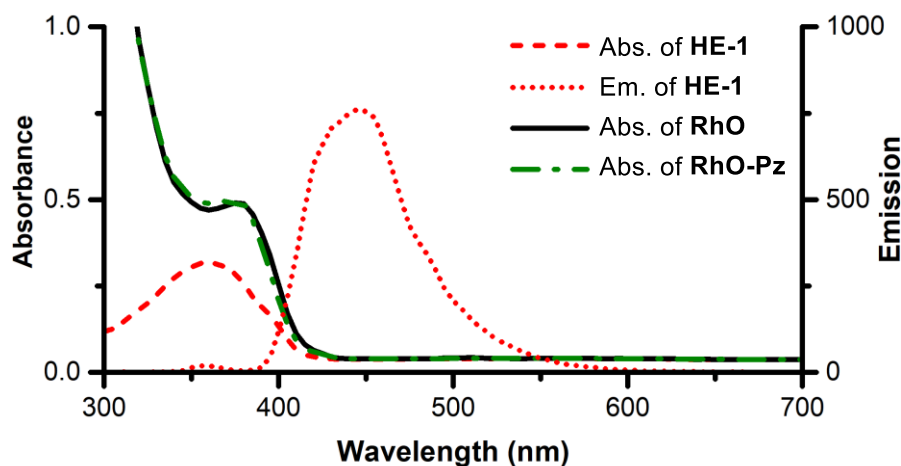


Figure 53. UV/Vis absorption and luminescence spectra measured for the β -functionalization reaction. Concentrations for absorption spectra in 1,4-dioxane: **HE-1** = 0.05 mM, **RhO** = 0.05 mM, **RhO-Pz** = 0.05 mM. Concentration for emission spectrum of **HE-1** in 1,4-dioxane = 0.5 mM.

4) Cyclic Voltammetry

The LUMO activation of α,β -unsaturated *N*-acyl pyrazole by bidentate coordination is supported by the cyclic voltammetry studies. As clearly shown in **Figure 54**, the free substrate **18a** showed one chemically irreversible reduction process with the cathodic peak potential $E_p = -2.59$ V vs Fc/Fc^+ . In

stark contrast, **RhO-Pz** could be reduced with a potential at approximately -1.62 V vs. Fc/Fc^+ and oxidized at approximately $+1.32$ V vs Fc/Fc^+ , both in chemically irreversible processes. A large difference in reduction potential by almost 1 V reflects the strong LUMO-lowering activation provided by the bis-cyclometalated Lewis acid.

Furthermore, **HE-1** could be oxidised in a chemically irreversible process with an anodic peak potential ($E_p^{(\text{HE-1})+/\text{HE-1}}$) at approximately 0.50 V vs Fc/Fc^+ . According to luminescence emission (**Figure 53**, maximum wavelength = 455 nm, corresponding to 2.73 eV), the redox potential of photoexcited **HE-1** $E_p^{(\text{HE-1})+/\text{HE-1}^*}$ is estimated as -2.23 V vs Fc/Fc^+ , which is feasible to reduce **RhO-Pz** but not free **18a**. These results reasonably explain the origin of the excellent chemoselectivity of the present transformation.

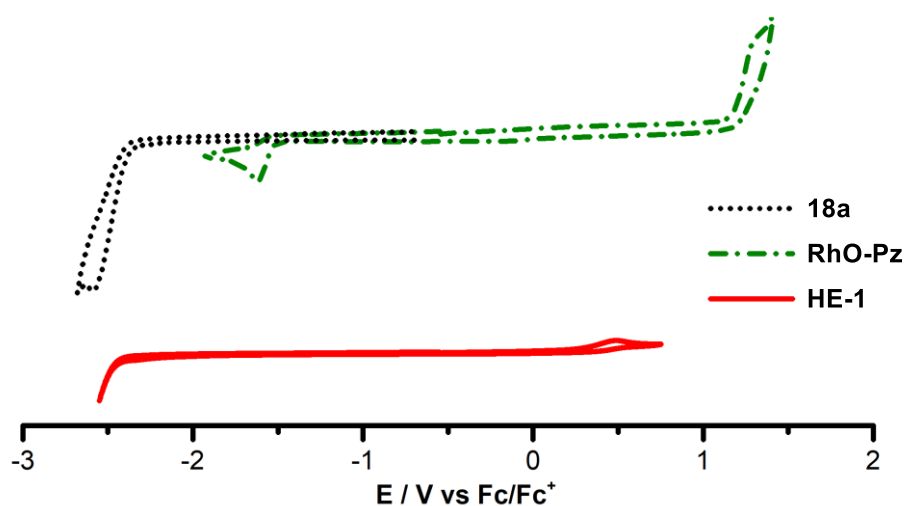


Figure 54. CV spectra of compounds **18a**, **RhO-Pz**, and **HE-1**.

6) Stern-Volmer quenching experiments

To further support the selective SET process between photoexcited **HE*** and intermediate **A**, two sets of Stern-Volmer quenching experiments were performed, with the photoredox mediator Hantzsch ester alone and with the mixture of Hantzsch ester and **RhO** (2:1), respectively. Firstly, the solutions of **HE-1** (0.5 mM in 1,4-dioxane) containing different amount of quencher were excited at $\lambda = 360$ nm and the emission were measured at 455 nm. As shown in **Figure 55**, **RhO-Pz** and **RhO** can quench the luminescence while substrate **18a** or substrate **19a** is not capable of quenching the excited **HE-1**. Since the **[Rh]** complexes could also absorb the excitation light competitively, an inner filter effect by **RhO-Pz** and **RhO** needs to be considered.

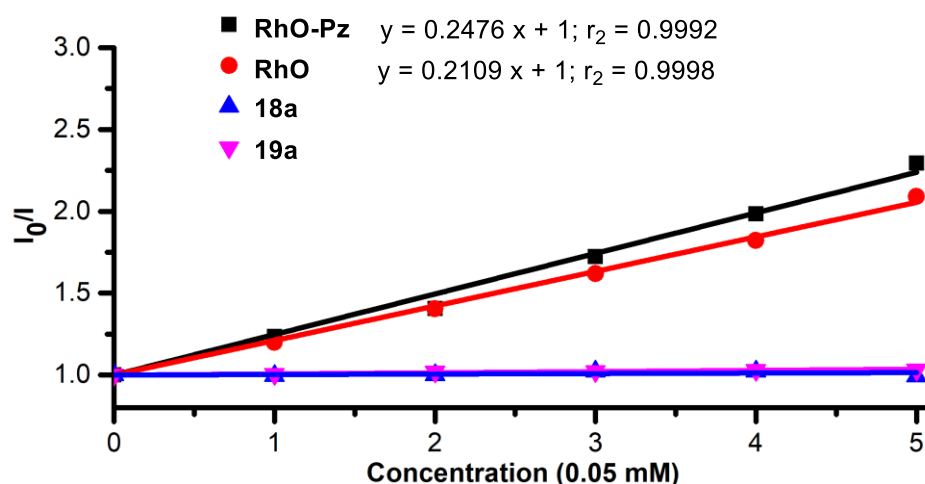


Figure 55. Stern-Volmer plots of the quenching on **HE-1**. I_0 and I are respective luminescence intensities of the solution of **HE-1** in the absence and presence of the indicated concentrations of the corresponding quencher. [**HE-1**] = 0.5 mM, Ex = 360 nm, Em = 455 nm.

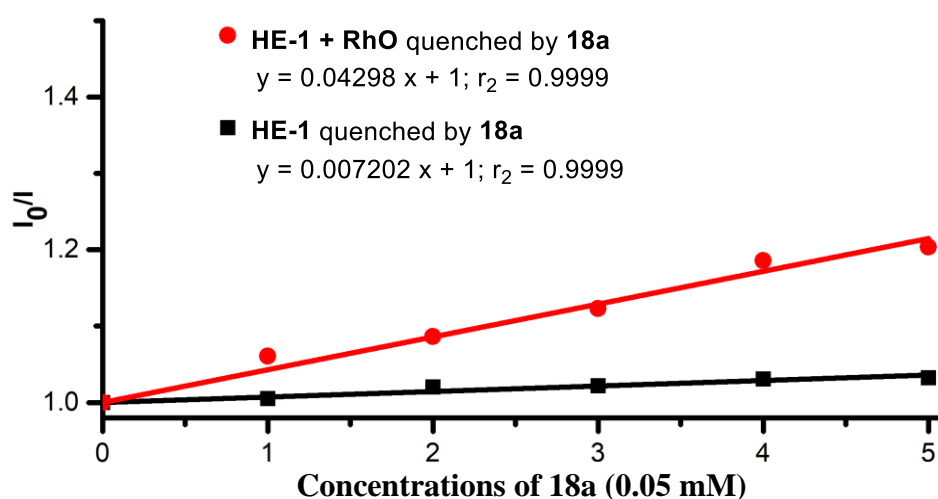


Figure 56. Stern-Volmer plots of the quenching experiments by **18a**. I_0 and I are respective luminescence intensities of the solution of **HE-1** (black one) or the mixture of **HE-1** and **RhO** (red one) in the absence and presence of the indicated concentrations of the quencher **18a**. Ex = 360 nm, Em = 455 nm.

Considering the similar absorption of **RhO-Pz** and **RhO** (Figure 53), pathways other than inner filter of Rh-species might contribute to the slightly stronger quenching effect of **RhO-Pz** compared with the effect by **RhO** (Figure 55). With this in mind, a second set of quenching experiments were conducted. Accordingly, free **18a** was used to quench the mixture of **HE-1** (0.5 mM) and **RhO** (0.25 mM). As a result, **18a** can quench the luminescence of the mixture of **HE-1** and **RhO** slightly while

almost no quenching effect was observed toward the solution of **HE-1** alone (**Figure 56**). Since the ligand exchange rate of chiral-at-rhodium complex is very fast, the in situ generated **RhO-Pz** is supposed to form immediately, and then to undergo single electron transfer with photoexcited **HE-1**, which has been demonstrated to be thermodynamically favorable by CV studies (**Figure 54**).

In summary, quenching experiments indicate that **RhO** bound substrate, the major existing species of rhodium complexes, is most likely responsible for the oxidative quenching of excited **HE***.

7) Evidences for a radical pathway

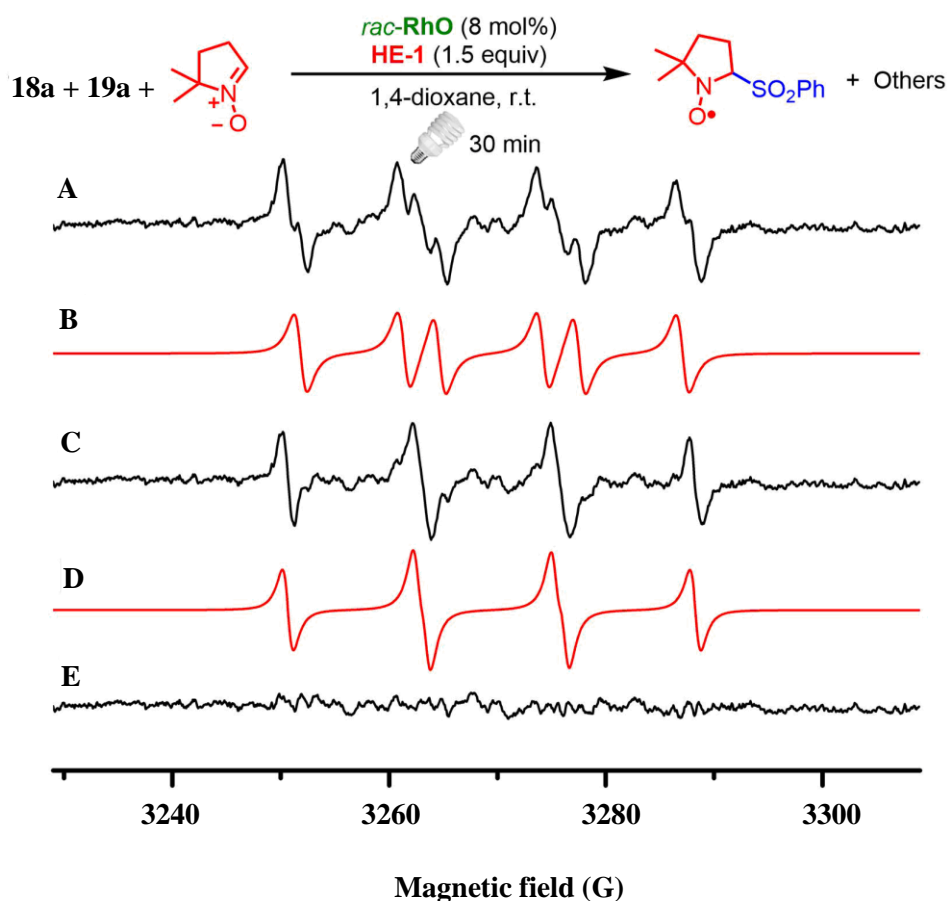


Figure 57. EPR experiments on the β -functionalization reaction with the addition of DMPO (X band, r.t.). **A**: experimental signals; **B**: simulated signal 1 ($g = 2.006$, $\alpha_N = 9.5$ G, $\alpha_H^\beta = 12.9$ G); **C**: residual of signals (A–B); **D**: simulated signals 2 ($g = 2.006$, $\alpha_N = 12.0$ G, $\alpha_H^\beta = 12.8$ G); **E**: residual of signals (C–D).

Several experiments support the proposed radical pathway. First, the title reaction **18a + 19a** \rightarrow **20a + 21a** was greatly inhibited upon adding 2,2,6,6-tetramethyl-piperidinoxy (TEMPO) or

2,6-di-*tert*-4-methylphenol (BHT) as radical scavengers. Second, when the reaction was monitored by electron paramagnetic resonance (EPR) using 5,5-dimethyl-1-pyrroline *N*-oxide (DMPO) as free radical spin-trapping agent, mixed signals containing two radical species were observed, one of which was proposed to be phenyl sulfonyl radical (**Figure 57**, $g = 2.006$, $a_N = 9.5$ G, $a_H^\beta = 12.9$ G).¹⁶ Third, a quantum yield of 0.09 was determined for the title reaction, which is consistent with the proposed mechanism being devoid of any chain process.

3.2.6 Conclusions

In conclusion, this chapter introduced an unusual reaction scheme in which a chiral rhodium complex enables the catalytic enantioselective functionalization of a photo-generated carbon radical employing cheap and readily available Hantzsch ester as photoredox mediator and reductant. Intriguingly, in this radical allylation reaction using allyl sulfones as reagents, the leaving sulfonyl radicals could be trapped by electron deficient alkenes and transformed into valuable enantioenriched S-containing building blocks, thereby minimizing waste generation. The simple reaction setup and the mild reaction conditions as well as the demonstrated compatibility with a wide range of functionality render this robust catalytic system an appealing process.

For the first time in the Meggers group, the rhodium bound allyl radical species (also called rhodium bound β -enolate radical) was generated and applied to an enantioselective conversion.¹⁷ This opened a new testing ground to develop novel chemistry of chiral-at-rhodium catalysts. Almost at the same time, Zijun Zhou in Meggers/Gong group at Xiamen University discovered an interesting PECT induced radical-radical recombination mechanism for a redox neutral β -amination of α,β -unsaturated 2-acyl imidazoles, which is proposed to proceed through a similar rhodium bound allyl radical intermediate.¹⁸ After that, Wei Yuan from Meggers/Gong group at Xiamen University expanded the PECT system to a β -alkylation by the merger with a 1,5-HAT process.¹⁹ Notably, this kind of radical species could also be generated oxidatively and applied to a radical-radical recombination, achieving an elegant asymmetric β -C-H functionalization as developed by Jiajia Ma.²⁰ On the other hand, based on the unique properties of **HE**, 4-substituted Hantzsch esters were employed as radical reservoirs for a catalytic asymmetric radical conjugate addition by Francisco F. de Assis.²¹

To be highlighted, Dr. Shipeng Luo and the author of this thesis contributed equally to this work.

Under the direction of Prof. E. Meggers, the author of this thesis conceived the design, found the reaction, optimized the conditions and did a part of scope investigation. Shipeng Luo finished the scope and transformations of products, got the single crystals for the assignment of product configurations, did robustness screening and conducted the mechanistic studies.

References

- 1 L. Zhang, E. Meggers, *Acc. Chem. Res.* **2017**, *50*, 320-330.
- 2 L. Zhang, E. Meggers, *Acc. Chem. Res.* **2017**, *50*, 320-330.
107-162; b) A. Studer, D. P. Curran, *Angew. Chem. Int. Ed.* **2016**, *55*, 58-102.
- 3 a) G. Pandey, *Top. Curr. Chem.* **1993**, *168*, 175; b) J. Twilton, C. Le, P. Zhang, M. H. Shaw, R. W. Evans, D. W. C. MacMillan, *Nat. Rev. Chem.* **2017**, *1*, 0052.
- 4 R. Brimioulle, D. Lenhart, M. M. Maturi, T. Bach, *Angew. Chem. Int. Ed.* **2015**, *54*, 3872-3890.
- 5 For selected examples, see: a) L. J. Rono, H. G. Yayla, D. Y. Wang, M. F. Armstrong, R. R. Knowles, *J. Am. Chem. Soc.* **2013**, *135*, 17735-17738; b) O. Gutierrez, J. C. Tellis, D. N. Primer, G. A. Molander, M. C. Kozlowski, *J. Am. Chem. Soc.* **2015**, *137*, 4896-4899; c) D. Uraguchi, N. Kinoshita, T. Kizu, T. Ooi, *J. Am. Chem. Soc.* **2015**, *137*, 13768-13771; d) C. Wang, J. Qin, X. Shen, R. Riedel, K. Harms, E. Meggers, *Angew. Chem. Int. Ed.* **2016**, *55*, 685-688; e) Q. M. Kainz, C. D. Matier, A. Bartoszewicz, S. L. Zultanski, J. C. Peters, G. C. Fu, *Science* **2016**, *351*, 681-684.
- 6 M. T. Pirnot, D. A. Rankic, D. B. C. Martin, D. W. C. MacMillan, *Science* **2013**, *339*, 1593-1596.
- 7 J. Du, K. L. Skubi, D. M. Schultz, T. P. Yoon, *Science* **2014**, *344*, 392-396.
- 8 M. Silvi, C. Verrier, Y. P. Rey, L. Buzzetti, P. Melchiorre, *Nat. Chem.* **2017**, *9*, 868-873.
- 9 a) X.-Q. Zhu, Y.-C. Liu, J.-P. Cheng, *J. Org. Chem.* **1999**, *64*, 8980-8981; b) J. Jung, J. Kim, G. Park, Y. You, E. J. Cho, *Adv. Synth. Catal.* **2016**, *358*, 74-80; c) W. Chen, H. Tao, W. Huang, G. Wang, S. Li, X. Cheng, G. Li, *Chem. Eur. J.* **2016**, *22*, 9546-9550.
- 10 For a review on the reaction of sulfonyl radicals, see: a) M. P. Bertrand, *Org. Prep. Proced. Int.* **1994**, *26*, 257; for selected examples on sulfone-based radical traps, see: b) A.-P. Schaffner, P. Renaud, *Angew. Chem. Int. Ed.* **2003**, *42*, 2658-2660; c) J. Zhang, Y. Li, F. Zhang, C. Hu, Y. Chen, *Angew. Chem. Int. Ed.* **2016**, *55*, 1872-1875; d) Y. Zhu, X. Wen, S. Song, N. Jiao, *ACS Catal.* **2016**,

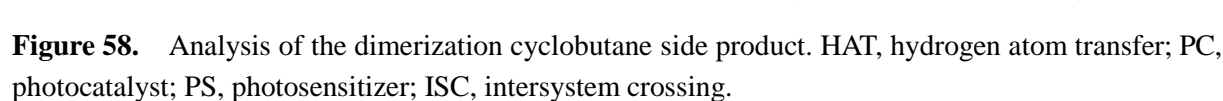
- 6465-6472.
- 11 a) H. Huo, K. Harms, E. Meggers, *J. Am. Chem. Soc.* **2016**, *138*, 6936-6939; b) C. Wang, K. Harms, E. Meggers, *Angew. Chem. Int. Ed.* **2016**, *55*, 13495-13498.
 - 12 J. Ma, X. Shen, K. Harms, E. Meggers, *Dalton Trans.* **2016**, *45*, 8320-8323.
 - 13 C. Wang, L.-A. Chen, H. Huo, X. Shen, K. Harms, L. Gong, E. Meggers, *Chem. Sci.* **2015**, *6*, 1094-1100.
 - 14 Y. Zheng, K. Harms, L. Zhang, E. Meggers, *Chem. Eur. J.* **2016**, *22*, 11977-11981.
 - 15 For a selected application of robustness screening, see: K. D. Collins, A. Rühling, F. Glorius, *Nat. Protoc.* **2014**, *9*, 1348-1353.
 - 16 V. Cholvad, K. Szaboova, A. Staško, O. Nuyken, B. Voit, *Magn. Reson. Chem.* **1991**, *29*, 402-404.
 - 17 X. Huang, S. Luo, O. Burghaus, R. D. Webster, K. Harms, E. Meggers, *Chem. Sci.* **2017**, *8*, 7126-7131.
 - 18 Z. Zhou, Y. Li, B. Han, L. Gong, E. Meggers, *Chem. Sci.* **2017**, *8*, 5757-5763.
 - 19 W. Yuan, Z. Zhou, L. Gong, E. Meggers, *Chem. Commun.* **2017**, *53*, 8964-8967.
 - 20 J. Ma, A. R. Rosales, X. Huang, K. Harms, R. Riedel, O. Wiest, E. Meggers, *J. Am. Chem. Soc.* **2017**, *139*, 17245-17248.
 - 21 F. F. de Assis, X. Huang, M. Akiyama, R. A. Pilli, E. Meggers, *J. Org. Chem.* **2018**, *83*, 10922-10932.

3.3 Direct Visible-Light-Excited Asymmetric Lewis Acid Catalysis of Intermolecular [2+2] Photocycloaddition

3.3.1 Side Product Inspired Reaction Design and Research Background

As mentioned in Chapter 3.2, a cyclobutane side product **17** was obtained as major product in some cases using β -phenyl α,β -unsaturated 2-acyl imidazole **26a** as substrate. For example, the photoredox conditions designed for the Minisci reaction gave the cyclobutane **17** without the formation of any desired β -arylation product (**Figure 58a**). Initially, a radical mechanism consisting of sequential photoinduced electron transfer/Giese-type radical conjugate addition/intramolecular radical cyclization was proposed to explain the undesired homo-[2+2] photodimerization (**Figure 58c**).¹ But later, the cyclobutane **17** could also be observed under conditions using benzil as visible-light-activated HAT mediator (**Figure 58b**). Since the well-known triplet sensitizer benzil is unable to reduce the rhodium bound substrate, a triplet energy transfer mechanism might be operative (**Figure 58d**).² The excited triplet rhodium bound substrate, which could be formed via a photosensitizer mediated energy transfer, undergoes a head-to-head photocycloaddition, thereby delivering the cyclobutane product. This implied an unprecedented catalysis scheme, in which direct bond formations occur at the electronically excited states being devoid of any charge separation, might be accessible by chiral-at-metal catalysts.

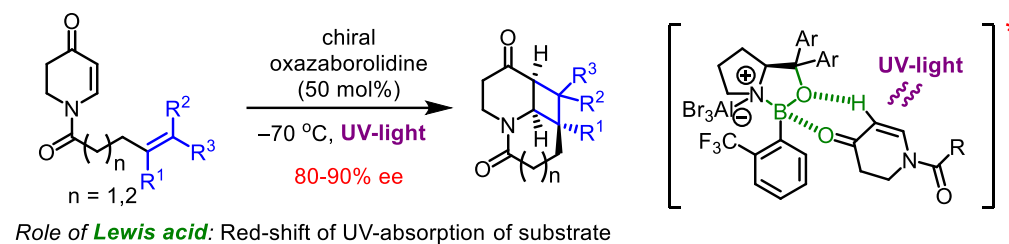
Electronically excited states feature distinctive reactivity that is often impossible to achieve by non-photochemical methods. On the other hand, visible-light-induced asymmetric catalysis is among the most economic and sustainable strategies for the synthesis of enantioenriched molecules.³ Most photochemistry reported to date involves photoinduced electron transfer,⁴ often called photoredox catalysis, to generate intermediate radical ions and free radicals. But steering the reaction course of such highly reactive intermediates in a stereocontrolled and catalytic fashion is very difficult and therefore often leads to a narrow scope.⁵ This renders visible-light-activated reactions that occur directly from an electronically excited state, without any charge separation, an appealing alternative.⁶ Controlling stereoselective reactions of such excited states in a catalytic and asymmetric fashion is therefore of high interest but largely unexplored.⁷



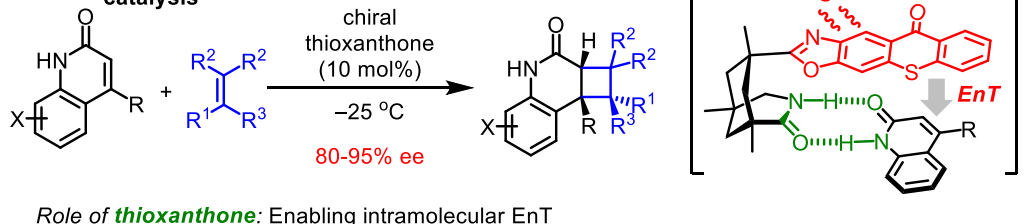
98

limited substrate scope might restrict its applications.

a) Bach, Lewis acid catalysis



b) Bach, H-bonding catalysis



c) Yoon, Dual chiral Lewis acid/photosensitizer

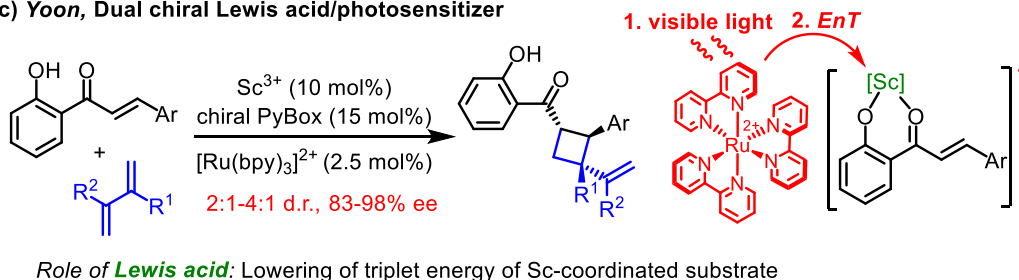


Figure 59. Previous strategies for stereocontrolled reactions from electronically excited states.

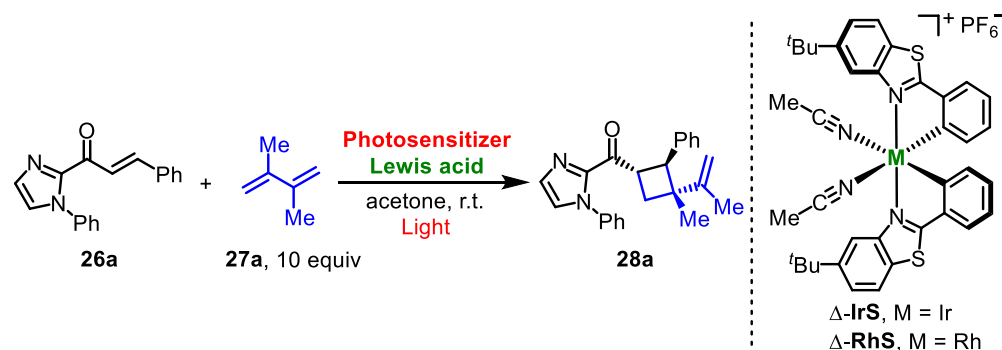
These facts spurred the author of this thesis to develop more general and highly stereocontrolled reactions directly from the visible-light-excited states. This chapter introduces how the author discloses a previously elusive simplified catalytic system that only relies on a single chiral-at-metal Lewis acid, to achieve asymmetric intermolecular [2+2] photocycloadditions providing a wide range of cyclobutanes with up to >99% ee and up to >20:1 d.r.

3.3.2 Reaction Development

Based on the analysis of the homo-[2+2] photocycloaddition and inspired by Yoon's dual-catalyst conditions, the diene **27a** was chosen to trap the triplet state of a chiral-at-rhodium catalyst bound α,β -unsaturated 2-acyl imidazole **26a**, in combination with the employment of benzil as

photosensitizer. Encouragingly, the desired cyclobutane **28a** could be obtained in excellent yield with 13:1 d.r. and 94% ee after the photolysis with blue LEDs in the presence of 4.0 mol% of Δ -**RhS** and one equivalent of benzil (**Table 11**, entry 1). To simplify conditions by moving away from dual catalysis, the chiral-at-iridium complex Δ -**IrS** was tested as a single catalyst (entry 2). Unfortunately, although the [2+2] photocycloaddition product **28a** was generated in 75% yield and with 5:1 d.r., the product was formed as a racemic mixture. Surprisingly, using the single rhodium analogue Δ -**RhS** instead, the reaction proceeded smoothly spot-to-spot to provide the cycloaddition product **28a** in almost quantitative yield with high stereoselectivity (entry 3, 99% NMR yield, 14:1 d.r., 99.5% ee). In addition, a more powerful 24 W blue LEDs lamp performed better than a 21 W CFL (entry 4).

Table 11. Initial experiments leading to a single chiral-at-rhodium catalyst system.^[a]



Δ -**IrS**, M = Ir
 Δ -**RhS**, M = Rh

Entry	LA	PS [mol%]	Light	Yield [%]	D.r.	Ee [%]
1	Δ - RhS	Benzil (100)	24 W Blue LEDs	93	13:1	94
2	Δ - IrS	None	24 W Blue LEDs	75	5:1	0
3	Δ - RhS	None	24 W Blue LEDs	99	14:1	99.5
4 ^[b]	Δ - RhS	None	21 W CFL	86	13:1	98

[a] Reaction conditions: **26a** (0.10 mmol), **27a** (1.0 mmol), Lewis acid (4.0 mol%), photosensitizer in acetone (0.2 M, 0.5 mL) were stirred at room temperature for 16 h; NMR yield; ee was determined by HPLC on a chiral stationary phase. [b] 40 h.

This single catalyst system turned out to be very robust (**Table 12**). Reducing catalyst loading to 2.0 mol% and the amount of diene to 3.0 equiv did not influence the reaction efficiency (entries 1-3). Even with a reduced Rh-catalyst loading of just 0.5 mol%, an excellent enantioselectivity of 96% ee was observed (entry 5). Interestingly, the reaction can be executed under “open-flask” conditions — under air and in the presence of residual water — without significantly affecting the reaction outcome

(entries 7,8). The transformation is insensitive to the polarity of the solvent as acetone could be replaced by DMF or CH_2Cl_2 (entries 9,10), indicating that free radical and/or radical ion intermediates might not be involved. Control experiments confirm that both visible light (entry 11) and catalyst (entry 12) are indispensable. Without catalyst, asymmetric induction is obviously not feasible but small amounts of racemic product are formed.

Table 12. Robustness of the [2+2] photocycloaddition.^[a]

$\text{26a} + \text{27a} \xrightarrow[\text{acetone, r.t., 16 h, blue LEDs}]{\Delta\text{-RhS}} \text{28a}$

Entry	[Rh] Loading	27a	Variation	Yield [%]	D.r.	Ee [%]
1	4.0 mol%	10 equiv	None	99	14:1	99.5
2	2.0 mol%	10 equiv	None	99	14:1	99
3	2.0 mol%	3 equiv	None	99 (97)	14:1	99
4	1.0 mol%	3 equiv	None	96	13:1	98
5	0.5 mol%	3 equiv	24 h	98	12:1	96
6	0.2 mol%	3 equiv	40 h	84	11:1	87
7	2.0 mol%	3 equiv	Air	97	14:1	99
8	2.0 mol%	3 equiv	Air, 1% H_2O	96	13:1	99
9	2.0 mol%	3 equiv	DMF as solv.	95	13:1	98
10	2.0 mol%	3 equiv	CH_2Cl_2 as solv.	99	14:1	99
11	2.0 mol%	3 equiv	Dark	0	n.a.	n.a.
12	0 mol%	3 equiv	None	19	6:1	0

[a] Reaction conditions: **26a** (0.10 mmol), **27a**, $\Delta\text{-RhS}$, in acetone (0.2 M, 0.5 mL) were stirred at room temperature for 16 h; NMR yield, isolated yield is provided in parentheses; ee was determined by HPLC on a chiral stationary phase.

Overall, a simple and robust reaction scheme that only relies on a single chiral-at-rhodium catalyst is developed for a highly asymmetric [2+2] photocycloaddition. The conditions based on using 2.0 mol% of $\Delta\text{-RhS}$ are selected for the further scope investigations (**Table 12**, entry 3).

3.3.3 Substrate Scope

As displayed in **Figure 60**, a variety of α,β -unsaturated imidazoles bearing different substituents at the β -aryl moiety provided the [2+2] addition products in good to excellent yields (up to 97%), high diastereoselectivities (up to 16:1 d.r.), and essentially complete enantioselectivities (up to >99% ee) independent of the electronic nature or position of the substituents (**28a-j**). Importantly, the imidazole moiety can be replaced by other coordinating groups, such as pyridine (**28k**) and the synthetically very useful pyrazole (**28l-q**), providing the potential for further transformations. Interestingly, a conjugate extended enone undergoes the [2+2] photocycloaddition in high stereo- and chemoselectivity with the exclusive bond formation on the double bond adjacent to carbonyl group (**28j**).

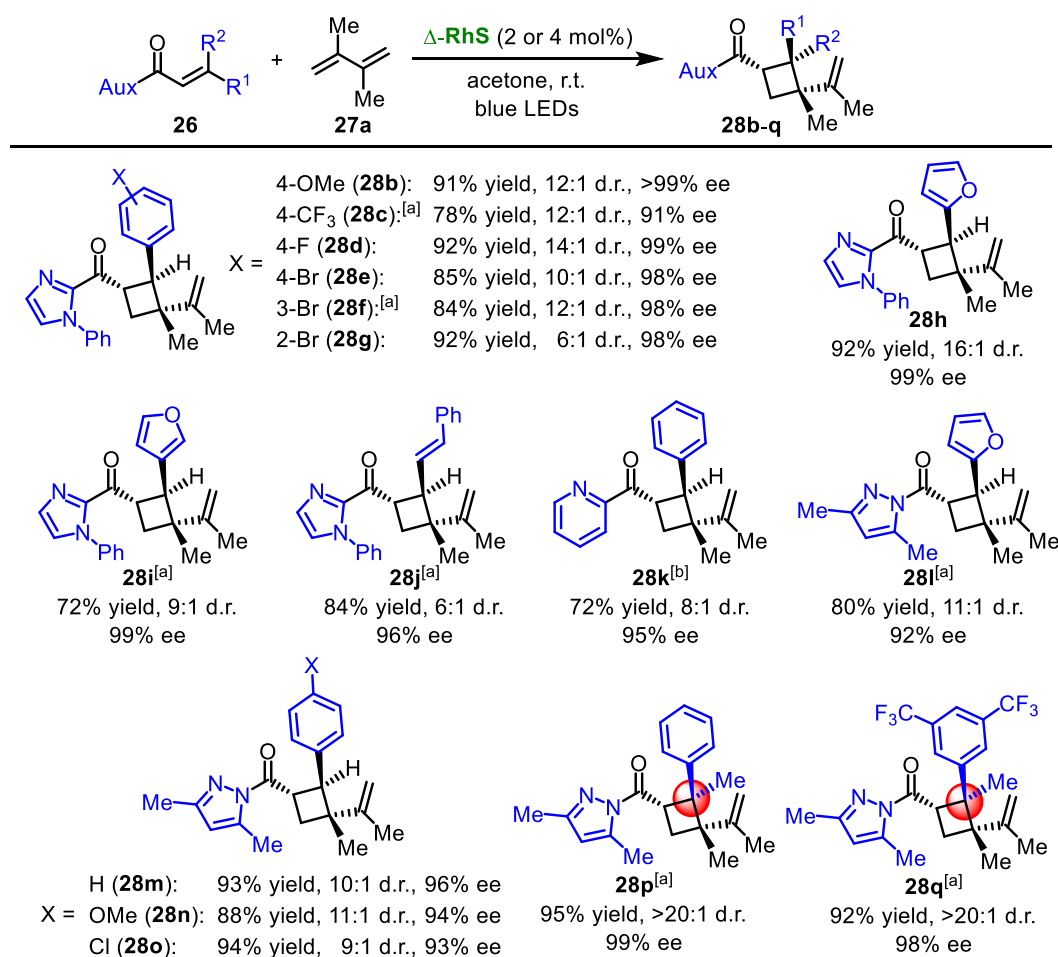


Figure 60. Scope of the [2+2] photocycloaddition with respect to α,β -unsaturated carbonyl compounds. Reaction conditions: see **Table 12** entry 3. [a] 4.0 mol% of Δ -RhS and 10 equiv of **27a**. [b] MeCN/acetone 1:1 instead of acetone. Configurations were assigned with crystal structures of **28e** and a derivative of **28p**.

Next the scope was expanded to more general alkenes (**Figure 61**). Although the reaction of styrene with the standard imidazole substrate **26a** gave cyclobutane **28r** only in 1:1 d.r. value, an β,β -di-substituted α,β -unsaturated *N*-acyl pyrazole substrate delivered excellent stereochemical control, producing the cycloaddition product **28s** in 16:1 d.r. with 99% ee. Besides the diene and styrene, a wide range of alkenes were well accommodated in this transformation, including a vinyl ether (**28t**), an enyne (**28u**), and substituted styrenes (**28s**, **28v-z**). Furthermore, this transformation tolerates heterocycles like furan (**28h-i**, **28l**) and thiophene (**28w**) and can be applied to the late-stage modification of complex biomolecule (**28z**). Notably, an example of intramolecular reaction worked as well, generating complex bicyclic compound **28aa** in a highly effective and asymmetric way.

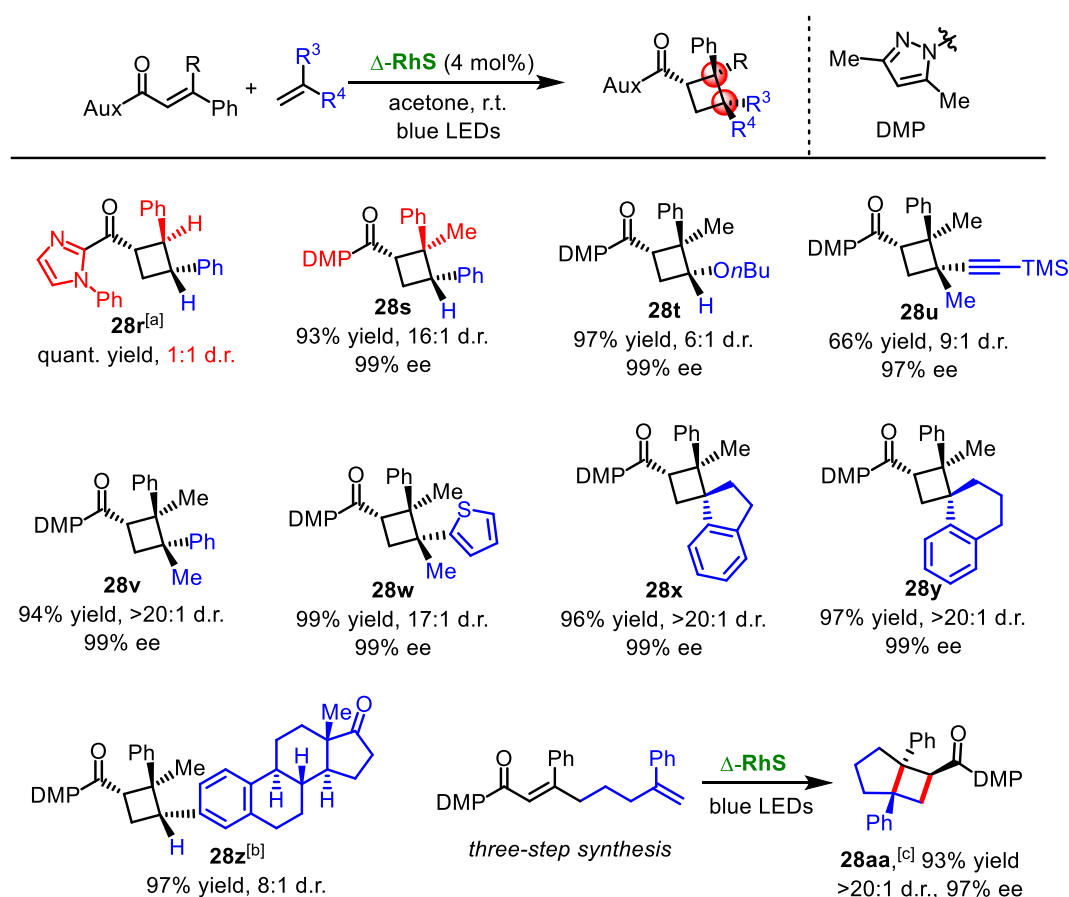


Figure 61. Scope of the [2+2] photocycloaddition with respect to alkenes. Reaction conditions: see **Table 12** entry 3. [a] with *rac*-RhS, NMR yield, ee not determined. [b] Performed with 3.0 equiv of estrone derived alkene in CH₂Cl₂ (0.2 M, 0.5 mL). [c] Intramolecular reaction: substrate (0.10 mmol) and Δ -RhS (4.0 mol%) in acetone (0.2 M, 0.5 mL).

It is worth noting that cyclobutanes with three contiguous stereogenic centers and vicinal all-carbon quaternary stereocenters can be constructed in a single step using this new methodology in high yields, with excellent d.r. and ee (**28p-q**, **28u-y**), highlighting the versatility of this protocol in building molecular complexity in a catalytic, asymmetric fashion.¹³

More challenging simple aliphatic alkenes and internal alkenes did not provide any desired products when the typical coordinative substrates were used (**Figure 62**, **28ab-ae**). Interestingly, by using 3-mono-substituted pyrazole as auxiliary, the photocycloadditions with cyclohexene did occur in moderate yields with moderate diastereoselectivities (**28af-ah**). The reaction efficiency and d.r. value could be higher (**28ai**, 98% yield, with 13:1 d.r., 99% ee) in the reaction with cycloheptene and using 3-*para*-methoxyphenyl pyrazole as auxiliary. Further investigation with respect to the scope of aliphatic (internal) alkenes and mechanistic studies to understand the effect of auxiliary is ongoing.

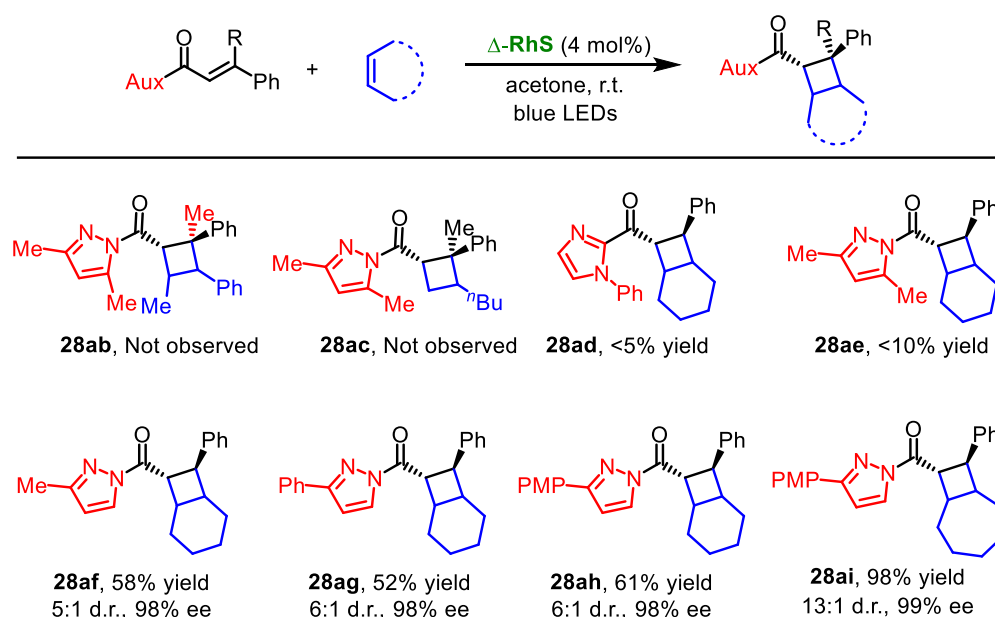


Figure 62. Auxiliary enabled [2+2] photocycloaddition with aliphatic (internal) alkenes.

There are some limitations as shown in **Figure 63**. A conjugated π ground at β -position is necessary for the reaction (for failed examples, see **28aj,ak**) and α,α -di-substituted carbonyl compounds failed to undergo the photocycloaddition (**28al**). Besides, a thiazole containing alkene and a phenylglycine derived alkene are not compatible (**28am,an**). In addition, a vinyl ether designed for the intramolecular photocycloaddition is not tolerated either (**28ao**).

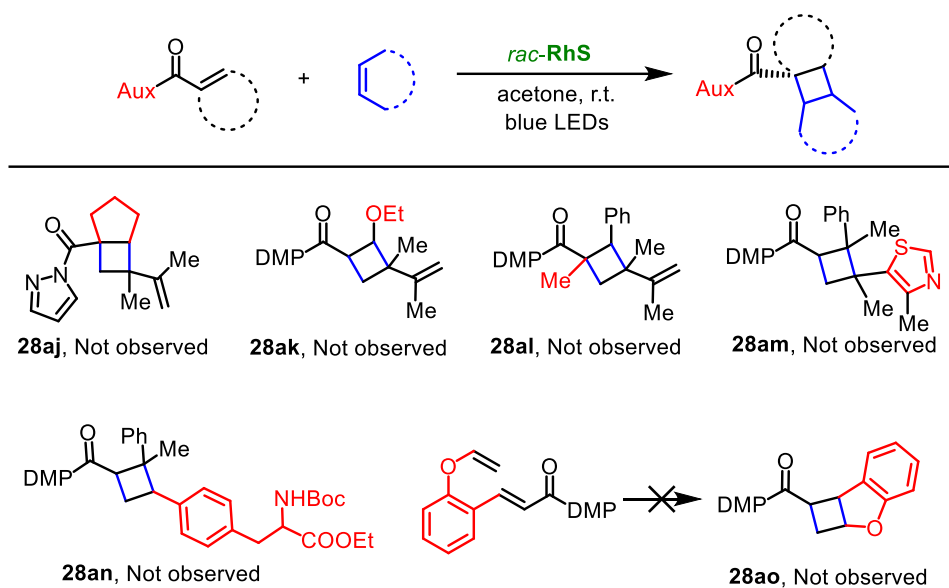


Figure 63. Limitations of the scope of the [2+2] photocycloaddition.

In summary, this novel methodology provides a very simple protocol to access structurally complex cyclobutanes in a catalytic and highly stereoselective fashion and therefore constitutes a valuable complement to existing protocols. Useful catalytic asymmetric photoinduced¹⁰ and thermal¹⁴ [2+2] cycloadditions have been reported before. However, the here introduced methodology is unique in its ability to install two adjacent all-carbon quaternary stereocenters (optionally spiro centers) in an intermolecular and highly stereocontrolled fashion. Furthermore, by tuning the auxiliary of enone substrate, the extension to aliphatic (internal) olefins, which can hardly be achieved by other reaction systems, highlights the versatility of this chiral-at-rhodium catalyst based method.

3.3.4 Mechanistic Studies

1) Identification of the key rhodium/substrate complex as visible-light-absorbing antenna

Firstly, the substrate coordinated rhodium complex **RhS-Im** formed immediately in quantitative yield once the bis-acetonitrile catalyst **RhS** was mixed with the 2-acyl imidazole **26a** (**Figure 64**). This indicates that the rhodium/substrate complex is the active catalytic species in the reaction solution. Then, two representative rhodium/substrate complexes **RhS-Im** and **RhS-Pz**, which were firstly characterized by Haohua Huo,¹⁵ were synthesized separately (**Figure 65**) and subjected to the further mechanistic investigations.

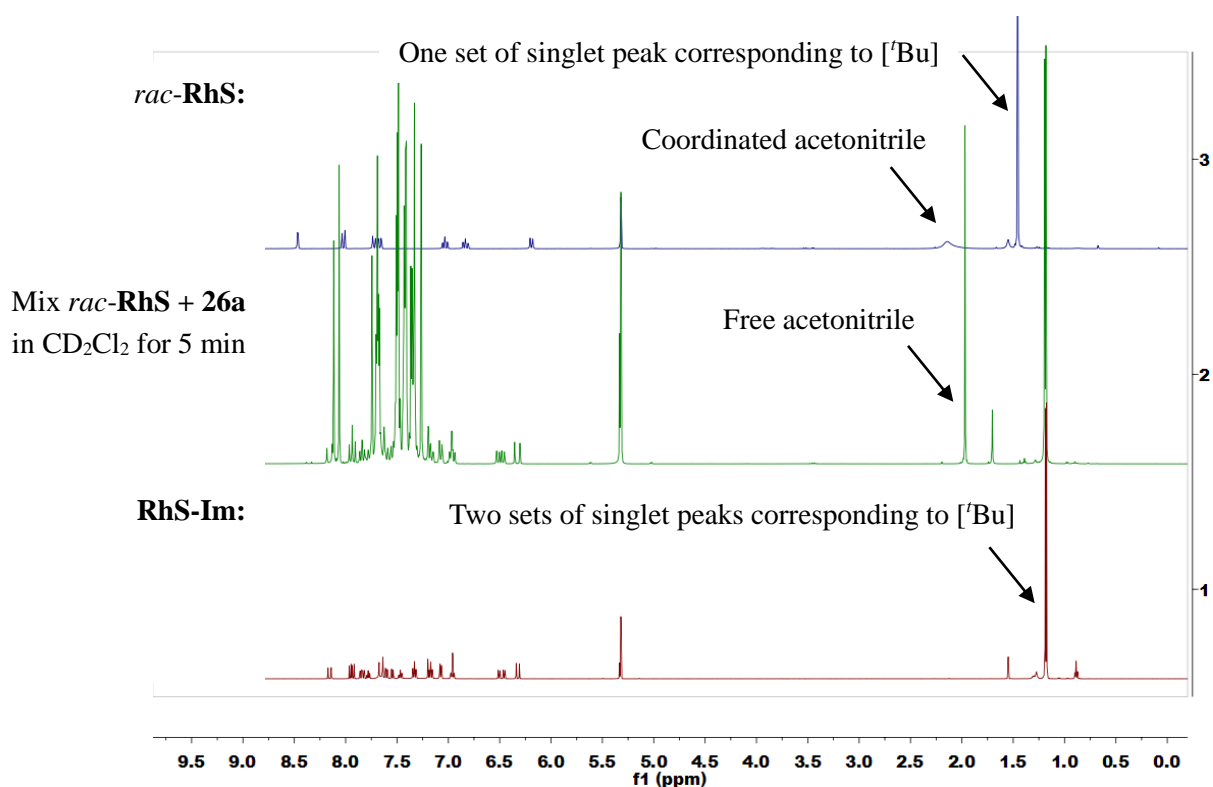


Figure 64. ^1H NMR experiments (300 M, CD_2Cl_2) demonstrating the fast generation of **RhS-Im** complex. Ratio of *rac*-**RhS**/**26a** = 1:1.

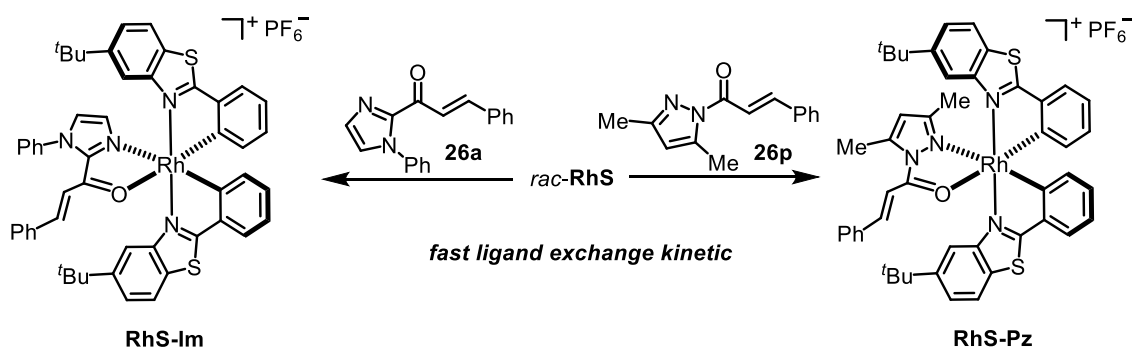


Figure 65. Two key rhodium/substrate complexes synthesized for mechanistic studies of the [2+2] photocycloaddition.

Secondly, UV/Vis absorption spectra show greatly enhanced absorption of catalyst bound substrates compared with the free substrates (**Figure 66**). Notably, free substrate **26a** has a very weak absorption in visible light region, thus explaining the background racemic reaction without catalyst (**Table 12** entry 12). Additionally, the imidazole bound complex **RhS-Im** shows much higher absorbance than the pyrazole bound congener **RhS-Pz** in near UV/visible light region, Interestingly,

the β -methyl α,β -unsaturated *N*-acyl pyrzaole coordinated analogue **RhO-Pz** has almost the identical absorption spectrum compared with **RhO** (Figure 53).

Thirdly, according to Beer-Lambert Law, molar extinction coefficients at 400 nm were determined on a Spectra Max M5 microplate reader. Significantly, **RhS-Pz** ($\epsilon_{400} = 34950 \text{ M}^{-1}\text{cm}^{-1}$) has a molar extinction coefficient that is 169 times higher than the free substrate **26a** ($\epsilon_{400} = 207 \text{ M}^{-1}\text{cm}^{-1}$).

Therefore, the rhodium/substrate complex was demonstrated to serve as a light harvesting antenna and suppress most of the background reaction, thereby providing up to almost complete enantioselectivities of >99% ee.

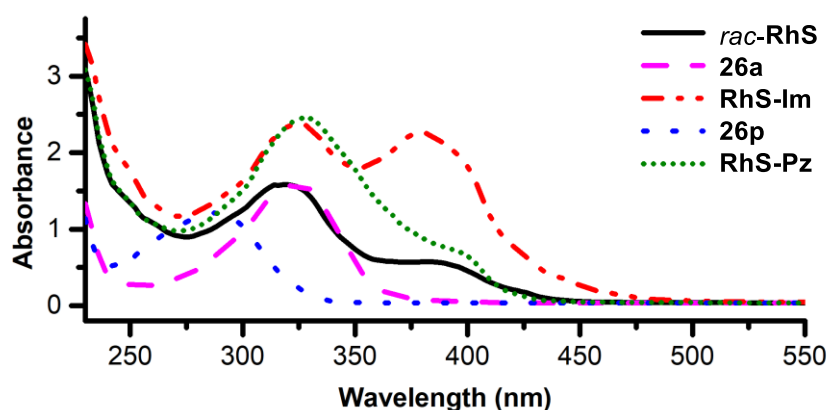


Figure 66. UV/Vis absorption spectra measured in the [2+2] photocycloaddition. Recorded in CH_2Cl_2 with the concentration of 0.05 mM.

2) Cyclic voltammetry studies excluding out the possibility of a redox mechanism

With the help of Prof. Dr. Webster, the voltammetry analysis of **Rh-Im** solution was performed. As shown in **Figure 67a**, **RhS-Im** could be reduced in a chemically reversible process at approximately -1.13 V vs Fc/Fc^+ and oxidized in a chemically irreversible process at approximately 1.23 V vs Fc/Fc^+ . Based on these results and the calculated $S_0\text{-}T_1$ gap (2.01 eV, see below), the redox potentials of the excited state **RhS-Im** can be estimated as $E^{[\text{RhS-Im}]^*/[\text{RhS-Im}]\cdot-} = +0.88 \text{ V}$ and $E^{[\text{RhS-Im}]\cdot-/[\text{RhS-Im}]^*} = -0.78 \text{ V}$ vs Fc/Fc^+ (**Figure 67b**). Based on these redox potentials, the excited **RhS-Im** is unable to oxidize or reduce the alkene substrate, such as styrene (**Figure 67c**). Furthermore, the reduced or oxidized rhodium/substrate complexes (**RhS-Im** $^{\cdot-}$ or **RhS-Im** $^{\cdot+}$) are not capable of facilitating the electron transfer with styrene either. Hence, a photoredox process is very unlikely.

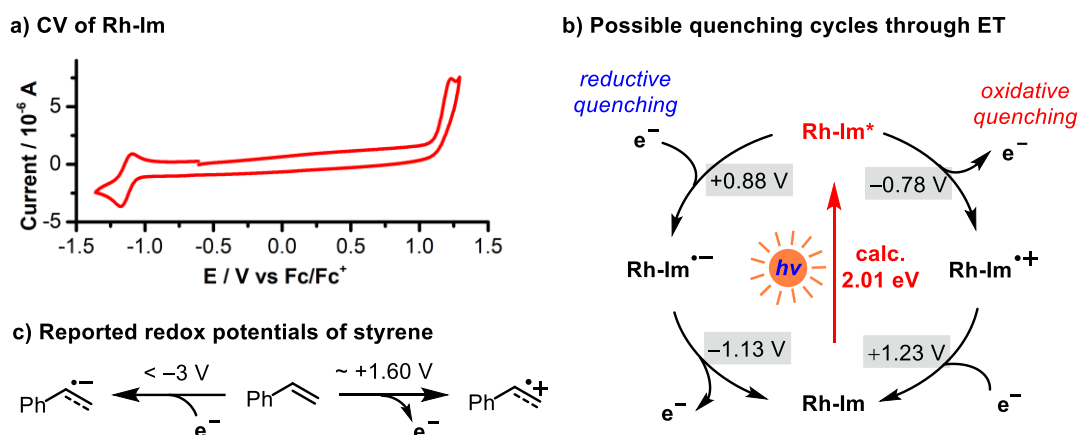


Figure 67. Cyclic voltammetry disapproving of a redox mechanism for the [2+2] photocycloaddition. All potentials refer to Fc/Fc⁺. Redox potentials of styrene, see reference 16.

3) Evidences for the excited triplet versus singlet state chemistry

Most of the established visible-light-activated [2+2] cycloadditions were reported to proceed through the triplet state of one of the involved alkenes.¹⁰ In the current reaction, the direct stereocontrolled reaction of the intermediate rhodium/substrate complex occurs in its first excited triplet state (T₁ state). This is supported by a number of experiments:

Table 13. Effect of sensitizers on the [2+2] photocycloaddition.^[a]

Entry	Catalyst [mol%]	Yield [%]	D.r.	Ee [%]
1	Δ-RhS (2.0)	99	14:1	99
2	Δ-IrS (2.0)	63	5:1	0
3	Benzil (40)	68	5:1	0
4	[Ir(ppy) ₂ (dtbbpy)](PF ₆) (2.0)	60	5:1	0
5	[Ir(dFCF ₃ ppy) ₂ (bpy)](PF ₆) (2.0)	65	5:1	0

[a] Reaction conditions: see **Table 12** entry 3.

(a) **Control experiments employing triplet sensitizer:** The racemic [2+2] cycloaddition **26a** + **27a** → **28a** can be catalyzed by well-known triplet sensitizers, such as benzil and iridium based photosensitizers (**Table 13**, entries 3-5). In addition, the relatively lower yields obtained in entries 2-5

is owing to the homo-[2+2] of **26a**. The formation of cyclobutane **17** also indicates the involvement of excited free substrate in these cases. Interestingly, the iridium based chiral-at-metal complex Δ -IrS provided a similar reaction outcome with these racemic photosensitizers (entry 2). Further studies to explain the performance of IrS are described in chapter 3.4.

(b) Control experiments employing triplet quencher: The reaction **26a** + **27a** \rightarrow **28a** is significantly inhibited by the triplet quencher 2,5-dimethylhexa-2,4-diene, supporting the involvement of excited triplet state intermediates (**Figure 68a**).

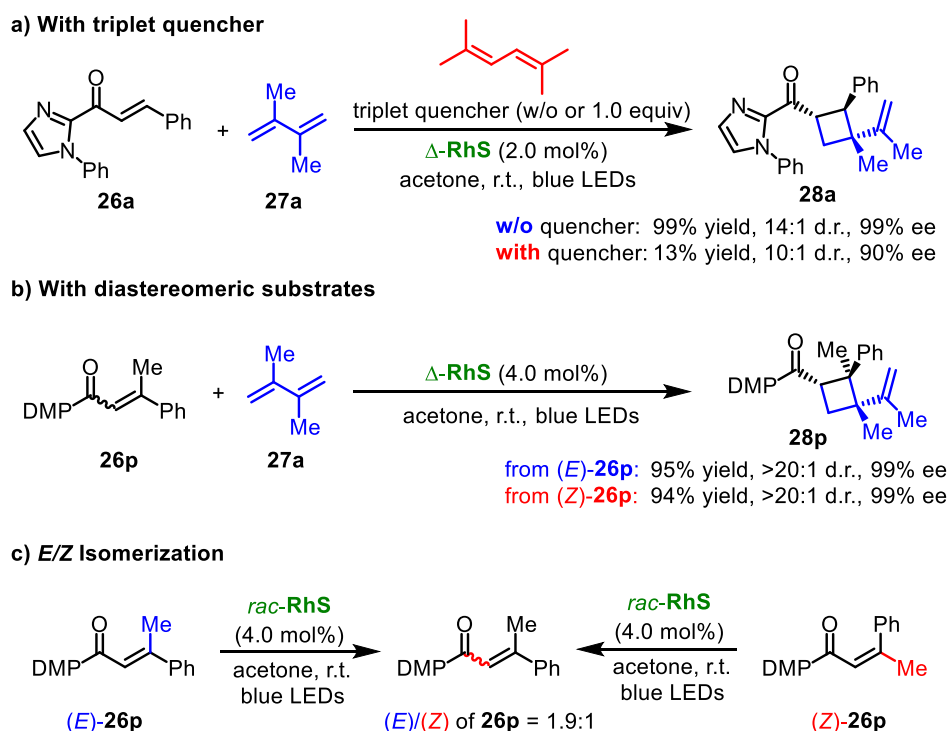


Figure 68. Control experiments supporting a triplet mechanism for the [2+2] photocycloaddition.

(c) Photocycloadditions with diastereomeric substrates: For [2+2] photocycloadditions through the first excited singlet state (S_1 state), the addition is expected to be stereospecific in contrast to [2+2] photocycloadditions through the T_1 state which form an intermediate 1,4-diradical leading to the loss of the substrate's configuration information. To probe this stereochemical aspect, the diastereomers (E)-**26p** and (Z)-**26p** were subjected to the standard conditions, respectively (**Figure 68b**). As the result, both diastereomers provided a product with identical stereochemistry as determined by ^1H NMR and HPLC analysis. Furthermore, photolysis of (E)-**26p** or (Z)-**26p** under blue LEDs with RhS led to the E/Z isomerization (with a same ratio of 1.9:1, **Figure 68c**). This observation

is consistent with the recent publications reported by Gilmour,¹⁷ which demonstrate $E \rightarrow Z$ isomerization of cinnamic esters proceeds through a triplet energy transfer mechanism.

Since the diastereomeric substrates are in equilibrium under the reaction conditions, the [2+2] photocycloaddition experiments with (*E*)- and (*Z*)-**26p** are not conclusive. However, the observed *E/Z*-isomerization suggests the involvement of a triplet rhodium/substrate intermediate from which the isomerization occurs.

(d) Detection of single oxygen generation in the presence of molecular oxygen: Quenching of excited triplet states by molecular oxygen leads to the formation of singlet oxygen. To verify the involvement of a rhodium/substrate complex in its triplet state upon irradiation, 9,10-dimethylantracene, known as a singlet oxygen trap,¹⁸ was added to the model reaction **26a** + **27a** \rightarrow **28a**. As expected, singlet oxygen trapping product **29** was isolated in 51% yield along with the formation of **28a** in 15% NMR yield, after 2 h irradiation in O₂-saturated acetone (**Figure 69a**).

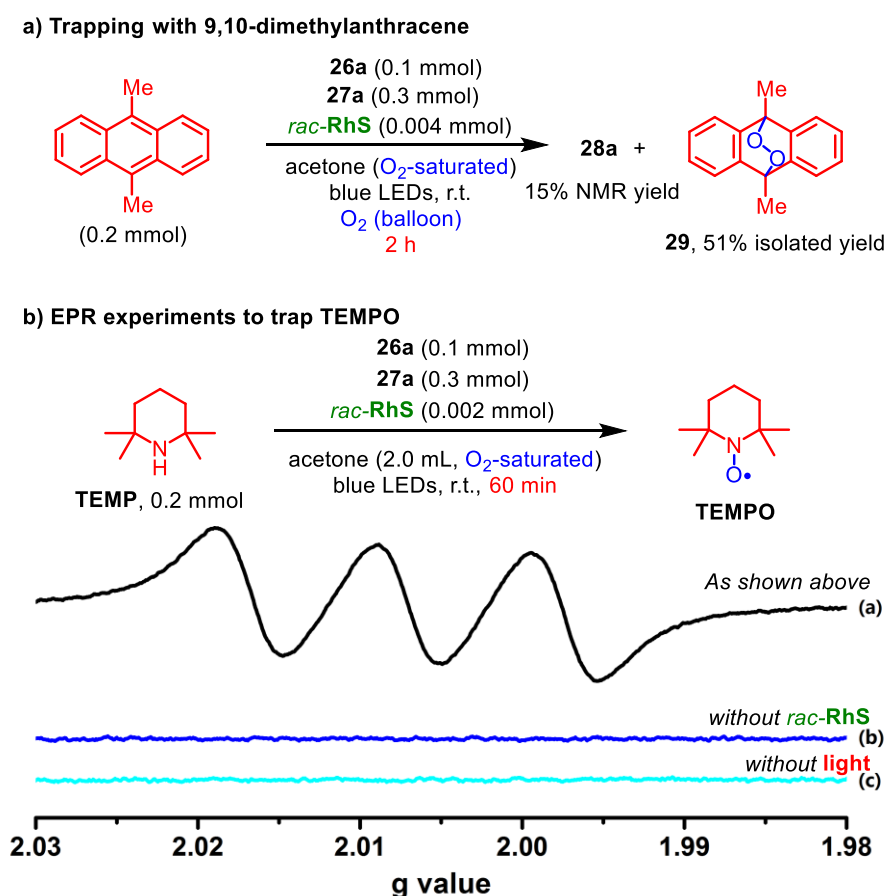


Figure 69. Experiments probing the formation of singlet oxygen in the presence of dioxygen. EPR (X band) experiments were conducted at room temperature.

According to well-developed methods, the reaction of singlet oxygen with 2,2,6,6-tetramethylpiperidine (TEMP) can generate the stable nitroxide radical TEMPO.¹⁹ Indeed, when adding TEMP to the reaction of **26a** + **27a** \rightarrow **28a** under oxygenated conditions, EPR signals with three lines corresponding to TEMPO were observed (**Figure 69b**). In addition, no signal was recorded without **RhS** or under dark conditions.

These results clearly verify the formation of singlet oxygen with the current catalytic system in the presence of molecular oxygen, and strongly supports the involvement of the excited triplet state rhodium/substrate complex.

4) Effect of molecular oxygen on the rhodium catalyzed [2+2] photocycloadditions

As mentioned in **Table 12**, the model photocycloaddition reaction **26a** + **27a** \rightarrow **28a** can be executed in the presence of air without compromising the outcome of the reaction. It is very interesting to further investigate the effect of dioxygen on this newly developed catalytic system. In order to bias the expected competition between oxygen quenching and alkene reaction, a more bulky substrate **26p** was chosen because it is expected to react somewhat more slowly with alkenes. Specifically, reactions of **26p** with two alkenes were performed under nitrogen and oxygen atmosphere, and monitored after 5 and 16 hours of irradiation, respectively (**Figure 70a,b**). As the result, the oxygen-saturated reactions proceed a little bit more slowly, showing moderate interference of molecular oxygen by quenching the excited triplet state of the rhodium/substrate complex.

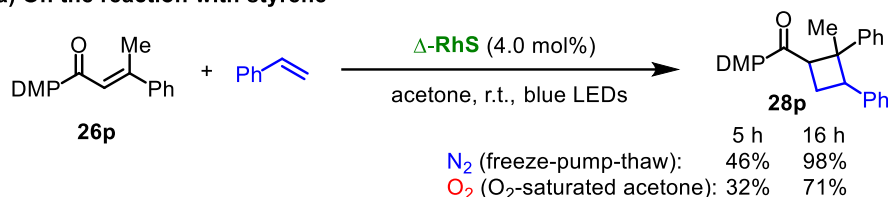
In order to assess if this is consistent with a triplet mechanism, the following aspects need to be considered: (1) *Quenching rate constants*: Molecular oxygen has been determined to quench the excited triplet state of enones with ca. $5 \times 10^9 \text{ M}^{-1}\text{s}^{-1}$ (diffusion controlled).²⁰ On the other hand, alkenes have been determined to quench triplet excited states of enones also very rapidly with rate constants in the range of 10^7 to $>10^9 \text{ M}^{-1}\text{s}^{-1}$, thus reaching diffusion control depending on the particular substrates.^{20,21} (2) *Concentrations*: An air-saturated solution contains around 2.4 mM dissolved O_2 .²² In comparison, the concentration of the alkene **27a** under the standard experimental conditions is 600 mM, being 250-fold higher.

Thus, considering the substrate concentrations and the triplet quenching rate constants of triplet state enones by molecular oxygen, the ability to perform the photocycloaddition in the presence of air can be rationalized and is not contradictory to a mechanism of the rhodium/substrate excited triplet

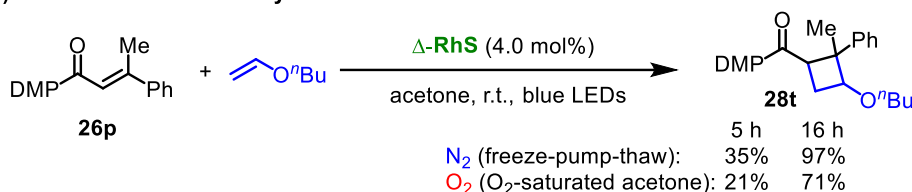
state.

In addition, there are several precedents in the literature in which the reactions via triplet energy transfer can be performed under air conditions.¹⁷ As for the current transformation, the racemic reaction **26a** + **27a** → **28a** catalyzed by a well-known triplet sensitizer [Ir(dFCF₃ppy)₂(bpy)](PF₆) can be performed with O₂ too (**Figure 70c**). Furthermore, the **RhS** catalyzed *E* → *Z* isomerization of **26p**, which is supposed to go through a triplet mechanism, is not sensitive to O₂ either (**Figure 70d**).

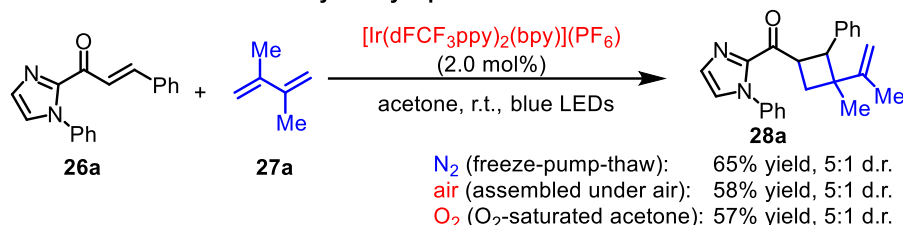
a) On the reaction with styrene



b) On the reaction with vinyl ether



c) On the racemic reaction catalyzed by a photosensitizer



d) On *E/Z* isomerization

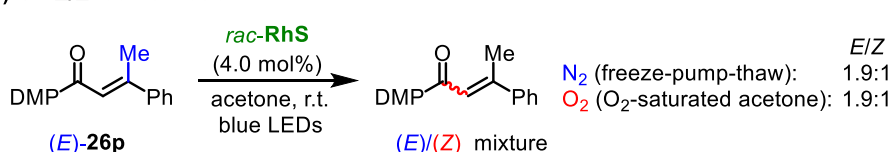


Figure 70. Effect of O₂ on the [2+2] photocycloaddition.

5) Computational studies

To further investigate the properties of the excited states, computational studies were conducted by the collaboration with T. R. Quinn and Prof. O. Wiest. The calculations reveals that in the T₁ state of the rhodium/substrate complex **RhS-Im**, the spin density is localized at the alkene carbons (**Figure 71**), consistent with the observed reactivity towards [2+2] cycloadditions. This should also lead to configurational lability of the alkene, which accounting for the observed *E* → *Z* isomerization (**Figure**

68c). Besides, the triplet energy of coordinated substrate is not significantly lower than the free substrate, which is different from Yoon's report¹¹ in which a great decrease of triplet energy after Lewis acid binding (lowering by 88 kJ/mol) is the key for high stereochemical induction.

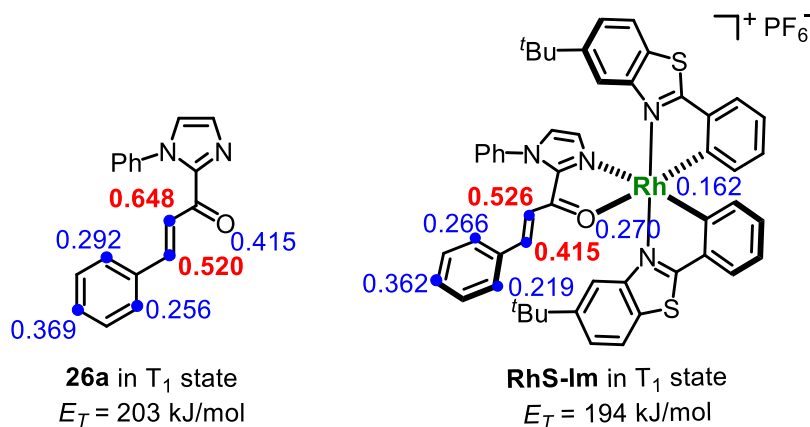


Figure 71. Calculated spin density distribution and triplet energy of the excited **26a** and **RhS-Im**.

6) Quantum yield measurement

It has long been known that Lewis acids can alter the course of photocycloaddition reactions, and in particular increase the quantum yield by more than 10 folds.^{8d} To examine the effect of chiral-at-rhodium catalyst, the model reaction **26a** + **27a** \rightarrow **28a** was chosen to determine the quantum yield under open air conditions. As a result, a quantum yield of 0.27 was observed, highlighting the high efficiency of this photoreaction enabled by the chiral-at-rhodium Lewis acid.

7) Proposed mechanism

Supported by the above experiments, a proposed mechanism is depicted in **Figure 72**. Initially, α,β -unsaturated carbonyl compound coordinates to the rhodium catalyst via an established *N,O*-chelate (intermediate **I**) and then is excited by visible light to its lowest singlet state (S_1 , intermediate **II**). After intersystem crossing (ISC), the excited triplet state (T_1 , intermediate **III**) reacts directly with alkene co-substrate under control of the stereochemistry by the metal-centered chirality, generating the rhodium-bound 1,4-diradical intermediate **IV**. After ISC and cyclization, the Rh-coordinated [2+2] cycloaddition product (intermediate **V**) is formed. A subsequent release of product and re-coordination of unreacted substrate then closes the catalytic cycle. It is worth pointing out that this mechanism scheme is distinctive from previous reports on the photocycloadditions of electronically excited states (**Figure 59**). A single chiral-at-metal rhodium catalyst bound substrate enables the direct

visible-light-excitation with greatly enhanced absorption, and the bond formation occurs directly at the excited states. As the result, this mild and simple reaction system provides a robust [2+2] photocycloaddition with broad substrate scope and excellent asymmetric induction.

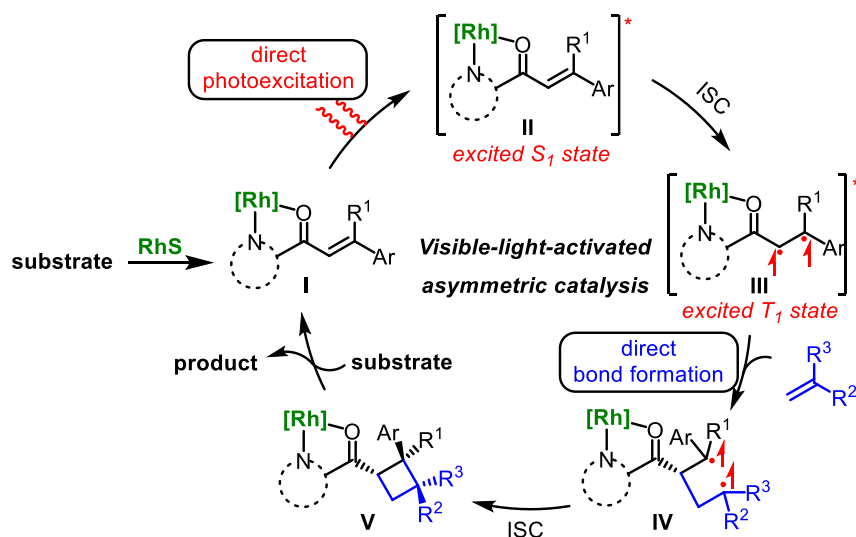


Figure 72. Proposed mechanism of the [2+2] photocycloaddition.

3.3.5 Conclusions

In conclusion, this chapter introduced the development of a previously elusive reaction scheme where a substrate-coordinated chiral Lewis acid is activated by visible light to catalyze a highly stereoselective [2+2] cycloaddition reaction, thus acting both as the visible light harvesting antenna to convert a coordinated substrate into its excited triplet state and, at the same time, serving as the chiral entity to achieve an excellent asymmetric induction.²³ The enhancement of the intrinsic blue light absorption by Lewis acid coordination ensures the selective direct visible-light-excitation, thereby accounting for the extremely high asymmetric induction.

From a synthetic perspective, the rhodium-catalyzed visible-light activated [2+2] cycloaddition is synthetically highly attractive. Based on a simple reaction setup and a single chiral catalyst with low loading (down to 0.5 mol%), complex cyclobutanes can be accessed with excellent diastereo- and enantioselectivities, including cyclobutanes with vicinal all-carbon quaternary stereocenters. The reaction is very robust, tolerating air and water, and displays little solvent dependence, thus providing a large flexibility in adjusting reaction conditions.

This work was highlighted in *Science* **2017**, 357, 265 and *Synfacts*, **2017**, 1061, respectively. Further investigations on photophysical properties of the key rhodium/substrate complexes and computational studies to understand the mechanism are ongoing. It is anticipated that this reaction design will spur more asymmetric photochemistry through stereocontrolled reactions of photoexcited substrate/catalyst complexes.

References

- 1 Z. Zhou, Y. Li, B. Han, L. Gong, E. Meggers, *Chem. Sci.* **2017**, 8, 5757-5763.
- 2 Indeed, after this work was published, a similar energy transfer mechanism was disclosed for the visible-light-activated [2+2] photodimerization of chalcones, see: T. Lei, C. Zhou, M.-Y. Huang, L.-M. Zhao, B. Yang, C. Ye, H. Xiao, Q.-Y. Meng, V. Ramamurthy, C.-H. Tung, L.-Z. Wu, *Angew. Chem. Int. Ed.* **2017**, 56, 15407-15410.
- 3 E. Meggers, *Chem. Commun.* **2015**, 51, 3290-3301.
- 4 C. K. Prier, D. A. Rankic, D. W. C. MacMillan, *Chem. Rev.* **2013**, 113, 5322-5363.
- 5 M. P. Sibi, S. Manyem, J. Zimmerman, *Chem. Rev.* **2003**, 103, 3263-3296.
- 6 A. Albini, *Synthesis* **1981**, 249-264.
- 7 For selected racemic transformations involving photosensitization, see a) Z. Lu, T. P. Yoon, *Angew. Chem. Int. Ed.* **2012**, 51, 10329-10332; b) E. Arceo, E. Montroni, P. Melchiorre, *Angew. Chem. Int. Ed.* **2014**, 53, 12064-12068; c) X.-D. Xia, J. Xuan, Q. Wang, L.-Q. Lu, J.-R. Chen, W.-J. Xiao, *Adv. Synth. Catal.* **2014**, 356, 2807-2812; d) E. R. Welin, C. Le, D. M. Arias-Rotondo, J. K. McCusker, D. W. C. MacMillan, *Science* **2017**, 355, 380-385.
- 8 a) H. Guo, E. Herdtweck, T. Bach, *Angew. Chem. Int. Ed.* **2010**, 49, 7782-7785; b) R. Brimioulle, T. Bach, *Science* **2013**, 342, 840-843; c) R. Brimioulle, T. Bach, *Angew. Chem. Int. Ed.* **2014**, 53, 12921-12924; d) R. Brimioulle, A. Bauer, T. Bach, *J. Am. Chem. Soc.* **2015**, 137, 5170-5176.
- 9 a) M. M. Maturi, T. Bach, *Angew. Chem. Int. Ed.* **2014**, 53, 7661-7664; b) A. Tröster, R. Alonso, A. Bauer, T. Bach, *J. Am. Chem. Soc.* **2016**, 138, 7808-7811.
- 10 S. Poplata, A. Tröster, Y.-Q. Zou, T. Bach, *Chem. Rev.* **2016**, 116, 9748-9815.
- 11 T. R. Blum, Z. D. Miller, D. M. Bates, I. A. Guzei, T. P. Yoon, *Science* **2016**, 354, 1391-1395.

- 12 M. N. Hopkinson, B. Sahoo, J.-L. Li, F. Glorius, *Chem. Eur. J.* **2014**, *20*, 3874-3886.
- 13 K. W. Quasdorf, L. E. Overman, *Nature* **2014**, *516*, 181-191.
- 14 Y. Xu, M. L. Conner, M. K. Brown, *Angew. Chem. Int. Ed.* **2015**, *54*, 11918-11928.
- 15 H. Huo, K. Harms, E. Meggers, *J. Am. Chem. Soc.* **2016**, *138*, 6936-6939.
- 16 a) N. P. Schepp, L. J. Johnston, *J. Am. Chem. Soc.* **1996**, *118*, 2872-2881; b) H. Senboku, H. Komatsu, Y. Fujimura, M. Tokuda, *Synlett* **2001**, 418-420.
- 17 J. B. Metternich, R. Gilmour, *J. Am. Chem. Soc.* **2015**, *137*, 11254-11257.
- 18 M. C. Carreño, M. González-López, A. Urbano, *Angew. Chem. Int. Ed.* **2006**, *45*, 2737-2741.
- 19 Y. Lion, M. Delmelle, A. Van De Vorst, *Nature* **1976**, *263*, 442-443.
20. a) R. Bonneau, *J. Am. Chem. Soc.* **1980**, *102*, 3816-3822; b) D. I. Schuster, D. A. Dunn, G. E. Heibel, P. B. Brown, J. M. Rao, J. Woning, R. Bonneau, *J. Am. Chem. Soc.* **1991**, *113*, 6245-6255.
21. D. I. Schuster, G. E. Heibel, P. B. Brown, N. J. Turro, C. V. Kumar, *J. Am. Chem. Soc.* **1988**, *110*, 8261-8263.
22. M. Quaranta, M. Murkovic, I. Klimant, I. Analyst **2013**, *138*, 6243-6245.
- 23 X. Huang, T. R. Quinn, K. Harms, R. D. Webster, L. Zhang, O. Wiest, E. Meggers, *J. Am. Chem. Soc.* **2017**, *139*, 9120-9123.

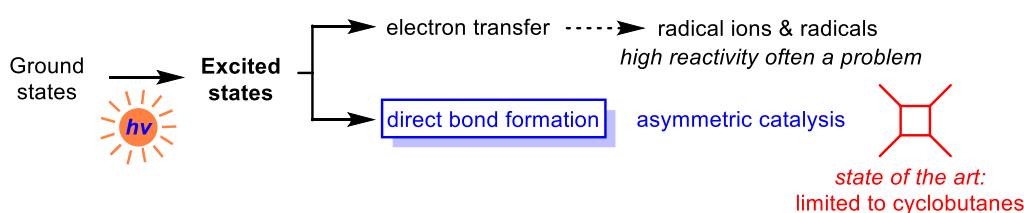
3.4 Catalytic Asymmetric Synthesis of 1-Pyrroline through Stereocontrolled Direct [2+3] Photocycloaddition from Excited State

3.4.1 Research Background and Reaction Design

The induction or activation of chemical reactions by visible light is an extremely valuable tool for synthetic organic chemistry.¹ Typically, photochemically excited species engage in single electron transfer with a substrate or reagent to generate radical ions and/or free radicals which then participate in a multitude of reaction schemes (**Figure 73a**).² However, reactions through radical ions and free radicals have severe drawbacks. For example, radical ions are extremely sensitive to solvent effects placing restriction to the reaction parameters, whereas the high reactivity of free radicals renders a control of their reaction pathway challenging, especially with respect to stereocontrol, and often leads to a narrow substrate scope.³ A highly attractive alternative constitute therefore bond forming reactions that occur directly from a photoexcited state without prior charge transfer to circumvent the mentioned disadvantages arising from intermediate free radicals and radical ions (**Figure 73a**).⁴ Due to the demand of optically pure compounds in the chemical and pharmaceutical industry, catalytic stereocontrolled reactions are of particular interest. Unfortunately, currently available methods for catalytic asymmetric reactions that occur from a photochemically excited state without any intermediate charge separation are limited to [2+2] photocycloadditions.^{5,6} This is probably owing to the lack of suitable, robust catalysts to enable new reaction patterns to intercept short-lived excited states and at the same time to provide efficient stereochemical induction.

Chapter 3.3 discloses a single rhodium catalyst based unique and versatile reaction system that enables the direct bond formation of the electronically excited state of catalyst/substrate complex, providing a practical synthetic route to enantioenriched cyclobutanes.⁷ However, this work and related reports from other groups⁶ did not address the prevalent restriction to cyclobutanes as structural motifs for such stereocontrolled bond forming reactions out of a photoexcited state. Although cyclobutanes built through [2+2] photocycloadditions are present in natural products, a direct access to other attractive structural motifs, by direct stereocontrolled reactions from photoexcited states would be highly desirable and furnish new powerful synthetic methodology.

a) Reactivity of photoexcited states



b) Hypothesis to access new structural motifs

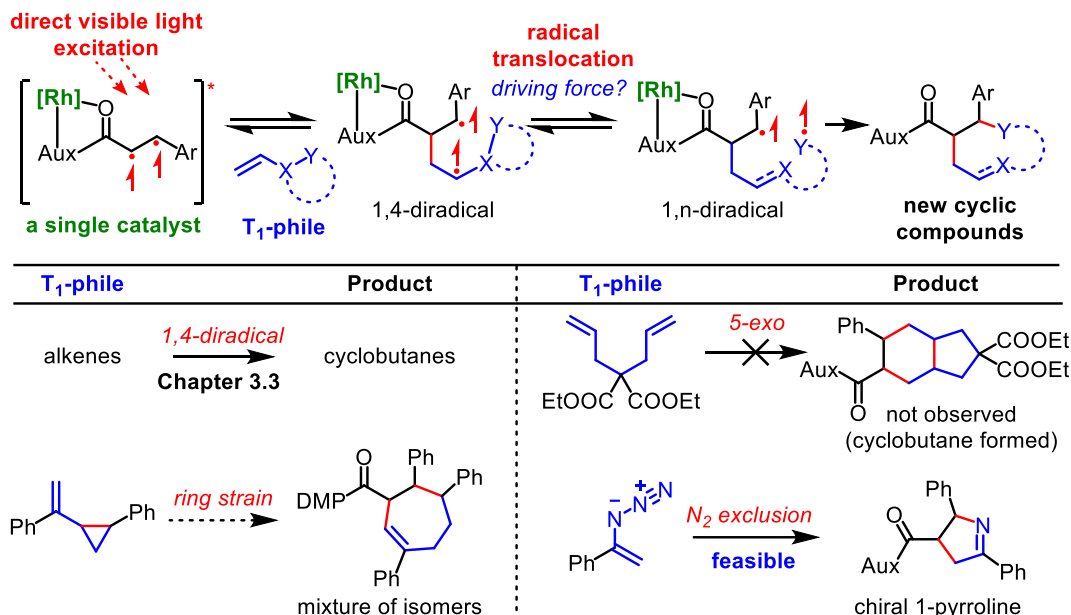


Figure 73. Chemistry of the photochemically excited states and effort to access new structural motifs by interference with the excited rhodium/substrate complex.

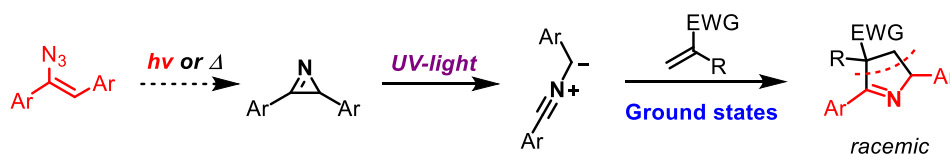
To explore new reaction manifolds of photoexcited molecules, several aspects need to be considered: 1) Since the first bond forming step might be reversible, a fast follow-up transformation or a stabilized 1,4-diradical species is required. 2) To avoid the ring closing of 1,4-diradical that would lead to the formation of previously reported cyclobutanes, a driving force is needed for the radical translocation process generating 1,n-diradical, which could result in new cyclic compound (**Figure 73b**). With these aspects in mind, several triplet-state-philes (T_1 -philes) were tested. For example, a cyclopropyl olefin could participate in the photocycloadditions, but a mixture of unidentified isomers including the desired 7-membered cyclic molecule was obtained. And a 1,6-diene, which was designed to undergo a 5-exo radical cyclization to give a bicyclic product, preferred [2+2] photocycloaddition delivering cyclobutane as major product. Finally, driven by the release of N_2 , a vinyl azide succeeded in trapping the triplet state as well as the subsequent rearrangement and ring closure processes, leading to a previously elusive structural motif, 1-pyrroline.

1-Pyrrolines are widely found in biologically active molecules such as natural products and drugs, and constitute versatile synthetic intermediates by conversion to functionalized pyrrolidines.⁸ Catalytic asymmetric methods to directly access this important heterocycle are little developed and limited to a few reports including the partial hydrogenation of pyrroles⁹, 1,3-cycloadditions of azlactones¹⁰ or α -isocyano esters¹¹ with acceptor-substituted alkenes, and some other addition/cyclization protocols.¹²

On the other hand, vinyl azides are well-known to act as nucleophiles,¹³ radical acceptors¹⁴ or triplet energy acceptors,¹⁵ but their ability to directly undergo cycloaddition with photoexcited alkenes has not been reported. In contrast, the reported photochemical reactivity of vinyl azide might do harm to the desired transformation. As reported by Padwa *et al.* in pioneering work,¹⁶ the photolysis of vinyl azides led to aryl azirines could form nitrile ylides and be subsequently trapped by ground state electron-deficient alkenes to afford racemic 1-pyrrolines with a constitution that differs from desired product from excited state chemistry (**Figure 74a**).

This chapter reports a direct [2+3] photocycloaddition of photoexcited acceptor substituted alkenes with vinyl azides in a catalytic and asymmetric fashion toward the synthesis of non-racemic chiral 1-pyrrolines with virtually perfect diastereoselectivity and enantioselectivities of up to >99% ee. (**Figure 74b**). This novel reaction discloses new reactivity of vinyl azide towards the direct bond formation reaction with excited states, and expands the scope of the electronically excited state chemistry by constructing previously inaccessible enantioenriched 1-pyrrolines.

a) Previous photoreaction of vinyl azide (ground state 1,3-dipolar cycloaddition)



b) This work: unprecedented reaction with photoexcited state

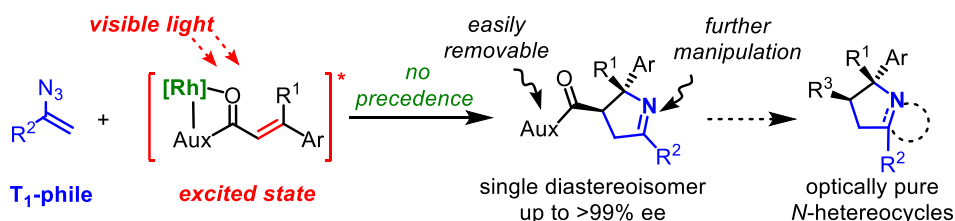
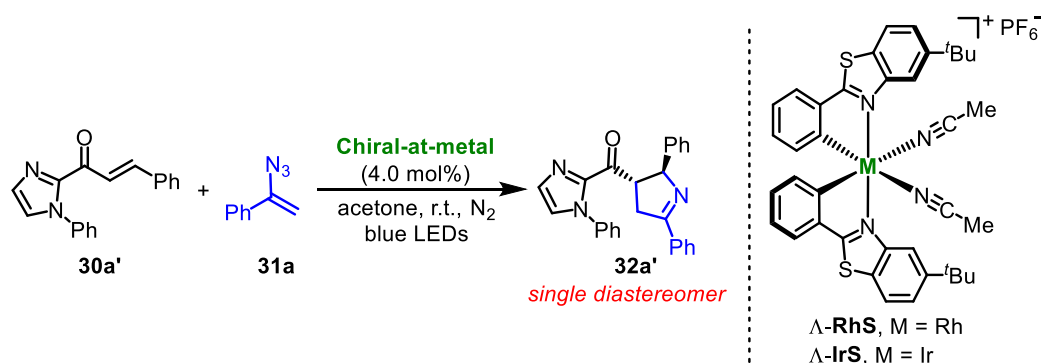


Figure 74. New chemistry of photochemically excited state and new access to chiral *N*-heterocycles provided by exploring unprecedented reactivity of vinyl azides.

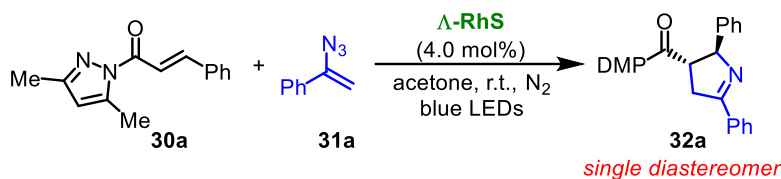
3.4.2 Reaction Development

Table 14. [2+3] Photocycloaddition with an α,β -unsaturated 2-acyl imidazole.^[a]

Entry	Catalyst	31a [equiv]	Variations	Yield [%]	Ee [%]
1	Λ - RhS	3.0	None	41	49
2	Λ - IrS	3.0	None	76	0
3	None	3.0	None	60	0
4	Λ - RhS	3.0	Dark	0	n.a.
5	Λ - RhS	3.0	CH_2Cl_2 instead of acetone	30	64
6	Λ - RhS	1.5	CH_2Cl_2 instead of acetone	26	72
7	Λ - RhS	1.25	CH_2Cl_2 instead of acetone	24	74

[a] Reaction conditions: **30a'** (0.10 mmol), **31a**, and chiral catalyst (4.0 mol%) in acetone (0.2 M, 0.5 mL) were stirred at room temperature under N_2 atmosphere with irradiation of blue LEDs (24 W) for 16 h; NMR yield; ee was determined by HPLC on a chiral stationary phase.

Based on the previously introduced [2+2] photocycloadditions,⁷ this work commenced with the reaction of β -phenyl α,β -unsaturated 2-acyl imidazole **30a'** with vinyl azide **31a** catalyzed by a single chiral bis-cyclometalated rhodium complex Λ -**RhS**. Gratifyingly, the expected 1-pyrroline **32a'** formed as a single diastereoisomer, albeit in only 41% yield with an unsatisfactory enantioselectivity of 49% ee (**Table 14**, entry 1). Similar to the reported [2+2] photocycloaddition, the iridium congener Λ -**IrS** could not give any enantioselectivity and light excitation is essential for the transformation (entries 2,4). Surprisingly, a significant uncatalyzed background reaction is observed with the formation of racemic product in 60% yield (entry 3), which might contribute to the low ee obtained for **32a'**. In addition, preliminary screening indicated that the amount of vinyl azide and the solvent have important effect on the reaction outcome (entries 5-7).

Table 15. [2+3] Photocycloaddition with an α,β -unsaturated *N*-acyl pyrazole.^[a]

Entry	Δ -RhS	31a [equiv]	Variations	Yield [%]	Ee [%]
1	4 mol%	3.0	None	63	49
2	None	3.0	None	<5	n.a.
3	4 mol%	3.0	MeCN instead of acetone	80	6
4	4 mol%	3.0	THF, DMSO or PhCl as sol.	<50	<44
5	4 mol%	3.0	CH ₂ Cl ₂ instead of acetone	28	73
6	4 mol%	1.5	CH ₂ Cl ₂ instead of acetone	27	91
7	8 mol%	1.25	CH ₂ Cl ₂ instead of acetone	34	93
8	8 mol%	1.25	None	54	86

[a] Reaction conditions: **30a** (0.10 mmol), **31a**, and Δ -RhS in acetone (0.2 M, 0.5 mL) were stirred at room temperature under N_2 atmosphere with irradiation of blue LEDs (24 W) for 16 h; NMR yield; ee was determined by HPLC on a chiral stationary phase.

Next, a *N*-acyl pyrazole **30a** was chosen for further optimization because it has almost no background reaction due to its much weaker absorption in near UV/Visible light region (**Figure 66**). As listed in **Table 15**, screening of various solvents led to a higher ee of 73% when CH₂Cl₂ was used (entry 5). While MeCN was employed, the reaction proceeded in 80% yield but only with 6% ee (entry 3). Importantly, decreasing the equivalence of vinyl azide **31a** to 1.25 equiv resulted in the formation of 1-pyrroline **32a** in 93% ee, albeit with 34% yield (entry 7). This implied that this new visible-light-activated [2+3] cycloaddition is more complicated than the previously developed [2+2] photocycloaddition which is very insensitive to reaction conditions. In addition, a higher yield of 54% could be obtained for **32a** by using acetone as solvent, however, with the compromise of enantioselectivity (86% ee, entry 8). All these results indicated that ligand exchange might be a limiting step, especially considering the potential product inhibition on catalyst.

Table 16. Effect of auxiliary and solvent on the [2+3] photocycloaddition.^[a]

Entry	Cat. [mol%]	30	Variations	Yield [%]	Ee [%]
1	Λ -RhS (8)	30a	None	32a , 54	86
2	Λ -RhS (8)	30b	None	32b , 75	72
3	Λ -RhS (8)	30c	None	32c , 83	87
4	Λ -RhS (8)	30c	CH ₂ Cl ₂ (0.2 M) as solvent	32c , 55	84
5	Λ -RhS (8)	30c	CDCl ₃ (0.2 M) as sol.	32c , 93	92
6	Λ -RhS (8)	30c	CDCl ₃ (0.1 M) as sol.	32c , 98	95
7	Λ -RhS (4)	30c	CDCl ₃ (0.1 M) as sol.	32c , 80	92
8	Λ -RhS (4)	30d	CDCl ₃ (0.1 M) as sol.	32d , 82	92
9	Λ -RhS (4)	30e	CDCl ₃ (0.1 M) as sol.	32e , 80	92
10	Λ -RhS (4)	30f	CDCl ₃ (0.1 M) as sol.	32f , 92 (90)	94
11	Λ -RhS (4)	30f	CHCl ₃ (0.1 M) as sol.	32f , 90	94
12	Λ -RhS (4)	30f	CDCl ₃ (0.1 M) as sol., open air	32f , 90	94
13	Λ -IrS (4)	30f	CDCl ₃ (0.1 M) as sol., open air	32f , 50	0
14	None	30f	CDCl ₃ (0.1 M) as sol., open air	32f , 7	n.a.
15	Λ -RhS (4)	30f	CDCl ₃ (0.1 M), air, dark	32f , 0	n.a.

[a] Reaction conditions: **30** (0.10 mmol), **31a** (0.125 mmol), and chiral catalyst in acetone (0.2 M, 0.5 mL) were stirred at room temperature under N₂ atmosphere with irradiation of blue LEDs (24 W) for 16 h; NMR yield, isolated yield is provided in parentheses; ee was determined by HPLC on a chiral stationary phase.

Based on these results, pyrazoles with different substitution patterns were tested (**Table 16**). While a methyl group at the 5-position (R²) was not good for the yield (entry 1), a single phenyl substituent at the 3-position (R¹) of the pyrazole produced 1-pyrroline **32c** with an increased yield of 83% with 87% ee (entry 3). Optimization of solvent and concentration led to an improved outcome of **32c** with 98% yield and 95% ee in CDCl₃ under more diluted conditions (entries 3-6). In order to reduce the catalyst loading, the effect of other auxiliary was evaluated (entries 7-10). As a result, 3-(4-methoxyphenyl) pyrazole provided the best choice for the present [2+3] photocycloaddition,

allowing to reduce the catalyst loading to 4 mol%, and delivering desired product **32f** in 92% yield with 94% ee (entry 10). No differences were found between CDCl₃, which was used to conveniently determine NMR yields, and CHCl₃ (entry 11). Importantly, this simple and mild protocol could be conducted under air without the need for inert conditions, which renders it very practical (entry 12). It is noteworthy that the iridium analogue Λ -**IrS** also provided the 1-pyrroline **3f** (50% yield) albeit without any enantioselectivity (entry 13). Control experiments demonstrated that the current transformation relies both on rhodium catalyst (entry 14) and visible light (entry 15).

Overall, optimal results for the asymmetric [2+3] photocycloaddition with vinyl azide were obtained by using a single chiral-at-rhodium catalyst (4.0 mol%) and 3-PMP pyrazole as auxiliary under simple open air conditions (**Table 16**, entry 12).

3.4.3 Mechanistic Studies

1) Proposed catalytic cycle

The proposed mechanism for this [2+3] photocycloaddition is shown in **Figure 75**. The coordination of substrate **30** to the chiral rhodium catalyst generates the substrate/catalyst complex **I**, which upon visible light excitation generates the excited state **I***, most likely in its triplet excited state. The following direct reaction of the excited state **I*** with the vinyl azide co-substrate **31** affords the catalyst bound diradical intermediate **II** under generation of a new C-C bond. The stereochemistry of this bond formation is controlled by the metal-centered chirality of the rhodium complex. Subsequent extrusion of dinitrogen delivers the catalyst bound iminyl radical intermediate **III**,¹⁷ which then undergoes a stereospecific cyclization generating the product coordinated complex **IV**. Release of product from the rhodium catalyst and coordination of new substrate **30** then initiates a new catalytic cycle. Since the reaction is insensitive to air, it can be assumed that the diradical intermediates **II** and **III** are very short-lived and thus cannot engage in other side reactions. This reveals the advantages of such direct bond forming reactions from a photoexcited state over processes that occur through initial electron transfer. This mechanism is based on previous [2+2] photocycloaddition and further supported by a series of experiments shown below.

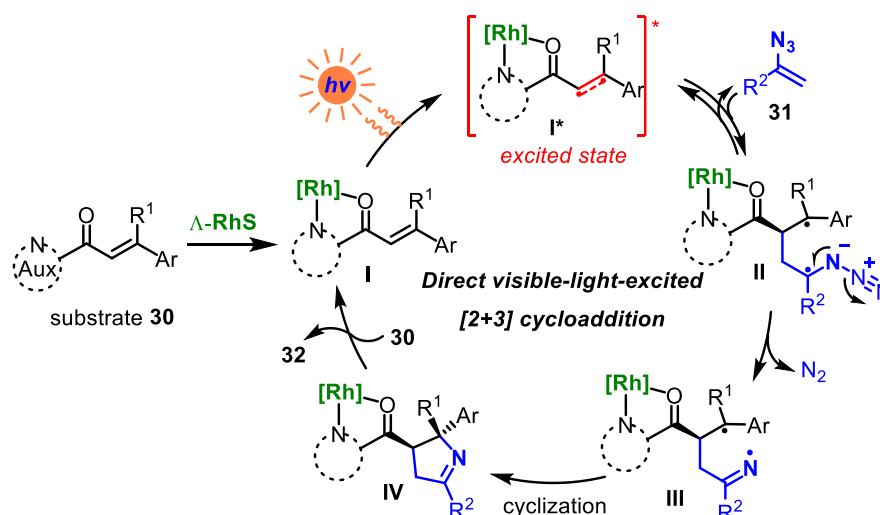


Figure 75. Proposed mechanism of the [2+3] photocycloaddition.

2) Identification of the key catalyst/substrate intermediate

The proposed formation of intermediate **I** in **Figure 75** is confirmed by a crystal structure of the pyrazole substrate **30f** bound racemic catalyst **RhS** complex (**RhS-PPz**), as shown in **Figure 76**. Interestingly, it further reveals a π - π stacking between the cyclometalating benzothiazole moiety of the rhodium catalyst and the *p*-methoxyphenyl moiety of the pyrazole auxiliary which might explain the superiority of this auxiliary by modulating binding constant, steric and/or electronic effects.¹⁸

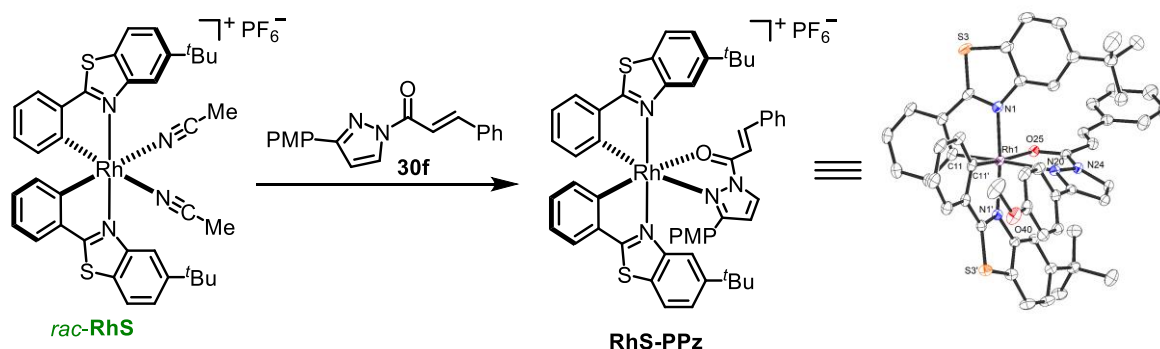


Figure 76. Synthesis and a crystal structure of the key rhodium/substrate intermediate **RhS-PPz**.

3) UV/Vis absorption spectra

UV-Vis absorption spectra in **Figure 77** show that free substrate **30f** has a weak absorption in the visible light region, thereby accounting for the background racemic reaction without catalyst (**Table 16**, entry 14). Notably, the visible light absorption of substrate **30f** is greatly enhanced upon binding to

the rhodium catalyst (**RhS-PPz**). Therefore, in the reaction mixture the intermediate **I** is selectively photoexcited to generate the photoexcited intermediate **I*** from which the direct bond formation with vinyl azide occurs. This is crucial in order to suppress any background reaction resulting from the photoactivation of the free α,β -unsaturated *N*-acyl pyrazole substrate, which would otherwise deteriorate the overall enantioselectivity.

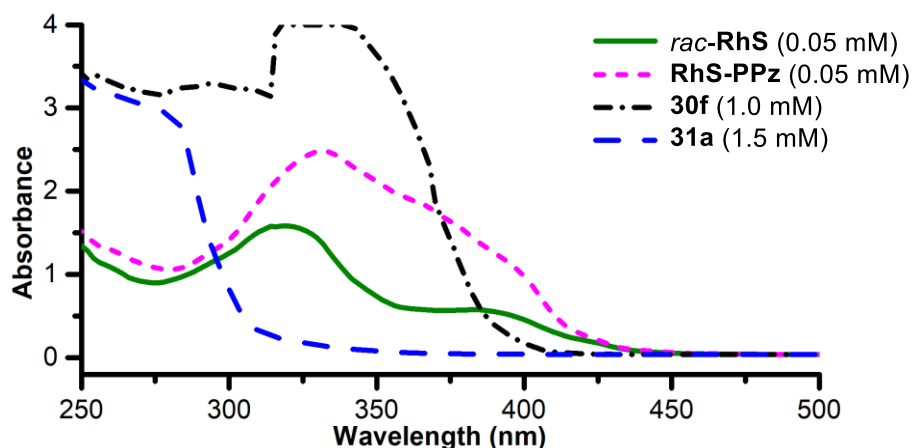


Figure 77. UV/Vis absorption spectra obtained in the study of the [2+3] photocycloaddition.

Interestingly, although appearing as a yellow liquid, vinyl azide **31a** does not absorb visible light significantly. But according to literature report, vinyl azide is supposed to be activated through energy transfer, which would lead to the generation of 2*H*-azirine **33**, a side product that was observed during the condition optimization process. But under optimal conditions, no undesired photoinduced rearrangement to 2*H*-azirine **33** was detected, which means that the excited intermediate **I*** bearing the optimized auxiliary apparently undergoes a direct cycloaddition instead of triplet energy transfer to the vinyl azide co-substrate.

In addition, the possibility of such azirines acting as viable intermediates in this catalytic cycle is ruled out since independently synthesized 2*H*-azirine **33** was demonstrated to not react with **30f** in the presence of **RhS** and visible light (**Figure 78a**). Furthermore, the quantum yield for the reaction **30f** + **31a** \rightarrow **32f** was determined as $\Phi = 0.19$, supporting the proposal that the photoreaction does not involve a chain process and instead at least one single photon is required for each formed product molecule (**Figure 78b**).

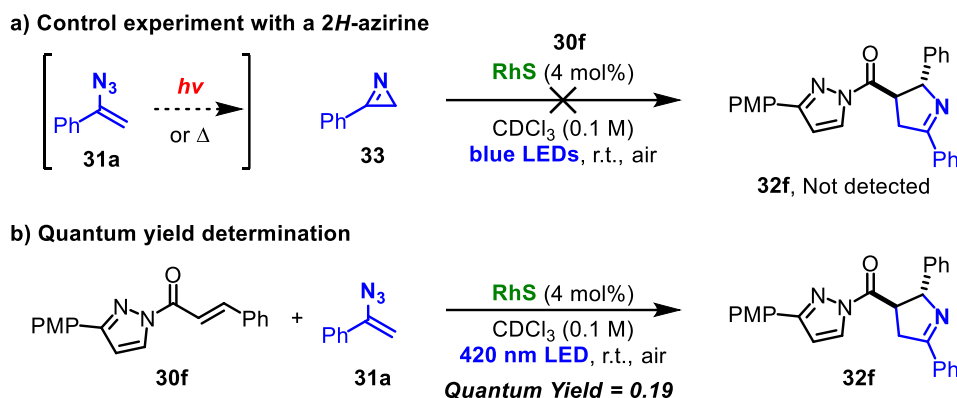


Figure 78. Control experiment with 2*H*-azirine and quantum yield measurement.

4) A computational study to interpret the results obtained with IrS as the catalyst

A remaining problem was why the iridium congener **IrS** could not provide any enantioselectivity in both [2+2] and [2+3] photocycloadditions. In sharp contrast to the chiral-at-rhodium complex, the analogue chiral **IrS** performed like a racemic photosensitizer, such as benzil, in the aspects of yield, diastereoselectivities and enantioselectivity (**Table 13**). Although, **IrS** is known to have slower ligand exchange kinetics than **RhS**,¹⁹ which is further supported by calculations (**Figure 79**), this should give products in lower ee rather than racemic product.

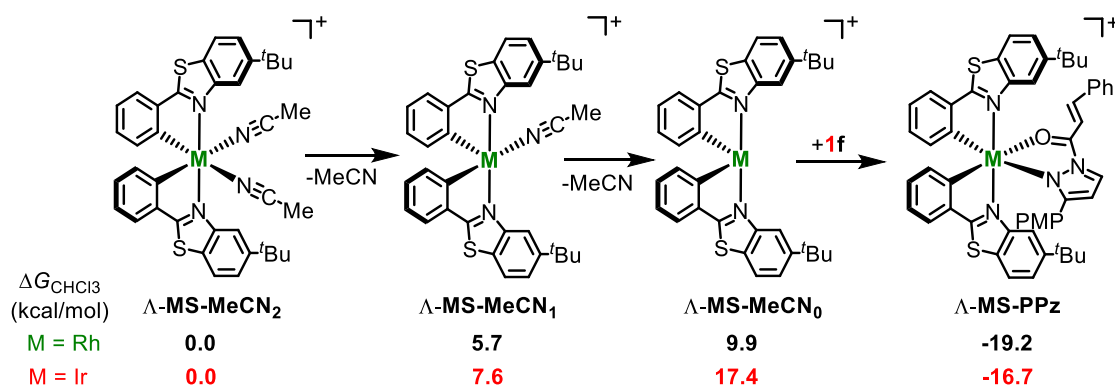


Figure 79. Calculated energy profiles for ligand exchanges with **RhS** and **IrS**.

To address this issue, a computational study on triplet energy and spin distribution of excited **RhS-PPz** and **IrS-PPz** was conducted. As a result, these two excited complexes have an identical triplet energy, but differ significantly in spin density distribution. As shown in **Figure 80**, most of the spin density in the triplet state of **RhS-PPz** is mainly localized at the alkene carbons of the coordinated substrate, at which position the chemoselective cycloaddition occurs, whereas in the triplet state of

IrS-PPz the iridium center possesses the majority of the spin density. This distinct difference in the nature of the excited state might account for the reactivity differences. Photoexcited **IrS-PPz** is not capable of undergoing a direct reaction with vinyl azides but instead serves as a photosensitizer to transfer its triplet energy to free substrate, and thereby leading to the formation of racemic photocycloaddition products.

It is noteworthy that these calculations were done by Xinyao from Peking University. Further investigations on photophysical properties and excited state properties of catalyst/substrate complexes are ongoing in collaboration with the Paola Ceroni group and Mu-Hyun Baik's group.

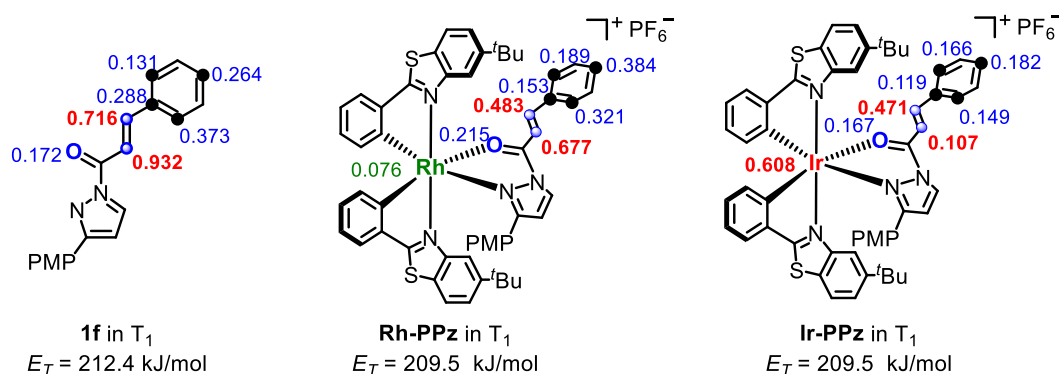


Figure 80. Calculated spin distribution and energy of the excited triplet states of **30f**, **RhS-PPz**, and **IrS-PPz**.

5) Interceptions for some of the reaction outcomes

The current [2+3] photocycloaddition is more sensitive to reaction conditions, such as solvent, the amount of vinyl azide, and different auxiliaries, when compared with the [2+2] photocycloaddition introduced in chapter 3.3. An additional N_2 exclusion/radical translocation is involved in this [2+3] cycloaddition. If this additional step is not effective enough, the initial C-C bond is just cleaved and the starting materials form back fast, which could lead to low yield. Furthermore, other pathways might influence the stereoselectivity of the target reaction. (**Figure 81**). For example, the excited rhodium complexes could transfer energy to free substrate, leading to formation of racemic product. This could explain the obtained low ee for the reaction of dimethyl pyrazole substrate **30a**. Although **30a** has no uncatalyzed background reaction (**Table 15**), the methyl group at the 5-position of the pyrazole provides steric hindrance, which might slow down the first bond forming thus accounting for the low yield and ee. Besides, in the presence of excess amount of vinyl azide, the reaction with

excited free substrate competes with the Lewis acid accelerated desired pathway, thus resulting in inferior enantioselectivity. Furthermore, product bound rhodium complex could also act as sensitizer, transferring energy to the free substrate and inhibit the desired transformation. Therefore, careful optimization of reaction conditions with the choice of a suitable auxiliary is very important for this [2+3] photocycloaddition.

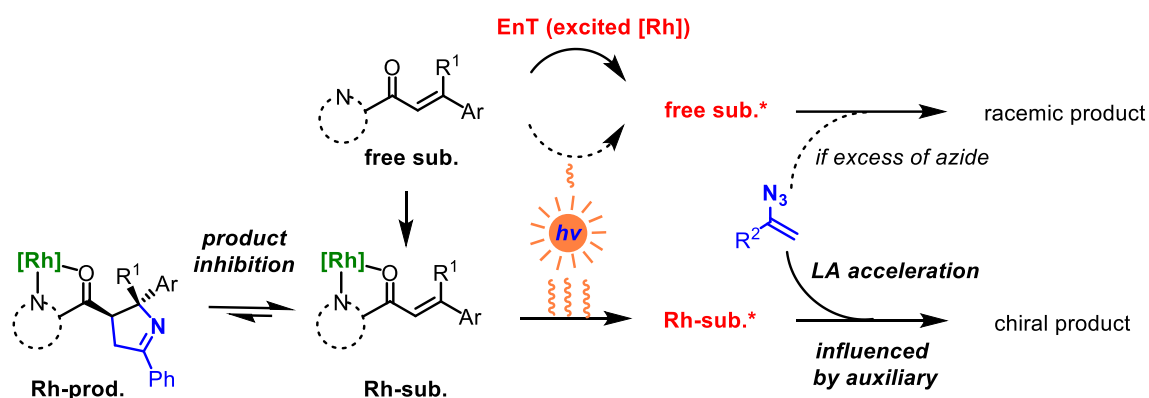


Figure 81. Hypothesis to explain the factors that affect the outcome of the [2+3] photocycloaddition.

3.4.4 Substrate Scope and Synthetic Applications

With the mechanistic picture in mind, the generality of the single chiral rhodium catalyst enabled [2+3] photocycloaddition was evaluated using 3-(4-methoxyphenyl)pyrazole as the auxiliary. As shown in **Figure 82**, different patterns of substitution at the β -aryl moiety of *N*-acyl pyrazoles **30** were well tolerated, regardless of electronic nature (**32g-l**) or position (**32g**, **32m-n**) of the substituents. Heteroaryl frameworks were proved to be compatible as demonstrated by the effective formation of thienyl- and indolyl- substituted 1-pyrrolines (**32o-p**). Notably, this protocol is amenable to the construction of complex 1-pyrrolines bearing a quaternary stereocenter (**32q-s**) reflecting the robustness of this single rhodium catalysis. In particular, enantioenriched 1-pyrroline **32s** containing a spiro center could be built in excellent yield (94%) with almost complete enantioselectivity of >99% ee. Additionally, α,β -unsaturated *N*-acyl pyrazoles (*E*)-**30q** and (*Z*)-**30q** gave the product **32q** in similar yields with identical stereochemistry as an indicator for the involvement of the diradical intermediates **II/III**, which also makes the protocol more practical since the preparation of starting materials could be easier without the concern of *E/Z* isomers. To be mentioned, electron rich aryl

substituted *N*-acyl pyrazole work better than electron deficient one as indicated by the comparison between **32q** and **32r**.

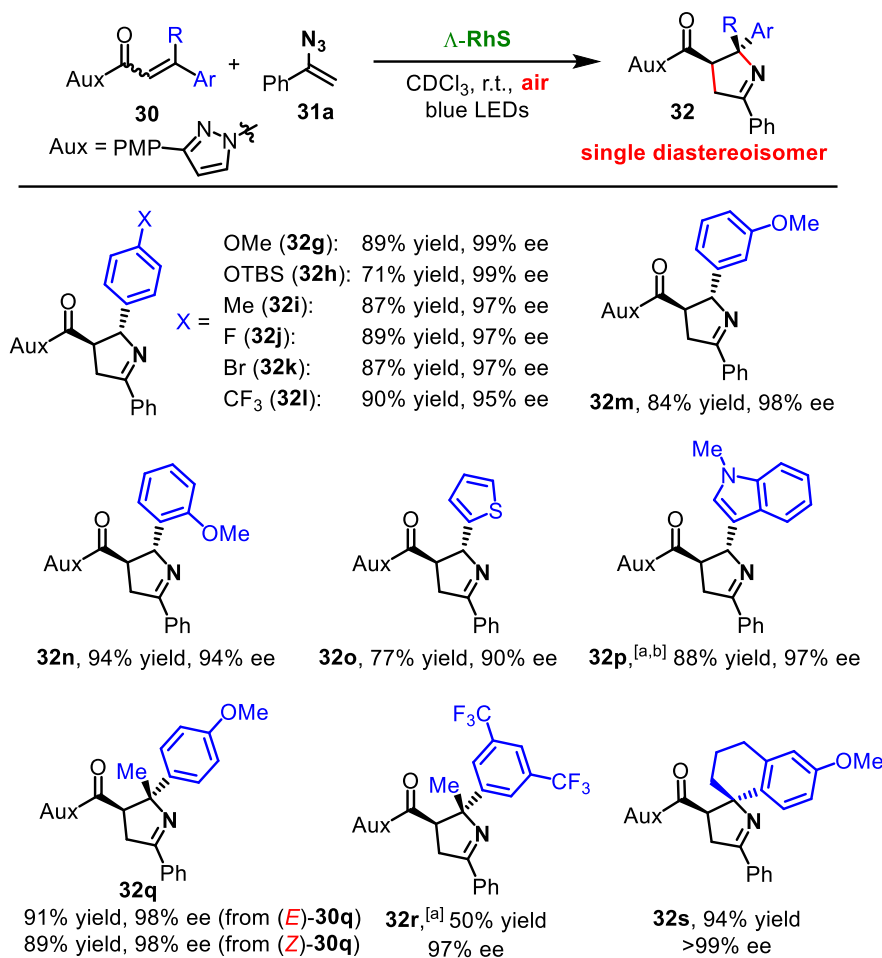


Figure 82. Substrate scope of the [2+3] photocycloaddition with respect to *N*-acyl pyrazole. Reaction conditions: see **Table 16** entry 12. [a] 8.0 mol% of Δ -RhS under nitrogen atmosphere. [b] CDCl₃ (2.0 mL). The relative and absolute configuration of 1-pyrrolines was unambiguously assigned by the crystal structure of **32k**.

Gratifyingly, various functionalized vinyl azides were readily accommodated (**Figure 83**), including not only aryl vinyl azides (**32ft-x**) but also more challenging alkyl vinyl azides (**32z-ab**). Although vinyl azides bearing an electron rich substitution at the phenyl group gave a decreased ee value (**32t**, 90% ee), the reaction outcome was not influenced by steric hindrance (**32v-x**). Furthermore, a free hydroxyl group (**32aa**) as well as C=C double bonds (**32ab**) were tolerated, thereby highlighting the good functional group compatibility of the current protocol. To be mentioned, for some cases, performing the reaction under nitrogen atmosphere with an increased catalyst loading (8.0 mol%) is

beneficial for reaction efficiency (for examples, see **32p**, **32t**, and **32ab**).

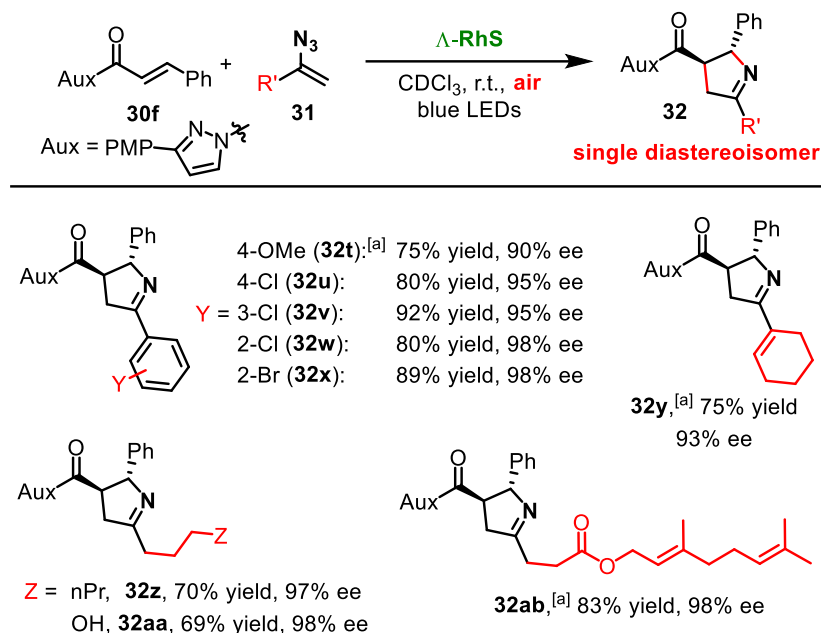


Figure 83. Substrate scope of the [2+3] photocycloaddition with respect to vinyl azide. Reaction conditions: see Table 16 entry 12. [a] 8.0 mol% of Δ -RhS under nitrogen atmosphere.

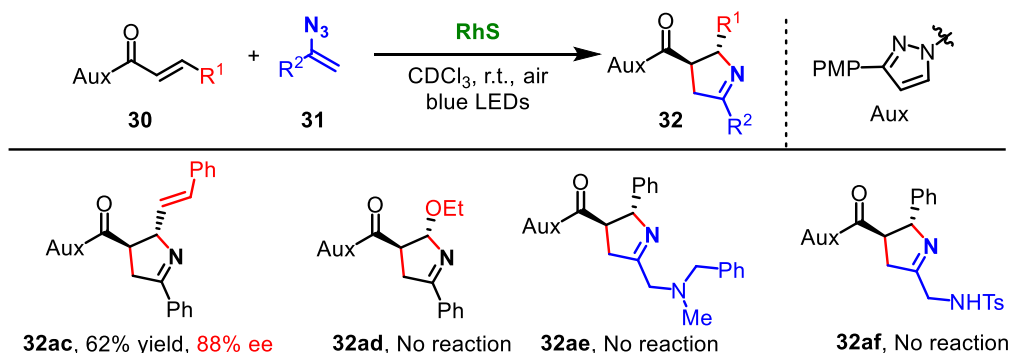


Figure 84. Scope limitations of the present [2+3] photocycloaddition.

Limitations of this reaction are shown in **Figure 84**. A δ -phenyl $\alpha,\beta/\gamma,\delta$ -unsaturated substrate furnished the 1-pyrroline **32ac** in moderate yield with excellent chemoselectivity, however the enantioselectivity of **32ac** was only 88% ee. An aromatic group at the β -position is required for this type of direct bond formation from the photoexcited state, as a β -ethoxyl *N*-acyl pyrazole failed to give the target product **32ad**. In addition, two vinyl azides containing different *N*-moieties were not competent for the photocycloaddition for unknown reasons.

30f + Ethisterone derivative 34

$\xrightarrow[\text{acetone, r.t., N}_2, \text{blue LEDs}]{\Delta\text{-RhS (8.0 mol\%)}}$

35, 86% yield >20:1 d.r.

30g, 3 mmol, 1.00 g **31a**, 1.25 equiv

Δ -RhS (4.0 mol%)
 CHCl₃, r.t., **air**
 blue LEDs

32g, 1.16 g
 86% yield, 99% ee

36, 94% yield, >20:1 d.r.
+ 99% of Auxiliary

32g, 99% ee

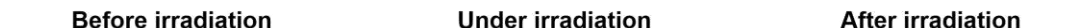
37, 95% yield
17:1 d.r., 98% ee

Aux = PMP-

Aux-H, **40**

38, 99% yield, 98% ee
+ 99% of Auxiliary

39, 68% yield, 98% ee



Encouraged by the mild conditions and broad substrate scope, the synthetic potential of this protocol was examined (**Figure 85**). First of all, a structurally complicated steroid substituted 1-pyrroline **35** could be obtained by the [2+3] photocycloaddition with ethisterone derived vinyl azide **34** in 86% yield obtaining almost a single stereoisomer (**Figure 85a**). Besides, this transformation was demonstrated to be applicable to a gram scale synthesis without loss of efficiency (**Figure 85b**). A simple set-up under air condition highlights its practicability (**Figure 86**). Although the present methodology relies on a bidentate coordination mode of the substrate, *N*-acyl pyrazoles constitute very desirable synthons which can easily be transformed into other functionalities, as shown in **Figure 85c**, for a clean and mild conversion to the amide **36** and ester **38**. Importantly, the auxiliary 3-(4-methoxyphenyl)pyrazole **40** was fully recovered in these conversions. Furthermore, 1-pyrroline with a prochiral cyclic imine group is applicable for further stereoselective synthetic manipulation as highlighted by the synthesis of a carbapenem analogue **37** and a pyrrolidine **39**.

3.4.5 Conclusions

In conclusion, this chapter demonstrates an important expansion of catalytic asymmetric reactions occurring via direct stereocontrolled bond forming reactions of photoexcited states.²⁰ Previously restricted to the class of cyclobutanes, an unprecedented economical access to the prevalent enantioenriched 1-pyrrolines was developed based on a visible-light-activated [2+3] photocycloaddition of alkenes with vinyl azides. The employed robust rhodium-based chiral-at-metal Lewis acid catalyst is key to the successful implementation of this methodology. Upon binding to the alkene substrate, it provides a unique handle for selective visible light excitation. Triplet spin of the corresponding excited substrate/catalyst complex is mainly localized at the alkene carbons so that an efficient reaction with the vinyl azide co-substrate can occur. All reactive intermediates remain bound to the catalysts, thus leading to a robust catalytic scheme (no exclusion of air necessary) with excellent stereocontrol.

In addition to the conceptual appeal, the synthetic usefulness of this protocol is indicated by the simple reaction setup with a single catalyst and no necessity for inert reaction conditions, exceptional stereoselectivity with virtual perfect diastereoselectivity and up to >99% ee, a broad substrate scope that gives access to a large variety of chiral 1-pyrrolines including quaternary stereocenters, and the

ability to use these 1-pyrrolines as building blocks for conversions into biologically relevant chiral pyrrolidines. Further discovery of new types of stereocontrolled reactions with electronically excited molecules could be anticipated.

References

- 1 a) N. Hoffmann, *Chem. Rev.* **2008**, *108*, 1052-1103; b) D. M. Schultz, T. P. Yoon, *Science* **2014**, *343*, 1239-1276.
- 2 J. Twilton, C. Le, P. Zhang, M. H. Shaw, R. W. Evans, D. W. C. MacMillan, *Nat. Rev. Chem.* **2017**, *1*, 0052.
- 3 A. Studer, D. P. Curran, *Angew. Chem. Int. Ed.* **2016**, *55*, 58-102.
- 4 F. Strieth-Kalthoff, M. J. James, M. Teders, L. Pitzer, F. Glorius, *Chem. Soc. Rev.* **2018**, *47*, 7190-7202.
- 5 For a review, see: S. Poplata, A. Tröster, Y.-Q. Zou, T. Bach, *Chem. Rev.* **2016**, *116*, 9748-9815.
- 6 For selected examples, see: a) R. Brimioulle, T. Bach, *Science* **2013**, *342*, 840-843; b) A. Tröster, R. Alonso, A. Bauer, T. Bach, *J. Am. Chem. Soc.* **2016**, *138*, 7808-7811; c) T. R. Blum, Z. D. Miller, D. M. Bates, I. A. Guzei, T. P. Yoon, *Science* **2016**, *354*, 1391-1395.
- 7 X. Huang, T. R. Quinn, K. Harms, R. D. Webster, L. Zhang, O. Wiest, E. Meggers, *J. Am. Chem. Soc.* **2017**, *139*, 9120-9123.
- 8 a) G. Dannhardt, W. Kiefer, *Arch. Pharm.* **2001**, *334*, 183-188; b) M.-G. A. Shvekhgeimer, *Chem. Heterocycl. Comp.* **2003**, *39*, 405-448.
- 9 D.-S. Wang, Z.-S. Ye, Q.-A. Chen, Y.-G. Zhou, C.-B. Yu, H.-J. Fan, Y. Duan, *J. Am. Chem. Soc.* **2011**, *133*, 8866-8869.
- 10 A. D. Melhado, M. Luparia, F. D. Toste, *J. Am. Chem. Soc.* **2007**, *129*, 12638-12639.
- 11 S. Padilla, J. Adrio, J. C. Carretero, *J. Org. Chem.* **2012**, *77*, 4161-4166.
- 12 a) H. Kawai, Y. Sugita, E. Tokunaga, H. Sato, M. Shiro, N. Shibata, *Chem. Commun.* **2012**, *48*, 3632-3634; b) T. Hashimoto, K. Maruoka, *Chem. Rev.* **2015**, *115*, 5366-5412.
- 13 B. Hu, S. G. DiMaggio, *Org. Biomol. Chem.* **2015**, *13*, 3844-3855.
- 14 a) Y.-F. Wang, S. Chiba, *J. Am. Chem. Soc.* **2009**, *131*, 12570-12572; b) W. Shu, A. Lorente, E.

- Gómez-Bengoa, C. Nevado, *Nat. Commun.* **2017**, 8, 13832.
- 15 S. Rajam, A. V. Jadhav, Q. Li, S. K. Sarkar, P. N. D. Singh, A. Rohr, T. C. S. Pace, R. Li, J. A. Krause, C. Bohne, B. S. Ault, A. D. Gudmundsdottir, *J. Org. Chem.* **2014**, 79, 9325-9334.
- 16 a) A. Padwa, J. Smolanoff, *J. Am. Chem. Soc.* **1971**, 93, 548-550; b) A. Padwa, M. Dharan, J. Smolanoff, S. I. Wetmore, *J. Am. Chem. Soc.* **1973**, 95, 1954-1961.
- 17 X. Sun, X. Li, S. Song, Y. Zhu, Y.-F. Liang, N. Jiao, *J. Am. Chem. Soc.* **2015**, 137, 6059-6066.
- 18 A. J. Neel, M. J. Hilton, M. S. Sigman, F. D. Toste, *Nature* **2017**, 543, 637-646.
- 19 X. Shen, K. Harms, M. Marsch, E. Meggers, *Chem. Eur. J.* **2016**, 22, 9102-9105.
- 20 X. Huang, X. Li, X. Xie, K. Harms, R. Riedel, E. Meggers, *Nat. Commun.* **2017**, 8, 2245.

3.5 Asymmetric [3+2] Photocycloaddition Enabled by Visible Light Excitation of Catalyst Bound Cyclopropanes

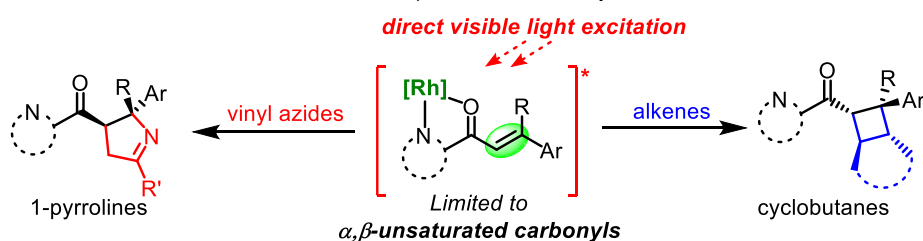
3.5.1 Research Background and Reaction Design

This thesis has illustrated a simplified catalytic system in which only a single rhodium-based chiral Lewis acid is required for a visible-light-activated asymmetric [2+2] photocycloaddition with alkenes (Chapter 3.3)¹ and a [2+3] photocycloaddition with vinyl azides (Chapter 3.4)² (**Figure 87a**). These transformations show unique advantages of photocycloadditions as a powerful synthetic tool that allow to construct carbo- and heterocycles with the formation of several new bonds and one or more stereocenters in a step- and atom-economic fashion.³ However, performing photocycloadditions in a catalytic asymmetric fashion is still a formidable challenge because of difficulties to suppress the uncatalyzed background photoreaction from the reactive photoexcited state of a substrate that is not associated with the chiral catalyst.⁴ Only a few examples of catalytic asymmetric photocycloadditions have been reported and they typically deal with [2+2] photocycloadditions of α,β -unsaturated carbonyls as the most frequently used substrates.⁵ Besides the previously described examples in this thesis, Bach introduced chiral Lewis-acid-catalyzed [2+2] photocycloadditions with UV-light.⁶ With respect to visible light, Bach⁷ and recently also Yoon⁸ reported catalytic asymmetric [2+2] photocycloadditions mediated through hydrogen-bonding interactions. Furthermore, Yoon developed some elegant asymmetric [2+2] photocycloadditions using a combination out of chiral Lewis acid catalyst and photocatalyst.⁹ New methodology activating other types of molecules to access prevalent new chiral cyclic scaffolds is highly desirable.

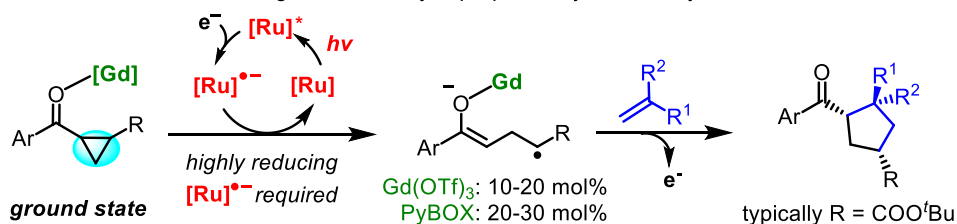
Cyclopropanes are very versatile synthetic building blocks due to ring opening induced by the inherent ring strain.¹⁰ Most of the cyclopropanes used for cycloadditions are highly activated bearing donor-acceptor substituents that predispose toward ring opening.¹¹ On the other hand, ring opening of cyclopropanes initiated by radical processes has been reported for decades and their applications for intramolecular cyclization were well studied.¹² However, only a single catalytic asymmetric photocycloaddition based on cyclopropanes has been reported. In 2016, the Yoon group¹³ introduced an elegant enantioselective [3+2] photocycloaddition between aryl cyclopropyl ketones and alkenes catalyzed by a combination out of gadolinium PyBOX chiral Lewis acid and [Ru(bpy)₃](PF₆)₂ as

photoredox catalyst (**Figure 87b**). Mechanistically, this cycloaddition is initiated by a photoredox catalyst mediated single electron reduction of the cyclopropyl ketones bound to the Lewis acid in the ground state. Besides photoinduced electron transfer,¹⁴ Alemán recently demonstrated that cyclopropanes can also undergo stereocontrolled direct reactions from the electronically excited state as revealed with an iridium-sensitized stereocontrolled ring expansion of chiral nitro cyclopropanes (**Figure 87c**).¹⁵ Despite their limitations with respect to scope, these two studies demonstrate that acceptor-substituted cyclopropanes are promising building blocks for photoinduced ring opening that occurs either directly from the excited state or by photoinduced electron transfer.

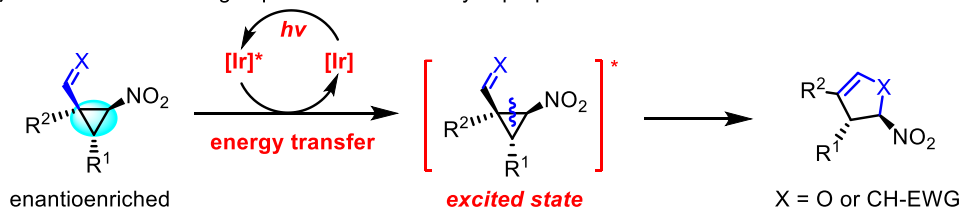
a) Previous work: Direct bond formations on photoexcited catalyst bound enones



b) Yoon's work: Reduction of ground state cyclopropanes by dual catalysis



c) Alemán's work: Ring expansion of excited cyclopropanes



d) This hypothesis: Direct visible light excitation of catalyst bound cyclopropanes

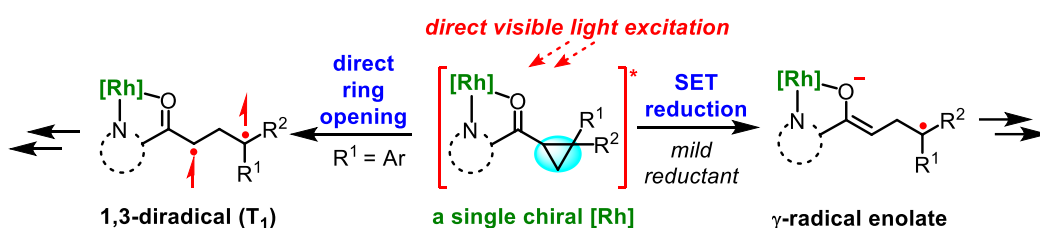


Figure 87. Strategies to broaden the scope of photocycloadditions from α,β -unsaturated carbonyls to acceptor-substituted cyclopropanes.

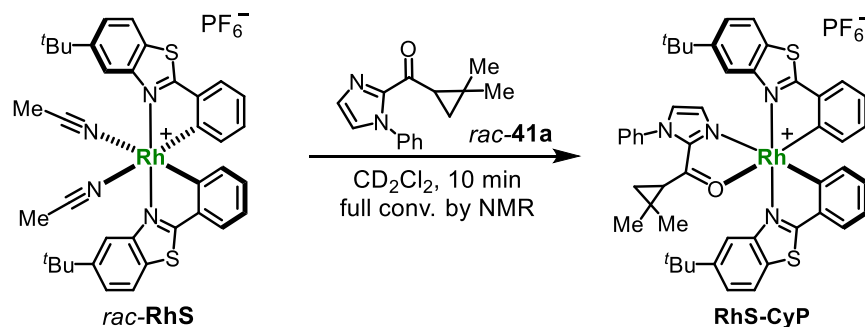
Inspired by these studies and based on the previous [2+2] and [2+3] photocycloadditions, the author of this thesis envisioned that if a cyclopropyl ketone could bind to the chiral-at-rhodium catalyst and be excited by visible light, the thereby formed excited cyclopropane/catalyst complex would undergo a facile single electron reduction followed by ring opening, generating γ -radical enolate, or a direct ring opening of the excited state giving 1,3-diradical species (**Figure 87d**). Trapping these highly reactive radical intermediates with the stereochemistry controlled by metal centered chirality would enable new catalytic asymmetric photocycloadditions. Herein, this chapter describes how the author accomplished this hypothesis and expanded the scope of rhodium catalyzed asymmetric photocycloadditions to simple mono-acceptor-substituted cyclopropanes affording previously inaccessible chiral cyclopentane and cyclopentene derivatives.

3.5.2 Development of [3+2] Photocycloaddition with Alkenes

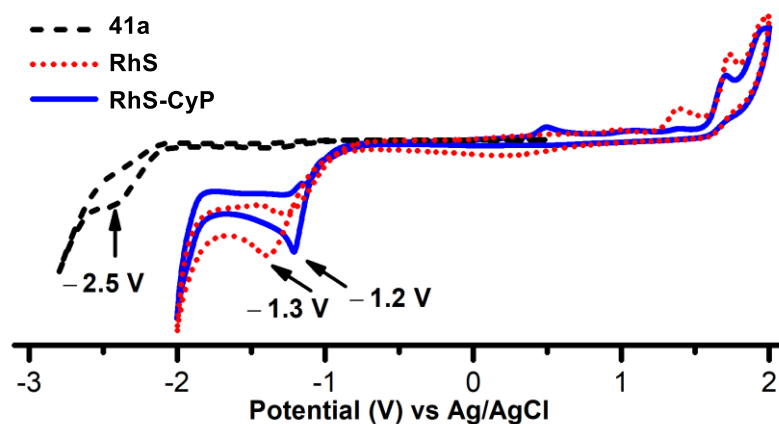
To accomplish the hypothesis, two main challenges needed to be addressed: first, to identify an efficient way to generate the photoexcited state of the cyclopropane substrates, and second to cope with the highly negative reduction potential of typical cyclopropanes, which is reported to be more negative than -2 V vs Ag/AgCl.¹²

Geminal β,β -dimethyl cyclopropane **41a** was selected to start the experimental study, considering that it produces less number of possible diastereomers. Gratifyingly, upon coordination of **41a** to the bis-cyclometalated Rh-based Lewis acid catalyst **RhS**, a new species forms immediately that is assigned to be rhodium bound cyclopropane, **RhS-CyP** (**Figure 88a**). Cyclic voltammetry reveals that the complex **RhS-CyP** ($E^{[\text{RhS-CyP}]/[\text{RhS-CyP}]^-} = -1.2$ V vs Ag/AgCl) has a greatly decreased reduction potential by $\Delta E = 1.3$ V compared with the noncoordinated cyclopropane **41a** ($E^{1a/1a^-} = -2.5$ V vs Ag/AgCl), thereby rendering it accessible for reduction under mild conditions (**Figure 88b**). Furthermore, in contrast to the free cyclopropane **41a**, the **RhS-CyP** complex absorbs visible light with a broad absorption band around 400 nm (**Figure 88c**). In collaboration with Dr. Marianna Marchini and Prof. Paola Ceroni from the University of Bologna, Italy, the emission spectrum of **RhS-CyP** was recorded at low temperature (77 K). According to the emission maximum at 507 nm (with a lifetime of 0.12 ms), a triplet state energy of 2.5 eV can be calculated which corresponds to a roughly estimated reduction potential of $+1.3$ V vs Ag/AgCl for the excited state **RhS-CyP**.

a) Fast formation of RhS-CyP



b) Cyclic voltammograms



c) Absorption/emission spectra

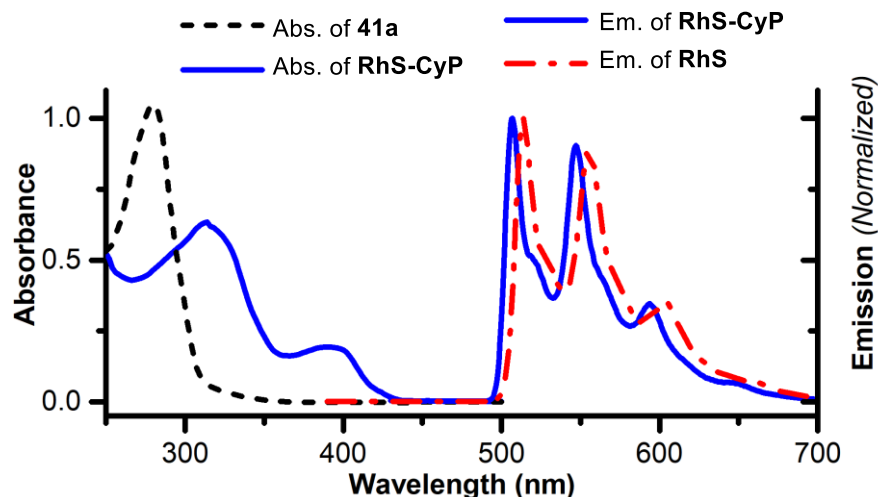
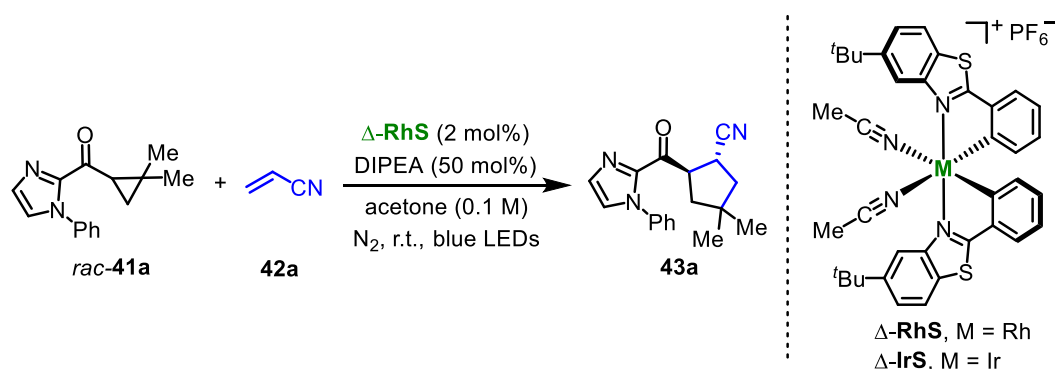


Figure 88. Changes of the photophysical and redox properties of cyclopropyl ketone **41a** upon **RhS** coordination. b) Cyclic voltammetry recorded in CH_2Cl_2 containing $0.1 \text{ M } n\text{Bu}_4\text{NPF}_6$ at $22 \pm 2^\circ\text{C}$. Scan rate = 0.1 V/s . The current was normalized. c) Absorption spectra measured at room temperature in CH_2Cl_2 (**41a**, 0.2 mM; **RhS-CyP**, 0.02 mM). Emission spectra recorded at 77 K with excitation at 400 nm.

These results indicate that the photoexcited **RhS-CyP** complex should be accessible to single electron reduction by a weak reductant, such as diisopropylethylamine (DIPEA, $E^{\text{DIPEA}\cdot+/ \text{DIPEA}} = +1.0$ V vs Ag/AgCl). Indeed, irradiating a mixture of **41a**, acrylonitrile **42a**, and 2.0 mol% of Δ -**RhS** with substoichiometric amount of DIPEA afforded the desired cycloaddition product cyclopentane **43a** in quantitative yield with perfect enantioselectivity (99% ee) and as a single diastereomer (**Table 17**, entry 1). Control experiments clearly demonstrated that **RhS**, reducing agent, visible light, and inert atmosphere with the exclusion of dioxygen are all indispensable for this highly efficient transformation (entries 2, 5-7). Inorganic base without reducing ability, like Na_2HPO_4 , did not facilitate the desired ring opening (entry 3). And the iridium analogue **IrS** could hardly give detectable amount of product (entry 4).

Table 17. [3+2] Photocycloaddition of a simple cyclopropane with acrylonitrile.^[a]



Entry	Catalyst	Variations	Yield [%]	D.r.	Ee [%]
1	Δ - RhS	None	98	>20:1	99
2	RhS	Without DIPEA	0	n.a.	n.a.
3 ^[b]	RhS	Na_2HPO_4 instead of DIPEA	0	n.a.	n.a.
4 ^[b]	IrS	None	<10	n.d.	n.d.
5	None	None	0	n.a.	n.a.
6	RhS	Dark	0	n.a.	n.a.
7	RhS	Under air	0	n.a.	n.a.

[a] Reaction conditions: **41a** (0.1 mmol), **42a** (2.5 equiv), DIPEA (50 mol%) and catalyst (2.0 mol%) in acetone (0.1 M) were stirred at room temperature under N_2 atmosphere with irradiation of blue LEDs (24 W) for 16 h; NMR yield; ee was determined by HPLC on a chiral stationary phase. [b] 4.0 mol% of catalyst with 10 equiv of **42a** and 2.0 equiv of base in 0.05 mmol scale.

Next, the 2-phenyl cyclopropane **44a** was subjected to the newly developed reaction system (**Figure 89**). In the presence of DIPEA, the desired cyclopentane **45a** was obtained in perfect yield and enantioselectivity, but with a low diastereoselectivity of 2.1:1. Interestingly, without any reducing agent, the reaction also worked smoothly, although the ee was a little bit lower. This implies that, instead of photoinduced SET reductive ring opening, the cycloaddition of cyclopropane bearing an aromatic substituent might proceed through direct ring expansion at the level of the excited state. Further attempts to improve the diastereoselectivity were made by modification of catalyst in the absence of DIPEA. As shown in **Figure 89**, catalysts that are more bulky in the coordination pocket gave slightly higher d.r. values, while introducing substituents at cyclometalating phenyl moiety was not helpful. Additionally, the related **RhO**, which features a less steric congestion than **RhS** congener, delivered much lower d.r. and ee values.

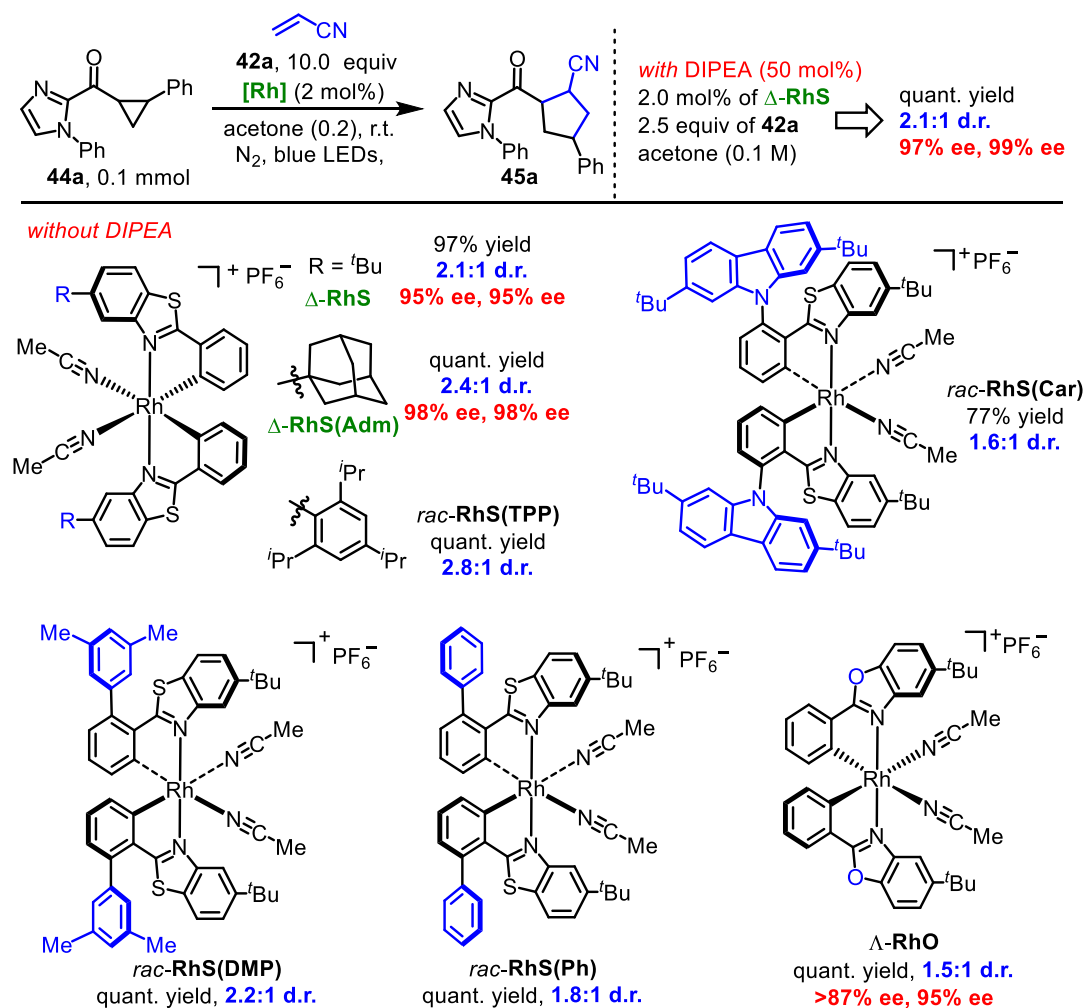


Figure 89. Effort to improve the diastereoselectivity of **45a** by catalyst modification. NMR yield.

Furthermore, synthetically more useful acyl cyclopropanes with pyrazole as auxiliary were tested (**Figure 90**). Unfortunately, under optimal conditions (**Table 17**, entry 1), no reaction occurred for the cyclopropane bearing 3,5-dimethyl pyrazole (**41b**), which is ascribed to the difficulty in reduction of an amide and the instability of the corresponding enolate. Actually, for a substrate with two electron withdrawing groups at the cyclopropyl ring (**41d**), full conversion was obtained. However, two unidentified isomers were formed in 3.7:1 ratio and with disappointing 15% ee for the major isomer. Finally, extensive screening led to the generation of a 3-PMP pyrazole substituted cyclopentane in moderate yield (50% NMR yield, starting from **41c**) under conditions with a modified bis-cyclometalated rhodium complex (**RhS(OMe)**) using *N,N*-dimethylaniline as reducing agent that is known to be easier oxidized ($E^{\text{amine.}+/ \text{amine}} = 0.71 \text{ V vs SCE}$,¹⁶ in MeCN).

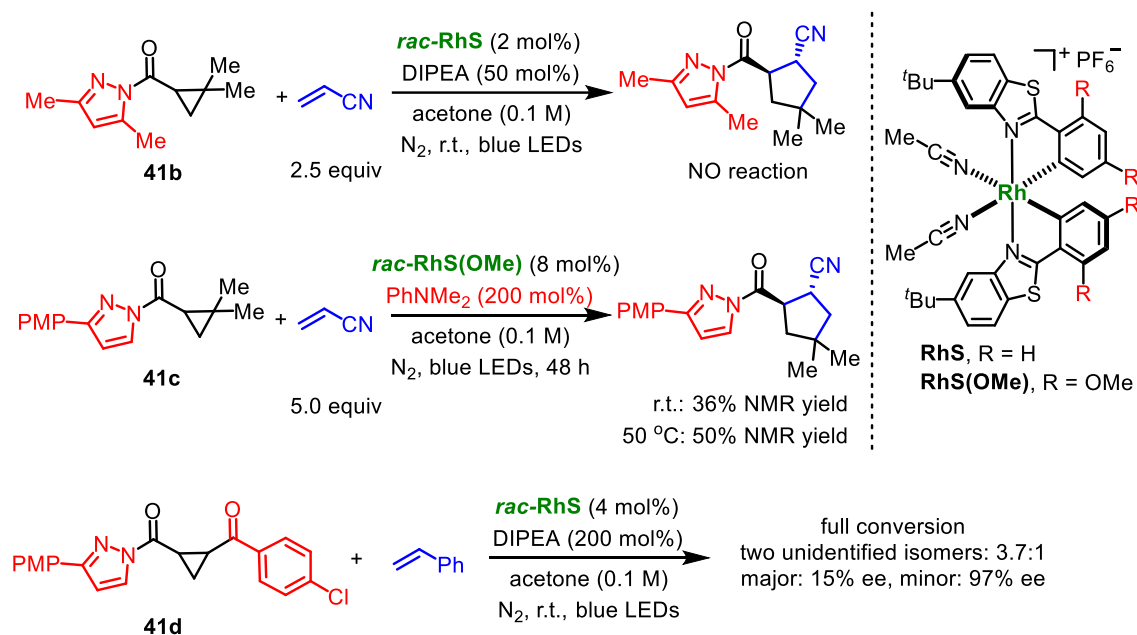


Figure 90. Effort to extend the scope of the [3+2] photocycloaddition to synthetically useful substrates with *N*-pyrazole as auxiliary.

In summary, mono-acceptor-substituted cyclopropanes were designed to undergo a [3+2] photocycloaddition with alkenes via photoinduced SET or direct ring opening at the excited state. Employing an imidazolyl group as auxiliary, good yields and enantioselectivities could be obtained with a single chiral-at-rhodium catalyst, but the attempts to apply synthetically more desirable pyrazoles as auxiliaries gave inferior results.

3.5.3 Extension to [3+2] Photocycloaddition with Alkynes

Table 18. Conditions optimization for [3+2] photocycloaddition with alkyne.^[a]

rac-41a, R = Ph
 rac-41e, R = Mes

46a

Catalyst
base
 solvent (0.1 M)
 N_2 , r.t., blue LEDs

47a, R = Ph
 47b, R = Mes

Entry	Catalyst [mol%]	Base	Solvent	Yield [%]	Ee [%]
1	$\Delta\text{-RhS}$ (4.0)	DIPEA	Acetone	47a , 57	87
2	$\Delta\text{-RhS}$ (4.0)	Et_3N	Acetone	47a , 75	88
3	$\Delta\text{-RhS}$ (4.0)	2,6-lutidine	Acetone	47a , 0	n.a.
4	$\Delta\text{-RhS}$ (4.0)	K_2CO_3	Acetone	47a , 0	n.a.
5	$\Delta\text{-RhS}$ (4.0)	Et_3N	CH_2Cl_2	47a , 82	81
6	$\Delta\text{-RhS}$ (4.0)	Et_3N	MeCN	47a , 57	77
7	$\Delta\text{-RhS}$ (4.0)	Et_3N	DMF	47a , 55	88
8	$\Delta\text{-RhS}$ (4.0)	Et_3N	PhCl	47a , 97	88
9	$\Delta\text{-RhS}$ (4.0)	Et_3N	THF	47a , 95 (92)	89
10	$\Delta\text{-RhS}$ (4.0)	Et_3N	1,4-dioxane	47a , 54	91
11	$\Delta\text{-RhS}$ (8.0)	Et_3N	THF	47a , 91	91
12	$\Delta\text{-RhS}$ (8.0)	Et_3N	1,4-dioxane	47a , 80	92
13	$\Delta\text{-RhO}$ (4.0)	Et_3N	THF	47a , 97	63
14	$\Delta\text{-RhS(Adm)}$ (4.0)	Et_3N	THF	47a , 75	93
15	$\Delta\text{-IrS}$ (4.0)	Et_3N	THF	47a , <10	81
16 ^[b]	$\Delta\text{-RhS}$ (4.0)	Et_3N	THF	47b , 99 (95)	98

[a] Reaction conditions: **41** (0.05 mmol), **46a** (5 equiv), base (2.0 equiv), and catalyst in the indicated solvent (0.1 M) were stirred at room temperature under N_2 atmosphere with irradiation of blue LEDs (24 W) for 16 h; NMR yield; ee was determined by HPLC on a chiral stationary phase. Isolated yields are provided in parenthesis. [b] **41e** was employed as substrate.

Based on these results, the author of this thesis tried to apply the strategy to the cycloaddition of cyclopropane with alkyne (**Table 18**). This is more challenging due to the relatively low reactivity of alkynes toward radical addition.¹⁷ Encouragingly, by using 4.0 mol% of catalyst in combination with 2.0 equiv of DIPEA, the desired cyclopentene **47a** was formed in moderate yield (57% NMR yield)

and with 87% ee for the reaction of **41a** with phenylacetylene **46a** (entry 1). Again, other bases, such as 2,6-lutidine and K_2CO_3 without reducing ability, could not facilitate the reaction (entries, 3,4). Et_3N was proved to be better for the photocycloaddition with alkyne, giving 75% yield with 88% ee (entry 2). Solvent screening revealed that PhCl and THF provided excellent yields (97% and 95%, respectively) with good enantioselectivities (88%-89% ee, entries 5-10). Besides, 1,4-dioxane delivered the highest ee of 91% among the solvents tested, albeit in a moderate yield of 54% (entry 10). Increasing the catalytic loading to 8.0 mol% led to improved results with the formation of **47a** in yield $\geq 80\%$ with enantioselectivities $\geq 91\%$ ee (entries 11,12). Other catalysts were evaluated as well (entries 13-15). Consistent with previous observations, a sterically highly demanding complex $\Delta\text{-RhS(Adm)}$ ¹⁸ gave the best enantioselectivities among these catalysts (93% ee, entry 14). Furthermore, the reaction catalyzed by the iridium congener $\Delta\text{-IrS}$ was very sluggish, which was presumably caused by the slow ligand exchange kinetics (entry 15). Guided by the previous investigations on the origins of asymmetric induction in Lewis acid catalyzed enolate chemistry (Chapter 3.1),¹⁹ a more bulky mesityl group was introduced as the *N*-substituent of the imidazolyl moiety. As expected, cyclopentene **47b** was formed in 99% NMR yield, 95% isolated yield with excellent 98% ee with 4.0 mol% of $\Delta\text{-RhS}$ and 2.0 equiv of Et_3N using THF as solvent (entry 16). Therefore, these conditions were used for the further substrate scope studies with respect to the synthesis of cyclopentenenes.

3.5.4 Substrate Scope

Firstly, the scope of [3+2] photocycloadditions with respect to alkenes was investigated under the mild conditions (**Figure 91**). A wide range of Michael acceptors (**43a-g**), styrenes (**43h-q**) and an enyne (**43r**) were able to participate in the cycloadditions generating cyclopentanes in 63% to 99% yields, with diastereoselectivities of 8:1 to $>20:1$ d.r. value, and up to complete enantioselectivities ($>99\%$ ee for **43p** and **43r**). In general, electron deficient olefins worked better, which is in accord with the electron rich nature of the γ -radical enolate intermediate (see **Figure 87d**), while a *para*-methoxy styrene could only work at the elevated temperature of 50 °C delivering compound **43i** in 70% yield with only 90% ee. Heterocycles like pyridines (**43n-o**) and functional groups that are vulnerable to highly reducing conditions, including carbonyls (**43c**, **43u**), sulfonyl (**43f**), cyano (**43l**),

C(sp²)-F bond (**43j**) and trifluoromethyl (**43p-q**), were compatible highlighting the mildness and versatility of the current catalytic system. It is noteworthy that cyclopentanes bearing an all-carbon quaternary center could be synthesized with excellent stereoselectivities (**43g** and **43p-r**, >20:1 d.r., ≥99% ee). Furthermore, biologically relevant structures derived from glucofuranose (**43s**), aspartame (**43t**), and fenofibrate (**43u**) could be constructed effectively.

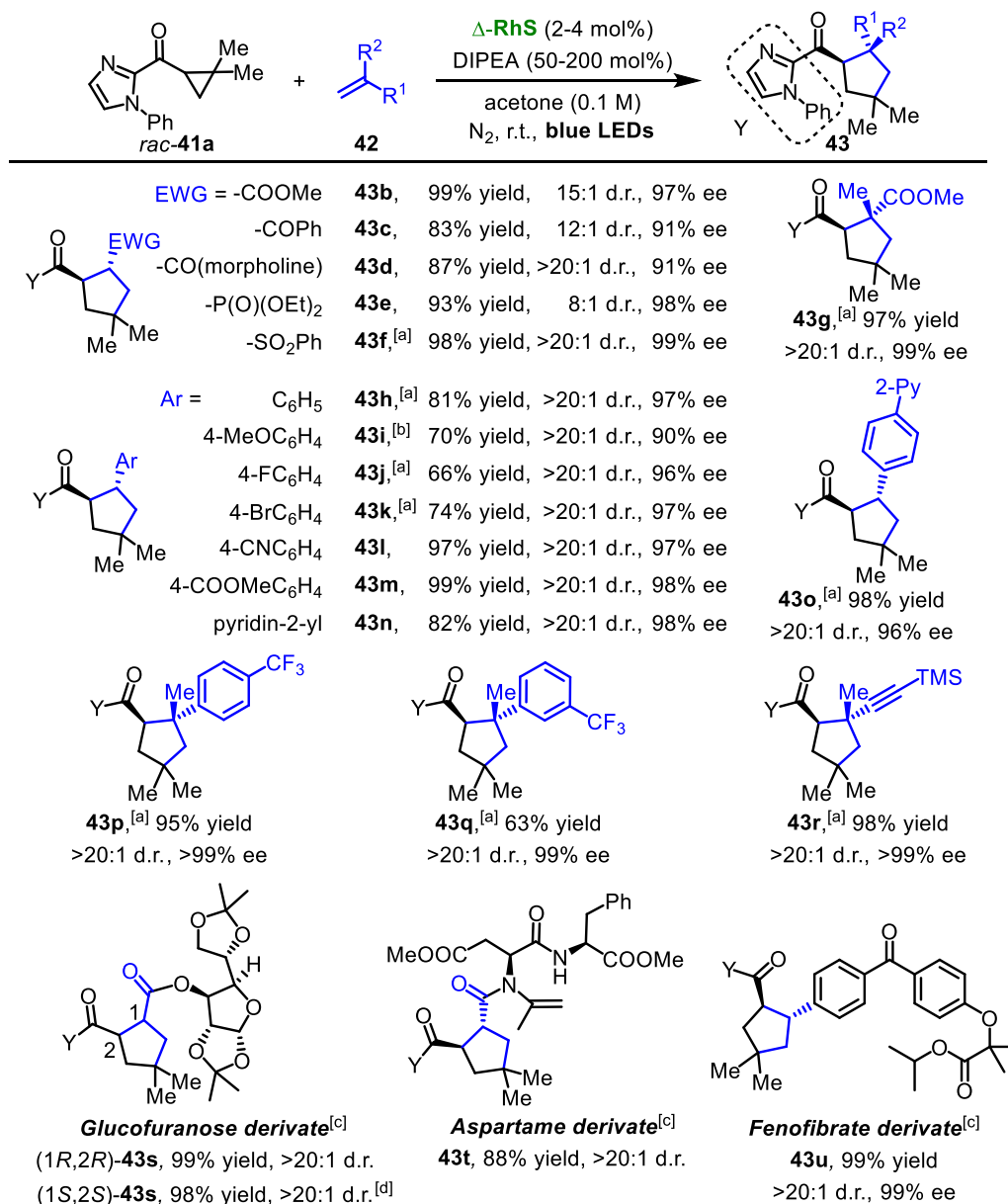


Figure 91. Substrate scope of the [3+2] photocycloaddition with respect to alkenes. Reaction conditions: see Table 17 entry 1. [a][b][c] DIPEA (2.0 equiv) and Δ -RhS (4.0 mol%) were employed. [b] 50 °C. [c] Optically pure alkenes (1.25 equiv) were employed. [d] Δ -RhS was employed. Structure of **43k** was determined by X-ray crystallography and all other compounds were assigned accordingly.

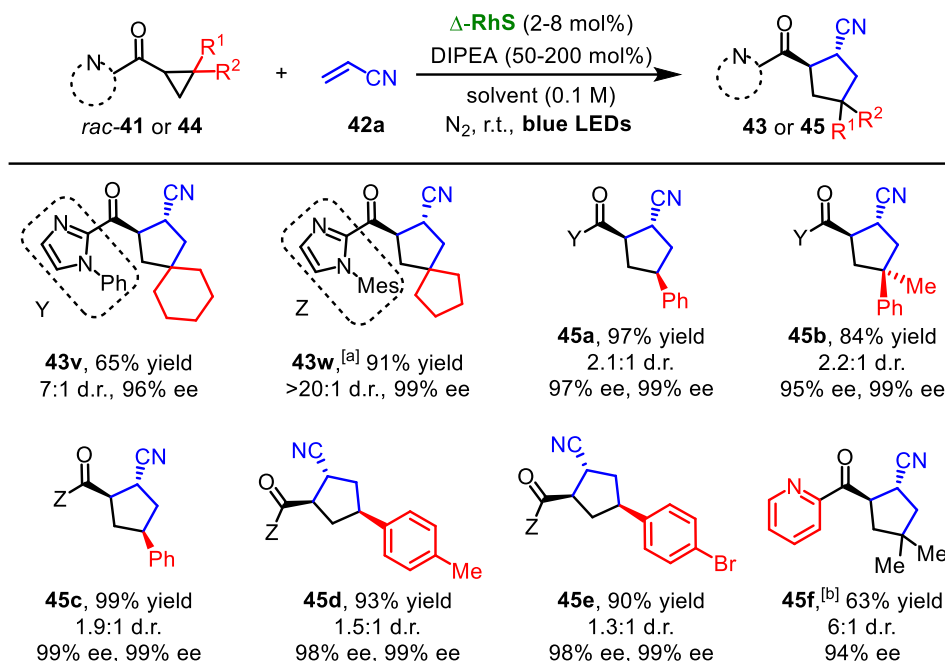


Figure 92. Substrate scope of the [3+2] photocycloaddition with respect to acceptor-substituted cyclopropanes. Reaction conditions: see **Table 17** entry 1. [a] DIPEA (2.0 equiv) and Δ -RhS (4.0 mol%). [b] DIPEA (2.0 equiv) and Δ -RhS (8.0 mol%) in acetone/MeCN (1:1).

Next, acyl cyclopropanes with imidazolyl auxiliary were subjected to the single chiral rhodium catalytic system (**Figure 92**). Alkyl (**43v-w**) or aryl (**45a-e**) substituents at the cyclopropyl ring were well accommodated furnishing desired cyclic products in 65-99% yield with up to 99% enantioselectivities. Notably, spirocyclic compounds could be obtained with good results in the cases of **43v-w**. However, cyclopropanes with two different substituents at the 2-position of the cyclopropyl ring led to the formation of products with poor d.r. values (**45a-e**). This can be rationalized with the flexibility of the corresponding γ -radical enolate intermediate which makes enantioface differentiation of the pro-chiral radical Csp² very challenging. In addition, a pyridyl group could also be employed as the coordinating group with synthetically acceptable efficiency (**45f**).

Figure 93 shows the limitation of this method. A very electron rich vinyl ether and two internal alkenes failed to undergo the photocycloadditions (**45g-i**), which can be attributed to the mismatched reactivity with the key radical enolate intermediate. The 4-vinylpyridine, which could competitively coordinate to the catalyst, is not tolerated (**45j**). In addition, a mono-methyl substituted acyl cyclopropane is somehow unable to react with acrylonitrile (**45k**).

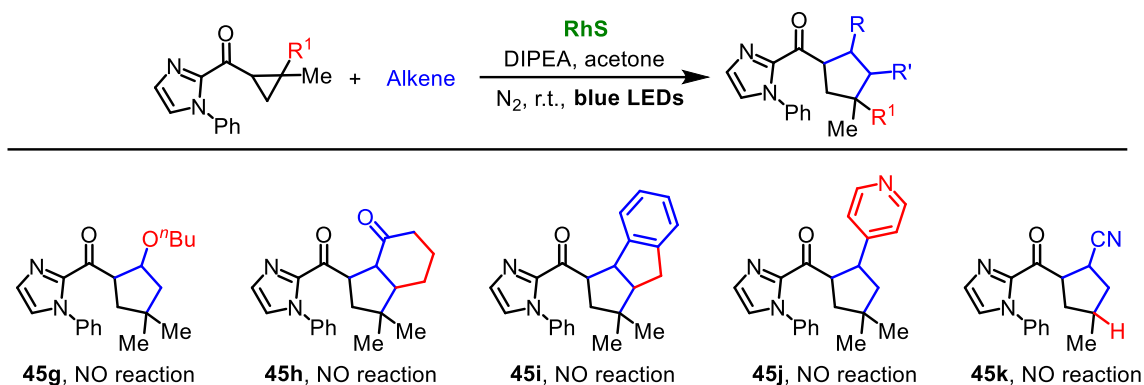


Figure 93. Limitations of the [3+2] photocycloaddition of cyclopropanes with alkenes.

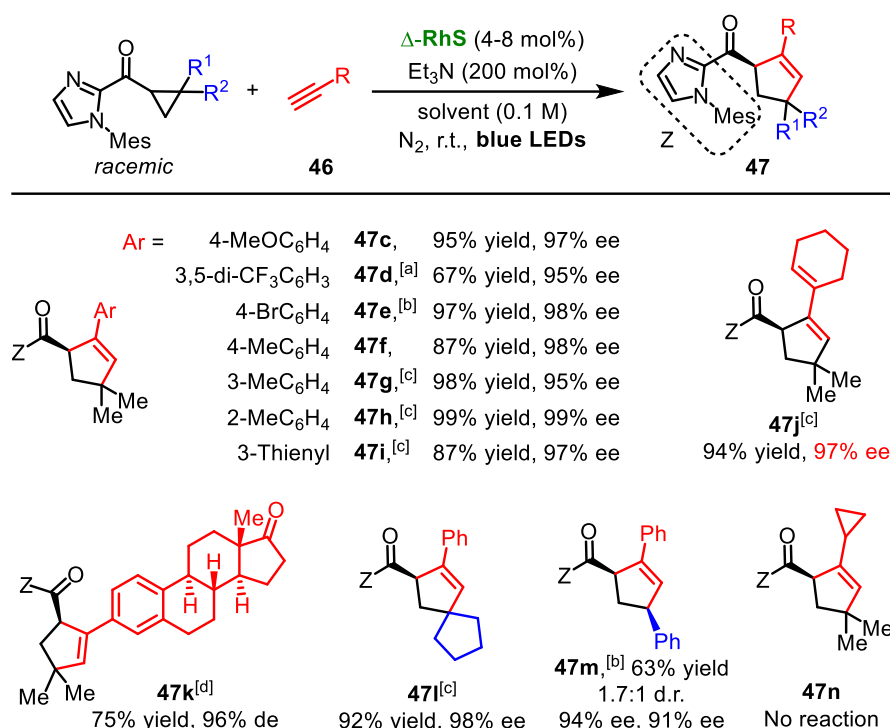


Figure 94. Substrate scope of the [3+2] photocycloaddition with respect to alkynes. Reaction condition: see **Table 18** entry 16 but with 2.5 equiv of alkyne. [a] Acetone instead of THF. [b] Alkyne (5.0 equiv) and Δ -RhS (8.0 mol%) in PhCl. [c] Alkyne (5.0 equiv) and Δ -RhS (4.0 mol%) in PhCl. [d] Optically pure alkyne (1.25 equiv) and Δ -RhS (8.0 mol%) in PhCl.

Finally, the scope of [3+2] photocycloadditions with alkynes is summarized in **Figure 94**. This transformation tolerated large electronic perturbation (**47a-f**) and different substituted pattern (**47f-h**) on the aromatic moiety of alkynes. Different from the scope of alkenes, an aryl alkyne with 4-methoxy group worked smoothly, forming **47c** in 95% yield with 97% ee. A thiophene (**47i**), an enyne (**47j**), and an estrone derivative (**47k**) were well accommodated, highlighting the functional group tolerance of this protocol. But aliphatic alkynes are not feasible for the desired cycloaddition (**47n**). Finally, two

represented cyclopropyl ketones were proved to be competent (**47l-m**).

3.5.5 Mechanistic Studies

1) Proposed mechanism

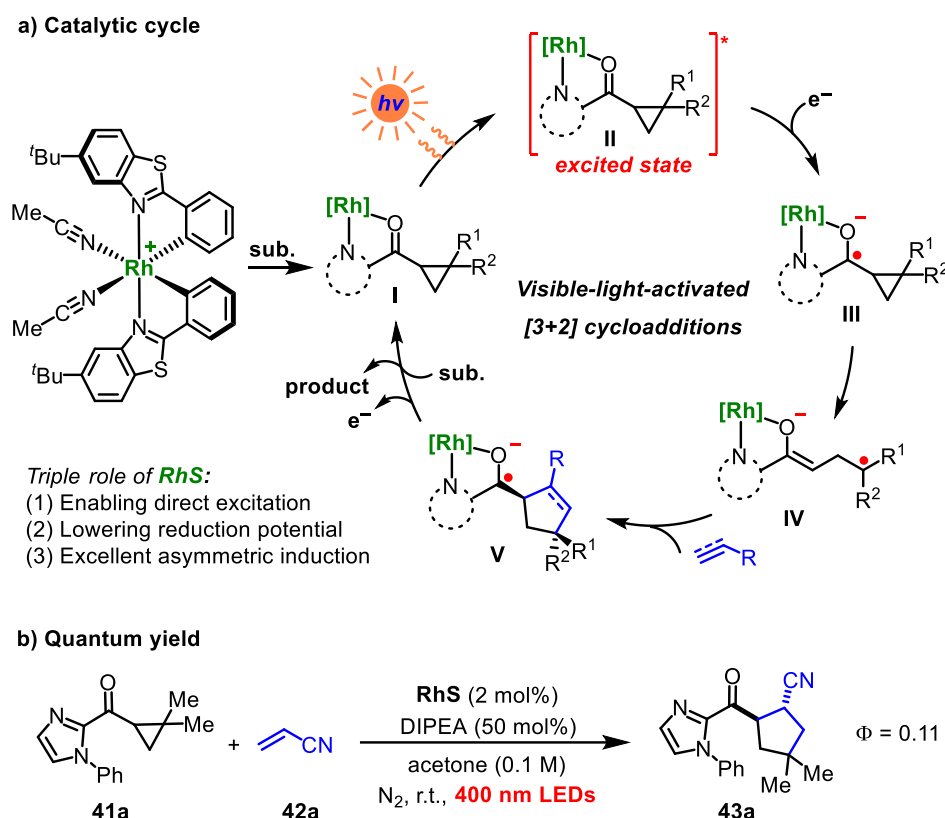


Figure 95. Proposed mechanism of the [3+2] photocycloadditions and quantum yield determination.

Based on the investigation of the photophysical and redox properties of the rhodium-coordinated cyclopropane (**Figure 88**), a proposed mechanism is depicted in **Figure 95**. Initially, the catalyst/substrate complex (intermediate **I**) forms upon bidentate coordination of the cyclopropane substrate to the rhodium complex **RhS**. After photoexcitation, intermediate **II** serves as a strong oxidant to become reduced by a tertiary amine generating the intermediate **III** which subsequently ring-opens¹² to form a rhodium-coordinated enolate radical intermediate **IV**. Subsequent radical cycloaddition with an alkene or an alkyne affords the corresponding ketyl radical intermediate **V**. This highly reducing ketyl radical **V** can either donate an electron to the oxidized amine radical cation for the regeneration of tertiary amine or to the photoexcited intermediate **II** propagating a chain process.

Finally, ligand exchange regenerates the catalyst/substrate complex **I** completing the catalytic cycle with the release of the cycloaddition products.

2) Discussion of the key SET step

As an example, the redox potential of excited **RhS-CyP** is calculated as +1.3 V vs Ag/AgCl based on the ground state potential and excited triplet energy (**Figure 88**), while the peak potential to oxidize DIPEA is +1.0 V vs Ag/AgCl (**Figure 96**). This supports a feasible SET transfer between a mild reducing agent and the photoexcited **RhS**/substrate complex (intermediate **II**), rather than any other ground state intermediates or non-coordinated substrate, which highlights this unique design of the direct photoexcitation of catalyst bound substrate. This system only relies on catalytic amounts of a mild reducing initiator, thus ensuring high chemoselectivity and excellent functional group tolerance. Furthermore, electron transfer is expected to happen with the excited triplet state instead of the singlet state, considering the longer life-time of the triplet state of Rh complexes because of the efficient inter system crossing in the presence of the heavy rhodium atom.²⁰ In addition, based on photophysical studies and cyclic voltammetry, the SET reduction of the **RhS-CyP** complex is supposed to be ligand centered, thus leading to the observed reactivity.

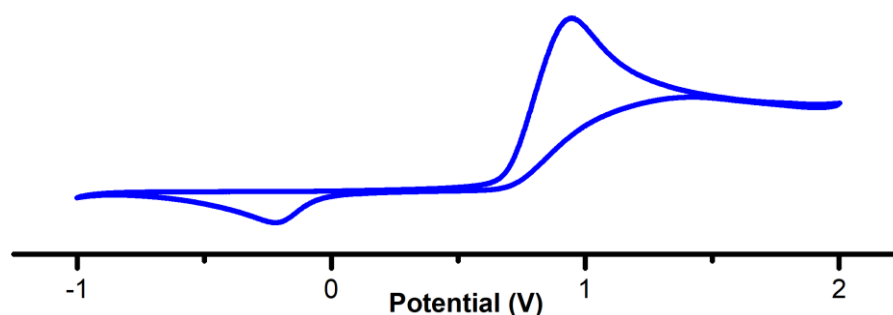


Figure 96. Cyclic voltammogram of DIPEA. Recorded in CH₂Cl₂ containing 0.1 M ⁿBu₄NPF₆ at a scan rate = 0.1 V/s.

3) Quantum yield measurement

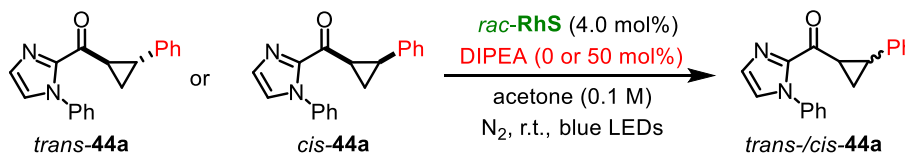
According to the proposed mechanism, at least one photon is required for the generation of a molecule of product, even if a chain mechanism is involved. Indeed, the quantum yield of the reaction **41a + 42a** \rightarrow **43a** was determined as 0.11 (**Figure 95b**), by a simplified procedure using a Powermeter

as the detector (see experimental part for details). This value disfavors the chain propagation through the electron transfer from ketyl radical intermediate **V** to the ground state intermediate **I**. But the chain process involving single electron transfer from ketyl radical intermediate **V** to the excited catalyst/substrate (intermediate **II**) could not be excluded out.

4) An alternative mechanism via direct ring opening at the excited state

For cyclopropanes with an aromatic substituent, a direct ring opening upon photoexcitation could happen. Such substrate undergoes [3+2] photocycloaddition without additional amine although the reaction is a little more sluggish (**Figure 89**). Furthermore, the *cis*-configured cyclopropane *cis*-**44a** converts to the *trans*-diastereomer *trans*-**44a** upon photolysis in the presence or absence of an amine, indicating a reversible ring opening/closure upon excitation (**Table 19**).

Table 19. *Cis*- to *trans*-isomerization of aryl cyclopropane **44a**.^[a]



Entry	Starting cyclopropane	DIPEA	Recovered cyclopropane [<i>trans</i> / <i>cis</i>]
1	<i>trans</i> - 44a	none	>25:1
2	<i>trans</i> - 44a	50 mol%	>25:1
3	<i>cis</i> - 44a	none	>25:1
4	<i>cis</i> - 44a	50 mol%	>25:1

[a] Reaction conditions: aryl cyclopropane **44a** (0.05 mmol), *rac*-**RhS** (4.0 mol%), DIPEA (0 or 50 mol%) in acetone (0.1 M) were stirred at room temperature under N₂ atmosphere with irradiation of blue LEDs (24 W) for 16 h; *Trans/cis* ratio was determined by crude ¹H NMR. In all entries, >90% of cyclopropane was recovered.

5) Competitive coordination of substrate and product to RhS

As indicated by in situ NMR experiments, both **41a** and **43a** could bind to **RhS** quickly, which again shows that the bis-cyclometalated rhodium catalyst is coordinatively very labile. In order to differ the coordination affinity of substrate and product with **RhS**, a competing experiment was conducted. To a solution of **41a/43a** (1:0.8), *rac*-**RhS** (1.0 equiv refers to **41a**) was added. After

mixing for 30 minutes, the crude ^1H NMR spectrum clearly showed that only the substrate coordinated Rh complex (**RhS-CyP**) was formed while all **43a** remained free without the formation of catalyst/product complex (**Figure 97**).

These results imply that compared with the product, the substrate has a much higher coordination constant with **RhS**. Besides, only the substrate-coordinated Rh complexes would undergo the following transformation leading to continuous consumption of substrate. Therefore, good conversions without significant catalyst inhibition by the product are reasonable in the current system.

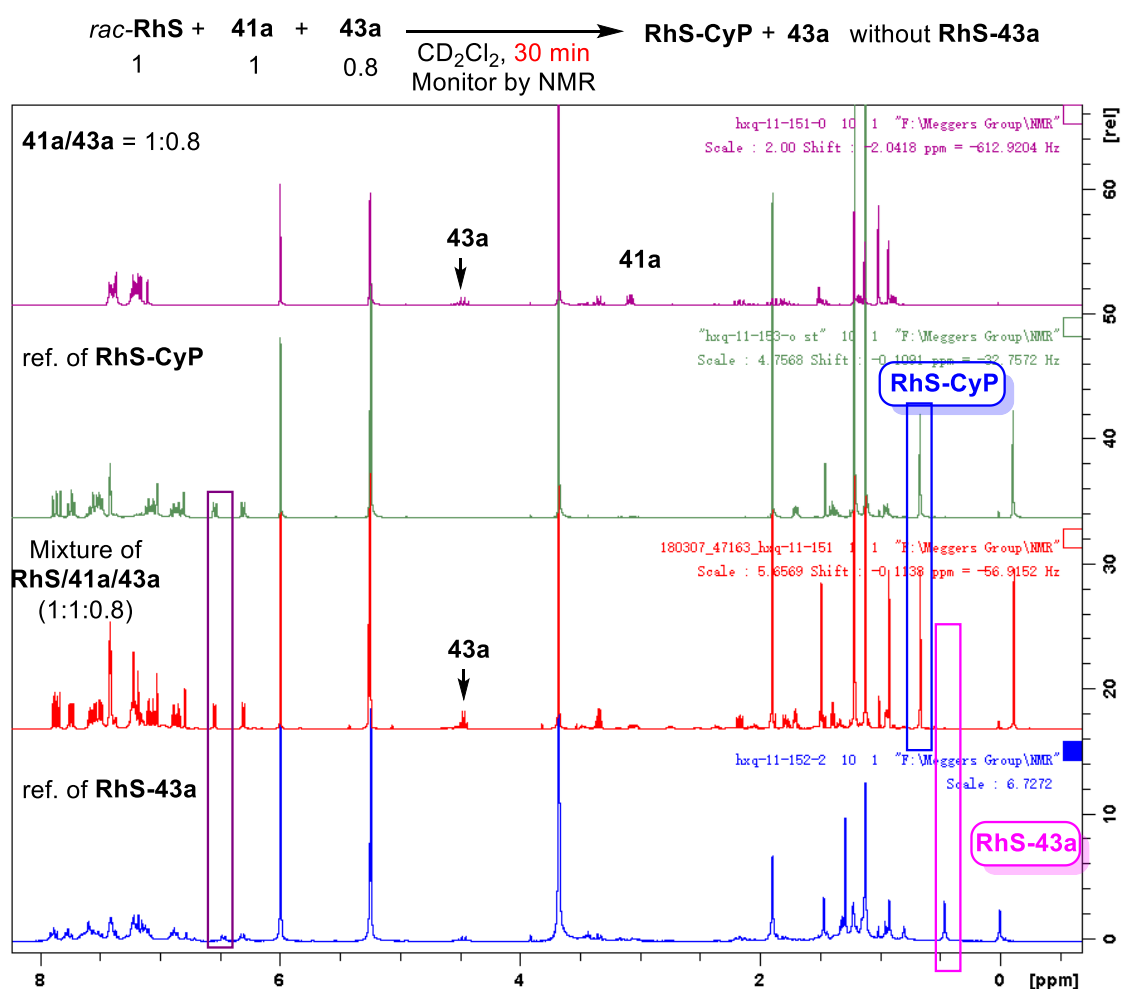


Figure 97. Competitive coordination of **41a** and **43a** to **RhS** as demonstrated by ^1H NMR experiments (300 or 500 M in CD_2Cl_2). The third spectrum: mix *rac*-**RhS** (0.02 mmol), **41a** (0.02 mmol) and **43a** (ratio of **41a/43a** = 1:0.8 as indicated in the first spectrum), 1,3,5-trimethoxybenzene (0.02 mmol, internal standard), and CD_2Cl_2 in a NMR tube for 30 minutes.

6) Triple role of RhS

Noteworthy are the essential multiple roles of the chiral rhodium Lewis acid catalyst **RhS**. Substrate coordination lowers the reduction potential of the rhodium-bound cyclopropyl ketone and enables a direct photochemical excitation using visible light, thereby creating a strongly oxidizing excited state which can be reduced by a mild reducing agent. This explains the high functional group tolerance and the absence of any background reaction which is a prerequisite for obtaining very high enantioselectivities. Importantly, all reactive intermediates, including excited states and radical species, remain bound to the single chiral catalyst throughout the catalytic cycle and thereby providing a very robust catalytic system with a selective photoexcitation and photoreactivity of the catalyst-bound substrate and high stereocontrol in the following radical chemistry. This is distinct from Yoon's work¹³ which employed two catalysts to separate the stereodetermining bond formation from the photochemical transformation, in which a highly reducing species derived from a reduced additional photocatalyst is required to activate the ground state Lewis acid bound cyclopropane (typically with two electron withdrawing groups).

3.5.6 Conclusions

In conclusion, this chapter disclosed a conceptually straightforward and effective method for the catalytic asymmetric [3+2] photocycloaddition of cyclopropanes by employing a single rhodium-based chiral Lewis acid catalyst.²¹ The cyclopropane/catalyst complex serves as the visible-light-absorbing intermediate and its photoexcited state constitutes a strong oxidant to facilitate a reductive ring opening of the cyclopropane under mild conditions in an overall photoinduced electron transfer catalysis. Notably, not only a wide range of alkenes but also phenylacetylenes, which have not been utilized for intermolecular catalytic asymmetric photocycloadditions before,²² are capable of trapping the catalyst-bound radical intermediate. Different from previous studies on direct bond formation of excited enones, a mild SET reduction of the photoexcited states enables these asymmetric [3+2] photocycloadditions providing new approaches to chiral cyclopentanes and cyclopentenones that complement the previously reported access to cyclobutanes¹ and 1-pyrrolines².

Chapters 3.3, 3.4, and 3.5 showed the versatility of the chiral-at-rhodium Lewis acid catalyst for catalyzing a set of highly asymmetric photocycloadditions that only rely on a single chiral catalyst

with loadings of 0.5-8 mol%, feature simple and mild reaction conditions, provide high yields (up to 99%) with excellent enantioselectivities (up to >99% ee), and display broad substrate scopes with high functional group tolerance.

The key to the success of this reaction is the utilization of the photoexcited rhodium bound cyclopropyl ketone as strong oxidant to trigger the SET process. On the other hand, the Kang group demonstrated that a rhodium bound enone could also directly undergo visible-light-excitation and then initial follow-up SET oxidation of a suitable substrate.²³ Specifically, tetrahydroisoquinoline derived α -amino alkyl radical formation and its stereoselective addition to an α,β -unsaturated 2-acyl imidazole were successfully achieved by using a single chiral-at-rhodium catalyst. On the contrast, the related Giese type radical additions previously developed by Meggers group require two catalysts. Shortly after that, Jiajia Ma from the Meggers group disclosed a single chiral-at-rhodium complex catalyzed reductive coupling of *N*-(acyloxy)phthalimide and α,β -unsaturated *N*-acyl pyrazole in the presence of Hantzsch ester as terminal reductant and proton source.²⁴ This robust protocol provided an efficient approach to enantioenriched β -substituted γ -aminobutyric acid derivatives, optionally containing fluorinated quaternary stereocenters. New asymmetric transformations based on the photoexcited chiral-at-rhodium catalyst/substrate complex are anticipated.

References

- 1 X. Huang, T. R. Quinn, K. Harms, R. D. Webster, L. Zhang, O. Wiest, E. Meggers, *J. Am. Chem. Soc.* **2017**, *139*, 9120-9123.
- 2 X. Huang, X. Li, X. Xie, K. Harms, R. Riedel, E. Meggers, *Nat. Commun.* **2017**, *8*, 2245.
- 3 a) F. Mueller, J. Mattay, *Chem. Rev.* **1993**, *93*, 99-117; b) J. Iriondo-Alberdi, M. F. Greaney, *Eur. J. Org. Chem.* **2007**, 4801-4815.
- 4 R. Brimioulle, D. Lenhart, M. M. Maturi, T. Bach, *Angew. Chem. Int. Ed.* **2015**, *54*, 3872-3890.
- 5 S. Poplata, A. Tröster, Y.-Q. Zou, T. Bach, *Chem. Rev.* **2016**, *116*, 9748-9815.
- 6 a) R. Brimioulle, T. Bach, *Science* **2013**, *342*, 840-843; b) R. Brimioulle, A. Bauer, T. Bach, *J. Am. Chem. Soc.* **2015**, *137*, 5170-5176.
- 7 a) M. M. Maturi, T. Bach, *Angew. Chem. Int. Ed.* **2014**, *53*, 7661-7664; b) A. Tröster, R. Alonso, A.

- Bauer, T. Bach, *J. Am. Chem. Soc.* **2016**, *138*, 7808-7811.
- 8 K. L. Skubi, J. B. Kidd, H. Jung, I. A. Guzei, M.-H. Baik, T. P. Yoon, *J. Am. Chem. Soc.* **2017**, *139*, 17186-17192.
- 9 a) J. Du, K. L. Skubi, D. M. Schultz, T. P. Yoon, *Science* **2014**, *344*, 392-396; b) T. R. Blum, Z. D. Miller, D. M. Bates, I. A. Guzei, T. P. Yoon, *Science* **2016**, *354*, 1391-1395.
- 10 C. Ebner, E. M. Carreira, *Chem. Rev.* **2017**, *117*, 11651-11679.
- 11 H.-U. Reissig, R. Zimmer, *Chem. Rev.* **2003**, *103*, 1151-1196.
- 12 a) J. M. Tanko, R. E. Drumright, *J. Am. Chem. Soc.* **1990**, *112*, 5362-5363; b) J. M. Tanko, R. E. Drumright, *J. Am. Chem. Soc.* **1992**, *114*, 1844-1854; c) J. Cossy, N. Furet, S. BouzBouz, *Tetrahedron* **1995**, *51*, 11751-11764; d) G. A. Molander, C. Alonso-Alija, *Tetrahedron* **1997**, *53*, 8067-8084.
- 13 A. G. Amador, E. M. Sherbrook, T. P. Yoon, *J. Am. Chem. Soc.* **2016**, *138*, 4722-4725.
- 14 M. Julliard, M. Chanon, *Chem. Rev.* **1983**, *83*, 425-506.
- 15 J. Luis-Barrera, V. Laina-Martín, T. Rigotti, F. Peccati, X. Solans-Monfort, M. Sodupe, R. Mas-Ballester, M. Liras, J. Alemán, *Angew. Chem. Int. Ed.* **2017**, *56*, 7826-7830.
- 16 S. Fukuzumi, K. Ohkubo, T. Suenobu, K. Kato, M. Fujitsuka, O. Ito, *J. Am. Chem. Soc.* **2001**, *123*, 8459-8467.
- 17 U. Wille, *Chem. Rev.* **2013**, *113*, 813-853.
- 18 S. Luo, X. Zhang, Y. Zheng, K. Harms, L. Zhang, E. Meggers, *J. Org. Chem.* **2017**, *82*, 8995-9005.
- 19 S. Chen, X. Huang, E. Meggers, K. N. Houk, *J. Am. Chem. Soc.* **2017**, *139*, 17902-17907.
- 20 a) J. E. Hillis, M. K. DeArmond, *J. Lumin.* **1971**, *4*, 273-290; b) T. L. Kelly, J. F. Endicott, *J. Am. Chem. Soc.* **1972**, *94*, 278-279.
- 21 X. Huang, J. Lin, T. Shen, K. Harms, M. Marchini, P. Ceroni, E. Meggers, *Angew. Chem. Int. Ed.* **2018**, *57*, 5454-5458.
- 22 A special class of alkynes, acetylenedicarboxylates have been reported to undergo enantioselective [2+2] photocycloadditions by Bach, see ref. 7a.
- 23 S.-X. Lin, G.-J. Sun, Q. Kang, *Chem. Commun.* **2017**, *53*, 7665-7668.
- 24 J. Ma, J. Lin, L. Zhao, K. Harms, M. Marsch, X. Xie, E. Meggers, *Angew. Chem. Int. Ed.* **2018**, *57*, 11193-11197.

3.6 Electricity Driven Asymmetric Lewis Acid Catalysis

3.6.1 Reaction Design and Research Background

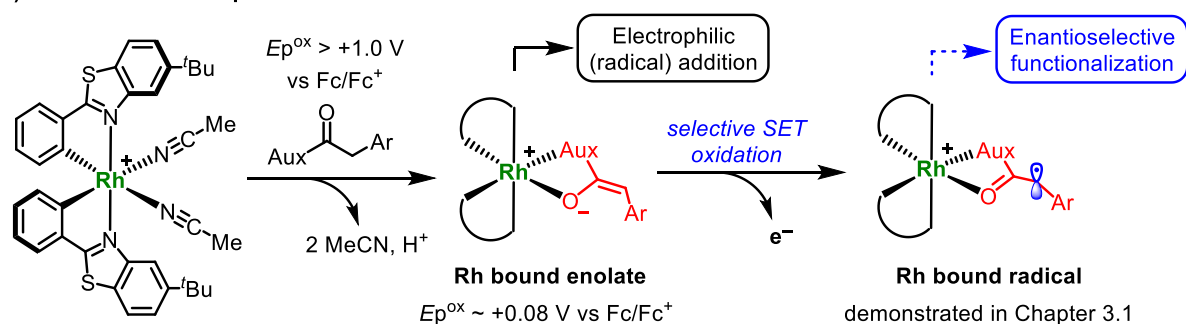
Bis-cyclometalated chiral-at-metal rhodium complexes have been demonstrated to be a versatile, novel class of chiral Lewis acids.¹ Among their diverse reactivity, HOMO activation of carbonyl compounds through bidentate coordination and deprotonation will form well-defined catalyst bound enolate intermediates (**Figure 98a**). These enolate species have been used not only as nucleophiles in the ground states toward a variety of asymmetric electrophilic additions,² but also as visible-light-absorbing antennas which after photoexcitation become highly reducing initiators for redox processes.³ In addition, chapter 3.1 clearly discloses a significantly lower redox potential by ~1.0 V of rhodium bound enolate compared with the parent carbonyl substrate.⁴ As a result, this enolate species could also be a reductive quencher (in the ground state) participating in an additional photoredox catalysis, thereby forming a rhodium bound α -carbonyl radical that is well-demonstrated in chapter 3.1. However, systematic studies and effective functionalization of this kind of radical species remain unexplored.

The author of this thesis envisioned that substrate binding to the catalyst and deprotonation would raise the HOMO and trigger a mild and selective SET oxidation to provide electron deficient rhodium bound radicals, which might be trapped by electron-rich silyl enol ethers in a stereocontrolled fashion generating non-racemic chiral 1,4-dicarbonyls (**Figure 98b**). Selective oxidative cross coupling of two enolates is a direct and attractive way for the construction of synthetically valuable unsymmetrical 1,4-dicarbonyls and much progress has been made over the last few decades.⁵ However, owing to the difficulty in suppressing the concomitant homo-coupling⁶ and also the lack of efficient catalytic asymmetric systems, only few enantioselective versions that rely on SOMO activation of aldehydes by chiral amines were reported.⁷ This SOMO catalysis employs stoichiometric amount of ceric ammonium nitrate (CAN) as oxidant, which is not attractive from the perspective of green chemistry. Hence, a robust catalytic asymmetric scheme to enable the effective and sustainable oxidative enolates cross coupling is highly desirable.

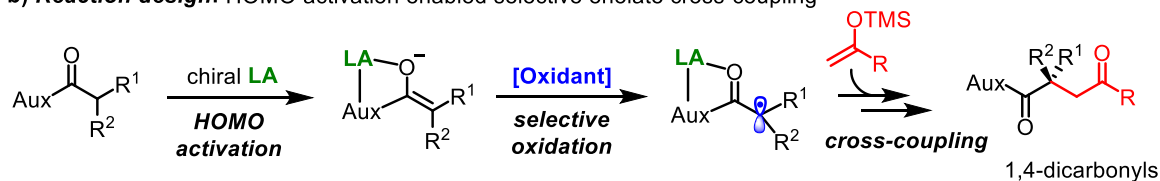
During the mechanistic investigations of the asymmetric amination described in chapter 3.1, a 1,4-dicarbonyl compound **9ba** was isolated in 42% yield when a silyl enol ether **8a** was added to the

photoredox reaction mixture (**Figure 98c**). Inspired by this result, an electricity driven asymmetric Lewis acid catalysis for the highly selective enolates cross coupling was developed which is described in this chapter. Notably, compared with the visible-light-driven system that requires two catalysts and uses an acceptor-substituted azide as sacrificed oxidant with the formation of the side product derived from chemical oxidation, this newly developed electrosynthesis features unique advantages, including simple and mild conditions, less waste generation and higher functional group tolerance.

a) HOMO activation upon enolate formation



b) Reaction design: HOMO activation enabled selective enolate cross-coupling



- Challenges:**
- 1) Concomitant homo-coupling by-products
 - 2) Asymmetric induction (2 examples based on SOMO catalysis)
 - 3) [Oxidant]: possible side products from the incorporation of chemical oxidant

c) Initial finding during the mechanistic study of photoredox amination (Chapter 3.1)

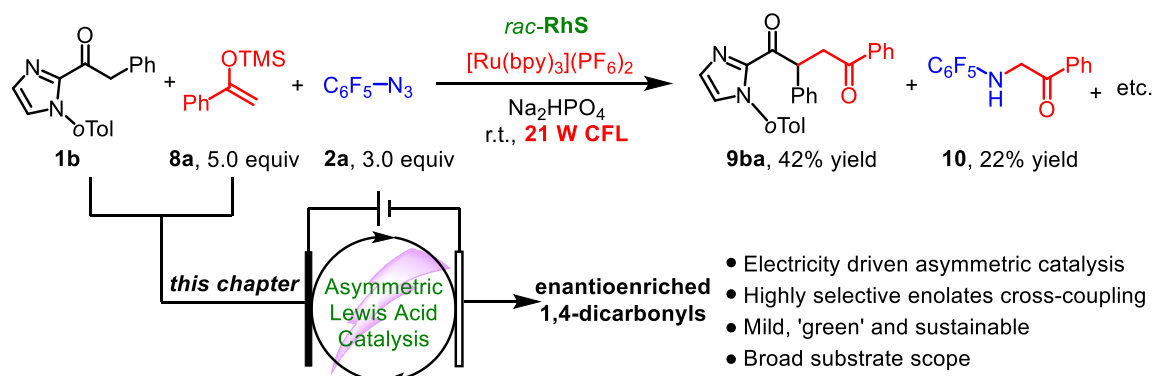
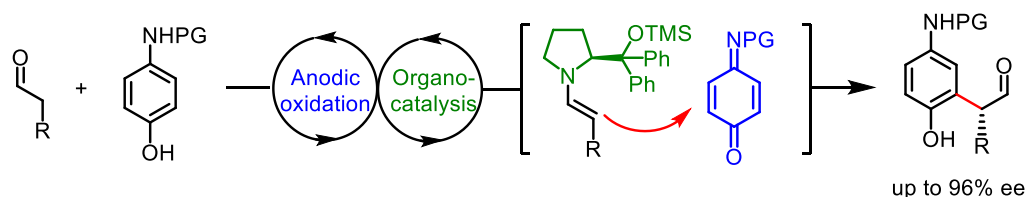


Figure 98. Rational design leading to an electricity driven asymmetric Lewis acid catalysis for highly selective cross coupling of enolates.

Organic electrosynthesis employs electrons as reagents which avoids the use of stoichiometric amounts of chemical oxidants or reductants and has therefore long been recognized as a sustainable synthetic platform for redox reactions.⁸ Likewise, asymmetric catalysis is considered an economic and efficient strategy to provide homochiral compounds for the production of drugs, agricultural chemicals, flavors, fragrances, and materials.⁹ Merging organic electrosynthesis with asymmetric catalysis is therefore an area of great significance. However, key challenges have hampered the development of electricity driven asymmetric catalysis. First, the oxidatively or reductively generated intermediate radical ions, radicals, or ions must be interfaced with a catalytic cycle but their high reactivity often provides ample opportunities for non-catalyzed side reactions which affect overall yields and enantioselectivities. Second, many catalysts display a limited compatibility with the conditions in an electrochemical cell due to redox instability and interactions with the electrolyte. This might explain why catalytic asymmetric electrochemistry is still in its infancy with a limited number of different concepts and usually modest enantioselectivities.¹⁰

a) *Jørgensen's work:*



b) *Luo's work:*

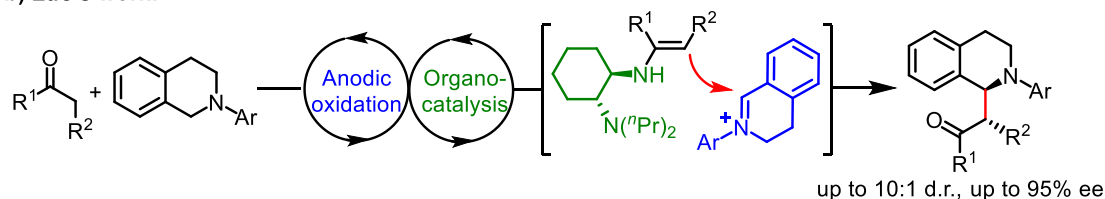


Figure 99. Two highly asymmetric electrochemical transformations that separate the asymmetric catalysis from electrochemical oxidation.

There are two highly asymmetric examples of electrochemical transformations, which benefit from the separation of electrochemical oxidation and asymmetric catalysis (**Figure 99**).¹¹ Generally speaking, an electrophile is generated by anodic oxidation of a suitable, easily oxidizable precursor, and this electrochemical step is subsequently followed up with enantioselective enamine catalysis. For example, Jørgensen demonstrated that the anodic oxidation of electron-rich aminophenols is compatible with enantioselective enamine catalysis (**Figure 99a**),^{11a} whereas Luo reported a

combination of an anodic oxidation of tetrahydroisoquinolines with enantioselective enamine catalysis for enabling an asymmetric α -functionalization of simple ketones (**Figure 99b**).^{11b} Although notable enantioselectivities of up to 96% ee were obtained, this method suffers from the oxidative sensitivity of the chiral amine catalyst and enamine intermediate which therefore strongly limits the choice of electrophile precursors. And in principle, these anodic oxidations could be replaced by other oxidation methods.

In a different electrochemical activation strategy, the active asymmetric catalyst was generated electrochemically. For example, a chiral *N*-oxyl radical achieved a kinetic resolution of amines and alcohols as reported by Kashiwagi and co-workers.¹² However, the direct interaction with the electrode requires a redox active and stable chiral catalyst and is typically plagued with low enantioselectivities.¹³ Therefore, often an additional redox mediator is employed which allows lower potentials and offers higher chemoselectivity.¹⁴ Some elegant catalytic systems have been successfully applied to indirect electrolysis with mediators, such as iodine-assisted osmium/chiral ligand systems,¹⁵ chiral metal salen complexes,¹⁶ and some enzymatic systems¹⁷.

A simplified appealing strategy uses only a single catalyst which not only provides the asymmetric induction but also facilitates the electrochemical process through an activation of one substrate. Although acid/base catalysts are well-known to activate the frontier molecular orbitals of substrates, their applications in asymmetric electrochemistry are underexplored. Few examples that use enamine activation toward facile anodic oxidation have been reported but with limited scopes and inferior stereoselectivities.¹⁸ For the first time, this chapter presents a unique electricity driven asymmetric Lewis acid catalysis for intermolecular cross coupling of enolates. Notably, the chiral Lewis acid is both involved in the electrochemical step and the asymmetric induction. At the end of this chapter, other electrochemical reactions catalyzed by the chiral-at-metal Lewis acid are described.

3.6.2 Reaction Development

Recently, organic electrosynthesis has experienced a renaissance promoted not only by the employment of novel or reanimated concepts, but also the invention of general and standard electrochemical devices for organic synthesis.¹⁹ Actually, this study commenced with a commercially available ElectraSyn 2.0 that was recently devised by Baran in collaboration with the company IKA

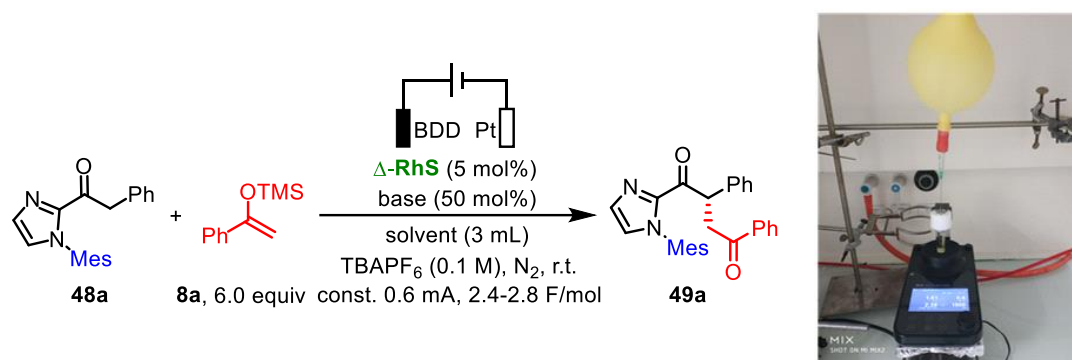
Inc.²⁰ After extensive attempts, an undivided electrochemical cell consisting of a boron-doped diamond (BDD) anode and a platinum (Pt) cathode under a relative low potential with TBAPF₆ as electrolyte was found to be compatible with the chiral-at-rhodium catalysis. Based on previous conclusions on the origin of asymmetric induction in chiral-at-rhodium catalyzed enolate chemistry, a bulky *N*-mesityl 2-acyl imidazole **48a** was chosen as substrate for initial experiments. To test the hypothesis, the solution of **48a**, silyl enol ether **8a**, 2,6-lutidine (50 mol%), and TBAPF₆ in THF/MeOH (1:2) was electrolyzed under a constant current of 0.6 mA. Encouragingly, the desired 1,4-dicarbonyl **49a** was obtained with an excellent enantioselectivity of 99% ee catalyzed by 5.0 mol% of Δ -**RhS**, albeit with a moderate yield (Table 20, entry 1). Extensive screening of solvents (entries 1-5) and bases (entries 6-9) led to the result that using a mixture of THF/MeOH as solvent and 2,6-lutidine as the soluble organic base was the most suitable condition for the current electrolysis. The addition of HFIP, a widely-used additive in electrochemical reactions, was not helpful (entry 5). The yield of **49a** could not be improved further (50-60%), which might be due to the lower reactivity of the highly congested rhodium bound radical intermediate bearing a *N*-mesityl imidazolyl auxiliary.

Hence, 2-acyl imidazole **48b** with a smaller phenyl as the *N*-substituent was selected for further optimization. Table 21 shows the effects of different parameters on the reaction **48b** + **8a** \rightarrow **49b**. Firstly, the bis-cyclometalated iridium based catalyst Δ -**IrS** could give the formation of desired 1,4-dicarbonyl **49b** in 27% yield with an excellent enantioselectivity of 98% ee (entry 1). Interestingly, a newly synthesized rhodium complex Δ -**RhS**(TMS), bearing more bulky trimethylsilyl (TMS) instead of *tert*-butyl groups, improved the yield of **49b** to 82% without affecting the enantioselectivity (entry 3). The possible reason for this might be less product decomposition when a more steric demanding catalyst is used.

Other electrodes were evaluated as well. While platinum as anodic material resulted in great inhibition of product formation, a graphite or a reticulated vitreous carbon (RVC) anode had little influence on reaction efficiency compared with the BDD anode (entries 3-6). For further investigations, the cheaper graphite anode was chosen as the standard anode material which delivered optimal conditions for **49b** (82% NMR yield, 79% isolated yield, 97% ee, entry 6). As shown in entry 7, a cheaper electrolyte LiClO₄ could be an alternative which gave satisfactory results. But a BF₄⁻ salt resulted in a less clean reaction with a decreased yield of 44% (entry 8). Electrolysis under a constant current of 1.5 mA could also generate **49b** in good yield with excellent ee (entry 9), thereby shortening

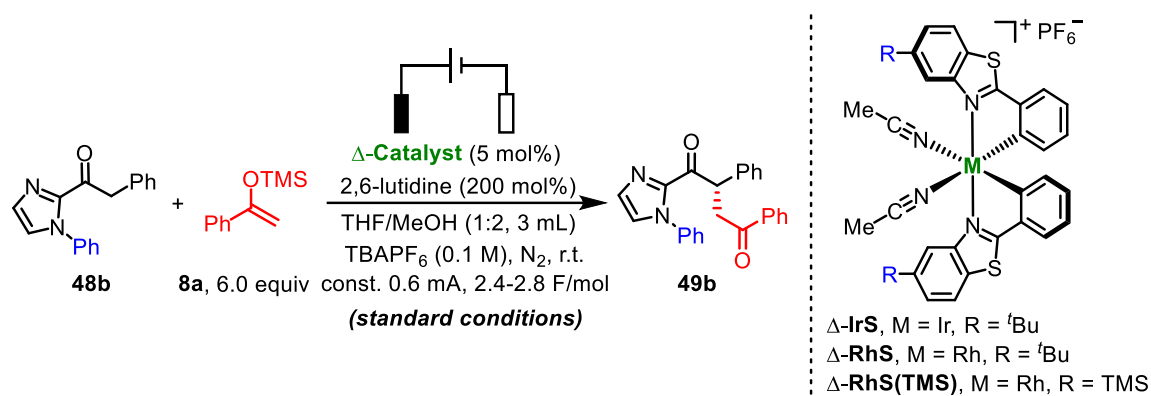
the reaction time. Besides, the reaction could take place under a quite low potential of 0.8 V vs Ag/AgCl indicating a mild and selective electron transfer process (entry 10). Furthermore, two control experiments were performed. In the absence of any catalyst, the undesirable homo-coupling of **8a** was observed as the major reaction without any formation of the hetero-coupling product **49b** (entry 11). In the presence of catalyst but absence of an external base, the product **49b** was generated in a significantly lower yield of just 46%, which could be attributed to in situ generated base from cathode reduction (entry 12).

Table 20. Initial experiments for electricity driven enolates cross coupling.^[a]



Entry	Base	Solvent	Yield [%]	Ee [%]
1	2,6-lutidine	THF/MeOH (1:2)	50-60 ^[b]	99
2	2,6-lutidine	MeOH (1:2)	50-60 ^[b]	99
3	2,6-lutidine	Acetone/MeOH (1:2)	50-60 ^[b]	99
4	2,6-lutidine	MeCN/MeOH (1:2)	Mess	n.d.
5	2,6-lutidine	THF/MeOH/HFIP (1:2, 2.0 equiv)	50-60 ^[b]	n.d.
6	Na ₂ HPO ₄	THF/MeOH (1:2)	36 ^[c]	n.d.
7	NaOAc	THF/MeOH (1:2)	31 ^[c]	n.d.
8	DABCO	THF/MeOH (1:2)	31 ^[c]	n.d.
9	NaOMe	THF/MeOH (1:2)	43 ^[c]	n.d.

[a] Reaction conditions: in an ElectraSyn 2.0 cell, **48a** (0.10 mmol), **8a** (0.60 mmol), Δ -RhS (5.0 mol%), base (50 mol%), and TBAPF₆ (0.30 mmol) in solvent (3.0 mL) were electrolyzed under a constant current of 0.6 mA with the electricity consumption of 2.4-2.8 F/mol. Ee was determined by HPLC on a chiral stationary phase. [b] Approximate yield since the product was isolated as a mixture. [c] NMR yield.

Table 21. Optimizations of the electricity driven asymmetric enolates cross coupling.^[a]

Entry	Catalyst	Electrodes	Derivations from S.C.	Yield [%]	Ee [%]
1	Δ -IrS	BDD-Pt	None	27	98
2	Δ -RhS	BDD-Pt	None	45	97
3	Δ -RhS(TMS)	BDD-Pt	None	82	97
4	Δ -RhS(TMS)	Pt-Pt	None	<10	n.d.
5	Δ -RhS(TMS)	RVC-Pt	None	80	93
6	Δ -RhS(TMS)	Graphite-Pt	None	82 (79)	97
7	Δ -RhS(TMS)	Graphite-Pt	LiClO ₄ instead of TBAPF ₆	79	95
8	Δ -RhS(TMS)	Graphite-Pt	TBAPF ₄ instead of TBAPF ₆	44	95
9	Δ -RhS(TMS)	Graphite-Pt	Const. 1.5 mA instead	80	96
10	Δ -RhS(TMS)	Graphite-Pt	Const. 0.8 V vs Ag/AgCl	72	97
11 ^[b]	None	Graphite-Pt	None	0	n.a.
12	Δ -RhS(TMS)	Graphite-Pt	Without 2,6-lutidine	46	96

[a] Reaction conditions: in an ElectraSyn 2.0 cell, **48b** (0.10 mmol), **8a** (0.60 mmol), catalyst (5.0 mol%), 2,6-lutidine (200 mol%), and TBAPF₆ (0.30 mmol) in THF/MeOH (1:2, 3.0 mL) were electrolyzed under a constant current of 0.6 mA with the electricity consumption of 2.4-2.8 F/mol. NMR yield, isolated yield is provided in parentheses; ee was determined by HPLC on a chiral stationary phase. [b] Homo-coupling of **8a** was the major side reaction.

Overall, a practical set-up based on the ElectraSyn 2.0 and the optimal conditions that rely on a new **RhS(TMS)** catalyst have been disclosed for the asymmetric electrochemical cross coupling of two enolates providing a previously elusive approach to chiral 1,4-dicarbonyls (**Table 21**, entry 6).

3.6.3 Substrate Scope

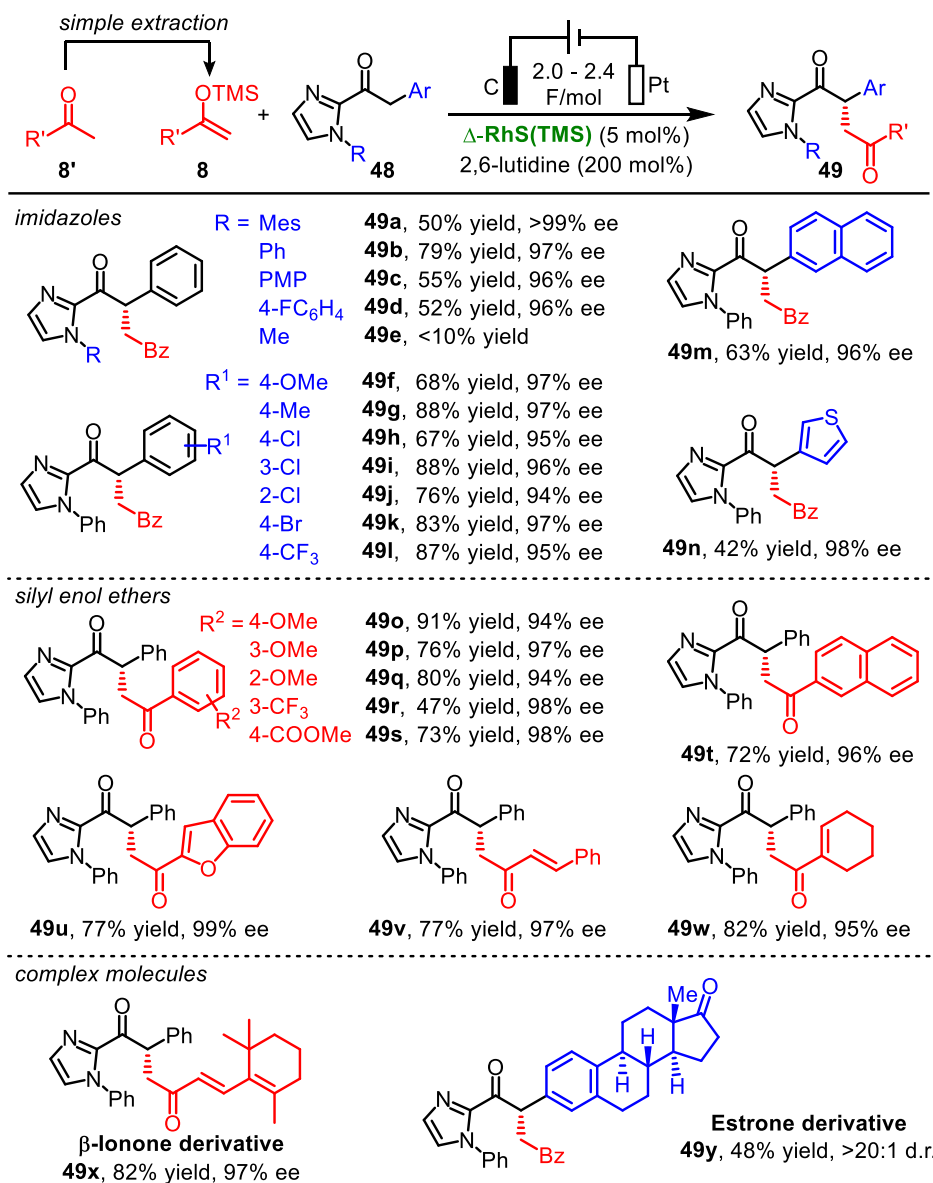


Figure 100. Substrate scope of the electrocyclic reaction with the generation of tertiary carbon stereocenters. Reaction conditions: see **Table 21** entry 6. The structure of **49k** was determined by X-ray crystallography and all other compounds were assigned accordingly.

The investigation on the substrate scope started with variations of the 2-acyl imidazole substrate. As shown in **Figure 100**, different groups at the *N*-atom of the imidazole auxiliary showed different efficiencies (**49a-e**). A bulky mesityl group resulted in the highest ee (**49a**, >99% ee) while a low yield of the 1,4-diketone was obtained using a methyl group (**49e**, <10% yield). This reaction exhibited broad tolerance with respect to the electronic property and substitution pattern of substituents on the

aromatic ring at the stereogenic carbon (**49f-l**, 67-88% yields with 94-97% ee). Additionally, 1,4-dicarbonyl products containing a 2-naphthyl (**49m**) and a 2-thienyl (**49n**) moiety could be produced in acceptable yields with excellent enantioselectivities, respectively.

On the other hand, a wide range of aryl substituted silyl enol ethers **8** underwent the cross coupling smoothly, delivering **49o-u** in yields of 47-91% with up to 99% ee. The compatibility of this protocol was further showcased with a benzofuran **49u**, and by the effective generation of two complicated natural product derivatives (a β -ionone derivative **49x** and an estrone derivative **49y**). It is noteworthy that all silyl enol ethers used were prepared and subjected to the electrochemical conditions described herein through simple extraction without tedious distillation.

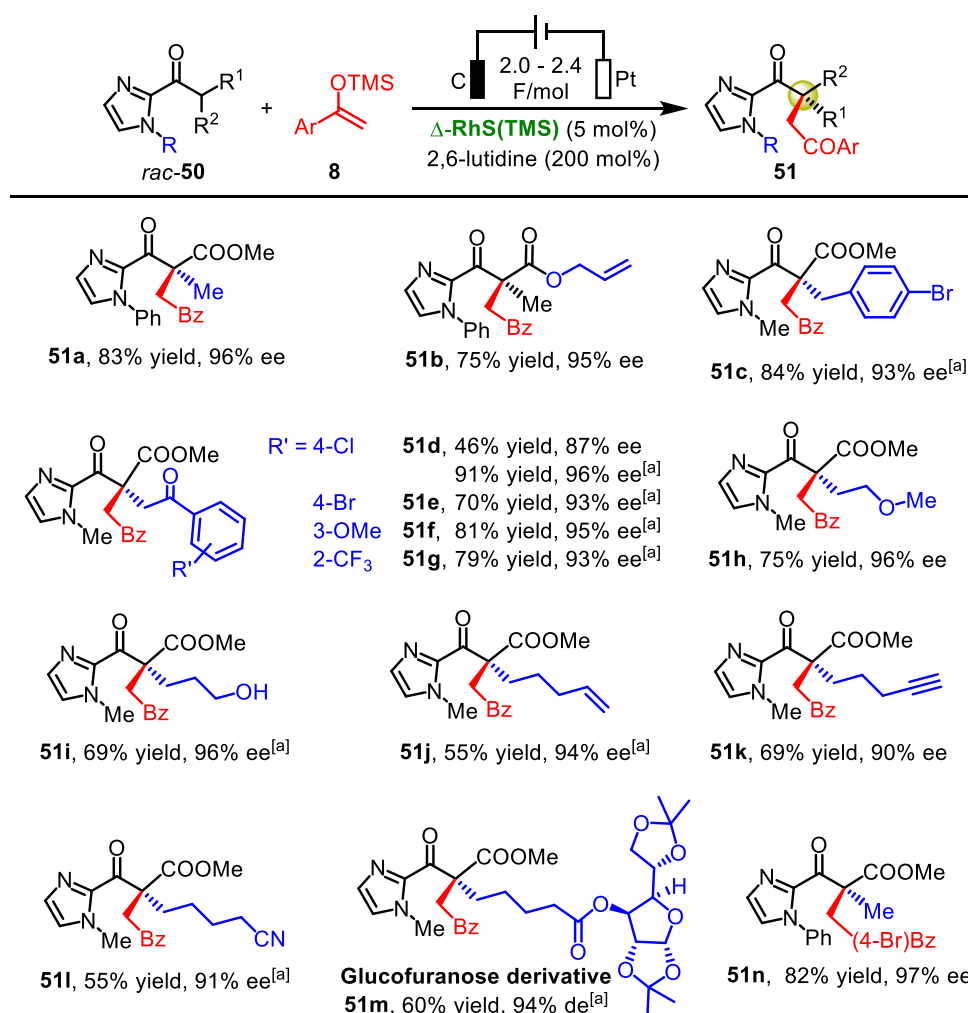


Figure 101. Substrate scope of the electrosynthesis with the generation of all-carbon quaternary centers. Reaction conditions: see **Table 21** entry 6. The structure of **51n** was determined by X-ray crystallography and all other compounds were assigned accordingly. [a] Δ -RhS (5.0 mol%) instead.

After many efforts (see failed examples in **Figure 102**), the substrate scope was expanded to more challenging racemic tertiary acyl imidazoles (**Figure 101**). Various enantioenriched carbonyl compounds bearing an all-carbon quaternary stereocenter were successfully constructed by the electrochemical method, which otherwise would be difficult to accomplish by traditional methods. Satisfactory yields and ee could be obtained by tuning the substituents on the imidazole and/or catalyst addressing the challenge of low reactivity of the tertiary carbon radicals. For example, the reaction of **50d** bearing a smaller methyl group at the *N*-atom of the imidazolyl auxiliary, catalyzed by the Δ -**RhS** provided **51d** with much higher yield and ee (91% yield, 96% ee), compared with the reaction catalyzed by Δ -**RhS**(TMS) (46% yield, 87% ee). Interestingly, the stereogenic carbons with two similar phenacyl substituents were formed with excellent enantioselectivities (**51d-g**, 93-96% ee). Remarkably, this transformation is extremely mild and effective as highlighted by the tolerance of many sensitive functional groups, including a free hydroxyl (**51i**), terminal C=C double bond (**51j**) and C \equiv C triplet bond (**51k**), and a glucofuranose (**51m**).

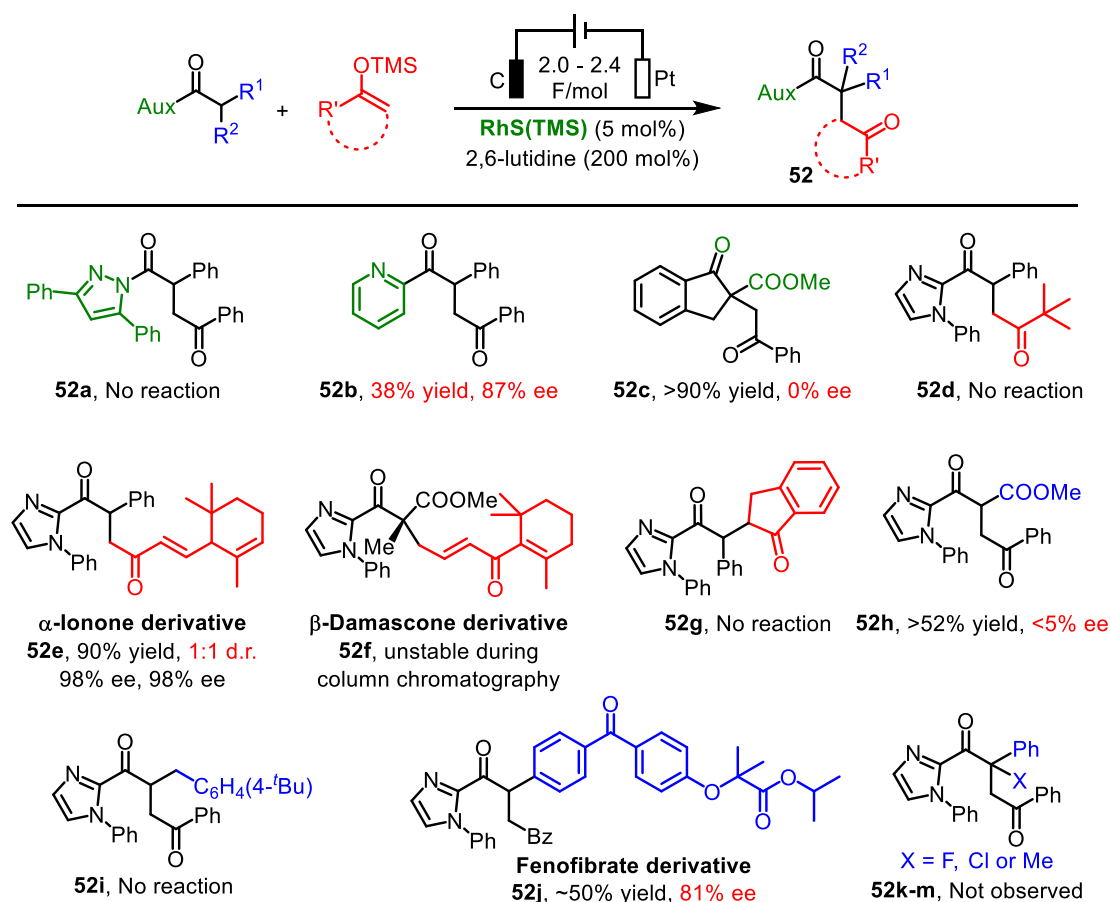


Figure 102. Limitations of the present electrochemical synthesis.

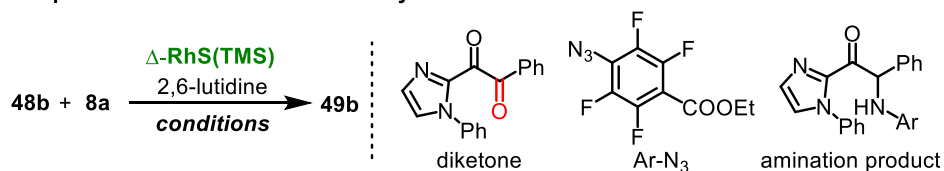
Some unsuccessful examples are listed in **Figure 102**. First, this catalysis heavily relies on the *N,O*-bidentate coordination of 2-acyl imidazole substrates. *N*-Acyl pyrazole failed to undergo the anodic oxidation while homo-coupling of silyl enol ether was observed in this case (**52a**). Besides, 2-pyridinyl auxiliary gave inferior results (**52b**), while a *O,O*-coordinating substrate could not give any enantioselectivity (**52c**). Second, a conjugated terminal enol ether is required for effective trapping of the radical intermediate as indicated by the failed attempts to generate products **52d** and **52g**. Third, an aromatic or an ester group at the stereogenic carbon is necessary for the formation of rhodium bound enolate intermediate (as suggested by the case of **52i**), which is in accord with previous observations.¹ Unfortunately, some complicated molecules could not be obtained with satisfactory results (**52e-f**, **52j**). In addition, other kind of quaternary carbons are not accessible by the current method (**52k-m**).

To highlight the advantages of this electrochemical protocol, the efficiency of different oxidative systems was compared (**Figure 103a**). Firstly, a chemical oxidation method was explored. Ceric ammonium nitrate (CAN) is a commonly used oxidant in SOMO catalysis,⁷ but proved unsuitable for this coupling since **49b** was only generated in 8% yield and with 81% ee (**Figure 103a**, entry 2). Besides, Fe(acac)₃, which was demonstrated as effective SET oxidant in a reported enolates cross coupling reaction,⁵ failed to fulfill this transformation (**Figure 103a**, entry 3). Photoredox catalysis that is recognized as a powerful method for performing redox reactions under mild conditions²¹ was able to facilitate the transformation. However, when the mixture was irradiated with a compact fluorescent lamp (CFL) using molecular oxygen as the terminal oxidant,²² the coupling product **49b** was only formed in 11% yield together with an unavoidable oxygenated diketone side product (**Figure 103a**, entry 4). In addition, when the previously developed dual-catalyst system was used together with an aryl azide as oxidant, 35% yield of **49b** could be obtained, albeit with 63% ee, whereas the amination product was found to be the major product (64% yield) (**Figure 103a**, entry 5). These results highlight the unique advantages of electrochemistry for the here reported catalytic asymmetric hetero-coupling in terms of cleanliness of conversion, yield, and enantioselectivity. The controlled electrochemical delivery of electrons ensures a clean transformation under mild redox conditions without the formation of undesirable side products which are observed under photoredox conditions or with chemical oxidants.

Also, a two-step one-pot procedure, which directly started from the acetophenone **8a'**, furnished

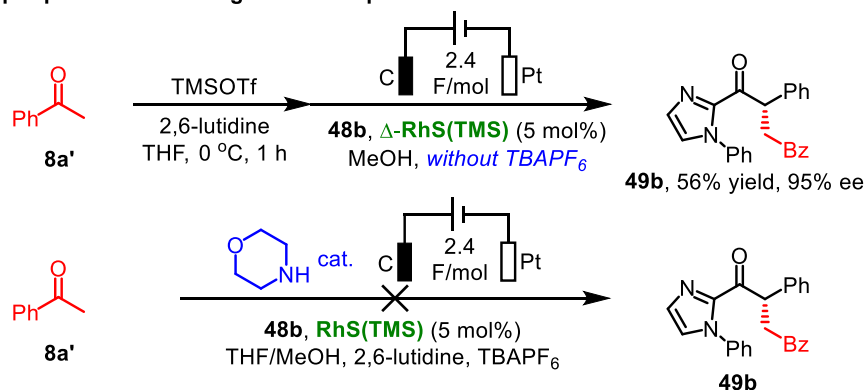
49b in a reasonable yield of 56% with 95% ee even in the absence of additional electrolyte (**Figure 103b**). But the attempt utilizing in situ formed catalytic amount of enamine instead of excess of silyl enol ester failed to produce the desired product.

a) Comparisons of different oxidation systems



Entry	Derivations from Electrolysis	Yield of 49b / ee	Other materials
1 ^[a]	None [C(+)-Pt(-), const. 0.6 mA]	79% / 97%	-
2 ^[b]	CAN (2.0 equiv)	8% / 81%	decomposed
3 ^[b]	Fe(acac)₃ (2.0 equiv)	0% / n.a.	48b (60%)
4 ^[b]	O₂ (balloon), 21 W CFL	11% / 86%	48b (74%), diketone (9%)
5 ^[b]	[Ru(bpy)₃](PF₆)₂, 21 W CFL, Ar-N₃ (2.0 equiv), acetone	35% / 63%	amination product (64%)

b) One-pot procedure starting from acetophenone



c) Cleavage of imidazolyl group

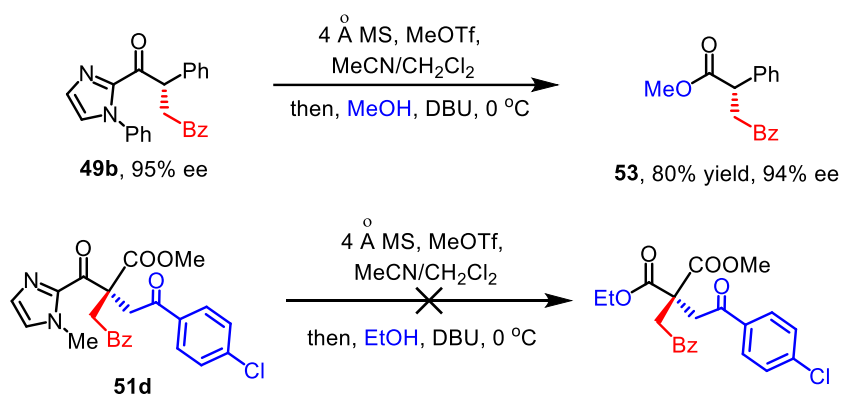
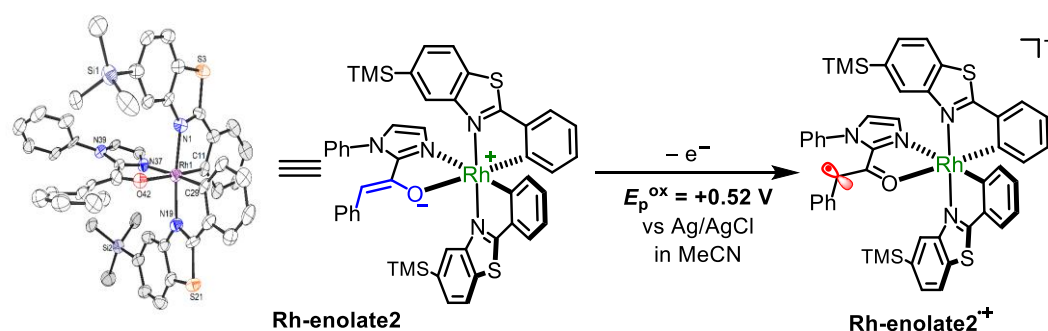


Figure 103. Comparisons of different synthetic methodologies and scope for synthetic applications of the electrosynthesis. [a] **Table 21**, entry 6. [b] As shown but without the electrochemical set-up and TBAPF₆.

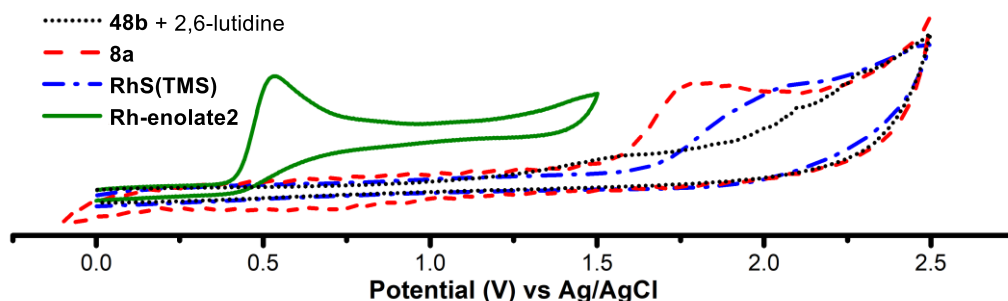
In addition, the cleavage of the imidazolyl group in 1,4-dicarbonyl compound **49b** was demonstrated, which led to ester **53** in 80% yield without a significant decrease of optical purity (**Figure 103c**). Unfortunately, product **51d** with a quaternary stereocenter is not compatible under these conditions, which might be due to the sluggish ethanol addition to the ionic intermediate caused by the high steric hindrance.

3.6.4 Mechanistic Studies

a) Characterization of the key enolate intermediate



b) Cyclic voltammograms



c) TEMPO trapping

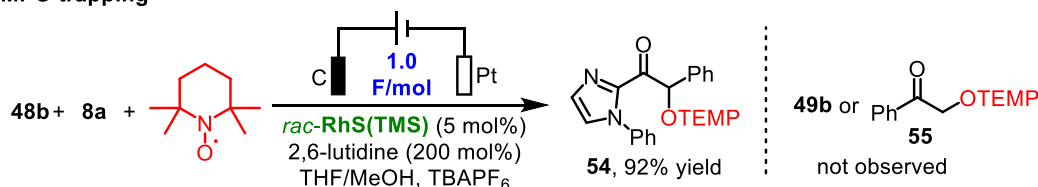


Figure 104. Mechanistic studies on the present electrosynthesis. Voltammetric experiments were conducted in MeCN containing 0.1 M TBAPF₆ at 22 ± 2 °C with a scan rate of 0.1 V s^{-1} . The current was normalized.

Mechanistic experiments were performed to understand the mechanism, the origin of the mild coupling conditions, and the observed high stereoselectivities (**Figure 104**). First, the key rhodium

bound enolate intermediate **Rh-enolate2** was synthesized and characterized. A crystal structural reveals a strong shielding of the *Re* face of the Δ -configured rhodium coordinated enolate by a very bulky trimethylsilyl group, which guarantees a high asymmetric induction (**Figure 104a**). Furthermore, the enolate complex **Rh-enolate2** also displays a very low oxidation potential of +0.52 V vs Ag/AgCl (**Figure 104b**). For comparison, voltammetry showed that the free acyl imidazole **48b** is unlikely to oxidize at a potential lower than 2 V vs Ag/AgCl (under conditions with 2,6-lutidine) and silyl enol ether **8a** is oxidized irreversibly at the potential of +1.72 vs Ag/AgCl. Thus, cyclic voltammetry clearly elucidates that it is not the silyl enol ether which is getting oxidized electrochemically but instead the intermediate rhodium enolate complex. Catalyst bound enolate formation effectively reduces the oxidation potential by around 1.5 V (HOMO activation) and thereby permits the selective SET oxidation for the generation of a catalyst bound reactive radical intermediate. To support this scenario, (2,2,6,6-tetramethylpiperidin-1-yl)oxyl (TEMPO) was used to trap this radical cation intermediate **Rh-enolate2**⁺. Indeed, a standard electrolysis with 1.0 F/mol of electricity in the presence of TEMPO provided the TEMPO-trapping product **54** in high yield with high current efficiency (both in 92%) without any formation of **8a** derived TEMPO-adduct **55** (**Figure 104c**), which is indicative of intermediate **Rh-enolate2**⁺. All these results strongly support that the formation of the chiral rhodium based enolate intermediate promotes the anodic oxidation and accounts for the mild conditions with high selectivity.

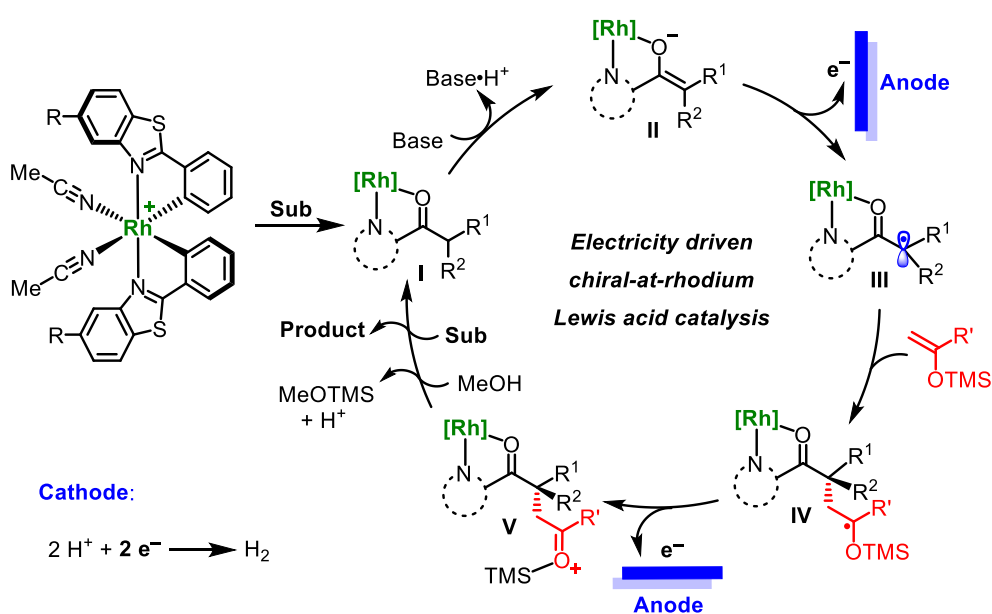


Figure 105. Proposed catalytic cycle for the present electrosynthesis.

Based on these experiments, a mechanism is shown in **Figure 105**. The catalysis initiates with the formation of rhodium bound substrate (int. **I**). A deprotonation generates the key enolate intermediate **II**. Subsequent single electron anodic oxidation selectively delivers rhodium bound radical intermediate **III**, which is trapped by electron rich silyl enol ethers, affording a secondary ketyl radical species (int. **IV**). Then, a second anodic single electron oxidation furnishes intermediate **V**. Finally, desilylation and substrate/product exchange complete the catalytic cycle. On the other hand, reduction of proton releases hydrogen gas at the cathode, thereby achieving proton and electron conservation.

3.6.5 Extensions to Other Transformations

1) α -Oxygenation with TEMPO

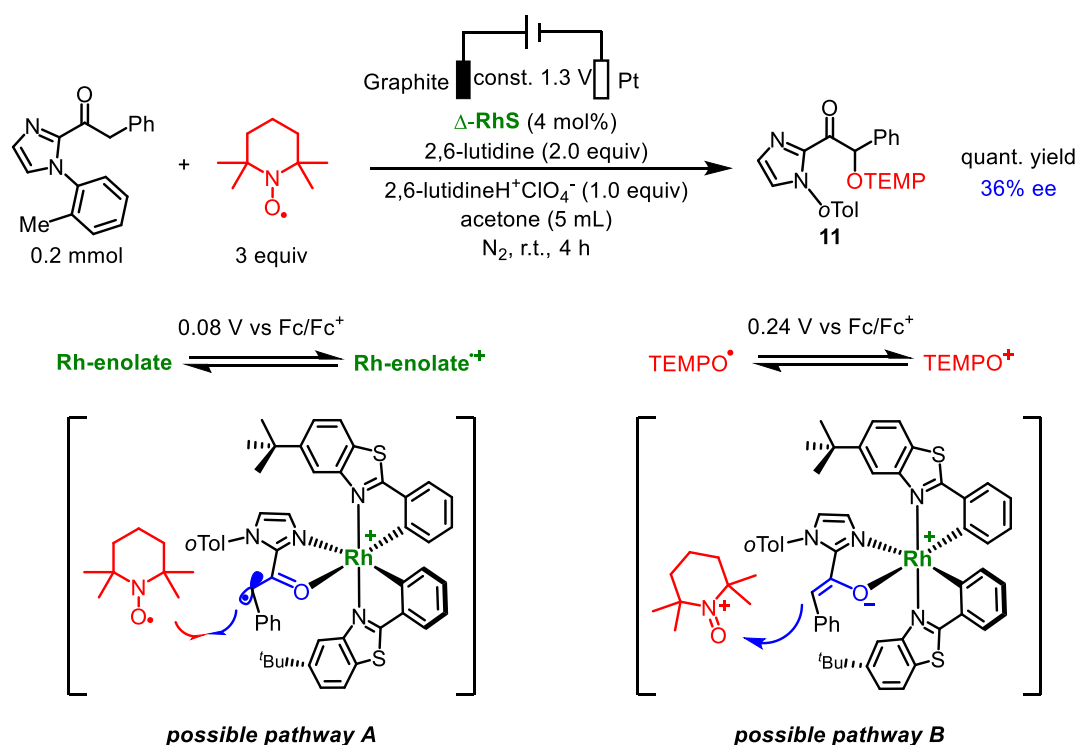


Figure 106. Electricity driven chiral Lewis acid catalyzed α -oxygenation with TEMPO.

Based on this newly-developed electricity driven chiral Lewis acid catalysis, a lot of transformations could be achieved. First of all, as mentioned above, the TEMPO adduct **11** was formed in excellent yield by electrolysis and a preliminary test reaction gave an enantioselectivity of 36% ee (**Figure 106**). Mechanistically, recombination of rhodium bound carbon centered radical with

free TEMPO radical might be operative (pathway A). But the anodic oxidation of TEMPO to TEMPO⁺ ($E_{1/2} = +0.24$ V vs Fc/Fc⁺)²³ followed by nucleophilic addition of rhodium bound enolate could not be completely excluded (pathway A). Considering that the redox potential of this key Rh-enolate species ($E_p^{[\text{Rh-enolate}]/[\text{Rh-enolate}]} = +0.08$ V vs Fc/Fc⁺, see Chapter 3.1)⁴ is slightly lower than TEMPO radical, pathway A is more favourable.

2) C-S Bond formation

Secondly, asymmetric dehydrogenative C-S bond formation was accomplished by this chiral-at-rhodium based electrochemical method. Preliminary experiments show that an α -thiolated carbonyl compound **56** could be generated in moderate yield with an encouraging enantioselectivity of 85% ee (**Figure 107**). During the reaction, disulfide was generated firstly, indicating the formation of intermediate sulfur radicals. This electron deficient pentafluoro sulphur-centered radical could add to the rhodium bound enolate intermediate (pathway A). Alternatively, the coupling of rhodium bound radical cation intermediate with disulfide or a sulfur centered radical is also possible (pathway B).²⁴ Further investigations are needed to clarify the reaction mechanism.

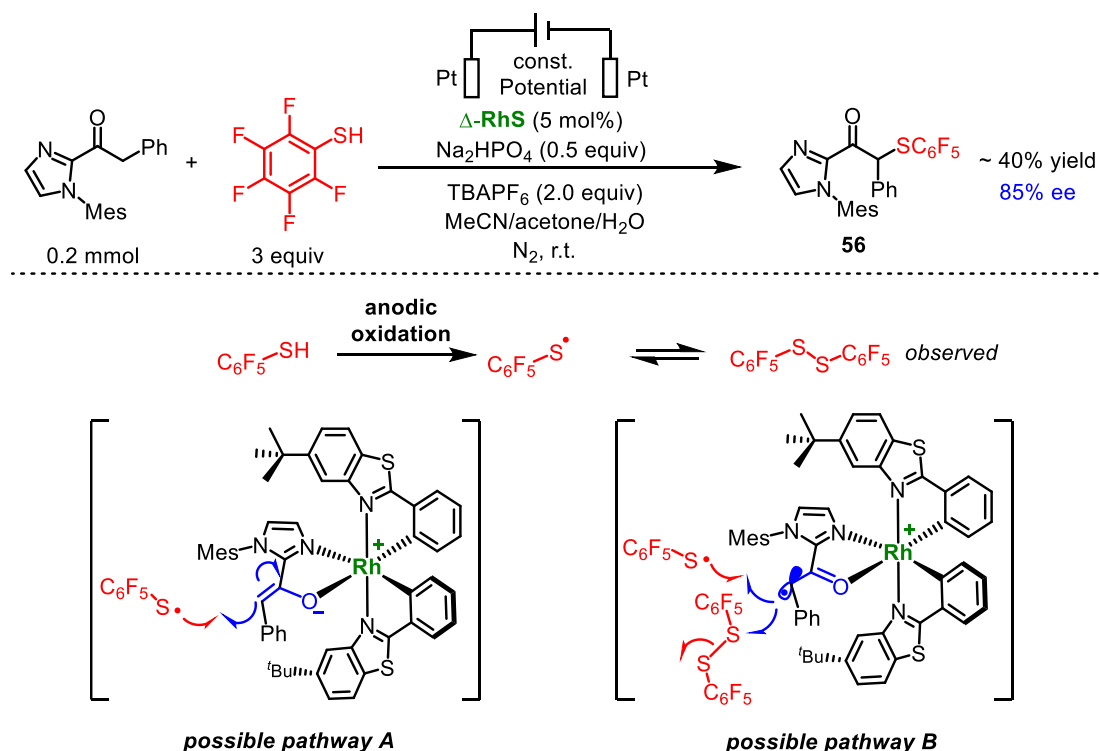
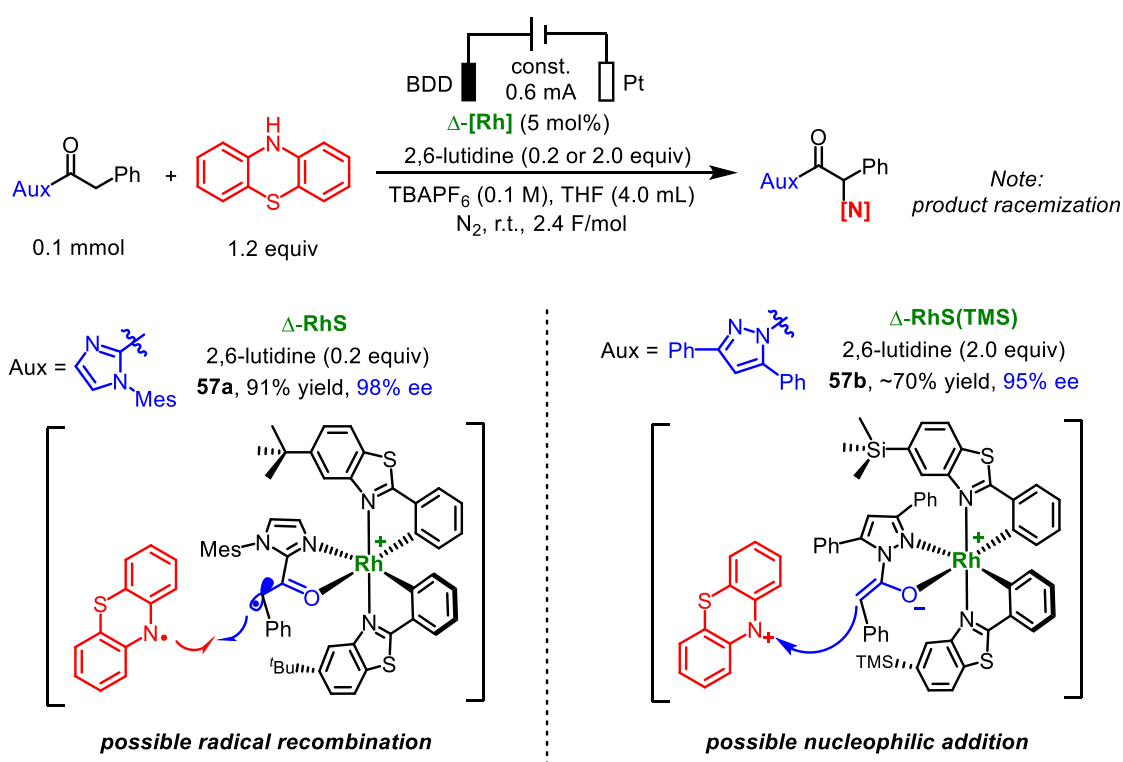


Figure 107. Electricity driven chiral Lewis acid catalyzed C-S formation.

3) α -Amination with 10*H*-phenothiazine

Thirdly, the enantioselective electrochemical α -amination was catalyzed by the chiral-at-rhodium complexes using 10*H*-phenothiazine, which is vulnerable to oxidation, as amino source (**Figure 108**). After extensive optimization, 91% yield with 98% ee for the generation of the α -amino 2-acyl imidazole product **57a** could be achieved. A radical-radical cross coupling mechanism is proposed,²⁵ based on cyclic voltammetry studies that reveal very close redox potentials between rhodium bound enolate ($E_{\text{p}^{\text{ox}}} = 0.52 \text{ V}$ vs Ag/AgCl, see **Figure 104a**) and 10*H*-phenothiazine (for the first SET oxidation process, $E_{1/2} = 0.64 \text{ V}$ vs Ag/AgCl, see **Figure 108**).



Key proof: CV of 10*H*-phenothiazine

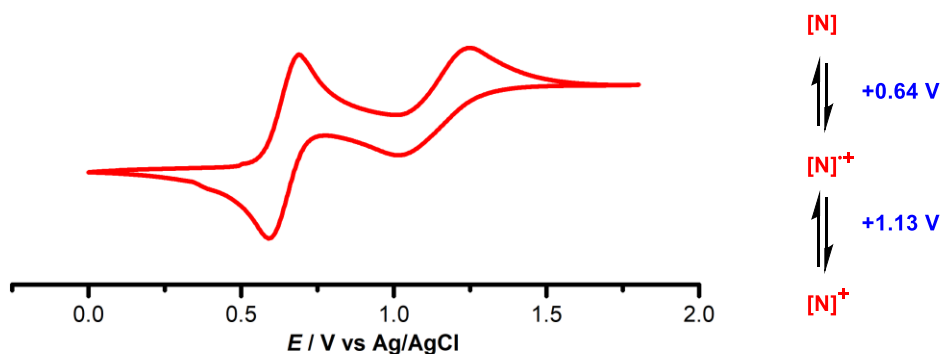


Figure 108. Electricity driven chiral Lewis acid catalyzed α -amination with 10*H*-phenothiazine.

Notably, an *N*-acyl pyrazolyl group was successfully applied as the auxiliary, delivering the amination product **57b** in around 70% yield with 95% ee with Δ -RhS(TMS) as catalyst. Since the oxidation of the corresponding rhodium bound enolate is more difficult, a nucleophilic addition to the nitrogen cation is proposed. To be noted, these products are easily racemized. Further investigations on substrate scope and mechanism were performed by Jiahui Lin, a M.Sc. student in the Meggers group.

4) Three-component carbo-oxygenation of alkene

Fourthly, a highly enantioselective three-component reaction of 2-acyl imidazole, 1,1-diphenyl ethylene and methanol was enabled by the electricity driven chiral Lewis acid catalysis, providing dual C-C/C-O bonds formation product **58** in 51% yield with excellent 99% ee (**Figure 109**). Obviously, the facile anodic oxidation of rhodium bound enolate generates a radical cation intermediate, which is trapped by the alkene forming secondary stabilized benzylic radical species. Subsequently, further SET oxidation of this benzylic radical gives a carbocation that is attacked by solvent methanol producing the final product. Noteworthy is the almost complete asymmetric induction, which again highlights the power and robustness of the Meggers' chiral-at-metal catalysts.

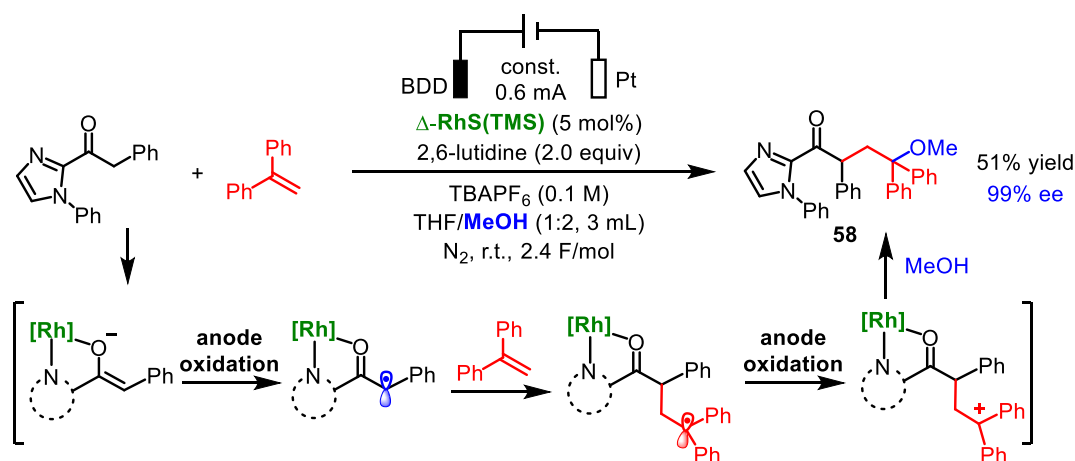


Figure 109. Electricity driven chiral Lewis acid catalyzed three-component reaction.

5) Cascade anodic dehydrogenation and [2+2] photocycloaddition

An interesting cascade reaction combining electro oxidative dehydrogenation and visible-light-activated [2+2] photocycloaddition is illustrated in **Figure 110**. Powered by electricity and visible light, a single chiral-at-metal rhodium catalyzed reaction of α,β -saturated 2-acyl imidazole

with diene afforded the corresponding cyclobutane **59** in 77% yield with excellent stereocontrol (13:1 d.r., >99% ee). Interestingly, alternating the polarity between two electrodes in every 3 minutes is very important for getting a good yield.

From a mechanistic aspect, the rhodium catalyst is involved in both the dehydrogenation and the [2+2] cycloaddition steps. Initially, a rhodium bound enolate forms in the presence of DABCO as base. Then, the dual activated allylic/benzylic C-H bond is abstracted by the anodically oxidized DABCO⁺, thereby forming the key rhodium bound β -enolate radical. Further anodic SET oxidation of this enolate radical gives the rhodium coordinated α,β -unsaturated 2-acyl imidazole. Finally, a subsequent visible-light-activated [2+2] photocycloaddition (see Chapter 3.3)²⁶ furnishes the cyclobutane product. Activation of the C-H bond upon rhodium enolate formation and the subsequent generation of β -enolate radical species have been demonstrated by Jiajia Ma.^{3b} Besides, as a proof to the mechanism, the corresponding α,β -unsaturated 2-acyl imidazole could be observed and isolated during the reaction.

Unfortunately, the scope of this very appealing combination of electro- and photochemistry appears to be quiet limited. For example, changing the substituent in the aryl moiety provided poor yields (**28a**). The reasons for this sensitivity are unclear and need to be investigated further.

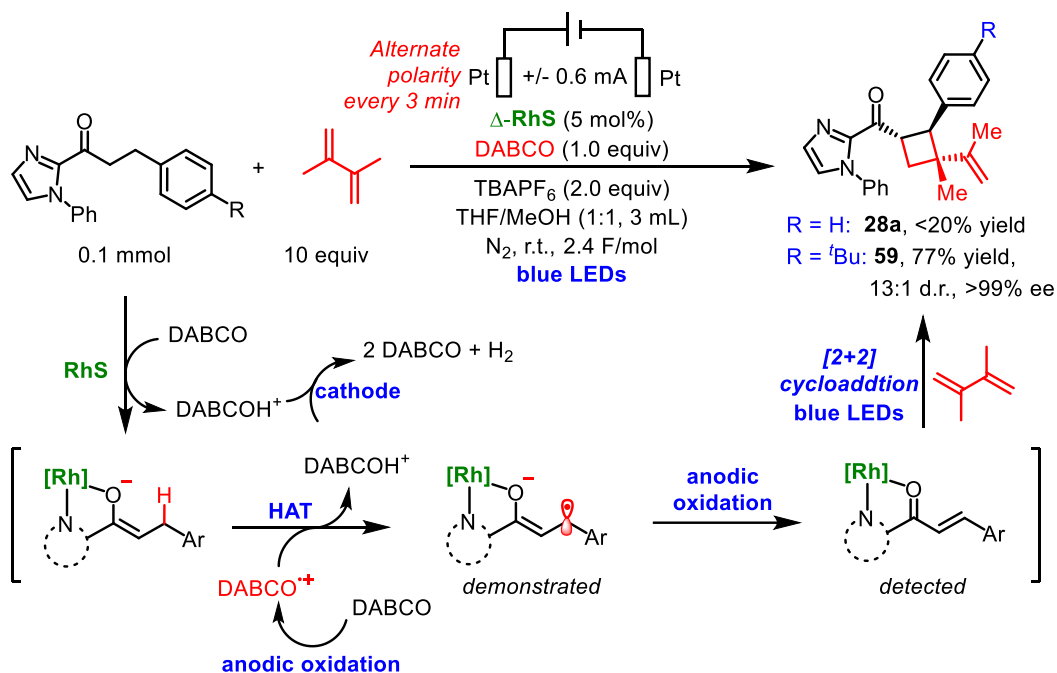


Figure 110. Electricity driven chiral Lewis acid catalyzed oxidative [2+2] photocycloaddition.

6) Anodic oxidative cyclization

Finally, an electrochemical oxidative cyclization of an enone with 1-phenylpyrrolidine was discovered (**Figure 111**). Although no enantioselectivity was obtained, a potentially useful cyclic motif **60**, namely 1,2,3,3a,4,5-hexahydropyrrolo[1,2-*a*]quinolone, could be constructed in 42% NMR yield. A possible mechanism starts with SET oxidation and deprotonation to generate electron-rich α -amino carbon centered radical. The subsequent Giese type radical conjugate addition forms the first C-C bond with the generation of an electron-deficient α -carbonyl carbon centered radical. Then, a subsequent intramolecular radical addition to the *N*-phenyl moiety and oxidative aromatization produce the final product.

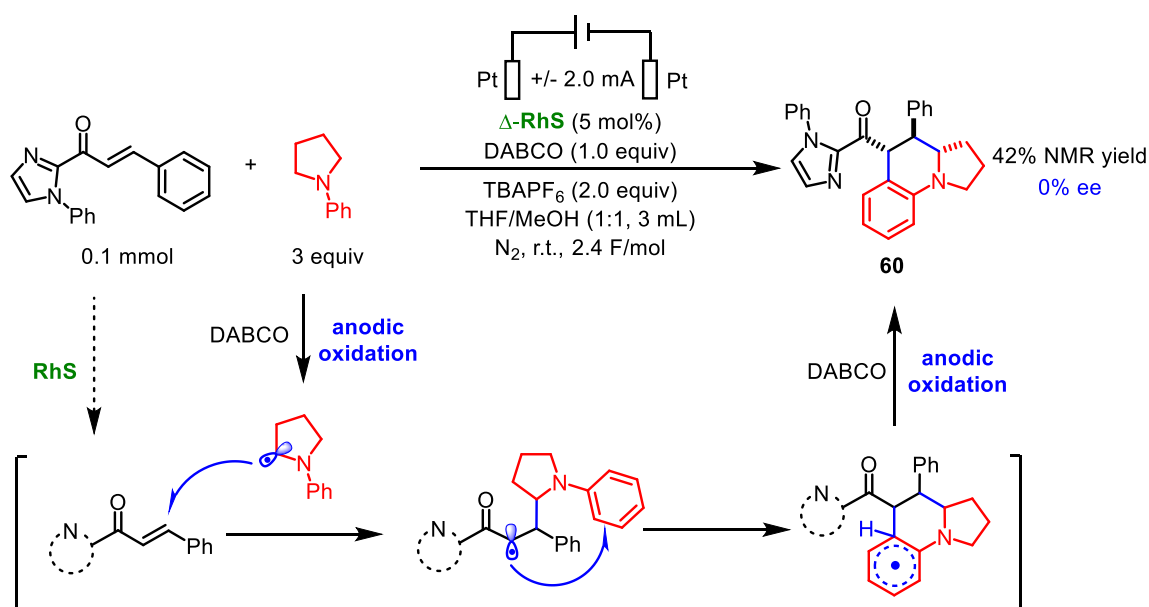


Figure 111. Electricity driven oxidative cyclization.

3.6.6 Conclusions

In conclusion, this chapter introduced an unprecedented versatile electricity driven chiral Lewis acid catalysis.²⁷ By intertwining electrochemical oxidation with chiral Lewis acid catalysis, a simple, sustainable, and highly enantioselective oxidative cross coupling of 2-acyl imidazoles with silyl enol ethers was achieved. This method provides a new avenue to synthetically useful chiral 1,4-dicarbonyls, including products bearing all-carbon quaternary stereocenters that are challenging to be accessed by conventional methods. The mild reaction conditions with high chemoselectivity and high functional

group tolerance can be traced back to the ability of the rhodium catalyst to strongly reduce the oxidation potential by the formation of a catalyst bound enolate intermediate. Thus the chiral Lewis acid catalyst fulfills several important functions by facilitating oxidation via complexation of the substrate, by staying bound to the oxidatively formed radical intermediate and thereby preventing unwanted side reactions such as homo-coupling, and by providing a high asymmetric induction in the course of the C-C bond formation

Furthermore, a series of interesting catalytic asymmetric electrochemical reactions were developed based on this newly-devised electricity driven chiral Lewis acid catalysis, including an α -amination, an electro- and photochemistry relay [2+2] cycloaddition, and an alkene three-component difunctionalization. As proof of principle studies, these results demonstrate the versatility and potential of combining asymmetric Lewis acid catalysis with electrochemistry. It is anticipated that the design and achievements described in this chapter will spur the development of novel activation strategies in the area of catalytic asymmetric electrosynthesis.

References

- 1 L. Zhang, E. Meggers, *Acc. Chem. Res.* **2017**, *50*, 320-330.
- 2 C. Wang, L.-A. Chen, H. Huo, X. Shen, K. Harms, L. Gong, E. Meggers, *Chem. Sci.* **2015**, *6*, 1094-1100.
- 3 a) X. Shen, K. Harms, M. Marsch, E. Meggers, *Chem. Eur. J.* **2016**, *22*, 9102-9105; b) J. Ma, A. R. Rosales, X. Huang, K. Harms, R. Riedel, O. Wiest, E. Meggers, *J. Am. Chem. Soc.* **2017**, *139*, 17245-17248.
- 4 X. Huang, R. D. Webster, K. Harms, E. Meggers, *J. Am. Chem. Soc.* **2016**, *138*, 12636-12642.
- 5 M. P. DeMartino, K. Chen, P. S. Baran, *J. Am. Chem. Soc.* **2008**, *130*, 11546-11560.
- 6 L. Næsborg, L. A. Leth, G. J. Reyes-Rodríguez, T. A. Palazzo, V. Corti, K. A. Jørgensen *Chem. Eur. J.* **2018**, *24*, 14844-14848.
- 7 a) H.-Y. Jang, J.-B. Hong, D. W. C. MacMillan, *J. Am. Chem. Soc.* **2007**, *129*, 7004-7005; b) P. Tisovský, M. Mečiarová, R. Šebesta, *Org. Biomol. Chem.* **2014**, *12*, 9446-9452.
- 8 a) M. Yan, Y. Kawamata, P. S. Baran, *Chem. Rev.* **2017**, *117*, 13230-13319; b) K. D. Moeller, *Chem.*

- Rev. **2018**, *118*, 4817-4833.
- 9 B. M. Trost, *Proc. Natl. Acad. Sci. USA* **2004**, *101*, 5348-5355.
 - 10 Z.-Y. Cao, J. Zhou, in *Multicatalyst System in Asymmetric Catalysis*, John Wiley & Sons, Inc., **2014**, pp. 475-500.
 - 11 a) K. L. Jensen, P. T. Franke, L. T. Nielsen, K. Daasbjerg, K. A. Jørgensen, *Angew. Chem. Int. Ed.* **2010**, *49*, 129-133; b) N. Fu, L. Li, Q. Yang, S. Luo, *Org. Lett.* **2017**, *19*, 2122-2125.
 - 12 a) Y. Kashiwagi, F. Kurashima, C. Kikuchi, J.-i. Anzai, T. Osa, J. M. Bobbitt, *Chem. Commun.* **1999**, 1983-1984; b) Y. Kashiwagi, F. Kurashima, S. Chiba, J.-i. Anzai, T. Osa, J. M. Bobbitt, *Chem. Commun.* **2003**, 114-115.
 - 13 J.-C. Moutet, C. Duboc-Toia, S. Ménage, S. Tingry, *Adv. Mater.* **1999**, *10*, 665-667.
 - 14 R. Francke, R. D. Little, *Chem. Soc. Rev.* **2014**, *43*, 2492-2521.
 - 15 a) S. Torii, P. Liu, N. Bhuvaneswari, C. Amatore, A. Jutand, *J. Org. Chem.* **1996**, *61*, 3055-3060; b) B. H. Nguyen, A. Redden, K. D. Moeller, *Green Chem.* **2014**, *16*, 69-72.
 - 16 a) H. Tanaka, M. Kuroboshi, H. Takeda, H. Kanda, S. Torii, *J. Electroanal. Chem.* **2001**, *507*, 75-81; b) B.-L. Chen, H.-W. Zhu, Y. Xiao, Q.-L. Sun, H. Wang, J.-X. Lu, *Electrochem. Commun.* **2014**, *42*, 55-59.
 - 17 a) R. Yuan, S. Watanabe, S. Kuwabata, H. Yoneyama, *J. Org. Chem.* **1997**, *62*, 2494-2499; b) F. Hollmann, K. Hofstetter, T. Habicher, B. Hauer, A. Schmid, *J. Am. Chem. Soc.* **2005**, *127*, 6540-6541; c) V. Hölzl, K. Otto, A. Schmid, *Adv. Synth. Catal.* **2007**, *349*, 1337-1340.
 - 18 a) N.-N. Bui, X.-H. Ho, S.-i. Mho, H.-Y. Jang, *Eur. J. Org. Chem.* **2009**, 5309-5312; b) X.-H. Ho, S.-i. Mho, H. Kang, H.-Y. Jang, *Eur. J. Org. Chem.* **2010**, 4436-4441.
 - 19 A. Wiebe, T. Gieshoff, S. Möhle, E. Rodrigo, M. Zirbes, S. R. Waldvogel, *Angew. Chem. Int. Ed.* **2018**, *57*, 5594-5619.
 - 20 M. Yan, Y. Kawamata, P. S. Baran, *Angew. Chem. Int. Ed.* **2017**, *57*, 4149-4155.
 - 21 J. Twilton, C. Le, P. Zhang, M. H. Shaw, R. W. Evans, D. W. C. MacMillan, *Nat. Rev. Chem.* **2017**, *1*, 0052.
 - 22 Y. Tan, W. Yuan, L. Gong, E. Meggers, *Angew. Chem. Int. Ed.* **2015**, *54*, 13045-13048.
 - 23 J. C. Siu, G. S. Sauer, A. Saha, R. L. Macey, N. Fu, T. Chauviré, K. M. Lancaster, S. Lin, *J. Am. Chem. Soc.* **2018**, *140*, 12511-12520.

- 24 P. Wang, S. Tang, P. Huang, A. Lei, *Angew. Chem. Int. Ed.* **2017**, *56*, 3009-3013.
- 25 S. Tang, S. Wang, Y. Liu, H. Cong, A. Lei, *Angew. Chem. Int. Ed.* **2018**, *57*, 4737-4741.
- 26 X. Huang, T. R. Quinn, K. Harms, R. D. Webster, L. Zhang, O. Wiest, E. Meggers, *J. Am. Chem. Soc.* **2017**, *139*, 9120-9123.
- 27 X. Huang, Q. Zhang, J. Lin, K. Harms, E. Meggers, *Nat. Catal.* **2019**, *2*, 34-40.

Chapter 4. Summary and Outlook

4.1 Summary

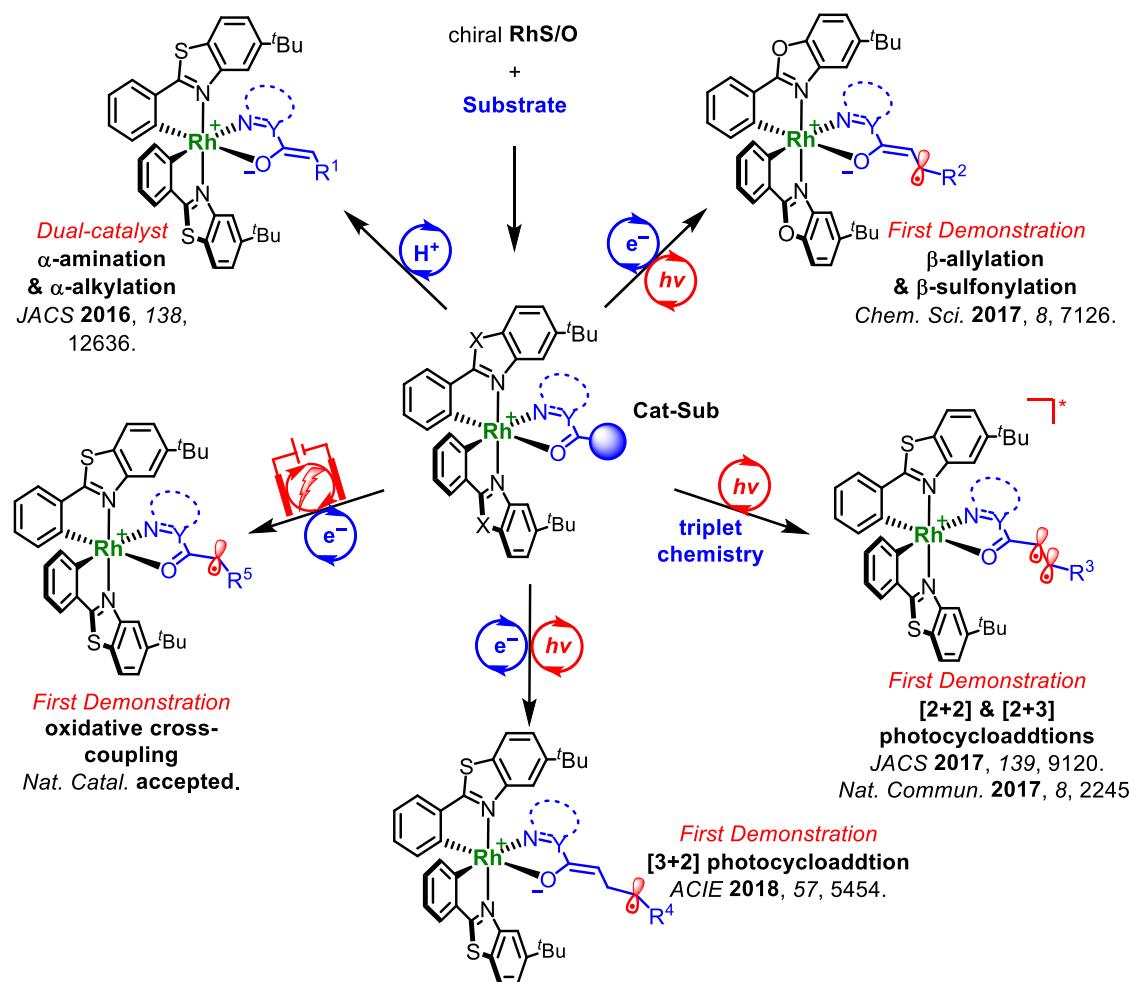


Figure 112. Overview of the discoveries of this thesis: visible light or electricity driven asymmetric chiral-at-rhodium catalysis for various novel transformations. (Unified with Λ -configured intermediates)

With the goal of developing efficient and sustainable methodologies to synthesize enantioenhanced molecules, this thesis focused on exploring novel asymmetric chiral-at-rhodium catalysis using visible light or electricity as activation energy. In all newly developed synthetic strategies, chiral catalyst/substrate complexes form in situ and are transformed into a series of reactive intermediates, among which β -enolate radicals, excited triplet states, γ -enolate radicals, and α -carbonyl radicals are demonstrated for the first time (**Figure 112**). The reaction courses of these reactive

intermediates are controlled by the metal-centered chirality, leading to several highly stereoselective visible light or electricity induced catalysis:

1. Dual-catalyst for α -amination/alkylation with azides/diazo esters

Chapter 3.1 presented a visible-light-activated asymmetric α -amination/alkylation of 2-acyl imidazoles catalyzed by the combination of chiral-at-metal **RhS** and a photoredox catalyst $[\text{Ru}(\text{bpy})_3](\text{PF}_6)_2$ (**Figure 113**). Enabled by a dual-catalyst strategy, this novel proton- and redox-neutral method provided yields of up to 99% and excellent enantioselectivities of up to >99% ee with broad functional group tolerance. Mechanistic investigations suggest that an intermediate rhodium enolate complex acts as a reductive quencher to initiate a radical process with the aryl azides and α -diazo carboxylic esters serving as precursors for nitrogen and carbon-centered radicals, respectively. This marks the first report on using aryl azides and α -diazo carboxylic esters as substrates for asymmetric catalysis under photoredox conditions. These reagents have the advantage that molecular nitrogen is the leaving group and sole by-product in these reactions. The detailed mechanistic studies in this work are expected to provide useful direction and inspiration for the design of new visible-light-activated asymmetric reactions.

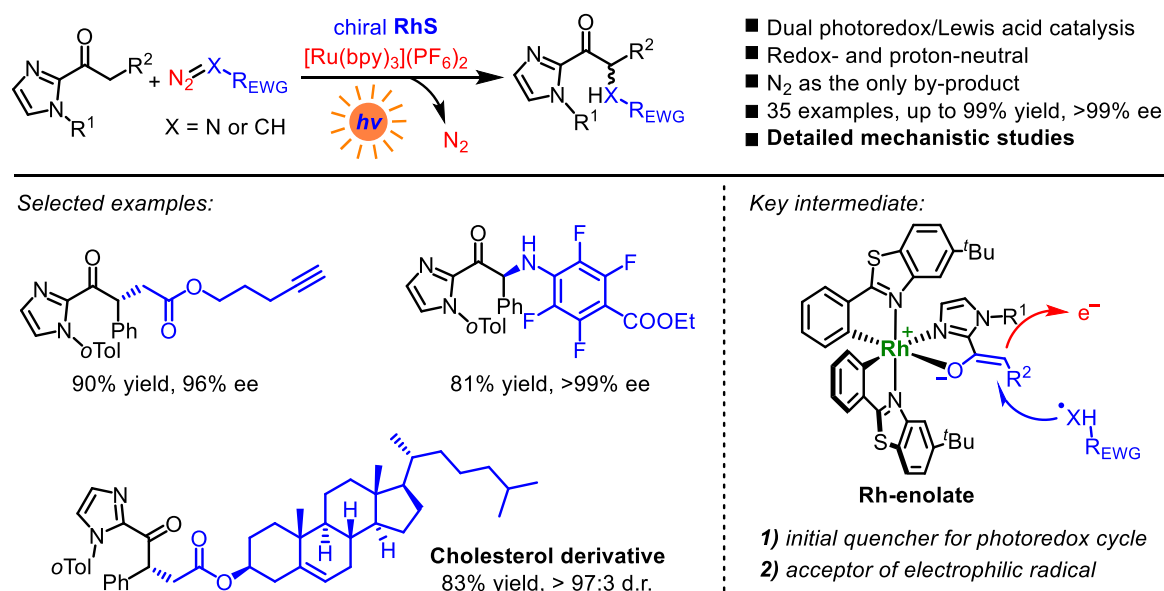


Figure 113. Summary of α -amination/alkylation with dual-catalyst. *JACS*, **2016**, *138*, 12636.

2. Combining the catalytic enantioselective reaction of visible-light-generated radicals with a by-product utilization system

Chapter 3.2 introduced a unique visible-light-induced asymmetric scheme that utilizes a single chiral catalyst for two distinct processes. The chiral bis-cyclometalated rhodium complex **RhO** enabled the stereocontrolled chemistry of photo-generated carbon-centered radicals and at the same time catalyzed an enantioselective sulfonyl radical addition to an alkene (**Figure 114**). Specifically, the Rh-coordinated prochiral radicals, which were generated through selective SET reduction by photoexcited Hantzsch esters, were trapped by allyl sulfones in a highly stereocontrolled fashion, providing radical allylation products with up to 97% ee. The hereby formed fragmented sulfonyl radicals were utilized via an enantioselective radical addition to form chiral sulfones, which minimizes waste generation. The robustness and FG compatibilities of this system was demonstrated by additions of a series of common chemical functionalities. For the first time, the rhodium bound β -enolate radical species was generated and applied for an enantioselective conversion, which paves a new way to develop novel chemistry based on chiral-at-rhodium catalysts.

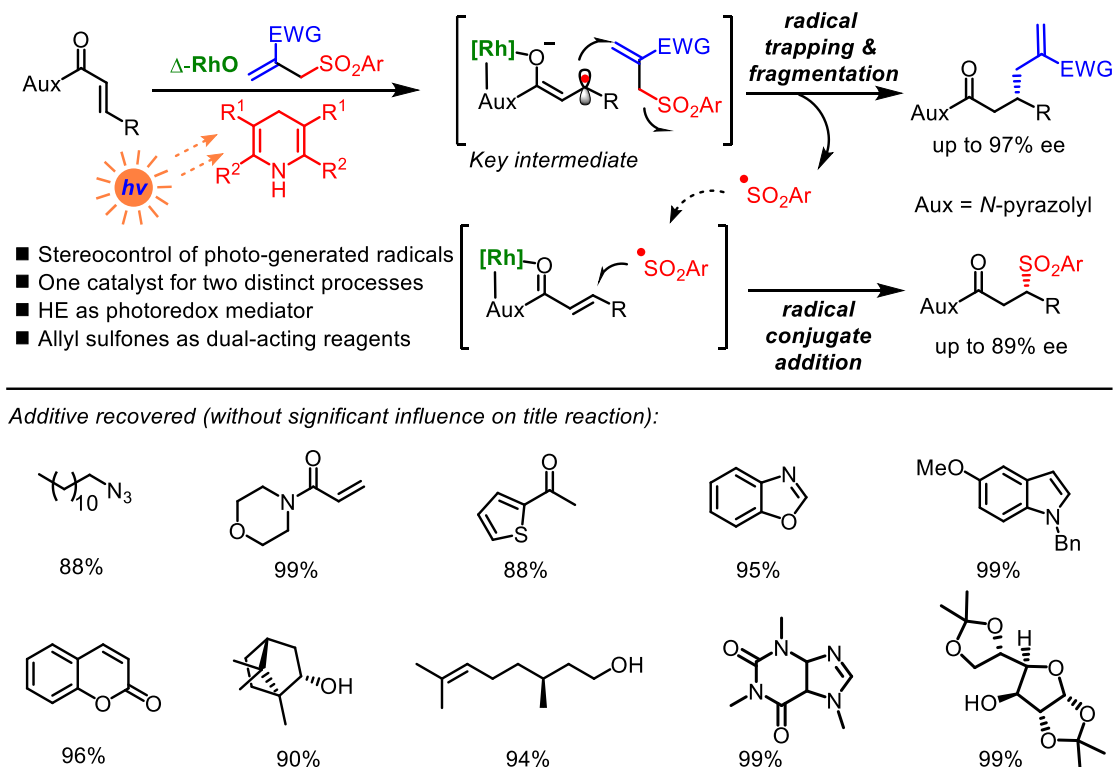
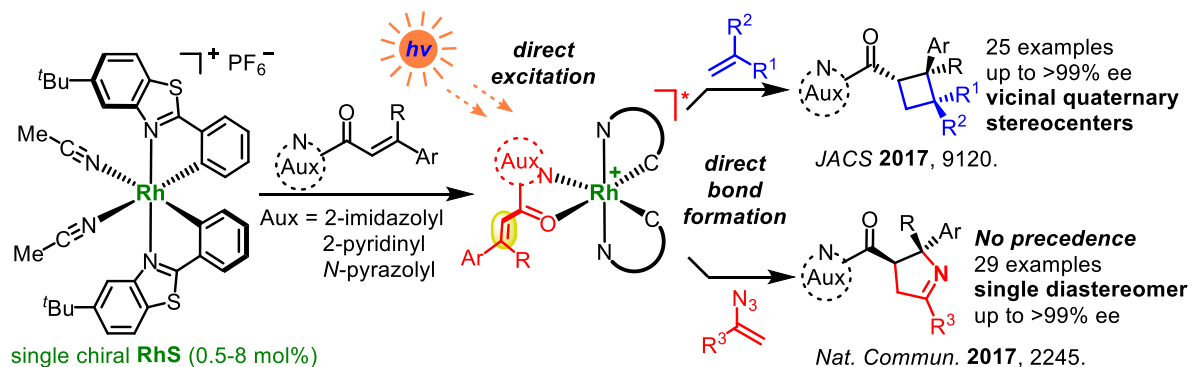
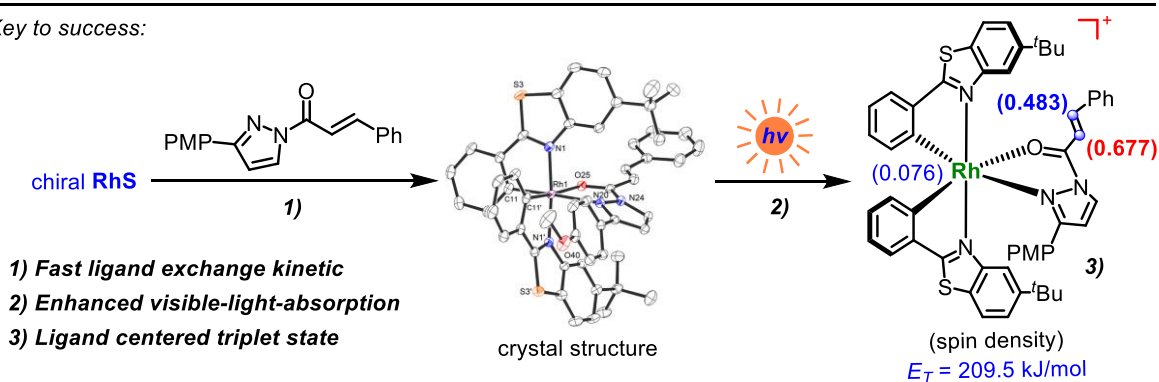


Figure 114. Summary of a single **RhO** enabled two distinct processes. *Chem. Sci.* **2017**, *8*, 7126.

3. Stereocontrolled direct bond formations upon directly visible-light-excited state



Key to success:



Selected examples:

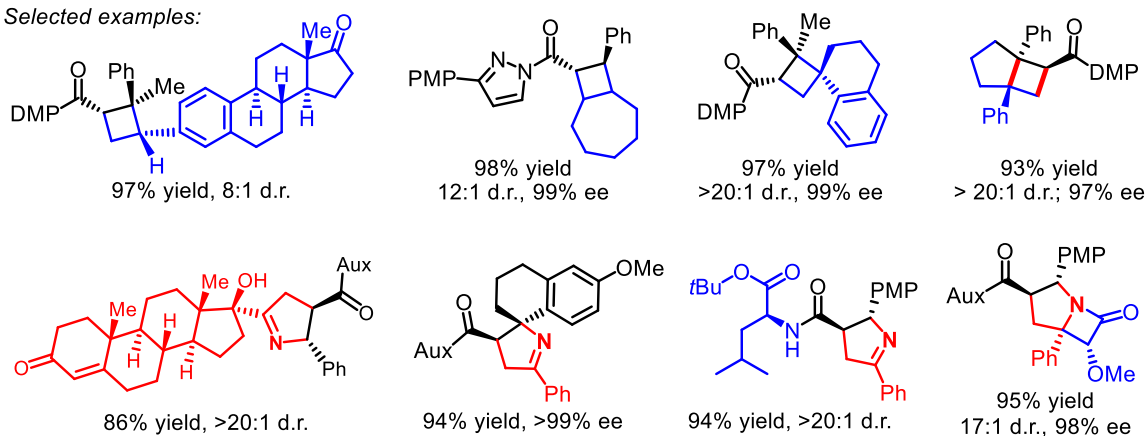


Figure 115. Summary of a single **RhS** enabled [2+2] and [2+3] photocycloadditions via direct visible-light-excitation and direct bond formation on electronically excited state.

Chapters 3.3 and 3.4 showed a simple and robust catalysis scheme to control the stereochemistry of photo-excited states that only relies on a single chiral-at-metal Lewis acid catalyst **RhS** (Figure 115). The substrate/catalyst complex absorbs visible light and generates the excited state that directly reacts with a co-substrate in a highly stereocontrolled fashion. Starting from simple cinnamic derivatives, a wide range of cyclobutanes via [2+2] photocycloadditions with alkenes, and various 1-pyrrolines through previously elusive [2+3] photocycloadditions with vinyl azides were successfully

constructed. These asymmetric photoreactions only require a single chiral catalyst with loading of 0.5-8 mol%, feature simple and mild reaction conditions, provide high yields (up to 99%) with excellent enantioselectivities (up to >99% ee), and display broad substrate scopes with high functional group tolerance. The key to the success is that upon substrate/catalyst complexation, greatly enhanced absorption is achieved, thus achieving selective visible-light-excitation and inhibiting the background racemic reactions. All reactive intermediates remain bound to the single catalyst thereby providing a robust catalytic scheme with excellent stereocontrol.

This strategy is very attractive because it not only provides a simpler and more efficient solution to stereocontrolled [2+2] photocycloadditions, but also expands the scope of stereocontrolled bond forming reactions of photoexcited intermediates to an unprecedented [2+3] photocycloaddition. And this newly-developed concept for stereocontrolled direct bond formation of directly visible-light-excited state is anticipated to be applied for more asymmetric catalysis.

4. Asymmetric [3+2] photocycloadditions enabled by selected SET reduction of directly visible-light-excited catalyst bound cyclopropanes

Chapter 3.5 introduced a single chiral-at-rhodium catalyst enabled visible-light-activated asymmetric [3+2] photocycloadditions between cyclopropanes and alkenes or alkynes to provide access to enantioenriched cyclopentanes and cyclopentenones, respectively, in 63-99% yields and with excellent enantioselectivities of up to >99% ee (**Figure 116**). A single **RhS** (2-8 mol%) which after coordination to the cyclopropane generates the visible-light-absorbing complex, lowers the reduction potential of the cyclopropane, and provides the asymmetric induction and overall stereocontrol. Complimentary to the above mentioned direct bond formation of excited catalyst/substrate complex, a mild single electron transfer reduction of the excited state induces the ring opening of cyclopropane, which leads to a previously elusive rhodium bound γ -enolate radical intermediate and ultimately delivers the new non-racemic chiral cyclic scaffolds. This method enriches the reactivity of chiral-at-metal rhodium-based Lewis acid by expanding the substrate of catalytic asymmetric photocycloadditions to simple mono-acceptor-substituted cyclopropanes affording previously inaccessible chiral cyclopentane and cyclopentene derivatives.

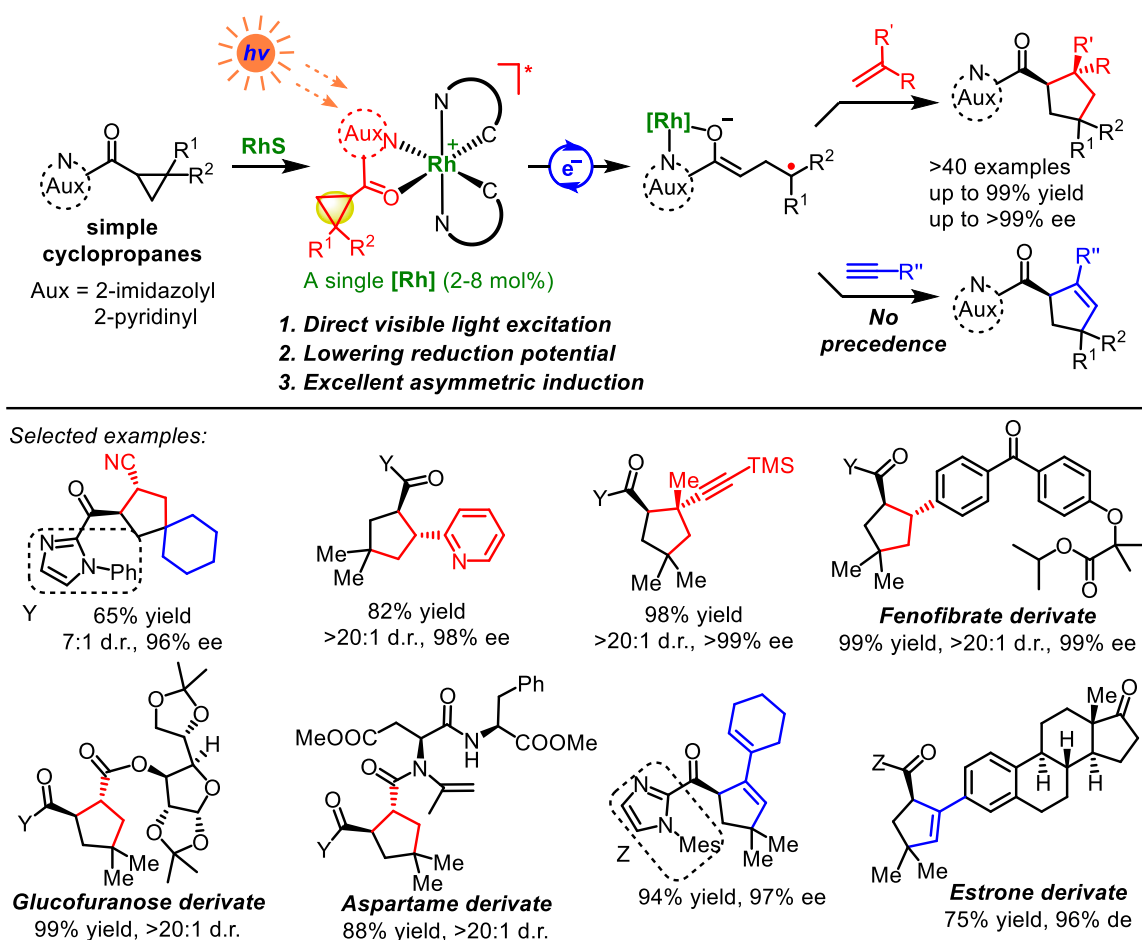
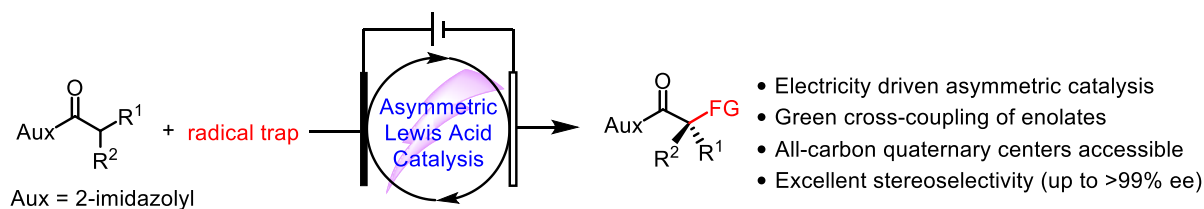


Figure 116. Summary of a single **RhS** enabled [3+2] photocycloaddition. *ACIE* **2018**, 57, 5454.

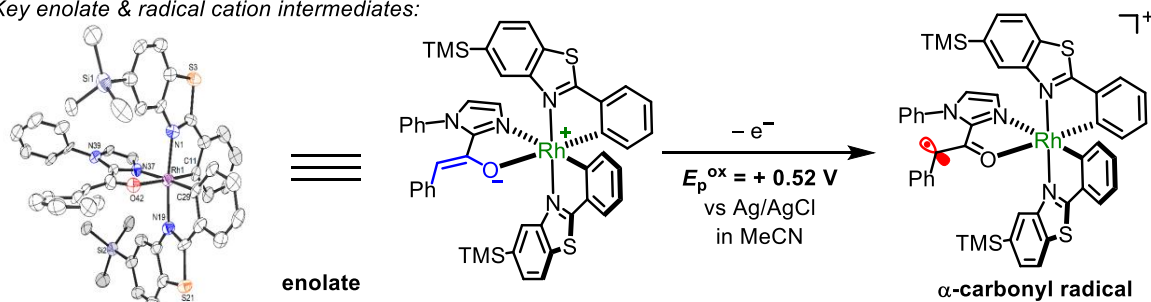
5. Electricity driven asymmetric Lewis acid catalysis

Chapter 3.6 showed the first example of electrochemical chiral-at-rhodium catalysis (**Figure 117**). Driven by electricity, the oxidative cross coupling of 2-acyl imidazoles with silyl enol ethers provides a sustainable avenue to synthetically useful enantioenriched 1,4-dicarbonyls, including products bearing all-carbon quaternary stereocenters which are difficult to obtain by conventional methods. A chiral-at-metal rhodium catalyst activates a substrate towards anodic oxidation by raising the HOMO upon enolate formation, which enables mild and selective anodic conditions, high chemo- and enantioselectivities (up to >99% ee), and a broad substrate scope. Thus the chiral **RhS** fulfills several important functions by facilitating oxidation via complexation of the substrate, by staying bound to the highly reactive electrochemically formed radical intermediate and thereby preventing unwanted side reactions, and by providing a high asymmetric induction in the course of follow-up bond formation. This work demonstrates the potential of combining asymmetric Lewis acid catalysis with

electrochemistry and it is expected to inspire further development of catalytic asymmetric electrosynthesis.



Key enolate & radical cation intermediates:



Selected examples:

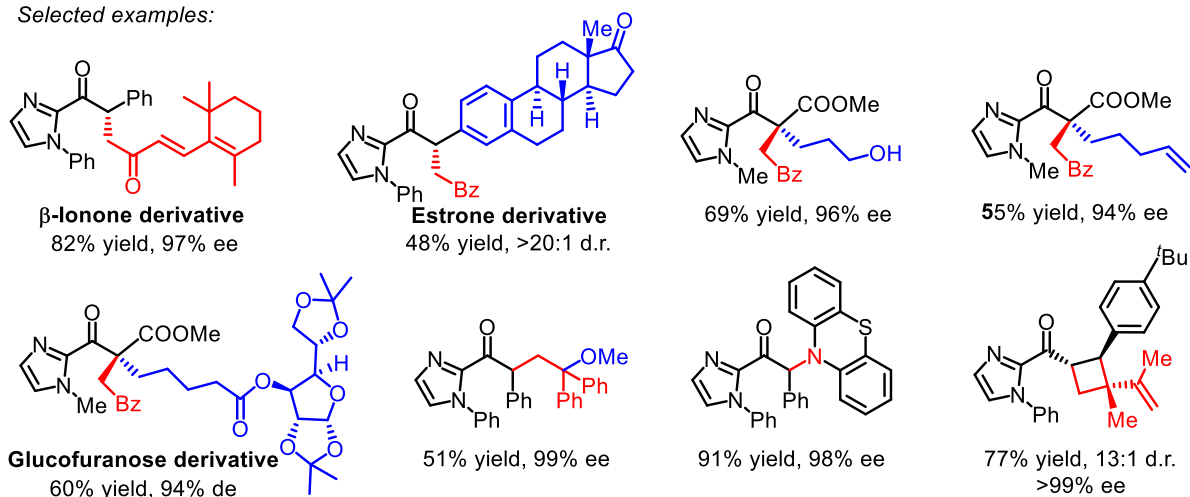


Figure 117. Summary of the electricity driven asymmetric chiral-at-rhodium catalysis. *Nat. Catal.* **2019**, 2, 34-40.

Overall, this thesis greatly expands the reactivity of the chiral-at-metal rhodium catalysts recently developed in the Meggers group. Several previously unknown rhodium bound radical-type intermediates were generated upon visible light irradiation or using electricity as environmentally friendly energy source. For the first time, highly efficient and stereocontrolled [2+2]/[2+3] photocycloadditions directly from the electronically excited state were achieved, which are superior over the previously developed catalytic photosystems. Notably, an elegant electricity driven chiral

Lewis acid catalysis has been disclosed and shed new light on catalytic asymmetric electrosynthesis. From the viewpoint of synthetic applications, novel and efficient methodologies for the synthesis of a wide range of enantioenriched structural units were developed. Enantioenriched α -aminated/alkylated carbonyls, β -functionalized carbonyls, cyclobutanes, cyclopentanes and cyclopentenes were synthesized, most of which are reported for the first time. This is in line with the growing demand of generating non-racemic chiral molecules. The generality and versatility of the privileged chiral-at-metal catalysts used in this thesis may indicate the potential of these complexes to be a general solution to the central challenge of stereoinduction in photochemical and/or electrochemical asymmetric catalysis.

4.2 Outlook

The recent work by the Meggers group clearly shows the versatility and robust reactivity of bis-cyclometalated chiral-at-metal rhodium(III) complexes. Therefore, it is very promising to explore other new reactions for the catalytic asymmetric synthesis of non-racemic chiral molecules based on the developed catalysts by taking into account the reaction modes of photochemically or electrochemically activated catalyst/substrate complexes.

1) Achieve asymmetric electrochemical reduction by LUMO activation

Catalytic asymmetric electrosynthesis remains underexplored. Chapter 3.6 demonstrates the ability of the chiral **RhS** catalyst for facilitating enantioselective electrochemical oxidations through HOMO activation of ketones. On the contrast, LUMO activation of a suitable substrate is known to be achieved by the Lewis acid coordination, which should make a selective SET reduction of catalyst bound substrate possible. In consideration of the inherent advantage of electrochemistry which provides electrons as clean and sustainable reductant, it is of significant interest to explore electricity driven asymmetric reduction reactions.

2) Explore new reactivity of photoexcited catalyst/substrate complex

As revealed in this thesis, one of the unique properties of the chiral-at-metal catalysis is that the in situ formed catalyst/substrate complex can be directly excited by visible light while at the same time provides excellent asymmetric induction. Hence, a simple single chiral-at-metal catalytic scheme is effective for SET processes and direct bond formations. Considering that the visible-light-excited state of **IrS** bound enone is defined as MLCT, investigations on previously untouched MLCT catalysis are highly desirable. While the corresponding **[Rh]**-intermediate is proved to be ligand centered, HAT chemistry using **RhS** could be anticipated. Besides, it is very attractive to test the asymmetric Paternò-Büchi reaction which has not been reported. But this is possibly accomplished using chiral-at-metal catalyst based on the assumption that the spin of the excited catalyst bound carbonyl complex might localize at the carbonyl group.

3) Extension to other classes of substrates

As a major shortage, these chiral-at-metal catalysis heavily rely on a *N,O*-bidentate coordination. Enantioselective hydrogenation and alkynylation of simple acetophenones have been successfully achieved where metal hydride or metal acetylide intermediates are proposed, respectively. Based on these results, it is interesting to test the reactivity of related species, which feature σ -bond connection between the metal and a substrate, under redox conditions provided by photochemistry and/or electrochemistry. Once this new coordination mode is feasible, approaches to new type of non-racemic chiral products could be achieved. Furthermore, if *N*-acylhydrazone could be applied as substrate, chiral amines would be obtained, rather than the currently formed carbonyl compounds.

On the other hand, design and modification of the octahedral chiral-at-metal structure might lead to new generations of catalysts with the potential of discovering unprecedented asymmetric catalysis. In this context, two directions could be envisioned:

4) Modify the cyclometalating ligands

Modification of the ligands could be built on several aspects. Introducing electron-rich(poor) groups in the phenyl moiety of the benzothiazoles could alter the Lewis acidity and redox potential of the catalyst, which provides the possibility of activating new substrates. A systematic investigation on the effect of substitution on the cyclometalating ligands is desirable. In addition, although difficult to synthesize, a kind of completely new complex with two different achiral ligands is expected to activate mono-coordinated substrates if the two free coordinating sites differ enough.

5) Change the central metal

Applying earth-abundant base metal complex for catalysis is an important trend in organic chemistry. The correct combination of metal with ligand could unlock new types of catalytic transformations. In particular, many Fe and Co based complexes are known to be octahedral and the unique redox flexibility of these metals is extremely attractive for chiral-at-metal catalysis.

Chapter 5. Experimental Part

5.1 General Materials and Methods

The chiral-at-metal **Ir/Rh** catalysts were synthesized according to the procedures developed by the Meggers group.¹ All small-scale photoreactions were performed in a Schlenk tube (10 mL) with magnetic stirring. Electrochemical reactions were performed in a 5 mL vial using the ElectraSyn 2.0.² The general procedures are described in the corresponding chapters.

Solvents and Reagents

Anhydrous solvents were distilled under nitrogen from calcium hydride (CH_2Cl_2 , and CH_3CN), magnesium turnings/iodine (MeOH) or sodium/benzophenone (Et_2O , THF and toluene), or bought from commercial suppliers (1,4-dioxane, DMF and DMSO). Unless otherwise mentioned, HPLC grade solvents including 2-methoxyethanol, EtOH, acetone, and PhCl were used directly without further drying. All reagents were purchased from Acros, Alfa Aesar, Sigma Aldrich, TCI, ChemPur and Fluorochem and used without further purification.

Chromatographic Methods

The course of the reactions and the column chromatographic elution were monitored by thin layer chromatography (TLC) [Macherey-Nagel (ALUGRAM®Xtra Sil G/UV254)]. Flash column chromatography was performed with silica gel 60 M from Macherey-Nagel (irregular shaped, 230-400 mesh, pH 6.8, pore volume: $0.81 \text{ mL} \times \text{g}^{-1}$, mean pore size: 66 \AA , specific surface: $492 \text{ m}^2 \times \text{g}^{-1}$, particle size distribution: $0.5\% < 25 \text{ }\mu\text{m}$ and $1.7\% > 71 \text{ }\mu\text{m}$, water content: 1.6%).

Nuclear Magnetic Resonance Spectroscopy (NMR)

^1H NMR, proton decoupled ^{13}C NMR and ^{19}F NMR spectra were recorded on Bruker Avance 250 (250 MHz), Bruker Avance 300 (300 MHz) Bruker AM (500 MHz) or Bruker AM (600 MHz) spectrometers at ambient temperature. NMR standards were used as follows: ^1H NMR spectroscopy: $\delta = 7.26 \text{ ppm}$ (CDCl_3), 5.32 ppm (CD_2Cl_2), 2.50 ppm ($(\text{CD}_3)_2\text{SO}$); ^{13}C NMR spectroscopy: $\delta = 77.0 \text{ ppm}$

(CDCl₃), 53.8 ppm (CD₂Cl₂), 39.52 ppm ((CD₃)₂SO); ¹⁹F NMR spectroscopy: δ = 0 ppm (CFCl₃). The characteristic signals were specified from the low field to high field with the chemical shifts given in ppm on the δ scale. ¹H NMR spectra peak multiplicities indicated as singlet (s), broad singlet (br s), doublet (d), doublet of doublet (dd), doublet of triplet (dt), doublet of doublet of doublet (ddd), triplet (t), triplet of doublet (td), triplet of triplet (tt), quartet (q), multiplet (m).

NMR yields were determined using 1,1,2,2-tetrachloroethane (a liquid) or 1,3,5-trimethoxybenzene (a solid, mainly used in chapter 3.6) as internal standard.

High-Performance Liquid Chromatography (HPLC)

Chiral HPLC was performed with an Agilent 1200 Series, Agilent 1260 Series HPLC System or Shimadzu Lc-2030c. All the HPLC conditions were detailed in the individual procedures. The type of the columns, mobile phase and the flow rate were specified in the individual procedures.

Infrared Spectroscopy (IR)

IR spectra were recorded on a Bruker Alpha FT-IR spectrometer. The absorption bands were indicated as wave numbers ν (cm⁻¹). All substances were measured as films or solids.

Mass Spectrometry (MS)

High-resolution mass spectra were recorded on a Bruker En Apex Ultra 7.0 TFT-MS instrument. Ionic masses are given in units of m/z for the isotopes with the highest natural abundance.

Circular Dichroism Spectroscopy (CD)

CD spectra were recorded on a JASCO J-810 CD spectropolarimeter. The parameters used are as follows: from 600 nm to 200 nm; data pitch (0.5 nm); band width (1 nm); response (1 second); sensitivity (standard); scanning speed (50 nm/min); accumulation (5 times). The concentration of the compounds for the measurements was 0.2 mM. The formula for converting θ to ϵ is shown as below.

$$\Delta\epsilon = \frac{\theta[m\text{ deg}]}{32980 \times c(\text{mol} / L) \times L(\text{cm})}$$

c = concentration of the sample; L = thickness of the measurement vessel

UV/Vis Analysis Spectroscopy and Stern-Volmer Quenching Experiments

UV/Vis measurements and quenching experiments were taken on a Spectra Max M5 microplate reader in a 10.0 mm quartz cuvette.

Optical Rotation Polarimeter

Optical rotations were measured on a Krüss P8000-T or Perkin-Elmer 241 polarimeter with $[\alpha]_D^{22}$ values reported in degrees with concentrations reported in g/100 mL.

Cyclic Voltammetry

For chapters 3.1, 3.2 and 3.3: Voltammetric experiments were conducted with a computer controlled Eco Chemie Autolab PGSTAT302N potentiostat in a Metrohm electrochemical cell containing a 1 mm diameter planar platinum and glassy carbon (GC) disk electrodes (eDAQ). A ferrocene/ferrocenium (Fc/Fc^+) redox couple as an internal standard.

For chapters 3.5 and 3.6: Voltammetric experiments were conducted with a computer controlled Eco Chemie Autolab PGSTAT204 potentiostat in a Metrohm electrochemical cell containing a 1 mm diameter planar platinum electrode, a Ag wire electrode and a Ag/AgCl/KCl(3 M) reference electrode. All solution used for the voltammetric experiment was deoxygenated by nitrogen gas and measurement was performed at room temperature (22 ± 2 °C).

Electron Paramagnetic Resonance (EPR)

The EPR spectrometer is from Bruker (model esp300), with a modified Varian rectangular X-band cavity. All the samples for EPR were measured at room temperature.

Quantum Yield Measurement

All the light sensitive operations were processed in the darkroom under red light.

For chapters 3.1, 3.3 and 3.4: The method was designed according to a published procedure with slight modifications.³ A 150 W xenon lamp (50% of light intensity, 420 ± 5 nm bandpass filter) was used as the light source. Photon flux of the spectrophotometer was determined by standard ferrioxalate actinometry. The yields of products were determined by GC measurement (FID detector, column: HP-5)

For chapters 3.2 and 3.5: Quantum yields were determined by a method and setups developed by the Riedle group.⁴ As light source a 420 nm LED (chapter 3.5) or a 400 nm LED (chapter 3.5) was employed. A powermeter was used as detector. The yields of products were determined by ¹H-NMR with an internal standard. A detailed procedure is described in section 5.6.4.

Light Source

A 21 W compact fluorescent lamp (CFL, OSRAM DULUX® SUPERSTAR Micro Twist) or 24 W Blue LEDs (Hongchangzhaoming from Chinese Taobao, <https://hongchang-led.taobao.com>) served as light sources. See **Figure 118** and **Figure 119**, respectively, for their emission spectra.

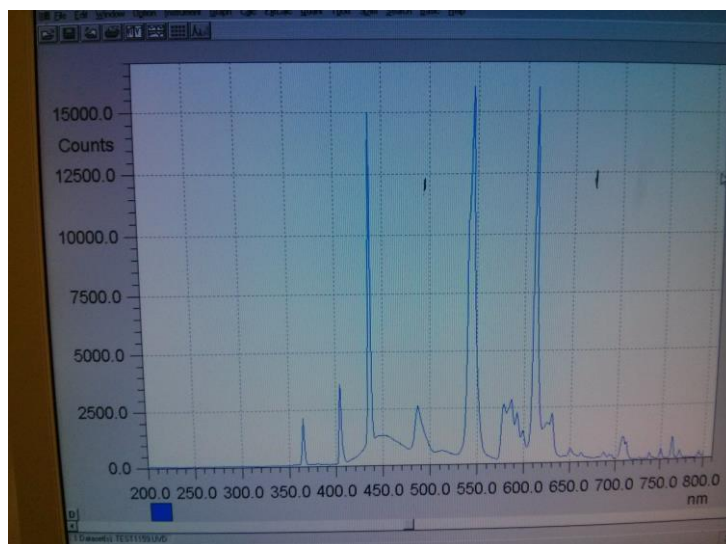


Figure 118. Emission spectrum of the 21 W CFL lamp. Picture from Christian P. Haas.

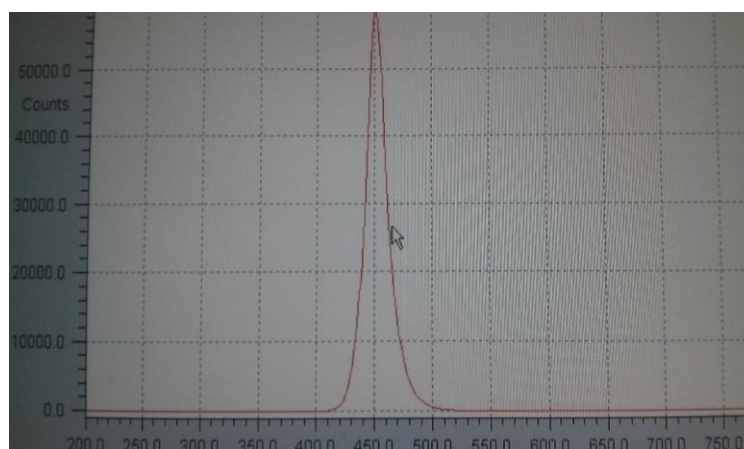
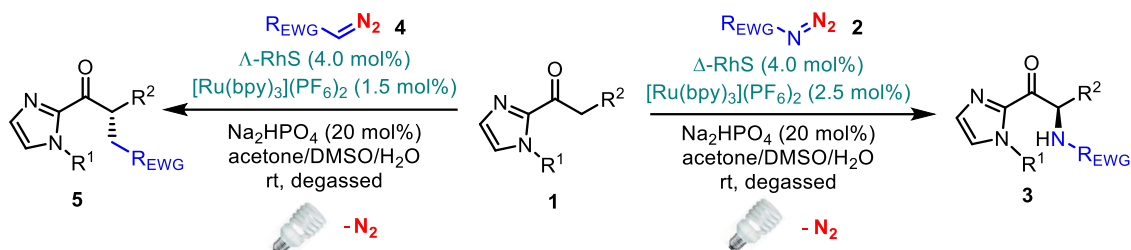


Figure 119. Emission spectrum of the 23 W blue LEDs lamp. Picture from Christian P. Haas.

5.2 Photoinduced Asymmetric α -Amination and α -Alkylation

5.2.1 General Procedure

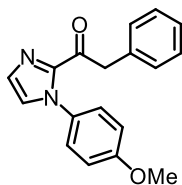


A dried 10 mL Schlenk tube was charged with 2-acyl imidazole **1** (0.10 mmol), Δ/Λ -**RhS** (3.5 mg, 4 mol%), $[\text{Ru}(\text{bpy})_3](\text{PF}_6)_2$ (2.2 mg, 2.5 mol% or 1.3 mg, 1.5 mol%) and Na_2HPO_4 (2.8 mg, 20 mol%). The tube was purged with nitrogen. Then acetone/DMSO (9:1, 0.5 mL, 0.2 M) was added via syringe, followed by H_2O (36.0 mg, 20 equiv). Azide **2** or diazo compound **4** (3.0 equiv) was added under nitrogen atmosphere with stirring. The reaction mixture was degassed via freeze-pump-thaw for three cycles. After the mixture was thoroughly degassed, the vial was sealed and positioned approximately 5 cm from a 21 W compact fluorescent lamp. The reaction was stirred at room temperature for the indicated time (monitored by TLC) under nitrogen atmosphere. Afterwards, the mixture was diluted with CH_2Cl_2 . The combined organic layers were concentrated under reduced pressure. The residue was purified by flash chromatography on silica gel (*n*-hexane/EtOAc) to afford the products **3** or **5**, respectively. Racemic samples were obtained by carrying out the reactions with *rac*-**RhS**. The enantiomeric excess was determined by chiral HPLC analysis.

5.2.2 Synthesis of Substrates

2-Acyl imidazoles **1** were synthesized according to the recently published procedures.⁵ Azides **2** were synthesized according to reported procedures.⁶ Diazo compounds **4** were synthesized according to reported literature.⁷

The data of novel substrates are shown below



1-(1-(4-Methoxyphenyl)-1H-imidazol-2-yl)-2-phenylethan-1-one (1c)

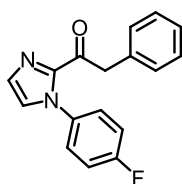
A white solid.

^1H NMR (300 MHz, CDCl_3) δ 7.35-7.18 (m, 6H), 7.18-7.10 (m, 3H), 6.94-6.87 (m, 2H), 4.44 (s, 2H), 3.82 (s, 3H).

^{13}C NMR (75 MHz, CDCl_3) δ 188.5, 159.7, 142.9, 134.5, 131.1, 129.9, 129.5, 128.4, 127.7, 126.9, 126.7, 114.1, 55.5, 45.6.

IR (film): ν (cm^{-1}) 3105, 3030, 2914, 1685, 1592, 1494, 1452, 1390, 1340, 1307, 1208, 1147, 1079, 1023, 991, 958, 912, 887, 840, 789, 761, 721, 696, 590, 542, 512, 480, 454.

HRMS (ESI, m/z) calcd for $\text{C}_{18}\text{H}_{17}\text{N}_2\text{O}_2$ $[\text{M}+\text{H}]^+$: 293.1285, found: 293.1286.



1-(1-(4-Fluorophenyl)-1H-imidazol-2-yl)-2-phenylethan-1-one (1d)

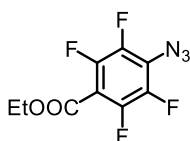
A white solid.

^1H NMR (300 MHz, CDCl_3) δ 7.37-7.17 (m, 9H), 7.16-7.08 (m, 2H), 4.48 (s, 2H).

^{13}C NMR (75 MHz, CDCl_3) δ 188.6, 162.5 (d, $J = 247.5$ Hz), 142.9, 134.3, 134.2, 129.91, 129.86, 128.5, 127.7 (d, $J = 8.8$ Hz), 127.4, 126.8, 115.9 (d, $J = 23.0$ Hz), 45.6.

IR (film): ν (cm^{-1}) 3159, 3077, 1683, 1508, 1449, 1399, 1219, 1147, 1027, 962, 911, 842, 793, 727, 701, 623, 537.

HRMS (EI, m/z) calcd for $\text{C}_{17}\text{H}_{13}\text{FN}_2\text{O}$ $[\text{M}]^+$: 280.1012, found: 280.1004.



Ethyl 4-azido-2,3,5,6-tetrafluorobenzoate (2c)

2c was synthesized by SNAr from corresponding ethyl 2,3,4,5,6-pentafluorobenzoate according to literature^{6c} as a yellow liquid.

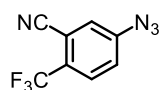
¹H NMR (500 MHz, CDCl₃) δ 4.43 (q, J = 7.0 Hz, 2H), 1.39 (t, J = 7.3 Hz, 3H).

¹³C NMR (125 MHz, CDCl₃) δ 159.3, 146.4-146.1 (m), 144.3-144.0 (m), 141.6-141.3 (m), 139.6-139.3 (m), 123.2-123.0 (m), 108.3-107.9 (m), 62.7, 14.0.

¹⁹F NMR (282 MHz, CDCl₃) δ -139.41 - -139.57 (m, 2F), -151.45 - -151.60 (m, 2F).

IR (film): ν (cm⁻¹) 2990, 2170, 2126, 1733, 1645, 1484, 1419, 1368, 1325, 1250, 1201, 993, 915, 864, 748.

HRMS (ESI, m/z) calcd for C₉H₅F₄N₃O₂Na [M+Na]⁺: 286.0210, found: 286.0210.



5-Azido-2-(trifluoromethyl)benzonitrile (2f)

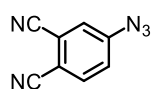
2f was synthesized by diazotization-azidation from corresponding aniline according to literature^{6a} as a grey solid.

¹H NMR (300 MHz, CDCl₃) δ 7.82 (d, J = 8.4 Hz, 1H), 7.38 (d, J = 2.1 Hz, 1H), 7.30 (dd, J_1 = 8.1 Hz, J_2 = 2.1 Hz, 1H).

¹³C NMR (75 MHz, CDCl₃) δ 145.6, 136.3, 135.3 (q, J = 33.4 Hz), 122.3, 121.8 (q, J = 272.6 Hz), 117.7 (q, J = 5.2 Hz), 115.0, 105.7 (q, J = 1.7 Hz).

IR (film): ν (cm⁻¹) 2387, 2226, 2113, 1606, 1493, 1432, 1314, 1262, 1178, 1124, 1044, 905, 839, 733, 675, 634, 548.

HRMS (ESI, m/z) calcd for C₈H₃F₃N₄Na [M+Na]⁺: 235.0202, found: 235.0202.



4-Azidophthalonitrile (2g)

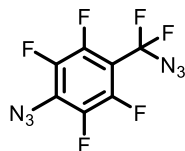
2g was synthesized by diazotization-azidation from corresponding aniline according to literature^{6a} as a grey solid.

¹H NMR (300 MHz, CDCl₃) δ 7.79 (d, J = 8.4 Hz, 1H), 7.40 (d, J = 1.8 Hz, 1H), 7.35 (dd, J_1 = 8.1 Hz, J_2 = 2.1 Hz, 1H).

^{13}C NMR (75 MHz, CDCl_3) δ 146.0, 135.1, 123.8, 123.3, 117.7, 115.0, 114.5, 111.3.

IR (film): ν (cm^{-1}) 2233, 2122, 1764, 1589, 1558, 1483, 1413, 1306, 1263, 1212, 1173, 1131, 890, 843, 753, 605, 521.

HRMS (ESI, m/z) calcd for $\text{C}_8\text{H}_3\text{N}_5\text{Na}$ $[\text{M}+\text{Na}]^+$: 192.0281, found: 192.0281.

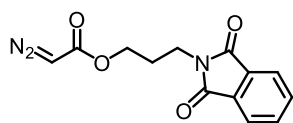


1-(Azidodifluoromethyl)-2,3,4,5,6-pentafluorobenzene (2h)

2h was synthesized by S_{N} reaction from corresponding perfluoro benzylic iodide according to literature^{6d} as a yellow liquid.

^{19}F NMR (282 MHz, CDCl_3) δ -64.19 - -64.92 (m, 2F), -139.56 - -140.22 (m, 2F), -149.90 - -150.93 (m, 2F).

IR (film): ν (cm^{-1}) 2126, 1651, 1490, 1426, 1334, 1250, 1164, 1054, 999, 975, 848, 782.



3-(1,3-Dioxoisindolin-2-yl)propyl 2-diazoacetate (4b)

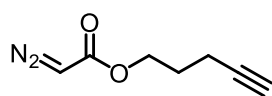
A yellow oil.

^1H NMR (300 MHz, CDCl_3) δ 7.88-7.81 (m, 2H), 7.75-7.68 (m, 2H), 4.69 (s, 1H), 4.21 (t, J = 6.2 Hz, 2H), 3.80 (t, J = 6.9 Hz, 2H), 2.11-2.00 (m, 2H).

^{13}C NMR (125 MHz, CDCl_3) δ 168.2, 134.0, 132.0, 123.3, 62.2, 46.2, 34.9, 27.7. (Missing one ^{13}C signal)

IR (film): ν (cm^{-1}) 3104, 2955, 2110, 1771, 1703, 1616, 1464, 1441, 1395, 1362, 1240, 1184, 1048, 986, 899, 794, 718, 526, 501.

HRMS (ESI, m/z) calcd for $\text{C}_{13}\text{H}_{11}\text{N}_3\text{O}_4\text{Na}$ $[\text{M}+\text{Na}]^+$: 296.0642, found: 296.0642.



Pent-4-yn-1-yl 2-diazoacetate (4d)

A yellow liquid.

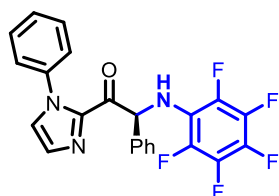
^1H NMR (300 MHz, CDCl_3) δ 4.73 (s, 1H), 4.25 (t, $J = 6.2$ Hz, 2H), 2.27 (td, $J_1 = 7.2$ Hz, $J_2 = 2.7$ Hz, 2H), 1.96 (t, $J = 2.7$ Hz, 1H), 1.91-1.82 (m, 2H).

^{13}C NMR (75 MHz, CDCl_3) δ 166.6, 82.8, 69.0, 63.3, 46.0, 27.7, 15.1.

IR (film): ν (cm^{-1}) 3296, 3114, 2961, 2107, 1682, 1443, 1396, 1359, 1296, 1239, 1179, 1086, 1035, 992, 738, 635, 556, 479.

HRMS (ESI, m/z) calcd for $\text{C}_7\text{H}_8\text{N}_2\text{O}_2\text{Na}$ $[\text{M}+\text{Na}]^+$: 175.0478, found: 175.0478.

5.2.3 Experimental and Characterization Data of Novel Products



(S)-2-((Perfluorophenyl)amino)-2-phenyl-1-(1-phenyl-1H-imidazol-2-yl)ethan-1-one (**3aa**)

According to the general procedure, the reaction of 2-phenyl-1-(1-phenyl-1H-imidazol-2-yl)ethan-1-one **1a** (26.2 mg, 0.10 mmol), 1-azido-2,3,4,5,6-pentafluorobenzene **2a** (62.7 mg, 3.0 equiv), $\Delta\text{-RhS}$ (3.5 mg, 4 mol%), $[\text{Ru}(\text{bpy})_3](\text{PF}_6)_2$ (2.2 mg, 2.5 mol%), Na_2HPO_4 (2.8 mg, 20 mol%) and H_2O (36.0 mg, 20 equiv) in acetone/DMSO (9:1, 0.5 mL, 0.2 M) under nitrogen atmosphere with visible light for 8 hours, afforded 36.3 mg (82%) of **3aa** as a yellow oil. Enantiomeric excess was established by HPLC analysis using a Chiralpak IC column, ee = 98% (HPLC: IC, 254 nm, *n*-hexane/isopropanol = 95:5, flow rate 1 mL/min, 25 °C, t_r (major) = 5.7 min, t_r (minor) = 4.9 min). $[\alpha]_{\text{D}}^{22} = +150.0^\circ$ (c 1.0, CH_2Cl_2).

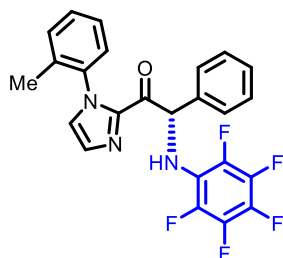
^1H NMR (500 MHz, CDCl_3) δ 7.51-7.54 (m, 5H), 7.33 (d, $J = 1.0$ Hz, 1H), 7.32-7.27 (m, 2H), 7.26-7.21 (m, 1H), 7.18 (d, $J = 0.5$ Hz, 1H), 7.14-7.11 (m, 2H), 6.74 (d, $J = 9.0$ Hz, 1H), 5.36 (d, $J = 9.5$ Hz, 1H).

^{13}C NMR (125 MHz, CDCl_3) δ 188.1, 140.8, 137.7, 136.8, 130.5, 129.11, 129.07, 128.8, 128.4, 128.1, 127.7, 125.5, 63.4-63.2 (m).

^{19}F NMR (282 MHz, CDCl_3) δ -157.35 - -157.51 (m, 2F), -164.25 - -164.46 (m, 2F), -170.41 (tt, $J_1 = 22.28$ Hz, $J_2 = 5.92$ Hz, 1F).

IR (film): ν (cm⁻¹) 3367, 1688, 1596, 1517, 1449, 1398, 1346, 1305, 1263, 1188, 1154, 1107, 1072, 1021, 976, 911, 839, 761, 732, 694, 625, 585, 548, 526, 498, 461.

HRMS (ESI, m/z) calcd for C₂₃H₁₄F₅N₃ONa [M+ Na]⁺: 466.0949, found: 466.0946.



(S)-2-((Perfluorophenyl)amino)-2-phenyl-1-(1-(*o*-tolyl)-1*H*-imidazol-2-yl)ethan-1-one (3ba)

According to the general procedure, the reaction of 2-phenyl-1-(1-(*o*-tolyl)-1*H*-imidazol-2-yl)ethan-1-one **1b** (27.6 mg, 0.10 mmol), 1-azido-2,3,4,5,6-pentafluorobenzene **2a** (62.7 mg, 3.0 equiv), Δ -**RhS** (3.5 mg, 4 mol%), [Ru(bpy)₃](PF₆)₂ (2.2 mg, 2.5 mol%), Na₂HPO₄ (2.8 mg, 20 mol%) and H₂O (36.0 mg, 20 equiv) in acetone/DMSO (9:1, 0.5 mL, 0.2 M) under nitrogen atmosphere with visible light for 13 hours, afforded 36.1 mg (79%) of **3ba** as a white solid. Enantiomeric excess was established by HPLC analysis using a Chiralpak OD-H column, ee = 99.1% (HPLC: OD-H, 254 nm, *n*-hexane/isopropanol = 95:5, flow rate 1 mL/min, 25 °C, t_r (major) = 7.5 min, t_r (minor) = 6.8 min). $[\alpha]_D^{22} = +156.4^\circ$ (*c* 1.0, CH₂Cl₂).

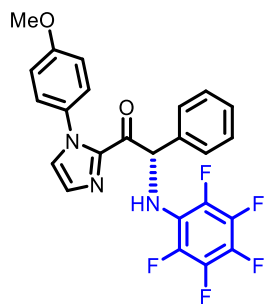
¹H NMR (500 MHz, CDCl₃) δ 7.47-7.31 (m, 5H), 7.30-7.18 (m, 5H), 7.09 (d, J = 1.0 Hz, 1H), 6.78 (d, J = 8.0 Hz, 1H, other rotamer), 6.76-6.68 (m, 1H), 5.41-5.28 (m, 1H), 2.04 (s, 3H, other rotamer), 1.41 (s, 3H).

¹³C NMR (125 MHz, CDCl₃) δ 186.0, 185.9, 141.3, 141.2, 137.2, 137.1, 136.7, 134.7, 134.2, 130.81, 130.78, 130.7, 129.5, 129.4, 128.8, 128.7, 128.4, 128.3, 128.1, 128.0, 127.18, 127.16, 126.7, 126.6, 126.4, 126.0, 63.3 (t, J = 3.4 Hz), 63.0 (t, J = 3.7 Hz), 17.2, 16.1. (Mixture of two rotation isomers).

¹⁹F NMR (282 MHz, CDCl₃) δ -157.30 - -157.68 (m, 2F), -164.31 - -164.51 (m, 2F), -170.31 - -170.69 (m, 1F).

IR (film): ν (cm⁻¹) 3370, 2923, 1300, 1686, 1515, 1459, 1400, 1023, 980, 959, 768, 700, 673, 647, 618, 558.

HRMS (ESI, m/z) calcd for C₂₄H₁₆F₅N₃ONa [M+Na]⁺: 480.1106, found: 480.1102.



(S)-1-(1-(4-Methoxyphenyl)-1H-imidazol-2-yl)-2-((perfluorophenyl)amino)-2-phenylethan-1-one (3ca)

According to the general procedure, the reaction of 1-(1-(4-methoxyphenyl)-1H-imidazol-2-yl)-2-phenylethan-1-one **1c** (29.2 mg, 0.10 mmol), 1-azido-2,3,4,5,6-pentafluorobenzene **2a** (62.7 mg, 3.0 equiv), Δ -**RhS** (3.5 mg, 4 mol%), [Ru(bpy)₃](PF₆)₂ (2.2 mg, 2.5 mol%), Na₂HPO₄ (2.8 mg, 20 mol%) and H₂O (36.0 mg, 20 equiv) in acetone/DMSO (9:1, 0.5 mL, 0.2 M) under nitrogen atmosphere with visible light for 6 hours, afforded 37.7 mg (80%) of **3ca** as a yellow oil. Enantiomeric excess was established by HPLC analysis using a Chiralpak IC column, ee = 99% (HPLC: IC, 254 nm, *n*-hexane/isopropanol = 90:10, flow rate 1 mL/min, 25 °C, *t_r* (major) = 6.3 min, *t_r* (minor) = 5.3 min). $[\alpha]_D^{22} = +173.0^\circ$ (*c* 1.0, CH₂Cl₂).

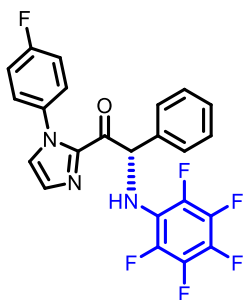
¹H NMR (500 MHz, CDCl₃) δ 7.48-7.44 (m, 2H), 7.32-7.27 (m, 3H), 7.25-7.20 (m, 1H), 7.14 (d, *J* = 1.0 Hz, 1H), 7.07-7.02 (m, 2H), 6.97-6.91 (m, 2H), 6.73 (d, *J* = 9.0 Hz, 1H), 5.36 (d, *J* = 9.0 Hz, 1H), 3.86 (s, 3H).

¹³C NMR (125 MHz, CDCl₃) δ 186.0, 159.8, 140.8, 136.8, 130.4, 128.8, 128.3, 128.10, 128.06 126.6, 114.2, 63.2 (t, *J* = 3.5 Hz), 55.5. (Missing one ¹³C signal)

¹⁹F NMR (282 MHz, CDCl₃) δ -157.74 - -157.90 (m, 2F), -164.67 - -164.89 (m, 2F), -170.85 (tt, *J₁* = 22.00 Hz, *J₂* = 5.78 Hz, 1F).

IR (film): ν (cm⁻¹) 3367, 2964, 2791, 1687, 1608, 1515, 1453, 1397, 1346, 1298, 1249, 1177, 1109, 1071, 1020, 976, 911, 836, 779, 732, 698, 675, 625, 585, 499.

HRMS (ESI, *m/z*) calcd for C₂₄H₁₆F₅N₃O₂Na [M+Na]⁺: 496.1055, found: 496.1054.



(S)-1-(1-(4-Fluorophenyl)-1*H*-imidazol-2-yl)-2-((perfluorophenyl)amino)-2-phenylethan-1-one
(3da)

According to the general procedure, the reaction of 1-(1-(4-fluorophenyl)-1*H*-imidazol-2-yl)-2-phenylethan-1-one **1d** (28.0 mg, 0.10 mmol), 1-azido-2,3,4,5,6-pentafluorobenzene **2a** (62.7 mg, 3.0 equiv), Δ -**RhS** (3.5 mg, 4 mol%), [Ru(bpy)₃](PF₆)₂ (2.2 mg, 2.5 mol%), Na₂HPO₄ (2.8 mg, 20 mol%) and H₂O (36.0 mg, 20 equiv) in acetone/DMSO (9:1, 0.5 mL, 0.2 M) under nitrogen atmosphere with visible light for 14 hours, afforded 34.9 mg (76%) of **3da** as a yellow oil. Enantiomeric excess was established by HPLC analysis using a Chiralpak AD-H column, ee = 98% (HPLC: AD-H, 254 nm, *n*-hexane/isopropanol = 90:10, flow rate 1 mL/min, 25 °C, *t_r* (major) = 7.0 min, *t_r* (minor) = 5.4 min). $[\alpha]_D^{22} = +150.0^\circ$ (*c* 1.0, CH₂Cl₂).

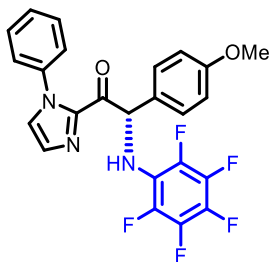
¹H NMR (500 MHz, CDCl₃) δ 7.48-7.43 (m, 2H), 7.32 (d, *J* = 1.0 Hz, 1H), 7.31-7.27 (m, 2H), 7.26-7.21 (m, 1H), 7.16-7.09 (m, 5H), 6.72 (d, *J* = 9.5 Hz, 1H), 5.32 (d, *J* = 9.5 Hz, 1H).

¹³C NMR (125 MHz, CDCl₃) δ 186.2, 162.6 (d, *J* = 249.3), 140.9, 136.7, 133.6 (d, *J* = 3.3 Hz), 130.7, 128.9, 128.4, 128.1, 127.5, 127.4 (d, *J* = 8.4 Hz), 116.1 (d, *J* = 22.9 Hz), 63.3 (t, *J* = 3.3 Hz).

¹⁹F NMR (282 MHz, CDCl₃) δ -111.60 (s, 1F), -157.36 - -157.51 (m, 2F), -164.17 - -164.38 (m, 2F), -170.23 (tt, *J₁* = 21.86 Hz, *J₂* = 6.06 Hz, 1F).

IR (film): ν (cm⁻¹) 3368, 1687, 1514, 1452, 1399, 1345, 1310, 1227, 1154, 1099, 1070, 1023, 978, 914, 842, 784, 735, 699, 625, 585, 545, 464, 423.

HRMS (ESI, *m/z*) calcd for C₂₃H₁₄F₆N₃O [M+H]⁺: 462.1036, found: 462.1031.



(S)-2-(4-Methoxyphenyl)-2-((perfluorophenyl)amino)-1-(1-phenyl-1*H*-imidazol-2-yl)ethan-1-one (3ea)

According to the general procedure, the reaction of 2-(4-methoxyphenyl)-1-(1-phenyl-1*H*-imidazol-2-yl)ethan-1-one **1e** (29.2 mg, 0.10 mmol), 1-azido-2,3,4,5,6-pentafluorobenzene **2a** (62.7 mg, 3.0 equiv), Δ -**RhS** (3.5 mg, 4 mol%), [Ru(bpy)₃](PF₆)₂ (2.2 mg, 2.5 mol%), DIPEA (2.6 mg, 20 mol%) and H₂O (36.0 mg, 20 equiv) in acetone/DMSO (9:1, 1.0 mL, 0.1 M) under nitrogen atmosphere with visible light for 17 hours, afforded 33.6 mg (71%) of **3ea** as a yellow oil. Enantiomeric excess was established by HPLC analysis using a Chiralpak OD-H column, ee = 99.1% (HPLC: OD-H, 254 nm, *n*-hexane/isopropanol = 95:5, flow rate 1 mL/min, 25 °C, *t_r* (major) = 10.1 min, *t_r* (minor) = 8.6 min). [α]_D²² = +202.6° (*c* 1.0, CH₂Cl₂).

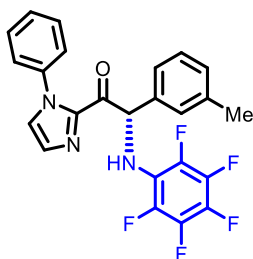
¹H NMR (500 MHz, CDCl₃) δ 7.51-7.42 (m, 3H), 7.39-7.34 (m, 2H), 7.32-7.30 (m, 1H), 7.18-7.10 (m, 1H), 7.15-7.10 (m, 2H), 6.84-6.78 (m, 2H), 6.67 (br s, 1H), 5.30 (br s, 1H), 3.75 (s, 3H).

¹³C NMR (125 MHz, CDCl₃) δ 186.0, 159.5, 140.8, 137.7, 130.5, 129.4, 129.11, 129.06, 128.6, 127.6, 125.6, 114.3, 62.6 (t, *J* = 3.3 Hz), 55.1.

¹⁹F NMR (282 MHz, CDCl₃) δ -157.30 - -157.47 (m, 2F), -164.32 - -164.55 (m, 2F), -170.46 (tt, *J₁* = 22.00 Hz, *J₂* = 5.78 Hz, 1F).

IR (film): ν (cm⁻¹) 3353, 2931, 2963, 1670, 1603, 1512, 1468, 1446, 1399, 1306, 1258, 1175, 1098, 1023, 979, 956, 913, 818, 786, 761, 731, 691, 573.

HRMS (EI, *m/z*) calcd for C₂₄H₁₆F₅N₃O₂ [M]⁺: 473.1163, found: 473.1173.



(S)-2-((Perfluorophenyl)amino)-1-(1-phenyl-1H-imidazol-2-yl)-2-(*m*-tolyl)ethan-1-one (3fa)

According to the general procedure, the reaction of 1-(1-phenyl-1H-imidazol-2-yl)-2-(*m*-tolyl)ethan-1-one **1f** (27.6 mg, 0.10 mmol), 1-azido-2,3,4,5,6-pentafluorobenzene **2a** (62.7 mg, 3.0 equiv), Δ -RhS (3.5 mg, 4 mol%), [Ru(bpy)₃](PF₆)₂ (2.2 mg, 2.5 mol%), Na₂HPO₄ (2.8 mg, 20 mol%) and H₂O (36.0 mg, 20 equiv) in acetone/DMSO (9:1, 0.5 mL, 0.2 M) under nitrogen atmosphere with visible light for 7 hours, afforded 35.1 mg (77%) of **3fa** as a brown solid. Enantiomeric excess was established by HPLC analysis using a Chiralpak AD-H column, ee = 98% (HPLC: AD-H, 254 nm, *n*-hexane/isopropanol = 90:10, flow rate 1 mL/min, 25 °C, *t_r* (major) = 6.4 min, *t_r* (minor) = 4.7 min). $[\alpha]_D^{22} = +177.0^\circ$ (*c* 1.0, CH₂Cl₂).

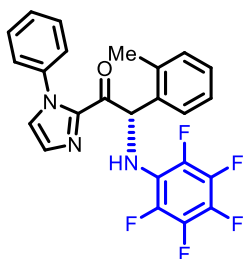
¹H NMR (500 MHz, CDCl₃) δ 7.51-7.40 (m, 3H), 7.32 (d, *J* = 1.5 Hz, 1H), 7.29-7.27 (m, 2H), 7.26-7.24 (m, 2H, other rotamer), 7.23-7.18 (m, 1H), 7.18 (d, *J* = 1.5 Hz, 1H), 7.17-7.10 (m, 2H), 7.07-7.06 (m, 1H), 7.05-7.03 (m, 1H, other rotamer), 6.69 (d, *J* = 14.5, 1H), 5.32-5.26 (m, 1H), 2.31 (s, 3H).

¹³C NMR (125 MHz, CDCl₃) δ 186.2, 140.9, 138.6, 137.7, 136.6, 130.5, 129.2, 129.10, 129.05, 128.7, 127.7, 125.6, 125.2, 63.3 (t, *J* = 5.9 Hz), 21.4. (Missing one ¹³C signal)

¹⁹F NMR (282 MHz, CDCl₃) δ -157.36 - -157.52 (m, 2F), -164.30 - -164.52 (m, 2F), -170.53 (tt, *J₁* = 22.00 Hz, *J₂* = 5.78 Hz, 1F).

IR (film): ν (cm⁻¹) 3371, 1682, 1519, 1447, 1395, 1306, 1025, 980, 957, 915, 843, 768, 727, 697, 670, 637, 591, 555, 516, 460.

HRMS (ESI, *m/z*) calcd for C₂₄H₁₆F₅N₃ONa [M+Na]⁺: 480.1106, found: 480.1106.



(S)-2-((Perfluorophenyl)amino)-1-(1-phenyl-1H-imidazol-2-yl)-2-(o-tolyl)ethan-1-one (3ga)

According to the general procedure, the reaction of 1-(1-phenyl-1H-imidazol-2-yl)-2-(o-tolyl)ethan-1-one **1g** (27.6 mg, 0.10 mmol), 1-azido-2,3,4,5,6-pentafluorobenzene **2a** (62.7 mg, 3.0 equiv), Δ -RhS (3.5 mg, 4 mol%), [Ru(bpy)₃](PF₆)₂ (2.2 mg, 2.5 mol%), Na₂HPO₄ (2.8 mg, 20 mol%) and H₂O (36.0 mg, 20 equiv) in acetone/DMSO (9:1, 0.5 mL, 0.2 M) under nitrogen atmosphere with visible light for 10 hours, afforded 25.0 mg (55%) of **3ga** as a white solid. Enantiomeric excess was established by HPLC analysis using a Chiralpak AD-H column, ee = 98% (HPLC: AD-H, 254 nm, *n*-hexane/isopropanol = 90:10, flow rate 1 mL/min, 25 °C, *t_r* (major) = 6.0 min, *t_r* (minor) = 4.6 min). $[\alpha]_D^{22} = +214.2^\circ$ (*c* 1.0, CH₂Cl₂).

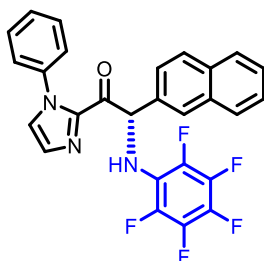
¹H NMR (500 MHz, CDCl₃) δ 7.49-7.41 (m, 3H), 7.25 (d, *J* = 0.5 Hz, 1H), 7.24-7.18 (m, 3H), 7.17-7.14 (m, 2H), 7.14-7.11 (m, 2H), 6.90 (br s, 1H), 4.86 (br s, 1H), 2.72 (s, 3H).

¹³C NMR (125 MHz, CDCl₃) δ 187.3, 141.4, 138.3, 137.7, 135.0, 131.5, 130.3, 129.1, 129.0, 128.6, 127.5, 126.6, 126.4, 125.5, 60.4 (t, *J* = 3.6 Hz), 19.4.

¹⁹F NMR (282 MHz, CDCl₃) δ -157.40 - -157.56 (m, 2F), -164.25 - -164.47 (m, 2F), -170.29 (tt, *J₁* = 22.00 Hz, *J₂* = 5.64 Hz, 1F).

IR (film): ν (cm⁻¹) 3366, 3128, 2923, 2855, 1692, 1597, 1514, 1464, 1402, 1351, 1307, 1247, 1211, 1152, 1120, 1086, 1011, 964, 912, 875, 844, 787, 761, 733, 691, 653, 625, 579, 561, 508.

HRMS (ESI, *m/z*) calcd for C₂₄H₁₆F₅N₃ONa [M+Na]⁺: 480.1106, found: 480.1105.



(S)-2-(Naphthalen-2-yl)-2-((perfluorophenyl)amino)-1-(1-phenyl-1H-imidazol-2-yl)ethan-1-one

(3ha)

According to the general procedure, the reaction of 2-(naphthalen-2-yl)-1-(1-phenyl-1H-imidazol-2-yl)ethan-1-one **1h** (31.2 mg, 0.10 mmol), 1-azido-2,3,4,5,6-pentafluorobenzene **2a** (62.7 mg, 3.0 equiv), Δ -**RhS** (3.5 mg, 4 mol%), $[\text{Ru}(\text{bpy})_3](\text{PF}_6)_2$ (2.2 mg, 2.5 mol%), Na_2HPO_4 (2.8 mg, 20 mol%) and H_2O (36.0 mg, 20 equiv) in acetone/DMSO (9:1, 0.5 mL, 0.2 M) under nitrogen atmosphere with visible light for 17 hours, afforded 24.8 mg (50%) of **3ha** as a yellow oil. Enantiomeric excess was established by HPLC analysis using a Chiralpak AD-H column, ee = 95% (HPLC: AD-H, 254 nm, *n*-hexane/isopropanol = 90:10, flow rate 1 mL/min, 25 °C, t_r (major) = 8.3 min, t_r (minor) = 6.4 min). $[\alpha]_D^{22} = +260.2^\circ$ (c 1.0, CH_2Cl_2).

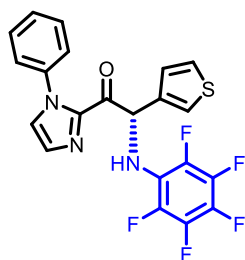
^1H NMR (500 MHz, CDCl_3) δ 7.98 (s, 1H), 7.85-7.81 (m, 1H), 7.80-7.76 (m, 2H), 7.55 (dd, $J_1 = 8.5$ Hz, $J_2 = 1.5$ Hz, 1H), 7.50-7.41 (m, 5H), 7.33 (d, $J = 1.0$ Hz, 1H), 7.16 (d, $J = 1.0$ Hz, 1H), 7.14-7.10 (m, 2H), 6.93-6.88 (m, 1H) 5.50-5.45 (m, 1H).

^{13}C NMR (125 MHz, CDCl_3) δ 185.8, 140.8, 137.6, 134.2, 133.3, 133.1, 130.6, 129.1, 128.8, 128.21, 128.16, 127.8, 127.6, 126.5, 126.3, 125.6, 125.0, 63.3 (t, $J = 3.6$ Hz). (Missing one ^{13}C signal)

^{19}F NMR (282 MHz, CDCl_3) δ -157.32 - -157.49 (m, 2F), -164.18 - -164.39 (m, 2F), -170.29 (tt, $J_1 = 22.00$ Hz, $J_2 = 5.92$ Hz, 1F).

IR (film): ν (cm^{-1}) 3367, 1687, 1597, 1517, 1448, 1398, 1305, 1266, 1180, 1154, 1123, 1099, 1022, 971, 909, 843, 813, 734, 691, 668, 641, 610, 544, 503, 474.

HRMS (ESI, m/z) calcd for $\text{C}_{27}\text{H}_{16}\text{F}_5\text{N}_3\text{ONa}$ $[\text{M}+\text{Na}]^+$: 516.1106, found: 516.1106.

**(S)-2-((Perfluorophenyl)amino)-1-(1-phenyl-1H-imidazol-2-yl)-2-(thiophen-3-yl)ethan-1-one****(3ia)**

According to the general procedure, the reaction of 1-(1-phenyl-1H-imidazol-2-yl)-2-(thiophen-3-yl)ethan-1-one **1i** (26.8 mg, 0.10 mmol), 1-azido-2,3,4,5,6-pentafluorobenzene **2a** (62.7 mg, 3.0 equiv), Δ -**RhS** (3.5 mg, 4 mol%), $[\text{Ru}(\text{bpy})_3](\text{PF}_6)_2$ (2.2 mg, 2.5 mol%), DIPEA (2.6 mg, 20 mol%) and H_2O

(36.0 mg, 20 equiv) in acetone/DMSO (9:1, 1.0 mL, 0.1 M) under nitrogen atmosphere with visible light for 40 hours, afforded 19.0 mg (42%) of **3ia** as a yellow oil. Enantiomeric excess was established by HPLC analysis using a Chiralpak AD-H column, ee = 93% (HPLC: AD-H, 254 nm, *n*-hexane/isopropanol = 90:10, flow rate 1 mL/min, 25 °C, *t_r* (major) = 7.8 min, *t_r* (minor) = 6.2 min). $[\alpha]_{\text{D}}^{22} = +123.8^{\circ}$ (*c* 0.4, CH₂Cl₂).

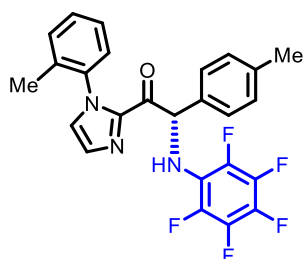
¹H NMR (500 MHz, CDCl₃) δ 7.50-7.44 (m, 3H), 7.38-7.35 (m, 1H), 7.34 (d, *J* = 1.0 Hz, 1H), 7.23 (dd, *J*₁ = 5.0 Hz, *J*₂ = 3.0 Hz, 1H), 7.21 (d, *J* = 1.0 Hz, 1H), 7.18-7.14 (m, 2H), 7.07 (dd, *J*₁ = 5.0 Hz, *J*₂ = 1.0 Hz, 1H), 6.83 (d, *J* = 9.5 Hz, 1H), 5.21 (d, *J* = 9.5 Hz, 1H).

¹³C NMR (125 MHz, CDCl₃) δ 185.5, 140.7, 137.6, 137.5, 130.6, 129.2, 129.1, 127.8, 126.5, 126.3, 125.6, 124.6, 59.3 (t, *J* = 3.9 Hz).

¹⁹F NMR (282 MHz, CDCl₃) δ -157.70 - -157.86 (m, 2F), -164.51 - -164.72 (m, 2F), -170.50 (tt, *J*₁ = 22.14 Hz, *J*₂ = 5.50 Hz, 1F).

IR (film): ν (cm⁻¹) 3364, 1687, 1599, 1515, 1448, 1397, 1348, 1305, 1260, 1182, 1151, 1098, 1021, 972, 912, 840, 763, 731, 693, 664, 546, 460.

HRMS (ESI, *m/z*) calcd for C₂₁H₁₂F₅N₃OSNa [M+Na]⁺: 472.0513, found: 472.0510.



(S)-2-((Perfluorophenyl)amino)-2-(*p*-tolyl)-1-(1-(*o*-tolyl)-1*H*-imidazol-2-yl)ethan-1-one (3ja**)**

According to the general procedure, the reaction of 2-(*p*-tolyl)-1-(1-(*o*-tolyl)-1*H*-imidazol-2-yl)ethan-1-one **1j** (29.0 mg, 0.10 mmol), 1-azido-2,3,4,5,6-pentafluorobenzene **2a** (62.7 mg, 3.0 equiv), Δ-**RhS** (3.5 mg, 4 mol%), [Ru(bpy)₃](PF₆)₂ (2.2 mg, 2.5 mol%), DIPEA (2.6 mg, 20 mol%) and H₂O (36.0 mg, 20 equiv) in acetone/DMSO (9:1, 1.0 mL, 0.1 M) under nitrogen atmosphere with visible light for 12 hours, afforded 37.5 mg (80%) of **3ja** as a yellow oil. Enantiomeric excess was established by HPLC analysis using a Chiralpak OD-H column, ee = 99.4% (HPLC: OD-H, 254 nm, *n*-hexane/isopropanol = 90:10, flow rate 1 mL/min, 25 °C, *t_r* (major) = 7.1 min, *t_r* (minor) = 6.0 min). $[\alpha]_{\text{D}}^{22} = +241.0^{\circ}$ (*c* 1.0, CH₂Cl₂).

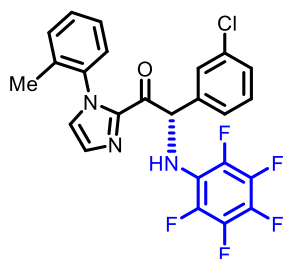
^1H NMR (500 MHz, CDCl_3) δ 7.42-7.27 (m, 5H), 7.26-7.19 (m, 2H), 7.10-7.03 (m, 3H), 6.80 (d, J = 8.0 Hz, 1H, other rotamer), 6.71-6.64 (m, 1H), 5.40-5.23 (m, 1H), 2.27 (s, 3H, other rotamer), 2.25 (s, 3H), 2.03 (s, 3H, other rotamer), 1.46 (s, 3H).

^{13}C NMR (125 MHz, CDCl_3) δ 186.1, 186.0, 141.4, 141.3, 138.2, 138.1, 137.3, 137.2, 134.7, 134.3, 133.7, 130.83, 130.76, 130.73, 130.68, 129.6, 129.5, 129.43, 129.37, 128.00, 127.9, 127.1, 126.7, 126.6, 126.5, 126.1, 63.0 (t, J = 3.3 Hz), 62.8 (t, J = 3.9 Hz), 21.11, 21.08, 17.2, 16.3. (Mixture of two rotation isomers).

^{19}F NMR (282 MHz, CDCl_3) δ -157.51 - -157.75 (m, 2F), -164.54 - -164.75 (m, 2F), -170.61 - -170.96 (m, 1F).

IR (film): ν (cm^{-1}) 3368, 2925, 2857, 1687, 1517, 1453, 1400, 1346, 1303, 1262, 1186, 1153, 1095, 1021, 967, 912, 851, 803, 765, 727, 653, 616, 555, 496, 455.

HRMS (ESI, m/z) calcd for $\text{C}_{25}\text{H}_{18}\text{F}_5\text{N}_3\text{ONa}$ $[\text{M}+\text{Na}]^+$: 494.1262, found: 494.1263.



(S)-2-(3-Chlorophenyl)-2-((perfluorophenyl)amino)-1-(1-(*o*-tolyl)-1*H*-imidazol-2-yl)ethan-1-one (3ka)

According to the general procedure, the reaction of 2-(3-chlorophenyl)-1-(1-(*o*-tolyl)-1*H*-imidazol-2-yl)ethan-1-one **1k** (31.1 mg, 0.10 mmol), 1-azido-2,3,4,5,6-pentafluorobenzene **2a** (62.7 mg, 3.0 equiv), Δ -**RhS** (3.5 mg, 4 mol%), $[\text{Ru}(\text{bpy})_3](\text{PF}_6)_2$ (2.2 mg, 2.5 mol%), Na_2HPO_4 (2.8 mg, 20 mol%) and H_2O (36.0 mg, 20 equiv) in acetone/DMSO (9:1, 0.5 mL, 0.2 M) under nitrogen atmosphere with visible light for 48 hours, afforded 23.3 mg (47%) of **3ka** as a white solid. Enantiomeric excess was established by HPLC analysis using a Chiralpak OD-H column, ee = 97% (HPLC: OD-H, 254 nm, *n*-hexane/isopropanol = 95:5, flow rate 1 mL/min, 25 °C, t_r (major) = 7.7 min, t_r (minor) = 6.9 min). $[\alpha]_{\text{D}}^{22} = +162.0^\circ$ (c 1.0, CH_2Cl_2).

^1H NMR (500 MHz, CDCl_3) δ 7.47-7.43 (m, 1H), 7.43-7.32 (m, 4H), 7.28-7.18 (m, 4H), 7.13-7.10 (m, 1H), 6.83 (d, J = 8.0 Hz, 1H, other rotamer), 6.72-6.64 (m, 1H), 5.40-5.28 (m, 1H), 2.03 (s, 3H, other

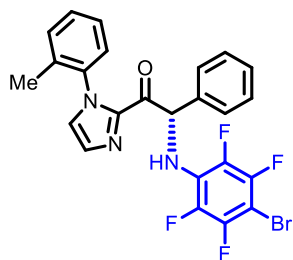
rotamer), 1.48 (s, 3H).

^{13}C NMR (125 MHz, CDCl_3) δ 185.3, 185.2, 141.0, 140.9, 139.0, 138.9, 137.03, 136.95, 134.7, 134.64, 134.60, 134.2, 131.0, 130.94, 130.86, 130.1, 130.0, 129.6, 129.5, 128.63, 128.58, 128.2, 128.1, 127.50, 127.48, 126.8, 126.7, 126.4, 126.2, 126.0, 62.6 (t, $J = 3.8$ Hz), 62.4 (t, $J = 3.5$ Hz), 17.2, 16.2. (Mixture of two rotation isomers).

^{19}F NMR (282 MHz, CDCl_3) δ -157.89 - -158.16 (m, 2F), -164.29 - -164.51 (m, 2F), -170.25 - -170.61 (m, 1F).

IR (film): ν (cm^{-1}) 3366, 1684, 1517, 1446, 1397, 1303, 1187, 1155, 1081, 1024, 981, 956, 911, 846, 765, 723, 696, 664, 630, 585, 554, 453.

HRMS (ESI, m/z) calcd for $\text{C}_{24}\text{H}_{15}\text{ClF}_5\text{N}_3\text{ONa}$ $[\text{M}+\text{Na}]^+$: 514.0716, found: 514.0715.



(S)-2-((4-Bromo-2,3,5,6-tetrafluorophenyl)amino)-2-phenyl-1-(1-(*o*-tolyl)-1*H*-imidazol-2-yl)ethan-1-one (3bb)

According to the general procedure, the reaction of 2-phenyl-1-(1-(*o*-tolyl)-1*H*-imidazol-2-yl)ethan-1-one **1b** (27.6 mg, 0.10 mmol), 1-azido-4-bromo-2,3,5,6-tetrafluorobenzene **2b** (80.7 mg, 3.0 equiv), Δ -**RhS** (3.5 mg, 4 mol%), $[\text{Ru}(\text{bpy})_3](\text{PF}_6)_2$ (2.2 mg, 2.5 mol%), Na_2HPO_4 (2.8 mg, 20 mol%) and H_2O (36.0 mg, 20 equiv) in acetone/DMSO (9:1, 0.5 mL, 0.2 M) under nitrogen atmosphere with visible light for 5 hours, afforded 46.5 mg (90%) of **3bb** as a white solid. Enantiomeric excess was established by HPLC analysis using a Chiralpak OD-H column, ee = 99.4% (HPLC: OD-H, 254 nm, *n*-hexane/isopropanol = 95:5, flow rate 1 mL/min, 25 °C, t_r (major) = 8.3 min, t_r (minor) = 7.4 min). $[\alpha]_{\text{D}}^{22} = +150.8^\circ$ (c 1.0, CH_2Cl_2).

^1H NMR (500 MHz, CDCl_3) δ 7.50-7.43 (m, 2H), 7.42-7.19 (m, 8H), 7.11-7.09 (m, 1H), 6.86-6.81 (m, 1H, other rotamer), 6.81-6.75 (m, 1H), 5.67-5.61 (m, 1H), 5.60-5.56 (m, 1H, other rotamer), 2.04 (s, 3H, other rotamer), 1.41 (s, 3H).

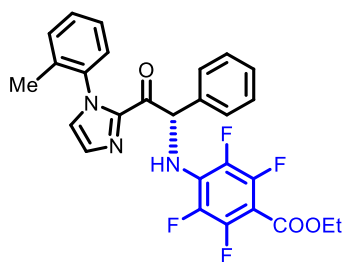
^{13}C NMR (125 MHz, CDCl_3) δ 185.8, 185.7, 146.2-145.8 (m), 144.3-144.0 (m), 141.4-141.0 (m),

139.2-138.7 (m), 137.3-136.9 (m), 136.8, 134.7, 134.3, 130.82, 130.80, 130.77, 130.7, 129.5, 129.4, 128.84, 128.76, 128.38, 128.35 128.1, 128.0, 127.21, 127.18 126.7, 126.6, 126.4, 126.0, 62.5 (t, $J = 3.7$ Hz), 62.2 (t, $J = 3.8$ Hz), 17.2, 16.0. (Mixture of two rotation isomers).

^{19}F NMR (282 MHz, CDCl_3) δ -136.00 - -136.20 (m, 2F), -156.03 - -156.31 (m, 2F).

IR (film): ν (cm^{-1}) 3350, 2923, 2856, 1688, 1641, 1495, 1455, 1404, 1299, 1148, 1074, 1026, 981, 948, 913, 858, 762, 736, 702, 675, 619, 579, 494, 454.

HRMS (ESI, m/z) calcd for $\text{C}_{24}\text{H}_{16}\text{BrF}_4\text{N}_3\text{O}_2\text{Na}$ $[\text{M}+\text{Na}]^+$: 540.0305, found: 540.0305.



Ethyl (S)-2,3,5,6-tetrafluoro-4-((2-oxo-1-phenyl-2-(1-(*o*-tolyl)-1*H*-imidazol-2-yl)ethyl)amino)benzoate (3bc**)**

According to the general procedure, the reaction of 2-phenyl-1-(1-(*o*-tolyl)-1*H*-imidazol-2-yl)ethan-1-one **1b** (27.6 mg, 0.10 mmol), ethyl 4-azido-2,3,5,6-tetrafluorobenzoate **2c** (78.9 mg, 3.0 equiv), Δ -**RhS** (3.5 mg, 4 mol%), $[\text{Ru}(\text{bpy})_3](\text{PF}_6)_2$ (2.2 mg, 2.5 mol%), Na_2HPO_4 (2.8 mg, 20 mol%) and H_2O (36.0 mg, 20 equiv) in acetone/DMSO (9:1, 0.5 mL, 0.2 M) under nitrogen atmosphere with visible light for 6 hours, afforded 41.3 mg (81%) of **3bc** as a white solid. Enantiomeric excess was established by HPLC analysis using a Chiralpak AD-H column, ee = 99.6% (HPLC: AD-H, 254 nm, *n*-hexane/isopropanol = 90:10, flow rate 1 mL/min, 25 °C, t_r (major) = 8.7 min, t_r (minor) = 5.3 min). $[\alpha]_{\text{D}}^{22} = +101.0^\circ$ (c 1.0, CH_2Cl_2).

^1H NMR (300 MHz, CDCl_3) δ 7.51-7.44 (m, 2H), 7.43-7.18 (m, 8H), 7.12-7.09 (m, 1H), 6.92-6.82 (m, 1H), 6.77 (d, $J = 7.8$ Hz, 1H, other rotamer), 5.94-5.81 (m, 1H), 4.34 (q, $J = 7.1$ Hz, 2H), 2.04 (s, 3H, other rotamer), 1.40 (s, 3H), 1.34 (t, $J = 7.4$ Hz, 3H).

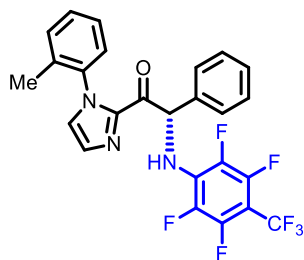
^{13}C NMR (125 MHz, CDCl_3) δ 185.4, 185.2, 160.6-160.4 (m), 147.0-147.3 (m), 145.3-145.0 (m), 141.1, 140.9, 138.1-137.7 (m), 137.04, 136.98, 136.7, 136.1-135.8 (m), 134.7, 134.2, 130.9, 130.81, 130.80, 130.77, 129.5, 129.4, 129.12, 129.09, 129.06, 129.03, 129.00, 128.9, 128.8, 128.5, 128.4, 128.1, 128.0, 127.31, 127.28, 126.7, 126.6, 126.4, 126.0, 62.6 (t, $J = 3.8$ Hz), 62.3 (t, $J = 3.8$ Hz), 61.6,

17.2, 16.0, 14.1. (Mixture of two rotation isomers).

^{19}F NMR (282 MHz, CDCl_3) δ -140.71 - -140.86 (m, 2F), -158.78 - -156.97 (m, 2F).

IR (film): ν (cm^{-1}) 3349, 2973, 2932, 1718, 1687, 1651, 1533, 1495, 1452, 1399, 1371, 1310, 1233, 1154, 1022, 986, 957, 913, 842, 789, 759, 699, 624, 561.

HRMS (ESI, m/z) calcd for $\text{C}_{27}\text{H}_{21}\text{F}_4\text{N}_3\text{O}_3\text{Na}$ $[\text{M}+\text{Na}]^+$: 534.1411, found: 534.1416.



(S)-2-Phenyl-2-((2,3,5,6-tetrafluoro-4-(trifluoromethyl)phenyl)amino)-1-(1-(*o*-tolyl)-1*H*-imidazol-2-yl)ethan-1-one (3bd)

According to the general procedure, the reaction of 2-phenyl-1-(1-(*o*-tolyl)-1*H*-imidazol-2-yl)ethan-1-one **1b** (27.6 mg, 0.10 mmol), 1-azido-2,3,5,6-tetrafluoro-4-(trifluoromethyl)benzene **2d** (77.7 mg, 3.0 equiv), Δ -**RhS** (3.5 mg, 4 mol%), $[\text{Ru}(\text{bpy})_3](\text{PF}_6)_2$ (2.2 mg, 2.5 mol%), Na_2HPO_4 (2.8 mg, 20 mol%) and H_2O (36.0 mg, 20 equiv) in acetone/DMSO (9:1, 0.5 mL, 0.2 M) under nitrogen atmosphere with visible light for 6 hours, afforded 35.6 mg (70%) of **3bd** as a yellow oil. Enantiomeric excess was established by HPLC analysis using a Chiralpak AD-H column, ee = 99% (HPLC: OD-H, 254 nm, *n*-hexane/isopropanol = 90:10, flow rate 1 mL/min, 25 °C, t_r (major) = 5.1 min, t_r (minor) = 4.1 min). $[\alpha]_{\text{D}}^{22} = +127.8^\circ$ (c 1.0, CH_2Cl_2).

^1H NMR (500 MHz, CDCl_3) δ 7.51-7.44 (m, 2H), 7.43-7.19 (m, 8H), 7.12-7.09 (m, 1H), 6.91-6.87 (m, 1H), 6.87-6.82 (m, 1H, other rotamer), 6.77 (d, J = 8.0 Hz, 1H, other rotamer), 5.97-5.91 (m, 1H), 5.89-5.83 (m, 1H, other rotamer), 2.04 (s, 3H, other rotamer), 1.39 (s, 3H).

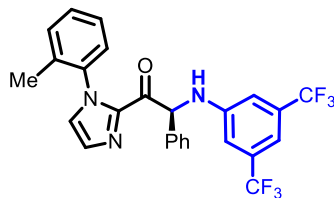
^{13}C NMR (125 MHz, CDCl_3) δ 185.2, 185.1, 141.1, 140.8, 137.02, 136.96, 136.6, 134.7, 134.2, 130.93, 130.85, 130.8, 129.53, 129.47, 129.0, 128.9, 128.6, 128.5, 128.1, 128.0, 127.38, 127.36, 126.8, 126.7, 126.4, 126.0, 63.0 (t, J = 3.6 Hz), 62.7 (t, J = 3.9 Hz), 17.2, 16.1. (Mixture of two rotation isomers).

^{19}F NMR (282 MHz, CDCl_3) δ -55.1 (t, J = 20.87, 3F), -143.25 - -143.50 (m, 2F), -158.28 - -158.50 (m, 2F).

IR (film): ν (cm^{-1}) 3373, 1688, 1655, 1539, 1505, 1457, 1400, 1330, 1304, 1235, 1179, 1130, 1078,

1025, 983, 957, 911, 884, 835, 764, 734, 703, 672, 626, 560, 494.

HRMS (ESI, m/z) calcd for $C_{23}H_{16}F_7N_3ONa$ $[M+Na]^+$: 530.1074, found: 530.1075.



(S)-2-((3,5-Bis(trifluoromethyl)phenyl)amino)-2-phenyl-1-(1-(*o*-tolyl)-1*H*-imidazol-2-yl)ethan-1-one (3be)

According to the general procedure, the reaction of 2-phenyl-1-(1-(*o*-tolyl)-1*H*-imidazol-2-yl)ethan-1-one **1b** (27.6 mg, 0.10 mmol), 1-azido-3,5-bis(trifluoromethyl)benzene **2e** (76.6 mg, 3.0 equiv), Δ -**RhS** (3.5 mg, 4 mol%), $[Ru(bpy)_3](PF_6)_2$ (2.2 mg, 2.5 mol%), Na_2HPO_4 (2.8 mg, 20 mol%) and H_2O (36.0 mg, 20 equiv) in acetone/DMSO (9:1, 0.5 mL, 0.2 M) under nitrogen atmosphere with visible light for 7 hours, afforded 29.8 mg (59%) of **3be** as a colorless oil. Enantiomeric excess was established by HPLC analysis using a Chiralpak OD-H column, ee = 98% (HPLC: OD-H, 254 nm, *n*-hexane/isopropanol = 95:5, flow rate 1 mL/min, 25 °C, t_r (major) = 8.5 min, t_r (minor) = 7.0 min). $[\alpha]_D^{22} = +97.0^\circ$ (c 1.0, CH_2Cl_2).

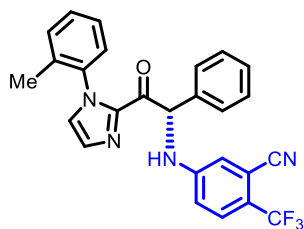
1H NMR (300 MHz, $CDCl_3$) δ 7.60-7.53 (m, 2H), 7.43-7.16 (m, 8H), 7.13-7.09 (m, 2H), 6.98-6.94 (m, 2H), 6.78 (d, J = 7.8 Hz, 1H, other rotamer), 6.56-6.49 (m, 1H), 5.79 (d, J = 7.2 Hz, 1H), 5.73 (d, J = 7.2 Hz, 1H, other rotamer), 2.00 (s, 3H, other rotamer), 1.40 (s, 3H).

^{13}C NMR (125 MHz, $CDCl_3$) δ 186.0, 185.9, 146.5, 146.4, 141.4, 141.3, 137.1, 137.0, 136.1, 134.6, 134.2, 132.3 (q, J = 97.5 Hz) 130.80, 130.78, 130.72, 130.7, 129.43, 129.37, 129.0, 128.9, 128.39, 128.38, 128.2, 128.1, 127.4, 126.0, 123.4 (q, J = 271.1 Hz), 112.61, 112.58, 110.6-110.4 (m), 61.9, 61.7, 17.2, 16.0 (Mixture of two rotation isomers).

^{19}F NMR (282 MHz, $CDCl_3$) δ -63.40 (6F), -63.40 (other rotamer).

IR (film): ν (cm^{-1}) 3381, 3066, 2927, 1674, 1624, 1501, 1450, 1394, 1274, 1172, 1126, 1028, 996, 969, 927, 867, 762, 726, 690, 644, 606, 529, 405.

HRMS (EI, m/z) calcd for $C_{26}H_{19}F_6N_3O$ $[M]^+$: 503.1432, found: 503.1447.



(S)-5-((2-Oxo-1-phenyl-2-(1-(*o*-tolyl)-1*H*-imidazol-2-yl)ethyl)amino)-2-(trifluoromethyl)benzonitrile (3bf**)**

According to the general procedure, the reaction of 2-phenyl-1-(1-(*o*-tolyl)-1*H*-imidazol-2-yl)ethan-1-one **1b** (27.6 mg, 0.10 mmol), 5-azido-2-(trifluoromethyl)benzonitrile **2f** (63.6 mg, 3.0 equiv), Δ -**RhS** (3.5 mg, 4 mol%), [Ru(bpy)₃](PF₆)₂ (2.2 mg, 2.5 mol%), Na₂HPO₄ (2.8 mg, 20 mol%) and H₂O (36.0 mg, 20 equiv) in acetone/DMSO (9:1, 0.5 mL, 0.2 M) under nitrogen atmosphere with visible light for 6 hours, afforded 33.9 mg (74%) of **3bf** as a yellow solid. Enantiomeric excess was established by HPLC analysis using a Chiralpak AD-H column, ee = 96% (HPLC: AD-H, 254 nm, *n*-hexane/isopropanol = 80:20, flow rate 1 mL/min, 25 °C, *t_r* (major) = 8.9 min, *t_r* (minor) = 16.0 min). $[\alpha]_D^{22} = +114.4^\circ$ (*c* 1.0, CH₂Cl₂).

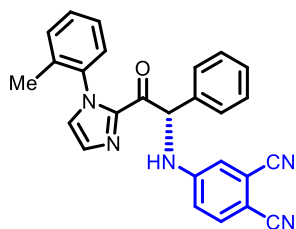
¹H NMR (500 MHz, CDCl₃) δ 7.57-7.50 (m, 2H), 7.48-7.45 (m, 1H), 7.43-7.17 (m, 8H), 7.15-7.13 (m, 1H), 6.89 (dd, *J*₁ = 7.5 Hz, *J*₂ = 2.0 Hz, 1H), 6.75 (d, *J* = 8.0 Hz, 1H, other rotamer), 6.70-6.65 (m, 1H), 6.53 (d, *J* = 6.5 Hz, 1H), 6.49 (d, *J* = 6.5 Hz, 1H, other rotamer), 6.14-6.10 (m, 1H), 2.00 (s, 3H, other rotamer), 1.37 (s, 3H).

¹³C NMR (125 MHz, CDCl₃) δ 185.2, 185.1, 148.8, 148.7, 141.1, 141.0, 136.9, 136.8, 136.1, 135.60, 135.57, 134.6, 134.24, 134.15, 134.0, 130.9, 130.83, 130.79, 129.5, 129.4, 129.1, 129.0, 128.6, 128.2, 128.0, 127.6, 126.72, 126.67, 126.3, 126.0, 123.5, 121.3, 116.9, 114.6, 111.2, 96.2, 61.6, 61.3, 17.2, 16.0. (Mixture of two rotation isomers).

¹⁹F NMR (282 MHz, CDCl₃) δ -63.097 (3F), -63.102 (3F, other rotamer).

IR (film): ν (cm⁻¹) 3336, 2922, 2223, 1697, 1608, 1522, 1497, 1447, 1402, 1352, 1274, 1172, 1131, 1025, 842, 768, 738, 701, 673, 557, 454.

HRMS (ESI, *m/z*) calcd for C₂₆H₁₉F₃N₄ONa [M+Na]⁺: 483.1403, found: 483.1405.



(S)-4-((2-Oxo-1-phenyl-2-(1-(*o*-tolyl)-1*H*-imidazol-2-yl)ethyl)amino)phthalonitrile (3bg)

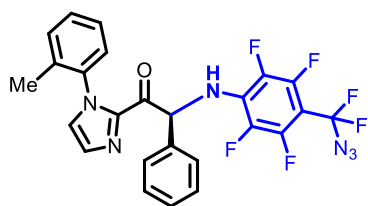
According to the general procedure, the reaction of 2-phenyl-1-(1-(*o*-tolyl)-1*H*-imidazol-2-yl)ethan-1-one **1b** (27.6 mg, 0.10 mmol), 4-azidophthalonitrile **2g** (50.7 mg, 3.0 equiv), Δ -**RhS** (3.5 mg, 4 mol%), [Ru(bpy)₃](PF₆)₂ (2.2 mg, 2.5 mol%), Na₂HPO₄ (2.8 mg, 20 mol%) and H₂O (36.0 mg, 20 equiv) in acetone/DMSO (9:1, 0.5 mL, 0.2 M) under nitrogen atmosphere with visible light for 6 hours, afforded 37.0 mg (89%) of **3bg** as a yellow solid. Enantiomeric excess was established by HPLC analysis using a Chiralpak AD-H column, ee = 99% (HPLC: AD-H, 254 nm, *n*-hexane/isopropanol = 60:40, flow rate 1 mL/min, 25 °C, *t_r* (major) = 8.2 min, *t_r* (minor) = 17.3 min). $[\alpha]_D^{22} = +111.4^\circ$ (*c* 1.0, CH₂Cl₂).

¹H NMR (500 MHz, CDCl₃) δ 7.56-7.50 (m, 2H), 7.44-7.37 (m, 2H), 7.37-7.23 (m, 5H), 7.22-7.16 (m, 2H), 7.15-7.13 (m, 1H), 6.86-6.83 (m, 1H), 6.78-6.72 (m, 1H), 6.78-6.72 (m, 1H, other rotamer), 6.50 (d, *J* = 6.5 Hz, 1H), 6.46 (d, *J* = 6.5 Hz, 1H, other rotamer), 6.21-6.15 (m, 1H), 2.01 (s, 3H, other rotamer), 1.36 (s, 3H).

¹³C NMR (125 MHz, CDCl₃) δ 184.9, 184.8, 148.9, 148.8, 141.0, 140.9, 136.9, 136.8, 135.3, 135.2, 134.6, 134.5, 134.1, 130.94, 130.86, 130.82, 130.79, 129.5, 129.4, 129.14, 129.10, 128.7, 128.1, 128.0, 127.7, 126.70, 126.66, 126.3, 126.0, 117.0, 116.6, 116.4, 115.8, 102.2, 61.5, 61.3, 17.2, 15.9. (Mixture of two rotation isomers)

IR (film): ν (cm⁻¹) 3366, 3063, 2923, 2220, 1685, 1596, 1514, 1454, 1398, 1346, 1304, 1257, 1023, 968, 910, 832, 764, 731, 703, 673, 521, 492, 453,

HRMS (ESI, *m/z*) calcd for C₂₆H₁₉N₅ONa [M+Na]⁺: 440.1482, found: 440.1482.



(S)-2-((4-(Azidodifluoromethyl)-2,3,5,6-tetrafluorophenyl)amino)-2-phenyl-1-(1-(*o*-tolyl)-1*H*-imi

dazol-2-yl)ethan-1-one (3bh)

According to the general procedure, the reaction of 2-phenyl-1-(1-(*o*-tolyl)-1*H*-imidazol-2-yl)ethan-1-one **1b** (27.6 mg, 0.10 mmol), 1-azido-4-(azidodifluoromethyl)-2,3,5,6-tetrafluorobenzene **2h** (84.6 mg, 3.0 equiv), Δ -**RhS** (3.5 mg, 4 mol%), [Ru(bpy)₃](PF₆)₂ (2.2 mg, 2.5 mol%), Na₂HPO₄ (2.8 mg, 20 mol%) and H₂O (36.0 mg, 20 equiv) in acetone/DMSO (9:1, 0.5 mL, 0.2 M) under nitrogen atmosphere with visible light for 11 hours, afforded 25.5 mg (48%) of **3bh** as a colorless oil. Enantiomeric excess was established by HPLC analysis using a Chiralpak OD-H column, ee = 98% (HPLC: OD-H, 254 nm, *n*-hexane/isopropanol = 95:5, flow rate 1 mL/min, 25 °C, *t_r* (major) = 8.8 min, *t_r* (minor) = 7.6 min). [α]_D²² = +128.2° (*c* 1.0, CH₂Cl₂).

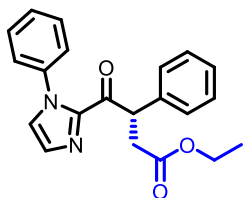
¹H NMR (500 MHz, CDCl₃) δ 7.50-7.43 (m, 2H), 7.42-7.18 (m, 8H), 7.11-7.09 (m, 1H), 6.90-6.85 (m, 1H), 6.85-6.81 (m, 1H, other rotamer), 6.76 (d, *J* = 8.0 Hz, 1H, other rotamer), 5.90-5.85 (m, 1H), 5.83-5.78 (m, 1H, other rotamer), 2.03 (s, 3H, other rotamer), 1.39 (s, 3H).

¹³C NMR (125 MHz, CDCl₃) δ 185.3, 185.2, 141.1, 140.9, 137.05, 136.98, 136.7, 134.7, 134.2, 130.9, 130.84, 130.81, 129.52, 129.46, 128.94, 128.85, 128.1, 128.0, 127.4, 127.3, 126.75, 126.65, 126.4, 126.0, 62.6 (t, *J* = 3.4 Hz), 62.2 (t, *J* = 3.7 Hz), 17.2, 16.0 (Mixture of two rotation isomers).

¹⁹F NMR (282 MHz, CDCl₃) δ -62.93 (t, *J* = 24.82, 2F), -142.24 - -142.54 (m, 2F), -157.67 - -157.90 (m, 2F).

IR (film): ν (cm⁻¹) 3373, 2962, 2927, 2145, 1689, 1655, 1536, 1500, 1456, 1428, 1400, 1320, 1275, 1229, 1148, 1028, 979, 953, 912, 865, 786, 763, 730, 697, 670, 626, 562, 488, 454, 393.

HRMS (ESI, *m/z*) calcd for C₂₅H₁₆F₆N₆ONa [M+Na]⁺: 553.1182, found: 553.1182.

**Ethyl (S)-4-oxo-3-phenyl-4-(1-phenyl-1*H*-imidazol-2-yl)butanoate (5aa)**

According to the general procedure, the reaction of 2-phenyl-1-(1-phenyl-1*H*-imidazol-2-yl)ethan-1-one **1a** (26.2 mg, 0.10 mmol), ethyl 2-diazoacetate **4a** (34.2 mg, 3.0 equiv), Δ -**RhS** (3.5 mg, 4 mol%), [Ru(bpy)₃](PF₆)₂ (1.3 mg, 1.5 mol%), Na₂HPO₄ (2.8 mg, 20 mol%) and H₂O (36.0 mg, 20 equiv) in acetone/DMSO (9:1, 0.5 mL, 0.2 M) under nitrogen atmosphere with visible light for 15

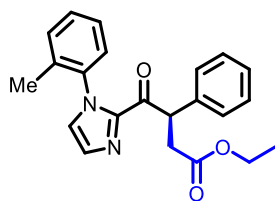
hours, afforded 32.7 mg (94%) of **5aa** as a yellow solid. Enantiomeric excess was established by HPLC analysis using a Chiralpak OD-H column, ee = 92% (HPLC: OD-H, 254 nm, *n*-hexane/isopropanol = 90:10, flow rate 1 mL/min, 25 °C, *t_r* (major) = 15.0 min, *t_r* (minor) = 11.1 min). $[\alpha]_{\text{D}}^{22} = +213.6^{\circ}$ (*c* 1.0, CH₂Cl₂).

¹H NMR (500 MHz, CDCl₃) δ 7.44-7.39 (m, 5H), 7.32-7.27 (m, 2H), 7.27 (d, *J* = 1.5 Hz, 1H), 7.25-7.21 (m, 1H), 7.19-7.15 (m, 2H), 7.11 (d, *J* = 1.0 Hz, 1H), 5.60 (dd, *J₁* = 10.5 Hz, *J₂* = 5.0 Hz, 1H), 4.07 (qd, *J₁* = 7.0 Hz, *J₂* = 1.0 Hz, 2H), 3.30 (dd, *J₁* = 17.0 Hz, *J₂* = 10.5 Hz, 1H), 2.70 (dd, *J₁* = 17.0 Hz, *J₂* = 5.0 Hz, 1H), 1.16 (t, *J* = 7.3 Hz, 3H).

¹³C NMR (125 MHz, CDCl₃) δ 189.4, 171.8, 142.4, 138.3, 137.6, 129.9, 128.9, 128.7, 128.6, 127.3, 127.0, 125.6, 60.6, 48.8, 37.4, 14.1. (Missing one ¹³C signal)

IR (film): ν (cm⁻¹) 2980, 2930, 1722, 1678, 1495, 1449, 1401, 1373, 1329, 1302, 1245, 1187, 1152, 1097, 1029, 939, 906, 756, 694, 585, 530.

HRMS (ESI, *m/z*) calcd for C₂₁H₂₁N₂O₃ [M+H]⁺: 349.1547, found: 349.1548.



Ethyl (*R*)-4-oxo-3-phenyl-4-(1-(*o*-tolyl)-1*H*-imidazol-2-yl)butanoate (**5ba**)

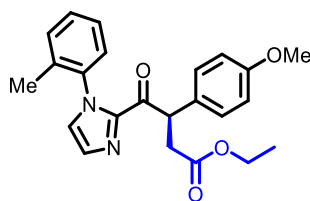
According to the general procedure, the reaction of 2-phenyl-1-(1-(*o*-tolyl)-1*H*-imidazol-2-yl)ethan-1-one **1b** (27.6 mg, 0.10 mmol), ethyl 2-diazoacetate **4a** (34.2 mg, 3.0 equiv), Λ -**RhS** (3.5 mg, 4 mol%), [Ru(bpy)₃](PF₆)₂ (1.3 mg, 1.5 mol%), Na₂HPO₄ (2.8 mg, 20 mol%) and H₂O (36.0 mg, 20 equiv) in acetone/DMSO (9:1, 0.5 mL, 0.2 M) under nitrogen atmosphere with visible light for 15 hours, afforded 35.9 mg (99%) of **5ba** as a yellow oil. Enantiomeric excess was established by HPLC analysis using a Chiralpak OD-H column, ee = 97% (HPLC: OD-H, 254 nm, *n*-hexane/isopropanol = 90:10, flow rate 1 mL/min, 25 °C, *t_r* (major) = 9.8 min, *t_r* (minor) = 11.7 min). $[\alpha]_{\text{D}}^{22} = -238.4^{\circ}$ (*c* 1.0, CH₂Cl₂).

¹H NMR (500 MHz, CDCl₃) δ 7.43-7.18 (m, 10H), 7.03 (d, *J* = 1.0 Hz, 1H), 6.90 (d, *J* = 8.0 Hz, 1H, other rotamer), 5.65-5.58 (m, 1H), 4.10-4.03 (m, 2H), 3.34-3.25 (m, 1H), 2.74-2.64 (m, 1H), 2.04 (s, 3H), 1.55 (s, 3H, other rotamer), 1.20-1.14 (m, 3H).

^{13}C NMR (125 MHz, CDCl_3) δ 189.35, 189.25, 171.6, 142.9, 142.8, 137.84, 137.80, 137.7, 137.6, 134.9, 134.3, 130.6, 130.5, 130.2, 130.1, 129.0, 128.9, 128.7, 128.61, 128.56, 128.5, 127.23, 127.19, 126.5, 126.41, 126.38, 126.1, 60.5, 48.61, 48.58, 37.4, 37.0, 17.1, 16.4, 14.05, 14.02. (Mixture of two rotation isomers)

IR (film): ν (cm^{-1}) 3111, 3061, 2981, 2931, 1729, 1682, 1594, 1495, 1453, 1403, 1375, 1305, 1243, 1178, 1093, 1026, 941, 909, 848, 762, 699, 670, 587, 529, 455.

HRMS (ESI, m/z) calcd for $\text{C}_{22}\text{H}_{22}\text{N}_2\text{O}_3\text{Na}$ $[\text{M}+\text{Na}]^+$: 385.1523, found: 385.1525



Ethyl (*R*)-3-(4-methoxyphenyl)-4-oxo-4-(1-(*o*-tolyl)-1*H*-imidazol-2-yl)butanoate (5la**)**

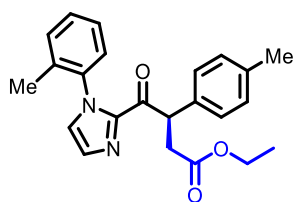
According to the general procedure, the reaction of 2-(4-methoxyphenyl)-1-(1-(*o*-tolyl)-1*H*-imidazol-2-yl)ethan-1-one **11** (30.6 mg, 0.10 mmol), ethyl 2-diazoacetate **4a** (34.2 mg, 3.0 equiv), Λ -**RhS** (3.5 mg, 4 mol%), $[\text{Ru}(\text{bpy})_3](\text{PF}_6)_2$ (1.3 mg, 1.5 mol%), Na_2HPO_4 (2.8 mg, 20 mol%) and H_2O (36.0 mg, 20 equiv) in acetone/DMSO (9:1, 0.5 mL, 0.2 M) under nitrogen atmosphere with visible light for 15 hours, afforded 38.1 mg (97%) of **5la** as a yellow solid. Enantiomeric excess was established by HPLC analysis using a Chiralpak IC column, ee = 95% (HPLC: IC, 254 nm, *n*-hexane/isopropanol = 80:20, flow rate 1 mL/min, 25 °C, t_r (major) = 13.1 min, t_r (minor) = 14.8 min). $[\alpha]_{\text{D}}^{22} = -239.4^\circ$ (c 1.0, CH_2Cl_2).

^1H NMR (500 MHz, CDCl_3) δ 7.38-7.26 (m, 5H), 7.25-7.18 (m, 2H), 7.03-7.01 (m, 1H), 6.89 (d, J = 8.0 Hz, 1H, other rotamer), 6.84-6.78 (m, 2H), 5.58-5.51 (m, 1H), 4.09-4.02 (m, 2H), 3.76 (s, 3H), 3.29-3.20 (m, 1H), 2.71-2.61 (m, 1H), 2.03 (s, 3H), 1.57 (s, 3H, other rotamer), 1.20-1.13 (m, 3H).

^{13}C NMR (125 MHz, CDCl_3) δ 189.5, 189.4, 171.7, 158.8, 143.0, 142.9, 137.9, 134.9, 134.3, 130.6, 130.08, 130.06, 129.7, 129.6, 129.0, 128.9, 126.5, 126.44, 126.39, 126.33, 126.31, 126.1, 114.1, 114.0, 60.5, 55.2, 47.83, 47.76, 37.4, 37.1, 17.2, 16.5, 14.1, 14.0. (Mixture of two rotation isomers)

IR (film): ν (cm^{-1}) 2971, 2933, 1728, 1674, 1606, 1507, 1452, 1340, 1302, 1243, 1178, 1106, 1091, 1024, 940, 906, 848, 766, 719, 536.

HRMS (ESI, m/z) calcd for $\text{C}_{23}\text{H}_{24}\text{N}_2\text{O}_4\text{Na}$ $[\text{M}+\text{Na}]^+$: 415.1628, found: 415.1629.



Ethyl (*R*)-4-oxo-3-(*p*-tolyl)-4-(1-(*o*-tolyl)-1*H*-imidazol-2-yl)butanoate (5ja**)**

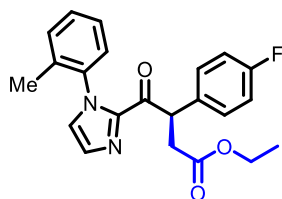
According to the general procedure, the reaction of 2-(*p*-tolyl)-1-(1-(*o*-tolyl)-1*H*-imidazol-2-yl)ethan-1-one **1j** (29.0 mg, 0.10 mmol), ethyl 2-diazoacetate **4a** (34.2 mg, 3.0 equiv), Λ -**RhS** (3.5 mg, 4 mol%), [Ru(bpy)₃](PF₆)₂ (2.2 mg, 2.5 mol%), Na₂HPO₄ (2.8 mg, 20 mol%) and H₂O (36.0 mg, 20 equiv) in acetone/DMSO (9:1, 2.0 mL, 0.05 M) under nitrogen atmosphere with visible light for 24 hours, afforded 35.5 mg (94%) of **5ja** as a yellow solid. Enantiomeric excess was established by HPLC analysis using a Chiralpak OD-H column, ee = 96% (HPLC: OD-H, 254 nm, *n*-hexane/isopropanol = 95:5, flow rate 1 mL/min, 25 °C, *t_r* (major) = 10.5 min, *t_r* (minor) = 13.2 min). $[\alpha]_D^{22} = -272.8^\circ$ (*c* 1.0, CH₂Cl₂).

¹H NMR (500 MHz, CDCl₃) δ 7.39-7.21 (m, 7H), 7.12-7.06 (m, 2H), 7.03-7.01 (m, 1H), 6.91 (d, *J* = 8.0 Hz, 1H, other rotamer), 5.60-5.53 (m, 1H), 4.10-4.02 (m, 2H), 3.31-3.24 (m, 1H), 2.71-2.62 (m, 1H), 2.30 (s, 3H), 2.29 (s, 3H, other rotamer), 2.04 (s, 3H), 1.59 (s, 3H, other rotamer), 1.21-1.14 (m, 3H).

¹³C NMR (125 MHz, CDCl₃) δ 189.5, 189.4, 171.7, 142.3, 142.8, 137.9, 137.8, 136.8, 134.9, 134.6, 134.5, 134.3, 130.6, 130.5, 130.11, 130.09, 129.4, 129.3, 128.95, 128.89, 128.4, 126.5, 126.41, 126.35, 126.30, 126.29, 126.1, 60.4, 48.21, 48.20, 37.4, 37.1, 21.0, 17.2, 16.6, 14.05, 14.01. (Mixture of two rotation isomers)

IR (film): ν (cm⁻¹) 3172, 2981, 2924, 1731, 1680, 1500, 1445, 1405, 1373, 1321, 1179, 1032, 942, 907, 767, 717, 534.

HRMS (ESI, *m/z*) calcd for C₂₃H₂₄N₂O₃Na [M+Na]⁺: 399.1679, found: 399.1677.



Ethyl (*R*)-3-(4-fluorophenyl)-4-oxo-4-(1-(*o*-tolyl)-1*H*-imidazol-2-yl)butanoate (5ma**)**

According to the general procedure, the reaction of 2-(4-fluorophenyl)-1-(1-(*o*-tolyl)-1*H*-imidazol-2-yl)ethan-1-one **1m** (29.4 mg, 0.10 mmol), ethyl 2-diazoacetate **4a** (34.2 mg, 3.0 equiv), Λ -**RhS** (3.5 mg, 4 mol%), [Ru(bpy)₃](PF₆)₂ (1.3 mg, 1.5 mol%), Na₂HPO₄ (2.8 mg, 20 mol%) and H₂O (36.0 mg, 20 equiv) in acetone/DMSO (9:1, 1.0 mL, 0.1 M) under nitrogen atmosphere with visible light for 16 hours, afforded 36.5 mg (96%) of **5ma** as a yellow solid. Enantiomeric excess was established by HPLC analysis using a Chiralpak OD-H column, ee = 98% (HPLC: OD-H, 254 nm, *n*-hexane/isopropanol = 90:10, flow rate 1 mL/min, 25 °C, *t*_r (major) = 7.6 min, *t*_r (minor) = 8.7 min). $[\alpha]_D^{22} = -205.8^\circ$ (*c* 1.0, CH₂Cl₂).

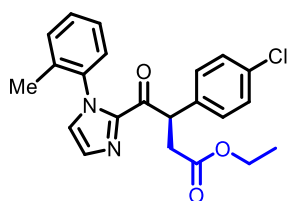
¹H NMR (500 MHz, CDCl₃) δ 7.40-7.26 (m, 5H), 7.25-7.17 (m, 2H), 7.04-7.02 (m, 1H), 6.99-6.92 (m, 2H), 6.90 (dd, *J*₁ = 8.0 Hz, *J*₂ = 1.0 Hz, 1H, other rotamer), 5.62-5.54 (m, 1H), 4.08-4.01 (m, 2H), 3.28-3.20 (m, 1H), 2.71-2.60 (m, 1H), 2.02 (s, 3H), 1.56 (s, 3H, other rotamer), 1.19-1.12 (m, 3H).

¹³C NMR (125 MHz, CDCl₃) δ 189.2, 189.1, 171.51, 171.49, 163.0, 161.0, 142.7, 142.6, 137.79, 137.75, 134.9, 134.2, 133.41, 133.39, 133.35, 133.32, 130.7, 130.6, 130.23, 130.21, 130.16, 130.1, 129.1, 129.0, 126.6, 126.5, 126.4, 126.0, 115.64, 115.59, 115.5, 115.4, 60.6, 47.8, 47.7, 37.4, 37.0, 17.1, 16.5, 14.1, 14.0. (Mixture of two rotation isomers)

¹⁹F NMR (282 MHz, CDCl₃) δ -115.32 (1F), -115.39 (1F, other rotamer).

IR (film): ν (cm⁻¹) 3119, 2985, 2926, 1723, 1683, 1502, 1454, 1403, 1376, 1313, 1225, 1185, 1159, 1096, 1022, 941, 908, 842, 803, 766, 716, 544, 492, 454.

HRMS (ESI, *m/z*) calcd for C₂₂H₂₁FN₂O₃Na [M+Na]⁺: 403.1428, found: 403.1425.



Ethyl (*R*)-3-(4-chlorophenyl)-4-oxo-4-(1-(*o*-tolyl)-1*H*-imidazol-2-yl)butanoate (**5na**)

According to the general procedure, the reaction of 2-(4-chlorophenyl)-1-(1-(*o*-tolyl)-1*H*-imidazol-2-yl)ethan-1-one **1n** (31.1 mg, 0.10 mmol), ethyl 2-diazoacetate **4a** (34.2 mg, 3.0 equiv), Λ -**RhS** (3.5 mg, 4 mol%), [Ru(bpy)₃](PF₆)₂ (2.2 mg, 2.5 mol%), Na₂HPO₄ (2.8 mg, 20 mol%) and H₂O (36.0 mg, 20 equiv) in acetone/DMSO (9:1, 2.0 mL, 0.05 M) under nitrogen atmosphere with visible light for 22 hours, afforded 39.0 mg (98%) of **5na** as a white solid. Enantiomeric excess was established by HPLC

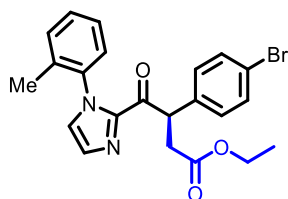
analysis using a Chiralpak IC column, ee = 95% (HPLC: IC, 254 nm, *n*-hexane/isopropanol = 85:15, flow rate 1 mL/min, 25 °C, t_r (major) = 7.3 min, t_r (minor) = 8.7 min). $[\alpha]_D^{22} = -208.4^\circ$ (*c* 1.0, CH₂Cl₂).

¹H NMR (500 MHz, CDCl₃) δ 7.39-7.26 (m, 5H), 7.26-7.17 (m, 4H), 7.04-7.03 (m, 1H), 6.91 (dd, $J_1 = 8.0$ Hz, $J_2 = 1.0$ Hz, 1H, other rotamer), 5.61-5.54 (m, 1H), 4.08-4.01 (m, 2H), 3.16-3.06 (m, 1H), 2.72-2.62 (m, 1H), 2.04 (s, 3H), 1.81 (s, 3H, other rotamer), 1.20-1.14 (m, 3H).

¹³C NMR (125 MHz, CDCl₃) δ 189.0, 188.9, 171.3, 171.2, 142.80, 142.77, 137.83, 137.81, 136.1, 135.9, 135.0, 134.2, 134.1, 134.0, 130.7, 130.6, 130.45, 130.41, 130.2, 129.1, 129.0, 128.6, 128.5, 128.43, 128.40, 126.9, 126.8, 126.7, 126.55, 126.50, 126.43, 126.37, 126.1, 60.6, 45.7, 45.6, 36.7, 36.5, 17.2, 16.9, 14.03, 14.00. (Mixture of two rotation isomers)

IR (film): ν (cm⁻¹) 2974, 2925, 1731, 1682, 1493, 1458, 1401, 1374, 1254, 1185, 1148, 1087, 1035, 943, 906, 769, 717, 531.

HRMS (ESI, *m/z*) calcd for C₂₂H₂₁ClN₂O₃Na [M+Na]⁺: 419.1133, found: 419.1131.



Ethyl (*R*)-3-(4-bromophenyl)-4-oxo-4-(1-(*o*-tolyl)-1*H*-imidazol-2-yl)butanoate (**5oa**)

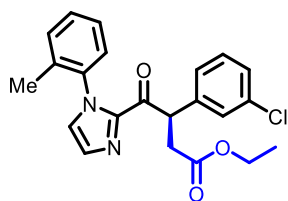
According to the general procedure, the reaction of 2-(4-bromophenyl)-1-(1-(*o*-tolyl)-1*H*-imidazol-2-yl)ethan-1-one **1o** (35.5 mg, 0.10 mmol), ethyl 2-diazoacetate **4a** (34.2 mg, 3.0 equiv), Λ -**RhS** (3.5 mg, 4 mol%), [Ru(bpy)₃](PF₆)₂ (2.2 mg, 2.5 mol%), Na₂HPO₄ (2.8 mg, 20 mol%) and H₂O (36.0 mg, 20 equiv) in acetone/DMSO (9:1, 2.0 mL, 0.05 M) under nitrogen atmosphere with visible light for 38 hours, afforded 41.0 mg (93%) of **5oa** as a white solid. Enantiomeric excess was established by HPLC analysis using a Chiralpak IC column, ee = 95% (HPLC: IC, 254 nm, *n*-hexane/isopropanol = 85:15, flow rate 1 mL/min, 25 °C, t_r (major) = 7.8 min, t_r (minor) = 9.1 min). $[\alpha]_D^{22} = -183.2^\circ$ (*c* 1.0, CH₂Cl₂).

¹H NMR (500 MHz, CDCl₃) δ 7.42-7.17 (m, 9H), 7.05-7.02 (m, 1H), 6.91 (d, $J = 8.0$ Hz, 1H, other rotamer), 5.60-5.53 (m, 1H), 4.08-4.02 (m, 2H), 3.27-3.19 (m, 1H), 2.70-2.61 (m, 1H), 2.01 (s, 3H), 1.59 (s, 3H, other rotamer), 1.19-1.12 (m, 3H).

^{13}C NMR (125 MHz, CDCl_3) δ 188.9, 188.8, 171.43, 171.41, 142.6, 142.5, 137.74, 137.71, 136.20, 136.17, 134.9, 134.2, 133.20, 133.19, 130.7, 130.6, 130.24, 130.21, 130.0, 129.12, 129.06, 128.9, 128.8, 126.7, 126.63, 126.58, 126.5, 126.4, 126.0, 60.6, 47.97, 47.95, 37.2, 36.9, 17.1, 16.6, 14.1, 14.0. (Mixture of two rotation isomers)

IR (film): ν (cm^{-1}) 2980, 2929, 1730, 1683, 1491, 1454, 1403, 1374, 1309, 1240, 1178, 1014, 941, 909, 766, 722, 532.

HRMS (ESI, m/z) calcd for $\text{C}_{22}\text{H}_{21}\text{BrN}_2\text{O}_3\text{Na}$ $[\text{M}+\text{Na}]^+$: 463.0628, found: 463.0624.



Ethyl (*R*)-3-(3-chlorophenyl)-4-oxo-4-(1-(*o*-tolyl)-1*H*-imidazol-2-yl)butanoate (**5ka**)

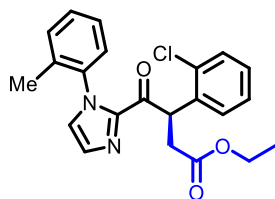
According to the general procedure, the reaction of 2-(3-chlorophenyl)-1-(1-(*o*-tolyl)-1*H*-imidazol-2-yl)ethan-1-one **1k** (31.1 mg, 0.10 mmol), ethyl 2-diazoacetate **4a** (34.2 mg, 3.0 equiv), Λ -**RhS** (3.5 mg, 4 mol%), $[\text{Ru}(\text{bpy})_3](\text{PF}_6)_2$ (1.3 mg, 1.5 mol%), Na_2HPO_4 (2.8 mg, 20 mol%) and H_2O (36.0 mg, 20 equiv) in acetone/DMSO (9:1, 0.5 mL, 0.2 M) under nitrogen atmosphere with visible light for 26 hours, afforded 36.5 mg (92%) of **5ka** as a yellow oil. Enantiomeric excess was established by HPLC analysis using a Chiralpak IC column, ee = 95% (HPLC: IC, 254 nm, *n*-hexane/isopropanol = 80:20, flow rate 1 mL/min, 25 °C, t_r (major) = 7.1 min, t_r (minor) = 12.2 min). $[\alpha]_{\text{D}}^{22} = -223.0^\circ$ (c 1.0, CH_2Cl_2).

^1H NMR (500 MHz, CDCl_3) δ 7.40-7.18 (m, 9H), 7.06-7.04 (m, 1H), 6.31 (dd, $J_1 = 8.0$ Hz, $J_2 = 1.0$ Hz, 1H, other rotamer), 5.61-5.55 (m, 1H), 4.09-4.02 (m, 2H), 3.28-3.21 (m, 1H), 2.71-2.62 (m, 1H), 2.02 (s, 3H), 1.62 (s, 3H, other rotamer), 1.20-1.13 (m, 3H).

^{13}C NMR (125 MHz, CDCl_3) δ 188.70, 188.65, 171.4, 171.3, 142.7, 142.6, 139.72, 139.69, 137.73, 137.69, 134.7, 134.40, 134.38, 134.2, 130.7, 130.34, 130.31, 129.91, 129.88, 129.12, 129.06, 128.64, 128.59, 127.5, 126.88, 126.85, 126.69, 126.67, 126.6, 126.5, 126.4, 126.1, 60.6, 48.22, 48.20, 37.3, 36.9, 17.1, 16.5, 14.1, 14.0. (Mixture of two rotation isomers)

IR (film): ν (cm^{-1}) 2982, 2930, 1730, 1683, 1454, 1402, 1376, 1304, 1241, 1180, 1088, 1025, 942, 908, 766, 724, 690, 454.

HRMS (ESI, m/z) calcd for $C_{22}H_{21}ClN_2O_3Na$ $[M+Na]^+$: 419.1133, found: 419.1131.



Ethyl (*R*)-3-(2-chlorophenyl)-4-oxo-4-(1-(*o*-tolyl)-1*H*-imidazol-2-yl)butanoate (5pa**)**

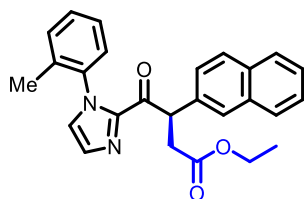
According to the general procedure, the reaction of 2-(2-chlorophenyl)-1-(1-(*o*-tolyl)-1*H*-imidazol-2-yl)ethan-1-one **1p** (31.1 mg, 0.10 mmol), ethyl 2-diazoacetate **4a** (34.2 mg, 3.0 equiv), Λ -**RhS** (3.5 mg, 4 mol%), $[Ru(bpy)_3](PF_6)_2$ (1.3 mg, 1.5 mol%), Na_2HPO_4 (2.8 mg, 20 mol%) and H_2O (36.0 mg, 20 equiv) in acetone/DMSO (9:1, 0.5 mL, 0.2 M) under nitrogen atmosphere with visible light for 15 hours, afforded 32.2 mg (81%) of **5pa** as a yellow oil. Enantiomeric excess was established by HPLC analysis using a Chiralpak IC column, ee = 97% (HPLC: IC, 254 nm, *n*-hexane/isopropanol = 85:15, flow rate 1 mL/min, 25 °C, t_r (major) = 12.9 min, t_r (minor) = 15.6 min). $[\alpha]_D^{22} = -309.8^\circ$ (c 1.0, CH_2Cl_2).

1H NMR (500 MHz, $CDCl_3$) δ 7.43-7.21 (m, 6H), 7.20-7.08 (m, 3H), 7.04-7.02 (m, 1H), 7.01 (d, J = 8.0 Hz, 1H, other rotamer), 6.03-5.95 (m, 1H), 4.50-4.03 (m, 2H), 3.16-3.06 (m, 1H), 2.72-2.62 (m, 1H), 2.04 (s, 3H), 1.81 (s, 3H, other rotamer), 1.20-1.14 (m, 3H).

^{13}C NMR (125 MHz, $CDCl_3$) δ 189.0, 188.9, 171.3, 171.2, 142.80, 142.77, 137.83, 137.81, 136.1, 135.9, 135.0, 134.2, 134.1, 134.0, 130.7, 130.6, 130.45, 130.41, 130.2, 129.1, 129.0, 128.6, 128.5, 128.43, 128.40, 126.9, 126.8, 126.7, 126.55, 126.50, 126.43, 126.37, 126.1, 60.6, 45.7, 45.6, 36.7, 36.5, 17.2, 16.9, 14.03, 14.00. (Mixture of two rotation isomers)

IR (film): ν (cm^{-1}) 2982, 2929, 1731, 1683, 1451, 1403, 1375, 1299, 1242, 1180, 1033, 940, 909, 759, 727, 458.

HRMS (ESI, m/z) calcd for $C_{22}H_{22}ClN_2O_3$ $[M+H]^+$: 397.1313, found: 397.1315.



Ethyl (*R*)-3-(naphthalen-2-yl)-4-oxo-4-(1-(*o*-tolyl)-1*H*-imidazol-2-yl)butanoate (5qa**)**

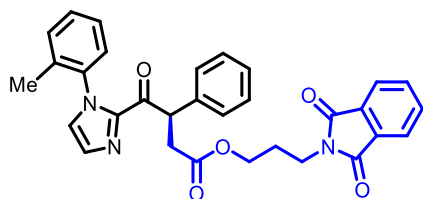
According to the general procedure, the reaction of 2-(naphthalen-2-yl)-1-(1-(*o*-tolyl)-1*H*-imidazol-2-yl)ethan-1-one **1q** (32.6 mg, 0.10 mmol), ethyl 2-diazoacetate **4a** (34.2 mg, 3.0 equiv), Λ -**RhS** (3.5 mg, 4 mol%), [Ru(bpy)₃](PF₆)₂ (1.3 mg, 1.5 mol%), Na₂HPO₄ (2.8 mg, 20 mol%) and H₂O (36.0 mg, 20 equiv) in acetone/DMSO (9:1, 0.5 mL, 0.2 M) under nitrogen atmosphere with visible light for 15 hours, afforded 35.4 mg (86%) of **5qa** as a colorless oil. Enantiomeric excess was established by HPLC analysis using a Chiralpak IC column, ee = 95% (HPLC: IC, 254 nm, *n*-hexane/isopropanol = 85:15, flow rate 1 mL/min, 25 °C, *t_r* (major) = 15.3 min, *t_r* (minor) = 17.7 min). [α]_D²² = -297.6° (*c* 1.0, CH₂Cl₂).

¹H NMR (500 MHz, CDCl₃) δ 7.83 (d, *J* = 12.5 Hz, 1H), 7.79-7.74 (m, 3H), 7.56-7.50 (m, 1H), 7.46-7.40 (m, 2H), 7.38-7.27 (m, 3H), 7.24-7.17 (m, 2H), 7.01-6.98 (m, 1H), 6.85 (d, *J* = 8.0 Hz, 1H, other rotamer), 5.80-5.73 (m, 1H), 4.10-4.03 (m, 2H), 3.41-3.32 (m, 1H), 2.81-2.72 (m, 1H), 2.05 (s, 3H), 1.52 (s, 3H, other rotamer), 1.20-1.13 (m, 3H).

¹³C NMR (125 MHz, CDCl₃) δ 189.2, 189.1, 171.7, 171.6, 142.9, 142.8, 137.8, 135.2, 134.9, 134.3, 133.4, 132.5, 130.61, 130.58, 130.22, 130.16, 129.1, 129.0, 128.40, 128.35, 127.9, 127.8, 127.6, 127.5, 126.6, 126.52, 126.46, 126.4, 126.1, 126.0, 125.87, 125.85, 60.6, 48.80, 48.77, 37.5, 37.2, 17.2, 16.6, 14.09, 14.05. (Mixture of two rotation isomers)

IR (film): ν (cm⁻¹) 3056, 2981, 2929, 1729, 1682, 1498, 1453, 1403, 1376, 1262, 1241, 1178, 1154, 1024, 941, 908, 816, 763, 728, 479.

HRMS (ESI, *m/z*) calcd for C₂₆H₂₄N₂O₃Na [M+Na]⁺: 435.1679, found: 435.1678.



3-(1,3-Dioxoisindolin-2-yl)propyl (R)-4-oxo-3-phenyl-4-(1-(*o*-tolyl)-1*H*-imidazol-2-yl)butanoate (5bb**)**

According to the general procedure, the reaction of 2-phenyl-1-(1-(*o*-tolyl)-1*H*-imidazol-2-yl)ethan-1-one **1b** (27.6 mg, 0.10 mmol), 3-(1,3-dioxoisindolin-2-yl)propyl 2-diazoacetate **4b** (82.0 mg, 3.0 equiv), Λ -**RhS** (3.5 mg, 4 mol%), [Ru(bpy)₃](PF₆)₂ (1.3 mg, 1.5 mol%), Na₂HPO₄ (2.8 mg, 20 mol%) and H₂O (36.0 mg, 20 equiv) in acetone/DMSO (9:1, 0.5 mL, 0.2 M) under nitrogen

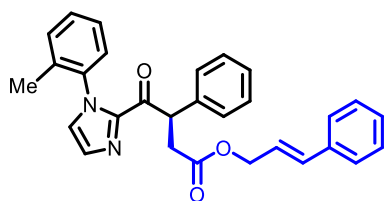
atmosphere with visible light for 16 hours, afforded 51.3 mg (98%) of **5bb** as a white solid. Enantiomeric excess was established by HPLC analysis using a Chiralpak IC column, ee = 96% (HPLC: IC, 254 nm, *n*-hexane/isopropanol = 50:50, flow rate 0.5 mL/min, 25 °C, *t_r* (major) = 58.0 min, *t_r* (minor) = 50.5 min). $[\alpha]_{\text{D}}^{22} = -106.8^{\circ}$ (*c* 1.0, CH₂Cl₂).

¹H NMR (500 MHz, CDCl₃) δ 7.87-7.80 (m, 2H), 7.75-7.66 (m, 2H), 7.38-7.23 (m, 7H), 7.23-7.17 (m, 3H), 7.01-7.00 (m, 1H), 6.87 (d, *J* = 7.5 Hz, 1H, other rotamer), 5.61-5.54 (m, 1H), 4.09-3.98 (m, 2H), 3.76-3.67 (m, 2H), 3.29-3.19 (m, 1H), 2.68-2.59 (m, 1H), 2.01 (s, 3H), 1.98-1.90 (m, 2H), 1.52 (s, 3H, other rotamer).

¹³C NMR (125 MHz, CDCl₃) δ 189.2, 189.1, 171.6, 171.60, 168.2, 142.9, 142.8, 137.83, 137.80, 137.6, 137.5, 134.9, 134.3, 134.1, 133.9, 132.0, 130.65, 130.56, 130.1, 129.02, 128.96, 128.70, 128.66, 128.6, 127.3, 127.2, 126.54, 126.50, 126.44, 126.39, 126.1, 123.3, 62.0, 48.59, 48.55, 37.2, 36.7, 35.0, 34.9, 27.5, 17.2, 16.5. (Mixture of two rotation isomers)

IR (film): ν (cm⁻¹) 2953, 2928, 1771, 1708, 1683, 1496, 1445, 1398, 1243, 1172, 1086, 1046, 941, 907, 765, 717, 524, 466.

HRMS (ESI, *m/z*) calcd for C₃₁H₂₇N₃O₅Na [M+Na]⁺: 544.1843, found: 544.1848.



Cinnamyl (*R*)-4-oxo-3-phenyl-4-(1-(*o*-tolyl)-1*H*-imidazol-2-yl)butanoate (**5bc**)

According to the general procedure, the reaction of 2-phenyl-1-(1-(*o*-tolyl)-1*H*-imidazol-2-yl)ethan-1-one **1b** (27.6 mg, 0.10 mmol), cinnamyl 2-diazoacetate **4c** (60.7 mg, 3.0 equiv), Λ -**RhS** (3.5 mg, 4 mol%), [Ru(bpy)₃](PF₆)₂ (1.3 mg, 1.5 mol%), Na₂HPO₄ (2.8 mg, 20 mol%) and H₂O (36.0 mg, 20 equiv) in acetone/DMSO (9:1, 0.5 mL, 0.2 M) under nitrogen atmosphere with visible light for 10 hours, afforded 26.3 mg (58%) of **5bc** as a yellow oil. Enantiomeric excess was established by HPLC analysis using a Chiralpak IC column, ee = 98% (HPLC: IC, 254 nm, *n*-hexane/isopropanol = 85:15, flow rate 1 mL/min, 25 °C, *t_r* (major) = 14.9 min, *t_r* (minor) = 17.8 min). $[\alpha]_{\text{D}}^{22} = -168.6^{\circ}$ (*c* 1.0, CH₂Cl₂).

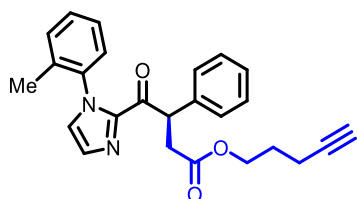
¹H NMR (500 MHz, CDCl₃) δ 7.42-7.36 (m, 2H), 7.36-7.29 (m, 6H), 7.29-7.24 (m, 4H), 7.24-7.17 (m,

3H), 7.17-7.14 (m, 1H, other rotamer), 7.00 (dd, $J_1 = 3.5$ Hz, $J_2 = 1.0$ Hz, 1H), 6.89 (dd, $J_1 = 8.0$ Hz, $J_2 = 1.0$ Hz, 1H, other rotamer), 6.57 (d, $J = 15.5$ Hz, 1H), 6.56 (d, $J = 15.5$ Hz, 1H, other rotamer), 6.21-6.12 (m, 1H), 5.67-5.60 (m, 1H), 4.72-4.61 (m, 2H), 3.39-3.30 (m, 1H), 2.79-2.70 (m, 1H), 1.98 (s, 3H), 1.54 (s, 3H, other rotamer).

^{13}C NMR (125 MHz, CDCl_3) δ 189.27, 189.18, 171.5, 171.4, 142.9, 142.8, 137.84, 137.79, 137.6, 137.5, 136.2, 134.9, 134.3, 133.93, 133.85, 130.61, 130.55, 130.21, 130.20, 129.0, 128.9, 128.73, 128.68, 128.59, 128.57, 128.51, 128.48, 128.0, 127.30, 127.27, 126.6, 126.52, 126.46, 126.44, 126.42, 126.39, 126.0, 123.1, 123.0, 65.13, 65.12, 48.7, 48.6, 37.41, 37.0, 17.1, 16.5. (Mixture of two rotation isomers)

IR (film): ν (cm^{-1}) 3059, 3030, 2927, 1732, 1682, 1495, 1451, 1404, 1308, 1242, 1161, 1091, 965, 939, 907, 759, 732, 695, 546, 454.

HRMS (ESI, m/z) calcd for $\text{C}_{29}\text{H}_{26}\text{N}_2\text{O}_3\text{Na}$ $[\text{M}+\text{Na}]^+$: 473.1836, found: 473.1837.



Pent-4-yn-1-yl (*R*)-4-oxo-3-phenyl-4-(1-(*o*-tolyl)-1*H*-imidazol-2-yl)butanoate (5bd**)**

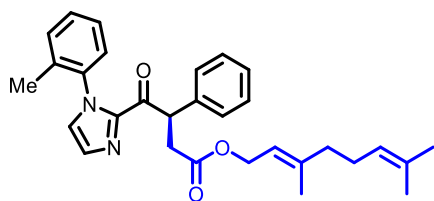
According to the general procedure, the reaction of 2-phenyl-1-(1-(*o*-tolyl)-1*H*-imidazol-2-yl)ethan-1-one **1b** (27.6 mg, 0.10 mmol), pent-4-yn-1-yl 2-diazoacetate **4d** (45.7 mg, 3.0 equiv), Λ -**RhS** (3.5 mg, 4 mol%), $[\text{Ru}(\text{bpy})_3](\text{PF}_6)_2$ (1.3 mg, 1.5 mol%), Na_2HPO_4 (2.8 mg, 20 mol%) and H_2O (36.0 mg, 20 equiv) in acetone/DMSO (9:1, 0.5 mL, 0.2 M) under nitrogen atmosphere with visible light for 18 hours, afforded 36.0 mg (90%) of **5bd** as a yellow oil. Enantiomeric excess was established by HPLC analysis using a Chiralpak OD-H column, ee = 96% (HPLC: OD-H, 254 nm, *n*-hexane/isopropanol = 90:10, flow rate 1 mL/min, 25 °C, t_r (major) = 12.2 min, t_r (minor) = 14.6 min). $[\alpha]_{\text{D}}^{22} = -201.4^\circ$ (c 1.0, CH_2Cl_2).

^1H NMR (500 MHz, CDCl_3) δ 7.42-7.26 (m, 7H), 7.25-7.19 (m, 3H), 7.04-7.03 (m, 1H), 6.89 (d, $J = 7.5$ Hz, 1H, other rotamer), 5.65-5.57 (m, 1H), 4.17-4.07 (m, 2H), 3.36-3.29 (m, 1H), 2.75-2.66 (m, 1H), 2.22-2.13 (m, 2H), 2.04 (s, 3H), 1.97-1.93 (m, 1H), 1.80-1.73 (m, 2H), 1.55 (s, 3H, other rotamer).

^{13}C NMR (125 MHz, CDCl_3) δ 189.2, 189.1, 171.6, 171.5, 142.8, 142.7, 137.78, 137.76, 137.6, 137.4, 134.8, 134.3, 130.6, 130.5, 130.2, 130.1, 129.0, 128.9, 128.70, 128.66, 128.5, 127.29, 127.25, 126.51, 126.48, 126.43, 126.40, 126.39, 126.0, 83.0, 68.9, 63.1, 63.0, 48.64, 48.56, 37.3, 36.9, 27.42, 27.38, 17.2, 16.4, 15.05, 15.00. (Mixture of two rotation isomers)

IR (film): ν (cm^{-1}) 3289, 2959, 2927, 1731, 1682, 1495, 1453, 1403, 1362, 1306, 1243, 1170, 1089, 1026, 941, 908, 763, 700, 639, 525.

HRMS (ESI, m/z) calcd for $\text{C}_{25}\text{H}_{24}\text{N}_2\text{O}_3\text{Na}$ $[\text{M}+\text{Na}]^+$: 423.1679, found: 423.1679.



(*E*)-3,7-Dimethylocta-2,6-dien-1-yl (R)-4-oxo-3-phenyl-4-(1-(*o*-tolyl)-1*H*-imidazol-2-yl)butanoate (5be**)**

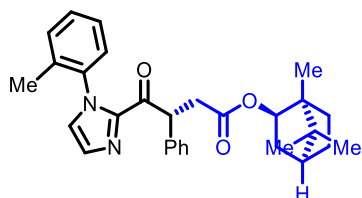
According to the general procedure, the reaction of 2-phenyl-1-(1-(*o*-tolyl)-1*H*-imidazol-2-yl)ethan-1-one **1b** (27.6 mg, 0.10 mmol), (*E*)-3,7-dimethylocta-2,6-dien-1-yl 2-diazoacetate **4e** (66.7 mg, 3.0 equiv), Δ -**RhS** (3.5 mg, 4 mol%), $[\text{Ru}(\text{bpy})_3](\text{PF}_6)_2$ (1.3 mg, 1.5 mol%), Na_2HPO_4 (2.8 mg, 20 mol%) and H_2O (36.0 mg, 20 equiv) in acetone/DMSO (9:1, 0.5 mL, 0.2 M) under nitrogen atmosphere with visible light for 24 hours, afforded 38.6 mg (82%) of **5be** as a yellow oil. Enantiomeric excess was established by HPLC analysis using a Chiralpak OD-H column, ee = 96% (HPLC: OD-H, 254 nm, *n*-hexane/isopropanol = 90:10, flow rate 1 mL/min, 25 °C, t_r (major) = 7.7 min, t_r (minor) = 9.1 min). $[\alpha]_D^{22} = -170.2^\circ$ (*c* 0.4, CH_2Cl_2).

^1H NMR (500 MHz, CDCl_3) δ 7.42-7.24 (m, 7H), 7.24-7.17 (m, 3H), 7.03-7.01 (m, 1H), 6.89 (d, J = 7.5 Hz, 1H, other rotamer), 5.64-5.57 (m, 1H), 5.27-5.22 (m, 1H), 5.10-5.05 (m, 1H), 4.55-4.49 (m, 2H), 3.35-3.26 (m, 1H), 2.75-2.65 (m, 1H), 2.11-1.97 (m, 4H), 2.04 (s, 3H), 1.69 (s, 3H), 1.65 (s, 3H), 1.64 (s, 3H, other rotamer), 1.61 (s, 3H), 1.55 (s, 3H, other rotamer).

^{13}C NMR (125 MHz, CDCl_3) δ 189.4, 189.3, 171.7, 143.0, 142.8, 142.1, 142.0, 137.9, 137.8, 137.7, 137.6, 134.9, 134.3, 131.8, 130.60, 130.56, 130.2, 130.1, 129.0, 128.9, 128.7, 128.63, 128.59, 128.58, 127.23, 127.20, 126.5, 126.45, 126.39, 126.37, 126.1, 123.7, 118.2, 118.1, 61.50, 48.65, 48.62, 39.5, 37.4, 37.0, 26.2, 25.7, 17.7, 17.2, 16.5, 16.4. (Mixture of two rotation isomers)

IR (film): ν (cm⁻¹) 2968, 2922, 2858, 1731, 1685, 1496, 1451, 1405, 1310, 1240, 1167, 940, 908, 763, 738, 700, 547.

HRMS (ESI, m/z) calcd for C₃₀H₃₄N₂O₃Na [M+Na]⁺: 493.2462, found: 493.2462.



(1S,2R,4S)-1,7,7-Trimethylbicyclo[2.2.1]heptan-2-yl (R)-4-oxo-3-phenyl-4-(1-(*o*-tolyl)-1H-imidazol-2-yl)butanoate (5bf)

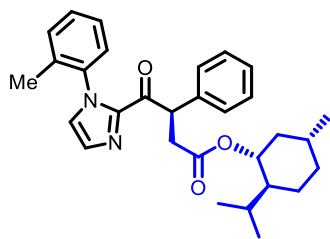
According to the general procedure, the reaction of 2-phenyl-1-(1-(*o*-tolyl)-1H-imidazol-2-yl)ethan-1-one **1b** (27.6 mg, 0.10 mmol), (1S,2R,4S)-1,7,7-trimethylbicyclo[2.2.1]heptan-2-yl 2-diazoacetate **4f** (66.7 mg, 3.0 equiv), Λ -**RhS** (3.5 mg, 4 mol%), [Ru(bpy)₃](PF₆)₂ (1.3 mg, 1.5 mol%), Na₂HPO₄ (2.8 mg, 20 mol%) and H₂O (36.0 mg, 20 equiv) in acetone/DMSO (9:1, 0.5 mL, 0.2 M) under nitrogen atmosphere with visible light for 24 hours, afforded 43.4 mg (92%) of **5bf** as a yellow solid. Diastereomer ratio was established by ¹H NMR and HPLC analysis using a Chiralpak OD-H column, d.r. > 98:2 (HPLC: OD-H, 254 nm, *n*-hexane/isopropanol = 99:1, flow rate 1 mL/min, 25 °C, t_r (major) = 17.8 min, t_r (minor) = 25.5 min). [α]_D²² = -180.0° (*c* 1.0, CH₂Cl₂).

¹H NMR (500 MHz, CDCl₃) δ 7.44-7.17 (m, 10H), 7.04-7.01 (m, 1H), 6.86 (d, *J* = 8.0 Hz, 1H, other rotamer), 5.67-5.50 (m, 1H), 4.87-4.76 (m, 1H), 3.39-3.25 (m, 1H), 2.79-2.70 (m, 1H), 2.32-2.21 (m, 1H), 2.05 (s, 3H), 1.89-1.60 (m, 3H), 1.52 (s, 3H, other rotamer), 1.30-1.06 (m, 2H), 1.51 (s, 3H, other rotamer), 0.95-0.83 (m, 7H), 0.72 (s, 3H), 0.70 (s, 3H, other rotamer).

¹³C NMR (125 MHz, CDCl₃) δ 189.3, 189.2, 171.9, 171.8, 142.89, 142.87, 137.81, 137.79, 137.6, 137.5, 134.8, 134.3, 130.6, 130.5, 130.13, 130.09, 129.0, 128.9, 128.8, 128.7, 128.62, 128.60, 128.58, 127.22, 127.19, 126.5, 126.42, 126.35, 126.1, 80.2, 48.8, 48.61, 48.59, 48.5, 47.70, 47.66, 44.74, 44.73, 37.5, 37.1, 36.45, 36.35, 27.82, 27.77, 27.0, 26.9, 19.6, 18.7, 17.2, 16.4, 13.3, 13.28. (Mixture of two rotation isomers)

IR (film): ν (cm⁻¹) 2953, 2878, 1728, 1684, 1495, 1453, 1404, 1306, 1253, 1181, 1155, 1022, 942, 910, 763, 731, 703, 549.

HRMS (ESI, m/z) calcd for C₃₀H₃₄N₂O₃Na [M+Na]⁺: 493.2462, found: 493.2462.



(1*R*,2*S*,5*R*)-2-Isopropyl-5-methylcyclohexyl (R)-4-oxo-3-phenyl-4-(1-(*o*-tolyl)-1*H*-imidazol-2-yl)butanoate (5bg)

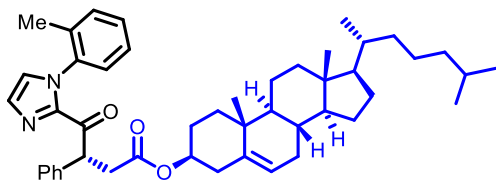
According to the general procedure, the reaction of 2-phenyl-1-(1-(*o*-tolyl)-1*H*-imidazol-2-yl)ethan-1-one **1b** (27.6 mg, 0.10 mmol), (1*R*,2*S*,5*R*)-2-isopropyl-5-methylcyclohexyl 2-diazoacetate **4g** (67.2 mg, 3.0 equiv), Λ -**RhS** (3.5 mg, 4 mol%), [Ru(bpy)₃](PF₆)₂ (1.3 mg, 1.5 mol%), Na₂HPO₄ (2.8 mg, 20 mol%) and H₂O (36.0 mg, 20 equiv) in acetone/DMSO (9:1, 0.5 mL, 0.2 M) under nitrogen atmosphere with visible light for 13 hours, afforded 44.2 mg (93%) of **5bg** as a colorless oil. Diastereomer ratio was established by ¹H NMR and HPLC analysis using a Chiralpak IC column, d.r. >99:1 (HPLC: IC, 254 nm, *n*-hexane/isopropanol = 98:2, flow rate 1 mL/min, 25 °C, *t_r* (major) = 30.4 min, *t_r* (minor) = 22.0 min). [α]_D²² = −220.6° (*c* 0.4, CH₂Cl₂).

¹H NMR (500 MHz, CDCl₃) δ 7.42-7.16 (m, 10H), 7.03-7.00 (m, 1H), 6.84 (d, *J* = 7.5 Hz, 1H, other rotamer), 5.62-5.54 (m, 1H), 4.62-4.53 (m, 1H), 3.30-3.17 (m, 1H), 2.74-2.65 (m, 1H), 2.03 (s, 3H), 1.88-1.83 (m, 1H), 1.66-1.60 (m, 2H), 1.51 (s, 3H, other rotamer), 1.47-1.23 (m, 3H), 1.02-0.75 (m, 9H), 0.66-0.60 (m, 3H).

¹³C NMR (125 MHz, CDCl₃) δ 189.3, 171.3, 171.3, 143.0, 142.9, 137.8, 137.6, 137.5, 134.9, 134.3, 130.6, 130.14, 130.10, 129.03, 128.96, 128.68, 128.66, 128.6, 127.3, 127.2, 126.47, 126.45, 126.40, 126.37, 126.1, 74.49, 74.47, 49.0, 48.8, 46.8, 46.7, 40.7, 37.7, 37.3, 34.2, 31.3, 26.03, 25.97, 23.33, 23.26, 21.99, 21.95, 20.73, 20.68, 17.3, 16.4, 16.21, 16.15. (Mixture of two rotation isomers)

IR (film): ν (cm^{−1}) 2954, 2926, 2867, 1726, 1684, 1496, 1454, 1405, 1373, 1306, 1246, 1178, 1153, 1091, 980, 941, 909, 763, 730, 702, 549.

HRMS (ESI, *m/z*) calcd for C₃₀H₃₆N₂O₃Na [M+Na]⁺: 495.2618, found: 495.2619.



(3*S*,8*S*,9*S*,10*R*,13*R*,14*S*,17*R*)-10,13-Dimethyl-17-((*R*)-6-methylheptan-2-yl)-2,3,4,7,8,9,10,11,12,13,14,15,16,17-tetradecahydro-1*H*-cyclopenta[*a*]phenanthren-3-yl (R)-4-oxo-3-phenyl-4-(1-(*o*-tolyl)-1*H*-imidazol-2-yl)butanoate (5bh)

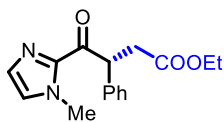
According to the general procedure, the reaction of 2-phenyl-1-(1-(*o*-tolyl)-1*H*-imidazol-2-yl)ethan-1-one **1b** (41.4 mg, 0.15 mmol), cholesteryl 2-diazoacetate **4h** (45.4 mg, 0.10 mmol), Λ -**RhS** (3.5 mg, 4 mol%), [Ru(bpy)₃](PF₆)₂ (2.2 mg, 2.5 mol%), Na₂HPO₄ (2.8 mg, 20 mol%) and H₂O (36.0 mg, 20 equiv) in acetone/DMSO (9:1, 2.0 mL, 0.05 M) under nitrogen atmosphere with visible light for 60 hours, afforded 58.1 mg (83%) of **5bh** as a white solid. Diastereomer ratio was established by ¹H NMR and HPLC analysis using a Chiralpak IC column, d.r. > 97:3 (HPLC: IC, 254 nm, *n*-hexane/isopropanol = 85:15, flow rate 1 mL/min, 25 °C, *t_r* (major) = 15.5 min, *t_r* (minor) = 8.9 min). [α]_D²² = −116.6° (*c* 0.4, CH₂Cl₂).

¹H NMR (500 MHz, CDCl₃) δ 7.42-7.17 (m, 10H), 7.03-7.01 (m, 1H), 6.88 (d, *J* = 7.5 Hz, 1H, other rotamer), 5.62-5.56 (m, 1H), 5.35-5.31 (m, 1H), 4.56-4.57 (m, 1H), 3.30-3.22 (m, 1H), 2.73-2.62 (m, 1H), 2.25-2.17 (m, 2H), 2.04 (s, 3H), 2.03-1.90 (m, 2H), 1.88-1.70 (m, 3H), 1.60-0.98 (m, 21H), 1.54 (s, 3H, other rotamer), 0.98 (s, 3H), 0.97 (s, 3H, other rotamer), 0.91 (d, *J* = 6.5 Hz, 3H), 0.87 (d, *J* = 6.5 Hz, 3H), 0.86 (d, *J* = 7.0 Hz, 3H), 0.67 (s, 3H).

¹³C NMR (125 MHz, CDCl₃) δ 189.4, 189.3, 171.1, 171.0, 142.9, 142.8, 139.7, 139.6, 137.85, 137.83, 137.7, 137.6, 134.9, 134.3, 130.61, 130.59, 130.10, 130.07, 129.02, 128.96, 128.7, 128.6, 127.23, 127.20, 126.5, 126.4, 126.1, 122.50, 122.46, 74.25, 74.23, 56.6, 56.1, 49.93, 49.92, 48.7, 48.6, 42.3, 39.7, 39.5, 37.92, 37.87, 37.8, 37.4, 36.9, 36.52, 36.50, 36.1, 35.8, 31.9, 31.84, 31.79, 28.20, 28.0, 27.6, 27.5, 24.2, 23.8, 22.8, 22.5, 21.0, 19.3, 18.7, 17.3, 16.5, 11.8. (Mixture of two rotation isomers)

IR (film): ν (cm^{−1}) 2939, 2864, 1730, 1685, 1496, 1458, 1406, 1373, 1245, 1176, 1007, 940, 909, 763, 730, 703, 547.

HRMS (ESI, *m/z*) calcd for C₄₇H₆₂N₂O₃Na [M+Na]⁺: 725.4653, found: 725.4666.



Ethyl (*R*)-4-(1-methyl-1*H*-imidazol-2-yl)-4-oxo-3-phenylbutanoate (**5ra**)

According to the general procedure, the reaction of 1-(1-methyl-1*H*-imidazol-2-yl)-2-phenylethan-1-one **1r** (20.0 mg, 0.10 mmol), ethyl 2-diazoacetate **4a** (34.2 mg, 3.0 equiv), Λ -**RhS** (3.5 mg, 4 mol%), [Ru(bpy)₃](PF₆)₂ (1.3 mg, 1.5 mol%), Na₂HPO₄ (2.8 mg, 20 mol%) and H₂O (36.0 mg, 20 equiv) in acetone/DMSO (9:1, 0.5 mL, 0.2 M) under nitrogen atmosphere (degassed by freeze-pump-thaw cycles) with 21 W CFL for 15 hours, afforded 26.0 mg (91%) of **5ra** as a yellow oil.

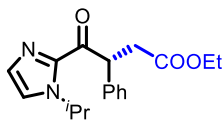
Enantiomeric excess of **5ra** was established by HPLC analysis as 87% ee. (HPLC: Agilent 1200 Series HPLC System, Daicel Chiralpak AS-H column (250 × 4.6 mm), 254 nm, *n*-hexane/isopropanol = 90:10, flow rate 1 mL/min, 25 °C, *t_r* (major) = 12.8 min, *t_r* (minor) = 11.7 min). [α]_D²² = -126.0° (*c* 1.0, CH₂Cl₂).

¹H NMR (300 MHz, CDCl₃) δ 7.48-7.41 (m, 2H), 7.33-7.25 (m, 2H), 7.24-7.17 (m, 1H), 7.16-7.14 (m, 1H), 6.97 (s, 1H), 5.61 (dd, *J*₁ = 10.5 Hz, *J*₂ = 5.1 Hz, 1H), 4.08 (q, *J* = 7.2 Hz, 2H), 3.95 (s, 3H), 3.39 (dd, *J*₁ = 16.8 Hz, *J*₂ = 10.5 Hz, 1H), 2.77 (dd, *J*₁ = 16.8 Hz, *J*₂ = 5.1 Hz, 1H), 1.17 (t, *J* = 7.1 Hz, 3H).

¹³C NMR (75 MHz, CDCl₃) δ 190.9, 171.8, 142.5, 138.0, 129.5, 128.7, 128.6, 127.2, 127.1, 60.5, 48.5, 37.5, 36.0, 14.0.

IR (film): ν (cm⁻¹) 3122, 2981, 2935, 1729, 1673, 1458, 1404, 1372, 1330, 1290, 1242, 1179, 1092, 1027, 992, 955, 911, 845, 779, 744, 699, 560, 529.

HRMS (ESI, *m/z*) calcd for C₁₆H₁₉N₂O₃ [M+H]⁺: 287.1390, found: 287.1396.



Ethyl (*R*)-4-(1-isopropyl-1*H*-imidazol-2-yl)-4-oxo-3-phenylbutanoate (**5sa**)

According to the general procedure, the reaction of 1-(1-isopropyl-1*H*-imidazol-2-yl)-2-phenylethan-1-one **1s** (22.8 mg, 0.10 mmol), ethyl 2-diazoacetate **4a** (34.2 mg, 3.0 equiv), Λ -**RhS** (3.5 mg, 4 mol%), [Ru(bpy)₃](PF₆)₂ (1.3 mg, 1.5 mol%), Na₂HPO₄ (2.8 mg, 20 mol%) and H₂O (36.0 mg, 20 equiv) in acetone/DMSO (9:1, 0.5 mL, 0.2 M) under nitrogen atmosphere (degassed by freeze-pump-thaw cycles) with 21 W CFL for 15 hours, afforded 28.7 mg (91%) of **5sa** as a yellow oil.

Enantiomeric excess of **5sa** was established by HPLC analysis as 89% ee. (HPLC: Agilent 1200 Series

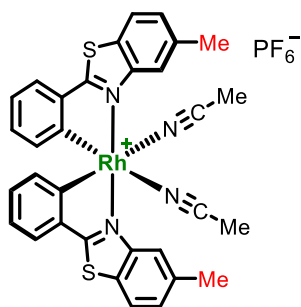
HPLC System, Daicel Chiralpak AS-H column (250 × 4.6 mm), 254 nm, *n*-hexane/isopropanol = 90:10, flow rate 1 mL/min, 25 °C, t_r (major) = 8.1 min, t_r (minor) = 7.0 min). $[\alpha]_D^{22} = -146.2^\circ$ (*c* 1.0, CH₂Cl₂).

¹H NMR (300 MHz, CDCl₃) δ 7.39-7.31 (m, 2H), 7.25-7.15 (m, 2H), 7.16-7.07 (m, 3H), 5.56 (dd, $J_1 = 10.5$ Hz, $J_2 = 5.1$ Hz, 1H), 5.40 (hept, $J = 6.6$ Hz, 1H), 3.99 (q, $J = 7.2$ Hz, 2H), 3.29 (dd, $J_1 = 16.5$ Hz, $J_2 = 10.2$ Hz, 1H), 2.68 (dd, $J_1 = 16.5$ Hz, $J_2 = 5.1$ Hz, 1H), 1.36 (d, $J = 6.9$ Hz, 3H), 1.24 (d, $J = 6.9$ Hz, 3H), 1.08 (t, $J = 7.2$ Hz, 3H).

¹³C NMR (75 MHz, CDCl₃) δ 191.1, 171.7, 141.9, 138.2, 129.9, 128.6, 128.5, 127.1, 121.2, 60.5, 49.1, 49.0, 37.7, 23.5, 23.4, 14.0.

IR (film): ν (cm⁻¹) 3143, 2980, 2932, 1731, 1673, 1457, 1394, 1330, 1298, 1250, 1173, 1090, 1028, 988, 951, 911, 849, 736, 699, 642, 579, 523.

HRMS (ESI, m/z) calcd for C₁₈H₂₃N₂O₃ [M+H]⁺: 315.1703, found: 315.1709.



Λ -**RhS(Me)** was obtained from 5-methyl-2-phenylbenzo[d]thiazole as a yellow solid.¹

¹H NMR (500 MHz, CD₂Cl₂) δ 8.22 (s, 2H), 7.94 (d, $J = 8.3$ Hz, 2H), 7.64 (dd, $J_1 = 7.6$ Hz, $J_2 = 1.3$ Hz, 2H), 7.44 (dd, $J_1 = 8.3$ Hz, $J_2 = 1.0$ Hz, 2H), 7.01 (td, $J_1 = 7.5$ Hz, $J_2 = 1.0$ Hz, 2H), 6.81 (td, $J_1 = 7.6$ Hz, $J_2 = 1.4$ Hz, 2H), 6.17 (d, $J = 7.9$ Hz, 2H), 2.57 (s, 6H), 2.21 (s, 6H).

¹³C NMR (125 MHz, CD₂Cl₂) δ 176.8, 160.9 (m), 150.1, 140.3, 139.1, 133.3, 131.2, 129.1, 128.4, 126.2, 124.5, 123.0, 122.3 (m), 120.8, 22.0, 3.4.

IR (film): ν (cm⁻¹) 3059, 2936, 2313, 2284, 1578, 1557, 1482, 1464, 1441, 1416, 1318, 1297, 1274, 1246, 1161, 1123, 1027, 993, 939, 836, 758, 747, 731, 722, 698, 657, 644, 579, 557.

HRMS (ESI, m/z) calcd for C₂₈H₂₀N₂RhS₂ [M-(MeCN)₂-(PF₆⁻)]: 551.0123, found: 551.0113.

CD (CH₃OH) for Λ -**RhS(Me)**: λ , nm ($\Delta\epsilon$, M⁻¹cm⁻¹) 407 (-38), 366 (+58), 349 (+51), 300 (-86), 263 (+31), 258 (+31), 242 (+41), 230 (-24), 214 (+99).

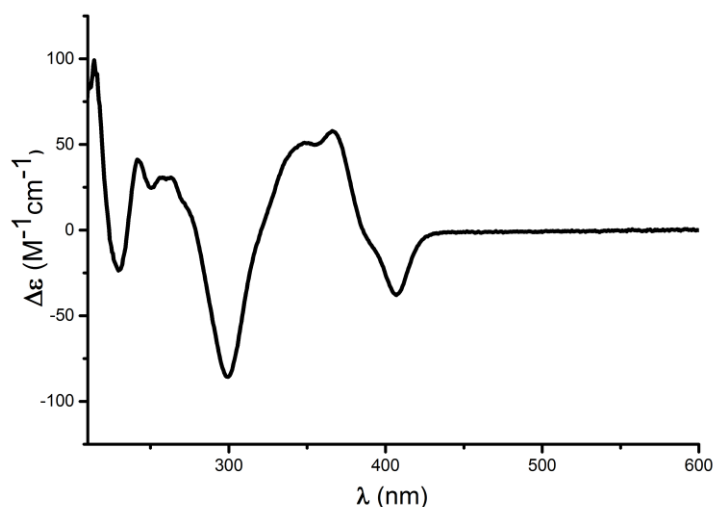


Figure 120. CD spectrum of Λ -**RhS(Me)**. Recorded in CH_3OH (0.2 mM).

5.2.4 Removal of 2-Aryl Imidazolyl Group

As shown in **Figure 30**, the directing imidazole moiety was cleaved according to the previous report with slight modification.^{8a} 4 Å MS (169 mg, 100 mg/0.1 mmol of **5ba**) was added to a solution of (*R*)-**5ba** (61 mg, 0.169 mmol) in CH_3CN (0.1 M) under nitrogen atmosphere. The suspension was stirred vigorously under a positive pressure of nitrogen for 3 h at 0 °C. Then methyl trifluoromethanesulfonate (30.5 mg, 0.186 mmol, 1.1 equiv) was added dropwise at 0 °C. After being stirred at 0 °C for 6 h, EtOH (1.0 mL) and DBU (28.3 mg, 0.186 mmol, 1.1 equiv) were subsequently added to the reaction mixture at 0 °C. After being stirred at 0 °C for 60 min, 10 mL of saturated NaHCO_3 aqueous solution was added. And the mixture was extracted with CH_2Cl_2 , washed with NaHCO_3 aqueous solution, water. The organic layer was dried and the solvent was evaporated and the residue was purified by flash chromatography on silica gel ($\text{EtOAc}/n\text{-hexane} = 1:50$) to give 34.1 mg (*R*)-**6** (81%) as a colorless oil.

Enantiomeric excess of (*R*)-**6** was established by HPLC analysis using a Chiralpak AD-H column, 95% ee (HPLC: AD-H, $n\text{-hexane}/\text{isopropanol} = 95:5$, flow rate 1 mL/min, 25 °C, t_r (major) = 7.0 min, t_r (minor) = 8.0 min). $[\alpha]_{\text{D}}^{22} = -97.6^\circ$ (c 1.0, CH_2Cl_2).

Literature report^{8b} for (*S*)-**6**: 77% ee (HPLC: AD-H, $n\text{-hexane}/\text{isopropanol} = 95:5$, flow rate 1 mL/min,

Retention times: 6.69 min [(*R*)-enantiomer], 7.68 min [(*S*)-enantiomer]. $[\alpha]_{\text{D}}^{29} = +51.25$ (c 1.19, CHCl_3). All other spectroscopic data of **6** are in agreement with literature report.^{8b}

5.2.5 Single-Crystal X-Ray Diffraction Studies

Single crystals of **Rh-enolate1** suitable for X-ray diffraction were obtained by slow diffusion from a solution of **Rh-enolate1** (20 mg) in CH_2Cl_2 (1.0 mL) layered with *n*-hexane (0.5 mL) at room temperature for several days in a NMR tube.

Single crystals of **5oa** suitable for X-ray diffraction were obtained by slow diffusion from a solution of **5oa** (30 mg) in CH_2Cl_2 (0.5 mL) layered with *n*-hexane (0.5 mL) at - 20 °C for several days in a NMR tube.

X-ray data were collected with a Bruker 3 circuit D8 Quest diffractometer with $\text{MoK}\alpha$ radiation (microfocus tube with multilayer optics) and Photon 100 CMOS detector at 100 K. Scaling and absorption correction was performed by using the SADABS software package of Bruker. Structures were solved using direct methods in SHELXT and refined using the full matrix least squares procedure in SHELXL-2014. The hydrogen atoms were placed in calculated positions and refined as riding on their respective C atom, and Uiso(H) was set at 1.2 Ueq(Csp^2) and 1.5 Ueq(Csp^3). Disorder was refined using restraints for both the geometry and the anisotropic displacement factors.

The absolute configuration of **5oa** has been determined. See **Figure 35** for Crystal structure of **Rh-enolate1**. See **Figure 121** for Crystal structure of **5oa**

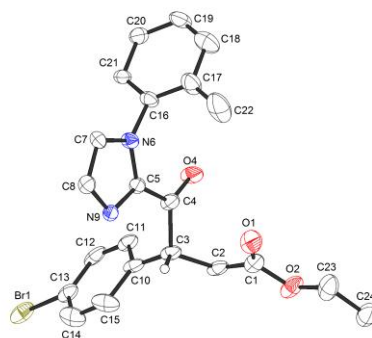


Figure 121. Crystal structure of **5oa**.

Table 22. Crystal data and structure refinement for **Rh-enolate1**.

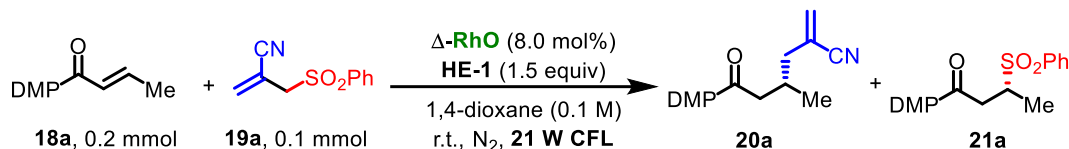
Crystal data	
CCDC number	1491052
Identification code	hxqC31_0m
Habitus, color	nugget, light green
Crystal size	0.23 x 0.13 x 0.10 mm ³
Crystal system	Monoclinic
Space group	P2 ₁ /n
Unit cell dimensions	$Z = 4$ $a = 11.6759(5) \text{ \AA}$ $\alpha = 90^\circ$ $b = 23.0296(9) \text{ \AA}$ $\beta = 92.6600(10)^\circ$ $c = 16.4573(7) \text{ \AA}$ $\gamma = 90^\circ$
Volume	4420.5(3) Å ³
Cell determination	9634 peaks with Theta 2.4 to 27.5 °
Empirical formula	C ₅₂ H ₄₇ N ₄ O Rh S ₂
Moiety formula	C ₅₂ H ₄₇ N ₄ O Rh S ₂
Formula weight	910.96
Density (calculated)	1.369 Mg/m ³
Absorption coefficient	0.524 mm ⁻¹
F(000)	1888
Data collection:	
Diffractometer type	Bruker D8 QUEST area detector
Wavelength	0.71073 Å
Temperature	100(2) K
Theta range for data collection	2.159 to 27.558 °
Index ranges	-15 ≤ h ≤ 15, -29 ≤ k ≤ 29, -21 ≤ l ≤ 21
Data collection software	APEX3 (Bruker AXS Inc., 2015)
Cell refinement software	SAINT V8.35A (Bruker AXS Inc., 2015)
Data reduction software	SAINT V8.35A (Bruker AXS Inc., 2015)
Solution and refinement:	
Reflections collected	155552
Independent reflections	10199 [R(int) = 0.0382]
Completeness to theta = 25.242 °	99.9 %
Observed reflections	9143 [I > 2(I)]
Reflections used for refinement	10199
Absorption correction	Semi-empirical from equivalents
Max. and min. transmission	0.95 and 0.90
Largest diff. peak and hole	0.413 and -0.701 e.Å ⁻³
Solution	Direct methods
Refinement	Full-matrix least-squares on F ²
Treatment of hydrogen atoms	Calculated positions, constr. ref.
Programs used	XT V2014/1 (Bruker AXS Inc., 2014) SHELXL-2014/7 (Sheldrick, 2014) DIAMOND (Crystal Impact) ShelXle (Hübschle, Sheldrick, Dittrich, 2011)
Data / restraints / parameters	10199 / 303 / 583
Goodness-of-fit on F ²	1.052
R index (all data)	wR2 = 0.0556
R index conventional [I > 2σ(I)]	R1 = 0.0227

Table 23. Crystal data and structure refinement for **50a**.

Crystal data		
CCDC number	1491053	
Identification code	hxqD53_0m	
Habitus, color	nugget, colorless	
Crystal size	0.27 x 0.22 x 0.15 mm ³	
Crystal system	Orthorhombic	
Space group	P2 ₁ 2 ₁ 2 ₁	Z = 4
Unit cell dimensions	a = 9.8543(4) Å	α = 90 °
	b = 13.1873(6) Å	β = 90 °
	c = 15.4684(7) Å	γ = 90 °
Volume	2010.14(15) Å ³	
Cell determination	9961 peaks with Theta 2.5 to 25.3 °	
Empirical formula	C ₂₂ H ₂₁ Br N ₂ O ₃	
Moiety formula	C ₂₂ H ₂₁ Br N ₂ O ₃	
Formula weight	441.32	
Density (calculated)	1.458 Mg/m ³	
Absorption coefficient	2.070 mm ⁻¹	
F(000)	904	
Data collection:		
Diffractometer type	Bruker D8 QUEST area detector	
Wavelength	0.71073 Å	
Temperature	100(2) K	
Theta range for data collection	2.451 to 25.288 °	
Index ranges	-11<=h<=11, -13<=k<=15, -18<=l<=18	
Data collection software	APEX3 (Bruker AXS Inc., 2015)	
Cell refinement software	SAINT V8.35A (Bruker AXS Inc., 2015)	
Data reduction software	SAINT V8.35A (Bruker AXS Inc., 2015)	
Solution and refinement:		
Reflections collected	29129	
Independent reflections	3633 [R(int) = 0.0358]	
Completeness to theta = 25.242 °	100.0 %	
Observed reflections	3507[I > 2(I)]	
Reflections used for refinement	3633	
Extinction coefficient	X = 0.0018(4)	
Absorption correction	Semi-empirical from equivalents	
Max. and min. transmission	0.75 and 0.65	
Flack parameter (absolute struct.)	0.005(4)	
Largest diff. peak and hole	0.720 and -0.920 e.Å ⁻³	
Solution	Direct methods	
Refinement	Full-matrix least-squares on F ²	
Treatment of hydrogen atoms	Calculated positions, constr. ref.	
Programs used	XT V2014/1 (Bruker AXS Inc., 2014)	
	SHELXL-2014/7 (Sheldrick, 2014)	
	DIAMOND (Crystal Impact)	
	ShelXle (Hübschle, Sheldrick, Dittrich, 2011)	
Data / restraints / parameters	3633 / 756 / 366	
Goodness-of-fit on F ²	1.152	
R index (all data)	wR2 = 0.0787	
R index conventional [I>2sigma(I)]	R1 = 0.0376	

5.3 Photoinduced Asymmetric β -Alkylation and β -Sulfonylation

5.3.1 General Procedure



Exemplary, a dried 10 mL Schlenk tube was charged with **19a** (20.7 mg, 0.10 mmol), Δ -**RhO** (6.6 mg, 8.0 mol%) and **HE-1** (42.2 mg, 0.15 mmol). The tube was purged with nitrogen for three times. Then, 1,4-dioxane (anhydrous, 1.0 mL, 0.10 M, bubbling with nitrogen gas for five minutes before addition) was added via syringe followed by addition of **18a** (32.8 mg, 0.2 mmol) under nitrogen atmosphere. The tube was sealed and positioned approximately 5 cm away from a 21 W compact fluorescent lamp. The reaction was stirred at room temperature for the indicated time (monitored by TLC) under nitrogen atmosphere. Afterwards, the mixture was diluted with CH_2Cl_2 . The combined organic layers were concentrated under reduced pressure. The residue was purified by flash chromatography on silica gel (*n*-hexane/EtOAc) to afford the products **20a** and **21a**. Racemic samples were obtained by carrying out the reactions with *rac*-**RhO**. The enantiomeric excess was determined by HPLC analysis on a chiral stationary phase.

5.3.2 Modifications for the Synthesis of Λ/Λ -**RhO**

Racemic **RhO** complex was synthesized according to the previous procedures,^{9a} in which the enantiopure **RhO** was obtained through a proline-mediated route resulting in a loss of at least 50% of rhodium complex. Herein, the resolution process was modified by using a chiral auxiliary (***R***)-**Aux**, namely (***R***)-3-fluoro-2-(4-phenyl-4,5-dihydrooxazol-2-yl)phenol, instead of proline. The corresponding complexes Λ/Λ -(***R***)-**RhO** are stable and could be separated by flash chromatography, thus improving the atom economy of the catalyst synthesis (**Figure 122**).

Accordingly, to the mixture of *rac*-**RhO** (249 mg, 0.3 mmol) and K_2CO_3 (82.8 mg, 0.6 mmol) in absolute ethanol (6.0 mL) was added (***R***)-3-fluoro-2-(4-phenyl-4,5-dihydrooxazol-2-yl)phenol ((***R***)-**Aux**, 91 mg, 0.33 mmol) in one portion. After stirring at 70 °C overnight, the reaction mixture was cooled to room temperature and concentrated to dryness. The residue was directly subjected to a

flash chromatography on silica gel (EtOAc/*n*-hexane = 1/100 to 1:10) giving Δ -(*R*)-RhO (117 mg, 45% yield) as a yellow solid and Λ -(*R*)-RhO (112 mg, 43% yield) as a yellow solid, respectively. The bis-acetonitrile catalysts could be obtained after removing of auxiliary following the previously reported procedures.^{9b}

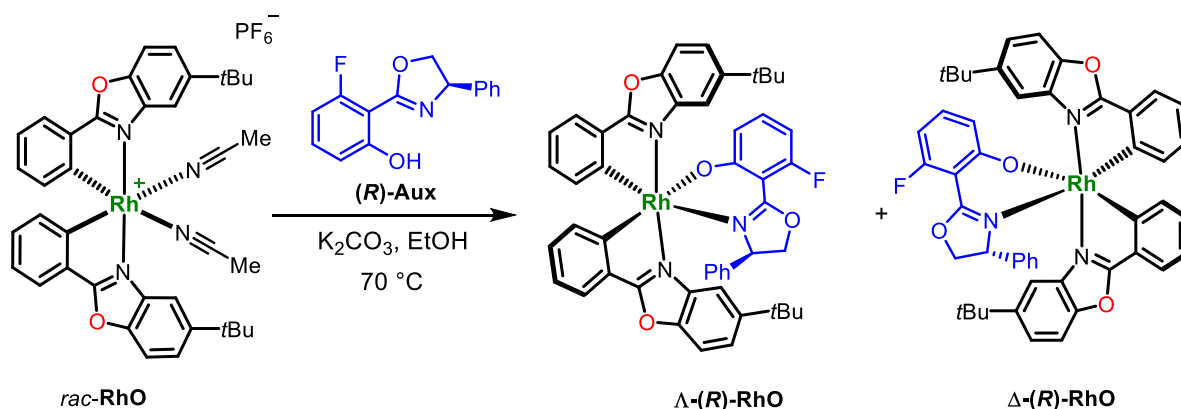


Figure 122. Modified resolution method for the synthesis of enantiopure RhO.

Δ -(*R*)-RhO

¹H NMR (500 MHz, CD₂Cl₂) δ 8.02-7.98 (m, 1H), 7.72-7.68 (m, 1H), 7.62-7.58 (m, 1H), 7.55-7.51 (m, 2H), 7.46 (dd, *J* = 8.8, 2.0 Hz, 1H), 7.36 (d, *J* = 8.8 Hz, 1H), 7.31-7.27 (m, 1H), 7.02-6.94 (m, 3H), 6.92-6.84 (m, 3H), 6.67 (d, *J* = 7.6 Hz, 1H), 6.64-6.48 (m, 3H), 6.37-6.33 (m, 1H), 6.21 (d, *J* = 7.6 Hz, 2H), 5.96 (ddd, *J* = 12.8, 7.8, 0.8 Hz, 1H), 4.92 (dd, *J* = 9.7, 4.6 Hz, 1H), 4.83 (dd, *J* = 9.7, 9.0 Hz, 1H), 4.11 (dd, *J* = 9.0, 4.6 Hz, 1H), 1.44 (s, 9H), 1.32 (s, 9H).

¹³C NMR (125 MHz, CD₂Cl₂) δ 175.23, 175.21, 172.0, 171.9, 170.54, 170.50, 169.3, 169.1, 167.1, 166.9, 165.44, 165.41, 164.1 (d, *J* = 257.5 Hz), 150.1, 150.0, 148.60, 148.56, 141.3, 139.1, 138.6, 134.5, 133.4, 133.3, 133.2, 131.9, 131.4, 131.11, 131.10, 130.8, 130.7, 127.9, 127.5 (2C), 125.7, 125.6, 123.7, 123.3, 123.1, 122.4, 120.60, 120.56, 115.3, 113.0, 111.3, 110.5, 100.2 (d, *J* = 6.4 Hz), 98.7 (d, *J* = 24.1 Hz), 75.0, 69.9, 35.5, 35.4, 31.81, 31.80.

IR (film): ν (cm⁻¹) 2958, 2904, 2869, 1622, 1589, 1528, 1478, 1445, 1374, 1273, 1224, 1092, 1031, 930, 813, 782, 732, 698, 529, 455,

HRMS (ESI, *m/z*) calcd for C₄₉H₄₄FN₃O₄Rh [M+H]⁺: 860.2365, found: 860.2357.

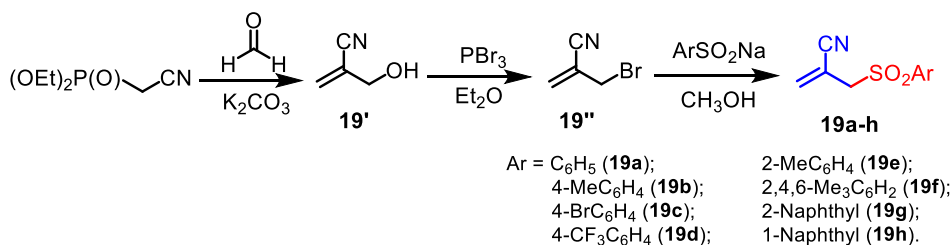
Λ -(R)-RhO

^1H NMR (500 MHz, CD_2Cl_2) δ 8.15-8.11 (m, 1H), 7.74-7.44 (m, 7H), 7.00-6.94 (m, 9H), 6.46-6.28 (m, 3H), 6.04-5.90 (m, 2H), 4.37 (dd, $J = 9.3, 7.8$ Hz, 1H), 4.24 (dd, $J = 16.8, 8.2$ Hz, 1H), 4.21 (dd, $J = 16.8, 8.2$ Hz, 1H), 1.43 (s, 9H), 1.30 (s, 9H).

^{13}C NMR (125 MHz, CD_2Cl_2) δ 175.03, 175.00, 172.0, 171.9, 171.81, 171.79, 168.5, 168.2, 168.0, 167.7, 165.51, 165.50, 163.2 (d, $J = 253.9$ Hz), 150.6, 149.6, 149.0, 148.2, 141.3, 139.1, 138.6, 135.6, 133.3, 132.6, 132.5, 131.3, 131.2, 130.5, 130.2, 128.5, 127.4, 127.2, 125.53, 125.50, 123.9, 123.5, 123.0, 122.3, 119.62, 119.60, 115.2, 114.2, 110.9, 110.8, 102.6 (d, $J = 8.3$ Hz), 98.5 (d, $J = 18.5$ Hz), 75.6, 69.3, 35.44, 35.37, 31.8, 31.6.

IR (film): ν (cm^{-1}) 2958, 2901, 2870, 1623, 1589, 1528, 1478, 1444, 1373, 1273, 1224, 1092, 1030, 979, 931, 814, 783, 733, 698, 529, 456.

HRMS (ESI, m/z) calcd for $\text{C}_{49}\text{H}_{44}\text{FN}_3\text{O}_4\text{Rh}$ $[\text{M}+\text{H}]^+$: 860.2365, found: 860.2357.

5.3.3 Synthesis of Substrates**1) Method A for the synthesis of compound 19a-h**

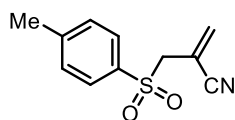
To a mixture of diethyl (cyanomethyl)phosphonate (20 mmol) and a 37% aqueous solution of formaldehyde (80 mmol), a saturated aqueous solution of potassium carbonate (37.5 mmol) was added at room temperature dropwise over 30 min. After stirring for an additional 2 h, the reaction was quenched with saturated aqueous ammonium chloride (20 mL). Afterwards, the reaction mixture was extracted with diethyl ether (3×12.5 mL). The organic layers were combined and dried over sodium sulfate. The solvent was evaporated, and the remaining colorless oil was purified by flash chromatography using pentane/ CH_2Cl_2 (2/1) giving the pure product **19'** as a colorless oil (70% yield).

To a solution of **19'** (14 mmol) in dry ether (20 mL) was added phosphorus(III) bromide (5 mmol) at -10 °C. The temperature was allowed to rise to 20 °C and stirring was continued for 3 h. Water (10 mL) was then added and the mixture was extracted with diethyl ether (3×30 mL). The organic phase

was washed with brine (20 mL), dried with sodium sulfate and concentrated under reduced pressure. The crude product was purified by column chromatography on silica gel (pentane/CH₂Cl₂, 1/1) to give **19''** as a colorless oil (89% yield).

To a solution of **19''** (2.0 mmol) in methanol (5 mL) was added corresponding sodium aryl sulfinate (3.0 mmol). After 2.5 h of reflux, the mixture was concentrated under reduced pressure, the thereby obtained residue was dissolved in EtOAc and the mixture was washed with water, brine, dried with Na₂SO₄, filtered and the filtrate was evaporated and purified by chromatography (EtOAc/*n*-hexane, 1/1) to give corresponding products **19a-h**.

The characteristic data of **19a** are in accord with literature.^{10a} Others are shown below.



2-(Tosylmethyl)acrylonitrile (**19b**)

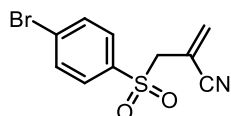
A white solid.

¹H NMR (300 MHz, CDCl₃) δ 7.83-7.76 (m, 2H), 7.43-7.36 (m, 2H), 6.20 (s, 1H), 5.98 (s, 1H), 3.91 (d, J = 0.8 Hz, 2H), 2.46 (s, 3H).

¹³C NMR (75 MHz, CDCl₃) δ 145.9, 139.3, 134.4, 130.1, 128.7, 116.5, 111.6, 59.8, 21.7.

IR (film): ν (cm⁻¹) 2985, 2226, 1315, 1288, 1144, 1084, 975, 813, 772, 676, 608, 580, 524.

HRMS (ESI, m/z) calcd for C₁₁H₁₁NO₂SN_a [M+Na]⁺: 244.0403, found: 244.0398.



2-(((4-Bromophenyl)sulfonyl)methyl)acrylonitrile (**19c**)

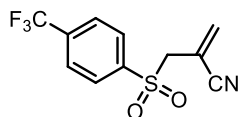
A white solid.

¹H NMR (300 MHz, CDCl₃) δ 8.13-7.85 (m, 4H), 6.26 (s, 1H), 6.05 (s, 1H), 3.98 (d, J = 0.8 Hz, 2H).

¹³C NMR (75 MHz, CDCl₃) δ 139.8, 139.7, 136.3, 132.9, 130.2, 116.4, 111.2, 59.8.

IR (film): ν (cm⁻¹) 2929, 2222, 1569, 1385, 1314, 1281, 1241, 1151, 1130, 1073, 1006, 968, 902, 819, 790, 709, 617, 579.

HRMS (ESI, m/z) calcd for C₁₀H₈NO₂SN_a [M+Na]⁺: 307.9351, found: 307.9347.


2-(((4-(Trifluoromethyl)phenyl)sulfonyl)methyl)acrylonitrile (19d)

A white solid.

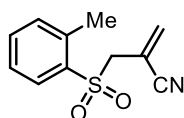
^1H NMR (300 MHz, CDCl_3) δ 8.08 (d, $J = 8.2$ Hz, 2H), 7.89 (d, $J = 8.2$ Hz, 2H), 6.26 (s, 1H), 6.05 (t, $J = 0.8$ Hz, 1H), 3.98 (d, $J = 0.8$ Hz, 2H).

^{13}C NMR (75 MHz, CDCl_3) δ 140.9, 140.0, 136.4 (q, $J = 33.2$ Hz), 129.4, 126.7 (q, $J = 3.6$ Hz), 122.9 (q, $J = 273.2$ Hz), 116.2, 111.0, 59.8.

^{19}F NMR (282 MHz, CDCl_3) δ -63.30 (s, 3F).

IR (film): ν (cm^{-1}) 2986, 2926, 2232, 1406, 1320, 1247, 1161, 1141, 1086, 1060, 1015, 972, 905, 844, 799, 698, 582.

HRMS (ESI, m/z) calcd for $\text{C}_{11}\text{H}_8\text{F}_3\text{NO}_2\text{SNa}$ $[\text{M}+\text{Na}]^+$: 298.0120, found: 298.0114.


2-((o-Tolylsulfonyl)methyl)acrylonitrile (19e)

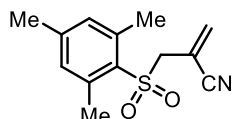
A white solid.

^1H NMR (300 MHz, CDCl_3) δ 7.97 (d, $J = 8.0$ Hz, 1H), 7.62-7.53 (m, 1H), 7.44-7.36 (m, 2H), 6.18 (s, 1H), 6.00 (s, 1H), 3.96 (s, 2H), 2.73 (s, 3H).

^{13}C NMR (75 MHz, CDCl_3) δ 139.3, 138.4, 135.5, 134.6, 133.0, 131.1, 126.8, 116.4, 111.3, 58.9, 20.4.

IR (film): ν (cm^{-1}) 2991, 2936, 2229, 1594, 1454, 1404, 1314, 1285, 1243, 1199, 1153, 1122, 1058, 960, 897, 806, 761, 698, 579.

HRMS (ESI, m/z) calcd for $\text{C}_{11}\text{H}_{11}\text{NO}_2\text{SNa}$ $[\text{M}+\text{Na}]^+$: 244.0403, found: 244.0398.


2-((Mesitylsulfonyl)methyl)acrylonitrile (19f)

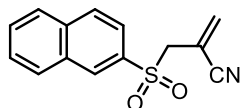
A white solid.

^1H NMR (300 MHz, CDCl_3) δ 7.00 (s, 2H), 6.20 (s, 1H), 6.00 (d, $J = 0.8$ Hz, 1H), 3.92 (d, $J = 0.8$ Hz, 2H), 2.66 (s, 6H), 2.33 (s, 3H).

^{13}C NMR (75 MHz, CDCl_3) δ 144.5, 140.5, 139.0, 132.5, 131.5, 116.6, 111.4, 59.5, 23.0, 21.1.

IR (film): ν (cm^{-1}) 2985, 2220, 1593, 1454, 1308, 3183, 1272, 1143, 971, 670, 605, 572.

HRMS (ESI, m/z) calcd for $\text{C}_{13}\text{H}_{15}\text{NO}_2\text{SNa}$ $[\text{M}+\text{Na}]^+$: 272.0716, found: 272.0710.



2-((Naphthalen-2-ylsulfonyl)methyl)acrylonitrile (19g)

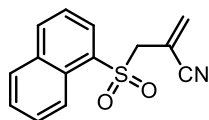
A white solid.

^1H NMR (300 MHz, CDCl_3) δ 8.75 (d, J = 8.4 Hz, 1H), 8.34-8.26 (m, 1H), 8.19 (d, J = 8.2 Hz, 1H), 8.01 (d, J = 8.0 Hz, 1H), 7.82-7.56 (m, 3H), 6.11 (s, 1H), 5.84 (s, 1H), 4.12 (s, 2H).

^{13}C NMR (75 MHz, CDCl_3) δ 139.1, 136.2, 134.2, 132.1, 132.0, 129.5, 129.2, 128.8, 127.2, 124.3, 123.4, 116.2, 111.3, 59.2.

IR (film): ν (cm^{-1}) 2929, 2234, 2186, 1505, 1311, 1256, 1164, 1114, 977, 905, 800, 770, 737, 640, 573, 538, 474.

HRMS (ESI, m/z) calcd for $\text{C}_{14}\text{H}_{11}\text{NO}_2\text{SNa}$ $[\text{M}+\text{Na}]^+$: 280.0403, found: 280.0396.



2-((Naphthalen-1-ylsulfonyl)methyl)acrylonitrile (19h)

A white solid.

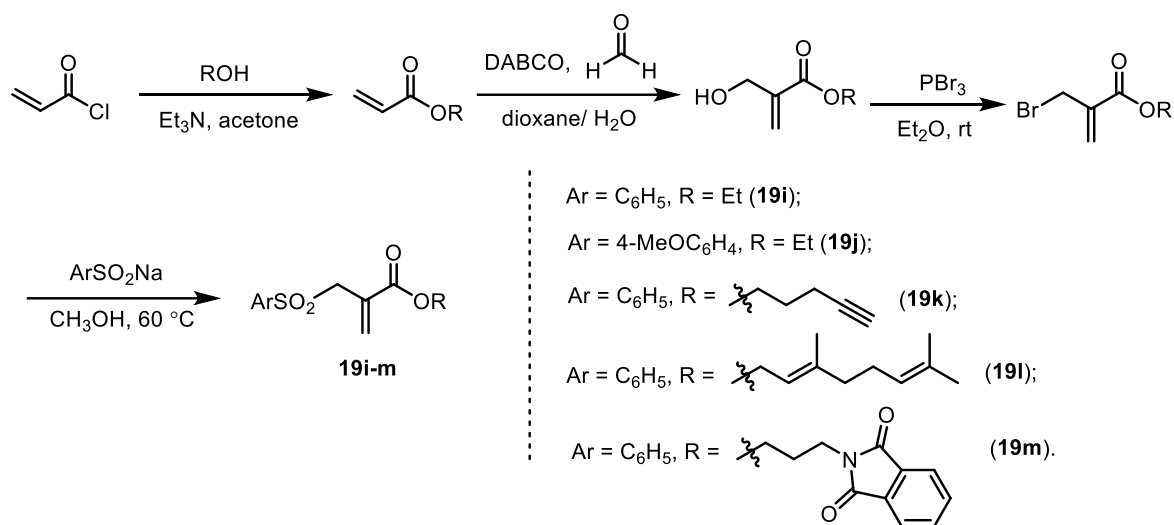
^1H NMR (300 MHz, CDCl_3) δ 8.51 (s, 1H), 8.10-7.84 (m, 4H), 7.77-7.59 (m, 2H), 6.20 (s, 1H), 5.97 (s, 1H), 4.01 (s, 2H).

^{13}C NMR (75 MHz, CDCl_3) δ 139.4, 135.7, 134.2, 132.0, 131.0, 129.9, 129.8, 129.6, 128.1, 128.0, 122.7, 116.5, 111.5, 59.8.

IR (film): ν (cm^{-1}) 2992, 2937, 2229, 1592, 1454, 1403, 1314, 1286, 1242, 1200, 1153, 1123, 1063, 959, 897, 761, 679, 578.

HRMS (ESI, m/z) calcd for $\text{C}_{14}\text{H}_{11}\text{NO}_2\text{SNa}$ $[\text{M}+\text{Na}]^+$: 280.0403, found: 280.0398.

2) Method B for the synthesis of compound 19i-m



To a solution of corresponding alcohol (ROH, 10 mmol) and triethylamine (15 mmol) in acetone (15 mL) was added acryloyl chloride (13 mmol) dropwise at 0 °C. After stirring at 0 °C for 30 min, the reaction mixture was warmed to room temperature and stirred for additional 5 h. The resulting mixture was concentrated, then taken up in EtOAc (50 mL) and washed with brine (3 × 10 mL). The organic extracts were dried over anhydrous Na₂SO₄, concentrated by rotary evaporation. Purification by column chromatography (*n*-hexane/EtOAc, 9/1) afforded the corresponding esters.

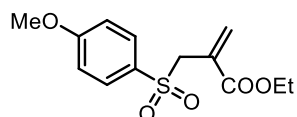
To a solution of a 37% aqueous solution of formaldehyde (7.0 mmol) and ester (5 mmol) in 5 mL 1,4-dioxane-water (1:1, v/v) was added DABCO (7.0 mmol) and the reaction progress was monitored by TLC. Upon completion, the reaction mixture was partitioned with EtOAc (50 mL) and water (20 mL). The organic layer was separated and washed with brine (5 mL), dried over anhydrous Na₂SO₄ and concentrated under reduced pressure. The crude product was purified by column chromatography on silica gel (EtOAc/*n*-hexane, 1/1) to afford corresponding hydroxyl ester.

To a solution of hydroxyl ester (5 mmol) in dry ether (10 mL) was added phosphorus(III) bromide (1.7 mmol) dropwise at −10 °C. The temperature was allowed to rise to 20 °C and stirring was continued for 3 h. Water (20 mL) was then added and the mixture was extracted with diethyl ether (3 × 10 mL). The organic phase was washed with saturated sodium chloride solution (5 mL), dried with sodium sulfate and concentrated under reduced pressure. The crude product was purified by column chromatography on silica gel (pentane/CH₂Cl₂, 1/1) to give corresponding bromo compound.

To a solution of bromo compound (2.0 mmol) in methanol (5 mL) was added corresponding sodium aryl sulfinate (3.0 mmol). After 2.5 h of reflux, the mixture was concentrated under reduced

pressure, the thereby obtained residue was dissolved in EtOAc and the mixture was washed with water, brine, dried with Na₂SO₄, filtered and the filtrate was evaporated and purified by chromatography (EtOAc/*n*-hexane, 1/1) to give corresponding products **19i-m**.

The characteristic data of **19i** are in accord with literature.^{10b} Others are shown below.



Ethyl 2-(((4-methoxyphenyl)sulfonyl)methyl)acrylate (19j)

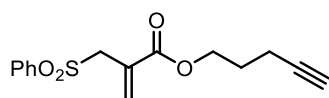
A colorless oil.

¹H NMR (300 MHz, CDCl₃) δ 7.78-7.72 (m, 2H), 7.00-6.94 (m, 2H), 6.47 (s, 1H), 5.88 (s, 1H), 4.12 (s, 2H), 4.03 (q, *J* = 7.1 Hz, 2H), 3.86 (s, 3H), 1.17 (t, *J* = 7.1 Hz, 3H).

¹³C NMR (75 MHz, CDCl₃) δ 164.8, 163.8, 133.0, 130.9, 130.0, 129.4, 114.2, 61.4, 57.7, 55.6, 14.0.

IR (film): ν (cm⁻¹) 2984, 1716, 1591, 1496, 1463, 1413, 1308, 1252, 1187, 1139, 1086, 1020, 962, 899, 837, 778, 670, 526.

HRMS (ESI, *m/z*) calcd for C₁₃H₁₆O₅SNa [M+Na]⁺: 307.0611, found: 307.0604.



Pent-4-yn-1-yl 2-((phenylsulfonyl)methyl)acrylate (19k)

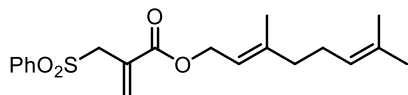
A white solid.

¹H NMR (300 MHz, CDCl₃) δ 7.90-7.84 (m, 2H), 7.68-7.62 (m, 1H), 7.59-7.51 (m, 2H), 6.51 (s, 1H), 5.92 (s, 1H), 4.16 (s, 2H), 4.09 (t, *J* = 6.3 Hz, 2H), 2.24 (td, *J* = 7.0, 2.6 Hz, 2H), 1.98 (t, 2.6 Hz, *J* = 1H), 1.84-1.74 (m, 2H).

¹³C NMR (75 MHz, CDCl₃) δ 164.7, 138.4, 133.9, 133.5, 129.1, 129.0, 128.7, 82.8, 69.1, 64.0, 57.5, 27.4, 15.2.

IR (film): ν (cm⁻¹) 3262, 1705, 1626, 1292, 1245, 1142, 1080, 749, 684, 523, 480.

HRMS (ESI, *m/z*) calcd for C₁₅H₁₆O₄SNa [M+Na]⁺: 315.0662, found: 315.0655.

**(E)-3,7-Dimethylocta-2,6-dien-1-yl 2-((phenylsulfonyl)methyl)acrylate (19l)**

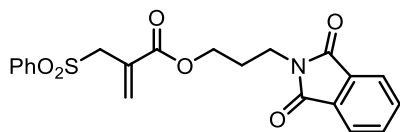
A colorless oil (*contains about 5% of Z-isomer derived from geraniol*).

^1H NMR (300 MHz, CDCl_3) δ 7.90-7.84 (m, 2H), 7.67-7.59 (m, 1H), 7.57-7.49 (m, 2H), 6.51 (s, 1H), 5.94 (s, 1H), 5.25-5.17 (m, 1H), 5.12-5.04 (m, 1H), 4.46 (d, $J = 7.1$ Hz, 2H), 4.16 (s, 2H), 2.13-1.95 (m, 4H), 1.69 (s, 3H), 1.66 (s, 3H), 1.61 (s, 3H).

^{13}C NMR (75 MHz, CDCl_3) δ 164.8, 142.6, 138.5, 133.8, 133.3, 131.9, 129.2, 129.0, 128.8, 123.6, 117.8, 62.4, 57.5, 39.5, 26.3, 25.7, 17.7, 16.5.

IR (film): ν (cm^{-1}) 2926, 1718, 1446, 1385, 1313, 1245, 1182, 1145, 1084, 965, 892, 809, 754, 660, 523.

HRMS (ESI, m/z) calcd for $\text{C}_{20}\text{H}_{26}\text{O}_4\text{SNa}$ $[\text{M}+\text{Na}]^+$: 385.1444, found: 385.1427.

**3-(1,3-Dioxoisindolin-2-yl)propyl 2-((phenylsulfonyl)methyl)acrylate (19m)**

A white solid.

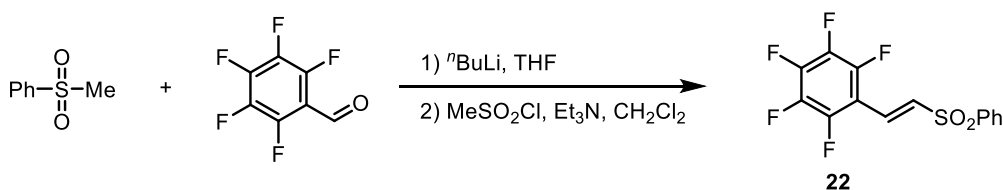
^1H NMR (300 MHz, CDCl_3) δ 7.90-7.82 (m, 4H), 7.77-7.69 (m, 2H), 7.66-7.49 (m, 3H), 6.49 (s, 1H), 5.89 (s, 1H), 4.14 (s, 2H), 4.02 (t, $J = 6.2$ Hz, 2H), 3.76 (t, $J = 6.9$ Hz, 2H), 2.02-1.92 (m, 2H).

^{13}C NMR (75 MHz, CDCl_3) δ 168.2, 164.6, 138.5, 134.1, 133.8, 133.7, 132.0, 129.1, 128.8, 123.3, 62.7, 57.5, 34.8, 27.5.

IR (film): ν (cm^{-1}) 2959, 1707, 1445, 1403, 1375, 1307, 1199, 1161, 1083, 1054, 969, 921, 791, 755, 681, 607, 558.

HRMS (ESI, m/z) calcd for $\text{C}_{21}\text{H}_{19}\text{NO}_6\text{SNa}$ $[\text{M}+\text{Na}]^+$: 436.0825, found: 436.0828.

3) Method C for the synthesis of compound 22



To a solution of methyl phenyl sulfone (1.25 g, 8.0 mmol) in THF (40 mL) cooled at $-78\text{ }^{\circ}\text{C}$, $n\text{-BuLi}$ (1.6 M in n -hexane, 5.5 mL, 8.8 mmol) was added dropwise under argon atmosphere. The resulting solution was stirred at $0\text{ }^{\circ}\text{C}$ for 30 min, and then cooled back to $-78\text{ }^{\circ}\text{C}$. A solution of 2,3,4,5,6-pentafluorobenzaldehyde (1.72g, 8.8 mmol) in THF (2.0 mL) was added dropwise and the temperature was allowed to slowly raise to room temperature, and the solution was stirred until methylphenylsulfone disappeared by TLC. A saturated aqueous solution of NH_4Cl (20 mL) was added, the organic layer was separated and the aqueous layer was extracted with CH_2Cl_2 ($3 \times 10\text{ mL}$). The combined organic layers were dried with Na_2SO_4 and evaporated under reduced pressure.

Without further purification, the resulting alcohol was dissolved in dry CH_2Cl_2 (25 mL) under argon atmosphere, cooled to $0\text{ }^{\circ}\text{C}$, then Et_3N (11.2 mL, 80 mmol) and methanesulfonyl chloride (0.93 mL, 12 mmol) were added continuously. After stirring at room temperature for 90 min, a saturated aqueous solution of NH_4Cl (30 mL) was added, the organic layer was separated and the aqueous layer was extracted with CH_2Cl_2 ($3 \times 15\text{ mL}$). The combined organic layers were dried (Na_2SO_4) and the solvent was evaporated. The residue was purified by flash chromatography (n -hexane/ EtOAc , 5/1) to afford compound **22** (1.73g, 65%) as a white solid.

(E)-1,2,3,4,5-Pentafluoro-6-(2-(phenylsulfonyl)vinyl)benzene (22)

^1H NMR (500 MHz, CDCl_3) δ 7.98-7.92 (m, 2H), 7.73-7.65 (m, 2H), 7.63-7.55 (m, 2H), 7.22 (d, $J = 16.8\text{ Hz}$, 1H).

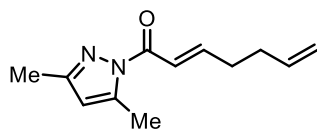
^{13}C NMR (125 MHz, CDCl_3) δ 147.6-147.2 (m), 144.2-143.8 (m), 140.8-140.2 (m), 139.5, 136.4-135.8 (m), 135.5-135.1 (m), 134.0, 129.6, 128.0, 125.9-125.7 (m), 108.4-107.8 (m).

^{19}F NMR (282 MHz, CDCl_3) δ $-138.10 - -138.32$ (m, 2F), $-148.58 - -148.82$ (m, 1F), $-160.56 - -160.84$ (m, 2F).

IR (film): ν (cm^{-1}) 1650, 1495, 1419, 1301, 1146, 1082, 1001, 963, 845, 816, 749, 685, 550.

HRMS (ESI, m/z) calcd for $\text{C}_{14}\text{H}_7\text{F}_5\text{O}_2\text{SNa}$ $[\text{M}+\text{Na}]^+$: 356.9979, found: 356.9970.

4) Others

**(E)-1-(3,5-Dimethyl-1H-pyrazol-1-yl)hepta-2,6-dien-1-one (18d)**

According to the reported procedure,^{10c} compound **18d** was obtained as a colorless liquid.

¹H NMR (300 MHz, CDCl₃) δ 7.40-7.16 (m, 2H), 6.00 (s, 1H), 5.95-5.75 (m, 1H), 5.14-5.00 (m, 2H), 2.60 (s, 3H), 2.51-2.41 (m, 2H), 2.36-2.24 (m, 2H), 2.28 (s, 3H).

¹³C NMR (75 MHz, CDCl₃) δ 165.1, 151.8, 150.4, 144.4, 137.1, 121.5, 115.5, 111.2, 32.2, 32.0, 14.6, 13.8.

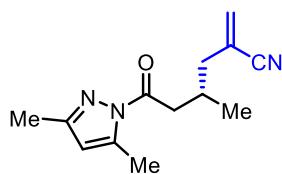
IR (film): ν (cm⁻¹) 2927, 1705, 1639, 1581, 1476, 1411, 1376, 1344, 1294, 1243, 1139, 960, 914, 805, 753, 700, 626, 586, 407.

HRMS (ESI, m/z) calcd for C₁₂H₁₆N₂ONa [M+Na]⁺: 227.1155, found: 227.1155.

Hantzsch esters were synthesized following a reported procedure.^{10d}

5.3.4 Experimental and Characterization Data of Novel Products**01) Table 10, entry 1**

According to the general procedure, the reaction of (*E*)-1-(3,5-dimethyl-1*H*-pyrazol-1-yl)but-2-en-1-one **18a** (32.8 mg, 0.20 mmol), 2-((phenylsulfonyl)methyl)acrylonitrile **19a** (20.8 mg, 0.10 mmol), Δ -**RhO** (6.6 mg, 8.0 mol%), diethyl 2,6-diethyl-1,4-dihydropyridine-3,5-dicarboxylate (42.2 mg, 1.5 equiv) in 1,4-dioxane (1.0 mL, 0.1 M) under nitrogen atmosphere with visible light for 24 hours at room temperature, afforded 19.6 mg (85%) of **20a** as a colorless oil and **21a** (28.2mg, 92%) as a yellow oil.

**(S)-6-(3,5-Dimethyl-1H-pyrazol-1-yl)-4-methyl-2-methylene-6-oxon-hexanenitrile (20a)**

Enantiomeric excess of **20a** was established by HPLC analysis using a Daicel Chiralpak OD-H

column, ee = 96% (HPLC: 254 nm, *n*-hexane/isopropanol = 99:1, flow rate 1.0 mL/min, 40 °C, *t_r* (major) = 6.8 min, *t_r* (minor) = 6.4 min).

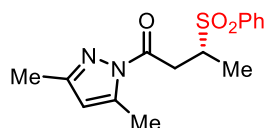
$[\alpha]_{\text{D}}^{22} = +21.1^{\circ}$ (*c* 1.0, CH₂Cl₂).

¹H NMR (300 MHz, CDCl₃) δ 5.95 (s, 1H), 5.91 (s, 1H), 5.78-5.75 (m, 1H), 3.13 (dd, *J* = 16.5, 5.8 Hz, 1H), 2.99 (dd, *J* = 16.5, 7.3 Hz, 1H), 2.54 (s, 3H), 2.52-2.38 (m, 2H), 2.23 (s, 3H), 2.23-2.09 (m, 1H), 1.07 (d, *J* = 6.6 Hz, 3H).

¹³C NMR (75 MHz, CDCl₃) δ 172.4, 152.0, 144.0, 132.0, 121.7, 118.6, 111.2, 41.5, 41.2, 28.5, 19.3, 14.5, 13.8.

IR (film): ν (cm⁻¹) 2965, 2929, 2221, 1722, 1583, 1437, 1379, 1333, 1240, 1171, 1137, 996, 960, 904, 805, 745, 642, 559.

HRMS (ESI, *m/z*) calcd for C₁₃H₁₇N₃ONa [M+Na]⁺: 254.1264, found: 254.1259.



(*R*)-1-(3,5-Dimethyl-1*H*-pyrazol-1-yl)-3-(phenylsulfonyl)butan-1-one (21a)

Enantiomeric excess of **21a** was established by HPLC analysis using a Daicel Chiralpak OD-H column, ee = 85% (HPLC: 254 nm, *n*-hexane/isopropanol = 95:5, flow rate 1.0 mL/min, 40 °C, *t_r* (major) = 12.0 min, *t_r* (minor) = 10.8 min).

$[\alpha]_{\text{D}}^{22} = +47.6^{\circ}$ (*c* 1.0, CH₂Cl₂).

¹H NMR (500 MHz, CDCl₃) δ 7.95-7.91 (m, 2H), 7.68-7.63 (m, 1H), 7.59-7.53 (m, 2H), 5.94 (s, 1H), 3.89-3.82 (m, 1H), 3.76 (dd, *J* = 17.4, 4.4 Hz, 1H), 3.27 (dd, *J* = 17.4, 8.8 Hz, 1H), 2.45 (s, 3H), 2.21 (s, 3H), 1.38 (d, *J* = 6.8 Hz, 3H).

¹³C NMR (125 MHz, CDCl₃) δ 170.0, 152.6, 144.1, 136.9, 133.8, 129.14, 129.12, 111.5, 56.1, 35.8, 14.3, 14.0, 13.8.

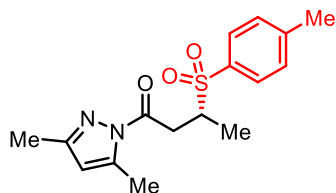
IR (film): ν (cm⁻¹) 2929, 1721, 1585, 1446, 1382, 1304, 1141, 1081, 1030, 986, 961, 911, 814, 757, 728, 688, 582, 547.

HRMS (ESI, *m/z*) calcd for C₁₅H₁₉N₂O₃S [M+H]⁺: 307.1111, found: 307.1107.

02) Table 10, entry 2

According to the general procedure, the reaction of (*E*)-1-(3,5-dimethyl-1*H*-pyrazol-1-yl)

but-2-en-1-one **18a** (32.8 mg, 0.20 mmol), 2-(tosylmethyl)acrylonitrile **19b** (22.1 mg, 0.10 mmol), Δ -**RhO** (6.6 mg, 8.0 mol%), diethyl 2,6-diethyl-1,4-dihydropyridine-3,5-dicarboxylate (42.2 mg, 1.5 equiv) in 1,4-dioxane (1.0 mL, 0.1 M) under nitrogen atmosphere with visible light for 24 hours at room temperature, afforded 16.1 mg (68%) of **20a** as a colorless oil and **21b** (21.4mg, 70%) as a yellow oil. Enantiomeric excess of **20a** was determined as 96% ee.



(R)-1-(3,5-Dimethyl-1H-pyrazol-1-yl)-3-tosylbutan-1-one (21b)

Enantiomeric excess of **21b** was established by HPLC analysis using a Daicel Chiralpak OD-H column, ee = 79% (HPLC: 254 nm, *n*-hexane/ isopropanol = 95:5, flow rate 1.0 mL/min, 40 °C, t_r (major) = 14.8 min, t_r (minor) = 11.0 min). $[\alpha]_D^{22} = +10.8^\circ$ (*c* 1.0, CH₂Cl₂).

¹H NMR (500 MHz, CDCl₃) δ 7.82-7.78 (m, 2H), 7.37-7.33 (m, 2H), 5.94 (s, 1H), 3.86-3.78 (m, 1H), 3.74 (dd, *J* = 17.4, 4.4 Hz, 1H), 3.24 (dd, *J* = 17.4, 8.8 Hz, 1H), 2.45 (s, 3H), 2.44 (s, 3H), 2.21 (s, 3H), 1.37 (d, *J* = 6.8 Hz, 3H).

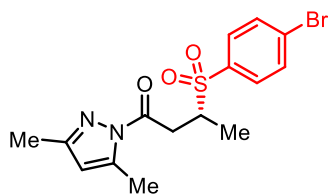
¹³C NMR (125 MHz, CDCl₃) δ 170.1, 152.5, 144.8, 144.1, 133.9, 129.8, 129.1, 111.5, 56.1, 35.9, 21.6, 14.3, 14.0, 13.8.

IR (film): ν (cm⁻¹) 2929, 1721, 1589, 1396, 1330, 1293, 1261, 1139, 1082, 1026, 987, 962, 908, 870, 758, 721, 640, 555.

HRMS (ESI, *m/z*) calcd for C₁₆H₂₀N₂O₃SN_a [M+Na]⁺: 343.1087, found: 343.1080.

03) Table 10, entry 3

According to the general procedure, the reaction of (*E*)-1-(3,5-dimethyl-1H-pyrazol-1-yl) but-2-en-1-one **18a** (32.8 mg, 0.20 mmol), 2-(((4-bromophenyl)sulfonyl)methyl)acrylonitrile **19c** (28.5 mg, 0.10 mmol), Δ -**RhO** (6.6 mg, 8.0 mol%), diethyl 2,6-diethyl-1,4-dihydropyridine-3,5-dicarboxylate (42.2 mg, 1.5 equiv) in 1,4-dioxane (1.0 mL, 0.1 M) under nitrogen atmosphere with visible light for 24 hours at room temperature, afforded 18.9 mg (81%) of **20a** as a colorless oil, and afforded **21c** (33.8 mg, 88%) as a white solid. Enantiomeric excess of **20a** was determined as 97% ee.



(*R*)-3-((4-bromophenyl)sulfonyl)-1-(3,5-dimethyl-1*H*-pyrazol-1-yl)butan-1-one (21c**)**

Enantiomeric excess of **21c** was established by HPLC analysis using a Daicel Chiralpak OD-H column, ee = 80% (HPLC: 254 nm, *n*-hexane/isopropanol = 95:5, flow rate 1.0 mL/min, 40 °C, *t_r* (major) = 12.9 min, *t_r* (minor) = 11.2 min). $[\alpha]_D^{22} = +13.1^\circ$ (*c* 1.0, CH₂Cl₂).

¹H NMR (500 MHz, CDCl₃) δ 7.80-7.76 (m, 2H), 7.71-7.67 (m, 2H), 5.96 (s, 1H), 3.89-3.81 (m, 1H), 3.76 (dd, *J* = 17.4, 4.8 Hz, 1H), 3.24 (dd, *J* = 17.4, 8.4 Hz, 1H), 2.45 (s, 3H), 2.21 (s, 3H), 1.40 (d, *J* = 6.8 Hz, 3H).

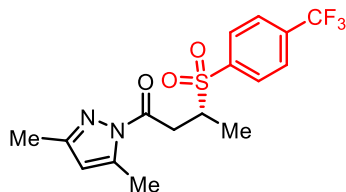
¹³C NMR (125 MHz, CDCl₃) δ 169.7, 152.7, 144.1, 135.9, 132.5, 130.7, 129.3, 111.6, 56.2, 35.8, 14.3, 13.9, 13.8.

IR (film): ν (cm⁻¹) 2981, 1727, 1575, 1446, 1384, 112, 1279, 1134, 1075, 988, 961, 914, 824, 761, 684, 576.

HRMS (ESI, *m/z*) calcd for C₁₅H₁₇BrN₂O₃SNa [M+Na]⁺: 407.0035, found: 407.0024.

04) Table 10, entry 4

According to the general procedure, the reaction of (*E*)-1-(3,5-dimethyl-1*H*-pyrazol-1-yl)but-2-en-1-one **18a** (32.8 mg, 0.20 mmol), 2-(((4-(trifluoromethyl)phenyl)sulfonyl)methyl) acrylonitrile **19d** (22.1 mg, 0.10 mmol), Δ -**RhO** (6.6 mg, 8.0 mol%), diethyl 2,6-diethyl-1,4-dihydropyridine-3,5-dicarboxylate (42.2 mg, 1.5 equiv) in 1,4-dioxane (1.0 mL, 0.1 M) under nitrogen atmosphere with visible light for 24 hours at room temperature, afforded 18.4 mg (78%) of **20a** as a colorless oil, and afforded 29.2 mg (78%) of **21d** as a white solid. Enantiomeric excess of **20a** was determined as 95% ee.



(*R*)-1-(3,5-Dimethyl-1*H*-pyrazol-1-yl)-3-((4-(trifluoromethyl)phenyl)sulfonyl)butan-1-one (21d**)**

Enantiomeric excess of **21d** was established by HPLC analysis using a Daicel Chiralpak OD-H

column, ee = 76% (HPLC: 254 nm, *n*-hexane/isopropanol = 95:5, flow rate 1.0 mL/min, 40 °C, t_r (major) = 10.3 min, t_r (minor) = 9.2 min). A white solid. $[\alpha]_D^{22} = +19.9^\circ$ (*c* 1.0, CH₂Cl₂).

¹H NMR (500 MHz, CDCl₃) δ 8.07 (d, *J* = 8.2 Hz, 2H), 7.82 (d, *J* = 8.2 Hz, 2H), 5.95 (s, 1H), 3.94-3.86 (m, 1H), 3.78 (dd, *J* = 17.4, 4.9 Hz, 1H), 3.24 (dd, *J* = 17.4, 8.3 Hz, 1H), 2.43 (s, 3H), 2.20 (s, 3H), 1.42 (d, *J* = 6.9 Hz, 3H).

¹³C NMR (125 MHz, CDCl₃) δ 169.6, 152.7, 144.2, 140.6, 135.5 (q, *J* = 33.2 Hz), 129.8, 126.2 (q, *J* = 3.6 Hz), 124.2, 123.0 (q, *J* = 273.2 Hz), 111.7, 56.2, 35.8, 14.2, 13.9, 13.8.

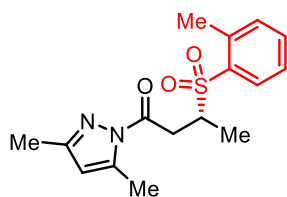
¹⁹F NMR (282 MHz, CDCl₃) δ -63.3 (s, 3F).

IR (film): ν (cm⁻¹) 2965, 1725, 1584, 1451, 1378, 1317, 1166, 1060, 1036, 984, 960, 890, 844, 743, 677, 545.

HRMS (ESI, *m/z*) calcd for C₁₆H₁₇F₃N₂O₃SNa [M+Na]⁺: 397.0804, found: 397.0794.

05) Table 10, entry 5

According to the general procedure, the reaction of (*E*)-1-(3,5-dimethyl-1*H*-pyrazol-1-yl)but-2-en-1-one **18a** (32.8 mg, 0.20 mmol), 2-((*o*-tolylsulfonyl)methyl)acrylonitrile **19e** (22.1 mg, 0.10 mmol), Δ -**RhO** (6.6 mg, 8.0 mol%), diethyl 2,6-diethyl-1,4-dihydropyridine-3,5-dicarboxylate (42.2 mg, 1.5 equiv) in 1,4-dioxane (1.0 mL, 0.1 M) under nitrogen atmosphere with visible light for 24 hours at room temperature, afforded 16.8 mg (71%) of **20a** as a colorless oil, and afforded 23.0 mg (72%) of **21e** as a yellow oil. Enantiomeric excess of **20a** was determined as 95% ee.



(*R*)-1-(3,5-Mimethyl-1*H*-pyrazol-1-yl)-3-(*o*-tolylsulfonyl)butan-1-one (**21e**)

Enantiomeric excess of **21e** was established by HPLC analysis using a Daicel Chiralpak OD-H column, ee = 86% (HPLC: 254 nm, *n*-hexane/isopropanol = 95:5, flow rate 1.0 mL/min, 40 °C, t_r (major) = 12.2 min, t_r (minor) = 10.8 min). $[\alpha]_D^{22} = +15.4^\circ$ (*c* 1.0, CH₂Cl₂).

¹H NMR (500 MHz, CDCl₃) δ 7.99 (d, *J* = 7.9 Hz, 1H), 7.51-7.47 (m, 1H), 7.35-7.29 (m, 2H), 5.93 (s, 1H), 3.99-3.91 (m, 1H), 3.75 (dd, *J* = 17.4, 4.4 Hz, 1H), 3.27 (dd, *J* = 17.4, 8.6 Hz, 1H), 2.73 (s, 3H), 2.43 (s, 3H), 2.20 (s, 3H), 1.40 (d, *J* = 6.8 Hz, 3H).

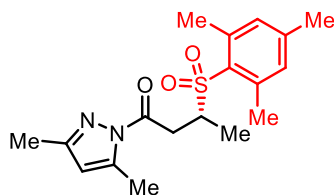
^{13}C NMR (125 MHz, CDCl_3) δ 170.1, 152.5, 144.0, 138.9, 135.2, 133.7, 132.8, 131.3, 126.3, 111.5, 54.8, 35.7, 20.5, 14.3, 13.7, 13.4.

IR (film): ν (cm^{-1}) 2981, 1722, 1586, 1452, 1382, 1308, 1144, 1031, 986, 961, 807, 758, 662, 554.

HRMS (ESI, m/z) calcd for $\text{C}_{16}\text{H}_{20}\text{N}_2\text{O}_3\text{SNa}$ $[\text{M}+\text{Na}]^+$: 343.1087, found: 343.1080.

06) Table 10, entry 6

According to the general procedure, the reaction of (*E*)-1-(3,5-dimethyl-1*H*-pyrazol-1-yl)but-2-en-1-one **18a** (32.8 mg, 0.20 mmol), 2-((mesitylsulfonyl)methyl)acrylonitrile **19f** (24.9 mg, 0.10 mmol), Δ -**RhO** (6.6 mg, 8.0 mol%), diethyl 2,6-diethyl-1,4-dihydropyridine-3,5-dicarboxylate (42.2 mg, 1.5 equiv) in 1,4-dioxane (1.0 mL, 0.1 M) under nitrogen atmosphere with visible light for 24 hours at 35 °C, afforded 13.5 mg (57%) of **20a** as a colorless oil, and afforded 20.9 mg (60%) of **21f** as a yellow oil. Enantiomeric excess of **20a** was determined as 94% ee.



(*R*)-1-(3,5-Dimethyl-1*H*-pyrazol-1-yl)-3-(mesitylsulfonyl)butan-1-one (**21f**)

Enantiomeric excess of **21f** was established by HPLC analysis using a Daicel Chiralpak IA column, ee = 89% (HPLC: 254 nm, *n*-hexane/isopropanol = 95:5, flow rate 1.0 mL/min, 40 °C, t_r (major) = 9.6 min, t_r (minor) = 10.9 min). $[\alpha]_D^{22} = -28.4^\circ$ (c 0.10, CH_2Cl_2).

^1H NMR (500 MHz, CDCl_3) δ 6.93 (s, 2H), 5.93 (s, 1H), 3.97-3.89 (m, 1H), 3.78 (dd, $J = 17.0, 4.6$ Hz, 1H), 3.27 (dd, $J = 17.0, 8.6$ Hz, 1H), 2.68 (s, 6H), 2.43 (s, 3H), 2.28 (s, 3H), 2.19 (s, 3H), 1.41 (d, $J = 6.9$ Hz, 3H).

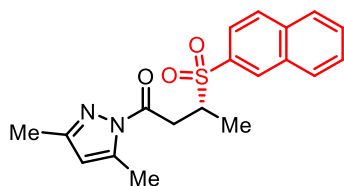
^{13}C NMR (125 MHz, CDCl_3) δ 170.3, 152.4, 144.0, 143.3, 140.8, 132.3, 131.1, 111.4, 55.4, 35.4, 23.0, 21.0, 14.3, 13.7, 13.2.

IR (film): ν (cm^{-1}) 2959, 1718, 1591, 1449, 1416, 1378, 1306, 1262, 1134, 1101, 1023, 962, 799, 749, 728, 681, 642, 569.

HRMS (ESI, m/z) calcd for $\text{C}_{18}\text{H}_{25}\text{N}_2\text{O}_3\text{S}$ $[\text{M}+\text{H}]^+$: 349.1580, found: 349.1573.

07) Table 10, entry 7

According to the general procedure, the reaction of (*E*)-1-(3,5-dimethyl-1*H*-pyrazol-1-yl)but-2-en-1-one **18a** (32.8 mg, 0.20 mmol), ethyl 2-((naphthalen-2-ylsulfonyl)methyl)acrylonitrile **19g** (25.7 mg, 0.10 mmol), Δ -**RhO** (6.6 mg, 8.0 mol%), diethyl 2,6-diethyl-1,4-dihydropyridine-3,5-dicarboxylate (42.2 mg, 1.5 equiv) in 1,4-dioxane (1.0 mL, 0.1 M) under nitrogen atmosphere with visible light for 24 hours at 35 °C, afforded 19.4 mg (82%) of **20a** as a colorless oil, and afforded 31.3 mg (88%) of **21g** as a yellow oil. Enantiomeric excess of **20a** was determined as 94% ee.

**(*R*)-1-(3,5-Dimethyl-1*H*-pyrazol-1-yl)-3-(naphthalen-2-ylsulfonyl)butan-1-one (**21g**)**

Enantiomeric excess of **21g** was established by HPLC analysis using a Daicel Chiralpak OD-H column, ee = 83% (HPLC: 254 nm, *n*-hexane/isopropanol = 95:5, flow rate 1.0 mL/min, 40 °C, *t_r* (major) = 13.5 min, *t_r* (minor) = 14.3 min). $[\alpha]_D^{22} = +39.2^\circ$ (*c* 1.0, CH₂Cl₂)

¹H NMR (300 MHz, CDCl₃) δ 8.80 (d, *J* = 8.6 Hz, 1H), 8.31 (d, *J* = 7.3 Hz, 1H), 8.11 (d, *J* = 8.2 Hz, 1H), 7.95 (d, *J* = 8.2 Hz, 1H), 7.75-7.53 (m, 3H), 5.89 (s, 1H), 4.22-4.08 (m, 1H), 3.82 (dd, *J* = 17.2, 4.4 Hz, 1H), 3.34 (dd, *J* = 17.2, 8.8 Hz, 1H), 2.39 (s, 3H), 2.14 (s, 3H), 1.39 (d, *J* = 6.8 Hz, 3H).

¹³C NMR (75 MHz, CDCl₃) δ 170.0, 152.4, 144.0, 135.3, 134.3, 132.2, 131.8, 129.3, 129.1, 128.7, 127.0, 124.5, 124.2, 111.4, 55.6, 35.8, 14.2, 13.8, 13.6.

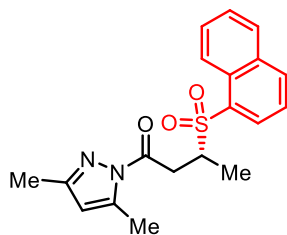
IR (film): ν (cm⁻¹) 2937, 1722, 1586, 1385, 1313, 1269, 1188, 1151, 1122, 964, 886, 805, 771, 742, 707, 663, 592.

HRMS (ESI, *m/z*) calcd for C₁₉H₂₀N₂O₃SNa [M+Na]⁺: 379.1087, found: 379.1078.

08) Table 10, entry 8

According to the general procedure, the reaction of (*E*)-1-(3,5-dimethyl-1*H*-pyrazol-1-yl)but-2-en-1-one **18a** (32.8 mg, 0.20 mmol), ethyl 1-((naphthalen-2-ylsulfonyl)methyl)acrylonitrile **19h** (25.7 mg, 0.10 mmol), Δ -**RhO** (6.6 mg, 8.0 mol%), diethyl 2,6-diethyl-1,4-dihydropyridine-3,5-dicarboxylate (42.2 mg, 1.5 equiv) in 1,4-dioxane (1.0 mL, 0.1 M) under nitrogen atmosphere with visible light for 24 hours at 35 °C, afforded 18.4 mg (78%) of **20a** as a colorless oil, and afforded 29.9

mg (84%) of **21h** as a yellow oil. Enantiomeric excess of **20a** was determined as 91% ee.



(R)-1-(3,5-Dimethyl-1H-pyrazol-1-yl)-3-(naphthalen-1-ylsulfonyl)butan-1-one (21h)

Enantiomeric excess of **21h** was established by HPLC analysis using a Daicel Chiralpak OD-H column, ee = 80% (HPLC: 254 nm, *n*-hexane/isopropanol = 95:5, flow rate 1.0 mL/min, 40 °C, *t_r* (major) = 18.7 min, *t_r* (minor) = 16.5 min. $[\alpha]_D^{22} = +15.6^\circ$ (*c* 1.0, CH₂Cl₂).

¹H NMR (300 MHz, CDCl₃) δ 8.50 (s, 1H), 8.03-7.87 (m, 4H), 7.71-7.57 (m, 2H), 5.88 (s, 1H), 4.02-3.88 (m, 1H), 3.84 (dd, *J* = 17.4, 4.6 Hz, 1H), 3.27 (dd, *J* = 17.4, 8.4 Hz, 1H), 2.36 (s, 3H), 2.19 (s, 3H), 1.43 (d, *J* = 6.8 Hz, 3H).

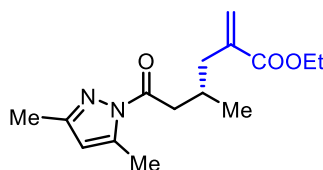
¹³C NMR (75 MHz, CDCl₃) δ 170.0, 152.5, 144.0, 135.4, 134.0, 132.1, 131.1, 129.4, 129.34, 129.30, 127.9, 127.6, 123.6, 111.5, 56.2, 36.0, 14.1, 14.0, 13.7.

IR (film): ν (cm⁻¹) 2924, 1721, 1586, 1451, 1382, 1305, 1122, 1073, 1029, 985, 961, 910, 862, 815, 752, 703, 644, 553, 474.

HRMS (ESI, *m/z*) calcd for C₁₉H₂₁N₂O₃S [M+H]⁺: 357.1267, found: 357.1259.

09) Table 10, entry 9

According to the general procedure, the reaction of (*E*)-1-(3,5-dimethyl-1H-pyrazol-1-yl)but-2-en-1-one **18a** (32.8 mg, 0.20 mmol), ethyl 2-((phenylsulfonyl)methyl)acrylate **19i** (25.4 mg, 0.10 mmol), Δ -**RhO** (6.6 mg, 8.0 mol%), diethyl 2,6-diethyl-1,4-dihydropyridine-3,5-dicarboxylate (42.2 mg, 1.5 equiv) in 1,4-dioxane (1.0 mL, 0.1 M) under nitrogen atmosphere with visible light for 24 hours at room temperature, afforded 18.3 mg (65%) of **20b** as a colorless oil, and afforded 20.8 mg (68%) of **21a** as a yellow oil. Enantiomeric excess of **21a** was determined as 84% ee.



Ethyl (*S*)-6-(3,5-dimethyl-1H-pyrazol-1-yl)-4-methyl-2-methylene-6-oxohexanoate (20b)

Enantiomeric excess of **20b** was established by HPLC analysis using a Daicel Chiralcel OJ-H column, ee = 94% (HPLC: 254 nm, *n*-hexane/isopropanol = 99:1, flow rate 1.0 mL/min, 25 °C, *t_r* (major) = 6.9 min, *t_r* (minor) = 7.6 min). $[\alpha]_{\text{D}}^{22} = +14.2^\circ$ (*c* 1.0, CH₂Cl₂).

¹H NMR (300 MHz, CDCl₃) δ 6.19 (d, *J* = 1.6 Hz, 1H), 5.93 (s, 1H), 5.57-5.53 (m, 1H), 4.19 (q, *J* = 7.2 Hz, 2H), 3.11 (dd, *J* = 16.4, 5.2 Hz, 1H), 2.93 (dd, *J* = 16.4, 7.4 Hz, 1H), 2.53 (s, 3H), 2.47-2.29 (m, 3H), 2.22 (s, 3H), 1.29 (t, *J* = 7.2 Hz, 3H), 1.00 (d, *J* = 6.4 Hz, 3H).

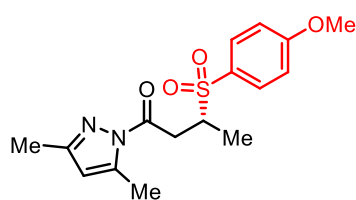
¹³C NMR (75 MHz, CDCl₃) δ 173.2, 167.2, 151.6, 144.0, 139.2, 126.2, 110.9, 60.6, 41.7, 39.1, 28.8, 19.8, 14.6, 14.2, 13.8.

IR (film): ν (cm⁻¹) 2967, 1718, 1630, 1583, 1440, 1409, 1377, 1329, 1242, 1185, 1148, 1025, 994, 959, 807, 746, 684, 553.

HRMS (ESI, *m/z*) calcd for C₁₅H₂₂N₂O₃Na [M+Na]⁺: 301.1523, found: 301.1527.

10) Table 10, entry 10

According to the general procedure, the reaction of (*E*)-1-(3,5-dimethyl-1*H*-pyrazol-1-yl)but-2-en-1-one **18a** (32.8 mg, 0.20 mmol), ethyl 2-(((4-methoxyphenyl)sulfonyl)methyl)acrylate **19j** (28.4 mg, 0.10 mmol), Δ -**RhO** (6.6 mg, 8.0 mol%), diethyl 2,6-diethyl-1,4-dihydropyridine-3,5-dicarboxylate (42.2 mg, 1.5 equiv) in 1,4-dioxane (1.0 mL, 0.1 M) under nitrogen atmosphere with visible light for 24 hours at 35 °C, afforded 18.3 mg (65%) of **20b** as a colorless oil, and afforded 21.2 mg (63%) of **21i** as a yellow oil. Enantiomeric excess of **20b** was determined as 92% ee.



(*R*)-1-(3,5-Dimethyl-1*H*-pyrazol-1-yl)-3-((4-methoxyphenyl)sulfonyl)butan-1-one (**21i**)

Enantiomeric excess of **21i** was established by HPLC analysis using a Daicel Chiralpak OD-H column, ee = 81% (HPLC: 254 nm, *n*-hexane/isopropanol = 90:10, flow rate 1.0 mL/min, 40 °C, *t_r* (major) = 14.4 min, *t_r* (minor) = 11.9 min). $[\alpha]_{\text{D}}^{22} = +10.0^\circ$ (*c* 1.0, CH₂Cl₂).

¹H NMR (500 MHz, CDCl₃) δ 7.87-7.81 (m, 2H), 7.03-7.67 (m, 2H), 5.94 (s, 1H), 3.88 (s, 3H), 3.85-3.71 (m, 2H), 3.27 (dd, *J* = 17.4, 8.8 Hz, 1H), 2.46 (s, 3H), 2.21 (s, 3H), 1.37 (d, *J* = 6.8 Hz, 3H).

¹³C NMR (125 MHz, CDCl₃) δ 170.1, 163.8, 152.5, 144.1, 131.3, 128.3, 114.3, 111.5, 56.3, 55.7, 36.0,

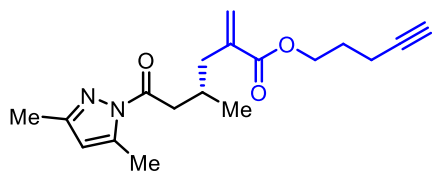
14.3, 14.1, 13.8.

IR (film): ν (cm⁻¹) 2922, 1716, 1587, 1457, 1372, 1310, 1264, 1130, 1080, 1020, 960, 842, 411, 758, 562.

HRMS (ESI, m/z) calcd for C₁₆H₂₀N₂O₄SNa [M+Na]⁺: 359.1036, found: 359.1027.

11) Table 10, entry 11

According to the general procedure, the reaction of (*E*)-1-(3,5-dimethyl-1H-pyrazol-1-yl)but-2-en-1-one **18a** (32.8 mg, 0.20 mmol), ethyl hex-4-yn-1-yl 2-((phenylsulfonyl)methyl)acrylate **19k** (30.6 mg, 0.10 mmol), Δ -**RhO** (6.6 mg, 8.0 mol%), diethyl 2,6-diethyl-1,4-dihydropyridine-3,5-dicarboxylate (42.2 mg, 1.5 equiv) in 1,4-dioxane (1.0 mL, 0.1 M) under nitrogen atmosphere with visible light for 24 hours at 35 °C, afforded 19.0 mg (60%) of **20c** as a colorless oil, and afforded 21.1 mg (69%) of **21a** as a yellow oil. Enantiomeric excess of **21a** was determined as 82% ee.



(*S*)-Pent-4-yn-1-yl-6-(3,5-dimethyl-1H-pyrazol-1-yl)-4-methyl-2-methylene-6-oxohexanoate (**20c**)

Enantiomeric excess of **20c** was established by HPLC analysis using a Daicel Chiralcel OJ-H column, ee = 92% (HPLC: 254 nm, *n*-hexane/isopropanol = 98:2, flow rate 1.0 mL/min, 25 °C, t_r (major) = 10.0 min, t_r (minor) = 11.8 min). $[\alpha]_D^{22} = +10.4^\circ$ (c 1.0, CH₂Cl₂).

¹H NMR (500 MHz, CDCl₃) δ 6.20 (d, J = 1.4 Hz, 1H), 5.94 (s, 1H), 5.59-5.56 (m, 1H), 4.24 (t, J = 6.3 Hz, 2H), 3.11 (dd, J = 16.4, 5.4 Hz, 1H), 2.94 (dd, J = 16.4, 7.4 Hz, 1H), 2.53 (s, 3H), 2.47-2.36 (m, 2H), 2.31 (td, J = 6.8, 2.6 Hz, 3H), 2.23 (s, 3H), 1.97 (t, J = 2.6 Hz, 1H), 1.96-1.87 (m, 2H), 1.00 (d, J = 6.4 Hz, 3H).

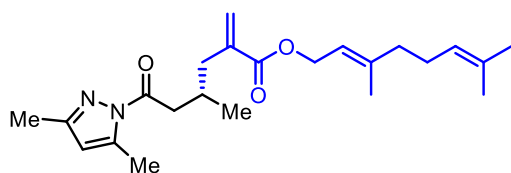
¹³C NMR (125 MHz, CDCl₃) δ 173.1, 167.0, 151.7, 144.0, 138.9, 126.6, 111.0, 83.1, 69.0, 63.2, 41.6, 39.1, 28.7, 27.5, 19.8, 15.3, 14.6, 13.8.

IR (film): ν (cm⁻¹) 3296, 2960, 2928, 1718, 1629, 1583, 1438, 1409, 1379, 1330, 1244, 1182, 1149, 1077, 996, 959, 809, 726, 637, 523.

HRMS (ESI, m/z) calcd for C₁₈H₂₄N₂O₃Na [M+Na]⁺: 339.1679, found: 339.1673.

12) Table 10, entry 12

According to the general procedure, the reaction of (*E*)-1-(3,5-dimethyl-1*H*-pyrazol-1-yl)but-2-en-1-one **18a** (32.8 mg, 0.20 mmol), (*E*)-3,7-dimethylocta-2,6-dien-1-yl 2-((phenylsulfonyl)methyl)acrylate **19l** (contains about 5% of *Z*-isomer derived from geraniol, 36.2 mg, 0.10 mmol), Δ -**RhO** (6.6 mg, 8.0 mol%), diethyl 2,6-diethyl-1,4-dihydropyridine-3,5-dicarboxylate (42.2 mg, 1.5 equiv) in 1,4-dioxane (1.0 mL, 0.1 M) under nitrogen atmosphere with visible light for 24 hours at 35 °C, afforded 23.9 mg (62%) of **20d** as a colorless oil, and afforded 22.0 mg (72%) of **21a** as a yellow oil. Enantiomeric excess of **21a** was determined as 83% ee.



(*E*)-3,7-Dimethylocta-2,6-dien-1-yl (S)-6-(3,5-dimethyl-1*H*-pyrazol-1-yl)-4-methyl-2-methylene-6-oxohexanoate (20d)

Enantiomeric excess of **20d** was established by HPLC analysis using a Daicel Chiralpak IG column, ee = 92% (HPLC: 254 nm, *n*-hexane/isopropanol = 99.1:0.9, flow rate 1.0 mL/min, 25 °C, t_r (major) = 12.4 min, t_r (minor) = 13.3 min). $[\alpha]_D^{22} = +15.7^\circ$ (*c* 1.0, CH₂Cl₂).

¹H NMR (500 MHz, CDCl₃) δ 6.20 (d, *J* = 1.4 Hz, 1H), 5.94 (s, 1H), 5.58-5.55 (m, 1H), 5.40-5.34 (m, 1H), 5.11-5.05 (m, 1H), 4.66 (d, 7.0 Hz, 2H), 3.11 (dd, *J* = 16.4, 5.4 Hz, 1H), 2.94 (dd, *J* = 16.4, 7.8 Hz, 1H), 2.53 (s, 3H), 2.47-2.29 (m, 3H), 2.22 (s, 3H), 2.13-2.01 (m, 4H), 1.71 (s, 3H), 1.67 (s, 3H), 1.60 (s, 3H), 1.00 (d, *J* = 6.4 Hz, 3H).

¹³C NMR (125 MHz, CDCl₃) δ 173.2, 167.2, 151.6, 144.0, 142.0, 139.1, 131.8, 126.3, 123.8, 118.4, 111.0, 61.7, 41.6, 39.5, 39.1, 28.7, 26.3, 25.7, 19.9, 17.7, 16.5, 14.6, 13.8.

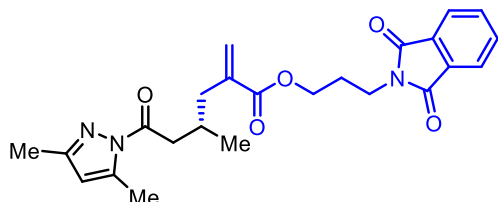
IR (film): ν (cm⁻¹) 3298, 3172, 2963, 2925, 2873, 1633, 1598, 1519, 1462, 1381, 1316, 1244, 1158, 1079, 1005, 956, 870, 770, 661, 544.

HRMS (ESI, *m/z*) calcd for C₂₃H₃₄N₂O₃Na [M+Na]⁺: 409.2462, found: 409.2454.

13) Table 10, entry 13

According to the general procedure, the reaction of (*E*)-1-(3,5-dimethyl-1*H*-pyrazol-1-yl)but-2-en-1-one **18a** (32.8 mg, 0.20 mmol), 3-(1,3-dioxoisindolin-2-yl)propyl 2-((phenylsulfonyl)

methyl)acrylate **19m** (41.3 mg, 0.10 mmol), Δ -**RhO** (6.6 mg, 8.0 mol%), diethyl 2,6-diethyl-1,4-dihydropyridine-3,5-dicarboxylate (42.2 mg, 1.5 equiv) in 1,4-dioxane (1.0 mL, 0.1 M) under nitrogen atmosphere with visible light for 24 hours at 35 °C, afforded 31.9 mg (73%) of **20e** as a colorless oil, and afforded 23.9 mg (78%) of **21a** as a yellow oil. Enantiomeric excess of **21a** was determined as 82% ee



(S)-3-(1,3-Dioxoisindolin-2-yl)propyl 6-(3,5-dimethyl-1H-pyrazol-1-yl)-4-methyl-2-methylene-6-oxohexanoate (20e)

Enantiomeric excess of **20e** was established by HPLC analysis using a Daicel Chiralcel OJ-H column, ee = 92% (HPLC: 254 nm, *n*-hexane/isopropanol = 80:20, flow rate 1.0 mL/min, 25 °C, t_r (major) = 17.4 min, t_r (minor) = 20.5 min). $[\alpha]_D^{22} = +13.7^\circ$ (*c* 1.0, CH₂Cl₂).

¹H NMR (500 MHz, CDCl₃) δ 7.84-7.80 (m, 2H), 7.72-7.68 (m, 2H), 6.17 (s, 1H), 5.92 (s, 1H), 5.55 (s, 1H), 4.17 (t, *J* = 6.2 Hz, 2H), 3.82 (t, *J* = 6.9 Hz, 2H), 3.10 (dd, *J* = 16.4, 5.4 Hz, 1H), 2.92 (dd, *J* = 16.4, 7.7 Hz, 1H), 2.51 (s, 3H), 2.45-2.33 (m, 2H), 2.32-2.26 (m, 1H), 2.21 (s, 3H), 2.11-2.04 (m, 2H), 0.99 (d, *J* = 6.4 Hz, 3H).

¹³C NMR (125 MHz, CDCl₃) δ 173.1, 168.2, 166.9, 151.6, 143.9, 138.7, 133.9, 132.0, 126.7, 123.2, 110.9, 62.0, 41.6, 39.0, 35.1, 28.7, 27.6, 19.8, 14.6, 13.8.

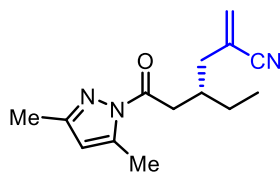
IR (film): ν (cm⁻¹) 2959, 2928, 1772, 1709, 1583, 1439, 1377, 1330, 1244, 1182, 1148, 1080, 1046, 959, 805, 747, 528.

HRMS (ESI, *m/z*) calcd for C₂₄H₂₇N₃O₅Na [M+Na]⁺: 460.1843, found: 460.1832.

14) Figure 48a, reaction of 18b

According to the general procedure, the reaction of (*E*)-1-(3,5-dimethyl-1H-pyrazol-1-yl)pent-2-en-1-one **18b** (35.6 mg, 0.20 mmol), 2-((phenylsulfonyl)methyl)acrylonitrile **19a** (20.8 mg, 0.10 mmol), Δ -**RhO** (6.6 mg, 8.0 mol%), diethyl 2,6-diethyl-1,4-dihydropyridine-3,5-dicarboxylate (42.2 mg, 1.5 equiv) in 1,4-dioxane (1.0 mL, 0.1 M) under nitrogen atmosphere with visible light for 48 hours at room temperature, afforded 20.1 mg (82%) of **20f** as a colorless oil, and afforded 27.2 mg

(85%) of **21j** as a yellow oil.



(S)-6-(3,5-Dimethyl-1H-pyrazol-1-yl)-4-ethyl-2-methylene-6-oxohexanenitrile (20f)

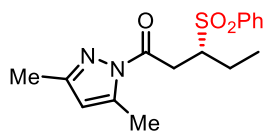
Enantiomeric excess of **20f** was established by HPLC analysis using a Daicel Chiralpak OD-H column, ee = 87% (HPLC: 254 nm, *n*-hexane/isopropanol = 99:1, flow rate 1.0 mL/min, 40 °C, *t_r* (major) = 6.8 min, *t_r* (minor) = 8.5 min). $[\alpha]_D^{22} = +4.0^\circ$ (*c* 1.0, CH₂Cl₂).

¹H NMR (500 MHz, CDCl₃) δ 5.96 (s, 1H), 5.90 (s, 1H), 5.77-5.75 (m, 1H), 3.14-3.04 (m, 2H), 2.53 (s, 3H), 2.38-2.31 (m, 3H), 2.23 (s, 3H), 1.55-1.43 (m, 2H), 0.95 (t, *J* = 7.4 Hz, 3H).

¹³C NMR (125 MHz, CDCl₃) δ 172.7, 151.9, 144.0, 132.1, 121.7, 118.7, 111.2, 38.7, 38.1, 34.6, 25.9, 14.6, 13.8, 10.8.

IR (film): ν (cm⁻¹) 2925, 2221, 1721, 1643, 1583, 1380, 1341, 1271, 1017, 959, 806, 745, 686, 578.

HRMS (ESI, *m/z*) calcd for C₁₄H₁₉N₃ONa [M+Na]⁺: 268.1420, found: 268.1417.



(R)-1-(3,5-Dimethyl-1H-pyrazol-1-yl)-3-(phenylsulfonyl)pentan-1-one (21j)

Enantiomeric excess of **21j** was established by HPLC analysis using a Daicel Chiralpak OD-H column, ee = 87% (HPLC: 254 nm, *n*-hexane/isopropanol = 95:5, flow rate 1.0 mL/min, 40 °C, *t_r* (major) = 12.6 min, *t_r* (minor) = 11.8 min). $[\alpha]_D^{22} = -4.2^\circ$ (*c* 1.0, CH₂Cl₂).

¹H NMR (500 MHz, CDCl₃) δ 7.94-7.90 (m, 2H), 7.65-7.61 (m, 1H), 7.56-7.50 (m, 2H), 5.94 (s, 1H), 3.85-3.79 (m, 1H), 3.77 (dd, *J* = 17.6, 6.3 Hz, 1H), 3.28 (dd, *J* = 17.6, 5.8 Hz, 1H), 2.43 (s, 3H), 2.22 (s, 3H), 2.11-2.01 (m, 1H), 1.72-1.62 (m, 1H), 1.02 (t, *J* = 7.4 Hz, 3H).

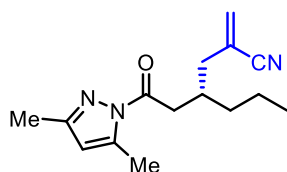
¹³C NMR (125 MHz, CDCl₃) δ 170.2, 152.4, 144.2, 137.6, 133.7, 129.1, 129.0, 111.5, 61.6, 33.7, 21.8, 14.3, 13.8, 11.2.

IR (film): ν (cm⁻¹) 2969, 2931, 1720, 1586, 1447, 1409, 1379, 1298, 1262, 1141, 1081, 959, 629, 693, 595, 563.

HRMS (ESI, *m/z*) calcd for C₁₆H₂₀N₂O₃SNa [M+Na]⁺: 343.1087, found: 343.1079.

15) Figure 48a, reaction of 18c

According to the general procedure, the reaction of (*E*)-1-(3,5-dimethyl-1*H*-pyrazol-1-yl)hex-2-en-1-one **18c** (38.5 mg, 0.20 mmol), 2-((phenylsulfonyl)methyl)acrylonitrile **19a** (20.8 mg, 0.10 mmol), Δ -**RhO** (6.6 mg, 8.0 mol%), diethyl 2,6-diethyl-1,4-dihydropyridine-3,5-dicarboxylate (42.2 mg, 1.5 equiv) in 1,4-dioxane (1.0 mL, 0.1 M) under nitrogen atmosphere with visible light for 40 hours at 35 °C, afforded 20.3 mg (78%) of **20g** as a colorless oil, and afforded 26.7 mg (80%) of **21k** as a yellow oil.

**(*S*)-6-(3,5-Dimethyl-1*H*-pyrazol-1-yl)-2-oxoethyl-2-methyleneheptanenitrile (**20g**)**

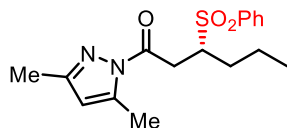
Enantiomeric excess of **20g** was established by HPLC analysis using a Daicel Chiralpak OD-H column, ee = 77% (HPLC: OD-H, 254 nm, *n*-hexane/isopropanol = 99:1, flow rate 1.0 mL/min, 40 °C, t_r (major) = 6.2 min, t_r (minor) = 5.5 min). $[\alpha]_D^{22} = +11.8^\circ$ (*c* 1.0, CH₂Cl₂).

¹H NMR (300 MHz, CDCl₃) δ 5.95 (s, 1H), 5.89 (s, 1H), 5.74 (s, 1H), 3.16-3.00 (m, 2H), 2.53 (s, 3H), 2.46-2.30 (m, 3H), 2.23 (s, 3H), 1.49-1.35 (m, 4H), 0.91 (t, *J* = 7.2 Hz, 3H).

¹³C NMR (75 MHz, CDCl₃) δ 172.7, 151.9, 144.0, 132.0, 121.8, 118.7, 111.2, 39.1, 38.6, 35.6, 33.0, 19.7, 14.5, 14.1, 13.8.

IR (film): ν (cm⁻¹) 2961, 2930, 2222, 1721, 1620, 1585, 1548, 1440, 1409, 1380, 1337, 1239, 1173, 1108, 958, 867, 805, 742, 648, 578, 412.

HRMS (ESI, *m/z*) calcd for C₁₅H₂₁N₃ONa [M+Na]⁺: 282.1577, found: 282.1579.

**(*R*)-1-(3,5-Dimethyl-1*H*-pyrazol-1-yl)-3-(phenylsulfonyl)hexan-1-one (**21k**)**

Enantiomeric excess of **21k** was established by HPLC analysis using a Daicel Chiralpak AD-H column, ee = 78% (HPLC: 254 nm, *n*-hexane/isopropanol = 95:5, flow rate 1.0 mL/min, 40 °C, t_r (major) = 13.0 min, t_r (minor) = 16.3 min). $[\alpha]_D^{22} = -7.0^\circ$ (*c* 1.0, CH₂Cl₂).

¹H NMR (300 MHz, CDCl₃) δ 7.96-7.88 (m, 2H), 7.68-7.44 (m, 3H), 5.94 (s, 1H), 3.96-3.84 (m, 1H), 3.76 (dd, *J* = 17.6, 6.4 Hz, 1H), 3.24 (dd, *J* = 17.6, 5.8 Hz, 1H), 2.41 (s, 3H), 2.21 (s, 3H), 2.08-1.90

(m, 1H), 1.67-1.29 (m, 3H), 0.89 (t, $J = 7.4$ Hz, 3H).

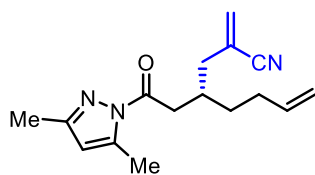
^{13}C NMR (75 MHz, CDCl_3) δ 170.2, 152.4, 144.1, 137.6, 133.6, 129.1, 129.0, 111.4, 60.2, 34.4, 30.5, 19.9, 14.2, 13.8, 13.7.

IR (film): ν (cm^{-1}) 2963, 2931, 2874, 1723, 1586, 1445, 1381, 1303, 1176, 1141, 1082, 1030, 999, 961, 933, 808, 730, 691, 591, 563, 410.

HRMS (ESI, m/z) calcd for $\text{C}_{17}\text{H}_{22}\text{N}_2\text{O}_3\text{SNa}$ $[\text{M}+\text{Na}]^+$: 357.1243, found: 357.1247.

16) Figure 48a, reaction of 18d

According to the general procedure, the reaction of (*E*)-1-(3,5-dimethyl-1*H*-pyrazol-1-yl)hepta-2,6-dien-1-one **18d** (40.9 mg, 0.20 mmol), 2-((phenylsulfonyl)methyl)acrylonitrile **19a** (20.8 mg, 0.10 mmol), Δ -**RhO** (6.6 mg, 8.0 mol%), diethyl 2,6-diethyl-1,4-dihydropyridine-3,5-dicarboxylate (42.2 mg, 1.5 equiv) in 1,4-dioxane (1.0 mL, 0.1 M) under nitrogen atmosphere with visible light for 40 hours at 35 °C, afforded 16.5 mg (61%) of **20h** as a colorless oil, and afforded 21.5 mg (62%) of **21l** as a yellow oil.



(*S*)-4-(2-(3,5-Dimethyl-1*H*-pyrazol-1-yl)-2-oxoethyl)-2-methyleneoct-7-enenitrile (**20h**)

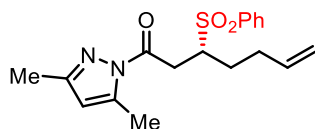
Enantiomeric excess of **20h** was established by HPLC analysis using a Daicel Chiralpak OD-H column, ee = 79% (HPLC: 254 nm, *n*-hexane/isopropanol = 99:1, flow rate 1.0 mL/min, 40 °C, t_r (major) = 6.9 min, t_r (minor) = 5.7 min). $[\alpha]_{\text{D}}^{22} = +6.0^\circ$ (c 1.0, CH_2Cl_2).

^1H NMR (300 MHz, CDCl_3) δ 5.95 (s, 1H), 5.90 (s, 1H), 5.87-5.71 (m, 2H), 5.07-4.93 (m, 2H), 3.08-3.02 (m, 2H), 2.53 (s, 3H), 2.48-2.32 (m, 3H), 2.23 (s, 3H), 2.18-2.08 (m, 2H), 1.58-1.48 (m, 2H).

^{13}C NMR (75 MHz, CDCl_3) δ 172.5, 152.0, 144.0, 137.9, 132.1, 121.6, 118.6, 115.1, 111.2, 39.0, 38.4, 32.8, 32.6, 30.7, 14.5, 13.8.

IR (film): ν (cm^{-1}) 2925, 2223, 1722, 1640, 1584, 1409, 1380, 1338, 1245, 1171, 1032, 959, 915, 806, 745, 644, 562, 410.

HRMS (ESI, m/z) calcd for $\text{C}_{16}\text{H}_{21}\text{N}_3\text{ONa}$ $[\text{M}+\text{Na}]^+$: 294.1577, found: 294.1580.



(*R*)-1-(3,5-Dimethyl-1*H*-pyrazol-1-yl)-3-(phenylsulfonyl)hept-6-en-1-one (21I**)**

Enantiomeric excess of **21I** was established by HPLC analysis using a Daicel Chiralpak AD-H column, ee = 83% (HPLC: 254 nm, *n*-hexane/isopropanol = 95:5, flow rate 1.0 mL/min, 40 °C, *t_r* (major) = 14.1 min, *t_r* (minor) = 17.2 min). [α]_D²² = -1.2° (*c* 1.0, CH₂Cl₂).

¹H NMR (300 MHz, CDCl₃) δ 7.95-7.89 (m, 2H), 7.66-7.48 (m, 3H), 5.94 (s, 1H), 5.78-5.62 (m, 1H), 5.03-4.93 (m, 2H), 3.98-3.86 (m, 1H), 3.78 (dd, *J* = 17.6, 6.4 Hz, 1H), 3.28 (dd, *J* = 17.6, 5.8 Hz, 1H), 2.41 (s, 3H), 2.22 (s, 3H), 2.26-2.04 (m, 3H), 1.76-1.64 (m, 1H).

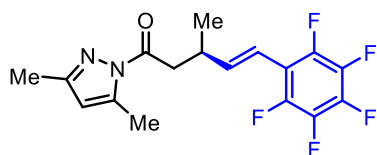
¹³C NMR (75 MHz, CDCl₃) δ 170.0, 152.4, 144.1, 137.6, 136.5, 133.7, 129.1, 129.0, 116.1, 111.4, 59.7, 34.4, 30.5, 27.7, 14.2, 13.7.

IR (film): ν (cm⁻¹) 2928, 1722, 1585, 1479, 1444, 1381, 1311, 1177, 1142, 1083, 1029, 916, 808, 732, 691, 588, 562, 410.

HRMS (ESI, *m/z*) calcd for C₁₈H₂₂N₂O₃SNa [M+Na]⁺: 369.1243, found: 369.1244.

17) Figure 48b, reaction of **22**

According to the general procedure, the reaction of (*E*)-1-(3,5-dimethyl-1*H*-pyrazol-1-yl) but-2-en-1-one **18a** (32.8 mg, 0.20 mmol), (*E*)-1,2,3,4,5-pentafluoro-6-(2-(phenylsulfonyl)vinyl) benzene **22** (25.7 mg, 0.10 mmol), Δ -RhO (6.6 mg, 8.0 mol%), diethyl 2,6-diethyl-1,4-dihydropyridine-3,5-dicarboxylate (42.2 mg, 1.5 equiv) in 1,4-dioxane (1.0 mL, 0.1 M) under nitrogen atmosphere with visible light for 48 hours at room temperature, afforded 21.1 mg (54%) of **23** as a colorless oil, and afforded 21.1 mg (59%) of **21a** as a yellow oil. Enantiomeric excess of **21a** was determined as 81% ee.



(*R,E*)-1-(3,5-Dimethyl-1*H*-pyrazol-1-yl)-3-methyl-5-(perfluorophenyl)pent-4-en-1-one (23**)**

Enantiomeric excess of **23** was established by HPLC analysis using a Daicel Chiralpak IG column, ee = 93% (HPLC: 254 nm, *n*-hexane/isopropanol = 99:1, flow rate 1.0 mL/min, 25 °C, *t_r* (major) = 11.4

min, t_r (minor) = 10.4 min). $[\alpha]_D^{22} = -12.0^\circ$ (c 0.5, CH_2Cl_2).

^1H NMR (500 MHz, CDCl_3) δ 6.56 (dd, J = 16.4, 7.6 Hz, 1H), 6.33 (dd, J = 16.4, 1.0 Hz, 1H), 5.96 (s, 1H), 3.28 (dd, J = 16.4, 7.6 Hz, 1H), 3.17 (dd, J = 16.4, 6.8 Hz, 1H), 3.12-3.04 (m, 1H), 2.53 (s, 3H), 2.24 (s, 3H), 1.23 (d, J = 6.8 Hz, 3H).

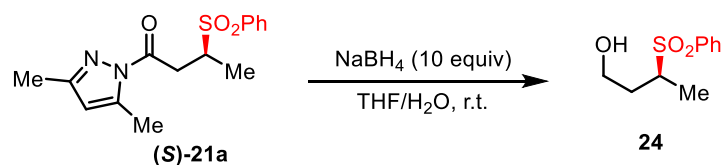
^{13}C NMR (125 MHz, CDCl_3) δ 172.2, 152.0, 144.3 (br), 144.1, 113.4, 111.2, 41.6, 34.6, 20.0, 14.6, 13.8.

^{19}F NMR (282 MHz, CDCl_3) δ -143.40 - -143.60 (m, 2F), -157.51 - -157.71 (m, 1F), -163.40 - -163.64 (m, 2F).

IR (film): ν (cm^{-1}) 2923, 1728, 1583, 1520, 1494, 1459, 1412, 1378, 1353, 1317, 1248, 1136, 997, 967, 802, 746.

HRMS (ESI, m/z) calcd for $\text{C}_{17}\text{H}_{15}\text{F}_5\text{N}_2\text{ONa}$ $[\text{M}+\text{Na}]^+$: 381.0997, found: 381.0987.

18) Figure 49a, reduction of (S)-21a



To a solution of (S)-1-(3,5-dimethyl-1H-pyrazol-1-yl)-3-(phenylsulfonyl)butan-1-one (S)-21a (*obtained by the reactions catalyzed by A-RhO*, 85% ee, 30.6 mg, 0.10 mmol) in THF/ H_2O (4/1, 1.0 mL, 0.1 M) at 0 °C was added NaBH_4 (38.0 mg, 1.0 mmol). The reaction mixture was stirred at room temperature for 6 hours. The reaction was quenched with aqueous 2 N HCl (1.0 mL) at room temperature and extracted with CH_2Cl_2 (4×10 mL). The combined organic layers were dried over anhydrous Na_2SO_4 , filtered, and concentrated under reduced pressure. The residue was purified by flash chromatography on silica gel ($\text{EtOAc}/n\text{-hexane}$ = 1:1) to afford **24** (20.9 mg, 0.098 mmol, yield: 98%) as a white solid.

(S)-3-(Phenylsulfonyl)butan-1-ol (24)

Enantiomeric excess of **24** was established by HPLC analysis using a Daicel Chiralpak OD-H column, ee = 85% (HPLC: 254 nm, $n\text{-hexane}/\text{isopropanol}$ = 90:10, flow rate 1.0 mL/min, 40 °C, t_r (major) = 19.1 min, t_r (minor) = 18.1 min). $[\alpha]_D^{22} = -15.8^\circ$ (c 1.0, CH_2Cl_2).

^1H NMR (300 MHz, CDCl_3) δ 7.93-7.85 (m, 2H), 7.70-7.54 (m, 3H), 3.86 (dt, J = 11.0, 5.6 Hz, 1H), 3.69 (ddd, J = 11.0, 8.4, 5.0 Hz, 1H), 3.41-3.28 (m, 1H), 2.31-2.17 (m, 2H), 1.69 (ddt, J = 14.1, 8.8,

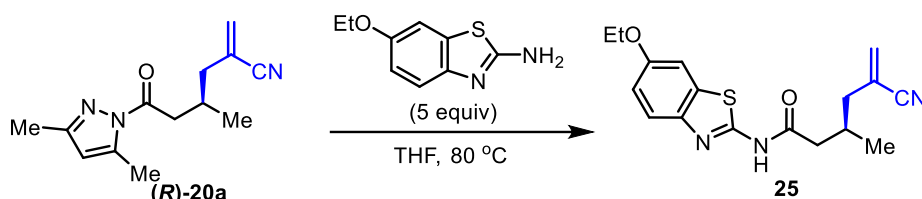
5.2 Hz, 1H), 1.27 (d, $J = 6.9$ Hz, 3H).

^{13}C NMR (75 MHz, CDCl_3) δ 137.2, 133.7, 129.1, 129.0, 59.3, 57.1, 32.2, 13.7.

IR (film): ν (cm^{-1}) 3341, 3208, 3143, 2928, 2876, 1581, 1447, 1380, 1294, 1140, 1060, 1005, 796, 766, 731, 691, 663, 589, 547.

HRMS (ESI, m/z) calcd for $\text{C}_{10}\text{H}_{14}\text{O}_3\text{SNa}$ $[\text{M}+\text{Na}]^+$: 237.0564, found: 237.0556.

19) Figure 49b, transamidation of (R)-20a



To a solution of (R)-6-(3,5-dimethyl-1H-pyrazol-1-yl)-4-methyl-2-methylene-6-oxohexanenitrile (R)-20a (obtained by the reactions catalyzed by A-RhO, 96% ee, 23.1 mg, 0.10 mmol) in THF (0.1 mL, 1 M) was added 6-ethoxybenzo[d]thiazol-2-amine (97.0 mg, 0.50 mmol). The reaction mixture was stirred at 80 °C for 40 hours. After the start material was converted completely, the reaction mixture was cooled to room temperature and concentrated under reduced pressure. The residue was purified by flash chromatography on silica gel (EtOAc/*n*-hexane = 1:1) to afford **25** (29.6 mg, 90% yield) as a white solid.

(R)-5-Cyano-N-(6-ethoxybenzo[d]thiazol-2-yl)-3-methylhex-5-enamide (25)

Enantiomeric excess of **25** was established by HPLC analysis using a Daicel Chiralpak OD-H column, ee = 96% (HPLC: 254 nm, *n*-hexane/isopropanol = 85:15, flow rate 1.0 mL/min, 40 °C, t_r (major) = 30.6 min, t_r (minor) = 22.9 min). $[\alpha]_{\text{D}}^{22} = -8.0^\circ$ (c 1.0, CH_2Cl_2).

^1H NMR (300 MHz, CDCl_3) δ 11.24 (br s, 1H), 7.64 (d, $J = 8.8$ Hz, 1H), 7.31 (d, $J = 2.5$ Hz, 1H), 7.06 (dd, $J = 8.8, 2.5$ Hz, 1H), 5.85 (s, 1H), 5.66 (s, 1H), 4.10 (q, $J = 7.0$, 2H), 2.55-2.27 (m, 4H), 2.12 (dd, $J = 13.6, 7.0$, 1H), 1.45 (t, $J = 7.0$, 3H), 0.98 (d, $J = 6.1$ Hz, 3H).

^{13}C NMR (75 MHz, CDCl_3) δ 169.9, 157.3, 156.3, 141.8, 133.2, 132.4, 121.1, 121.0, 118.4, 115.9, 105.3, 64.2, 41.2, 41.0, 29.2, 19.0, 14.8.

IR (film): ν (cm^{-1}) 3182, 2975, 2921, 2218, 2047, 1688, 1605, 1551, 1460, 1259, 1223, 1114, 1060, 942, 822, 747, 666.

HRMS (ESI, m/z) calcd for $\text{C}_{17}\text{H}_{19}\text{N}_3\text{O}_2\text{SNa}$ $[\text{M}+\text{Na}]^+$: 330.1271, found: 330.1264.

5.3.5 Single-Crystal X-Ray Diffraction Studies

Single crystals of **RhO-Pz** suitable for X-ray diffraction were obtained by slow diffusion from a solution of racemic **RhO-Pz** (20 mg) in CH₂Cl₂ (2.0 mL) layered with ethyl ether (1.0 mL) at room temperature for several days in a NMR tube.

Single crystals of **21d** suitable for X-ray diffraction were obtained by slow diffusion from a solution of **21d** (20 mg) in ethyl ether (0.5 mL) layered with *n*-hexane (0.5 mL) at 4 °C for several days in a NMR tube.

Single crystals of compound **25** suitable for X-ray diffraction were obtained by slow diffusion from a solution of **25** (30 mg), in CH₂Cl₂ (0.5 mL) layered with *n*-hexane (0.5 mL) at room temperature for several days in a NMR tube.

X-ray data were collected with a Bruker 3 circuit D8 Quest diffractometer with MoK α radiation (microfocus tube with multilayer optics) and Photon 100 CMOS detector at 100 K. Scaling and absorption correction was performed by using the SADABS software package of Bruker. Structures were solved using direct methods in SHELXT and refined using the full matrix least squares procedure in SHELXL-2014. The hydrogen atoms were placed in calculated positions and refined as riding on their respective C atom, and Uiso(H) was set at 1.2 Ueq(Csp²) and 1.5 Ueq(Csp³). Disorder was refined using restraints for both the geometry and the anisotropic displacement factors.

The absolute configuration of **21d** and **25** have been determined (**Figure 123**). See **Figure 52** for structure of **RhO-Pz**.

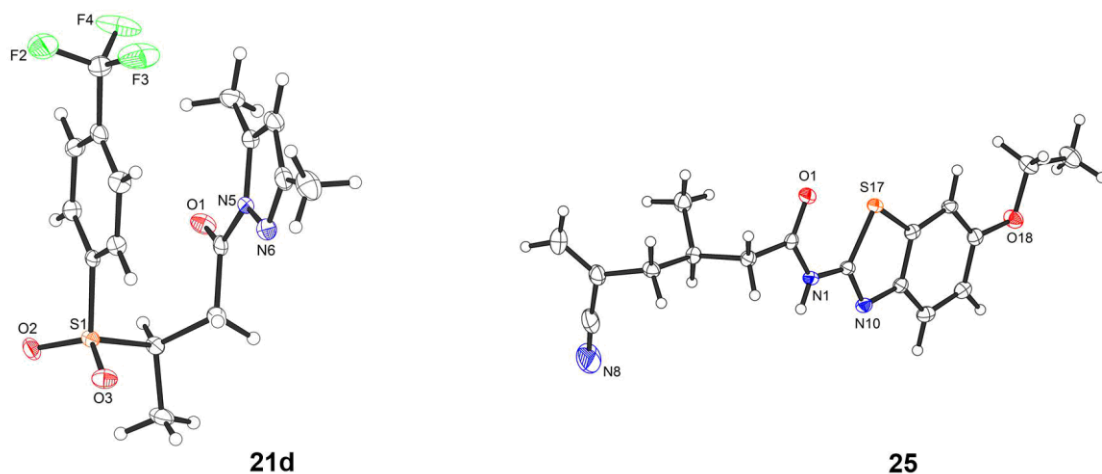


Figure 123. Crystal structures of compounds **21d** and **25**.

Table 24. Crystal data and structure refinement for **RhO-Pz**.

Crystal data		
CCDC number	1547314	
Identification code	hxqE104_0m	
Habitus, color	nugget, pale yellow	
Crystal size	0.34 x 0.25 x 0.23 mm ³	
Crystal system	Triclinic	
Space group	P-1	Z = 2
Unit cell dimensions	a = 11.9931(5) Å	α = 89.480(1)°.
	b = 13.7713(6) Å	β = 67.088(1)°.
	c = 14.7325(6) Å	γ = 79.592(1)°.
	Volume	2199.33(16) Å ³
3Cell determination	9783 peaks with Theta 2.6 to 27.5 °.	
Empirical formula	C ₄₄ H ₄₆ Cl ₂ F ₆ N ₄ O ₃ P Rh	
Moiety formula	C ₄₃ H ₄₄ N ₄ O ₃ Rh, F ₆ P, C H ₂ Cl ₂	
Formula weight	997.63	
Density (calculated)	1.506 Mg/m ³	
Absorption coefficient	0.616 mm ⁻¹	
F(000)	1020	
Data collection:		
Diffractionmeter type	Bruker D8 QUEST area detector	
Wavelength	0.71073 Å	
Temperature	100(2) K	
Theta range for data collection	2.248 to 27.564 °.	
Index ranges	-15<=h<=15, -17<=k<=17, -19<=l<=18	
Data collection software	APEX3 (Bruker AXS Inc., 2015)	
Cell refinement software	SAINT V8.35A (Bruker AXS Inc., 2015)	
Data reduction software	SAINT V8.35A (Bruker AXS Inc., 2015)	
Solution and refinement:		
Reflections collected	82467	
Independent reflections	10124 [R(int) = 0.0338]	
Completeness to theta = 25.242 °	99.9 %	
Observed reflections	9422[I > 2(I)]	
Reflections used for refinement	10124	
Absorption correction	Semi-empirical from equivalents	
Max. and min. transmission	0.87 and 0.82	
Largest diff. peak and hole	0.438 and -0.606 e.Å ⁻³	
Solution	Direct methods	
Refinement	Full-matrix least-squares on F ²	
Treatment of hydrogen atoms	Calculated positions, constr. ref.	
Programs used	XT V2014/1 (Bruker AXS Inc., 2014)	
	SHELXL-2014/7 (Sheldrick, 2014)	
	DIAMOND (Crystal Impact)	
	ShelXle (Hübschle, Sheldrick, Dittrich, 2011)	
Data / restraints / parameters	10124 / 144 / 590	
Goodness-of-fit on F ²	1.038	
R index (all data)	wR2 = 0.0560	
R index conventional [I>2sigma(I)]	R1 = 0.0223	

Table 25. Crystal data and structure refinement for **21d**.

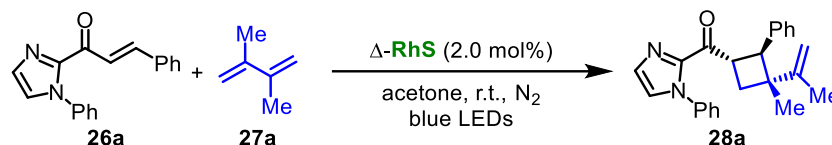
Crystal data		
CCDC number	1547315	
Identification code	hxq119b_0m	
Habitus, color	block, colorless	
Crystal size	0.31 x 0.13 x 0.08 mm ³	
Crystal system	Tetragonal	
Space group	P4 ₃ 2 ₁ 2	Z = 8
Unit cell dimensions	a = 7.1300(2) Å	α = 90°.
	b = 7.1300(2) Å	β = 90°.
	c = 66.238(2) Å	γ = 90°.
	3367.3(2) Å ³	
Volume	3367.3(2) Å ³	
Cell determination	9348 peaks with Theta 2.5 to 25.2 °	
Empirical formula	C ₁₆ H ₁₇ F ₃ N ₂ O ₃ S	
Moiety formula	C ₁₆ H ₁₇ F ₃ N ₂ O ₃ S	
Formula weight	374.37	
Density (calculated)	1.477 Mg/m ³	
Absorption coefficient	0.242 mm ⁻¹	
F(000)	1552	
Data collection:		
Diffractionmeter type	Bruker D8 QUEST area detector	
Wavelength	0.71073 Å	
Temperature	110(2) K	
Theta range for data collection	2.460 to 25.262 °	
Index ranges	-8<=h<=8, -8<=k<=8, -79<=l<=79	
Data collection software	APEX3 (Bruker AXS Inc., 2015)	
Cell refinement software	SAINT V8.37A (Bruker AXS Inc., 2015)	
Data reduction software	SAINT V8.37A (Bruker AXS Inc., 2015)	
Solution and refinement:		
Reflections collected	35175	
Independent reflections	3048 [R(int) = 0.0499]	
Completeness to theta = 25.242 °	99.9 %	
Observed reflections	2921[I > 2σ(I)]	
Reflections used for refinement	3048	
Absorption correction	Semi-empirical from equivalents	
Max. and min. transmission	0.98 and 0.84	
Flack parameter (absolute struct.)	0.00(3)	
Largest diff. peak and hole	0.308 and -0.260 e.Å ⁻³	
Solution	“Dual space”	
Refinement	Full-matrix least-squares on F ²	
Treatment of hydrogen atoms	Calculated positions, constr. ref.	
Programs used	XT V2014/1 (Bruker AXS Inc., 2014)	
	SHELXL-2014/7 (Sheldrick, 2014)	
	DIAMOND (Crystal Impact)	
	ShelXle (Hübschle, Sheldrick, Dittrich, 2011)	
Data / restraints / parameters	3048 / 0 / 229	
Goodness-of-fit on F ²	1.224	
R index (all data)	wR2 = 0.1020	
R index conventional [I>2sigma(I)]	R1 = 0.0479	

Table 26. Crystal data and structure refinement for **25**.

Crystal data		
CCDC number	1547316	
Identification code	lsp182_0m	
Habitus, color	plate, colorless	
Crystal size	0.45 x 0.40 x 0.04 mm ³	
Crystal system	Monoclinic	
Space group	P2 ₁	Z = 8
Unit cell dimensions	a = 15.7976(9) Å	α = 90 °
	b = 12.9960(8) Å	β = 112.625(2) °
	c = 17.9469(11) Å	γ = 90 °
	3401.0(4) Å ³	
Volume	3401.0(4) Å ³	
Cell determination	9782 peaks with Theta 2.7 to 26.4 °	
Empirical formula	C ₁₇ H ₁₉ N ₃ O ₂ S	
Moiety formula	C ₁₇ H ₁₉ N ₃ O ₂ S	
Formula weight	329.41	
Density (calculated)	1.287 Mg/m ³	
Absorption coefficient	0.203 mm ⁻¹	
F(000)	1392	
Data collection:		
Diffractionmeter type	Bruker D8 QUEST area detector	
Wavelength	0.71073 Å	
Temperature	100(2) K	
Theta range for data collection	2.144 to 26.420 °	
Index ranges	-19<=h<=19, -16<=k<=16, -22<=l<=19	
Data collection software	APEX3 (Bruker AXS Inc., 2015)	
Cell refinement software	SAINT V8.37A (Bruker AXS Inc., 2015)	
Data reduction software	SAINT V8.37A (Bruker AXS Inc., 2015)	
Solution and refinement:		
Reflections collected	40409	
Independent reflections	13945 [R(int) = 0.0372]	
Completeness to theta = 25.242 °	99.9 %	
Observed reflections	12300[I > 2σ(I)]	
Reflections used for refinement	13945	
Absorption correction	Semi-empirical from equivalents	
Max. and min. transmission	0.99 and 0.91	
Flack parameter (absolute struct.)	0.01(2)	
Largest diff. peak and hole	0.241 and -0.264 e.Å ⁻³	
Solution	Direct methods	
Refinement	Full-matrix least-squares on F ²	
Treatment of hydrogen atoms	CH calculated positions, constr. ref., NH located,	
isotr. ref.		
Programs used	XT V2014/1 (Bruker AXS Inc., 2014) SHELXL-2014/7 (Sheldrick, 2014) DIAMOND (Crystal Impact ShelXle (Hübschle, Sheldrick, Dittrich, 2011)	
Data / restraints / parameters	13945 / 1 / 853	
Goodness-of-fit on F ²	1.037	
R index (all data)	wR2 = 0.0759	
R index conventional [I>2sigma(I)]	R1 = 0.0353	

5.4 Asymmetric [2+2] Photocycloaddition

5.4.1 General Procedure

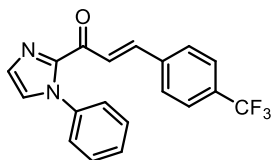


Exemplary, a dried 10 mL Schlenk tube was charged with α,β -unsaturated 2-acyl imidazole **26a** (27.4 mg, 0.10 mmol) and Δ -RhS (1.7 mg, 2 mol%). The tube was purged with nitrogen. Then, acetone (0.5 mL, 0.2 M) was added via syringe, followed by diene **27a** (24.6 mg, 3.0 equiv) under nitrogen atmosphere with stirring. The reaction mixture was degassed via freeze-pump-thaw for three cycles. After the mixture was thoroughly degassed, the vial was sealed and positioned in a water bath approximately 5 cm from a 24 W blue LEDs lamp. The temperature of the water bath was kept at 24~27 °C during the reaction. After stirring for the indicated time (monitored by TLC) under nitrogen atmosphere, the mixture was diluted with CH₂Cl₂. The combined organic layers were concentrated under reduced pressure. The crude residue was subjected to ¹H NMR to determine the d.r. value. Then, the mixture was purified by flash chromatography on silica gel (*n*-hexane/EtOAc) to afford the product **28a**. The enantiomeric excess was determined by chiral HPLC analysis. Racemic samples were obtained by carrying out the reactions with *rac*-RhS.

Note: the model reaction **26a** + **27a** → **28a** under open air conditions (assembled in air, sealed tube) without degassing works as well as the degassed reaction.

5.4.2 Synthesis of Substrates

α,β -Unsaturated 2-acyl imidazoles and *N*-acyl pyrazoles **26** were synthesized according to the recently published procedures.^{8a} α -Methyl styrenes were synthesized following a published procedure.^{11a} 3-Vinylestrone was synthesized following the reported procedure.^{11b} The data of new substrates are shown below.



(E)-1-(1-Phenyl-1H-imidazol-2-yl)-3-(4-(trifluoromethyl)phenyl)prop-2-en-1-one (26c)

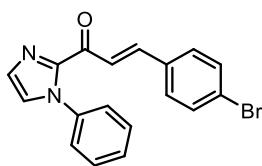
A yellow solid.

^1H NMR (300 MHz, CDCl_3) δ 8.14 (d, $J = 16.2$ Hz, 1H), 7.73 (d, $J = 15.9$ Hz, 1H), 7.77-7.72 (m, 2H), 7.64 (d, $J = 8.4$ Hz, 2H), 7.52-7.47 (m, 3H), 7.39-7.31 (m, 3H), 7.27-7.25 (m, 1H).

^{13}C NMR (125 MHz, CDCl_3) δ 178.7, 143.8, 141.7, 138.4, 138.2, 131.8 (q, $J = 32.5$ Hz), 130.0, 129.0, 128.9, 128.8, 127.6, 125.9, 125.8 (q, $J = 3.6$ Hz), 124.9, 123.8 (q, $J = 270.6$ Hz).

IR (film): ν (cm^{-1}) 3067, 2927, 1665, 1606, 1494, 1447, 1405, 1314, 1158, 1114, 1066, 1037, 975, 916, 885, 834, 797, 753, 692, 645, 592, 501.

HRMS (ESI, m/z) calcd for $\text{C}_{19}\text{H}_{13}\text{F}_3\text{N}_2\text{ONa}$ $[\text{M}+\text{Na}]^+$: 365.0872, found: 365.0871.



(E)-3-(4-Bromophenyl)-1-(1-phenyl-1H-imidazol-2-yl)prop-2-en-1-one (26e)

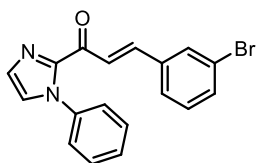
A yellow solid.

^1H NMR (300 MHz, CDCl_3) δ 8.06 (d, $J = 15.9$ Hz, 1H), 7.66 (d, $J = 15.9$ Hz, 1H), 7.54-7.51 (m, 4H), 7.50-7.45 (m, 3H), 7.37-7.31 (m, 3H), 7.24 (d, $J = 0.9$ Hz, 1H).

^{13}C NMR (75 MHz, CDCl_3) δ 178.9, 144.0, 142.3, 138.5, 133.8, 132.1, 130.1, 129.9, 129.0, 128.8, 127.4, 125.9, 124.8, 123.3.

IR (film): ν (cm^{-1}) 3107, 1659, 1603, 1486, 1444, 1396, 1307, 1151, 1040; 1005, 975, 911, 810, 771, 755, 690, 645, 524, 489.

HRMS (ESI, m/z) calcd for $\text{C}_{18}\text{H}_{13}\text{BrN}_2\text{ONa}$ $[\text{M}+\text{Na}]^+$: 375.0103, found: 375.0102.



(E)-3-(3-Bromophenyl)-1-(1-phenyl-1H-imidazol-2-yl)prop-2-en-1-one (26f)

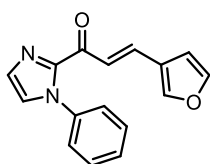
A yellow solid.

^1H NMR (300 MHz, CDCl_3) δ 8.06 (d, $J = 15.9$ Hz, 1H), 7.82 (t, $J = 1.8$ Hz, 1H), 7.64 (d, $J = 15.9$ Hz, 1H), 7.57-7.47 (m, 5H), 7.38-7.31 (m, 3H), 7.29-7.22 (m, 2H).

^{13}C NMR (75 MHz, CDCl_3) δ 178.7, 143.9, 141.9, 138.5, 137.0, 133.2, 131.1, 130.3, 130.0, 129.0, 128.8, 127.5, 127.4, 125.9, 124.0, 123.0.

IR (film): ν (cm^{-1}) 3108, 3064, 1659, 1599, 1556, 1494, 1445, 1387, 1303, 1194, 1150, 1073, 1040, 976, 887, 857, 787, 754, 668, 642, 575, 517, 428.

HRMS (ESI, m/z) calcd for $\text{C}_{18}\text{H}_{13}\text{BrN}_2\text{ONa}$ $[\text{M}+\text{Na}]^+$: 375.0103, found: 375.0103.



(E)-3-(Furan-3-yl)-1-(1-phenyl-1H-imidazol-2-yl)prop-2-en-1-one (26i)

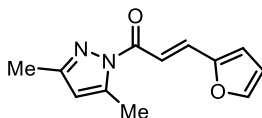
A yellow solid.

^1H NMR (300 MHz, CDCl_3) δ 7.76 (d, $J = 15.9$ Hz, 1H), 7.69-7.61 (m, 2H), 7.50-7.42 (m, 4H), 7.34-7.30 (m, 3H), 7.22 (d, $J = 0.9$ Hz, 1H), 6.76 (d, $J = 1.8$ Hz, 1H).

^{13}C NMR (75 MHz, CDCl_3) δ 179.1, 145.6, 144.4, 144.0, 138.6, 133.8, 129.7, 128.9, 128.7, 127.2, 125.9, 123.4, 122.6, 107.8.

IR (film): ν (cm^{-1}) 3107, 3022, 1658, 1591, 1550, 1491, 1442, 1404, 1306, 1213, 1151, 1045, 1003, 975, 858, 816, 758, 727, 697, 665, 617, 591, 566, 520, 446.

HRMS (ESI, m/z) calcd for $\text{C}_{16}\text{H}_{13}\text{N}_2\text{O}_2$ $[\text{M}+\text{H}]^+$: 265.0972, found: 265.0970.



(E)-1-(3,5-Dimethyl-1H-pyrazol-1-yl)-3-(furan-2-yl)prop-2-en-1-one (26l)

A white solid.

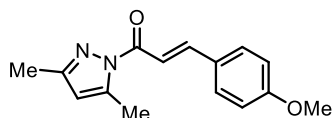
^1H NMR (300 MHz, CDCl_3) δ 7.78 (d, $J = 15.6$ Hz, 1H), 7.63 (d, $J = 15.6$ Hz, 1H), 7.52 (d, $J = 1.5$ Hz, 1H), 6.72 (d, $J = 3.6$ Hz, 1H), 6.49 (d, $J_1 = 3.3$ Hz, $J_2 = 1.8$ Hz, 1H), 6.00 (s, 1H), 2.61 (m, 3H), 2.28 (s, 3H).

^{13}C NMR (75 MHz, CDCl_3) δ 165.5, 151.8, 151.7, 145.0, 144.2, 132.0, 115.7, 115.6, 112.4, 111.3,

14.6, 13.8.

IR (film): ν (cm⁻¹) 3123, 2977, 2919, 1692, 1617, 1580, 1551, 1473, 1373, 1342, 1298, 1253, 1234, 1183, 1007, 960, 879, 861, 833, 748, 690, 590, 463.

HRMS (ESI, m/z) calcd for C₁₂H₁₂N₂O₂Na [M+Na]⁺: 239.0791, found: 239.0790.



(E)-1-(3,5-Dimethyl-1H-pyrazol-1-yl)-3-(4-methoxyphenyl)prop-2-en-1-one (26n)

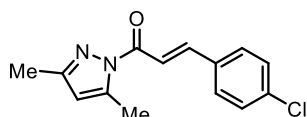
A white solid.

¹H NMR (300 MHz, CDCl₃) δ 7.88 (d, J = 15.6 Hz, 1H), 7.79 (d, J = 15.9 Hz, 1H), 7.67-7.60 (m, 2H), 6.96-6.90 (m, 2H), 6.00 (s, 1H), 3.85 (s, 3H), 2.63-2.61 (m, 3H), 2.29 (s, 3H).

¹³C NMR (75 MHz, CDCl₃) δ 165.8, 161.7, 151.7, 146.0, 144.3, 130.5, 127.7, 115.3, 114.3, 111.2, 55.4, 14.7, 13.8.

IR (film): ν (cm⁻¹) 3094, 3051, 2997, 2964, 2930, 1684, 1598, 1571, 1508, 1463, 1418, 1347, 1313, 1284, 1228, 1171, 1113, 1013, 959, 813, 763, 723, 550, 514, 445, 410.

HRMS (ESI, m/z) calcd for C₁₅H₁₆N₂O₂Na [M+Na]⁺: 279.1104, found: 279.1103.



(E)-1-(3,5-Dimethyl-1H-pyrazol-1-yl)-3-(4-chlorophenyl)prop-2-en-1-one (26o)

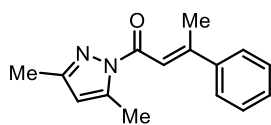
A white solid.

¹H NMR (300 MHz, CDCl₃) δ 7.92 (d, J = 15.9 Hz, 1H), 7.82 (d, J = 16.2 Hz, 1H), 7.63-7.57 (m, 2H), 7.41-7.34 (m, 2H), 6.02 (s, 1H), 2.63-2.61 (m, 3H), 2.29 (s, 3H).

¹³C NMR (75 MHz, CDCl₃) δ 165.2, 152.0, 144.5, 144.4, 136.4, 133.3, 129.8, 129.1, 118.6, 111.5, 14.6, 13.8.

IR (film): ν (cm⁻¹) 2978, 2923, 1695, 1616, 1579, 1483, 1404, 1370, 1349, 1231, 1170, 1090, 1004, 973, 803, 749, 621, 494, 403.

HRMS (ESI, m/z) calcd for C₁₄H₁₃ClN₂ONa [M+Na]⁺: 283.0609, found: 283.0608.

**(E)-1-(3,5-Dimethyl-1H-pyrazol-1-yl)-3-phenylbut-2-en-1-one (26p)**

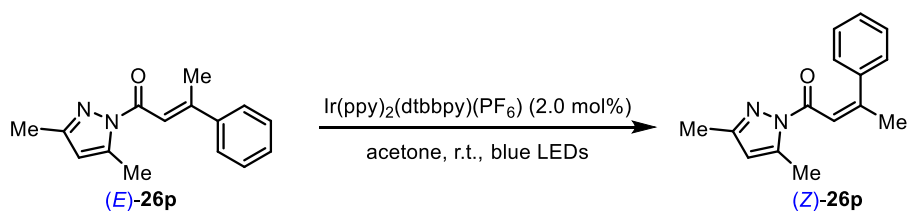
A white solid.

^1H NMR (300 MHz, CDCl_3) δ 7.61-7.56 (m, 2H), 7.55 (q, $J = 1.3$ Hz, 1H), 7.44-7.37 (m, 3H), 5.98 (s, 1H), 2.67 (d, $J = 1.5$ Hz, 3H), 2.63-2.61 (m, 3H), 2.25 (s, 3H).

^{13}C NMR (75 MHz, CDCl_3) δ 165.6, 157.8, 151.2, 144.2, 142.7, 129.2, 128.5, 126.7, 117.3, 111.0, 18.6, 14.7, 13.8.

IR (film): ν (cm^{-1}) 3115, 2926, 1691, 1603, 1573, 1442, 1410, 1377, 1350, 1313, 1277, 1224, 1022, 952, 876, 851, 827, 753, 740, 688, 579, 519, 493.

HRMS (ESI, m/z) calcd for $\text{C}_{15}\text{H}_{16}\text{N}_2\text{ONa}$ $[\text{M}+\text{Na}]^+$: 263.1155, found: 263.1154.



Substrate (Z)-**26p** was synthesized from (E)-**26p** according to literature with some modifications.^{11c}

The mixture of α,β -unsaturated *N*-acyl pyrazole (E)-**26p** (48.0 mg, 0.2 mmol) and $\text{Ir}(\text{ppy})_2(\text{dtbbpy})(\text{PF}_6)$ (3.7 mg, 2.0 mol%) in acetone (2.0 mL) was stirred under N_2 atmosphere with the irradiation of 24 W blue LEDs. After 20 h, the reaction mixture was concentrated *in vacuo* and purification by flash column chromatography yielded 37.1 mg (Z)-**26p** (77% yield).

(Z)-1-(3,5-Dimethyl-1H-pyrazol-1-yl)-3-phenylbut-2-en-1-one ((Z)-26p)

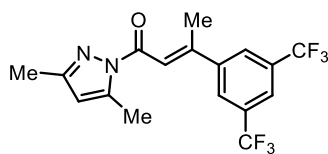
A white solid.

^1H NMR (300 MHz, CDCl_3) δ 7.40-7.31 (m, 3H), 7.29-7.24 (m, 2H), 7.17 (q, $J = 1.5$ Hz, 1H), 5.94 (s, 1H), 2.45-2.43 (m, 3H), 2.30 (d, $J = 1.5$ Hz, 3H), 2.28 (s, 3H).

^{13}C NMR (75 MHz, CDCl_3) δ 164.5, 157.8, 151.4, 144.3, 141.1, 128.1, 128.0, 126.8, 118.0, 111.8, 27.9, 14.5, 13.8.

IR (film): ν (cm^{-1}) 3056, 2976, 2927, 1708, 1626, 1577, 1484, 1437, 1408, 1376, 1319, 1251, 1205, 1174, 1141, 1082, 1053, 1027, 963, 913, 836, 763, 697, 624, 579, 533, 488, 427.

HRMS (ESI, m/z) calcd for $\text{C}_{15}\text{H}_{16}\text{N}_2\text{ONa}$ $[\text{M}+\text{Na}]^+$: 263.1155, found: 263.1154.



(*E*)-3-(3,5-Bis(trifluoromethyl)phenyl)-1-(3,5-dimethyl-1*H*-pyrazol-1-yl)but-2-en-1-one (26q)

A white solid.

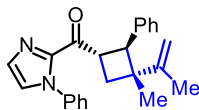
^1H NMR (300 MHz, CDCl_3) δ 7.96 (s, 2H), 7.89 (s, 1H), 7.54 (q, $J = 1.2$ Hz, 1H), 6.01 (s, 1H), 2.67 (d, $J = 1.2$ Hz, 3H), 2.63-2.61 (m, 3H), 2.26 (s, 3H).

^{13}C NMR (125 MHz, CDCl_3) δ 164.8, 153.3, 152.0, 144.7, 144.4, 132.0 (q, $J = 33.3$ Hz), 126.7 (q, $J = 3.0$ Hz), 123.2 (q, $J = 271.2$ Hz), 122.7-122.4 (m), 120.3, 111.5, 18.6, 14.7, 13.8.

IR (film): ν (cm^{-1}) 3158, 2979, 2927, 1697, 1612, 1578, 1447, 1365, 1320, 1278, 1226, 1171, 1118, 1021, 959, 902, 876, 846, 817, 760, 722, 687, 590, 523, 397.

HRMS (ESI, m/z) calcd for $\text{C}_{17}\text{H}_{14}\text{F}_6\text{N}_2\text{O}$ $[\text{M}+\text{Na}]^+$: 399.0903, found: 399.0901.

5.4.3 Experimental and Characterization Data of Novel Products



((1*S*,2*S*,3*R*)-3-Methyl-2-phenyl-3-(prop-1-en-2-yl)cyclobutyl)(1-phenyl-1*H*-imidazol-2-yl)methanone (28a)

According to the general procedure, the reaction of (*E*)-3-phenyl-1-(1-phenyl-1*H*-imidazol-2-yl)prop-2-en-1-one **26a** (27.4 mg, 0.10 mmol), 2,3-dimethylbuta-1,3-diene **27a** (24.6 mg, 3.0 equiv) and Δ -**RhS** (1.7 mg, 2 mol%) in acetone (0.5 mL, 0.2 M) under nitrogen atmosphere with blue LEDs for 16 hours, afforded 34.6 mg (97%, combined yield) of **28a** as a colorless oil; $[\alpha]_{\text{D}}^{22} = +128.6^\circ$ (c 1.0, CH_2Cl_2); d.r. value was determined through ^1H NMR of crude materials as 14:1; enantiomeric excess of the major diastereoisomer was established by HPLC analysis using a Chiralpak AD-H column, ee = 99% (HPLC: AD-H, 254 nm, n -hexane/isopropanol = 99:1, flow rate 1 mL/min, 25 $^\circ\text{C}$, t_{r} (major) = 14.1 min, t_{r} (minor) = 9.6 min).

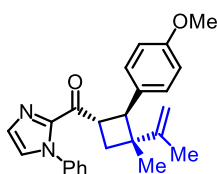
^1H NMR (500 MHz, CDCl_3) δ 7.48-7.45 (m, 3H), 7.34 (s, 1H), 7.33-7.26 (m, 6H), 7.22-7.17 (m, 2H), 4.89-4.79 (m, 3H), 4.07 (d, $J = 10.0$ Hz, 1H), 2.28 (t, $J = 10.0$ Hz, 1H), 2.22 (t, $J = 10.0$ Hz, 1H), 1.76

(s, 3H), 1.12 (s, 3H).

^{13}C NMR (125 MHz, CDCl_3) δ 191.4, 152.5, 142.7, 139.9, 138.4, 129.8, 128.9, 128.7, 128.2, 127.9, 127.4, 126.1, 125.9, 108.8, 47.6, 44.9, 40.0, 36.0, 21.3, 18.9.

IR (film): ν (cm^{-1}) 3071, 2963, 2864, 1676, 1596, 1495, 1445, 1403, 1306, 1225, 1149, 1101, 1057, 945, 892, 835, 759, 694, 538.

HRMS (ESI, m/z) calcd for $\text{C}_{24}\text{H}_{25}\text{N}_2\text{O}$ $[\text{M}+\text{H}]^+$: 357.1961, found: 357.1959.



((1S,2S,3R)-2-(4-Methoxyphenyl)-3-methyl-3-(prop-1-en-2-yl)cyclobutyl)(1-phenyl-1H-imidazol-2-yl)methanone (28b)

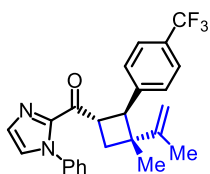
According to the general procedure, the reaction of (*E*)-3-(4-methoxyphenyl)-1-(1-phenyl-1*H*-imidazol-2-yl)prop-2-en-1-one **26b** (30.4 mg, 0.10 mmol), 2,3-dimethylbuta-1,3-diene **27a** (24.6 mg, 3.0 equiv) and Δ -**RhS** (1.7 mg, 2 mol%) in acetone (0.5 mL, 0.2 M) under nitrogen atmosphere with blue LEDs for 15 hours, afforded 35.3 mg (91%, combined yield) of **28b** as a colorless oil; $[\alpha]_{\text{D}}^{22} = +181.4^\circ$ (*c* 1.0, CH_2Cl_2); d.r. value was determined through ^1H NMR of crude materials as 12:1; enantiomeric excess of the major diastereoisomer was established by HPLC analysis using a Chiralpak AD-H column, ee >99% (HPLC: AD-H, 254 nm, *n*-hexane/isopropanol = 98:2, flow rate 1 mL/min, 25 °C, t_{r} (major) = 23.8 min, t_{r} (minor) = 14.7 min).

^1H NMR (500 MHz, CDCl_3) δ 7.46-7.41 (m, 3H), 7.30 (d, $J = 1.0$ Hz, 1H), 7.26-7.23 (m, 2H), 7.23-7.20 (m, 2H), 7.18 (d, $J = 1.5$ Hz, 1H), 6.83-6.79 (m, 2H), 4.82-4.74 (m, 3H), 3.94 (d, $J = 10.5$ Hz, 1H), 3.77 (s, 3H), 2.24 (t, $J = 10.0$ Hz, 1H), 2.16 (t, $J = 10.0$ Hz, 1H), 1.71-1.70 (m, 3H), 1.09 (s, 3H).

^{13}C NMR (125 MHz, CDCl_3) δ 191.5, 158.0, 152.7, 142.7, 138.4, 131.9, 129.8, 129.3, 128.9, 128.7, 127.4, 125.9, 113.3, 108.5, 55.2, 47.4, 44.9, 40.3, 35.7, 21.3, 18.9.

IR (film): ν (cm^{-1}) 3075, 2962, 2935, 2836, 1677, 1639, 1606, 1507, 1445, 1404, 1304, 1246, 1178, 1150, 1074, 1036, 941, 906, 890, 836, 762, 731, 690, 653, 597, 539.

HRMS (ESI, m/z) calcd for $\text{C}_{25}\text{H}_{27}\text{N}_2\text{O}_2$ $[\text{M}+\text{H}]^+$: 387.2067, found: 387.2060.



((1S,2S,3R)-3-Methyl-3-(prop-1-en-2-yl)-2-(4-(trifluoromethyl)phenyl)cyclobutyl)(1-phenyl-1H-imidazol-2-yl)methanone (28c)

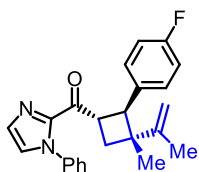
According to the general procedure, the reaction of (*E*)-1-(1-phenyl-1*H*-imidazol-2-yl)-3-(4-(trifluoromethyl)phenyl)prop-2-en-1-one **26c** (34.2 mg, 0.10 mmol), 2,3-dimethylbuta-1,3-diene **27a** (82.1 mg, 10.0 equiv) and Δ -**RhS** (3.5 mg, 4 mol%) in acetone (0.5 mL, 0.2 M) under nitrogen atmosphere with blue LEDs for 24 hours, afforded 33.3 mg (78%, combined yield) of **28c** as a colorless oil; $[\alpha]_D^{22} = +107.4^\circ$ (*c* 1.0, CH₂Cl₂); d.r. value was determined through ¹H NMR of crude materials as 12:1; enantiomeric excess of the major diastereoisomer was established by HPLC analysis using a Chiralpak AD-H column, ee = 91% (HPLC: AD-H, 254 nm, *n*-hexane/isopropanol = 95:5, flow rate 1 mL/min, 25 °C, *t_r* (major) = 7.9 min, *t_r* (minor) = 5.4 min).

¹H NMR (500 MHz, CDCl₃) δ 7.55-7.50 (m, 2H), 7.49-7.43 (m, 3H), 7.42-7.37 (m, 2H), 7.33 (s, 1H), 7.30-7.24 (m, 2H), 7.22 (s, 1H), 4.86-4.79 (m, 3H), 4.09 (d, *J* = 10.0 Hz, 1H), 2.29 (t, *J* = 10.0 Hz, 1H), 2.22 (t, *J* = 10.0 Hz, 1H), 1.74 (s, 3H), 1.10 (s, 3H).

¹³C NMR (125 MHz, CDCl₃) δ 191.0, 151.9, 144.07, 144.06, 142.5, 138.2, 129.9, 129.5, 129.0, 128.8, 128.5, 128.4, 128.3, 128.2, 127.6, 125.9, 125.3, 124.93, 124.90, 124.87, 124.8, 109.1, 47.3, 45.0, 40.0, 36.0, 21.3, 18.9. (Mixture of two diastereoisomers)

IR (film): ν (cm⁻¹) 2967, 2938, 2866, 1679, 1619, 1497, 1446, 1405, 1322, 1229, 1161, 1117, 1067, 1015, 942, 891, 839, 761, 690, 658, 597, 536.

HRMS (ESI, *m/z*) calcd for C₂₅H₂₄F₃N₂O [M+H]⁺: 425.1835, found: 425.1835.



((1S,2S,3R)-2-(4-Fluorophenyl)-3-methyl-3-(prop-1-en-2-yl)cyclobutyl)(1-phenyl-1H-imidazol-2-yl)methanone (28d)

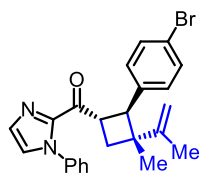
According to the general procedure, the reaction of (*E*)-3-(4-fluorophenyl)-1-(1-phenyl-1*H*-imidazol-2-yl)prop-2-en-1-one **26d** (29.2 mg, 0.10 mmol), 2,3-dimethylbuta-1,3-diene **27a** (24.6 mg, 3.0 equiv) and Δ -**RhS** (1.7 mg, 2 mol%) in acetone (0.5 mL, 0.2 M) under nitrogen atmosphere with blue LEDs for 14 hours, afforded 34.5 mg (92%, combined yield) of **28d** as a colorless oil; $[\alpha]_{\text{D}}^{22} = +131.2^\circ$ (*c* 1.0, CH₂Cl₂); d.r. value was determined through ¹H NMR of crude materials as 14:1; enantiomeric excess of the major diastereoisomer was established by HPLC analysis using a Chiralpak AD-H column, ee = 99% (HPLC: AD-H, 254 nm, *n*-hexane/isopropanol = 99:1, flow rate 1 mL/min, 25 °C, *t_r* (major) = 17.4 min, *t_r* (minor) = 9.4 min).

¹H NMR (500 MHz, CDCl₃) δ 7.49-7.45 (m, 3H), 7.34-7.32 (m, 1H), 7.30-7.24 (m, 4H), 7.22-7.20 (m, 1H), 7.01-6.94 (m, 2H), 4.86-4.76 (m, 3H), 4.01 (d, *J* = 10.0 Hz, 1H), 2.28 (t, *J* = 10.0 Hz, 1H), 2.21 (t, *J* = 10.0 Hz, 1H), 1.74 (s, 3H), 1.11 (s, 3H).

¹³C NMR (125 MHz, CDCl₃) δ 191.3, 161.5 (d, *J* = 242.6 Hz), 152.3, 142.7, 138.4, 135.6 (d, *J* = 2.6 Hz), 129.9, 129.6 (d, *J* = 7.5 Hz), 129.0, 128.8, 127.5, 125.9, 114.7 (d, *J* = 20.9 Hz), 108.8, 47.1, 44.8, 40.4, 35.9, 21.2, 18.9.

IR (film): ν (cm⁻¹) 3077, 2965, 2936, 2867, 1677, 1599, 1503, 1445, 1403, 1307, 1225, 1154, 1072, 1050, 890, 837, 760, 730, 690, 564, 537, 500.

HRMS (ESI, *m/z*) calcd for C₂₄H₂₃FN₂ONa [M+Na]⁺: 397.1687, found: 397.1685.



((1*S*,2*S*,3*R*)-2-(4-Bromophenyl)-3-methyl-3-(prop-1-en-2-yl)cyclobutyl)(1-phenyl-1*H*-imidazol-2-yl)methanone (28e**)**

According to the general procedure, the reaction of (*E*)-3-(4-bromophenyl)-1-(1-phenyl-1*H*-imidazol-2-yl)prop-2-en-1-one **26e** (35.3 mg, 0.10 mmol), 2,3-dimethylbuta-1,3-diene **27a** (24.6 mg, 3.0 equiv) and Δ -**RhS** (1.7 mg, 2 mol%) in acetone (0.5 mL, 0.2 M) under nitrogen atmosphere with blue LEDs for 15 hours, afforded 37.1 mg (85%, combined yield) of **28e** as a white solid; $[\alpha]_{\text{D}}^{22} = +185.8^\circ$ (*c* 1.0, CH₂Cl₂); d.r. value was determined through ¹H NMR of crude materials as 10:1; enantiomeric excess of the major diastereoisomer was established by HPLC analysis using a Chiralpak

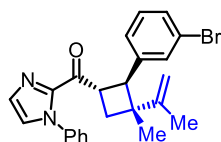
AD-H column, ee = 98% (HPLC: AD-H, 254 nm, *n*-hexane/isopropanol = 99:1, flow rate 1 mL/min, 25 °C, *t_r* (major) = 23.9 min, *t_r* (minor) = 11.3 min).

¹H NMR (500 MHz, CDCl₃) δ 7.47-7.43 (m, 3H), 7.41-7.37 (m, 2H), 7.31 (m, 1H), 7.28-7.22 (m, 2H), 7.20 (s, 1H), 7.18-7.13 (m, 2H), 4.81 (s, 1H), 4.79-4.72 (m, 2H), 3.96 (d, *J* = 10.0 Hz, 1H), 2.26 (t, *J* = 10.0 Hz, 1H), 2.18 (t, *J* = 10.0 Hz, 1H), 1.72 (s, 3H), 1.08 (s, 3H).

¹³C NMR (125 MHz, CDCl₃) δ 191.1, 152.1, 142.5, 138.9, 138.3, 131.0, 129.94, 129.86, 129.0, 128.8, 127.6, 125.9, 120.1, 108.9, 47.2, 44.8, 40.1, 35.8, 21.2, 18.9.

IR (film): ν (cm⁻¹) 3079, 2965, 2936, 2867, 1677, 1639, 1492, 1444, 1403, 1338, 1306, 1226, 1149, 1071, 1005, 904, 833, 761, 729, 692, 656, 537, 488.

HRMS (ESI, *m/z*) calcd for C₂₄H₂₃BrN₂ONa [M+Na]⁺: 457.0886, found: 457.0884.



((1*S*,2*S*,3*R*)-2-(3-Bromophenyl)-3-methyl-3-(prop-1-en-2-yl)cyclobutyl)(1-phenyl-1*H*-imidazol-2-yl)methanone (28f**)**

According to the general procedure, the reaction of (*E*)-3-(3-bromophenyl)-1-(1-phenyl-1*H*-imidazol-2-yl)prop-2-en-1-one **26f** (35.3 mg, 0.10 mmol), 2,3-dimethylbuta-1,3-diene **27a** (82.1 mg, 10.0 equiv) and Δ-**RhS** (3.5 mg, 4 mol%) in acetone (0.5 mL, 0.2 M) under nitrogen atmosphere with blue LEDs for 22 hours, afforded 36.6 mg (84%, combined yield) of **28f** as a colorless oil; [α]_D²² = +127.2° (*c* 1.0, CH₂Cl₂); d.r. value was determined through ¹H NMR of crude materials as 12:1; enantiomeric excess of the major diastereoisomer was established by HPLC analysis using a Chiralpak AD-H column, ee = 98% (HPLC: AD-H, 254 nm, *n*-hexane/isopropanol = 99:1, flow rate 1 mL/min, 25 °C, *t_r* (major) = 11.2 min, *t_r* (minor) = 9.5 min).

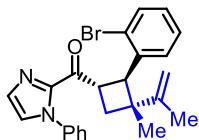
¹H NMR (500 MHz, CDCl₃) δ 7.47-7.42 (m, 4H), 7.34-7.24 (m, 4H), 7.23-7.19 (m, 2H), 7.13 (t, *J* = 7.8 Hz, 1H), 4.84 (s, 1H), 4.80 (s, 1H), 4.75 (q, *J* = 9.5 Hz, 1H), 4.01 (d, *J* = 9.5 Hz, 1H), 2.25 (t, *J* = 8.2 Hz, 1H), 2.22 (t, *J* = 8.0 Hz, 1H), 1.73 (s, 3H), 1.11 (s, 3H).

¹³C NMR (125 MHz, CDCl₃) δ 191.0, 152.0, 142.42, 142.40, 138.2, 131.1, 129.9, 129.5, 129.3, 128.9, 128.8, 127.5, 126.8, 125.9, 122.2, 109.0, 46.9, 45.0, 40.2, 36.1, 21.3, 18.9.

IR (film): ν (cm⁻¹) 3077, 2965, 2936, 2864, 1677, 1639, 1594, 1563, 1496, 1444, 1403, 1338, 1307,

1226, 1150, 1102, 1070, 996, 947, 890, 844, 813, 761, 692, 661, 536, 497, 438.

HRMS (ESI, m/z) calcd for $C_{24}H_{23}BrN_2ONa$ $[M+Na]^+$: 457.0886, found: 457.0883.



((1S,2R,3R)-2-(2-Bromophenyl)-3-methyl-3-(prop-1-en-2-yl)cyclobutyl)(1-phenyl-1H-imidazol-2-yl)methanone (28g)

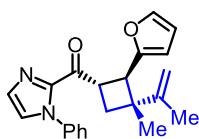
According to the general procedure, the reaction of (*E*)-3-(2-bromophenyl)-1-(1-phenyl-1*H*-imidazol-2-yl)prop-2-en-1-one **26g** (35.3 mg, 0.10 mmol), 2,3-dimethylbuta-1,3-diene **27a** (24.6 mg, 3.0 equiv) and Δ -**RhS** (1.7 mg, 2 mol%) in acetone (0.5 mL, 0.2 M) under nitrogen atmosphere with blue LEDs for 14 hours, afforded 40.1 mg (92%, combined yield) of **28g** as a colorless oil; $[\alpha]_D^{22} = +119.0^\circ$ (c 1.0, CH_2Cl_2); d.r. value was determined through 1H NMR of crude materials as 6:1; enantiomeric excess of the major diastereoisomer was established by HPLC analysis using a Chiralpak AD-H column, ee = 98% (HPLC: AD-H, 254 nm, *n*-hexane/isopropanol = 99:1, flow rate 1 mL/min, 25 °C, t_r (major) = 20.7 min, t_r (minor) = 10.9 min).

1H NMR (500 MHz, $CDCl_3$) δ 7.62 (d, J = 7.8 Hz, 1H), 7.49 (d, J = 8.0 Hz, 1H), 7.46-7.43 (m, 3H), 7.30 (t, J = 7.8 Hz, 1H), 7.27-7.23 (m, 3H), 7.15 (s, 1H), 7.04 (t, J = 7.5 Hz, 1H), 4.88 (q, J = 9.5 Hz, 1H), 4.77 (s, 1H), 4.76 (s, 1H), 4.36 (d, J = 10.0 Hz, 1H), 2.52 (t, J = 10.0 Hz, 1H), 2.05 (t, J = 9.8 Hz, 1H), 1.84 (s, 3H), 1.18 (s, 3H).

^{13}C NMR (125 MHz, $CDCl_3$) δ 190.7, 151.3, 142.7, 138.6, 138.3, 133.0, 130.3, 129.7, 129.0, 128.7, 127.9, 127.4, 126.8, 125.9, 125.3, 109.7, 47.9, 45.3, 40.9, 33.9, 21.4, 19.8.

IR (film): ν (cm^{-1}) 3064, 2965, 2868, 1678, 1637, 1595, 1496, 1443, 1403, 1339, 1309, 1226, 1150, 1074, 1050, 1023, 951, 890, 836, 756, 731, 691, 659, 540, 450.

HRMS (ESI, m/z) calcd for $C_{24}H_{23}BrN_2ONa$ $[M+Na]^+$: 457.0886, found: 457.0885.



((1S,2R,3R)-2-(Furan-2-yl)-3-methyl-3-(prop-1-en-2-yl)cyclobutyl)(1-phenyl-1H-imidazol-2-yl)m

ethanone (28h)

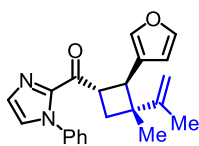
According to the general procedure, the reaction of (*E*)-3-(furan-2-yl)-1-(1-phenyl-1*H*-imidazol-2-yl)prop-2-en-1-one **26h** (26.4 mg, 0.10 mmol), 2,3-dimethylbuta-1,3-diene **27a** (24.6 mg, 3.0 equiv) and Δ -**RhS** (1.7 mg, 2 mol%) in acetone (0.5 mL, 0.2 M) under nitrogen atmosphere with blue LEDs for 16 hours, afforded 31.7 mg (92%, combined yield) of **28h** as a colorless oil; $[\alpha]_{\text{D}}^{22} = +117.8^\circ$ (*c* 1.0, CH₂Cl₂); d.r. value was determined through ¹H NMR of crude materials as 16:1; enantiomeric excess of the major diastereoisomer was established by HPLC analysis using a Chiralpak AD-H column, ee = 99% (HPLC: AD-H, 254 nm, *n*-hexane/isopropanol = 98:2, flow rate 1 mL/min, 25 °C, *t_r* (major) = 11.2 min, *t_r* (minor) = 8.2 min).

¹H NMR (500 MHz, CDCl₃) δ 7.47-7.42 (m, 3H), 7.32 (dd, *J*₁ = 2.0 Hz, *J*₂ = 1.0 Hz, 1H), 7.30 (d, *J* = 1.0 Hz, 1H), 7.29-7.24 (m, 2H), 7.29 (d, *J* = 1.0 Hz, 1H), 6.28 (dd, *J*₁ = 3.5 Hz, *J*₂ = 2.0 Hz, 1H), 6.22 (dt, *J*₁ = 3.0 Hz, *J*₂ = 1.0 Hz, 1H), 4.83-4.81 (m, 1H), 4.74-4.72 (m, 1H), 4.69 (q, *J* = 9.5 Hz, 1H), 3.88 (d, *J* = 10.0 Hz, 1H), 2.26-2.18 (m, 2H), 1.71-1.69 (m, 3H), 1.16 (s, 3H).

¹³C NMR (125 MHz, CDCl₃) δ 190.7, 154.7, 152.7, 142.5, 141.4, 138.3, 129.9, 128.9, 128.7, 127.3, 126.0, 109.9, 108.3, 106.9, 45.3, 41.9, 39.8, 35.7, 22.0, 18.0.

IR (film): ν (cm⁻¹) 3112, 3077, 2965, 2937, 2866, 1678, 1642, 1594, 1497, 1444, 1404, 1339, 1306, 1227, 1148, 1065, 1011, 955, 890, 827, 761, 732, 692, 657, 597, 536.

HRMS (ESI, *m/z*) calcd for C₂₂H₂₂N₂O₂Na [M+Na]⁺: 369.1573, found: 369.1572.



((1*S*,2*R*,3*R*)-2-(Furan-3-yl)-3-methyl-3-(prop-1-en-2-yl)cyclobutyl)(1-phenyl-1*H*-imidazol-2-yl)m ethanone (28i)

According to the general procedure, the reaction of (*E*)-3-(furan-3-yl)-1-(1-phenyl-1*H*-imidazol-2-yl)prop-2-en-1-one **26i** (26.4 mg, 0.10 mmol), 2,3-dimethylbuta-1,3-diene **27a** (82.1 mg, 10.0 equiv) and Δ -**RhS** (3.5 mg, 4 mol%) in acetone (0.5 mL, 0.2 M) under nitrogen atmosphere with blue LEDs for 20 hours, afforded 24.9 mg (72%, combined yield) of **28i** as a colorless oil; $[\alpha]_{\text{D}}^{22} = +89.6^\circ$ (*c* 1.0, CH₂Cl₂); d.r. value was determined through ¹H NMR of crude materials as 9:1; enantiomeric excess of the major diastereoisomer was established by HPLC analysis using a Chiralpak

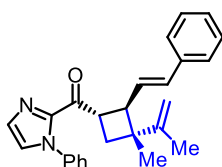
AD-H column, ee = 99% (HPLC: AD-H, 254 nm, *n*-hexane/isopropanol = 99:1, flow rate 1 mL/min, 25 °C, *t_r* (major) = 18.1 min, *t_r* (minor) = 11.5 min).

¹H NMR (500 MHz, CDCl₃) δ 7.49-7.45 (m, 3H), 7.44 (d, *J* = 1.0 Hz, 1H), 7.35 (t, *J* = 1.8 Hz, 1H), 7.32 (s, 1H), 7.30-7.26 (m, 2H), 7.21 (s, 1H), 6.36-6.34 (s, 1H), 4.75-4.73 (m, 2H), 4.57 (q, *J* = 9.5 Hz, 1H), 3.73 (d, *J* = 10.0 Hz, 1H), 2.27 (t, *J* = 10.0 Hz, 1H), 2.17 (t, *J* = 9.8 Hz, 1H), 1.70 (s, 3H), 1.18 (s, 3H).

¹³C NMR (125 MHz, CDCl₃) δ 191.3, 152.9, 142.7, 142.5, 140.3, 138.3, 129.8, 128.9, 128.7, 127.4, 126.0, 124.1, 111.1, 108.0, 44.3, 41.0, 40.3, 35.7, 21.9, 18.3.

IR (film): ν (cm⁻¹) 3113, 3077, 2963, 2934, 2864, 1677, 1641, 1595, 1496, 1444, 1403, 1338, 1307, 1226, 1154, 1063, 1029, 996, 896, 880, 826, 762, 730, 692, 657, 599, 537.

HRMS (ESI, *m/z*) calcd for C₂₂H₂₂N₂O₂Na [M+Na]⁺: 369.1573, found: 369.1572.



((1*S*,2*R*,3*R*)-3-Methyl-3-(prop-1-en-2-yl)-2-((*E*)-styryl)cyclobutyl)(1-phenyl-1*H*-imidazol-2-yl)methanone (28j**)**

According to the general procedure, the reaction of 5-phenyl-1-(1-phenyl-1*H*-imidazol-2-yl)penta-2,4-dien-1-one **26j** (30.0 mg, 0.10 mmol, *E/Z* mixture), 2,3-dimethylbuta-1,3-diene **27a** (82.1 mg, 10.0 equiv) and Δ-**RhS** (3.5 mg, 4 mol%) in acetone (0.5 mL, 0.2 M) under nitrogen atmosphere with blue LEDs for 15 hours, afforded 33.2 mg (84%, combined yield) of **28j**; d.r. value was determined through ¹H NMR of crude materials as 6:1. The separable major diastereoisomer was obtained as a colorless oil; [α]_D²² = +190.0° (*c* 1.0, CH₂Cl₂); enantiomeric excess was established by HPLC analysis using a Chiralpak AD-H column, ee = 96% (HPLC: AD-H, 254 nm, *n*-hexane/isopropanol = 99:1, flow rate 1 mL/min, 25 °C, *t_r* (major) = 17.1 min, *t_r* (minor) = 13.9 min).

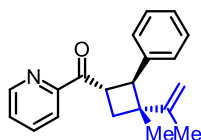
¹H NMR (500 MHz, CDCl₃) δ 7.47-7.43 (m, 3H), 7.37-7.33 (m, 2H), 7.30-7.25 (m, 5H), 7.21-7.16 (m, 2H), 6.48 (d, *J* = 16.0 Hz, 1H), 6.35 (dd, *J₁* = 16.0 Hz, *J₂* = 8.0 Hz, 1H), 4.68-4.66 (m, 2H), 4.47 (q, *J* = 9.5 Hz, 1H), 3.37 (t, *J* = 8.8 Hz, 1H), 2.24 (t, *J* = 10.3 Hz, 1H), 2.11 (dd, *J₁* = 10.5 Hz, *J₂* = 9.0 Hz, 1H), 1.66 (s, 3H), 1.31 (s, 3H).

¹³C NMR (125 MHz, CDCl₃) δ 191.3, 153.2, 142.7, 138.4, 137.4, 131.5, 129.7, 129.1, 128.9, 128.7,

128.4, 127.3, 127.1, 126.2, 125.9, 107.7, 47.7, 44.7, 41.2, 35.2, 21.7, 18.2.

IR (film): ν (cm⁻¹) 3074, 3026, 2962, 2933, 2863, 1677, 1642, 1597, 1496, 1445, 1403, 1307, 1226, 1149, 1051, 963, 887, 846, 807, 754, 690, 661, 536, 489.

HRMS (ESI, m/z) calcd for C₂₆H₂₆N₂ONa [M+Na]⁺: 405.1937, found: 405.1935.



((1S,2S,3R)-3-Methyl-2-phenyl-3-(prop-1-en-2-yl)cyclobutyl)(pyridin-2-yl)methanone (28k)

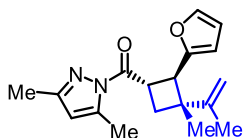
According to the general procedure, the reaction of (*E*)-3-phenyl-1-(pyridin-2-yl)prop-2-en-1-one **26k** (20.9 mg, 0.10 mmol), 2,3-dimethylbuta-1,3-diene **27a** (24.6 mg, 3.0 equiv) and Δ -RhS (1.7 mg, 2 mol%) in acetone/MeCN (0.5 mL, 1:1 v/v, 0.2 M) under nitrogen atmosphere with blue LEDs for 12 hours, afforded 21.0 mg (72%, combined yield) of **28k** as a white solid; $[\alpha]_D^{22} = +50.2^\circ$ (*c* 1.0, CH₂Cl₂); d.r. value was determined through ¹H NMR of crude materials as 8:1; enantiomeric excess of the major diastereoisomer was established by HPLC analysis using a Chiralpak AD-H column, ee = 95% (HPLC: AD-H, 254 nm, *n*-hexane/isopropanol = 99:1, flow rate 1 mL/min, 25 °C, *t_r* (major) = 11.7 min, *t_r* (minor) = 15.3 min).

¹H NMR (500 MHz, CDCl₃) δ 8.70-8.67 (m, 1H), 8.05 (d, *J* = 8.0 Hz, 1H), 7.81 (td, *J₁* = 8.0 Hz, *J₂* = 4.0 Hz, 1H), 7.45 (ddd, *J₁* = 7.5 Hz, *J₂* = 5.0 Hz, *J₃* = 1.0 Hz, 1H), 7.30-7.24 (m, 4H), 7.20-7.15 (m, 1H), 4.95-4.87 (m, 2H), 4.48-4.82 (m, 1H), 4.14 (d, *J* = 10.0 Hz, 1H), 2.27 (t, *J* = 10.0 Hz, 1H), 2.21 (t, *J* = 10.0 Hz, 1H), 1.78 (s, 3H), 1.14 (s, 3H).

¹³C NMR (125 MHz, CDCl₃) δ 202.0, 153.0, 152.6, 149.0, 140.1, 136.8, 128.2, 127.9, 127.1, 126.1, 122.3, 108.8, 47.8, 45.1, 38.7, 36.1, 21.5, 19.0.

IR (film): ν (cm⁻¹) 3057, 3027, 2958, 2866, 1681, 1640, 1578, 1434, 1374, 1333, 1272, 1232, 1203, 1060, 996, 963, 884, 853, 794, 741, 696, 637, 624, 570, 405.

HRMS (ESI, m/z) calcd for C₂₀H₂₂NO [M+H]⁺: 292.1696, found: 292.1695.



(3,5-Dimethyl-1*H*-pyrazol-1-yl)((1*S*,2*R*,3*R*)-2-(furan-2-yl)-3-methyl-3-(prop-1-en-2-yl)cyclobutyl) methanone (28l**)**

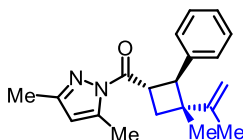
According to the general procedure, the reaction of (*E*)-1-(3,5-dimethyl-1*H*-pyrazol-1-yl)-3-(furan-2-yl)prop-2-en-1-one **26l** (21.6 mg, 0.10 mmol), 2,3-dimethylbuta-1,3-diene **27a** (82.1 mg, 10.0 equiv) and Δ -**RhS** (3.5 mg, 4 mol%) in acetone (0.5 mL, 0.2 M) under nitrogen atmosphere with blue LEDs for 18 hours, afforded 23.9 mg (80%, combined yield) of **28l** as a colorless oil; $[\alpha]_D^{22} = +39.6^\circ$ (*c* 1.0, CH₂Cl₂); d.r. value was determined through ¹H NMR of crude materials as 11:1; enantiomeric excess of the major diastereoisomer was established by HPLC analysis using a Chiralpak OD-H column, ee = 92% (HPLC: OD-H, 254 nm, *n*-hexane/isopropanol = 99.5:0.5, flow rate 0.6 mL/min, 25 °C, *t_r* (major) = 9.5 min, *t_r* (minor) = 11.3 min).

¹H NMR (500 MHz, CDCl₃) δ 7.34 (dd, *J*₁ = 2.0 Hz, *J*₂ = 1.0 Hz, 1H), 6.29 (dd, *J*₁ = 3.0 Hz, *J*₂ = 2.0 Hz, 1H), 6.21 (d, *J* = 3.0 Hz 1H), 5.94-5.93 (m, 1H), 4.87-4.86 (m, 1H), 4.78-4.77 (m, 1H), 4.54 (q, *J* = 9.7 Hz, 1H), 3.96 (d, *J* = 10.0 Hz, 1H), 2.52-2.51 (m, 3H), 2.31 (t, *J* = 10.5 Hz, 1H), 2.26-2.19 (m, 1H), 2.23 (s, 3H), 1.74 (s, 3H), 1.16 (s, 3H).

¹³C NMR (125 MHz, CDCl₃) δ 174.3, 154.5, 152.7, 152.0, 144.1, 141.4, 111.2, 110.0, 108.3, 107.0, 45.6, 42.7, 36.8, 35.8, 22.0, 18.1, 14.4, 13.8.

IR (film): ν (cm⁻¹) 3116, 3081, 2966, 2931, 2868, 1719, 1583, 1442, 1376, 1332, 1309, 1250, 1145, 1013, 987, 960, 891, 833, 804, 775, 731, 594, 552.

HRMS (ESI, *m/z*) calcd for C₁₈H₂₂N₂O₂Na [M+Na]⁺: 321.1573, found: 321.1572.



(3,5-Dimethyl-1*H*-pyrazol-1-yl)((1*S*,2*S*,3*R*)-3-methyl-2-phenyl-3-(prop-1-en-2-yl)cyclobutyl) methanone (28m**)**

According to the general procedure, the reaction of (*E*)-1-(3,5-dimethyl-1*H*-pyrazol-1-yl)-3-phenylprop-2-en-1-one **26m** (22.6 mg, 0.10 mmol), 2,3-dimethylbuta-1,3-diene **27a** (24.6 mg, 3.0

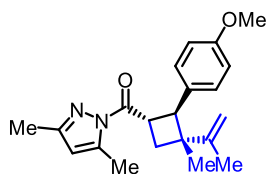
equiv) and Δ -**RhS** (1.7 mg, 2 mol%) in acetone (0.5 mL, 0.2 M) under nitrogen atmosphere with blue LEDs for 15 hours, afforded 28.8 mg (93%, combined yield) of **28m** as a colorless oil; $[\alpha]_D^{22} = +25.2^\circ$ (c 1.0, CH_2Cl_2); d.r. value was determined through ^1H NMR of crude materials as 10:1; enantiomeric excess of the major diastereoisomer was established by HPLC analysis using a Chiralcel OJ-H column, $ee = 96\%$ (HPLC: OJ-H, 254 nm, n -hexane/isopropanol = 99:1, flow rate 1 mL/min, 25 $^\circ\text{C}$, t_r (major) = 6.8 min, t_r (minor) = 12.8 min).

^1H NMR (500 MHz, CDCl_3) δ 7.34-7.28 (m, 4H), 7.27-7.20 (m, 1H), 5.98-5.97 (m, 1H), 4.94-4.92 (m, 1H), 4.88-4.85 (m, 1H), 4.70 (q, $J = 9.5$ Hz, 1H), 4.16 (d, $J = 10.0$ Hz, 1H), 2.55-2.54 (m, 3H), 2.37 (t, $J = 10.0$ Hz, 1H), 2.27 (s, 3H), 2.27-2.22 (m, 1H), 1.81-1.80 (m, 3H), 1.13 (s, 3H).

^{13}C NMR (125 MHz, CDCl_3) δ 174.9, 152.5, 152.0, 144.0, 139.6, 128.2, 127.9, 126.2, 111.2, 108.8, 48.2, 45.3, 36.8, 36.0, 21.3, 19.0, 14.5, 13.8.

IR (film): ν (cm^{-1}) 3083, 3029, 2965, 2931, 2867, 1719, 1581, 1487, 1444, 1381, 1338, 1313, 1249, 1169, 1025, 958, 890, 842, 804, 770, 734, 697, 629, 556.

HRMS (ESI, m/z) calcd for $\text{C}_{20}\text{H}_{24}\text{N}_2\text{ONa}$ $[\text{M}+\text{Na}]^+$: 331.1781, found: 331.1780.



(3,5-Dimethyl-1H-pyrazol-1-yl)((1S,2S,3R)-2-(4-methoxyphenyl)-3-methyl-3-(prop-1-en-2-yl)cyclobutyl)methanone (28n)

According to the general procedure, the reaction of (*E*)-1-(3,5-dimethyl-1H-pyrazol-1-yl)-3-(4-methoxyphenyl)prop-2-en-1-one **26n** (25.6 mg, 0.10 mmol), 2,3-dimethylbuta-1,3-diene **27a** (24.6 mg, 3.0 equiv) and Δ -**RhS** (1.7 mg, 2 mol%) in acetone (0.5 mL, 0.2 M) under nitrogen atmosphere with blue LEDs for 12 hours, afforded 29.8 mg (88%, combined yield) of **28n** as a colorless oil; $[\alpha]_D^{22} = +48.4^\circ$ (c 1.0, CH_2Cl_2); d.r. value was determined through ^1H NMR of crude materials as 11:1; enantiomeric excess of the major diastereoisomer was established by HPLC analysis using a Chiralpak OD-H column, $ee = 94\%$ (HPLC: OD-H, 254 nm, n -hexane/isopropanol = 99:1, flow rate 1 mL/min, 25 $^\circ\text{C}$, t_r (major) = 5.7 min, t_r (minor) = 6.7 min).

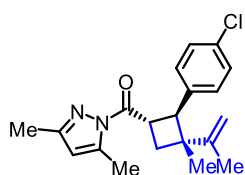
^1H NMR (500 MHz, CDCl_3) δ 7.25-7.21 (m, 2H), 6.85-6.81 (m, 2H), 5.94 (s, 1H), 4.87 (s, 1H),

4.82-4.80 (m, 1H), 4.62 (q, $J = 9.5$ Hz, 1H), 4.03 (d, $J = 10.0$ Hz, 1H), 3.78 (s, 3H), 2.51 (s, 3H), 2.33 (t, $J = 10.0$ Hz, 1H), 2.24 (s, 3H), 2.20 (t, $J = 10.0$ Hz, 1H), 1.76 (s, 3H), 1.10 (s, 3H).

^{13}C NMR (125 MHz, CDCl_3) δ 175.0, 158.1, 152.7, 151.9, 144.0, 131.7, 129.3, 113.3, 111.2, 108.6, 55.2, 47.9, 45.3, 37.1, 35.8, 21.3, 18.9, 14.5, 13.8.

IR (film): ν (cm^{-1}) 3081, 2962, 2933, 2836, 1719, 1611, 1581, 1512, 1443, 1381, 1337, 1310, 1246, 1176, 1033, 958, 889, 836, 806, 769, 737, 592, 556.

HRMS (ESI, m/z) calcd for $\text{C}_{21}\text{H}_{26}\text{N}_2\text{O}_2\text{Na}$ $[\text{M}+\text{Na}]^+$: 361.1886, found: 361.1885.



((1S,2S,3R)-2-(4-Chlorophenyl)-3-methyl-3-(prop-1-en-2-yl)cyclobutyl)(3,5-dimethyl-1H-pyrazol-1-yl)methanone (28o)

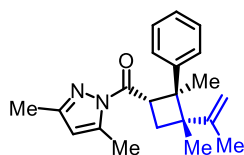
According to the general procedure, the reaction of (*E*)-1-(3,5-dimethyl-1H-pyrazol-1-yl)-3-(4-chlorophenyl)prop-2-en-1-one **26o** (26.1 mg, 0.10 mmol), 2,3-dimethylbuta-1,3-diene **27a** (24.6 mg, 3.0 equiv) and Δ -**RhS** (1.7 mg, 2 mol%) in acetone (0.5 mL, 0.2 M) under nitrogen atmosphere with blue LEDs for 12 hours, afforded 32.0 mg (94%, combined yield) of **28o** as a white solid; $[\alpha]_{\text{D}}^{22} = +30.2^\circ$ (c 1.0, CH_2Cl_2); d.r. value was determined through ^1H NMR of crude materials as 9:1; enantiomeric excess of the major diastereoisomer was established by HPLC analysis using a Chiralpak OD-H column, ee = 93% (HPLC: OD-H, 254 nm, *n*-hexane/isopropanol = 99.5:0.5, flow rate 0.6 mL/min, 25 $^\circ\text{C}$, t_{r} (major) = 9.8 min, t_{r} (minor) = 12.1 min).

^1H NMR (500 MHz, CDCl_3) δ 7.28-7.20 (m, 4H), 5.96-5.95 (m, 1H), 4.88-4.87 (m, 1H), 4.85-4.83 (m, 1H), 4.62 (q, $J = 9.7$ Hz, 1H), 4.07 (d, $J = 10.0$ Hz, 1H), 2.53-2.52 (m, 3H), 2.36 (t, $J = 10.0$ Hz, 1H), 2.24 (s, 3H), 2.24-2.18 (m, 1H), 1.78-1.77 (m, 3H), 1.09 (s, 3H).

^{13}C NMR (125 MHz, CDCl_3) δ 174.7, 152.2, 152.1, 144.1, 138.1, 132.1, 129.6, 128.1, 111.3, 109.0, 47.9, 45.2, 37.0, 35.8, 21.2, 18.9, 14.4, 13.8.

IR (film): ν (cm^{-1}) 3083, 2965, 2930, 2869, 1718, 1582, 1489, 1443, 1379, 1334, 1250, 1171, 1091, 1014, 959, 890, 836, 802, 766, 733, 661, 554, 497.

HRMS (ESI, m/z) calcd for $\text{C}_{20}\text{H}_{23}\text{ClN}_2\text{ONa}$ $[\text{M}+\text{Na}]^+$: 365.1391, found: 365.1390.



(3,5-Dimethyl-1*H*-pyrazol-1-yl)((1*S*,2*S*,3*S*)-2,3-dimethyl-2-phenyl-3-(prop-1-en-2-yl)cyclobutyl)methanone (28p**)**

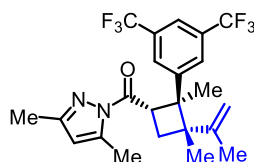
According to the general procedure, the reaction of (*E*)-1-(3,5-dimethyl-1*H*-pyrazol-1-yl)-3-phenylbut-2-en-1-one **26p** (24.0 mg, 0.10 mmol), 2,3-dimethylbuta-1,3-diene **27a** (82.1 mg, 10.0 equiv) and Δ -**RhS** (3.5 mg, 4 mol%) in acetone (0.5 mL, 0.2 M) under nitrogen atmosphere with blue LEDs for 19 hours, afforded 30.4 mg (95%, combined yield) of **28p** as a colorless oil; $[\alpha]_D^{22} = +117.6^\circ$ (*c* 1.0, CH₂Cl₂); d.r. value was determined through ¹H NMR of crude materials as >20:1; enantiomeric excess of the major diastereoisomer was established by HPLC analysis using a Chiralpak AD-H column, ee = 99% (HPLC: AD-H, 254 nm, *n*-hexane/isopropanol = 99:1, flow rate 0.6 mL/min, 25 °C, *t_r* (major) = 8.3 min, *t_r* (minor) = 14.8 min).

¹H NMR (500 MHz, CDCl₃) δ 7.69 (d, *J* = 8.0 Hz, 2H), 7.31 (t, *J* = 7.8 Hz, 2H), 7.20 (t, *J* = 7.3 Hz, 1H), 5.89 (s, 1H), 5.10 (dd, *J₁* = 10.5 Hz, *J₂* = 8.5 Hz, 1H), 4.97 (s, 1H), 4.91 (s, 1H), 2.95 (t, *J* = 10.5 Hz, 1H), 2.50 (s, 3H), 2.13 (s, 3H), 1.79 (dd, *J₁* = 10.5 Hz, *J₂* = 8.5 Hz, 1H), 1.78 (s, 3H), 1.36 (s, 3H), 0.99 (s, 3H).

¹³C NMR (125 MHz, CDCl₃) δ 173.7, 151.2, 149.1, 144.2, 143.5, 127.9, 127.3, 125.8, 111.7, 111.1, 53.7, 48.2, 38.9, 29.8, 24.7, 20.9, 20.4, 14.4, 13.5.

IR (film): ν (cm⁻¹) 3085, 3059, 2968, 2929, 2875, 1715, 1635, 1581, 1445, 1408, 1375, 1352, 1314, 1248, 1143, 1078, 1029, 960, 890, 829, 804, 772, 696, 576, 416.

HRMS (ESI, *m/z*) calcd for C₂₁H₂₆N₂ONa [M+Na]⁺: 345.1937, found: 345.1935.



((1*S*,2*S*,3*S*)-2-(3,5-Bis(trifluoromethyl)phenyl)-2,3-dimethyl-3-(prop-1-en-2-yl)cyclobutyl)(3,5-dimethyl-1*H*-pyrazol-1-yl)methanone (28q**)**

According to the general procedure, the reaction of (*E*)-3-(3,5-bis(trifluoromethyl)phenyl)-1-(3,5-dimethyl-1*H*-pyrazol-1-yl)but-2-en-1-one **26q** (37.6 mg, 0.10 mmol), 2,3-dimethylbuta-1,3-diene

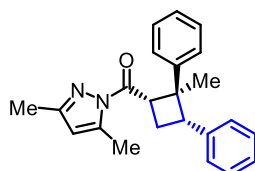
27a (82.1 mg, 10.0 equiv) and Δ -**RhS** (3.5 mg, 4 mol%) in acetone (0.5 mL, 0.2 M) under nitrogen atmosphere with blue LEDs for 22 hours, afforded 42.3 mg (92%, combined yield) of **28q** as a colorless oil; $[\alpha]_D^{22} = +73.0^\circ$ (c 1.0, CH_2Cl_2); d.r. value was determined through ^1H NMR of crude materials as >20:1; enantiomeric excess of the major diastereoisomer was established by HPLC analysis using a Chiralpak OD-H column, ee = 98% (HPLC: OD-H, 254 nm, n -hexane/isopropanol = 99.5:0.5, flow rate 0.6 mL/min, 25 $^\circ\text{C}$, t_r (major) = 11.0 min, t_r (minor) = 12.9 min).

^1H NMR (500 MHz, CDCl_3) δ 8.22 (s, 2H), 7.73 (s, 1H), 5.92 (s, 1H), 5.09 (dd, $J_1 = 10.0$ Hz, $J_2 = 8.5$ Hz, 1H), 5.04 (s, 1H), 4.93 (s, 1H), 3.03 (t, $J = 10.8$ Hz, 1H), 2.52 (s, 3H), 2.08 (s, 3H), 1.78 (dd, $J_1 = 11.0$ Hz, $J_2 = 8.0$ Hz, 1H), 1.76 (s, 3H), 1.38 (s, 3H), 0.96 (s, 3H).

^{13}C NMR (125 MHz, CDCl_3) δ 172.6, 152.2, 147.9, 147.1, 143.9, 130.6 (q, $J = 32.7$ Hz), 128.3-128.1 (m), 123.7 (q, $J = 271.0$ Hz), 120.0-119.8 (m), 112.8, 111.6, 53.4, 48.1, 38.9, 29.2, 24.9, 20.8, 20.2, 14.4, 13.2.

IR (film): ν (cm^{-1}) 3088, 2970, 2935, 2879, 1718, 1583, 1450, 1411, 1377, 1315, 1273, 1174, 1128, 1013, 960, 938, 895, 851, 806, 759, 704, 682, 412.

HRMS (ESI, m/z) calcd for $\text{C}_{23}\text{H}_{25}\text{F}_6\text{N}_2\text{O}$ $[\text{M}+\text{H}]^+$: 459.1866, found: 459.1863.



(3,5-Dimethyl-1H-pyrazol-1-yl)((1S,2S,3S)-2-methyl-2,3-diphenylcyclobutyl)methanone (28s)

According to the general procedure, the reaction of (*E*)-1-(3,5-dimethyl-1H-pyrazol-1-yl)-3-phenylbut-2-en-1-one **26p** (24.0 mg, 0.10 mmol), styrene (104.2 mg, 10.0 equiv) and Δ -**RhS** (3.5 mg, 4 mol%) in acetone (0.5 mL, 0.2 M) under nitrogen atmosphere with blue LEDs for 16 hours, afforded 31.9 mg (93%, combined yield) of **28s** as a colorless oil; $[\alpha]_D^{22} = -61.4^\circ$ (c 1.0, CH_2Cl_2); d.r. value was determined through ^1H NMR of crude materials as 16:1; enantiomeric excess of the major diastereoisomer was established by HPLC analysis using a Chiralpak OD-H column, ee = 99% (HPLC: OD-H, 254 nm, n -hexane/isopropanol = 99:1, flow rate 1 mL/min, 25 $^\circ\text{C}$, t_r (major) = 7.2 min, t_r (minor) = 6.7 min).

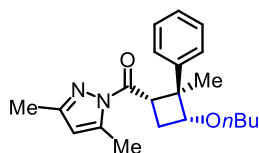
^1H NMR (500 MHz, CDCl_3) δ 7.52 (d, $J = 7.5$ Hz, 2H), 7.37-7.29 (m, 4H), 7.26-7.20 (m, 4H), 5.90 (s,

¹H), 4.80 (dd, $J_1 = 10.5$ Hz, $J_2 = 8.0$ Hz, 1H), 3.94 (dd, $J_1 = 11.0$ Hz, $J_2 = 8.5$ Hz, 1H), 3.04 (q, $J = 11.0$ Hz, 1H), 2.55 (s, 3H), 2.44 (dt, $J_1 = 11.0$ Hz, $J_2 = 8.5$ Hz, 1H), 1.98 (s, 3H), 1.09 (s, 3H).

¹³C NMR (125 MHz, CDCl₃) δ 173.1, 151.4, 148.8, 143.4, 139.6, 128.1, 128.0, 127.9, 126.5, 126.0, 125.8, 111.0, 52.3, 47.5, 44.7, 22.7, 18.1, 14.3, 13.4.

IR (film): ν (cm⁻¹) 3058, 3027, 2967, 2927, 1714, 1581, 1491, 1448, 1406, 1377, 1349, 1314, 1249, 1178, 1138, 1093, 1029, 1002, 961, 921, 843, 803, 761, 695, 629, 583, 551, 479, 398.

HRMS (ESI, m/z) calcd for C₂₃H₂₄N₂ONa [M+Na]⁺: 367.1781, found: 367.1780.



((1S,2S,3R)-3-Butoxy-2-methyl-2-phenylcyclobutyl)(3,5-dimethyl-1H-pyrazol-1-yl)methanone (28t)

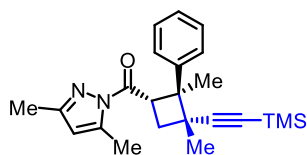
According to the general procedure, the reaction of (*E*)-1-(3,5-dimethyl-1H-pyrazol-1-yl)-3-phenylbut-2-en-1-one **26p** (24.0 mg, 0.10 mmol), 1-(vinylloxy)butane (100.2 mg, 10.0 equiv) and Δ -**RhS** (3.5 mg, 4 mol%) in acetone (0.5 mL, 0.2 M) under nitrogen atmosphere with blue LEDs for 12 hours, afforded 32.9 mg (97%, combined yield) of **28t**; d.r. value was determined through ¹H NMR of crude materials as 6:1. The separable major diastereoisomer was obtained as a white solid; $[\alpha]_D^{22} = +85.2^\circ$ (c 1.0, CH₂Cl₂); enantiomeric excess was established by HPLC analysis using a Chiralcel OJ-H column, ee = 99% (HPLC: OJ-H, 254 nm, *n*-hexane/isopropanol = 99:1, flow rate 1 mL/min, 25 °C, t_r (major) = 4.2 min, t_r (minor) = 5.2 min).

¹H NMR (500 MHz, CDCl₃) δ 7.69 (d, $J = 8.5$ Hz, 2H), 7.34 (t, $J = 7.5$ Hz, 2H), 7.25-7.21 (m, 1H), 5.92 (s, 1H), 4.78 (dd, $J_1 = 9.5$ Hz, $J_2 = 5.5$ Hz, 1H), 4.00 (t, $J = 7.0$ Hz, 1H), 3.28 (dt, $J_1 = 9.0$ Hz, $J_2 = 6.5$ Hz, 1H), 3.15 (dt, $J_1 = 9.5$ Hz, $J_2 = 7.0$ Hz, 1H), 2.87-2.81 (m, 1H), 2.56 (s, 3H), 2.15-2.10 (m, 1H), 2.08 (s, 3H), 1.44-1.37 (m, 2H), 1.31 (s, 3H), 1.26-1.19 (m, 2H), 0.82 (t, $J = 7.3$ Hz, 3H).

¹³C NMR (125 MHz, CDCl₃) δ 174.5, 151.6, 143.7, 143.6, 127.8, 127.5, 125.9, 111.0, 81.1, 69.1, 52.8, 43.1, 31.7, 27.3, 25.1, 19.2, 14.5, 13.9, 13.6.

IR (film): ν (cm⁻¹) 2957, 2924, 2869, 1706, 1581, 1488, 1452, 1412, 1376, 1350, 1310, 1240, 1180, 1156, 1107, 1072, 1026, 963, 915, 827, 764, 704, 656, 511, 455, 416.

HRMS (ESI, m/z) calcd for C₂₁H₂₈N₂O₂Na [M+Na]⁺: 363.2043, found: 363.2042.



(3,5-Dimethyl-1*H*-pyrazol-1-yl)((1*S*,2*S*,3*R*)-2,3-dimethyl-2-phenyl-3-((trimethylsilyl)ethynyl)cyclobutyl)methanone (28u)

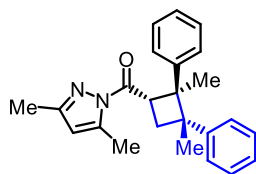
According to the general procedure, the reaction of (*E*)-1-(3,5-dimethyl-1*H*-pyrazol-1-yl)-3-phenylbut-2-en-1-one **26p** (24.0 mg, 0.10 mmol), trimethyl(3-methylbut-3-en-1-yn-1-yl)silane (138.3 mg, 10.0 equiv) and Δ -**RhS** (3.5 mg, 4 mol%) in acetone (0.5 mL, 0.2 M) under nitrogen atmosphere with blue LEDs for 15 hours, afforded 24.8 mg (66%, combined yield) of **28u** as a white solid; d.r. value was determined through ^1H NMR of crude materials as 9:1; $[\alpha]_{\text{D}}^{22} = +104.8^\circ$ (*c* 1.0, CH_2Cl_2); enantiomeric excess of the major diastereoisomer was established by HPLC analysis using a Chiralpak OD-H column, ee = 97% (HPLC: OD-H, 254 nm, *n*-hexane/isopropanol = 99:1, flow rate 0.6 mL/min, 25 $^\circ\text{C}$, t_{r} (major) = 6.0 min, t_{r} (minor) = 10.7 min).

^1H NMR (500 MHz, CDCl_3) δ 7.55-7.51 (m, 2H), 7.29-7.23 (m, 2H), 7.16 (tt, $J_1 = 7.0$ Hz, $J_2 = 1.5$ Hz, 1H), 5.97-5.96 (m, 1H), 5.14 (dd, $J_1 = 10.5$ Hz, $J_2 = 8.5$ Hz, 1H), 2.55 (t, $J = 10.5$ Hz, 1H), 2.54-2.52 (m, 3H), 2.39 (dd, $J_1 = 10.5$ Hz, $J_2 = 8.5$ Hz, 1H), 2.25 (s, 3H), 1.46 (s, 3H), 1.44 (s, 3H), -0.13 (s, 9H).

^{13}C NMR (125 MHz, CDCl_3) δ 173.1, 151.5, 147.5, 143.8, 127.3, 126.4, 125.7, 112.9, 111.3, 87.8, 54.6, 41.7, 40.3, 34.5, 23.0, 21.1, 14.5, 13.7, -0.2.

IR (film): ν (cm^{-1}) 3062, 2959, 2927, 2897, 2158, 1708, 1583, 1490, 1442, 1410, 1364, 1311, 1248, 1140, 1024, 958, 836, 757, 725, 695, 646, 506, 446.

HRMS (ESI, m/z) calcd for $\text{C}_{23}\text{H}_{31}\text{N}_2\text{OSi}$ $[\text{M}+\text{H}]^+$: 379.2200, found: 379.2196.



(3,5-Dimethyl-1*H*-pyrazol-1-yl)((1*S*,2*S*,3*S*)-2,3-dimethyl-2,3-diphenylcyclobutyl)methanone (28v)

According to the general procedure, the reaction of (*E*)-1-(3,5-dimethyl-1*H*-pyrazol-1-yl)-3-phenylbut-2-en-1-one **26p** (24.0 mg, 0.10 mmol), prop-1-en-2-ylbenzene (118.2 mg, 10.0 equiv) and Δ -**RhS** (3.5 mg, 4 mol%) in acetone (0.5 mL, 0.2 M) under nitrogen atmosphere with blue LEDs for

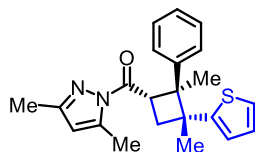
12 hours, afforded 33.8 mg (94%, combined yield) of **28v** as a colorless oil; $[\alpha]_D^{22} = +61.2^\circ$ (c 1.0, CH_2Cl_2); d.r. value was determined through ^1H NMR of crude materials as >20:1; enantiomeric excess of the major diastereoisomer was established by HPLC analysis using a Chiralpak OD-H column, ee = 99% (HPLC: OD-H, 254 nm, n -hexane/isopropanol = 99:1, flow rate 0.6 mL/min, 25 °C, t_r (major) = 11.6 min, t_r (minor) = 12.7 min).

^1H NMR (500 MHz, CDCl_3) δ 7.79-7.75 (m, 2H), 7.40-7.35 (m, 6H), 7.27-7.23 (m, 2H), 5.91-5.90 (m, 1H), 5.27 (dd, $J_1 = 10.0$ Hz, $J_2 = 8.0$ Hz, 1H), 3.36 (t, $J = 10.5$ Hz, 1H), 2.51-2.50 (m, 3H), 2.17 (s, 3H), 1.99 (dd, $J_1 = 11.0$ Hz, $J_2 = 8.0$ Hz, 1H), 1.20 (s, 3H), 1.08 (s, 3H).

^{13}C NMR (125 MHz, CDCl_3) δ 173.6, 151.3, 145.6, 144.3, 143.6, 128.1, 127.7, 127.5, 126.6, 126.02, 125.98, 111.1, 54.3, 46.8, 39.1, 29.1, 27.4, 21.5, 14.4, 13.6.

IR (film): ν (cm^{-1}) 3087, 3058, 3028, 2967, 2929, 2874, 1713, 1581, 1493, 1444, 1409, 1377, 1353, 1314, 1248, 1029, 1007, 957, 909, 840, 805, 772, 731, 697, 567, 418.

HRMS (ESI, m/z) calcd for $\text{C}_{24}\text{H}_{26}\text{N}_2\text{ONa}$ $[\text{M}+\text{Na}]^+$: 381.1937, found: 381.1937.



(3,5-Dimethyl-1H-pyrazol-1-yl)((1S,2S,3R)-2,3-dimethyl-2-phenyl-3-(thiophen-2-yl)cyclobutyl) methanone (28w**)**

According to the general procedure, the reaction of (*E*)-1-(3,5-dimethyl-1H-pyrazol-1-yl)-3-phenylbut-2-en-1-one **26p** (24.0 mg, 0.10 mmol), 2-(prop-1-en-2-yl)thiophene (138.2 mg, 10.0 equiv) and Δ -**RhS** (3.5 mg, 4 mol%) in acetone (0.5 mL, 0.2 M) under nitrogen atmosphere with blue LEDs for 20 hours, afforded 36.1 mg (99%, combined yield) of **28w** as a colorless oil; $[\alpha]_D^{22} = +90.6^\circ$ (c 1.0, CH_2Cl_2); d.r. value was determined through ^1H NMR of crude materials as 17:1; enantiomeric excess of the major diastereoisomer was established by HPLC analysis using a Chiralpak OD-H column, ee = 99% (HPLC: OD-H, 254 nm, n -hexane/isopropanol = 99:1, flow rate 0.6 mL/min, 25 °C, t_r (major) = 19.9 min, t_r (minor) = 13.1 min).

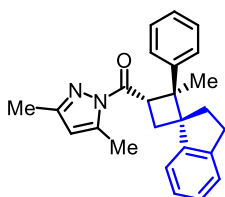
^1H NMR (500 MHz, CDCl_3) δ 7.78-7.74 (m, 2H), 7.35 (t, $J = 8.0$ Hz, 2H), 7.27 (t, $J = 2.0$ Hz, 1H), 7.25-7.21 (m, 1H), 7.08-7.04 (m, 2H), 5.97-5.96 (m, 1H), 5.20 (dd, $J_1 = 10.0$ Hz, $J_2 = 8.5$ Hz, 1H), 3.26 (t, $J = 10.8$ Hz, 1H), 2.55-2.54 (m, 3H), 2.27 (s, 3H), 2.14 (dd, $J_1 = 11.0$ Hz, $J_2 = 8.0$ Hz, 1H),

1.25 (s, 3H), 1.21 (s, 3H).

^{13}C NMR (125 MHz, CDCl_3) δ 173.3, 151.5, 150.5, 145.4, 143.8, 127.7, 127.0, 126.7, 126.0, 124.5, 123.8, 111.3, 54.9, 44.8, 39.2, 32.4, 28.0, 22.6, 14.5, 13.7.

IR (film): ν (cm^{-1}) 3062, 2967, 2928, 2870, 1713, 1582, 1444, 1409, 1377, 1352, 1313, 1259, 1240, 1177, 1142, 1077, 1007, 960, 919, 813, 765, 695, 627, 575, 534, 502, 475, 417.

HRMS (ESI, m/z) calcd for $\text{C}_{22}\text{H}_{24}\text{N}_2\text{OSNa}$ $[\text{M}+\text{Na}]^+$: 387.1502, found: 387.1498.



(3,5-Dimethyl-1*H*-pyrazol-1-yl)((1*S*,2*S*,3*S*)-2-methyl-2-phenyl-2',3'-dihydrospiro[cyclobutane-1,1'-inden]-3-yl)methanone (28x**)**

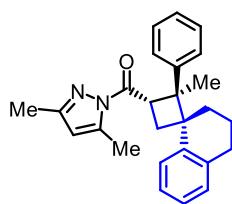
According to the general procedure, the reaction of (*E*)-1-(3,5-dimethyl-1*H*-pyrazol-1-yl)-3-phenylbut-2-en-1-one **26p** (24.0 mg, 0.10 mmol), 1-methylene-2,3-dihydro-1*H*-indene (130.2 mg, 10.0 equiv) and Δ -**RhS** (3.5 mg, 4 mol%) in acetone (0.5 mL, 0.2 M) under nitrogen atmosphere with blue LEDs for 20 hours, afforded 35.7 mg (96%, combined yield) of **28x** as a white solid; $[\alpha]_{\text{D}}^{22} = +37.0^\circ$ (c 1.0, CH_2Cl_2); d.r. value was determined through ^1H NMR of crude materials as >20:1; enantiomeric excess of the major diastereoisomer was established by HPLC analysis using a Chiralpak OD-H column, ee = 99% (HPLC: OD-H, 254 nm, *n*-hexane/isopropanol = 99:1, flow rate 0.6 mL/min, 25 $^\circ\text{C}$, t_{r} (major) = 7.5 min, t_{r} (minor) = 10.0 min).

^1H NMR (500 MHz, CDCl_3) δ 7.53 (d, J = 6.5 Hz, 1H), 7.44 (br s, 2H), 7.30-7.20 (m, 5H), 7.19-7.14 (m, 1H), 5.98 (s, 1H), 5.19 (dd, J_1 = 11.0 Hz, J_2 = 8.0 Hz, 1H), 3.22 (t, J = 10.8 Hz, 1H), 2.56 (s, 3H), 2.49 (dd, J_1 = 10.5 Hz, J_2 = 9.0 Hz, 1H), 2.41-2.35 (m, 1H), 2.34-2.26 (m, 1H), 2.29 (s, 3H), 2.05 (dd, J_1 = 11.0 Hz, J_2 = 8.0 Hz, 1H), 1.97 (dt, J_1 = 12.5 Hz, J_2 = 10.0 Hz, 1H), 1.41 (s, 3H).

^{13}C NMR (125 MHz, CDCl_3) δ 173.4, 151.4, 146.8, 145.6, 144.7, 143.9, 127.5, 127.2, 126.6, 125.91, 125.89, 125.7, 124.7, 111.3, 56.0, 55.9, 39.8, 38.0, 33.0, 30.7, 22.1, 14.5, 13.7.

IR (film): ν (cm^{-1}) 3059, 3024, 2965, 2930, 2854, 1713, 1582, 1477, 1448, 1409, 1377, 1315, 1247, 1177, 1140, 1099, 1070, 1023, 965, 937, 908, 845, 795, 760, 729, 701, 652, 623, 576.

HRMS (ESI, m/z) calcd for $\text{C}_{25}\text{H}_{26}\text{N}_2\text{ONa}$ $[\text{M}+\text{Na}]^+$: 393.1937, found: 393.1934.



(3,5-Dimethyl-1H-pyrazol-1-yl)((1S,2S,3S)-2-methyl-2-phenyl-3',4'-dihydro-2'H-spiro[cyclobutane-1,1'-naphthalen]-3-yl)methanone (28y)

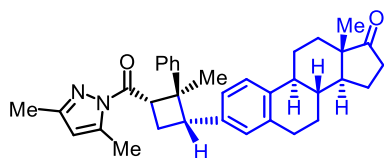
According to the general procedure, the reaction of (*E*)-1-(3,5-dimethyl-1H-pyrazol-1-yl)-3-phenylbut-2-en-1-one **26p** (24.0 mg, 0.10 mmol), 1-methylene-1,2,3,4-tetrahydronaphthalene (144.2 mg, 10.0 equiv) and Δ -**RhS** (3.5 mg, 4 mol%) in acetone (0.5 mL, 0.2 M) under nitrogen atmosphere with blue LEDs for 20 hours, afforded 37.2 mg (97%, combined yield) of **28y** as a colorless oil; $[\alpha]_D^{22} = +69.0^\circ$ (*c* 1.0, CH₂Cl₂); d.r. value was determined through ¹H NMR of crude materials as >20:1; enantiomeric excess of the major diastereoisomer was established by HPLC analysis using a Chiralpak OD-H column, ee = 99% (HPLC: OD-H, 254 nm, *n*-hexane/isopropanol = 99:1, flow rate 0.6 mL/min, 25 °C, *t_r* (major) = 8.6 min, *t_r* (minor) = 13.3 min).

¹H NMR (500 MHz, CDCl₃) δ 7.76 (d, *J* = 7.5 Hz, 1H), 7.61 (d, *J* = 7.0 Hz, 2H), 7.31-7.26 (m, 3H), 7.24-7.18 (m, 2H), 7.08 (d, *J* = 7.0 Hz, 1H), 5.91 (s, 1H), 5.36 (dd, *J₁* = 10.0 Hz, *J₂* = 8.5 Hz, 1H), 3.41 (dd, *J₁* = 11.5 Hz, *J₂* = 10.5 Hz, 1H), 2.58-2.49 (m, 2H), 2.54 (s, 3H), 2.41 (dt, *J₁* = 14.0 Hz, *J₂* = 4.5 Hz, 1H), 2.14 (s, 3H), 1.88 (dd, *J₁* = 11.5 Hz, *J₂* = 8.5 Hz, 1H), 1.64-1.55 (m, 1H), 1.31 (s, 3H), 1.26-1.17 (m, 1H), 0.73-0.62 (m, 1H).

¹³C NMR (125 MHz, CDCl₃) δ 174.0, 151.3, 144.2, 143.5, 138.6, 137.9, 129.5, 129.0, 128.2, 127.2, 126.3, 126.0, 124.7, 111.1, 55.1, 46.0, 39.5, 34.0, 31.5, 28.8, 21.9, 17.7, 14.3, 13.5.

IR (film): ν (cm⁻¹) 3059, 2933, 2878, 2844, 1712, 1582, 1487, 1444, 1408, 1376, 1353, 1315, 1251, 1178, 1136, 1071, 1033, 1007, 961, 911, 834, 754, 729, 697, 653, 565, 495, 410.

HRMS (ESI, *m/z*) calcd for C₂₆H₂₈N₂ONa [M+Na]⁺: 407.2094, found: 407.2091.



(8R,9S,13S,14S)-3-((1S,2S,3S)-3-(3,5-Dimethyl-1H-pyrazole-1-carbonyl)-2-methyl-2-phenylcyclobutyl)-13-methyl-6,7,8,9,11,12,13,14,15,16-decahydro-17H-cyclopenta[*a*]phenanthren-17-one (28z)

According to the general procedure, the reaction of (*E*)-1-(3,5-dimethyl-1*H*-pyrazol-1-yl)-3-phenylbut-2-en-1-one **26p** (24.0 mg, 0.10 mmol), 3-vinylestrone (84.1 mg, 3.0 equiv) and Δ -**RhS** (3.5 mg, 4 mol%) in CH_2Cl_2 (0.5 mL, 0.2 M) under nitrogen atmosphere with blue LEDs for 24 hours, afforded 50.6 mg (97%, combined yield) of **28z** as a yellow solid; $[\alpha]_{\text{D}}^{22} = +42.5^\circ$ (*c* 1.0, CH_2Cl_2); d.r. value was determined through ^1H NMR of crude materials as 8:1.

^1H NMR (600 MHz, CDCl_3) δ 7.52-7.49 (m, 2H), 7.35-7.31 (m, 2H), 7.24-7.20 (m, 2H), 7.01 (s, 1H), 6.99 (d, $J = 7.8$ Hz, 1H), 5.92-5.91 (m, 1H), 4.79 (dd, $J_1 = 10.2$ Hz, $J_2 = 7.8$ Hz, 1H), 3.85 (dd, $J_1 = 10.8$ Hz, $J_2 = 8.4$ Hz, 1H), 3.00 (q, $J = 10.8$ Hz, 1H), 2.92 (dd, $J_1 = 9.0$ Hz, $J_2 = 4.8$ Hz, 2H), 2.56-2.55 (m, 3H), 2.51 (dd, $J_1 = 19.2$ Hz, $J_2 = 9.0$ Hz, 1H), 2.43-2.28 (m, 3H), 2.20-1.95 (m, 4H), 2.01 (s, 3H), 1.68-1.42 (m, 6H), 1.13 (s, 3H), 0.92 (s, 3H).

^{13}C NMR (125 MHz, CDCl_3) δ 221.0, 173.2, 151.4, 149.0, 143.4, 137.9, 137.0, 136.1, 128.7, 127.8, 125.94, 125.92, 125.8, 125.0, 111.0, 52.4, 50.5, 48.0, 47.0, 44.4, 44.3, 38.1, 35.8, 31.6, 29.5, 26.5, 25.7, 23.1, 21.5, 18.4, 14.3, 13.8, 13.4.

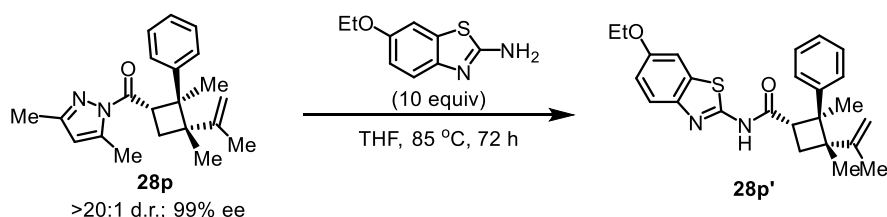
IR (film): ν (cm^{-1}) 2928, 2867, 1721, 1583, 1495, 1449, 1376, 1313, 1250, 1085, 1006, 964, 911, 816, 728, 646, 581.

HRMS (ESI, m/z) calcd for $\text{C}_{35}\text{H}_{40}\text{N}_2\text{O}_2\text{Na}$ $[\text{M}+\text{Na}]^+$: 543.2982, found: 543.2977.

5.4.4 Single-Crystal X-Ray Diffraction Studies

Single crystals of **28e** suitable for X-ray diffraction were obtained by slow evaporation of a solution of **28e** (30 mg) in Et_2O (1.0 mL) at room temperature for several days in a 10 mL vial.

Product **28p** was transformed to an amide **28p'** as shown below. Single crystals of **28p'** suitable for X-ray diffraction were obtained by slow evaporation of a solution of **28p'** (33 mg) in Et_2O (1.0 mL) at room temperature for several days in a NMR tube.



The mixture of **28p** (32.2 mg, 0.1 mmol) and 6-ethoxybenzo[d]thiazol-2-amine (194.3 mg, 10.0

equiv) in THF (0.5 mL) was heated at 85 °C under nitrogen atmosphere for 72 h. Then, the mixture was purified by flash chromatography on silica gel (*n*-hexane/EtOAc) to afford the products **28p'** (33.5 mg, 80% yield) as a white solid; d.r. value >20:1; $[\alpha]_D^{22} = +113.8^\circ$ (*c* 1.0, CH₂Cl₂); enantiomeric excess was established by HPLC analysis using a Chiralpak OD-H column, ee = 98% (HPLC: OD-H, 254 nm, *n*-hexane/isopropanol = 60:40, flow rate 1 mL/min, 25 °C, *t_r* (major) = 9.2 min, *t_r* (minor) = 23.6 min).

(1*S*,2*S*,3*S*)-*N*-(6-Ethoxybenzo[*d*]thiazol-2-yl)-2,3-dimethyl-2-phenyl-3-(prop-1-en-2-yl)cyclobutane-1-carboxamide (28p')

¹H NMR (300 MHz, CDCl₃) δ 9.05 (br s, 1H), 7.52 (d, *J* = 8.7 Hz, 1H), 7.34-7.28 (m, 2H), 7.26-7.11 (m, 4H), 6.94 (dd, *J₁* = 9.0 Hz, *J₂* = 2.7 Hz, 1H), 4.98 (s, 1H), 4.80 (s, 1H), 4.00 (q, *J* = 7.2 Hz, 2H), 3.86 (dd, *J₁* = 9.9 Hz, *J₂* = 8.4 Hz, 1H), 2.79 (t, *J* = 10.5 Hz, 1H), 1.76 (dd, *J₁* = 11.1 Hz, *J₂* = 7.8 Hz, 1H), 1.68 (s, 3H), 1.36 (t, *J* = 6.9 Hz, 3H), 1.29 (s, 3H), 0.85 (s, 3H).

¹³C NMR (125 MHz, CDCl₃) δ 170.7, 156.2, 155.8, 148.5, 143.3, 142.1, 133.3, 128.5, 126.67, 126.56, 121.1, 115.8, 112.0, 105.0, 64.1, 52.6, 48.4, 40.8, 28.9, 24.2, 20.6, 20.0, 14.8.

IR (film): ν (cm⁻¹) 3062, 2969, 2928, 2876, 1689, 1603, 1544, 1456, 1372, 1259, 1219, 1167, 1117, 1060, 1034, 941, 890, 818, 761, 698, 550, 433.

HRMS (ESI, *m/z*) calcd for C₂₅H₂₉N₂O₂S [M+H]⁺: 421.1944, found: 421.1941.

X-ray data were collected with a Bruker 3 circuit D8 Quest diffractometer with MoK α radiation (microfocus tube with multilayer optics) and Photon 100 CMOS detector at 100 K. Scaling and absorption correction was performed by using the SADABS software package of Bruker. Structures were solved using direct methods in SHELXT and refined using the full matrix least squares procedure in SHELXL-2014. The hydrogen atoms were placed in calculated positions and refined as riding on their respective C atom, and Uiso(H) was set at 1.2 Ueq(Csp²) and 1.5 Ueq(Csp³). Disorder was refined using restraints for both the geometry and the anisotropic displacement factors.

The relative and absolute configurations of **28e** (Figure 124) and **28p'** (Figure 125) have been determined.

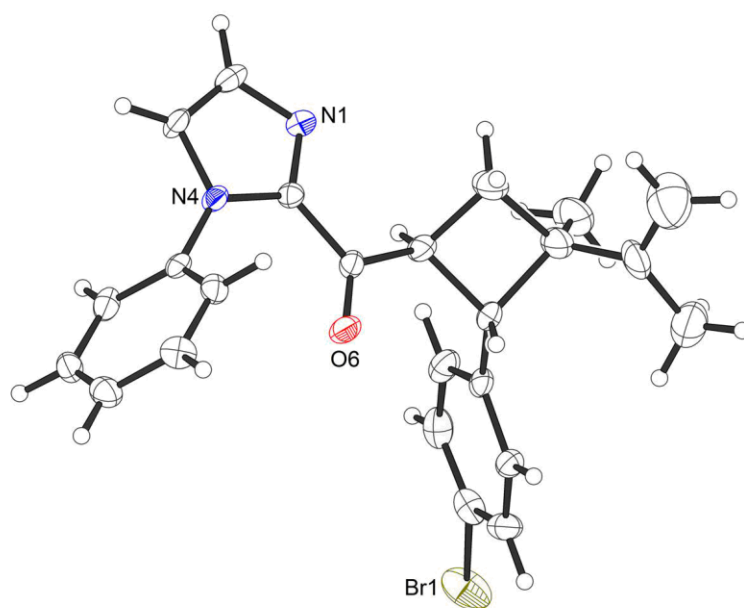


Figure 124. Crystal structure of compound **28e**.

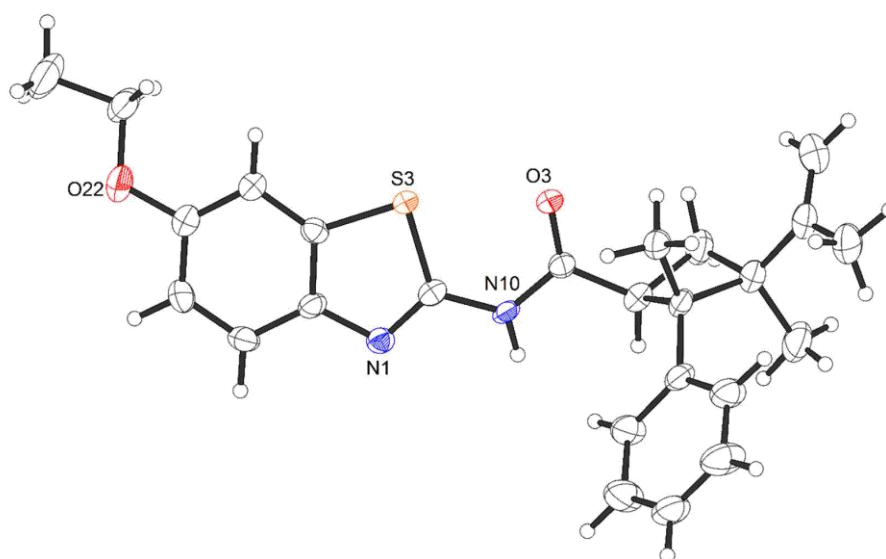


Figure 125. Crystal structure of compound **28p'**.

Table 27. Crystal data and structure refinement for **28e**.

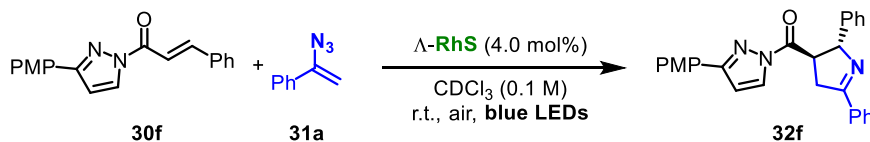
Crystal data	
CCDC number	1536749
Identification code	hxqG7_0m
Habitus, color	needle, colorless
Crystal size	0.64 x 0.13 x 0.06 mm ³
Crystal system	Orthorhombic
Space group	P2 ₁ 2 ₁ 2 ₁ Z = 4
Unit cell dimensions	a = 6.2276(6) Å α = 90 °
	b = 10.0974(9) Å β = 90 °
	c = 33.032(3) Å γ = 90 °
	2077.1(3) Å ³
Volume	9991 peaks with Theta 2.4 to 25.2 °
Cell determination	C ₂₄ H ₂₃ Br N ₂ O
Empirical formula	C ₂₄ H ₂₃ Br N ₂ O
Moiety formula	435.35
Formula weight	1.392 Mg/m ³
Density (calculated)	1.995 mm ⁻¹
Absorption coefficient	896
F(000)	
Data collection:	
Diffraction type	Bruker D8 QUEST area detector
Wavelength	0.71073 Å
Temperature	110(2) K
Theta range for data collection	2.364 to 25.270 °
Index ranges	-6 ≤ h ≤ 7, -12 ≤ k ≤ 11, -39 ≤ l ≤ 38
Data collection software	APEX3 (Bruker AXS Inc., 2015)
Cell refinement software	SAINT V8.37A (Bruker AXS Inc., 2015)
Data reduction software	SAINT V8.37A (Bruker AXS Inc., 2015)
Solution and refinement:	
Reflections collected	19907
Independent reflections	3772 [R(int) = 0.0548]
Completeness to theta = 25.242 °	99.9 %
Observed reflections	3515 [I > 2σ(I)]
Reflections used for refinement	3772.
Absorption correction	Semi-empirical from equivalents
Max. and min. transmission	0.7452 and 0.5119
Flack parameter (absolute struct.)	-0.004(4)
Largest diff. peak and hole	0.755 and -0.830 e.Å ⁻³
Solution	dual space algorithm
Refinement	Full-matrix least-squares on F ²
Treatment of hydrogen atoms	Calculated positions, constr. ref.
Programs used	XT V2014/1 (Bruker AXS Inc., 2014)
	SHELXL-2016/6 (Sheldrick, 2016)
	DIAMOND (Crystal Impact)
	ShelXle (Hübschle, Sheldrick, Dittrich, 2011)
Data / restraints / parameters	3772 / 183 / 284
Goodness-of-fit on F ²	1.048
R index (all data)	wR2 = 0.0975
R index conventional [I > 2σ(I)]	R1 = 0.0397

Table 28. Crystal data and structure refinement for **28p'**.

Crystal data		
CCDC number	1536750	
Identification code	lsp242_0m_sq	
Habitus, color	needle, colorless	
Crystal size	0.87 x 0.17 x 0.04 mm ³	
Crystal system	Orthorhombic	
Space group	P2 ₁ 2 ₁ 2	Z = 8
Unit cell dimensions	a = 22.0286(9) Å	α = 90 °
	b = 13.8772(6) Å	β = 90 °
	c = 15.9440(7) Å	γ = 90 °
Volume	4874.0(4) Å ³	
Cell determination	9411 peaks with Theta 2.6 to 24.8 °	
Empirical formula	C ₂₅ H ₂₈ N ₂ O ₂ S	
Moiety formula	C ₂₅ H ₂₈ N ₂ O ₂ S	
Formula weight	420.55	
Density (calculated)	1.146 Mg/m ³	
Absorption coefficient	0.154 mm ⁻¹	
F(000)	1792	
Data collection:		
Diffractionmeter type	Bruker D8 QUEST area detector	
Wavelength	0.71073 Å	
Temperature	110(2) K	
Theta range for data collection	2.154 to 25.285 °	
Index ranges	-26<=h<=25, -15<=k<=16, -19<=l<=18	
Data collection software	APEX3 (Bruker AXS Inc., 2015)	
Cell refinement software	SAINT V8.37A (Bruker AXS Inc., 2015)	
Data reduction software	SAINT V8.37A (Bruker AXS Inc., 2015)	
Solution and refinement:		
Reflections collected	31255	
Independent reflections	8868 [R(int) = 0.0649]	
Completeness to theta = 25.242 °	99.9 %	
Observed reflections	7140[I > 2σ(I)]	
Reflections used for refinement	8868	
.Absorption correction	Semi-empirical from equivalents	
Max. and min. transmission	0.7452 and 0.6600	
Flack parameter (absolute struct.)	0.06(4)	
Largest diff. peak and hole	0.273 and -0.240 e.Å ⁻³	
Solution	Duals space algorithm	
Refinement	Full-matrix least-squares on F ²	
Treatment of hydrogen atoms	CH calc., constr. ref., NH located, isotr. ref.	
Programs used	XT V2014/1 (Bruker AXS Inc., 2014)	
	SHELXL-2016/6 (Sheldrick, 2016)	
	DIAMOND (Crystal Impact)	
	ShelXle (Hübschle, Sheldrick, Dittrich, 2011)	
Data / restraints / parameters	8868 / 56 / 577	
Goodness-of-fit on F ²	1.016	
R index (all data)	wR2 = 0.1040	
R index conventional [I>2sigma(I)]	R1 = 0.0466	

5.5 Asymmetric [2+3] Photocycloaddition

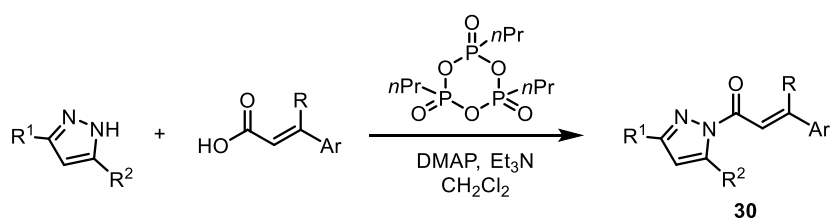
5.5.1 General Procedure



Exemplary, an oven-dried 10 mL Schlenk tube was charged with α,β -unsaturated *N*-acyl pyrazole **30f** (30.4 mg, 0.10 mmol) and Δ -**RhS** (3.5 mg, 4 mol%) under air. Then, CDCl_3 (1.0 mL, 0.1 M) was added via syringe, followed by vinyl azide **31a** (18.2 mg, 1.25 equiv) under open air atmosphere with stirring. The tube was sealed and positioned at approximately 8 cm from a 24 W blue LEDs lamp. After stirring for the indicated time (monitored by TLC), the mixture was directly subjected to ^1H NMR to determine the d.r. value. Then, all the mixture was collected and purified by flash chromatography on silica gel (*n*-hexane/EtOAc) to afford the product **32f**. The enantiomeric excess was determined by HPLC analysis on a chiral stationary phase. Racemic samples were obtained by carrying out the reactions with *rac*-**RhS**.

For products **32y-32ab** which might decompose in silica gel column, a fast flash chromatography is recommended.

5.5.2 Synthesis of Substrates

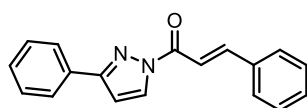


α,β -Unsaturated *N*-acyl pyrazoles **30** were synthesized according to published procedures with some modification.^{12a} To a solution of pyrazole (1.0 equiv) and α,β -unsaturated carboxyl acid (1.5 equiv) in CH_2Cl_2 (0.2 M) at room temperature, was added 1-propanephosphonic acid cyclic anhydride (CAS number: 68957-94-8; 50% solution in EtOAc; 1.5 equiv) dropwise. After stirring for 1 hour at room temperature, the mixture was cooled to 0 °C followed by the addition of DMAP (0.2 equiv) and Et_3N (3.0 equiv; dropwise). Then the reaction mixture was allowed to warm to room temperature with stirring. After a full conversion of pyrazole was detected by TLC (5-12 h), the mixture was poured into

HCl solution (1 M) and extracted with EtOAc for three times. The combined organic layers were washed with NaOH solution (2 M), saturated NaHCO₃ solution and brine. After dried with anhydrous Na₂SO₄, filtration and concentration under reduced pressure, the crude residue was purified by flash chromatography on silica gel (*n*-hexane/EtOAc) to afford the substrate **30** with yields from 75% to 95%. To obtain with better quality, the isolated product could be washed with Et₂O/*n*-hexane.

Vinyl azides **31** were prepared according to published procedures.^{12b,c}

The data of novel substrates are shown below.



(*E*)-3-Phenyl-1-(3-phenyl-1*H*-pyrazol-1-yl)prop-2-en-1-one (30c)

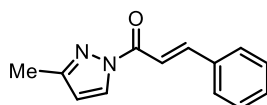
A white solid.

¹H NMR (500 MHz, CDCl₃) δ 8.43 (d, *J* = 3.0 Hz, 1H), 8.07 (d, *J* = 16.0 Hz, 1H), 8.03 (d, *J* = 16.0 Hz, 1H), 7.97-7.94 (m, 2H), 7.75-7.71 (m, 2H), 7.51-7.40 (m, 6H), 6.84 (d, *J* = 3.0 Hz, 1H).

¹³C NMR (75 MHz, CDCl₃) δ 163.7, 155.4, 147.6, 134.6, 132.0, 131.0, 130.0, 129.2, 129.0, 128.84, 128.79, 126.4, 116.0, 107.7.

IR (film): ν (cm⁻¹) 1698, 1612, 1532, 1499, 1452, 1400, 1345, 1301, 1213, 1095, 1072, 1036, 995, 954, 915, 874, 755, 681, 564.

HRMS (ESI, *m/z*) calcd for C₁₈H₁₄N₂ONa [M+Na]⁺: 297.1009, found: 297.0999.



(*E*)-1-(3-Methyl-1*H*-pyrazol-1-yl)-3-phenylprop-2-en-1-one (30d)

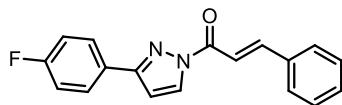
A white solid.

¹H NMR (300 MHz, CDCl₃) δ 8.28 (d, *J* = 3.0 Hz, 1H), 8.00 (d, *J* = 15.9 Hz, 1H), 7.87 (d, *J* = 15.9 Hz, 1H), 7.73-7.67 (m, 2H), 7.46-7.40 (m, 3H), 6.30 (d, *J* = 2.7 Hz, 1H), 2.38 (s, 3H).

¹³C NMR (75 MHz, CDCl₃) δ 163.4, 153.8, 147.3, 134.6, 130.9, 129.4, 128.9, 128.8, 116.2, 110.6, 14.0.

IR (film): ν (cm⁻¹) 2958, 1685, 1613, 1551, 1446, 1408, 1343, 1203, 1046, 989, 940, 861, 761, 713, 675, 569.

HRMS (ESI, m/z) calcd for $C_{13}H_{12}N_2ONa$ $[M+Na]^+$: 235.0853, found: 235.0842.



(E)-1-(3-(4-Fluorophenyl)-1H-pyrazol-1-yl)-3-phenylprop-2-en-1-one (30e)

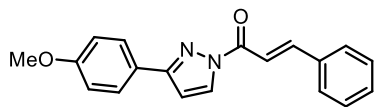
A white solid.

1H NMR (300 MHz, $CDCl_3$) δ 8.42 (d, J = 3.3 Hz, 1H), 8.06 (d, J = 16.2 Hz, 1H), 7.98 (d, J = 15.9 Hz, 1H), 7.95-7.89 (m, 2H), 7.75-7.70 (m, 2H), 7.48-7.43 (m, 3H), 7.21-7.12 (m, 2H), 6.78 (d, J = 2.7 Hz, 1H).

^{13}C NMR (75 MHz, $CDCl_3$) δ 163.6, 163.4 (d, J = 247.1 Hz), 154.4, 147.7, 134.6, 131.0, 130.1, 129.0, 128.8, 128.204 (d, J = 8.3 Hz), 128.205 (d, J = 2.9 Hz), 115.85, 115.79 (d, J = 21.6 Hz), 107.5.

IR (film): ν (cm^{-1}) 1688, 1612, 1507, 1430, 1398, 1340, 1298, 1219, 1155, 1092, 1052, 980, 949, 885, 840, 815, 758, 679, 624, 567.

HRMS (ESI, m/z) calcd for $C_{18}H_{13}FN_2ONa$ $[M+Na]^+$: 315.0904, found: 315.0905.



(E)-1-(3-(4-Methoxyphenyl)-1H-pyrazol-1-yl)-3-phenylprop-2-en-1-one (30f)

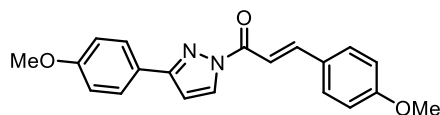
A white solid.

1H NMR (300 MHz, $CDCl_3$) δ 8.40 (d, J = 2.7 Hz, 1H), 8.06 (d, J = 15.9 Hz, 1H), 8.00 (d, J = 16.2 Hz, 1H), 7.92-7.85 (m, 2H), 7.76-7.70 (m, 2H), 7.48-7.41 (m, 3H), 7.04-6.96 (m, 2H), 6.77 (d, J = 3.0 Hz, 1H), 3.88 (s, 3H).

^{13}C NMR (75 MHz, $CDCl_3$) δ 163.6, 160.5, 155.2, 147.4, 134.7, 130.9, 129.9, 129.0, 128.8, 127.8, 124.7, 116.2, 114.2, 107.5, 55.4.

IR (film): ν (cm^{-1}) 2964, 1692, 1613, 1510, 1401, 1352, 1301, 1251, 1220, 1174, 1094, 1024, 950, 875, 833, 762, 678, 629, 567.

HRMS (ESI, m/z) calcd for $C_{19}H_{17}N_2O_2$ $[M+H]^+$: 305.1296, found: 305.1284.



(E)-3-(4-Methoxyphenyl)-1-(3-(4-methoxyphenyl)-1H-pyrazol-1-yl)prop-2-en-1-one (30g)

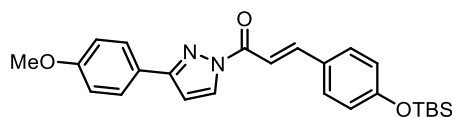
A white solid.

^1H NMR (300 MHz, CDCl_3) δ 8.40 (d, $J = 2.7$ Hz, 1H), 8.01 (d, $J = 15.9$ Hz, 1H), 7.91-7.83 (m, 3H), 7.71-7.65 (m, 2H), 7.02-6.93 (m, 4H), 6.75 (d, $J = 3.0$ Hz, 1H), 3.87 (s, 6H).

^{13}C NMR (75 MHz, CDCl_3) δ 163.9, 162.0, 160.4, 155.0, 147.2, 130.7, 129.8, 127.7, 127.5, 124.8, 114.4, 114.2, 113.5, 107.2, 55.4, 55.3.

IR (film): ν (cm^{-1}) 2999, 2932, 1690, 1596, 1568, 1509, 1428, 1395, 1342, 1294, 1251, 1216, 1173, 1092, 1032, 996, 955, 825, 767, 726, 627, 549.

HRMS (ESI, m/z) calcd for $\text{C}_{20}\text{H}_{19}\text{N}_2\text{O}_3$ $[\text{M}+\text{H}]^+$: 335.1401, found: 335.1390.



(E)-3-(4-((tert-Butyldimethylsilyl)oxy)phenyl)-1-(3-(4-methoxyphenyl)-1H-pyrazol-1-yl)prop-2-en-1-one (30h)

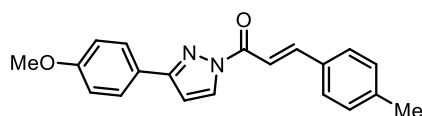
A white solid.

^1H NMR (300 MHz, CDCl_3) δ 8.39 (d, $J = 2.7$ Hz, 1H), 8.00 (d, $J = 15.9$ Hz, 1H), 7.91-7.82 (m, 3H), 7.66-7.59 (m, 2H), 7.02-6.95 (m, 2H), 6.94-6.86 (m, 2H), 6.74 (d, $J = 3.0$ Hz, 1H), 3.85 (s, 3H), 1.01 (s, 9H), 0.25 (s, 6H).

^{13}C NMR (75 MHz, CDCl_3) δ 163.8, 160.4, 158.5, 154.9, 147.1, 130.5, 129.8, 128.0, 127.7, 124.7, 120.5, 114.1, 113.7, 107.1, 55.2, 25.6, 18.2, -4.4.

IR (film): ν (cm^{-1}) 3144, 2932, 2893, 2857, 1696, 1594, 1508, 1466, 1428, 1400, 1348, 1250, 1220, 1170, 1094, 1035, 990, 950, 909, 831, 775, 733, 690, 630, 567, 527.

HRMS (ESI, m/z) calcd for $\text{C}_{25}\text{H}_{30}\text{N}_2\text{O}_3\text{SiNa}$ $[\text{M}+\text{Na}]^+$: 457.1918, found: 457.1911.



(E)-1-(3-(4-Methoxyphenyl)-1H-pyrazol-1-yl)-3-(p-tolyl)prop-2-en-1-one (30i)

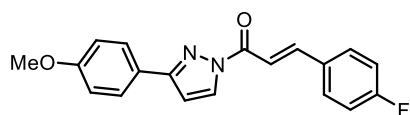
A white solid.

^1H NMR (300 MHz, CDCl_3) δ 8.40 (d, $J = 3.0$ Hz, 1H), 8.03 (d, $J = 15.9$ Hz, 1H), 7.95 (d, $J = 15.9$ Hz, 1H), 7.93-7.85 (m, 2H), 7.62 (d, $J = 8.1$ Hz, 2H), 7.25 (d, $J = 7.8$ Hz, 2H), 7.03-6.96 (m, 2H), 6.76 (d, $J = 2.7$ Hz, 1H), 3.87 (s, 3H), 2.41 (s, 3H).

^{13}C NMR (75 MHz, CDCl_3) δ 163.8, 160.5, 155.1, 147.5, 141.5, 132.0, 129.9, 129.7, 128.9, 127.7, 124.7, 115.0, 114.2, 107.3, 55.3, 21.6.

IR (film): ν (cm^{-1}) 3130, 2967, 1691, 1610, 1508, 1426, 1399, 1349, 1301, 1249, 1219, 1179, 1092, 1030, 951, 885, 838, 807, 767, 728, 688, 628, 526.

HRMS (ESI, m/z) calcd for $\text{C}_{20}\text{H}_{19}\text{N}_2\text{O}_2$ $[\text{M}+\text{H}]^+$: 319.1452, found: 319.1442.



(*E*)-3-(4-Fluorophenyl)-1-(3-(4-methoxyphenyl)-1*H*-pyrazol-1-yl)prop-2-en-1-one (30j)

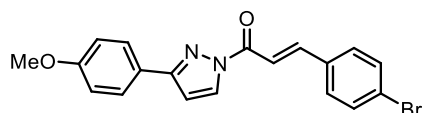
A white solid.

^1H NMR (300 MHz, CDCl_3) δ 8.40 (d, $J = 2.7$ Hz, 1H), 8.00 (d, $J = 15.9$ Hz, 1H), 7.93 (d, $J = 15.9$ Hz, 1H), 7.93-7.84 (m, 2H), 7.75-7.69 (m, 2H), 7.17-7.10 (m, 2H), 7.02-6.97 (m, 2H), 6.77 (d, $J = 2.7$ Hz, 1H), 3.87 (s, 3H).

^{13}C NMR (75 MHz, CDCl_3) δ 164.3 (d, $J = 251.0$ Hz), 163.5, 160.5, 155.3, 146.0, 130.9 (d, $J = 3.7$ Hz), 130.8 (d, $J = 9.1$ Hz), 129.9, 127.8, 124.6, 116.2 (d, $J = 22.0$ Hz), 115.9 (d, $J = 2.2$ Hz), 114.2, 107.5, 55.3.

IR (film): ν (cm^{-1}) 3085, 2960, 1710, 1592, 1505, 1426, 1394, 1341, 1292, 1240, 1210, 1162, 1091, 1032, 1007, 957, 877, 826, 763, 731, 626.

HRMS (ESI, m/z) calcd for $\text{C}_{19}\text{H}_{15}\text{FN}_2\text{O}_2\text{Na}$ $[\text{M}+\text{Na}]^+$: 345.1021, found: 345.1010.



(*E*)-3-(4-Bromophenyl)-1-(3-(4-methoxyphenyl)-1*H*-pyrazol-1-yl)prop-2-en-1-one (30k)

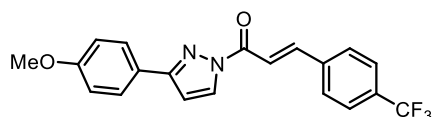
A white solid.

^1H NMR (300 MHz, CDCl_3) δ 8.39 (d, $J = 3.0$ Hz, 1H), 8.00 (d, $J = 16.2$ Hz, 1H), 7.94 (d, $J = 15.9$ Hz, 1H), 7.90-7.83 (m, 2H), 7.58-7.57 (m, 4H), 7.02-6.97 (m, 2H), 6.77 (d, $J = 2.7$ Hz, 1H), 3.87 (s, 3H).

^{13}C NMR (75 MHz, CDCl_3) δ 163.3, 160.6, 155.3, 145.8, 133.5, 132.2, 130.1, 129.9, 127.8, 125.3, 124.5, 116.8, 114.2, 107.6, 55.3.

IR (film): ν (cm^{-1}) 3081, 2963, 1691, 1611, 1511, 1485, 1403, 1345, 1299, 1243, 1218, 1169, 1095, 1036, 984, 944, 821, 767, 626, 528.

HRMS (ESI, m/z) calcd for $\text{C}_{19}\text{H}_{15}\text{BrN}_2\text{O}_2\text{Na}$ $[\text{M}+\text{Na}]^+$: 405.0209, found: 405.0204.



(E)-1-(3-(4-Methoxyphenyl)-1H-pyrazol-1-yl)-3-(4-(trifluoromethyl)phenyl)prop-2-en-1-one (30l)

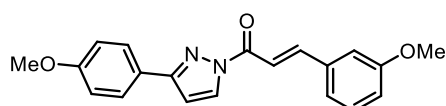
A white solid.

^1H NMR (300 MHz, CDCl_3) δ 8.39 (d, $J = 3.0$ Hz, 1H), 8.08 (d, $J = 16.2$ Hz, 1H), 8.00 (d, $J = 16.5$ Hz, 1H), 7.90-7.84 (m, 2H), 7.81 (d, $J = 8.1$ Hz, 2H), 7.70 (d, $J = 8.4$ Hz, 2H), 7.03-6.96 (m, 2H), 6.78 (d, $J = 3.0$ Hz, 1H), 3.87 (s, 3H).

^{13}C NMR (75 MHz, CDCl_3) δ 163.1, 160.6, 155.5, 145.1, 137.9 (q, $J = 1.3$ Hz), 132.2 (q, $J = 32.8$ Hz), 130.0, 128.8, 127.8, 125.9 (q, $J = 3.7$ Hz), 124.4, 123.8 (q, $J = 270.8$ Hz), 118.8, 114.2, 107.8, 55.3.

IR (film): ν (cm^{-1}) 3061, 2936, 1689, 1617, 1577, 1513, 1404, 1349, 1317, 1248, 1222, 1160, 1109, 1046, 983, 945, 878, 828, 791, 763, 739, 625, 594.

HRMS (ESI, m/z) calcd for $\text{C}_{20}\text{H}_{15}\text{F}_3\text{N}_2\text{O}_2\text{Na}$ $[\text{M}+\text{Na}]^+$: 395.0978, found: 395.0972.



(E)-3-(3-Methoxyphenyl)-1-(3-(4-methoxyphenyl)-1H-pyrazol-1-yl)prop-2-en-1-one (30m)

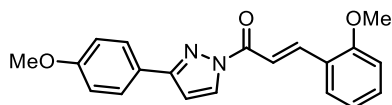
A white solid.

^1H NMR (300 MHz, CDCl_3) δ 8.40 (d, $J = 3.0$ Hz, 1H), 8.02 (d, $J = 16.5$ Hz, 1H), 7.97 (d, $J = 15.9$ Hz, 1H), 7.91-7.84 (m, 2H), 7.40-7.29 (m, 2H), 7.27-7.22 (m, 1H), 7.03-6.96 (m, 3H), 6.77 (d, $J = 2.7$ Hz, 1H), 3.88 (s, 3H), 3.87 (s, 3H).

^{13}C NMR (75 MHz, CDCl_3) δ 163.5, 160.5, 160.0, 155.2, 147.3, 136.0, 129.94, 129.90, 127.7, 124.6, 121.5, 116.7, 116.4, 114.2, 113.8, 107.5, 55.4, 55.3.

IR (film): ν (cm^{-1}) 2967, 2928, 1696, 1613, 1577, 1514, 1399, 1349, 1251, 1216, 1162, 1099, 1034, 988, 949, 830, 765, 726, 676, 628, 576.

HRMS (ESI, m/z) calcd for $C_{20}H_{19}N_2O_3$ $[M+H]^+$: 335.1390, found: 335.1386.



(E)-3-(2-Methoxyphenyl)-1-(3-(4-methoxyphenyl)-1H-pyrazol-1-yl)prop-2-en-1-one (30n)

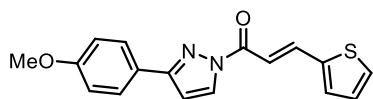
A white solid.

1H NMR (300 MHz, $CDCl_3$) δ 8.41 (d, $J = 15.9$ Hz, 1H), 8.40 (d, $J = 2.7$ Hz, 1H), 8.05 (d, $J = 16.2$ Hz, 1H), 7.91-7.85 (m, 2H), 7.77 (dd, $J_1 = 7.8$ Hz, $J_2 = 1.5$ Hz, 1H), 7.45-7.37 (m, 1H), 7.07-6.93 (m, 4H), 6.76 (d, $J = 3.0$ Hz, 1H), 3.94 (s, 3H), 3.87 (s, 3H).

^{13}C NMR (75 MHz, $CDCl_3$) δ 164.0, 160.4, 158.8, 154.9, 142.6, 132.2, 129.9, 129.1, 127.7, 124.8, 123.7, 120.7, 116.2, 114.2, 111.3, 107.1, 55.6, 55.3.

IR (film): ν (cm^{-1}) 2963, 2936, 1692, 1607, 1511, 1461, 1432, 1397, 1344, 1322, 1245, 1214, 1165, 1096, 1018, 990, 949, 834, 805, 750, 627, 583, 516.

HRMS (ESI, m/z) calcd for $C_{20}H_{19}N_2O_3$ $[M+H]^+$: 335.1390, found: 335.1386.



(E)-1-(3-(4-Methoxyphenyl)-1H-pyrazol-1-yl)-3-(thiophen-2-yl)prop-2-en-1-one (30o)

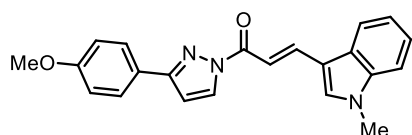
A white solid.

1H NMR (300 MHz, $CDCl_3$) δ 8.38 (d, $J = 3.0$ Hz, 1H), 8.14 (d, $J = 15.6$ Hz, 1H), 7.91-7.84 (m, 2H), 7.78 (d, $J = 15.6$ Hz, 1H), 7.49 (d, $J = 5.1$ Hz, 1H), 7.43 (d, $J = 3.6$ Hz, 1H), 7.12 (dd, $J_1 = 5.4$ Hz, $J_2 = 3.9$ Hz, 1H), 7.03-6.97 (m, 2H), 6.76 (d, $J = 2.7$ Hz, 1H), 3.87 (s, 3H).

^{13}C NMR (75 MHz, $CDCl_3$) δ 163.5, 160.5, 155.2, 140.1, 139.6, 132.2, 129.8, 129.7, 128.3, 127.7, 124.7, 114.8, 114.2, 107.4, 55.3.

IR (film): ν (cm^{-1}) 3077, 2913, 1683, 1597, 1507, 1424, 1396, 1338, 1280, 1239, 1215, 1167, 1089, 1031, 948, 828, 768, 706, 681, 626, 592, 522.

HRMS (ESI, m/z) calcd for $C_{17}H_{15}N_2O_2S$ $[M+H]^+$: 311.0849, found: 311.0844.



(*E*)-1-(3-(4-Methoxyphenyl)-1*H*-pyrazol-1-yl)-3-(1-methyl-1*H*-indol-3-yl)prop-2-en-1-one (30p)

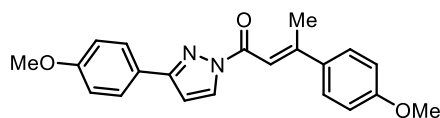
A yellow solid.

^1H NMR (500 MHz, CDCl_3) δ 8.43 (d, $J = 3.0$ Hz, 1H), 8.27 (d, $J = 16.0$ Hz, 1H), 8.13-8.08 (m, 1H), 7.96-7.89 (m, 3H), 7.54 (s, 1H), 7.42-7.34 (m, 3H), 7.04-7.00 (m, 2H), 6.75 (d, $J = 3.0$ Hz, 1H), 3.88 (s, 3H), 3.87 (s, 3H).

^{13}C NMR (125 MHz, CDCl_3) δ 164.7, 160.3, 154.6, 140.9, 138.2, 134.6, 129.8, 127.7, 126.3, 125.0, 123.3, 121.8, 120.9, 114.2, 113.2, 110.1, 109.9, 106.7, 55.3, 33.4.

IR (film): ν (cm^{-1}) 3098, 2951, 2913, 1677, 1595, 1509, 1463, 1397, 1369, 1344, 1281, 1240, 1217, 1178, 1097, 1067, 1036, 950, 830, 766, 734, 654, 630.

HRMS (ESI, m/z) calcd for $\text{C}_{22}\text{H}_{20}\text{N}_3\text{O}_2$ $[\text{M}+\text{H}]^+$: 358.1550, found: 358.1545.



(*E*)-3-(4-Methoxyphenyl)-1-(3-(4-methoxyphenyl)-1*H*-pyrazol-1-yl)but-2-en-1-one ((*E*)-30q)

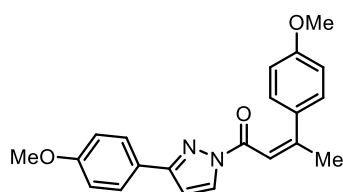
A white solid.

^1H NMR (300 MHz, CDCl_3) δ 8.38 (d, $J = 2.7$ Hz, 1H), 7.89-7.82 (m, 2H), 7.70 (q, $J = 1.5$ Hz, 1H), 7.67-7.61 (m, 2H), 7.01-6.93 (m, 4H), 6.72 (d, $J = 2.7$ Hz, 1H), 3.86 (s, 3H), 3.85 (s, 3H), 2.74 (d, $J = 1.2$ Hz, 3H).

^{13}C NMR (75 MHz, CDCl_3) δ 163.3, 161.0, 160.3, 159.3, 154.4, 134.4, 129.6, 128.2, 127.6, 124.9, 114.1, 113.9, 113.0, 106.7, 55.32, 55.26, 18.5.

IR (film): ν (cm^{-1}) 3001, 2930, 2838, 1683, 1594, 1567, 1509, 1435, 1396, 1348, 1286, 1246, 1217, 1176, 1093, 1023, 928, 829, 766, 736, 698, 536, 493.

HRMS (ESI, m/z) calcd for $\text{C}_{21}\text{H}_{21}\text{N}_2\text{O}_3$ $[\text{M}+\text{H}]^+$: 349.1547, found: 349.1542.



(Z)-3-(4-Methoxyphenyl)-1-(3-(4-methoxyphenyl)-1H-pyrazol-1-yl)but-2-en-1-one ((Z)-30q)

(Z)-30q was synthesized according to the previous procedure.^{11c}

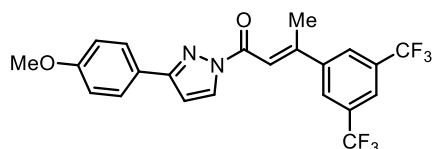
A white solid.

¹H NMR (500 MHz, CDCl₃) δ 8.26-8.22 (m, 1H), 7.89-7.83 (m, 2H), 7.36-7.33 (m, 1H), 7.32-7.27 (m, 2H), 7.01-6.95 (m, 2H), 6.94-6.89 (m, 2H), 6.69 (d, J = 3.0 Hz, 1H), 3.87 (s, 3H), 3.83 (s, 3H), 2.37 (d, J = 1.0 Hz, 3H).

¹³C NMR (125 MHz, CDCl₃) δ 162.3, 160.4, 160.3, 159.8, 154.8, 132.6, 129.8, 128.7, 127.7, 124.8, 114.9, 114.1, 113.4, 106.8, 55.3, 55.2, 28.1.

IR (film): ν (cm⁻¹) 3121, 2962, 2928, 1704, 1613, 1509, 1436, 1401, 1369, 1333, 1289, 1238, 1173, 1103, 1050, 1023, 943, 885, 829, 814, 789, 730, 686, 639, 555, 521.

HRMS (ESI, m/z) calcd for C₂₁H₂₁N₂O₃ [M+H]⁺: 349.1547, found: 349.1543.

**(E)-3-(3,5-Bis(trifluoromethyl)phenyl)-1-(3-(4-methoxyphenyl)-1H-pyrazol-1-yl)but-2-en-1-one (30r)**

A white solid.

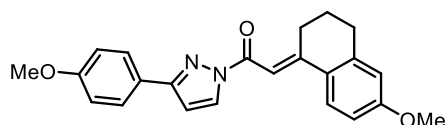
¹H NMR (500 MHz, CDCl₃) δ 8.39 (d, J = 3.0 Hz, 1H), 8.01 (s, 2H), 7.93 (s, 1H), 7.85-7.80 (m, 2H), 7.69 (q, J = 1.5 Hz, 1H), 7.00-6.95 (m, 2H), 6.77 (d, J = 3.0 Hz, 1H), 3.86 (s, 3H), 2.76 (d, J = 1.5 Hz, 3H).

¹³C NMR (125 MHz, CDCl₃) δ 162.6, 160.5, 155.6, 155.2, 144.6, 132.1 (q, J = 33.8 Hz), 129.8, 127.7, 126.9-126.6 (m), 124.3, 123.1 (q, J = 271.3 Hz), 123.0-122.7 (m), 118.3, 114.2, 107.6, 55.3, 18.9.

¹⁹F NMR (282 MHz, CDCl₃) δ -62.81 (s, 6F).

IR (film): ν (cm⁻¹) 3054, 2932, 1696, 1613, 1513, 1441, 1403, 1379, 1354, 1283, 1250, 1216, 1168, 1119, 1090, 1032, 938, 883, 836, 774, 679, 619, 580, 523.

HRMS (ESI, m/z) calcd for C₂₂H₁₆F₆N₂O₂Na [M+Na]⁺: 477.1008, found: 477.1001.



(E)-2-(6-Methoxy-3,4-dihydronaphthalen-1(2H)-ylidene)-1-(3-(4-methoxyphenyl)-1H-pyrazol-1-yl)ethan-1-one (30s)

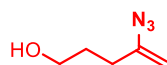
A white solid.

^1H NMR (300 MHz, CDCl_3) δ 8.37 (d, $J = 2.7$ Hz, 1H), 7.91 (d, $J = 9.0$ Hz, 1H), 7.89-7.82 (m, 3H), 7.02-6.95 (m, 2H), 6.72 (dd, $J_1 = 9.0$ Hz, $J_2 = 2.4$ Hz, 1H), 6.73-6.87 (m, 2H), 3.863 (s, 3H), 3.856 (s, 3H), 3.36 (td, $J_1 = 7.8$ Hz, $J_2 = 1.8$ Hz, 2H), 2.82 (d, $J = 6.0$ Hz, 2H), 1.95-1.85 (m, 2H).

^{13}C NMR (75 MHz, CDCl_3) δ 163.4, 161.4, 160.3, 159.4, 154.2, 143.1, 129.5, 127.6, 127.4, 127.2, 125.0, 114.1, 113.3, 113.1, 108.0, 106.5, 55.3(two MeO), 20.7, 29.3, 22.6.

IR (film): ν (cm^{-1}) 2927, 2837, 1683, 1579, 1504, 1434, 1397, 1331, 1299, 1221, 1174, 1097, 1036, 955, 889, 864, 828, 767, 716, 629, 594, 527, 413.

HRMS (ESI, m/z) calcd for $\text{C}_{23}\text{H}_{23}\text{N}_2\text{O}_3$ $[\text{M}+\text{H}]^+$: 375.1703, found: 375.1699.



4-Azidopent-4-en-1-ol (31i)

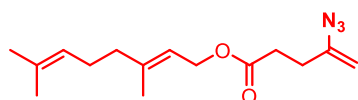
A yellow liquid.

^1H NMR (300 MHz, CDCl_3) δ 4.72-4.69 (m, 1H), 4.68-4.65 (m, 1H), 3.68 (t, $J = 6.2$ Hz, 2H), 2.22-2.15 (m, 2H), 1.81-1.69 (m, 2H).

^{13}C NMR (75 MHz, CDCl_3) δ 146.3, 98.3, 61.7, 30.2, 30.1.

IR (film): ν (cm^{-1}) 3318, 2931, 2875, 2092, 1627, 1441, 1265, 1048, 916, 843, 657, 541, 456.

HRMS (ESI, m/z) calcd for $\text{C}_5\text{H}_{10}\text{N}_3\text{O}$ $[\text{M}+\text{H}]^+$: 128.0818, *not found probably due to the decomposition.*



(E)-3,7-Dimethylocta-2,6-dien-1-yl 4-azidopent-4-enoate (31j)

A yellow liquid.

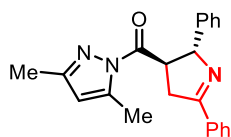
^1H NMR (300 MHz, CD_2Cl_2) δ 5.35-5.28 (m, 1H), 5.14-5.05 (m, 1H), 4.76-4.72 (m, 1H), 4.68-4.65 (m, 1H), 4.59 (d, $J = 7.2$ Hz, 2H), 2.52-2.44 (m, 2H), 2.41-2.33 (m, 2H), 2.16-2.00 (m, 4H), 1.70 (s, 3H), 1.69-1.66 (m, 3H), 1.61 (s, 3H).

^{13}C NMR (75 MHz, CD_2Cl_2) δ 172.4, 146.0, 142.7, 132.1, 124.1, 118.8, 98.7, 61.8, 39.9, 32.5, 29.4, 26.7, 25.7, 17.7, 16.5.

IR (film): ν (cm^{-1}) 2968, 2920, 2857, 2102, 1733, 1629, 1441, 1379, 1277, 1169, 1048, 955, 846, 634.

HRMS (ESI, m/z) calcd for $\text{C}_{15}\text{H}_{23}\text{N}_3\text{O}_2\text{Na}$ $[\text{M}+\text{Na}]^+$: 300.1682, found: 300.1679.

5.5.3 Experimental and Characterization Data of Novel Products



(3,5-Dimethyl-1H-pyrazol-1-yl)((2R,3R)-2,5-diphenyl-3,4-dihydro-2H-pyrrol-3-yl)methanone (32a)

As shown in **Table 16** entry 1, the reaction of (*E*)-1-(3,5-dimethyl-1H-pyrazol-1-yl)-3-phenylprop-2-en-1-one **30a** (22.6 mg, 0.10 mmol), (1-azidovinyl)benzene **31a** (18.2 mg, 1.25 equiv) and Λ -**RhS** (6.9 mg, 8 mol%) in acetone (0.5 mL, 0.2 M) under nitrogen atmosphere (degassed with freeze-pump-thaw) with blue LEDs for 18 hours, afforded **32a** as a white solid (54% NMR yield).

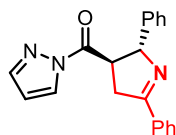
Only one single diastereoisomer was observed through ^1H NMR of crude materials. Enantiomeric excess of **32a** was established by HPLC analysis using a Chiralpak AS-H column, ee = 86% (HPLC: AS-H, 254 nm, *n*-hexane/isopropanol = 90:10, flow rate 1 mL/min, 40 °C, t_r (major) = 5.2 min, t_r (minor) = 8.6 min). $[\alpha]_{\text{D}}^{22} = -37.6^\circ$ (c 0.5, CH_2Cl_2).

^1H NMR (500 MHz, CDCl_3) δ 7.99-7.95 (m, 2H), 7.50-7.42 (m, 3H), 7.37-7.30 (m, 4H), 7.28-7.23 (m, 1H), 5.99-5.97 (m, 1H), 5.81-5.76 (m, 1H), 4.43 (ddd, $J_1 = 9.5$ Hz, $J_2 = 6.5$ Hz, $J_3 = 6.0$ Hz, 1H), 3.66 (ddd, $J_1 = 17.5$ Hz, $J_2 = 10.0$ Hz, $J_3 = 2.0$ Hz, 1H), 3.40 (ddd, $J_1 = 17.0$ Hz, $J_2 = 7.0$ Hz, $J_3 = 1.5$ Hz, 1H), 2.57 (d, $J = 1.0$ Hz, 3H), 2.19 (s, 3H).

^{13}C NMR (125 MHz, CDCl_3) δ 173.9, 171.5, 152.2, 144.3, 142.7, 133.7, 130.9, 128.5, 128.4, 128.0, 127.2, 127.0, 111.4, 78.3, 51.1, 40.5, 14.5, 13.8.

IR (film): ν (cm⁻¹) 3028, 2925, 1713, 1621, 1581, 1489, 1437, 1408, 1375, 1337, 1316, 1250, 1168, 1139, 1010, 958, 917, 864, 801, 759, 695, 613.

HRMS (ESI, m/z) calcd for C₂₂H₂₂N₃O [M+H]⁺: 344.1757, found: 344.1757.



((2R,3R)-2,5-Diphenyl-3,4-dihydro-2H-pyrrol-3-yl)(1H-pyrazol-1-yl)methanone (32b)

As shown in **Table 16** entry 2, the reaction of 3-phenyl-1-(1H-pyrazol-1-yl)prop-2-en-1-one **30b** (19.8 mg, 0.10 mmol), (1-azidovinyl)benzene **31a** (18.2 mg, 1.25 equiv) and Λ -**RhS** (6.9 mg, 8 mol%) in acetone (0.5 mL, 0.2 M) under nitrogen atmosphere (degassed with freeze-pump-thaw) with blue LEDs for 24 hours, afforded **32b** as a white solid (75% NMR yield).

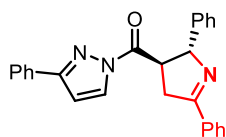
Only one single diastereoisomer was observed through ¹H NMR of crude materials. Enantiomeric excess of **32b** was established by HPLC analysis using a Chiralpak AS-H column, ee = 72% (HPLC: AS-H, 254 nm, *n*-hexane/isopropanol = 80:20, flow rate 1 mL/min, 40 °C, *t*_r (major) = 16.2 min, *t*_r (minor) = 7.5 min). [α]_D²² = -32.4° (*c* 1.0, CH₂Cl₂).

¹H NMR (300 MHz, CDCl₃) δ 8.31 (d, *J* = 2.7 Hz, 1H), 7.99-7.94 (m, 2H), 7.70 (d, *J* = 0.9 Hz, 1H), 7.52-7.41 (m, 3H), 7.37-7.24 (m, 5H), 6.48 (dd, *J*₁ = 2.7 Hz, *J*₂ = 1.2 Hz, 1H), 5.83 (dt, *J*₁ = 6.3 Hz, *J*₂ = 1.5 Hz, 1H), 4.46 (ddd, *J*₁ = 9.9 Hz, *J*₂ = 7.2 Hz, *J*₃ = 6.6 Hz, 1H), 3.71 (ddd, *J*₁ = 17.1 Hz, *J*₂ = 9.6 Hz, *J*₃ = 1.8 Hz, 1H), 3.43 (ddd, *J*₁ = 17.1 Hz, *J*₂ = 7.2 Hz, *J*₃ = 1.8 Hz, 1H).

¹³C NMR (125 MHz, CDCl₃) δ 172.5, 171.2, 144.2, 142.4, 133.6, 131.0, 128.7, 128.6, 128.0, 127.4, 126.8, 110.0, 78.6, 50.0, 40.7. (Missing one ¹³C signal)

IR (film): ν (cm⁻¹) 3124, 3091, 2924, 1719, 1613, 1573, 1535, 1491, 1448, 1419, 1381, 1312, 1270, 1247, 1198, 1101, 1028, 946, 915, 863, 832, 802, 751, 689, 641, 595.

HRMS (ESI, m/z) calcd for C₂₀H₁₈N₃O [M+H]⁺: 316.1455, found: 316.1445.



((2R,3R)-2,5-Diphenyl-3,4-dihydro-2H-pyrrol-3-yl)(3-phenyl-1H-pyrazol-1-yl)methanone (32c)

As shown in **Table 16** entry 7, the reaction of (*E*)-3-phenyl-1-(3-phenyl-1*H*-pyrazol-1-yl)prop-2-en-1-one **30c** (27.4 mg, 0.10 mmol), (1-azidovinyl)benzene **31a** (18.2 mg, 1.25 equiv) and Λ -**RhS** (3.5 mg, 4 mol%) in CDCl_3 (0.5 mL, 0.2 M) under nitrogen atmosphere (degassed with freeze-pump-thaw) with blue LEDs for 18 hours, afforded **32c** as a white solid (80% NMR yield).

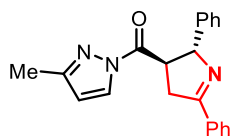
Only one single diastereoisomer was observed through ^1H NMR of crude materials. Enantiomeric excess of **32c** was established by HPLC analysis using a Chiralpak OD-H column, ee = 92% (HPLC: OD-H, 254 nm, *n*-hexane/isopropanol = 90:10, flow rate 1 mL/min, 25 °C, t_r (major) = 11.6 min, t_r (minor) = 15.4 min). $[\alpha]_{\text{D}}^{22} = +36.4^\circ$ (*c* 1.0, CH_2Cl_2).

^1H NMR (500 MHz, CDCl_3) δ 8.36 (d, $J = 3.0$ Hz, 1H), 8.04-7.99 (m, 2H), 7.79-7.75 (m, 2H), 7.53-7.35 (m, 10H), 7.34-7.29 (m, 1H), 6.83 (d, $J = 2.5$ Hz, 1H), 5.86-5.83 (m, 1H), 4.59 (ddd, $J_1 = 9.5$ Hz, $J_2 = 6.5$ Hz, $J_3 = 6.0$ Hz, 1H), 3.71 (ddd, $J_1 = 17.0$ Hz, $J_2 = 10.5$ Hz, $J_3 = 2.0$ Hz, 1H), 3.59 (ddd, $J_1 = 17.0$ Hz, $J_2 = 6.5$ Hz, $J_3 = 1.5$ Hz, 1H).

^{13}C NMR (125 MHz, CDCl_3) δ 172.3, 171.4, 155.5, 142.5, 133.6, 131.4, 130.9, 129.8, 129.2, 128.6, 128.5, 128.0, 127.3, 126.9, 126.3, 107.7, 79.2, 49.8, 40.0. (Missing one ^{13}C signal)

IR (film): ν (cm^{-1}) 3059, 3031, 1719, 1619, 1540, 1450, 1407, 1344, 1230, 1077, 1036, 944, 908, 799, 756, 688, 613, 555.

HRMS (ESI, m/z) calcd for $\text{C}_{26}\text{H}_{22}\text{N}_3\text{O}$ $[\text{M}+\text{H}]^+$: 392.1757, found: 392.1754.



((2*R*,3*R*)-2,5-Diphenyl-3,4-dihydro-2*H*-pyrrol-3-yl)(3-methyl-1*H*-pyrazol-1-yl)methanone (32d**)**

As shown in **Table 16** entry 8, the reaction of (*E*)-1-(3-methyl-1*H*-pyrazol-1-yl)-3-phenylprop-2-en-1-one **30d** (21.2 mg, 0.10 mmol), (1-azidovinyl)benzene **31a** (18.2 mg, 1.25 equiv) and Λ -**RhS** (3.5 mg, 4 mol%) in CDCl_3 (1.0 mL, 0.1 M) under nitrogen atmosphere (degassed with freeze-pump-thaw) with blue LEDs for 24 hours, afforded **32d** as a white solid (82% NMR yield).

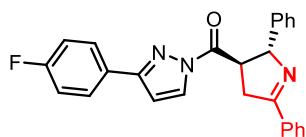
Only one single diastereoisomer was observed through ^1H NMR of crude materials. Enantiomeric excess of **32d** was established by HPLC analysis using a Chiralpak AS-H column, ee = 92% (HPLC: AS-H, 254 nm, *n*-hexane/isopropanol = 90:10, flow rate 1 mL/min, 40 °C, t_r (major) = 13.2 min, t_r (minor) = 9.3 min). $[\alpha]_{\text{D}}^{22} = -44.2^\circ$ (*c* 1.0, CH_2Cl_2).

^1H NMR (500 MHz, CDCl_3) δ 8.18 (d, J = 3.0 Hz, 1H), 7.98-7.94 (m, 2H), 7.51-7.41 (m, 3H), 7.36-7.30 (m, 4H), 7.29-7.24 (m, 1H), 6.28-6.26 (m, 1H), 5.81 (dt, J_1 = 6.0 Hz, J_2 = 2.0 Hz, 1H), 4.39 (ddd, J_1 = 10.0 Hz, J_2 = 7.5 Hz, J_3 = 6.5 Hz, 1H), 3.70 (ddd, J_1 = 16.5 Hz, J_2 = 9.5 Hz, J_3 = 1.5 Hz, 1H), 3.41 (ddd, J_1 = 17.0 Hz, J_2 = 7.0 Hz, J_3 = 1.5 Hz, 1H), 2.28 (s, 3H).

^{13}C NMR (125 MHz, CDCl_3) δ 172.0, 171.2, 154.1, 142.5, 133.6, 130.9, 129.3, 128.52, 128.46, 128.0, 127.3, 126.9, 110.8, 78.5, 50.0, 40.7, 13.9.

IR (film): ν (cm^{-1}) 3134, 2923, 1720, 1616, 1551, 1442, 1407, 1365, 1334, 1287, 1248, 1201, 1054, 1016, 951, 899, 862, 768, 691, 609, 550.

HRMS (ESI, m/z) calcd for $\text{C}_{21}\text{H}_{20}\text{N}_3\text{O}$ $[\text{M}+\text{H}]^+$: 330.1601, found: 330.1597.



((2R,3R)-2,5-Diphenyl-3,4-dihydro-2H-pyrrol-3-yl)(3-(4-fluorophenyl)-1H-pyrazol-1-yl)methanone (32e)

As shown in **Table 16** entry 9, the reaction of (*E*)-1-(3-(4-fluorophenyl)-1*H*-pyrazol-1-yl)-3-phenylprop-2-en-1-one **30e** (29.2 mg, 0.10 mmol), (1-azidovinyl)benzene **31a** (18.2 mg, 1.25 equiv) and Λ -**RhS** (3.5 mg, 4 mol%) in CDCl_3 (1.0 mL, 0.1 M) under nitrogen atmosphere (degassed with freeze-pump-thaw) with blue LEDs for 24 hours, afforded **32e** as a white solid (80% NMR yield).

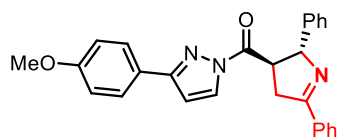
Only one single diastereoisomer was observed through ^1H NMR of crude materials. Enantiomeric excess of **32e** was established by HPLC analysis using a Chiralcel OJ-H column, ee = 92% (HPLC: OJ-H, 254 nm, *n*-hexane/isopropanol = 60:40, flow rate 1 mL/min, 40 °C, t_r (major) = 17.4 min, t_r (minor) = 11.6 min). $[\alpha]_{\text{D}}^{22} = +36.6^\circ$ (c 1.0, CH_2Cl_2).

^1H NMR (500 MHz, CDCl_3) δ 8.33 (d, J = 3.0 Hz, 1H), 8.01-7.96 (m, 2H), 7.72-7.66 (m, 2H), 7.54-7.43 (m, 3H), 7.37-7.27 (m, 5H), 7.12-7.05 (m, 2H), 6.77 (d, J = 3.0 Hz, 1H), 5.78 (dt, J_1 = 6.0 Hz, J_2 = 1.5 Hz, 1H), 4.55 (ddd, J_1 = 10.0 Hz, J_2 = 7.0 Hz, J_3 = 6.0 Hz, 1H), 3.68 (ddd, J_1 = 17.5 Hz, J_2 = 10.0 Hz, J_3 = 2.0 Hz, 1H), 3.59 (ddd, J_1 = 17.0 Hz, J_2 = 6.5 Hz, J_3 = 1.5 Hz, 1H).

^{13}C NMR (125 MHz, CDCl_3) δ 172.3, 171.4, 163.4 (d, J = 247.4 Hz), 154.6, 142.5, 133.6, 131.0, 130.0, 128.6, 128.5, 128.1 (d, J = 8.4 Hz), 128.0, 127.7 (d, J = 3.1 Hz), 127.4, 127.0, 115.7 (d, J = 21.5 Hz), 107.6, 79.4, 49.9, 40.1.

IR (film): ν (cm⁻¹) 3029, 2887, 1714, 1607, 1511, 1432, 1399, 1333, 1282, 1224, 1156, 1092, 1044, 936, 909, 837, 759, 691, 616, 555.

HRMS (ESI, m/z) calcd for C₂₆H₂₁FN₃O [M+H]⁺: 410.1663, found: 410.1658.



**((2*R*,3*R*)-2,5-Diphenyl-3,4-dihydro-2*H*-pyrrol-3-yl)(3-(4-methoxyphenyl)-1*H*-pyrazol-1-yl)
methanone (**32f**)**

As shown in **Table 16** entry 10, the reaction of (*E*)-1-(3-(4-methoxyphenyl)-1*H*-pyrazol-1-yl)-3-phenylprop-2-en-1-one **30f** (30.4 mg, 0.10 mmol), (1-azidovinyl)benzene **31a** (18.2 mg, 1.25 equiv) and Λ -**RhS** (3.5 mg, 4 mol%) in CDCl₃ (1.0 mL, 0.1 M) under nitrogen atmosphere (degassed with freeze-pump-thaw) with blue LEDs for 24 hours, afforded **32f** as a white solid (92% NMR yield, 90% isolated yield).

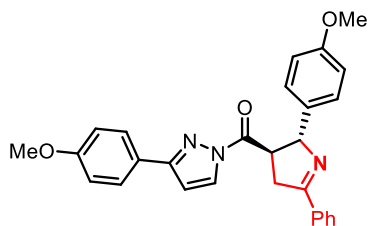
Only one single diastereoisomer was observed through ¹H NMR of crude materials. Enantiomeric excess of **32f** was established by HPLC analysis using a Chiralpak OD-H column, ee = 94% (HPLC: OD-H, 254 nm, *n*-hexane/isopropanol = 95:5, flow rate 1 mL/min, 40 °C, *t_r* (major) = 20.3 min, *t_r* (minor) = 24.0 min). [α]_D²² = +14.4° (*c* 1.0, CH₂Cl₂).

¹H NMR (500 MHz, CDCl₃) δ 8.31 (d, *J* = 3.0 Hz, 1H), 8.02-7.97 (m, 2H), 7.71-7.64 (m, 2H), 7.53-7.43 (m, 3H), 7.39-7.32 (m, 4H), 7.31-7.27 (m, 1H), 6.96-6.91 (m, 2H), 6.75 (d, *J* = 3.0 Hz, 1H), 5.82-5.78 (m, 1H), 4.55 (ddd, *J*₁ = 9.5 Hz, *J*₂ = 6.5 Hz, *J*₃ = 6.0 Hz, 1H), 3.86 (s, 3H), 3.69 (ddd, *J*₁ = 17.0 Hz, *J*₂ = 9.5 Hz, *J*₃ = 2.0 Hz, 1H), 3.57 (ddd, *J*₁ = 17.0 Hz, *J*₂ = 6.5 Hz, *J*₃ = 1.5 Hz, 1H).

¹³C NMR (125 MHz, CDCl₃) δ 172.3, 171.5, 160.5, 155.3, 142.5, 133.6, 131.0, 129.8, 128.54, 128.52, 128.0, 127.7, 127.4, 127.0, 124.2, 114.1, 107.5, 79.2, 55.3, 49.9, 40.1.

IR (film): ν (cm⁻¹) 2921, 2854, 1714, 1608, 1512, 1440, 1397, 1345, 1284, 1247, 1228, 1175, 1089, 1020, 937, 901, 836, 809, 770, 726, 691, 614, 558.

HRMS (ESI, m/z) calcd for C₂₇H₂₄N₃O₂ [M+H]⁺: 422.1863, found: 422.1857.



(3-(4-Methoxyphenyl)-1H-pyrazol-1-yl)((2R,3R)-2-(4-methoxyphenyl)-5-phenyl-3,4-dihydro-2H-pyrrol-3-yl)methanone (32g)

According to the general procedure, the reaction of (*E*)-3-(4-methoxyphenyl)-1-(3-(4-methoxyphenyl)-1H-pyrazol-1-yl)prop-2-en-1-one **30g** (33.4 mg, 0.10 mmol), (1-azidovinyl)benzene **31a** (18.2 mg, 1.25 equiv) and Λ -RhS (3.5 mg, 4 mol%) in CDCl_3 (1.0 mL, 0.1 M) under open air atmosphere with blue LEDs for 24 hours, afforded **32g** as a white solid (40.2 mg, 89% isolated yield).

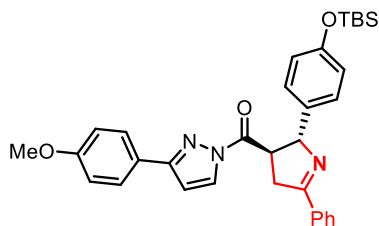
Only one single diastereoisomer was observed through ^1H NMR of crude materials. Enantiomeric excess of **32g** was established by HPLC analysis using a Chiralpak OD-H column, ee = 99% (HPLC: OD-H, 254 nm, *n*-hexane/isopropanol = 95:5, flow rate 1 mL/min, 40 °C, t_r (major) = 29.4 min, t_r (minor) = 36.1 min). $[\alpha]_D^{22} = +51.6^\circ$ (*c* 1.0, CH_2Cl_2).

^1H NMR (300 MHz, CDCl_3) δ 8.30 (d, $J = 2.7$ Hz, 1H), 8.01-7.95 (m, 2H), 7.72-7.65 (m, 2H), 7.52-7.41 (m, 3H), 7.32-7.26 (m, 2H), 6.97-6.84 (m, 4H), 6.75 (d, $J = 2.7$ Hz, 1H), 5.75-5.71 (m, 1H), 4.57-4.47 (m, 1H), 3.85 (s, 3H), 3.79 (s, 3H), 3.66 (ddd, $J_1 = 17.1$ Hz, $J_2 = 9.6$ Hz, $J_3 = 2.1$ Hz, 1H), 3.56 (ddd, $J_1 = 17.1$ Hz, $J_2 = 7.2$ Hz, $J_3 = 1.5$ Hz, 1H).

^{13}C NMR (75 MHz, CDCl_3) δ 172.4, 171.2, 160.5, 159.0, 155.3, 134.8, 133.7, 130.9, 129.8, 128.5, 128.1, 128.0, 127.7, 124.3, 114.1, 113.9, 107.5, 78.9, 55.32, 55.26, 50.0, 40.0.

IR (film): ν (cm^{-1}) 3057, 2962, 2911, 1713, 1610, 1511, 1435, 1405, 1352, 1334, 1300, 1246, 1173, 1029, 938, 905, 826, 771, 733, 692, 564.

HRMS (ESI, m/z) calcd for $\text{C}_{28}\text{H}_{26}\text{N}_3\text{O}_3$ $[\text{M}+\text{H}]^+$: 452.1969, found: 452.1963.



((2R,3R)-2-(4-((tert-Butyldimethylsilyl)oxy)phenyl)-5-phenyl-3,4-dihydro-2H-pyrrol-3-yl)(3-(4-methoxyphenyl)-1H-pyrazol-1-yl)methanone (32h)

According to the general procedure, the reaction of (*E*)-3-(4-((*tert*-butyldimethylsilyl)oxy)phenyl)-1-(3-(4-methoxyphenyl)-1*H*-pyrazol-1-yl)prop-2-en-1-one **30h** (43.4 mg, 0.10 mmol), (1-azidovinyl)benzene **31a** (18.2 mg, 1.25 equiv) and Λ -**RhS** (3.5 mg, 4 mol%) in CDCl₃ (1.0 mL, 0.1 M) under open air atmosphere with blue LEDs for 24 hours, afforded **32h** as a yellow oil (39.0 mg, 71% isolated yield).

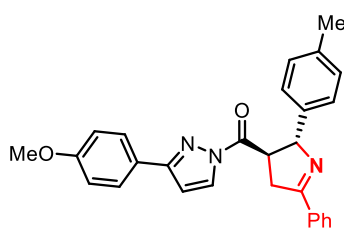
Only one single diastereoisomer was observed through ¹H NMR of crude materials. Enantiomeric excess of **32h** was established by HPLC analysis using a Chiralpak OD-H column, ee = 99% (HPLC: OD-H, 254 nm, *n*-hexane/isopropanol = 80:20, flow rate 1 mL/min, 40 °C, *t*_r (major) = 5.7 min, *t*_r (minor) = 6.5 min). [α]_D²² = +27.6° (*c* 1.0, CH₂Cl₂).

¹H NMR (300 MHz, CDCl₃) δ 8.30 (d, *J* = 3.0 Hz, 1H), 8.01-7.96 (m, 2H), 7.74-7.67 (m, 2H), 7.52-7.41 (m, 3H), 7.25-7.18 (m, 2H), 6.98-6.91 (m, 2H), 6.84-6.78 (m, 2H), 6.75 (d, *J* = 2.7 Hz, 1H), 5.76-5.70 (m, 1H), 4.57-4.47 (m, 1H), 3.86 (s, 3H), 3.67 (ddd, *J*₁ = 17.1 Hz, *J*₂ = 9.3 Hz, *J*₃ = 1.8 Hz, 1H), 3.55 (ddd, *J*₁ = 16.8 Hz, *J*₂ = 6.6 Hz, *J*₃ = 2.1 Hz, 1H), 0.99 (s, 9H), 0.19 (s, 3H), 0.18 (s, 3H).

¹³C NMR (75 MHz, CDCl₃) δ 172.4, 171.1, 160.5, 155.4, 155.0, 135.3, 133.8, 130.9, 129.8, 128.5, 128.03, 128.01, 127.7, 124.3, 120.0, 114.1, 107.4, 79.0, 55.3, 49.9, 40.0, 25.7, 18.2, -4.4, -4.5.

IR (film): ν (cm⁻¹) 2954, 2932, 2893, 2857, 1719, 1611, 1509, 1435, 1403, 1354, 1335, 1247, 1173, 1097, 1032, 908, 834, 801, 771, 730, 690, 559.

HRMS (ESI, *m/z*) calcd for C₃₃H₃₈N₃O₃Si [M+H]⁺: 552.2677, found: 552.2669.



(3-(4-Methoxyphenyl)-1*H*-pyrazol-1-yl)((2*R*,3*R*)-5-phenyl-2-(*p*-tolyl)-3,4-dihydro-2*H*-pyrrol-3-yl) methanone (32i**)**

According to the general procedure, the reaction of (*E*)-1-(3-(4-methoxyphenyl)-1*H*-pyrazol-1-yl)-3-(*p*-tolyl)prop-2-en-1-one **30i** (31.8 mg, 0.10 mmol), (1-azidovinyl)benzene **31a** (18.2 mg, 1.25 equiv) and Λ -**RhS** (3.5 mg, 4 mol%) in CDCl₃ (1.0 mL, 0.1 M) under open air atmosphere with blue LEDs for 24 hours, afforded **32i** as a white solid (38.1 mg, 87% isolated yield).

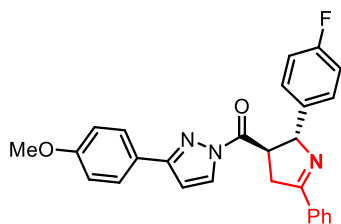
Only one single diastereoisomer was observed through ^1H NMR of crude materials. Enantiomeric excess of **32i** was established by HPLC analysis using a Chiralpak IC column, ee = 97% (HPLC: IC, 254 nm, *n*-hexane/isopropanol = 80:20, flow rate 1 mL/min, 40 °C, t_r (major) = 14.9 min, t_r (minor) = 13.8 min). $[\alpha]_{\text{D}}^{22} = +42.4^\circ$ (*c* 1.0, CH_2Cl_2).

^1H NMR (500 MHz, CDCl_3) δ 8.30 (d, $J = 3.0$ Hz, 1H), 8.00-7.96 (m, 2H), 7.69-7.65 (m, 2H), 7.51-7.43 (m, 3H), 7.26-7.23 (m, 2H), 7.17-7.12 (m, 2H), 6.95-6.90 (m, 2H), 6.74 (d, $J = 3.0$ Hz, 1H), 5.77-5.72 (m, 1H), 4.57-4.50 (m, 1H), 3.86 (s, 3H), 3.66 (ddd, $J_1 = 17.0$ Hz, $J_2 = 9.5$ Hz, $J_3 = 2.0$ Hz, 1H), 3.60-3.52 (m, 1H), 2.34 (s, 3H).

^{13}C NMR (125 MHz, CDCl_3) δ 172.4, 171.3, 160.5, 155.3, 139.6, 137.0, 133.7, 130.9, 129.8, 129.2, 128.5, 128.1, 127.7, 126.9, 124.3, 114.1, 107.5, 79.1, 55.3, 50.0, 40.0, 21.1.

IR (film): ν (cm^{-1}) 3058, 2953, 2914, 1717, 1613, 1511, 1434, 1398, 1339, 1292, 1245, 1176, 1091, 1027, 934, 902, 846, 813, 769, 728, 688, 559.

HRMS (ESI, m/z) calcd for $\text{C}_{28}\text{H}_{26}\text{N}_3\text{O}_2$ $[\text{M}+\text{H}]^+$: 436.2020, found: 436.2013.



((2*R*,3*R*)-2-(4-Fluorophenyl)-5-phenyl-3,4-dihydro-2*H*-pyrrol-3-yl)(3-(4-methoxyphenyl)-1*H*-pyrazol-1-yl)methanone (32j**)**

According to the general procedure, the reaction of (*E*)-3-(4-fluorophenyl)-1-(3-(4-methoxyphenyl)-1*H*-pyrazol-1-yl)prop-2-en-1-one **30j** (32.2 mg, 0.10 mmol), (1-azidovinyl)benzene **31a** (18.2 mg, 1.25 equiv) and Λ -**RhS** (3.5 mg, 4 mol%) in CDCl_3 (1.0 mL, 0.1 M) under open air atmosphere with blue LEDs for 24 hours, afforded **32j** as a white solid (39.0 mg, 89% isolated yield).

Only one single diastereoisomer was observed through ^1H NMR of crude materials. Enantiomeric excess of **32j** was established by HPLC analysis using a Chiralpak OD-H column, ee = 97% (HPLC: OD-H, 254 nm, *n*-hexane/isopropanol = 90:10, flow rate 1 mL/min, 40 °C, t_r (major) = 11.8 min, t_r (minor) = 14.6 min). $[\alpha]_{\text{D}}^{22} = +33.4^\circ$ (*c* 1.0, CH_2Cl_2).

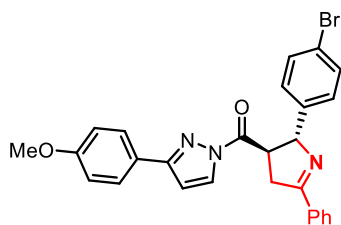
^1H NMR (300 MHz, CDCl_3) δ 8.31 (d, $J = 2.7$ Hz, 1H), 8.00-7.95 (m, 2H), 7.70-7.64 (m, 2H), 7.53-7.42 (m, 3H), 7.37-7.30 (m, 2H), 7.07-6.98 (m, 2H), 6.98-6.90 (m, 2H), 6.76 (d, $J = 2.7$ Hz, 1H),

5.78-5.72 (m, 1H), 4.56-4.45 (m, 1H), 3.86 (s, 3H), 3.68 (ddd, $J_1 = 17.4$ Hz, $J_2 = 9.3$ Hz, $J_3 = 2.1$ Hz, 1H), 3.57 (ddd, $J_1 = 17.1$ Hz, $J_2 = 6.9$ Hz, $J_3 = 1.2$ Hz, 1H).

^{13}C NMR (75 MHz, CDCl_3) δ 172.2, 171.7, 162.2 (d, $J = 243.8$ Hz), 160.6, 155.5, 138.4 (d, $J = 3.1$ Hz), 133.6, 131.1, 129.9, 128.61 (d, $J = 8.0$ Hz), 128.59, 128.1, 127.7, 124.2, 115.3 (d, $J = 21.2$ Hz), 114.2, 107.6, 78.6, 55.3, 50.0, 40.1.

IR (film): ν (cm^{-1}) 3138, 3061, 2964, 2913, 1719, 1608, 1506, 1400, 1336, 1246, 1224, 1177, 1028, 936, 904, 832, 772, 727, 689, 561.

HRMS (ESI, m/z) calcd for $\text{C}_{27}\text{H}_{23}\text{FN}_3\text{O}_2$ $[\text{M}+\text{H}]^+$: 440.1769, found: 440.1762.



((2*R*,3*R*)-2-(4-Bromophenyl)-5-phenyl-3,4-dihydro-2*H*-pyrrol-3-yl)(3-(4-methoxyphenyl)-1*H*-pyrazol-1-yl)methanone (32k**)**

According to the general procedure, the reaction of (*E*)-3-(4-bromophenyl)-1-(3-(4-methoxyphenyl)-1*H*-pyrazol-1-yl)prop-2-en-1-one **30k** (38.3 mg, 0.10 mmol), (1-azidovinyl)benzene **31a** (18.2 mg, 1.25 equiv) and Λ -**RhS** (3.5 mg, 4 mol%) in CDCl_3 (1.0 mL, 0.1 M) under open air atmosphere with blue LEDs for 24 hours, afforded **32k** as a white solid (43.6 mg, 87% isolated yield).

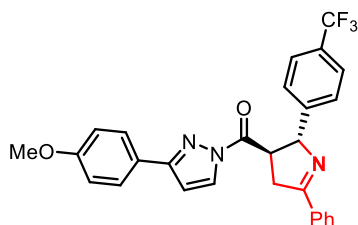
Only one single diastereoisomer was observed through ^1H NMR of crude materials. Enantiomeric excess of **32k** was established by HPLC analysis using a Chiralpak OD-H column, ee = 97% (HPLC: OD-H, 254 nm, *n*-hexane/isopropanol = 90:10, flow rate 1 mL/min, 40 °C, t_r (major) = 13.7 min, t_r (minor) = 15.8 min). $[\alpha]_{\text{D}}^{22} = +50.8^\circ$ (c 1.0, CH_2Cl_2).

^1H NMR (300 MHz, CDCl_3) δ 8.31 (d, $J = 3.0$ Hz, 1H), 8.01-7.94 (m, 2H), 7.67-7.60 (m, 2H), 7.55-7.42 (m, 5H), 7.27-7.21 (m, 2H), 7.00-6.92 (m, 2H), 6.76 (d, $J = 3.0$ Hz, 1H), 5.73-5.68 (m, 1H), 4.51 (ddd, $J_1 = 9.0$ Hz, $J_2 = 7.5$ Hz, $J_3 = 6.3$ Hz, 1H), 3.87 (s, 3H), 3.67 (ddd, $J_1 = 17.1$ Hz, $J_2 = 9.3$ Hz, $J_3 = 1.8$ Hz, 1H), 3.57 (ddd, $J_1 = 17.4$ Hz, $J_2 = 7.5$ Hz, $J_3 = 1.8$ Hz, 1H).

^{13}C NMR (75 MHz, CDCl_3) δ 172.00, 171.96, 160.6, 155.5, 141.8, 133.5, 131.6, 131.1, 129.8, 128.8, 128.6, 128.0, 127.7, 124.1, 121.3, 114.2, 107.6, 78.8, 55.3, 49.9, 40.0.

IR (film): ν (cm⁻¹) 2953, 2921, 1709, 1612, 1512, 1431, 1400, 1336, 1295, 1239, 1173, 1017, 945, 905, 834, 767, 727, 692, 620, 555.

HRMS (ESI, m/z) calcd for C₂₇H₂₃BrN₃O₂ [M+H]⁺: 500.0968, found: 500.0961.



(3-(4-Methoxyphenyl)-1H-pyrazol-1-yl)((2R,3R)-5-phenyl-2-(4-(trifluoromethyl)phenyl)-3,4-dihydro-2H-pyrrol-3-yl)methanone (32l**)**

According to the general procedure, the reaction of (*E*)-1-(3-(4-methoxyphenyl)-1H-pyrazol-1-yl)-3-(4-(trifluoromethyl)phenyl)prop-2-en-1-one **30l** (37.2 mg, 0.10 mmol), (1-azidovinyl)benzene **31a** (18.2 mg, 1.25 equiv) and Λ -**RhS** (3.5 mg, 4 mol%) in CDCl₃ (1.0 mL, 0.1 M) under open air atmosphere with blue LEDs for 24 hours, afforded **32l** as a white solid (44.2 mg, 90% isolated yield).

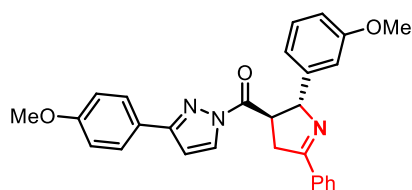
Only one single diastereoisomer was observed through ¹H NMR of crude materials. Enantiomeric excess of **32l** was established by HPLC analysis using a Chiralpak AD-H column, ee = 95% (HPLC: AD-H, 254 nm, *n*-hexane/isopropanol = 90:10, flow rate 1 mL/min, 40 °C, *t_r* (major) = 11.3 min, *t_r* (minor) = 13.1 min). [α]_D²² = +27.6° (*c* 1.0, CH₂Cl₂).

¹H NMR (500 MHz, CDCl₃) δ 8.32 (d, *J* = 3.0 Hz, 1H), 8.01-7.96 (m, 2H), 7.62-7.56 (m, 4H), 7.55-7.49 (m, 1H), 7.49-7.44 (m, 4H), 6.94-6.90 (m, 2H), 6.76 (d, *J* = 2.5 Hz, 1H), 5.81-5.77 (m, 1H), 4.53 (ddd, *J₁* = 9.5 Hz, *J₂* = 7.0 Hz, *J₃* = 6.5 Hz, 1H), 3.85 (s, 3H), 3.69 (ddd, *J₁* = 17.5 Hz, *J₂* = 9.5 Hz, *J₃* = 2.0 Hz, 1H), 3.64 (ddd, *J₁* = 17.0 Hz, *J₂* = 7.5 Hz, *J₃* = 1.5 Hz, 1H).

¹³C NMR (125 MHz, CDCl₃) δ 172.3, 171.9, 160.6, 155.5, 146.6, 133.3, 131.3, 130.0, 129.6 (q, *J* = 32.0 Hz), 128.6, 128.1, 127.6, 127.4, 125.5 (q, *J* = 3.8 Hz), 124.2 (q, *J* = 270.4 Hz), 123.9, 114.1, 107.8, 78.9, 55.3, 49.8, 40.1.

IR (film): ν (cm⁻¹) 3061, 2933, 1718, 1614, 1514, 1405, 1355, 1323, 1247, 1165, 1114, 1065, 1024, 908, 834, 800, 767, 691, 601.

HRMS (ESI, m/z) calcd for C₂₈H₂₃F₃N₃O₂ [M+H]⁺: 490.1737, found: 490.1729.



(3-(4-Methoxyphenyl)-1H-pyrazol-1-yl)((2R,3R)-2-(3-methoxyphenyl)-5-phenyl-3,4-dihydro-2H-pyrrol-3-yl)methanone (32m)

According to the general procedure, the reaction of (*E*)-3-(3-methoxyphenyl)-1-(3-(4-methoxyphenyl)-1H-pyrazol-1-yl)prop-2-en-1-one **30m** (33.4 mg, 0.10 mmol), (1-azidovinyl)benzene **31a** (18.2 mg, 1.25 equiv) and Λ -**RhS** (3.5 mg, 4 mol%) in CDCl_3 (1.0 mL, 0.1 M) under open air atmosphere with blue LEDs for 24 hours, afforded **32m** as a yellow solid (38.0 mg, 84% isolated yield).

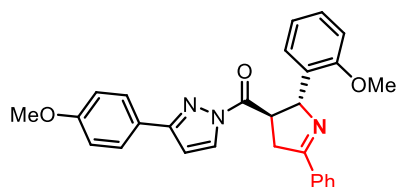
Only one single diastereoisomer was observed through ^1H NMR of crude materials. Enantiomeric excess of **32m** was established by HPLC analysis using a Chiralpak AD-H column, ee = 98% (HPLC: AD-H, 254 nm, *n*-hexane/isopropanol = 80:20, flow rate 1 mL/min, 40 °C, t_r (major) = 22.7 min, t_r (minor) = 15.1 min). $[\alpha]_D^{22} = +11.8^\circ$ (*c* 1.0, CH_2Cl_2).

^1H NMR (300 MHz, CDCl_3) δ 8.31 (d, $J = 2.7$ Hz, 1H), 8.02-7.95 (m, 2H), 7.73-7.66 (m, 2H), 7.54-7.41 (m, 3H), 7.26 (t, $J = 7.8$ Hz, 1H), 6.99-6.90 (m, 4H), 6.87-6.80 (m, 1H), 6.75 (d, $J = 3.0$ Hz, 1H), 5.80-5.76 (m, 1H), 4.61-4.51 (m, 1H), 3.85 (s, 3H), 3.75 (s, 3H), 3.69 (ddd, $J_1 = 17.4$ Hz, $J_2 = 9.9$ Hz, $J_3 = 1.8$ Hz, 1H), 3.55 (ddd, $J_1 = 17.1$ Hz, $J_2 = 6.9$ Hz, $J_3 = 1.8$ Hz, 1H).

^{13}C NMR (75 MHz, CDCl_3) δ 172.3, 171.4, 160.6, 159.8, 155.4, 144.2, 133.7, 131.0, 129.8, 129.5, 128.5, 128.0, 127.7, 124.3, 119.3, 114.1, 112.8, 112.7, 107.5, 79.1, 55.3, 55.2, 49.8, 40.3.

IR (film): ν (cm^{-1}) 3056, 2955, 2915, 1717, 1610, 1583, 1511, 1488, 1436, 1400, 1331, 1242, 1174, 1149, 1028, 943, 903, 833, 802, 768, 729, 692, 558.

HRMS (ESI, m/z) calcd for $\text{C}_{28}\text{H}_{26}\text{N}_3\text{O}_3$ $[\text{M}+\text{H}]^+$: 452.1969, found: 452.1962.



(3-(4-Methoxyphenyl)-1H-pyrazol-1-yl)((2R,3R)-2-(2-methoxyphenyl)-5-phenyl-3,4-dihydro-2H-pyrrol-3-yl)methanone (32n)

According to the general procedure, the reaction of (*E*)-3-(3-methoxyphenyl)-1-(3-(4-methoxyphenyl)-1*H*-pyrazol-1-yl)prop-2-en-1-one **30n** (33.4 mg, 0.10 mmol), (1-azidovinyl)benzene **31a** (18.2 mg, 1.25 equiv) and Λ -**RhS** (3.5 mg, 4 mol%) in CDCl₃ (1.0 mL, 0.1 M) under open air atmosphere with blue LEDs for 24 hours, afforded **32n** as a yellow oil (42.3 mg, 94% isolated yield).

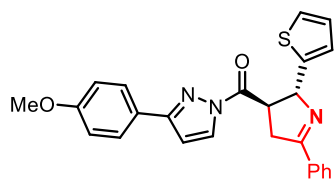
Only one single diastereoisomer was observed through ¹H NMR of crude materials. Enantiomeric excess of **32n** was established by HPLC analysis using a Chiralpak AD-H column, ee = 94% (HPLC: AD-H, 254 nm, *n*-hexane/isopropanol = 80:20, flow rate 1 mL/min, 40 °C, *t_r* (major) = 13.5 min, *t_r* (minor) = 11.5 min). [α]_D²² = +60.4° (*c* 1.0, CH₂Cl₂).

¹H NMR (300 MHz, CDCl₃) δ 8.38 (d, *J* = 3.0 Hz, 1H), 8.02-7.95 (m, 2H), 7.62-7.55 (m, 2H), 7.54-7.42 (m, 3H), 7.38 (dd, *J*₁ = 7.5 Hz, *J*₂ = 1.5 Hz, 1H), 7.24 (td, *J*₁ = 7.8 Hz, *J*₂ = 1.8 Hz, 1H), 6.97 (dd, *J*₁ = 7.5 Hz, *J*₂ = 0.9 Hz, 1H), 6.93-6.84 (m, 2H), 6.78-6.72 (m, 2H), 6.05-6.00 (m, 1H), 4.62-4.52 (m, 1H), 3.84 (s, 3H), 3.64 (ddd, *J*₁ = 17.4 Hz, *J*₂ = 10.5 Hz, *J*₃ = 2.4 Hz, 1H), 3.53 (ddd, *J*₁ = 17.1 Hz, *J*₂ = 7.5 Hz, *J*₃ = 1.8 Hz, 1H), 3.42 (s, 3H).

¹³C NMR (75 MHz, CDCl₃) δ 173.9, 170.8, 160.4, 156.4, 154.8, 134.0, 131.7, 130.8, 129.5, 128.5, 128.1, 128.0, 127.6, 127.0, 124.4, 120.5, 114.1, 110.0, 107.3, 75.8, 55.3, 54.7, 48.0, 41.5.

IR (film): ν (cm⁻¹) 3059, 3002, 2936, 1719, 1611, 1513, 1490, 1457, 1435, 1403, 1357, 1334, 1292, 1241, 1174, 1098, 1027, 953, 907, 838, 803, 756, 729, 692.

HRMS (ESI, *m/z*) calcd for C₂₈H₂₆N₃O₃ [M+H]⁺: 452.1969, found: 452.1961.



(3-(4-Methoxyphenyl)-1*H*-pyrazol-1-yl)((2*R*,3*R*)-5-phenyl-2-(thiophen-2-yl)-3,4-dihydro-2*H*-pyrrol-3-yl)methanone (32o**)**

According to the general procedure, the reaction of (*E*)-1-(3-(4-methoxyphenyl)-1*H*-pyrazol-1-yl)-3-(thiophen-2-yl)prop-2-en-1-one **30o** (31.0 mg, 0.10 mmol), (1-azidovinyl)benzene **31a** (18.2 mg, 1.25 equiv) and Λ -**RhS** (3.5 mg, 4 mol%) in CDCl₃ (1.0 mL, 0.1 M) under open air atmosphere with blue LEDs for 24 hours, afforded **32o** as a yellow solid (32.9 mg, 77% isolated yield).

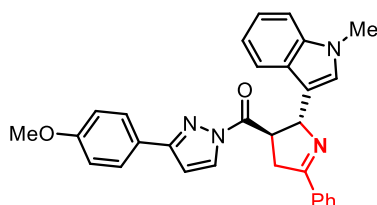
Only one single diastereoisomer was observed through ^1H NMR of crude materials. Enantiomeric excess of **32o** was established by HPLC analysis using a Chiralpak OD-H column, ee = 90% (HPLC: OD-H, 254 nm, *n*-hexane/isopropanol = 90:10, flow rate 1 mL/min, 40 °C, t_r (major) = 15.1 min, t_r (minor) = 17.4 min). $[\alpha]_D^{22} = +5.6^\circ$ (*c* 1.0, CH_2Cl_2).

^1H NMR (300 MHz, CDCl_3) δ 8.31 (d, $J = 3.0$ Hz, 1H), 8.00-7.94 (m, 2H), 7.82-7.74 (m, 2H), 7.54-7.41 (m, 3H), 7.24 (dd, $J_1 = 5.1$ Hz, $J_2 = 1.2$ Hz, 1H), 7.12-7.07 (m, 1H), 7.02-6.93 (m, 3H), 6.77 (d, $J = 3.0$ Hz, 1H), 6.09-6.05 (m, 1H), 4.73-4.64 (m, 1H), 3.86 (s, 3H), 3.71 (ddd, $J_1 = 17.1$ Hz, $J_2 = 9.6$ Hz, $J_3 = 1.8$ Hz, 1H), 3.55 (ddd, $J_1 = 17.1$ Hz, $J_2 = 6.9$ Hz, $J_3 = 1.2$ Hz, 1H).

^{13}C NMR (75 MHz, CDCl_3) δ 171.9, 171.5, 160.6, 155.6, 145.9, 133.5, 131.1, 129.9, 128.5, 128.1, 127.8, 126.8, 124.5, 124.32, 124.25, 114.2, 107.7, 75.0, 55.3, 50.0, 40.1.

IR (film): ν (cm^{-1}) 2956, 2935, 1714, 1607, 1513, 1434, 1399, 1346, 1288, 1233, 1177, 1087, 1020, 968, 898, 835, 807, 771, 695, 557.

HRMS (ESI, m/z) calcd for $\text{C}_{25}\text{H}_{22}\text{N}_3\text{O}_2\text{S}$ $[\text{M}+\text{H}]^+$: 428.1427, found: 428.1422.



(3-(4-Methoxyphenyl)-1H-pyrazol-1-yl)((2R,3R)-2-(1-methyl-1H-indol-3-yl)-5-phenyl-3,4-dihydro-2H-pyrrol-3-yl)methanone (32p**)**

According to the general procedure with some modifications, the reaction of (*E*)-1-(3-(4-methoxyphenyl)-1H-pyrazol-1-yl)-3-(1-methyl-1H-indol-3-yl)prop-2-en-1-one **30p** (35.7 mg, 0.10 mmol), (1-azidovinyl)benzene **31a** (18.2 mg, 1.25 equiv) and Λ -**RhS** (6.9 mg, 8 mol%) in CDCl_3 (2.0 mL, 0.05 M) under nitrogen atmosphere (degassed with freeze-pump-thaw) with blue LEDs for 24 hours, afforded **32p** as a yellow oil (42.0 mg, 88% isolated yield).

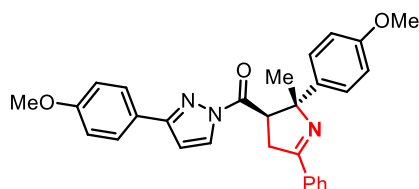
Only one single diastereoisomer was observed through ^1H NMR of crude materials. Enantiomeric excess of **32p** was established by HPLC analysis using a Chiralpak OD-H column, ee = 97% (HPLC: OD-H, 254 nm, *n*-hexane/isopropanol = 60:40, flow rate 1 mL/min, 40 °C, t_r (major) = 20.4 min, t_r (minor) = 25.5 min). $[\alpha]_D^{22} = +20.4^\circ$ (*c* 1.0, CH_2Cl_2).

^1H NMR (300 MHz, CDCl_3) δ 8.31 (d, J = 3.0 Hz, 1H), 8.04-7.98 (m, 2H), 7.67 (d, J = 7.8 Hz, 1H), 7.62-7.56 (m, 2H), 7.51-7.42 (m, 3H), 7.33-7.20 (m, 2H), 7.10-7.03 (m, 2H), 6.93-6.87 (m, 2H), 6.73 (d, J = 2.7 Hz, 1H), 6.10-6.04 (m, 1H), 4.88-4.78 (m, 1H), 3.85 (s, 3H), 3.77 (ddd, J_1 = 16.8 Hz, J_2 = 9.6 Hz, J_3 = 1.8 Hz, 1H), 3.70 (s, 3H), 3.59 (ddd, J_1 = 17.1 Hz, J_2 = 7.2 Hz, J_3 = 1.5 Hz, 1H).

^{13}C NMR (75 MHz, CDCl_3) δ 172.9, 170.3, 160.4, 155.2, 137.6, 134.0, 130.8, 129.7, 128.5, 128.0, 127.7, 126.8, 126.6, 124.3, 121.6, 119.8, 119.2, 115.7, 114.0, 109.2, 107.4, 73.2, 55.3, 48.6, 40.4, 32.6.

IR (film): ν (cm^{-1}) 3147, 3056, 2932, 1716, 1612, 1513, 1433, 1402, 1332, 1293, 1244, 1176, 1095, 1027, 904, 836, 800, 769, 730, 692, 644.

HRMS (ESI, m/z) calcd for $\text{C}_{30}\text{H}_{27}\text{N}_4\text{O}_2$ $[\text{M}+\text{H}]^+$: 475.2129, found: 475.2122.



(3-(4-Methoxyphenyl)-1H-pyrazol-1-yl)((2R,3R)-2-(4-methoxyphenyl)-2-methyl-5-phenyl-3,4-dihydro-2H-pyrrol-3-yl)methanone (32q**)**

According to the general procedure, the reaction of (*E*)-3-(4-methoxyphenyl)-1-(3-(4-methoxyphenyl)-1H-pyrazol-1-yl)but-2-en-1-one (*E*)-**30q** (34.8 mg, 0.10 mmol), (1-azidovinyl)benzene **31a** (18.2 mg, 1.25 equiv) and Λ -**RhS** (3.5 mg, 4 mol%) in CDCl_3 (1.0 mL, 0.1 M) under open air atmosphere with blue LEDs for 24 hours, afforded **32q** as a yellow solid (42.6 mg, 91% isolated yield).

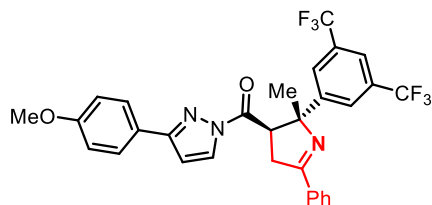
Only one single diastereoisomer was observed through ^1H NMR of crude materials. Enantiomeric excess of **32q** was established by HPLC analysis using a Chiralpak AD-H column, ee = 98% (HPLC: AD-H, 254 nm, *n*-hexane/isopropanol = 80:20, flow rate 1 mL/min, 40 °C, t_r (major) = 12.6 min, t_r (minor) = 10.2 min). $[\alpha]_{\text{D}}^{22} = +210.4^\circ$ (*c* 1.0, CH_2Cl_2).

^1H NMR (300 MHz, CDCl_3) δ 8.31 (d, J = 2.7 Hz, 1H), 8.04-7.99 (m, 2H), 7.68-7.61 (m, 2H), 7.52-7.42 (m, 5H), 6.98-6.92 (m, 2H), 6.90-6.83 (m, 2H), 6.77 (d, J = 2.7 Hz, 1H), 4.94 (dd, J_1 = 9.0 Hz, J_2 = 5.1 Hz, 1H), 3.87 (s, 3H), 3.80 (dd, J_1 = 17.1 Hz, J_2 = 5.4 Hz, 1H), 3.79 (s, 3H), 3.28 (dd, J_1 = 17.1 Hz, J_2 = 9.0 Hz, 1H), 1.58 (s, 3H).

^{13}C NMR (75 MHz, CDCl_3) δ 172.1, 170.0, 160.5, 158.4, 155.1, 140.0, 133.9, 130.8, 129.6, 128.5, 128.1, 127.7, 126.9, 124.3, 114.1, 113.4, 107.5, 81.3, 55.3, 55.2, 52.0, 39.0, 24.4.

IR (film): ν (cm^{-1}) 3061, 2962, 2934, 1715, 1612, 1511, 1436, 1402, 1351, 1335, 1295, 1241, 1176, 1100, 1028, 911, 831, 767, 729, 692.

HRMS (ESI, m/z) calcd for $\text{C}_{29}\text{H}_{28}\text{N}_3\text{O}_3$ $[\text{M}+\text{H}]^+$: 466.2125, found: 466.2118.



((2*R*,3*R*)-2-(3,5-Bis(trifluoromethyl)phenyl)-2-methyl-5-phenyl-3,4-dihydro-2*H*-pyrrol-3-yl)(3-(4-methoxyphenyl)-1*H*-pyrazol-1-yl)methanone (32r**)**

According to the general procedure with some modifications, the reaction of (*E*)-3-(3,5-bis(trifluoromethyl)phenyl)-1-(3-(4-methoxyphenyl)-1*H*-pyrazol-1-yl)but-2-en-1-one **30r** (45.4 mg, 0.10 mmol), (1-azidovinyl)benzene **31a** (18.2 mg, 1.25 equiv) and Λ -**RhS** (6.9 mg, 8 mol%) in CDCl_3 (1.0 mL, 0.1 M) under nitrogen atmosphere (degassed with freeze-pump-thaw) with blue LEDs for 45 hours, afforded **32r** as a yellow oil (28.4 mg, 50% isolated yield).

Only one single diastereoisomer was observed through ^1H NMR of crude materials. Enantiomeric excess of **32r** was established by HPLC analysis using a Chiralpak AD-H column, ee = 97% (HPLC: AD-H, 254 nm, *n*-hexane/isopropanol = 90:10, flow rate 1 mL/min, 40 °C, t_r (major) = 5.7 min, t_r (minor) = 4.0 min). $[\alpha]_{\text{D}}^{22} = +199.8^\circ$ (c 1.0, CH_2Cl_2).

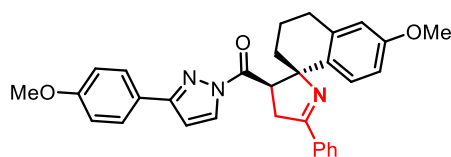
^1H NMR (300 MHz, CDCl_3) δ 8.33 (d, J = 2.7 Hz, 1H), 8.04-7.98 (m, 4H), 7.74 (s, 1H), 7.59-7.47 (m, 5H), 6.95-6.89 (m, 2H), 6.79 (d, J = 3.0 Hz, 1H), 4.96 (dd, J_1 = 9.0 Hz, J_2 = 5.7 Hz, 1H), 3.87 (s, 3H), 3.84 (dd, J_1 = 17.4 Hz, J_2 = 5.4 Hz, 1H), 3.31 (dd, J_1 = 17.4 Hz, J_2 = 9.0 Hz, 1H), 1.63 (s, 3H).

^{13}C NMR (75 MHz, CDCl_3) δ 172.2, 170.9, 160.7, 155.7, 150.3, 133.3, 131.4, 131.3 (q, J = 33.3 Hz), 129.7, 128.7, 128.2, 127.5, 126.3-126.2 (m), 123.7, 123.4 (q, J = 271.8 Hz), 121.1-120.9 (m), 114.1, 108.0, 80.6, 55.3, 51.7, 39.1, 24.6.

^{19}F NMR (282 MHz, CDCl_3) δ -63.45 (s, 6F).

IR (film): ν (cm^{-1}) 2979, 2936, 1718, 1614, 1515, 1405, 1366, 1276, 1241, 1172, 1125, 1029, 936, 904, 839, 767, 733, 684, 525.

HRMS (ESI, m/z) calcd for $C_{30}H_{24}F_6N_3O_2$ $[M+H]^+$: 572.1767, found: 572.1758.



((1*R*,3'*R*)-6-Methoxy-5'-phenyl-3,3',4,4'-tetrahydro-2*H*-spiro[naphthalene-1,2'-pyrrol]-3'-yl)(3-(4-methoxyphenyl)-1*H*-pyrazol-1-yl)methanone (32s**)**

According to the general procedure, the reaction of (*E*)-2-(6-methoxy-3,4-dihydronaphthalen-1(2*H*)-ylidene)-1-(3-(4-methoxyphenyl)-1*H*-pyrazol-1-yl)ethan-1-one **30s** (37.4 mg, 0.10 mmol), (1-azidovinyl)benzene **31a** (18.2 mg, 1.25 equiv) and Λ -**RhS** (3.5 mg, 4 mol%) in $CDCl_3$ (1.0 mL, 0.1 M) under open air atmosphere with blue LEDs for 24 hours, afforded **32s** as a yellow solid (46.2 mg, 94% isolated yield).

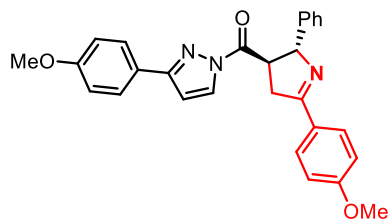
Only one single diastereoisomer was observed through 1H NMR of crude materials. Enantiomeric excess of **32s** was established by HPLC analysis using a Chiralpak OD-H column, ee = 99.6% (HPLC: OD-H, 254 nm, *n*-hexane/isopropanol = 80:20, flow rate 1 mL/min, 40 °C, t_r (major) = 8.1 min, t_r (minor) = 6.7 min). $[\alpha]_D^{22} = +144.6^\circ$ (c 1.0, CH_2Cl_2).

1H NMR (300 MHz, $CDCl_3$) δ 8.25 (br s, 1H), 7.97-7.92 (m, 2H), 7.49-7.41 (m, 3H), 7.25 (d, J = 9.0 Hz, 1H), 7.22-7.17 (m, 2H), 6.92 (dd, J_1 = 8.7 Hz, J_2 = 3.0 Hz, 1H), 6.84-6.78 (m, 2H), 6.67 (d, J = 2.7 Hz, 1H), 6.49 (d, J = 2.7 Hz, 1H), 5.03 (t, J = 9.0 Hz, 1H), 3.95 (dd, J_1 = 17.1 Hz, J_2 = 9.0 Hz, 1H), 3.83 (s, 3H), 3.79 (s, 3H), 3.48 (dd, J_1 = 17.4 Hz, J_2 = 9.6 Hz, 1H), 2.77-2.64 (m, 1H), 2.45 (dt, J_1 = 16.5 Hz, J_2 = 5.1 Hz, 1H), 1.95-1.81 (m, 3H), 1.22-1.06 (m, 1H).

^{13}C NMR (75 MHz, $CDCl_3$) δ 171.7, 168.0, 160.4, 158.4, 154.9, 138.4, 134.0, 133.8, 130.7, 129.1, 128.5, 128.0, 127.7, 124.1, 113.8, 113.4, 112.5, 107.5, 80.7, 55.2, 55.1, 53.3, 39.2, 31.9, 30.0, 19.9. (Missing one ^{13}C signal)

IR (film): ν (cm^{-1}) 3000, 2935, 2836, 1712, 1611, 1579, 1507, 1435, 1403, 1335, 1293, 1238, 1173, 1120, 1089, 1030, 942, 911, 837, 804, 765, 728, 691, 631, 559.

HRMS (ESI, m/z) calcd for $C_{31}H_{30}N_3O_3$ $[M+H]^+$: 492.2282, found: 492.2276.



(3-(4-Methoxyphenyl)-1H-pyrazol-1-yl)((2R,3R)-5-(4-methoxyphenyl)-2-phenyl-3,4-dihydro-2H-pyrrol-3-yl)methanone (32t**)**

According to the general procedure with some modifications, the reaction of (*E*)-1-(3-(4-methoxyphenyl)-1H-pyrazol-1-yl)-3-phenylprop-2-en-1-one **30f** (30.4 mg, 0.10 mmol), 1-(1-azidovinyl)-4-methoxybenzene **31b** (21.9 mg, 1.25 equiv) and Λ -**RhS** (6.9 mg, 8 mol%) in CDCl_3 (1.0 mL, 0.1 M) under nitrogen atmosphere (degassed with freeze-pump-thaw) with blue LEDs for 24 hours, afforded **32t** as a yellow oil (33.7 mg, 75% isolated yield).

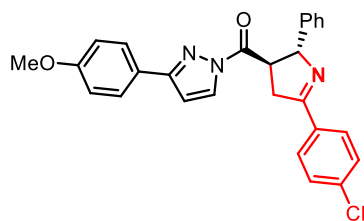
Only one single diastereoisomer was observed through ^1H NMR of crude materials. Enantiomeric excess of **32t** was established by HPLC analysis using a Chiralpak AD-H column, ee = 90% (HPLC: AD-H, 254 nm, *n*-hexane/isopropanol = 60:40, flow rate 1 mL/min, 40 °C, t_r (major) = 16.3 min, t_r (minor) = 23.4 min). $[\alpha]_D^{22} = +35.6^\circ$ (*c* 1.0, CH_2Cl_2).

^1H NMR (300 MHz, CDCl_3) δ 8.30 (d, $J = 3.0$ Hz, 1H), 7.97-7.91 (m, 2H), 7.71-7.64 (m, 2H), 7.41-7.25 (m, 5H), 7.00-6.90 (m, 4H), 6.74 (d, $J = 2.7$ Hz, 1H), 5.79-5.73 (m, 1H), 4.58-4.48 (m, 1H), 3.87 (s, 3H), 3.85 (s, 3H), 3.65 (ddd, $J_1 = 16.8$ Hz, $J_2 = 9.3$ Hz, $J_3 = 1.8$ Hz, 1H), 3.53 (ddd, $J_1 = 16.8$ Hz, $J_2 = 6.9$ Hz, $J_3 = 1.2$ Hz, 1H).

^{13}C NMR (75 MHz, CDCl_3) δ 172.4, 170.8, 161.9, 160.5, 155.3, 142.8, 129.8, 129.7, 128.5, 127.7, 127.3, 127.0, 126.5, 124.3, 114.1, 113.9, 107.4, 79.1, 55.4, 55.3, 49.9, 40.0.

IR (film): ν (cm^{-1}) 3004, 2959, 2837, 1717, 1608, 1512, 1431, 1403, 1336, 1296, 1245, 1173, 1096, 1027, 945, 908, 834, 802, 770, 729, 697, 556.

HRMS (ESI, m/z) calcd for $\text{C}_{28}\text{H}_{26}\text{N}_3\text{O}_3$ $[\text{M}+\text{H}]^+$: 452.1980, found: 452.1969.



((2*R*,3*R*)-5-(4-Chlorophenyl)-2-phenyl-3,4-dihydro-2*H*-pyrrol-3-yl)(3-(4-methoxyphenyl)-1*H*-pyrazol-1-yl)methanone (32u)

According to the general procedure, the reaction of (*E*)-1-(3-(4-methoxyphenyl)-1*H*-pyrazol-1-yl)-3-phenylprop-2-en-1-one **30f** (30.4 mg, 0.10 mmol), 1-(1-azidovinyl)-4-chlorobenzene **31c** (22.5 mg, 1.25 equiv) and Λ -**RhS** (3.5 mg, 4 mol%) in CDCl_3 (1.0 mL, 0.1 M) under open air atmosphere with blue LEDs for 24 hours, afforded **32u** as a yellow solid (36.5 mg, 80% isolated yield).

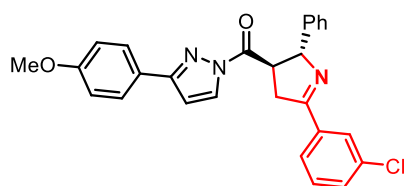
Only one single diastereoisomer was observed through ^1H NMR of crude materials. Enantiomeric excess of **32u** was established by HPLC analysis using a Chiralpak AD-H column, ee = 95% (HPLC: AD-H, 254 nm, *n*-hexane/isopropanol = 80:20, flow rate 0.6 mL/min, 40 °C, t_r (major) = 34.0 min, t_r (minor) = 31.6 min). $[\alpha]_D^{22} = +21.0^\circ$ (*c* 1.0, CH_2Cl_2).

^1H NMR (300 MHz, CDCl_3) δ 8.30 (d, $J = 3.3$ Hz, 1H), 7.94-7.88 (m, 2H), 7.70-7.64 (m, 2H), 7.46-7.40 (m, 2H), 7.37-7.27 (m, 5H), 6.96-6.89 (m, 2H), 6.75 (d, $J = 2.7$ Hz, 1H), 5.80-5.76 (m, 1H), 4.60-4.51 (m, 1H), 3.86 (s, 3H), 3.65 (ddd, $J_1 = 17.1$ Hz, $J_2 = 9.6$ Hz, $J_3 = 2.1$ Hz, 1H), 3.53 (ddd, $J_1 = 17.1$ Hz, $J_2 = 6.9$ Hz, $J_3 = 1.5$ Hz, 1H).

^{13}C NMR (75 MHz, CDCl_3) δ 172.2, 170.4, 160.6, 155.5, 142.4, 137.1, 132.2, 129.9, 129.4, 128.8, 128.6, 127.7, 127.5, 126.9, 124.2, 114.1, 107.6, 79.4, 55.3, 49.9, 40.0.

IR (film): ν (cm^{-1}) 3029, 2928, 2836, 1716, 1612, 1513, 1431, 1402, 1355, 1333, 1293, 1246, 1175, 1091, 1034, 946, 909, 832, 801, 769, 725, 697.

HRMS (ESI, m/z) calcd for $\text{C}_{27}\text{H}_{23}\text{ClN}_3\text{O}_2$ $[\text{M}+\text{H}]^+$: 456.1473, found: 456.1467.



((2*R*,3*R*)-5-(3-Chlorophenyl)-2-phenyl-3,4-dihydro-2*H*-pyrrol-3-yl)(3-(4-methoxyphenyl)-1*H*-pyrazol-1-yl)methanone (32v)

According to the general procedure, the reaction of (*E*)-1-(3-(4-methoxyphenyl)-1*H*-pyrazol-1-yl)-3-phenylprop-2-en-1-one **30f** (30.4 mg, 0.10 mmol), 1-(1-azidovinyl)-3-chlorobenzene **31d** (22.5 mg, 1.25 equiv) and Λ -**RhS** (3.5 mg, 4 mol%) in CDCl₃ (1.0 mL, 0.1 M) under open air atmosphere with blue LEDs for 24 hours, afforded **32v** as a yellow oil (41.8 mg, 92% isolated yield).

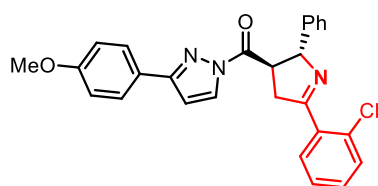
Only one single diastereoisomer was observed through ¹H NMR of crude materials. Enantiomeric excess of **32v** was established by HPLC analysis using a Chiralpak IG column, ee = 95% (HPLC: IG, 254 nm, *n*-hexane/isopropanol = 80:20, flow rate 1 mL/min, 40 °C, *t_r* (major) = 22.2 min, *t_r* (minor) = 18.3 min). [α]_D²² = +23.4° (*c* 1.0, CH₂Cl₂).

¹H NMR (300 MHz, CDCl₃) δ 8.31 (d, *J* = 3.0 Hz, 1H), 8.01 (t, *J* = 1.5 Hz, 1H), 7.83 (dt, *J₁* = 7.8 Hz, *J₂* = 1.5 Hz, 1H), 7.71-7.64 (m, 2H), 7.49-7.44 (m, 1H), 7.43-7.28 (m, 6H), 6.97-6.90 (m, 2H), 6.75 (d, *J* = 2.7 Hz, 1H), 5.84-5.78 (m, 1H), 4.62-4.51 (m, 1H), 3.86 (s, 3H), 3.65 (ddd, *J₁* = 17.1 Hz, *J₂* = 9.3 Hz, *J₃* = 2.1 Hz, 1H), 3.53 (ddd, *J₁* = 17.1 Hz, *J₂* = 7.2 Hz, *J₃* = 1.5 Hz, 1H).

¹³C NMR (75 MHz, CDCl₃) δ 172.1, 170.3, 160.6, 155.5, 142.2, 135.4, 134.7, 130.9, 129.84, 129.81, 128.6, 128.1, 127.7, 127.5, 126.9, 126.2, 124.2, 114.1, 107.6, 79.3, 55.3, 49.8, 40.0.

IR (film): ν (cm⁻¹) 3064, 3029, 2931, 1717, 1613, 1514, 1430, 1403, 1355, 1331, 1294, 1244, 1174, 1093, 1032, 949, 908, 837, 770, 729, 691.

HRMS (ESI, *m/z*) calcd for C₂₇H₂₃ClN₃O₂ [M+H]⁺: 456.1473, found: 456.1467.



((2*R*,3*R*)-5-(2-Chlorophenyl)-2-phenyl-3,4-dihydro-2*H*-pyrrol-3-yl)(3-(4-methoxyphenyl)-1*H*-pyrazol-1-yl)methanone (32w**)**

According to the general procedure, the reaction of (*E*)-1-(3-(4-methoxyphenyl)-1*H*-pyrazol-1-yl)-3-phenylprop-2-en-1-one **30f** (30.4 mg, 0.10 mmol), 1-(1-azidovinyl)-2-chlorobenzene **31e** (22.5 mg, 1.25 equiv) and Λ -**RhS** (3.5 mg, 4 mol%) in CDCl₃ (1.0 mL, 0.1 M) under open air atmosphere with blue LEDs for 24 hours, afforded **32w** as a yellow oil (36.3 mg, 80% isolated yield).

Only one single diastereoisomer was observed through ¹H NMR of crude materials. Enantiomeric excess of **32w** was established by HPLC analysis using a Chiralpak IG column, ee = 98% (HPLC: IG,

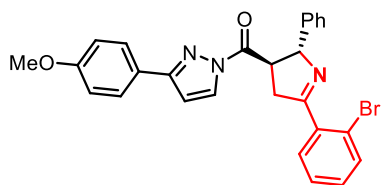
254 nm, *n*-hexane/isopropanol = 80:20, flow rate 1 mL/min, 40 °C, t_r (major) = 22.9 min, t_r (minor) = 15.5 min). $[\alpha]_D^{22} = +10.6^\circ$ (*c* 1.0, CH₂Cl₂).

¹H NMR (300 MHz, CDCl₃) δ 8.31 (d, *J* = 3.0 Hz, 1H), 7.81-7.96 (m, 1H), 7.71-7.65 (m, 2H), 7.48-7.27 (m, 8H), 6.96-6.90 (m, 2H), 6.75 (d, *J* = 3.0 Hz, 1H), 5.81-5.76 (m, 1H), 4.63-4.53 (m, 1H), 3.85 (s, 3H), 3.81 (ddd, *J*₁ = 17.4 Hz, *J*₂ = 9.6 Hz, *J*₃ = 2.1 Hz, 1H), 3.62 (ddd, *J*₁ = 17.7 Hz, *J*₂ = 7.5 Hz, *J*₃ = 1.8 Hz, 1H).

¹³C NMR (75 MHz, CDCl₃) δ 172.5, 172.2, 160.6, 155.5, 142.1, 134.3, 132.6, 130.9, 130.8, 130.3, 129.8, 128.5, 127.7, 127.4, 127.0, 126.9, 124.2, 114.1, 107.6, 78.8, 55.3, 50.5, 43.3.

IR (film): ν (cm⁻¹) 3062, 2933, 2836, 1717, 1610, 1513, 1431, 1403, 1355, 1331, 1294, 1246, 1175, 1028, 908, 836, 802, 755, 728, 700.

HRMS (ESI, *m/z*) calcd for C₂₇H₂₃ClN₃O₂ [M+H]⁺: 456.1473, found: 456.1467.



((2*R*,3*R*)-5-(2-Bromophenyl)-2-phenyl-3,4-dihydro-2*H*-pyrrol-3-yl)(3-(4-methoxyphenyl)-1*H*-pyrazol-1-yl)methanone (32x**)**

According to the general procedure, the reaction of (*E*)-1-(3-(4-methoxyphenyl)-1*H*-pyrazol-1-yl)-3-phenylprop-2-en-1-one **30f** (30.4 mg, 0.10 mmol), 1-(1-azidovinyl)-2-bromobenzene **31f** (28.0 mg, 1.25 equiv) and Λ -**RhS** (3.5 mg, 4 mol%) in CDCl₃ (1.0 mL, 0.1 M) under open air atmosphere with blue LEDs for 24 hours, afforded **32x** as a yellow solid (44.6 mg, 89% isolated yield).

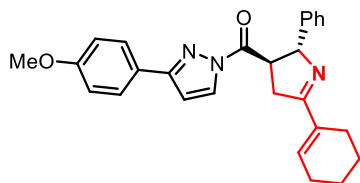
Only one single diastereoisomer was observed through ¹H NMR of crude materials. Enantiomeric excess of **32x** was established by HPLC analysis using a Chiralpak AD-H column, ee = 98% (HPLC: AD-H, 254 nm, *n*-hexane/isopropanol = 80:20, flow rate 1 mL/min, 40 °C, t_r (major) = 16.9 min, t_r (minor) = 10.4 min). $[\alpha]_D^{22} = +8.4^\circ$ (*c* 1.0, CH₂Cl₂).

¹H NMR (300 MHz, CDCl₃) δ 8.31 (d, *J* = 3.0 Hz, 1H), 7.71-7.61 (m, 4H), 7.48-7.27 (m, 7H), 6.96-6.90 (m, 2H), 6.74 (d, *J* = 2.7 Hz, 1H), 5.82-5.76 (m, 1H), 4.64-4.55 (m, 1H), 3.85 (s, 3H), 3.82 (ddd, *J*₁ = 18.0 Hz, *J*₂ = 9.6 Hz, *J*₃ = 2.1 Hz, 1H), 3.58 (ddd, *J*₁ = 17.4 Hz, *J*₂ = 7.2 Hz, *J*₃ = 1.5 Hz, 1H).

^{13}C NMR (75 MHz, CDCl_3) δ 173.6, 172.1, 160.6, 155.4, 142.0, 136.7, 133.4, 130.8, 130.5, 129.8, 128.5, 127.7, 127.44, 127.42, 127.0, 124.2, 121.1, 114.1, 107.6, 79.1, 55.3, 50.5, 43.4.

IR (film): ν (cm^{-1}) 3061, 2958, 2931, 2836, 1716, 1610, 1513, 1430, 1402, 1355, 1330, 1293, 1245, 1174, 1095, 1024, 947, 908, 836, 801, 751, 696.

HRMS (ESI, m/z) calcd for $\text{C}_{27}\text{H}_{23}\text{BrN}_3\text{O}_2$ $[\text{M}+\text{H}]^+$: 500.0968, found: 500.0962.



((2R,3R)-5-(Cyclohex-1-en-1-yl)-2-phenyl-3,4-dihydro-2H-pyrrol-3-yl)(3-(4-methoxyphenyl)-1H-pyrazol-1-yl)methanone (32y**)**

According to the general procedure with some modifications, the reaction of (*E*)-1-(3-(4-methoxyphenyl)-1H-pyrazol-1-yl)-3-phenylprop-2-en-1-one **30f** (30.4 mg, 0.10 mmol), 1-(1-azidovinyl)cyclohex-1-ene **31g** (18.7 mg, 1.25 equiv) and Λ -**RhS** (6.9 mg, 8 mol%) in CDCl_3 (1.0 mL, 0.1 M) under nitrogen atmosphere (degassed with freeze-pump-thaw) with blue LEDs for 24 hours, afforded **32y** as a yellow oil (31.8 mg, 75% isolated yield).

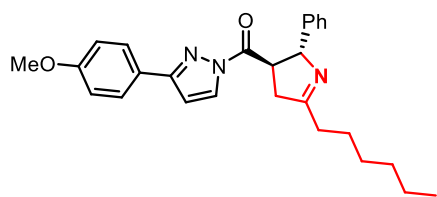
Only one single diastereoisomer was observed through ^1H NMR of crude materials. Enantiomeric excess of **32y** was established by HPLC analysis using a Chiralpak AD-H column, ee = 93% (HPLC: AD-H, 254 nm, *n*-hexane/isopropanol = 90:10, flow rate 1 mL/min, 40 °C, t_r (major) = 13.3 min, t_r (minor) = 11.7 min). $[\alpha]_{\text{D}}^{22} = -26.4^\circ$ (*c* 1.0, CH_2Cl_2).

^1H NMR (300 MHz, CDCl_3) δ 8.28 (d, J = 3.0 Hz, 1H), 7.70-7.63 (m, 2H), 7.35-7.22 (m, 5H), 6.96-6.89 (m, 2H), 6.72 (d, J = 2.7 Hz, 1H), 6.43 (t, J = 3.6 Hz, 1H), 5.67-5.62 (m, 1H), 4.42-4.33 (m, 1H), 3.85 (s, 3H), 3.40 (ddd, J_1 = 16.8 Hz, J_2 = 9.6 Hz, J_3 = 1.5 Hz, 1H), 3.26 (ddd, J_1 = 16.5 Hz, J_2 = 6.9 Hz, J_3 = 0.9 Hz, 1H), 2.57-2.48 (m, 2H), 2.28-2.21 (m, 2H), 1.80-1.61 (m, 4H).

^{13}C NMR (75 MHz, CDCl_3) δ 173.0, 172.6, 160.5, 155.2, 142.9, 135.9, 134.6, 129.8, 128.4, 127.7, 127.2, 126.9, 124.3, 114.1, 107.4, 78.9, 55.3, 49.7, 39.0, 26.1, 25.1, 22.3, 22.0.

IR (film): ν (cm^{-1}) 2930, 2837, 1717, 1608, 1513, 1432, 1402, 1354, 1333, 1293, 1244, 1175, 1094, 1027, 909, 836, 799, 766, 728, 697.

HRMS (ESI, m/z) calcd for $\text{C}_{27}\text{H}_{28}\text{N}_3\text{O}_2$ $[\text{M}+\text{H}]^+$: 426.2176, found: 426.2170.



((2*R*,3*R*)-5-Hexyl-2-phenyl-3,4-dihydro-2*H*-pyrrol-3-yl)(3-(4-methoxyphenyl)-1*H*-pyrazol-1-yl)methanone (32z**)**

According to the general procedure, the reaction of (*E*)-1-(3-(4-methoxyphenyl)-1*H*-pyrazol-1-yl)-3-phenylprop-2-en-1-one **30f** (30.4 mg, 0.10 mmol), 2-azidooct-1-ene **31h** (19.2 mg, 1.25 equiv) and Λ -**RhS** (3.5 mg, 4 mol%) in CDCl₃ (1.0 mL, 0.1 M) under open air atmosphere with blue LEDs for 24 hours, afforded **32z** as a yellow oil (30.1 mg, 70% isolated yield).

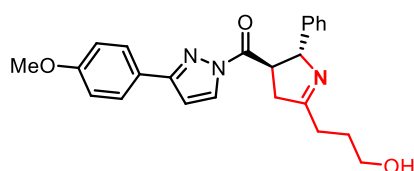
Only one single diastereoisomer was observed through ¹H NMR of crude materials. Enantiomeric excess of **32z** was established by HPLC analysis using a Chiralpak IG column, ee = 97% (HPLC: IG, 254 nm, *n*-hexane/isopropanol = 80:20, flow rate 1 mL/min, 40 °C, *t_r* (major) = 15.1 min, *t_r* (minor) = 12.5 min). [α]_D²² = +49.0° (*c* 1.0, CH₂Cl₂).

¹H NMR (300 MHz, CDCl₃) δ 8.28 (d, *J* = 2.7 Hz, 1H), 7.68-7.62 (m, 2H), 7.36-7.22 (m, 5H), 6.95-6.89 (m, 2H), 6.72 (d, *J* = 2.7 Hz, 1H), 5.57-5.52 (m, 1H), 4.43-4.34 (m, 1H), 3.85 (s, 3H), 3.22-3.04 (m, 2H), 2.52 (t, *J* = 8.3 Hz, 2H), 1.79-1.67 (m, 2H), 1.46-1.30 (m, 6H), 0.91 (t, *J* = 6.9 Hz, 3H).

¹³C NMR (75 MHz, CDCl₃) δ 177.2, 172.6, 160.5, 155.3, 142.6, 129.7, 128.4, 127.7, 127.2, 126.8, 124.3, 114.1, 107.4, 79.0, 55.3, 49.7, 42.2, 33.6, 31.5, 29.2, 26.5, 22.5, 14.0.

IR (film): ν (cm⁻¹) 2924, 2856, 1718, 1645, 1610, 1512, 1431, 1402, 1353, 1294, 1247, 1175, 1094, 1031, 950, 908, 837, 771, 698, 619, 525.

HRMS (ESI, *m/z*) calcd for C₂₇H₃₂N₃O₂ [M+H]⁺: 430.2489, found: 430.2484.



((2*R*,3*R*)-5-(3-Hydroxypropyl)-2-phenyl-3,4-dihydro-2*H*-pyrrol-3-yl)(3-(4-methoxyphenyl)-1*H*-pyrazol-1-yl)methanone (32aa**)**

According to the general procedure, the reaction of (*E*)-1-(3-(4-methoxyphenyl)-1*H*-pyrazol-1-yl)-3-phenylprop-2-en-1-one **30f** (30.4 mg, 0.10 mmol), 4-azidopent-4-en-1-ol **31i** (15.9 mg, 1.25 equiv) and Λ -**RhS** (6.9 mg, 8 mol%) in CDCl_3 (1.0 mL, 0.1 M) under nitrogen atmosphere (degassed with freeze-pump-thaw) with blue LEDs for 24 hours, afforded **32aa** as a yellow solid (38.0 mg, 69% isolated yield; 94% NMR yield, not stable in silica gel column).

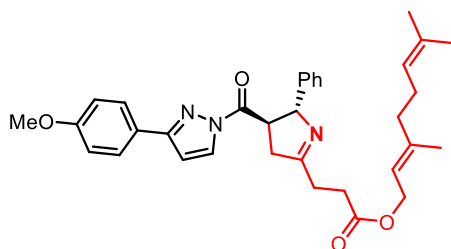
Only one single diastereoisomer was observed through ^1H NMR of crude materials. Enantiomeric excess of **32aa** was established by HPLC analysis using a Chiralpak AD-H column, ee = 98% (HPLC: AD-H, 254 nm, *n*-hexane/isopropanol = 90:10, flow rate 1 mL/min, 40 °C, t_r (major) = 23.7 min, t_r (minor) = 26.4 min). $[\alpha]_D^{22} = -45.2^\circ$ (*c* 1.0, CH_2Cl_2).

^1H NMR (300 MHz, CDCl_3) δ 8.27 (d, $J = 3.0$ Hz, 1H), 7.68-7.62 (m, 2H), 7.36-7.23 (m, 5H), 6.95-6.89 (m, 2H), 6.72 (d, $J = 3.3$ Hz, 1H), 5.60-5.55 (m, 1H), 4.46-4.37 (m, 1H), 3.99 (br s, 1H), 3.85 (s, 3H), 3.75 (t, $J = 5.7$ Hz, 2H), 3.25-3.07 (m, 2H), 2.72-2.51 (m, 2H), 2.06-1.96 (m, 2H).

^{13}C NMR (75 MHz, CDCl_3) δ 177.9, 172.2, 160.6, 155.4, 142.1, 129.8, 128.5, 127.7, 127.4, 126.6, 124.2, 114.1, 107.5, 78.6, 62.5, 55.3, 49.7, 42.9, 31.3, 28.7.

IR (film): ν (cm^{-1}) 3120, 2958, 2919, 2840, 1724, 1646, 1611, 1515, 1445, 1348, 1245, 1174, 1025, 955, 906, 836, 768, 730, 699, 609, 524.

HRMS (ESI, m/z) calcd for $\text{C}_{24}\text{H}_{26}\text{N}_3\text{O}_3$ $[\text{M}+\text{H}]^+$: 404.1969, found: 404.1964.



(*E*)-3,7-Dimethylocta-2,6-dien-1-yl 3-((2*R*,3*R*)-3-(3-(4-methoxyphenyl)-1*H*-pyrazole-1-carbonyl)-2-phenyl-3,4-dihydro-2*H*-pyrrol-5-yl)propanoate (32ab**)**

According to the general procedure with some modifications, the reaction of (*E*)-1-(3-(4-methoxyphenyl)-1*H*-pyrazol-1-yl)-3-phenylprop-2-en-1-one **30f** (30.4 mg, 0.10 mmol), (*E*)-3,7-dimethylocta-2,6-dien-1-yl 4-azidopent-4-enoate **31j** (34.7 mg, 1.25 equiv) and Λ -**RhS** (6.9 mg, 8 mol%) in CDCl_3 (1.0 mL, 0.1 M) under nitrogen atmosphere (degassed with freeze-pump-thaw) with blue LEDs for 24 hours, afforded **32ab** as a yellow solid (45.7 mg, 83% isolated yield; 92% NMR yield, not stable in silica gel column).

Only one single diastereoisomer was observed through ^1H NMR of crude materials. Enantiomeric excess of **32ab** was established by HPLC analysis using a Chiralpak OD-H column, ee = 98% (HPLC: OD-H, 254 nm, *n*-hexane/isopropanol = 90:10, flow rate 1 mL/min, 40 °C, t_r (major) = 10.5 min, t_r (minor) = 12.7 min). $[\alpha]_D^{22} = +80.6^\circ$ (*c* 1.0, CH_2Cl_2).

^1H NMR (500 MHz, CDCl_3) δ 8.27 (d, $J = 3.0$ Hz, 1H), 7.68-7.63 (m, 2H), 7.33-7.29 (m, 2H), 7.28-7.23 (m, 3H), 6.94-6.90 (m, 2H), 6.72 (d, $J = 3.0$ Hz, 1H), 5.56-5.50 (m, 1H), 5.36-5.31 (m, 1H), 5.09-5.04 (m, 1H), 4.67-4.58 (m, 2H), 3.38 (ddd, $J_1 = 9.5$ Hz, $J_2 = 6.5$ Hz, $J_3 = 5.5$ Hz, 1H), 3.85 (s, 3H), 3.20 (ddd, $J_1 = 17.0$ Hz, $J_2 = 9.5$ Hz, $J_3 = 1.5$ Hz, 1H), 3.10 (ddd, $J_1 = 17.5$ Hz, $J_2 = 6.5$ Hz, $J_3 = 1.0$ Hz, 1H), 2.94-2.81 (m, 2H), 2.80-2.70 (m, 2H), 2.12-2.05 (m, 2H), 2.04-1.99 (m, 2H), 1.69-1.67 (m, 6H), 1.59 (s, 3H).

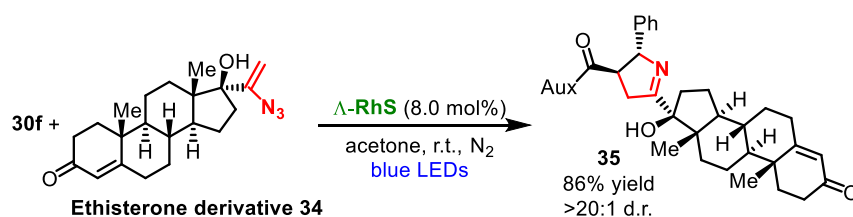
^{13}C NMR (125 MHz, CDCl_3) δ 175.3, 173.0, 172.4, 160.5, 155.3, 142.5, 142.2, 131.8, 129.7, 128.4, 127.7, 127.2, 126.8, 124.2, 123.7, 118.2, 114.1, 107.5, 78.8, 61.5, 55.3, 49.8, 42.7, 39.5, 30.7, 28.2, 26.2, 25.7, 17.7, 16.4.

IR (film): ν (cm^{-1}) 2961, 2918, 2848, 1722, 1651, 1611, 1513, 1432, 1402, 1354, 1293, 1247, 1173, 1095, 1031, 945, 905, 836, 771, 698.

HRMS (ESI, m/z) calcd for $\text{C}_{34}\text{H}_{40}\text{N}_3\text{O}_4$ $[\text{M}+\text{H}]^+$: 554.3013, found: 554.3003.

5.5.4 Synthetic Applications

1) Access to Ethisterone derivative 1-pyrroline **35**



(8*R*,9*S*,10*R*,13*S*,14*S*,17*S*)-17-(1-Azidovinyl)-17-hydroxy-10,13-dimethyl-1,2,6,7,8,9,10,11,12,13,14,15,16,17-tetradecahydro-3*H*-cyclopenta[*a*]phenanthren-3-one **34** was synthesized according to the reported procedure.^{12d} Ethisterone derived vinyl azide **34** is unstable in CDCl_3 . So acetone is chosen as solvent for this transformation.

According to the general procedure with some modifications, the reaction of (*E*)-1-(3-(4-methoxyphenyl)-1*H*-pyrazol-1-yl)-3-phenylprop-2-en-1-one **30f** (30.4 mg, 0.10 mmol), **34**

(44.4 mg, 1.25 equiv) and Λ -**RhS** (6.9 mg, 8 mol%) in **acetone** (1.0 mL, 0.1 M) under nitrogen atmosphere (degassed with freeze-pump-thaw) with blue LEDs for 48 hours, afforded **35** as a yellow solid (54.6 mg, 86%). $[\alpha]_{\text{D}}^{22} = +27.8^\circ$ (c 1.0, CH_2Cl_2).

A d.r. value of >20:1 was observed through ^1H NMR of crude materials. Reference sample was obtained by carrying out the reaction with *rac*-**RhS**.

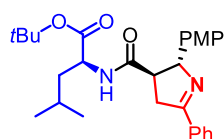
^1H NMR (500 MHz, CDCl_3) δ 8.27 (d, $J = 3.0$ Hz, 1H), 7.63-7.59 (m, 2H), 7.33-7.23 (m, 5H), 6.93-6.89 (m, 2H), 6.72 (d, $J = 3.0$ Hz, 1H), 5.73 (s, 1H), 5.62-5.56 (m, 1H), 4.50-4.43 (m, 1H), 3.84 (s, 3H), 3.82 (br s, 1H), 3.31 (ddd, $J_1 = 17.0$ Hz, $J_2 = 9.0$ Hz, $J_3 = 1.5$ Hz, 1H), 3.22 (ddd, $J_1 = 17.5$ Hz, $J_2 = 8.5$ Hz, $J_3 = 2.0$ Hz, 1H), 2.44-2.32 (m, 4H), 2.30-2.24 (m, 1H), 2.06-1.94 (m, 2H), 1.92-1.84 (m, 1H), 1.82-1.42 (m, 8H), 1.26-1.14 (m, 1H), 1.21 (s, 3H), 1.09-1.00 (m, 1H), 1.06 (s, 3H), 0.99-0.89 (m, 1H).

^{13}C NMR (125 MHz, CD_2Cl_2) δ 199.3, 182.2, 172.4, 171.4, 161.0, 155.7, 142.8, 130.1, 128.8, 128.0, 127.7, 127.1, 124.4, 124.0, 114.4, 107.9, 85.8, 77.6, 55.6, 54.2, 51.8, 50.1, 48.0, 42.9, 39.0, 36.6, 36.4, 36.1, 34.3, 33.2, 33.1, 32.2, 24.3, 21.1, 17.6, 14.7.

IR (film): ν (cm^{-1}) 3385, 2940, 2860, 1719, 1662, 1613, 1514, 1432, 1404, 1356, 1294, 1245, 1177, 1027, 951, 909, 836, 802, 773, 728, 698.

HRMS (ESI, m/z) calcd for $\text{C}_{40}\text{H}_{46}\text{N}_3\text{O}_4$ $[\text{M}+\text{H}]^+$: 632.3483, found: 632.3473.

2) Functional group conversions (Figure 85)



tert-Butyl ((2*R*,3*R*)-2-(4-methoxyphenyl)-5-phenyl-3,4-dihydro-2*H*-pyrrole-3-carbonyl)-*L*-leucinate (**36**)

According to literature report,^{13a} *L*-leucin-*tert*-butylester hydrochlorid (44.7 mg, 0.2 mmol), toluene (0.5 mL), and Et_3N (20.2 mg, 0.2 mmol) was added into a 10 mL Schlenk tube equipped with a stirring bar. After stirred at room temperature for 10 min, **32g** (45.2 mg, 0.1 mmol), 1-hydroxybenzotriazole (27.0 mg, 0.2 mmol), and toluene (1.0 mL) was added continuously. Then the tube was sealed and heated at 50 $^\circ\text{C}$ for 16 hours. The mixture was concentrated under reduced pressure and the crude

residue was subjected to ^1H NMR to determine the d.r. value. Then target product **36** was isolated by flash chromatography (*n*-Hexane/EtOAc) in 94% yield (43.8 mg). At the same time the auxiliary 3-(4-methoxyphenyl)-1*H*-pyrazole could be obtained in 99% yield (17.4 mg).

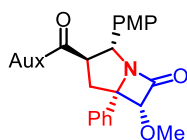
Only one single diastereoisomer (>20:1 d.r.) was observed through ^1H NMR of crude materials. Reference sample was obtained by carrying out the reaction with *rac*-**32g**. $[\alpha]_{\text{D}}^{22} = -23.4^\circ$ (*c* 1.0, CH_2Cl_2).

^1H NMR (300 MHz, CDCl_3) δ 7.93-7.86 (m, 2H), 7.47-7.36 (m, 3H), 7.23-7.15 (m, 2H), 6.93-6.84 (m, 2H), 5.71 (d, $J = 8.7$ Hz, 1H), 5.32-5.26 (m, 1H), 4.56 (td, $J_1 = 9.0$ Hz, $J_2 = 4.8$ Hz, 1H), 3.80 (s, 3H), 3.52 (ddd, $J_1 = 17.1$ Hz, $J_2 = 9.0$ Hz, $J_3 = 2.4$ Hz, 1H), 3.36 (ddd, $J_1 = 16.8$ Hz, $J_2 = 9.0$ Hz, $J_3 = 1.8$ Hz, 1H), 2.98-2.85 (m, 1H), 1.69-1.51 (m, 2H), 1.44 (s, 9H), 0.97 (d, $J = 6.3$ Hz, 3H), 0.94 (d, $J = 6.0$ Hz, 3H). (Missing the N-H signal)

^{13}C NMR (75 MHz, CDCl_3) δ 172.3, 172.2, 171.7, 159.1, 135.3, 133.9, 130.8, 128.4, 127.9, 114.1, 81.9, 80.0, 55.3, 54.5, 51.3, 42.0, 39.9, 27.9, 24.9, 22.8, 22.0. (Missing one ^{13}C signal)

IR (film): ν (cm^{-1}) 3287, 3062, 2857, 2823, 1731, 1644, 1616, 1539, 1512, 1453, 1371, 1335, 1297, 1243, 1147, 1037, 917, 825, 762, 731, 690, 578, 536.

HRMS (ESI, m/z) calcd for $\text{C}_{28}\text{H}_{37}\text{N}_2\text{O}_4$ $[\text{M}+\text{H}]^+$: 465.2748, found: 465.2743.



(2*R*,3*R*,5*S*,6*R*)-6-Methoxy-2-(4-methoxyphenyl)-3-(3-(4-methoxyphenyl)-1*H*-pyrazole-1-carbonyl)-5-phenyl-1-azabicyclo[3.2.0]heptan-7-one (37)

According to literature report,^{13b} **32g** (22.6 mg, 0.05 mmol), Et_3N (15.2 mg, 0.15 mmol), and CH_2Cl_2 (1.0 mL) was added into a 10 mL Schlenk tube equipped with a stirring bar. 2-Methoxyacetyl chloride (16.3 mg, 0.15 mmol, in 1.0 mL CH_2Cl_2) was added to the mixture dropwise at room temperature. Then the tube was sealed and heated at 50 $^\circ\text{C}$ for 16 hours. The mixture was concentrated under reduced pressure and the crude residue was subjected to ^1H NMR to determine the d.r. value. Then target product **37** was isolated by flash chromatography (*n*-Hexane/EtOAc) in 95% yield (24.9 mg).

A d.r. value of 17:1 was determined through ^1H NMR of crude materials. Reference sample was obtained by carrying out the reaction with *rac*-**32g**. Enantiomeric excess of **37** was established by

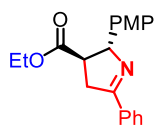
HPLC analysis using a Chiralpak OD-H column, ee = 98% (HPLC: OD-H, 254 nm, *n*-hexane/isopropanol = 80:20, flow rate 1 mL/min, 40 °C, t_r (major) = 20.0 min, t_r (minor) = 12.6 min). $[\alpha]_D^{22} = +188.8^\circ$ (*c* 1.0, CH₂Cl₂).

¹H NMR (500 MHz, CDCl₃) δ 8.24 (d, *J* = 3.0 Hz, 1H), 7.68-7.63 (m, 2H), 7.60-7.55 (m, 2H), 7.50-7.43 (m, 2H), 7.42-7.37 (m, 1H), 7.26-7.22 (m, 2H), 6.95-6.90 (m, 2H), 6.81-6.76 (m, 2H), 6.72 (d, *J* = 3.0 Hz, 1H), 5.57 (d, *J* = 8.0 Hz, 1H), 4.75-4.66 (m, 1H), 4.69 (s, 1H), 3.85 (s, 3H), 3.74 (s, 3H), 3.34 (dd, *J*₁ = 13.0 Hz, *J*₂ = 6.5, 1H), 3.16 (s, 3H), 2.56 (dd, *J*₁ = 12.5 Hz, *J*₂ = 10.5, 1H).

¹³C NMR (75 MHz, CDCl₃) δ 173.3, 170.3, 160.7, 159.1, 155.6, 137.5, 131.3, 129.9, 128.31, 128.27, 128.0, 127.7, 127.4, 124.0, 114.2, 113.9, 107.8, 90.4, 73.4, 64.0, 58.2, 55.3, 55.2, 54.8, 41.0.

IR (film): ν (cm⁻¹) 2999, 2884, 2835, 1763, 1716, 1673, 1612, 1550, 1514, 1433, 1406, 1335, 1295, 1246, 1217, 1175, 1142, 1093, 1023, 936, 907, 833, 774, 727, 700, 644, 577.

HRMS (ESI, *m/z*) calcd for C₃₁H₃₀N₃O₅ [M+H]⁺: 524.2180, found: 524.2188.



Ethyl (2*R*,3*R*)-2-(4-methoxyphenyl)-5-phenyl-3,4-dihydro-2*H*-pyrrole-3-carboxylate (**38**)

According to literature report,^{13a} **32g** (45.2 mg, 0.1 mmol), EtOH (0.8 mL), THF (0.2 mL), LiCl (21.2 mg, 0.5 mmol), and Et₃N (50.5 mg, 0.5 mmol) was added in sequence to a 10 mL Schlenk tube equipped with a stirring bar. After stirred at room temperature for 16 hours, the mixture was concentrated under reduced pressure and the crude residue was subjected to ¹H NMR to determine the d.r. value. Then target product **38** was isolated by flash chromatography (*n*-Hexane/EtOAc) in 99% yield (32.0 mg) at the same time the auxiliary 3-(4-methoxyphenyl)-1*H*-pyrazole could be obtained in 99% yield (17.4 mg).

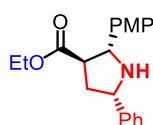
Only one single diastereoisomer was observed through ¹H NMR of crude materials. Reference sample was obtained by carrying out the reaction with *rac*-**32g**. Enantiomeric excess of **38** was established by HPLC analysis using a Chiralpak AD-H column, ee = 98% (HPLC: AD-H, 254 nm, *n*-hexane/isopropanol = 80:20, flow rate 1 mL/min, 40 °C, t_r (major) = 13.1 min, t_r (minor) = 9.5 min). $[\alpha]_D^{22} = +4.2^\circ$ (*c* 1.0, CH₂Cl₂).

^1H NMR (300 MHz, CDCl_3) δ 7.98-7.91 (m, 2H), 7.51-7.40 (m, 3H), 7.29-7.20 (m, 2H), 6.94-6.85 (m, 2H), 5.55-5.49 (m, 1H), 4.31-4.17 (m, 2H), 3.81 (s, 3H), 3.53-3.35 (m, 2H), 3.15 (td, $J_1 = 9.0$ Hz, $J_2 = 6.6$ Hz, 1H), 1.31 (t, $J = 7.1$ Hz, 3H).

^{13}C NMR (75 MHz, CDCl_3) δ 174.0, 171.3, 158.9, 135.4, 133.8, 130.9, 128.5, 127.9, 127.7, 114.0, 79.2, 61.0, 55.3, 51.3, 39.4, 14.2.

IR (film): ν (cm^{-1}) 2969, 2930, 2904, 2838, 1724, 1612, 1579, 1511, 1447, 1373, 1332, 1301, 1242, 1166, 1112, 1025, 870, 823, 762, 690, 586, 545.

HRMS (ESI, m/z) calcd for $\text{C}_{20}\text{H}_{22}\text{NO}_3$ $[\text{M}+\text{H}]^+$: 324.1594, found: 324.1590.



Ethyl (2*R*,3*R*,5*S*)-2-(4-methoxyphenyl)-5-phenylpyrrolidine-3-carboxylate (**39**)

38 (32.3 mg, 0.1 mmol), Pd/C (16 mg, 50%), and EtOAc (1.0 mL) was added in sequence to a 10 mL flask equipped with a stirring bar. After bubbling with H_2 for 5 minutes, the flask was allowed to stir at room temperature for 12 hours. The mixture was filtered and concentrated under reduced pressure. Then target product **39** was isolated by flash chromatography (*n*-Hexane/EtOAc) in 68% yield (22.2 mg, a white solid) as a single diastereoisomer.

Reference sample was obtained by carrying out the reaction with *rac*-**38**. Enantiomeric excess of **39** was established by HPLC analysis using a Chiralpak IC column, ee = 98% (HPLC: IC, 220 nm, *n*-hexane/isopropanol = 90:10, flow rate 1 mL/min, 40 °C, t_r (major) = 8.2 min, t_r (minor) = 7.2 min). $[\alpha]_{\text{D}}^{22} = -74.8^\circ$ (c 1.0, CH_2Cl_2).

^1H NMR (300 MHz, CDCl_3) δ 7.55-7.42 (m, 4H), 7.40-7.32 (m, 2H), 7.31-7.21 (m, 1H), 6.94-6.86 (m, 2H), 5.50 (d, $J = 7.8$ Hz, 1H), 4.45 (t, $J = 8.3$ Hz, 1H), 4.21-4.10 (m, 2H), 3.82 (s, 3H), 2.98-2.87 (m, 1H), 2.28-2.46 (m, 1H), 2.25-2.05 (br s, 1H), 2.16-2.02 (m, 1H), 1.23 (t, $J = 7.2$ Hz, 3H).

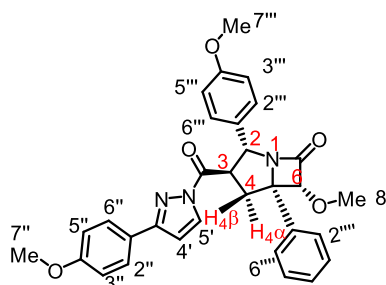
^{13}C NMR (75 MHz, CDCl_3) δ 174.7, 159.0, 144.0, 135.1, 128.4, 128.0, 127.1, 126.7, 113.8, 65.3, 61.3, 60.6, 55.3, 51.9, 38.8, 14.2.

IR (film): ν (cm^{-1}) 3315, 2975, 2941, 2834, 1724, 1609, 1508, 1451, 1375, 1345, 1299, 1242, 1168, 1099, 1033, 828, 755, 700, 579, 537.

HRMS (ESI, m/z) calcd for $\text{C}_{20}\text{H}_{24}\text{NO}_3$ $[\text{M}+\text{H}]^+$: 326.1751, found: 326.1746.

3) Determined of the configuration of **37** was by NMR spectroscopy

Sample of **37** dissolved in 0.6 mL of CDCl₃ were performed on a Bruker AVHD 500 MHz spectrometer equipped with a 5 mm TXI probe with z-gradient. NOESY experiments were performed with mixing time of 1.5 s. Chemical shifts are referenced with the rest solvent signal.



The NOESY cross peaks characteristic for the stereostructure of the molecule are presented in **Table 29**. With the known configuration at positions 2 and 3, through the observation of the NOE contacts among the substituents the configuration at positions 5 and 6 is unequivocally determined. There are additional NOESY cross peaks observed. A whole assignment to these signals are presented in **Figure 126**. The vicinal coupling constants observed are $^3J_{H_2H_3} = 8$ Hz, $^3J_{H_3H_{4\alpha}} = 6$ Hz, and $^3J_{H_3H_{4\beta}} = 10$ Hz. These values are consistent with the determined structure.

Table 29. NOESY cross peaks and molecular structure of compound **37**.

No.	Positions	Configuration	No.	Positions	Configuration
1	H-6 – CH ₃ -8		6	2'''/6''' – H-4 α	α -substitution of 5-Ph
2	H-2 – H-4 β	H-4 β	7	2'''/6''' – CH ₃ -8	cis-config. 5-Ph / 6-OMe
3	H-6 – H-4 β	α -substitution of H-6	8	2'''/6''' – H-3	trans-config. H-2 / H-3
4	H-3 – H-4 α	H-4 α	9	2'''/6''' – H-3	α -substitution at 5-Ph
5	2'''/6''' – 2'''/6'''	α -substitution of 5-Ph			

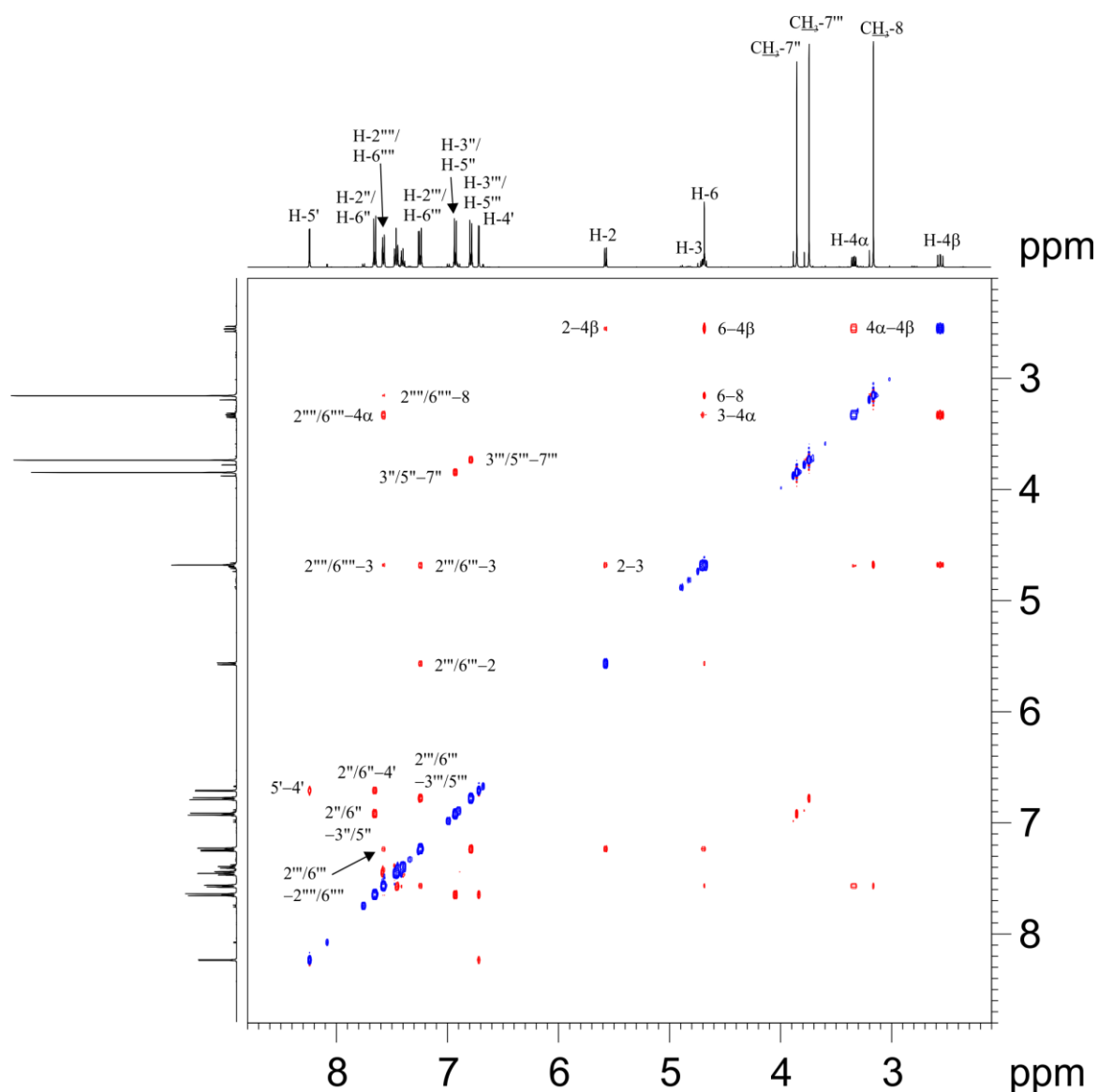
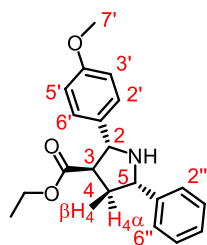


Figure 126. NOESY spectrum of compound **37** in CDCl_3 at 300 K, mixing time 1.5 s.

4) Determined of the configuration of **39** was by NMR spectroscopy



An assignment of the main NOESY cross peaks are given in **Figure 127**, with the known configuration at positions 2 and 3, strong NOE cross peak between H-3 and H-4 α was observed, which enabled the assignment of H-4 α . Strong NOE was observed between H-4 α and H-2''/H-6'', which

determined an α -substitution of phenyl group at position 5. In addition, a medium NOE contact was observed between H-2 and H-5, which verified the assigned configuration. The vicinal coupling constants observed are $^3J_{\text{H2H3}} = 7.8$ Hz, $^3J_{\text{H3H4}\alpha} = 10.5$ Hz, $^3J_{\text{H3H4}\beta} = 5.1$ Hz, $^3J_{\text{H4}\alpha\text{H4}\beta} = 13.0$ Hz, $^3J_{\text{H4}\alpha\text{H5}} = 8.1$ Hz, $^3J_{\text{H4}\beta\text{H5}} = 8.1$ Hz.

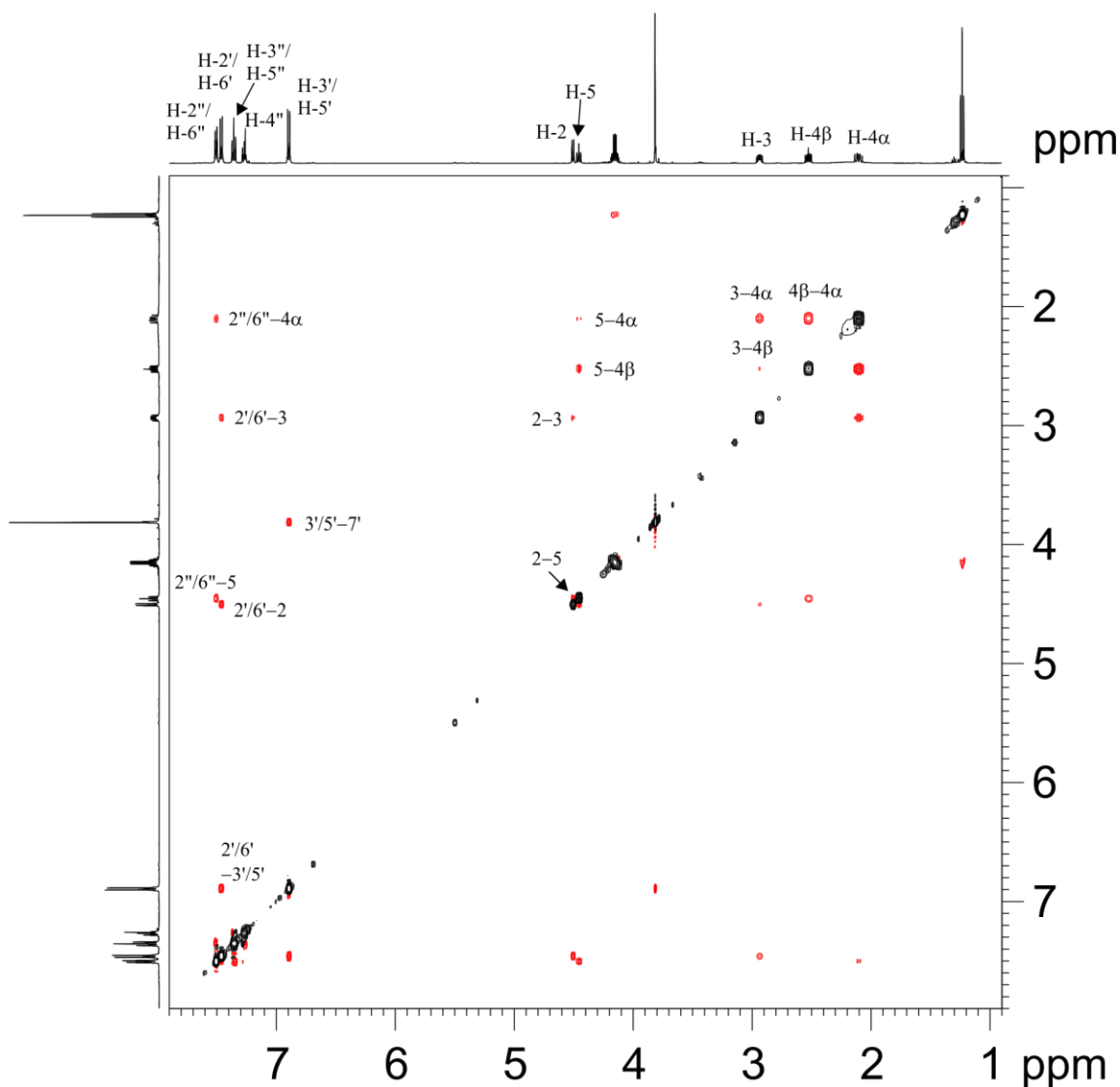


Figure 127. NOESY spectrum of compound **39** in CDCl_3 at 300 K, mixing time 1.5 s.

5.5.5 Single-Crystal X-Ray Diffraction Studies

Single crystals of **RhS-PPz** suitable for X-ray diffraction were obtained by slow diffusion of a solution of **RhS-PPz** (20 mg) in CH_2Cl_2 (0.5 mL) layered with Et_2O (0.5 mL) at room temperature for several days in a NMR tube.

Single crystals of **32k** suitable for X-ray diffraction were obtained by slow diffusion of a solution of **32k** (30 mg) in CH₂Cl₂ (0.5 mL) layered with *n*-hexane (0.5 mL) at room temperature for several days in a NMR tube.

X-ray data were collected with a STOE 4 circuit StadiVari diffractometer with CuK α radiation (microfocus tube with multilayer optics) and Dectris Pilatus 300K detector at 100 K. Scaling and absorption correction was performed by using the X-AREA/LANA software package of STOE. Structures were solved using direct methods in SHELXT and refined using the full matrix least squares procedure in SHELXL-2017. The hydrogen atoms were placed in calculated positions and refined as riding on their respective C atom, and Uiso(H) was set at 1.2 Ueq(Csp²) and 1.5 Ueq(Csp³). Disorder was refined using restraints for both the geometry and the anisotropic displacement factors.

The relative and absolute configuration of **32k** has been determined (**Figure 128**). The crystal structure of **RhS-PPz** was shown in **Figure 76**.

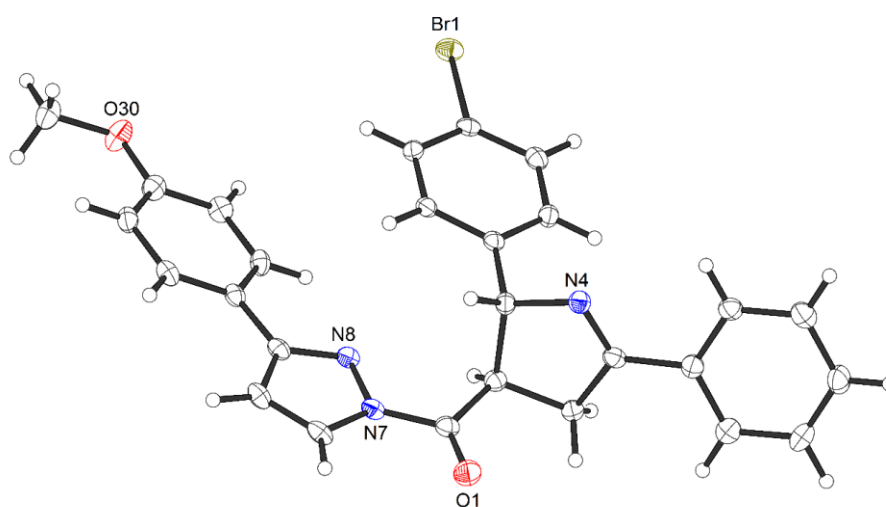


Figure 128. Crystal structure of compound **32k**.

Table 30. Crystal data and structure refinement for **RhS-PPz**.

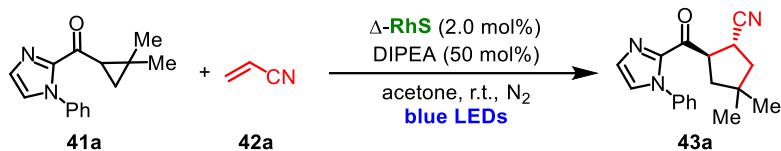
Crystal data		
CCDC number	1568748	
Identification code	hxqH72	
Habitus, color	block, yellow	
Crystal size	0.20 x 0.18 x 0.10 mm ³	
Crystal system	Monoclinic	
Space group	P2 ₁ /c	Z = 4
Unit cell dimensions	a = 13.7758(2) Å	α = 90°.
	b = 15.1202(1) Å	β = 96.139(1)°.
	c = 26.0113(3) Å	γ = 90°.
Volume	5386.9(1) Å ³	
Cell determination	56919 peaks with Theta 3.2 to 70.3 °	
Empirical formula	C _{55.89} H _{55.04} Cl _{0.74} F ₆ N ₄ O _{2.63} P Rh S ₂	
Moiety formula	C ₅₃ H ₄₈ N ₄ O ₂ Rh S ₂ , F ₆ P, 0.63(C ₄ H ₁₀ O), 0.37(C H ₂ Cl ₂)	
Formula weight	1163.07	
Density (calculated)	1.434 Mg/m ³	
Absorption coefficient	4.476 mm ⁻¹	
F(000)	2392	
Data collection:		
Diffractometer type	STOE STADIVARI	
Wavelength	1.54184 Å	
Temperature	100(2) K	
Theta range for data collection	3.227 to 69.719 °	
Index ranges	-16<=h<=7, -18<=k<=16, -31<=l<=30	
Data collection software	X-Area Pilatus3_SV 1.31.127.0 (STOE, 2016)	
Cell refinement software	X-Area Recipe 1.33.0.0 (STOE, 2015)	
Data reduction software	X-Area Integrate 1.71.0.0 (STOE, 2016)	
	X-Area LANA 1.68.2.0 (STOE, 2016)	
Solution and refinement:		
Reflections collected	49551	
Independent reflections	10012 [R(int) = 0.0208]	
Completeness to theta = 67.684 °	99.5 %	
Observed reflections	9039[I > 2σ(I)]	
Reflections used for refinement	10012	
Absorption correction	Semi-empirical from equivalents	
Max. and min. transmission	1.0000 and 0.3908	
Largest diff. peak and hole	0.871 and -0.406 e.Å ⁻³	
Solution	dual space algorithm	
Refinement	Full-matrix least-squares on F ²	
Treatment of hydrogen atoms	Calculated positions, constr ref.	
Programs used	XT V2014/1 (Bruker AXS Inc., 2014)	
	SHELXL-2016/6 (Sheldrick, 2016)	
	DIAMOND (Crystal Impact)	
	ShelXle (Hübschle, Sheldrick, Dittrich, 2011)	
Data / restraints / parameters	10012 / 49 / 730	
Goodness-of-fit on F ²	1.069	
R index (all data)	wR2 = 0.0741	
R index conventional [I>2sigma(I)]	R1 = 0.0266	

Table 31. Crystal data and structure refinement for **32k**.

Crystal data	
CCDC number	1568749
Identification code	hxqH27
Habitus, color	plate, colorless
Crystal size	0.17 x 0.17 x 0.04 mm ³
Crystal system	Monoclinic
Space group	P2 ₁
Unit cell dimensions	Z = 2
	a = 10.5089(2) Å
	b = 7.7040(1) Å
	c = 14.2627(2) Å
	$\alpha = 90^\circ$
	$\beta = 101.167(1)^\circ$
	$\gamma = 90^\circ$
Volume	1132.85(3) Å ³
Cell determination	28484 peaks with Theta 3.2 to 69.6 °
Empirical formula	C ₂₇ H ₂₂ Br N ₃ O ₂
Moiety formula	C ₂₇ H ₂₂ Br N ₃ O ₂
Formula weight	500.38
Density (calculated)	1.467 Mg/m ³
Absorption coefficient	2.713 mm ⁻¹
F(000)	512
Data collection:	
Diffractometer type	STOE STADIVARI
Wavelength	1.54184 Å
Temperature	100(2) K
Theta range for data collection	4.288 to 69.163 °
Index ranges	-10 ≤ h ≤ 12, -9 ≤ k ≤ 8, -17 ≤ l ≤ 8
Data collection software	X-Area Pilatus3_SV 1.31.127.0 (STOE, 2016)
Cell refinement software	X-Area Recipe 1.33.0.0 (STOE, 2015)
Data reduction software	X-Area Integrate 1.71.0.0 (STOE, 2016)
	X-Area LANA 1.68.2.0 (STOE, 2016)
Solution and refinement:	
Reflections collected	17616
Independent reflections	4091 [R(int) = 0.0176]
Completeness to theta = 67.684 °	99.3 %
Observed reflections	4006 [I > 2σ(I)]
Reflections used for refinement	4091
Absorption correction	Semi-empirical from equivalents
Max. and min. transmission	1.0000 and 0.4410
Flack parameter (absolute struct.)	-0.024(10)
Largest diff. peak and hole	0.285 and -0.244 e.Å ⁻³
Solution	dual space algorithm
Refinement	Full-matrix least-squares on F ²
Treatment of hydrogen atoms	Calculated positions, constr. ref.
Programs used	XT V2014/1 (Bruker AXS Inc., 2014)
	SHELXL-2016/6 (Sheldrick, 2016)
	DIAMOND (Crystal Impact)
	ShelXle (Hübschle, Sheldrick, Dittrich, 2011)
Data / restraints / parameters	4091 / 1 / 299
Goodness-of-fit on F ²	1.050
R index (all data)	wR2 = 0.0547
R index conventional [I > 2σ(I)]	R1 = 0.0208

5.6 Asymmetric [3+2] Photocycloaddition

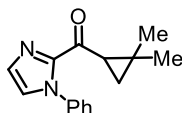
5.6.1 General Procedure



Exemplary, an oven-dried 10 mL Schlenk tube was charged with cyclopropane **41a** (24.0 mg, 0.10 mmol) and Δ -RhS (1.7 mg, 2 mol%). The tube was purged with nitrogen. Then, acetone (1.0 mL, 0.1 M) was added via syringe, followed by acrylonitrile **42a** (13.3 mg, 2.5 equiv) and DIPEA (6.5 mg, 0.5 equiv) under nitrogen atmosphere with stirring. The reaction mixture was degassed via freeze-pump-thaw for three cycles. After the mixture was thoroughly degassed, the vial was sealed and positioned at approximately 10 cm away from a 24 W blue LEDs lamp. After stirring for the indicated time (monitored by TLC), the mixture was diluted with CH_2Cl_2 . The combined mixture was concentrated under reduced pressure. The crude residue was subjected to 1H NMR to determine the d.r. value. Then, all the mixture was collected and purified by flash chromatography on silica gel (*n*-hexane/EtOAc) to afford the product **43a**. The enantiomeric excess was determined by HPLC analysis on a chiral stationary phase. Racemic samples were obtained by carrying out the reactions with *rac*-RhS.

5.6.2 Synthesis of Substrates

Cyclopropyl ketones were prepared via the well-established Weinreb ketone synthesis.⁵ All cyclopropanes are used in racemic. The data of novel substrates are shown below.



(2,2-Dimethylcyclopropyl)(1-phenyl-1H-imidazol-2-yl)methanone (**41a**)

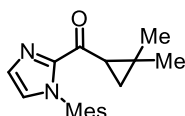
A white solid.

^1H NMR (300 MHz, CDCl_3) δ 7.48-7.40 (m, 3H), 7.30-7.22 (m, 3H), 7.16-7.10 (m, 1H), 3.16 (dd, $J_1 = 7.8$ Hz, $J_2 = 6.0$ Hz, 1H), 1.35-1.29 (m, 4H), 1.12 (s, 3H), 0.98 (dd, $J_1 = 7.8$ Hz, $J_2 = 3.9$ Hz, 1H).

^{13}C NMR (75 MHz, CDCl_3) δ 188.9, 144.6, 138.8, 129.4, 128.9, 128.5, 126.5, 125.9, 32.4, 28.5, 27.3, 24.1, 18.1.

IR (film): ν (cm^{-1}) 3100, 3067, 2996, 2955, 2870, 1663, 1494, 1441, 1410, 1370, 1298, 1093, 1024, 971, 894, 784, 760, 689, 642.

HRMS (ESI, m/z) calcd for $\text{C}_{15}\text{H}_{17}\text{N}_2\text{O}$ $[\text{M}+\text{H}]^+$: 241.1335, found: 241.1330.



(2,2-Dimethylcyclopropyl)(1-mesityl-1H-imidazol-2-yl)methanone (41e)

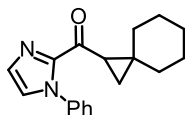
A white solid.

^1H NMR (300 MHz, CDCl_3) δ 7.38-7.35 (m, 1H), 6.97-6.91 (m, 3H), 3.17 (dd, $J_1 = 7.8$ Hz, $J_2 = 5.7$ Hz, 1H), 2.32 (s, 3H), 1.89 (s, 3H), 1.84 (s, 3H), 1.34-1.29 (m, 4H), 1.06 (s, 3H), 0.94 (dd, $J_1 = 7.8$ Hz, $J_2 = 3.6$ Hz, 1H).

^{13}C NMR (75 MHz, CDCl_3) δ 188.6, 144.5, 138.2, 135.3, 134.0, 133.9, 130.1, 128.9, 128.8, 125.1, 32.2, 28.2, 27.2, 23.6, 21.1, 18.0, 17.3, 17.2.

IR (film): ν (cm^{-1}) 3132, 3107, 2978, 2947, 2921, 2869, 1659, 1483, 1412, 1373, 1328, 1280, 1091, 1019, 974, 891, 850, 816, 775, 743, 585.

HRMS (ESI, m/z) calcd for $\text{C}_{18}\text{H}_{23}\text{N}_2\text{O}$ $[\text{M}+\text{H}]^+$: 283.1805, found: 283.1797.



(1-Phenyl-1H-imidazol-2-yl)(spiro[2.5]octan-1-yl)methanone (41f)

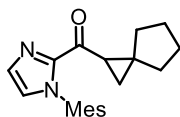
A colorless oil.

^1H NMR (300 MHz, CDCl_3) δ 7.48-7.41 (m, 3H), 7.30-7.28 (m, 1H), 7.28-7.22 (m, 2H), 7.17-7.14 (m, 1H), 3.16 (dd, $J_1 = 7.8$ Hz, $J_2 = 5.7$ Hz, 1H), 1.73-1.38 (m, 9H), 1.33 (dd, $J_1 = 5.7$ Hz, $J_2 = 3.9$ Hz, 1H), 1.28-1.12 (m, 1H), 0.96 (dd, $J_1 = 7.5$ Hz, $J_2 = 3.9$ Hz, 1H).

^{13}C NMR (75 MHz, CDCl_3) δ 188.6, 144.4, 138.9, 129.4, 128.9, 128.6, 126.4, 125.9, 37.8, 36.5, 31.7, 28.0, 26.2, 26.1, 25.9, 22.6.

IR (film): ν (cm⁻¹) 3109, 3063, 2923, 2850, 1666, 1596, 1495, 1442, 1411, 1330, 1305, 1208, 1147, 1107, 1057, 1034, 966, 891, 868, 758, 690, 638, 513.

HRMS (ESI, m/z) calcd for C₁₈H₂₁N₂O [M+H]⁺: 281.1648, found: 281.1641.



(1-Mesityl-1H-imidazol-2-yl)(spiro[2.4]heptan-1-yl)methanone (41g)

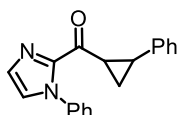
A colorless oil.

¹H NMR (300 MHz, CDCl₃) δ 7.37-7.34 (m, 1H), 6.96-6.91 (m, 3H), 3.33 (dd, $J_1 = 7.8$ Hz, $J_2 = 6.0$ Hz, 1H), 2.32 (s, 3H), 1.89 (s, 3H), 1.85 (s, 3H), 1.88-1.80 (m, 1H), 1.75-1.45 (m, 7H), 1.43 (dd, $J_1 = 5.7$ Hz, $J_2 = 3.9$ Hz, 1H), 1.17 (dd, $J_1 = 8.1$ Hz, $J_2 = 3.6$ Hz, 1H).

¹³C NMR (75 MHz, CDCl₃) δ 189.0, 144.4, 138.2, 135.2, 133.9, 130.1, 128.9, 128.8, 125.1, 39.3, 37.1, 31.9, 29.7, 26.0, 25.9, 23.0, 21.1, 17.3, 17.2. (Missing one ¹³C signal)

IR (film): ν (cm⁻¹) 3109, 2950, 2862, 1665, 1485, 1441, 1410, 1377, 1321, 1281, 1146, 1058, 982, 938, 894, 851, 819, 766, 738, 581.

HRMS (ESI, m/z) calcd for C₂₀H₂₅N₂O [M+H]⁺: 309.1961, found: 309.1956.



(1-Phenyl-1H-imidazol-2-yl)(2-phenylcyclopropyl)methanone (44a)

Trans-44a: A white solid.

¹H NMR (300 MHz, CDCl₃) δ 7.51-7.44 (m, 3H), 7.35-7.24 (m, 5H), 7.23-7.14 (m, 4H), 3.67-3.58 (m, 1H), 2.68-2.58 (m, 1H), 1.78-1.70 (m, 1H), 1.56-1.46 (m, 1H).

¹³C NMR (75 MHz, CDCl₃) δ 188.9, 143.5, 140.4, 138.5, 129.9, 128.9, 128.8, 128.4, 127.1, 126.4, 126.2, 126.0, 29.7, 29.4, 20.2.

IR (film): ν (cm⁻¹) 3108, 3061, 3031, 1667, 1598, 1495, 1437, 1409, 1311, 1149, 1043, 966, 910, 869, 832, 756, 692, 660, 560, 525.

HRMS (ESI, m/z) calcd for C₁₉H₁₇N₂O [M+H]⁺: 289.1335, found: 289.1328.

Cis-44a: A white solid. Cis-44a was synthesized from the corresponding *cis*-cyclopropyl carboxylic acid.^{14a}

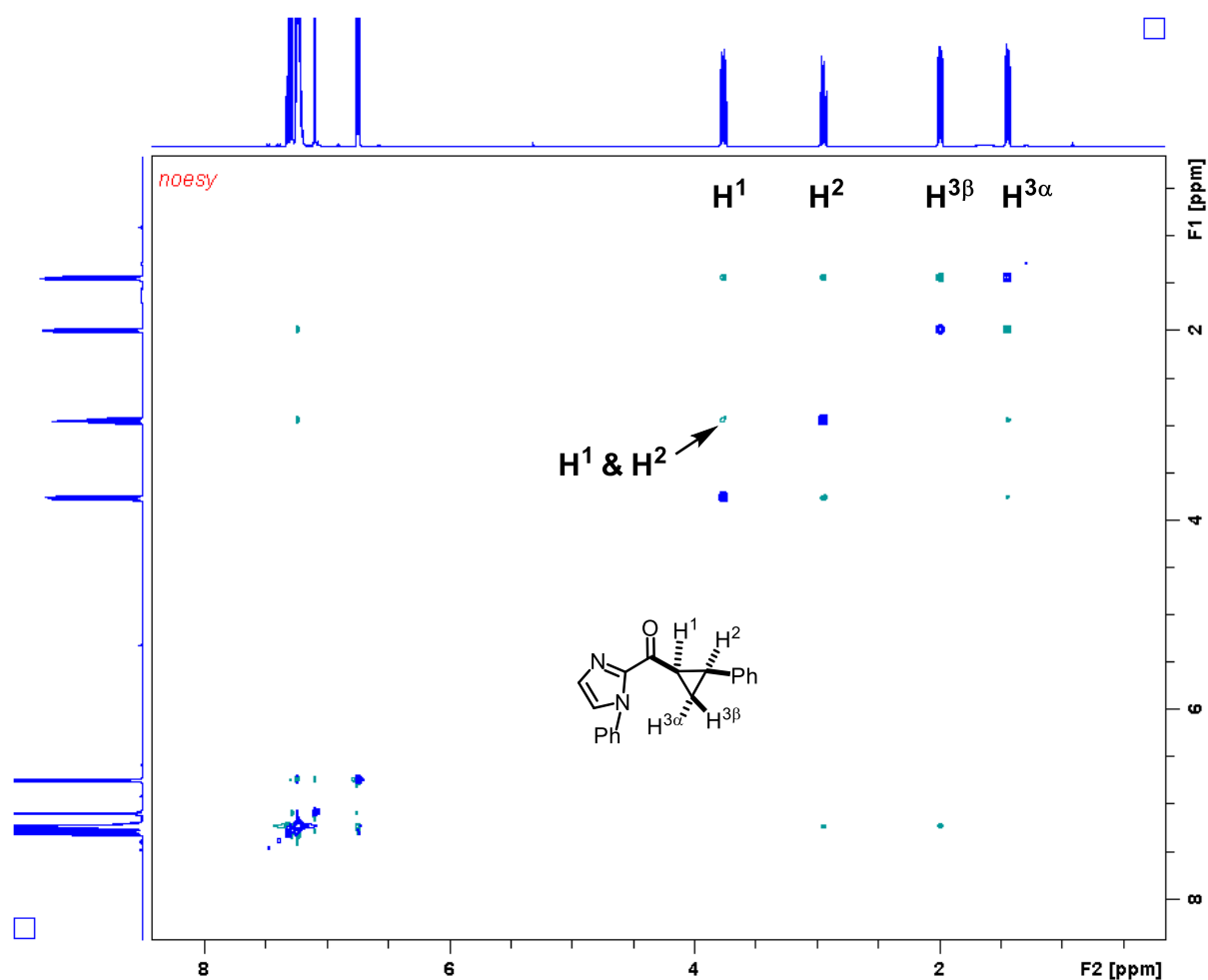
^1H NMR (300 MHz, CDCl_3) δ 7.38-7.20 (m, 9H), 7.14-7.10 (m, 1H), 6.80-6.73 (m, 2H), 3.84-3.74 (m, 1H), 3.03-2.91 (m, 1H), 2.06-1.97 (m, 1H), 1.52-1.42 (m, 1H).

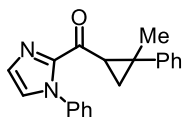
^{13}C NMR (75 MHz, CDCl_3) δ 186.0, 144.2, 138.1, 136.0, 129.6, 129.5, 128.7, 128.2, 127.8, 126.4, 126.3, 125.3, 29.8, 27.4, 11.1.

IR (film): ν (cm^{-1}) 3117, 3052, 3013, 1663, 1596, 1495, 1448, 1413, 1336, 1306, 1206, 1147, 1105, 1080, 1030, 970, 918, 883, 806, 759, 724, 692, 550, 509.

HRMS (ESI, m/z) calcd for $\text{C}_{19}\text{H}_{16}\text{N}_2\text{ONa}$ $[\text{M}+\text{Na}]^+$: 311.1155, found: 311.1163.

NOE spectrum of *cis*-**44a**:



**(2-Methyl-2-phenylcyclopropyl)(1-phenyl-1H-imidazol-2-yl)methanone (44b)**

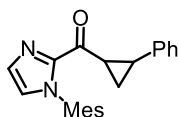
A white solid.

^1H NMR (300 MHz, CDCl_3) δ 7.51-7.43 (m, 5H), 7.38-7.27 (m, 5H), 7.26-7.17 (m, 2H), 3.36 (dd, $J_1 = 7.8$ Hz, $J_2 = 6.0$ Hz, 1H), 1.65 (dd, $J_1 = 6.3$ Hz, $J_2 = 4.2$ Hz, 1H), 1.49 (dd, $J_1 = 8.1$ Hz, $J_2 = 4.2$ Hz, 1H), 1.41 (s, 3H).

^{13}C NMR (75 MHz, CDCl_3) δ 188.3, 146.3, 144.5, 138.7, 129.7, 128.9, 128.6, 128.5, 127.6, 126.7, 126.4, 126.0, 35.3, 32.8, 21.9, 19.4.

IR (film): ν (cm^{-1}) 3058, 2987, 2928, 1666, 1594, 1493, 1410, 1369, 1337, 1300, 1068, 1031, 957, 906, 851, 760, 696, 658, 541.

HRMS (ESI, m/z) calcd for $\text{C}_{20}\text{H}_{19}\text{N}_2\text{O}$ $[\text{M}+\text{H}]^+$: 303.1492, found: 303.1485.

**(1-Mesityl-1H-imidazol-2-yl)(2-phenylcyclopropyl)methanone (44c)**

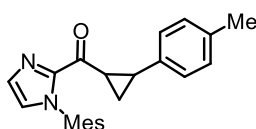
A white solid.

^1H NMR (300 MHz, CDCl_3) δ 7.38-7.36 (m, 1H), 7.32-7.23 (m, 2H), 7.22-7.12 (m, 3H), 7.02-7.00 (m, 1H), 6.96 (br s, 2H), 3.64-3.57 (m, 1H), 2.64-2.56 (m, 1H), 2.34 (s, 3H), 1.90 (s, 3H), 1.88 (s, 3H), 1.74-1.66 (m, 1H), 1.51-1.43 (m, 1H).

^{13}C NMR (75 MHz, CDCl_3) δ 188.8, 143.5, 140.5, 138.5, 134.9, 134.1, 133.9, 130.5, 128.9, 128.4, 126.4, 126.2, 125.7, 29.5, 29.1, 21.1, 20.2, 17.34, 17.32. (Missing one ^{13}C signal)

IR (film): ν (cm^{-1}) 3112, 3027, 2919, 2859, 1664, 1604, 1487, 1411, 1380, 1319, 1282, 1147, 1083, 1038, 969, 936, 910, 855, 767, 737, 698, 669, 533.

HRMS (ESI, m/z) calcd for $\text{C}_{22}\text{H}_{23}\text{N}_2\text{O}$ $[\text{M}+\text{H}]^+$: 331.1805, found: 331.1797.

**(1-Mesityl-1H-imidazol-2-yl)(2-(p-tolyl)cyclopropyl)methanone (44d)**

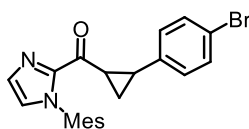
A white solid.

^1H NMR (300 MHz, CDCl_3) δ 7.39-7.36 (m, 1H), 7.12-7.02 (m, 4H), 7.02-7.00 (m, 1H), 6.97 (br s, 2H), 3.63-3.53 (m, 1H), 2.63-2.53 (m, 1H), 2.35 (s, 3H), 2.32 (s, 3H), 1.91 (s, 3H), 1.89 (s, 3H), 1.74-1.65 (m, 1H), 1.50-1.41 (m, 1H).

^{13}C NMR (75 MHz, CDCl_3) δ 188.9, 143.5, 138.4, 137.4, 135.9, 134.9, 134.1, 133.9, 130.5, 129.0, 128.9, 126.1, 125.6, 29.3, 29.0, 21.1, 20.9, 20.1, 17.31, 17.28. (Missing one ^{13}C signal)

IR (film): ν (cm^{-1}) 3144, 3114, 3013, 2948, 2920, 2860, 1664, 1487, 1439, 1410, 1378, 1322, 1047, 970, 943, 918, 872, 804, 771, 741, 532.

HRMS (ESI, m/z) calcd for $\text{C}_{23}\text{H}_{25}\text{N}_2\text{O}$ $[\text{M}+\text{H}]^+$: 345.1961, found: 345.1953.



(2-(4-Bromophenyl)cyclopropyl)(1-mesityl-1H-imidazol-2-yl)methanone (44e)

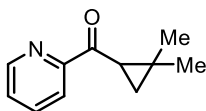
A white solid.

^1H NMR (300 MHz, CDCl_3) δ 7.42-7.34 (m, 3H), 7.05-6.97 (m, 3H), 6.96 (br s, 2H), 3.60-3.52 (m, 1H), 2.59-2.50 (m, 1H), 2.34 (s, 3H), 1.89 (s, 3H), 1.88 (s, 3H), 1.74-1.65 (m, 1H), 1.47-1.38 (m, 1H).

^{13}C NMR (75 MHz, CDCl_3) δ 188.4, 143.4, 139.6, 138.5, 134.8, 134.1, 133.9, 131.4, 130.6, 129.0, 128.0, 125.8, 120.1, 29.0, 28.7, 21.1, 20.0, 17.34, 17.32. (Missing one ^{13}C signal)

IR (film): ν (cm^{-1}) 3063, 2959, 2916, 2855, 1664, 1484, 1412, 1374, 1314, 1037, 1007, 968, 913, 857, 841, 806, 777, 751, 532.

HRMS (ESI, m/z) calcd for $\text{C}_{22}\text{H}_{22}\text{BrN}_2\text{O}$ $[\text{M}+\text{H}]^+$: 409.0910, found: 409.0900.



(2,2-Dimethylcyclopropyl)(pyridin-2-yl)methanone (44f)

A grey solid.

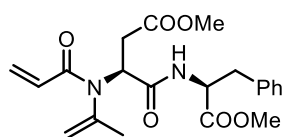
^1H NMR (300 MHz, CDCl_3) δ 8.73-8.68 (m, 1H), 8.02 (d, $J = 8.1$ Hz, 1H), 7.81 (td, $J_1 = 7.8$ Hz, $J_2 = 1.8$ Hz, 1H), 7.44 (ddd, $J_1 = 7.2$ Hz, $J_2 = 4.8$ Hz, $J_3 = 1.2$ Hz, 1H), 3.38 (dd, $J_1 = 7.5$ Hz, $J_2 = 5.7$ Hz,

¹H), 1.49 (dd, $J_1 = 5.7$ Hz, $J_2 = 3.9$ Hz, 1H), 1.33 (s, 3H), 1.18 (s, 3H), 1.08 (dd, $J_1 = 7.5$ Hz, $J_2 = 3.6$ Hz, 1H).

¹³C NMR (75 MHz, CDCl₃) δ 199.3, 154.8, 148.9, 136.7, 126.5, 121.5, 30.5, 28.9, 27.3, 25.0, 18.2.

IR (film): ν (cm⁻¹) 3058, 2994, 2943, 2870, 1667, 1575, 1443, 1384, 1312, 1273, 1211, 1116, 1089, 1038, 996, 910, 834, 797, 758, 711, 678, 646, 616.

HRMS (ESI, m/z) calcd for C₁₁H₁₄NO [M+H]⁺: 176.1070, found: 176.1070.



Methyl (S)-4-(((S)-1-methoxy-1-oxo-3-phenylpropan-2-yl)amino)-4-oxo-3-(N-(prop-1-en-2-yl)acrylamido)butanoate (42t)

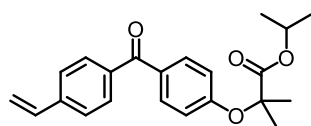
A white solid. **42t** was isolated as a minor product in the tandem esterification/acylation reaction of **aspartame** following a published procedure.^{14b}

¹H NMR (500 MHz, (CD₃)₂SO) δ 8.04 (d, $J = 7.8$ Hz, 1H), 7.27-7.21 (m, 2H), 7.21-7.18 (m, 1H), 7.18-7.14 (m, 2H), 6.43 (dd, $J_1 = 16.8$ Hz, $J_2 = 10.3$ Hz, 1H), 6.22 (dd, $J_1 = 16.8$ Hz, $J_2 = 2.0$ Hz, 1H), 5.73 (dd, $J_1 = 10.3$ Hz, $J_2 = 2.3$ Hz, 1H), 5.25 (t, $J = 7.4$ Hz, 1H), 5.12-5.10 (m, 1H), 4.63 (s, 1H), 4.49-4.42 (m, 1H), 3.61 (s, 3H), 3.57 (s, 3H), 3.03 (dd, $J_1 = 13.9$ Hz, $J_2 = 5.1$ Hz, 1H), 2.92 (dd, $J_1 = 13.8$ Hz, $J_2 = 9.4$ Hz, 1H), 2.87 (dd, $J_1 = 16.6$ Hz, $J_2 = 8.0$ Hz, 1H), 2.56 (dd, $J_1 = 16.6$ Hz, $J_2 = 6.8$ Hz, 1H), 1.58 (s, 3H).

¹³C NMR (125 MHz, (CD₃)₂SO) δ 171.5, 170.6, 169.3, 164.4, 141.6, 137.1, 129.1, 128.9, 128.3, 127.9, 126.6, 118.1, 53.8, 53.3, 52.0, 51.6, 36.3, 33.5, 22.1.

IR (film): ν (cm⁻¹) 3380, 2956, 1738, 1678, 1644, 1610, 1516, 1448, 1413, 1369, 1314, 1237, 1167, 1128, 1024, 986, 929, 897, 824, 750, 703, 548, 497, 392.

HRMS (ESI, m/z) calcd for C₂₁H₂₆N₂O₆Na [M+Na]⁺: 425.1683, found: 425.1678.



Isopropyl 2-methyl-2-(4-(4-vinylbenzoyl)phenoxy)propanoate (42u)

A white solid. **42u** was synthesized through a Suzuki cross coupling of **fenofibrate** with potassium vinyltrifluoroborate according to a published procedure.^{14c}

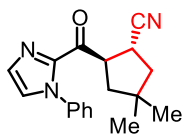
¹H NMR (300 MHz, CDCl₃) δ 7.79-7.70 (m, 4H), 7.52-7.46 (m, 2H), 6.90-6.83 (m, 2H), 6.78 (dd, $J_1 = 17.4$ Hz, $J_2 = 10.8$ Hz, 1H), 5.88 (d, $J = 17.7$ Hz, 1H), 5.39 (d, $J = 10.8$ Hz, 1H), 5.09 (sept, $J = 6.0$ Hz, 1H), 1.66 (s, 6H), 1.22 (s, 3H), 1.19 (s, 3H).

¹³C NMR (75 MHz, CDCl₃) δ 195.0, 173.2, 159.5, 141.1, 137.3, 136.1, 131.9, 130.8, 130.2, 126.0, 117.2, 116.3, 79.4, 69.3, 25.4, 21.5.

IR (film): ν (cm⁻¹) 3082, 2983, 2938, 2877, 1718, 1641, 1599, 1570, 1281, 1247, 1174, 1148, 1103, 971, 923, 854, 775, 669, 594.

HRMS (ESI, m/z) calcd for C₂₂H₂₄O₄Na [M+Na]⁺: 375.1567, found: 375.1556.

5.6.3 Experimental and Characterization Data of Novel Products



((1R,2R)-4,4-Dimethyl-2-(1-phenyl-1H-imidazole-2-carbonyl)cyclopentane-1-carbonitrile (**43a**))

According to the general procedure, the reaction of (2,2-dimethylcyclopropyl)(1-phenyl-1H-imidazol-2-yl)methanone **41a** (24.0 mg, 0.10 mmol), acrylonitrile **42a** (13.3 mg, 2.5 equiv), Δ -RhS (1.7 mg, 2 mol%) and DIPEA (6.5 mg, 0.5 equiv) in acetone (1.0 mL, 0.1 M) under nitrogen atmosphere with blue LEDs for 24 hours, afforded 28.8 mg (98% yield) of **43a** as a colorless oil.

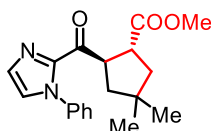
The d.r. value was determined through ¹H NMR of crude materials as >20:1; enantiomeric excess was established by HPLC analysis using a Chiralpak AD-H column, ee = 99% (HPLC: AD-H, 254 nm, *n*-hexane/isopropanol = 85:15, flow rate 1 mL/min, 40 °C, t_r (major) = 8.0 min, t_r (minor) = 10.7 min). $[\alpha]_D^{22} = -86.0^\circ$ (c 1.0, CH₂Cl₂).

¹H NMR (300 MHz, CDCl₃) δ 7.44-7.37 (m, 3H), 7.26-7.23 (m, 1H), 7.22-7.18 (m, 2H), 7.16-7.13 (m, 1H), 4.51 (q, $J = 9.2$ Hz, 1H), 3.39 (q, $J = 8.5$ Hz, 1H), 2.21 (dd, $J_1 = 12.9$ Hz, $J_2 = 9.3$ Hz, 1H), 1.89 (dd, $J_1 = 12.9$ Hz, $J_2 = 9.0$ Hz, 1H), 1.80 (dd, $J_1 = 12.9$ Hz, $J_2 = 8.1$ Hz, 1H), 1.48 (dd, $J_1 = 12.9$ Hz, $J_2 = 9.6$ Hz, 1H), 1.14 (s, 3H), 0.93 (s, 3H).

^{13}C NMR (75 MHz, CDCl_3) δ 189.3, 142.0, 138.1, 130.3, 129.03, 128.97, 127.7, 125.9, 122.4, 52.1, 46.2, 45.2, 40.3, 28.64, 28.55, 27.9.

IR (film): ν (cm^{-1}) 3112, 2957, 2868, 2239, 1681, 1596, 1496, 1448, 1402, 1337, 1305, 1150, 1069, 1033, 978, 910, 836, 797, 763, 731, 692, 659, 535.

HRMS (ESI, m/z) calcd for $\text{C}_{18}\text{H}_{20}\text{N}_3\text{O}$ $[\text{M}+\text{H}]^+$: 294.1601, found: 294.1593.



Methyl (1R,2R)-4,4-dimethyl-2-(1-phenyl-1H-imidazole-2-carbonyl)cyclopentane-1-carboxylate (43b)

According to the general procedure, the reaction of (2,2-dimethylcyclopropyl)(1-phenyl-1H-imidazol-2-yl)methanone **41a** (24.0 mg, 0.10 mmol), methyl acrylate **42b** (21.5 mg, 2.5 equiv), Δ -**RhS** (1.7 mg, 2 mol%) and DIPEA (6.5 mg, 0.5 equiv) in acetone (1.0 mL, 0.1 M) under nitrogen atmosphere with blue LEDs for 22 hours, afforded 32.5 mg (99% yield) of **43b** as a colorless oil.

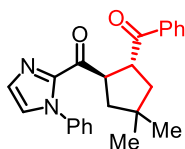
The d.r. value was determined through ^1H NMR of crude materials as 15:1; enantiomeric excess of the major diastereoisomer was established by HPLC analysis using a Chiralpak IG column, ee = 97% (HPLC: IG, 254 nm, *n*-hexane/isopropanol = 80:20, flow rate 1 mL/min, 25 °C, t_r (major) = 12.4 min, t_r (minor) = 15.4 min). $[\alpha]_D^{22} = -63.0^\circ$ (*c* 1.0, CH_2Cl_2).

^1H NMR (300 MHz, CDCl_3) δ 7.50-7.42 (m, 3H), 7.31-7.25 (m, 3H), 7.20-7.17 (m, 1H), 4.56 (q, J = 9.0 Hz, 1H), 3.62 (s, 3H, the corresponding peak of the minor diastereoisomer at 3.27), 4.48 (q, J = 9.0 Hz, 1H), 2.18 (dd, J_1 = 12.9 Hz, J_2 = 9.6 Hz, 1H), 1.89-1.82 (m, 2H), 1.61 (dd, J_1 = 12.6 Hz, J_2 = 9.3 Hz, 1H), 1.13 (s, 3H), 1.02 (s, 3H, the corresponding peak of minor diastereoisomer at 1.05).

^{13}C NMR (75 MHz, CDCl_3) δ 191.7, 175.3, 142.9, 138.5, 129.8, 128.9, 128.7, 127.0, 125.8, 51.7, 50.4, 45.9, 44.9, 44.0, 39.5, 29.11, 29.09.

IR (film): ν (cm^{-1}) 3134, 3110, 2952, 2867, 1730, 1681, 1597, 1504, 1493, 1445, 1404, 1369, 1306, 1247, 1196, 1172, 1150, 1041, 1003, 982, 905, 849, 806, 760, 693, 660, 535.

HRMS (ESI, m/z) calcd for $\text{C}_{19}\text{H}_{22}\text{N}_2\text{O}_3\text{Na}$ $[\text{M}+\text{Na}]^+$: 349.1523, found: 349.1520.



(1*R*,2*R*)-2-Benzoyl-4,4-dimethylcyclopentyl(1-phenyl-1*H*-imidazol-2-yl)methanone (43c)

According to the general procedure, the reaction of (2,2-dimethylcyclopropyl)(1-phenyl-1*H*-imidazol-2-yl)methanone **41a** (24.0 mg, 0.10 mmol), 1-phenylprop-2-en-1-one **42c** (33.1 mg, 2.5 equiv), Δ -**RhS** (1.7 mg, 2 mol%) and DIPEA (6.5 mg, 0.5 equiv) in acetone (1.0 mL, 0.1 M) under nitrogen atmosphere with blue LEDs for 24 hours, afforded 28.5 mg (77% yield) of the major diastereoisomer of **43c** as a yellow solid.

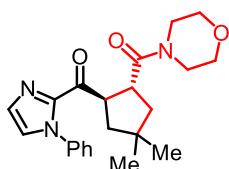
The d.r. value was determined through ^1H NMR of crude materials as 12:1, therefore the total yield is estimated as 83%. Enantiomeric excess of the major diastereoisomer was established by HPLC analysis using a Chiralpak AD-H column, ee = 91% (HPLC: AD-H, 254 nm, *n*-hexane/isopropanol = 85:15, flow rate 1 mL/min, 40 °C, t_r (major) = 9.1 min, t_r (minor) = 15.0 min). $[\alpha]_{\text{D}}^{22} = -65.2^\circ$ (*c* 1.0, CH_2Cl_2).

^1H NMR (300 MHz, CDCl_3) δ 7.94-7.88 (m, 2H), 7.54-7.46 (m, 1H), 7.45-7.36 (m, 5H), 7.29-7.27 (m, 1H), 7.24-7.18 (m, 2H), 7.14-7.12 (m, 1H), 4.86 (q, $J = 9.3$ Hz, 1H), 4.41 (q, $J = 9.0$ Hz, 1H), 2.31 (dd, $J_1 = 12.3$ Hz, $J_2 = 9.3$ Hz, 1H), 2.02 (dd, $J_1 = 12.6$ Hz, $J_2 = 9.9$ Hz, 1H), 1.77-1.66 (m, 2H), 1.12 (s, 3H), 1.09 (s, 3H).

^{13}C NMR (75 MHz, CDCl_3) δ 201.2, 192.3, 142.8, 138.5, 136.8, 132.7, 129.9, 128.9, 128.6, 128.4, 126.9, 125.9, 125.8, 49.5, 48.0, 46.2, 45.8, 40.2, 29.4, 29.0.

IR (film): ν (cm^{-1}) 3055, 2951, 2930, 2864, 1672, 1504, 1491, 1446, 1411, 1375, 1307, 1228, 1207, 1049, 873, 812, 786, 770, 705, 694, 661, 536.

HRMS (ESI, m/z) calcd for $\text{C}_{24}\text{H}_{24}\text{N}_2\text{O}_2\text{Na}$ $[\text{M}+\text{Na}]^+$: 395.1730, found: 395.1728.



(1*R*,2*R*)-4,4-Dimethyl-2-(1-phenyl-1*H*-imidazole-2-carbonyl)cyclopentyl(morpholino)methanone (43d)

According to the general procedure, the reaction of (2,2-dimethylcyclopropyl)(1-phenyl-1*H*-imidazol-2-yl)methanone **41a** (24.0 mg, 0.10 mmol), 1-morpholinoprop-2-en-1-one **42d** (35.3 mg, 2.5 equiv), Δ -**RhS** (1.7 mg, 2 mol%) and DIPEA (6.5 mg, 0.5 equiv) in acetone (1.0 mL, 0.1 M) under nitrogen atmosphere with blue LEDs for 24 hours, afforded 33.1 mg (87% yield) of **43d** as a colorless oil.

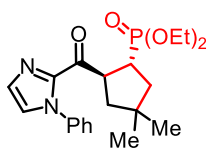
The d.r. value was determined through ^1H NMR of crude materials as >20:1; enantiomeric excess was established by HPLC analysis using a Chiralpak IG column, ee = 91% (HPLC: IG, 254 nm, *n*-hexane/isopropanol = 40:60, flow rate 1 mL/min, 40 °C, t_r (major) = 9.5 min, t_r (minor) = 20.7 min). $[\alpha]_D^{22} = -38.4^\circ$ (c 1.0, CH_2Cl_2).

^1H NMR (300 MHz, CDCl_3) δ 7.48-7.41 (m, 3H), 7.32-7.29 (m, 1H), 7.28-7.22 (m, 2H), 7.16-7.13 (m, 1H), 4.81 (q, $J = 9.0$ Hz, 1H), 3.68-3.45 (m, 9H), 2.32 (dd, $J_1 = 12.9$ Hz, $J_2 = 9.6$ Hz, 1H), 1.79 (dd, $J_1 = 12.3$ Hz, $J_2 = 9.0$ Hz, 1H), 1.68 (dd, $J_1 = 12.3$ Hz, $J_2 = 9.6$ Hz, 1H), 1.60 (dd, $J_1 = 12.6$ Hz, $J_2 = 9.6$ Hz, 1H), 1.17 (s, 3H), 1.02 (s, 3H).

^{13}C NMR (75 MHz, CDCl_3) δ 192.5, 173.0, 142.8, 138.6, 130.0, 128.9, 128.6, 126.9, 125.8, 66.9, 66.8, 51.0, 46.1, 46.0, 45.1, 42.3, 41.6, 39.8, 29.5, 29.4.

IR (film): ν (cm^{-1}) 2954, 2928, 2861, 1677, 1635, 1597, 1503, 1493, 1443, 1402, 1304, 1269, 1231, 1211, 1113, 1069, 1046, 911, 870, 806, 762, 728, 693, 536.

HRMS (ESI, m/z) calcd for $\text{C}_{22}\text{H}_{27}\text{N}_3\text{O}_3\text{Na}$ $[\text{M}+\text{Na}]^+$: 404.1945, found: 404.1942.



Diethyl ((1*R*,2*S*)-4,4-dimethyl-2-(1-phenyl-1*H*-imidazole-2-carbonyl)cyclopentyl)phosphonate (43e**)**

According to the general procedure, the reaction of (2,2-dimethylcyclopropyl)(1-phenyl-1*H*-imidazol-2-yl)methanone **41a** (24.0 mg, 0.10 mmol), diethyl vinylphosphonate **42e** (41.0 mg, 2.5 equiv), Δ -**RhS** (1.7 mg, 2 mol%) and DIPEA (6.5 mg, 0.5 equiv) in acetone (1.0 mL, 0.1 M) under nitrogen atmosphere with blue LEDs for 24 hours, afforded 37.5 mg (93% yield, total yield) of **43e** as a colorless oil as a mixture of two diastereoisomers.

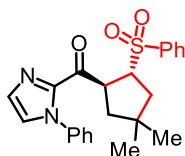
The d.r. value was determined through ^1H NMR of crude materials as 8:1; enantiomeric excess of the major diastereoisomer was established by HPLC analysis using a Chiralpak IG column, ee = 98% (HPLC: IG, 254 nm, *n*-hexane/isopropanol = 50:50, flow rate 1 mL/min, 40 °C, t_r (major) = 7.4 min, t_r (minor) = 24.1 min). $[\alpha]_D^{22} = -33.4^\circ$ (*c* 1.0, CH_2Cl_2).

^1H NMR (300 MHz, CDCl_3) δ 7.50-7.41 (m, 3H), 7.31-7.25 (m, 3H), 7.20-7.15 (m, 1H), 4.64-4.46 (m, 1H), 4.11-3.90 (m, 4H), 3.16-2.97 (m, 1H), 2.23-2.11 (m, 1H), 1.89-1.78 (m, 2H), 1.61 (dd, $J_1 = 12.9$ Hz, $J_2 = 8.1$ Hz, 1H), 1.26-1.16 (m, 6H), 1.15 (s, 3H), 0.99 (s, 3H, the corresponding peak of the minor diastereoisomer at 1.05).

^{13}C NMR (75 MHz, CDCl_3) δ 191.4 (d, $J = 2.3$ Hz), 142.8, 138.5, 129.8, 128.9, 128.6, 127.0, 125.7, 61.6 (d, $J = 5.4$ Hz), 61.5, (d, $J = 6.5$ Hz), 48.1, 47.1 (d, $J = 11.9$ Hz), 41.6 (d, $J = 2.3$ Hz), 40.2 (d, $J = 12.7$ Hz), 36.2 (d, $J = 146.4$ Hz), 29.0, 28.6, 16.4 (d, $J = 1.5$ Hz), 16.3 (d, $J = 1.9$ Hz).

IR (film): ν (cm^{-1}) 2954, 2868, 1683, 1504, 1493, 1445, 1404, 1237, 1053, 1020, 955, 900, 810, 761, 730, 693, 663, 564, 549, 532.

HRMS (ESI, m/z) calcd for $\text{C}_{21}\text{H}_{29}\text{N}_2\text{O}_4\text{PNa}$ $[\text{M}+\text{Na}]^+$: 427.1757, found: 427.1755.



((1S,2R)-4,4-Dimethyl-2-(phenylsulfonyl)cyclopentyl)(1-phenyl-1H-imidazol-2-yl)methanone (43f)

According to the general procedure, the reaction of (2,2-dimethylcyclopropyl)(1-phenyl-1H-imidazol-2-yl)methanone **41a** (24.0 mg, 0.10 mmol), (vinylsulfonyl)benzene **42f** (42.1 mg, 2.5 equiv), Δ -**RhS** (3.5 mg, 4 mol%) and DIPEA (25.8 mg, 2.0 equiv) in acetone (1.0 mL, 0.1 M) under nitrogen atmosphere with blue LEDs for 20 hours, afforded 40.1 mg (98% yield) of **43f** as a yellow solid.

The d.r. value was determined through ^1H NMR of crude materials as >20:1; enantiomeric excess was established by HPLC analysis using a Chiralpak IG column, ee = 99% (HPLC: IG, 254 nm, *n*-hexane/isopropanol = 50:50, flow rate 1 mL/min, 40 °C, t_r (major) = 10.4 min, t_r (minor) = 20.7 min). $[\alpha]_D^{22} = -13.4^\circ$ (*c* 1.0, CH_2Cl_2).

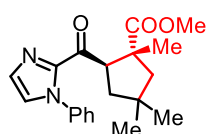
^1H NMR (300 MHz, CDCl_3) δ 7.90-7.83 (m, 2H), 7.60-7.52 (m, 1H), 7.48-7.38 (m, 5H), 7.31-7.28 (m, 1H), 7.16-7.13 (m, 1H), 7.23-7.06 (m, 2H), 4.80 (q, $J = 8.7$ Hz, 1H), 4.35 (q, $J = 9.0$ Hz, 1H), 2.24 (dd,

$J_1 = 12.9$ Hz, $J_2 = 9.9$ Hz, 1H), 2.10 (dd, $J_1 = 13.2$ Hz, $J_2 = 9.0$ Hz, 1H), 1.85 (dd, $J_1 = 13.2$ Hz, $J_2 = 9.3$ Hz, 1H), 1.61 (dd, $J_1 = 12.6$ Hz, $J_2 = 8.1$ Hz, 1H), 1.13 (s, 3H), 0.96 (s, 3H).

^{13}C NMR (75 MHz, CDCl_3) δ 189.5, 142.0, 138.5, 138.1, 133.3, 130.0, 128.9, 128.8, 128.7, 127.3, 125.7, 64.8, 47.8, 46.7, 40.9, 40.0, 28.7, 28.5. (Missing one ^{13}C signal)

IR (film): ν (cm^{-1}) 3124, 3062, 2952, 2868, 1685, 1496, 1450, 1407, 1340, 1294, 1144, 1080, 1033, 987, 916, 885, 808, 755, 716, 690, 601, 561, 496, 417.

HRMS (ESI, m/z) calcd for $\text{C}_{23}\text{H}_{24}\text{N}_2\text{O}_3\text{SNa}$ $[\text{M}+\text{Na}]^+$: 431.1400, found: 431.1397.



Methyl (1R,2R)-1,4,4-trimethyl-2-(1-phenyl-1H-imidazole-2-carbonyl)cyclopentane-1-carboxylate (43g)

According to the general procedure, the reaction of (2,2-dimethylcyclopropyl)(1-phenyl-1H-imidazol-2-yl)methanone **41a** (24.0 mg, 0.10 mmol), methyl methacrylate **42g** (25.0 mg, 2.5 equiv), Δ -RhS (3.5 mg, 4 mol%) and DIPEA (25.8 mg, 2.0 equiv) in acetone (1.0 mL, 0.1 M) under nitrogen atmosphere with blue LEDs for 24 hours, afforded 32.9 mg (97% yield) of **43g** as a yellow solid.

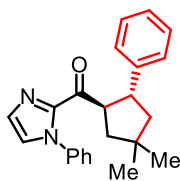
The d.r. value was determined through ^1H NMR of crude materials as >20:1; enantiomeric excess was established by HPLC analysis using a Chiralpak IG column, ee = 99% (HPLC: IG, 254 nm, *n*-hexane/isopropanol = 80:20, flow rate 1 mL/min, 25 °C, t_r (major) = 6.4 min, t_r (minor) = 8.3 min). $[\alpha]_D^{22} = -60.2^\circ$ (c 1.0, CH_2Cl_2).

^1H NMR (300 MHz, CDCl_3) δ 7.40-7.33 (m, 3H), 7.22-7.16 (m, 2H), 7.15-7.12 (m, 1H), 7.08-7.05 (m, 1H), 4.70 (dd, $J_1 = 12.6$ Hz, $J_2 = 6.6$ Hz, 1H), 3.62 (s, 3H, the corresponding peak of the minor diastereoisomer at 3.41), 2.20 (d, $J = 13.5$ Hz, 1H), 1.99 (t, $J = 12.6$ Hz, 1H), 1.56 (dd, $J_1 = 12.9$ Hz, $J_2 = 6.3$ Hz, 1H), 1.42 (d, $J = 13.5$ Hz, 1H), 1.09 (s, 3H), 1.03 (s, 3H), 1.01 (s, 3H).

^{13}C NMR (75 MHz, CDCl_3) δ 191.0, 177.7, 143.7, 138.5, 129.5, 128.9, 128.6, 127.0, 125.9, 53.9, 53.5, 53.1, 52.1, 42.2, 37.1, 31.1, 30.2, 21.5.

IR (film): ν (cm^{-1}) 2938, 2868, 1728, 1679, 1495, 1444, 1404, 1333, 1302, 1253, 1175, 1144, 1113, 1067, 1018, 994, 968, 899, 860, 823, 765, 688, 536.

HRMS (ESI, m/z) calcd for $\text{C}_{20}\text{H}_{24}\text{N}_2\text{O}_3\text{Na}$ $[\text{M}+\text{Na}]^+$: 363.1679, found: 363.1677.



((1*R*,2*R*)-4,4-Dimethyl-2-phenylcyclopentyl)(1-phenyl-1*H*-imidazol-2-yl)methanone (43h)

According to the general procedure, the reaction of (2,2-dimethylcyclopropyl)(1-phenyl-1*H*-imidazol-2-yl)methanone **41a** (24.0 mg, 0.10 mmol), styrene **42h** (26.1 mg, 2.5 equiv), Δ -**RhS** (3.5 mg, 4 mol%) and DIPEA (25.8 mg, 2.0 equiv) in acetone (1.0 mL, 0.1 M) under nitrogen atmosphere with blue LEDs for 24 hours, afforded 28.0 mg (81% yield) of **43h** as a colorless oil.

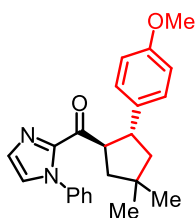
The d.r. value was determined through ^1H NMR of crude materials as >20:1; enantiomeric excess was established by HPLC analysis using a Chiralpak IG column, ee = 97% (HPLC: IG, 254 nm, *n*-hexane/isopropanol = 80:20, flow rate 1 mL/min, 25 °C, t_r (major) = 5.4 min, t_r (minor) = 6.2 min). $[\alpha]_D^{22} = -171.4^\circ$ (c 1.0, CH_2Cl_2).

^1H NMR (300 MHz, CDCl_3) δ 7.38-7.31 (m, 3H), 7.23-7.11 (m, 5H), 7.10-7.02 (m, 3H), 7.02-6.99 (m, 1H), 4.47-4.34 (q, $J = 9.8$ Hz, 1H), 3.64 (td, $J_1 = 11.4$ Hz, $J_2 = 7.6$ Hz, 1H), 2.16 (dd, $J_1 = 12.8$ Hz, $J_2 = 9.6$ Hz, 1H), 1.89 (dd, $J_1 = 12.6$ Hz, $J_2 = 7.6$ Hz, 1H), 1.71 (t, $J = 12.1$ Hz, 1H), 1.62 (dd, $J_1 = 12.8$ Hz, $J_2 = 9.3$ Hz, 1H), 1.13 (s, 3H), 1.03 (s, 3H).

^{13}C NMR (75 MHz, CDCl_3) δ 192.9, 143.6, 143.4, 138.4, 129.5, 128.9, 128.6, 128.2, 127.5, 126.8, 126.0, 125.7, 54.6, 50.2, 47.1, 46.8, 38.5, 30.7, 30.2.

IR (film): ν (cm^{-1}) 3060, 3029, 2949, 2863, 1679, 1596, 1495, 1447, 1403, 1304, 1149, 1069, 1032, 979, 894, 816, 756, 693, 663, 528.

HRMS (ESI, m/z) calcd for $\text{C}_{23}\text{H}_{25}\text{N}_2\text{O}$ $[\text{M}+\text{H}]^+$: 345.1961, found: 345.1953.



((1*R*,2*R*)-2-(4-Methoxyphenyl)-4,4-dimethylcyclopentyl)(1-phenyl-1*H*-imidazol-2-yl)methanone (43i)

According to the general procedure, the reaction of (2,2-dimethylcyclopropyl)(1-phenyl-1*H*-imidazol-2-yl)methanone **41a** (24.0 mg, 0.10 mmol), 1-methoxy-4-vinylbenzene **42i** (33.6 mg, 2.5 equiv), Δ -**RhS** (3.5 mg, 4 mol%) and DIPEA (25.8 mg, 2.0 equiv) in acetone (1.0 mL, 0.1 M) under nitrogen atmosphere at 50 °C with blue LEDs for 36 hours, afforded 26.3 mg (70% yield) of **43i** as a colorless oil.

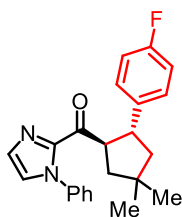
The d.r. value was determined through ^1H NMR of crude materials as >20:1; enantiomeric excess was established by HPLC analysis using a Chiralpak IG column, ee = 90% (HPLC: IG, 254 nm, *n*-hexane/isopropanol = 90:10, flow rate 1 mL/min, 25 °C, t_r (major) = 10.1 min, t_r (minor) = 12.0 min). $[\alpha]_D^{22} = -92.4^\circ$ (*c* 0.5, CH_2Cl_2).

^1H NMR (500 MHz, CDCl_3) δ 7.40-7.46 (m, 3H), 7.21 (d, $J = 1.0$ Hz, 1H), 7.20-7.17 (m, 2H), 7.16-7.12 (m, 2H), 7.10 (d, $J = 1.1$ Hz, 1H), 6.75-6.75 (m, 2H), 4.47-4.39 (m, 1H), 3.74 (s, 3H), 3.66 (td, $J_1 = 12.7$ Hz, $J_2 = 7.5$ Hz, 1H), 2.21 (dd, $J_1 = 12.9$ Hz, $J_2 = 9.6$ Hz, 1H), 1.93 (dd, $J_1 = 12.6$ Hz, $J_2 = 9.6$ Hz, 1H), 1.74 (t, $J = 12.3$ Hz, 1H), 1.67 (dd, $J_1 = 12.9$ Hz, $J_2 = 9.4$ Hz, 1H), 1.19 (s, 3H), 1.09 (s, 3H).

^{13}C NMR (125 MHz, CDCl_3) δ 193.0, 157.8, 143.3, 138.4, 135.6, 129.5, 128.9, 128.6, 128.4, 126.9, 125.7, 113.6, 55.2, 54.8, 50.3, 46.7, 46.4, 38.3, 30.8, 30.3.

IR (film): ν (cm^{-1}) 3062, 2948, 2863, 1678, 1605, 1506, 1447, 1403, 1304, 1244, 1177, 1149, 1032, 978, 891, 827, 761, 692, 662, 536.

HRMS (ESI, m/z) calcd for $\text{C}_{24}\text{H}_{27}\text{N}_2\text{O}_2$ $[\text{M}+\text{H}]^+$: 375.2067, found: 375.2063.



((1*R*,2*R*)-2-(4-Fluorophenyl)-4,4-dimethylcyclopentyl)(1-phenyl-1*H*-imidazol-2-yl)methanone (43j)

According to the general procedure, the reaction of (2,2-dimethylcyclopropyl)(1-phenyl-1*H*-imidazol-2-yl)methanone **41a** (24.0 mg, 0.10 mmol), 1-fluoro-4-vinylbenzene **42j** (30.5 mg, 2.5 equiv), Δ -**RhS** (3.5 mg, 4 mol%) and DIPEA (25.8 mg, 2.0 equiv) in acetone (1.0 mL, 0.1 M) under nitrogen atmosphere with blue LEDs for 26 hours, afforded 23.8 mg (66% yield) of **43j** as a colorless oil.

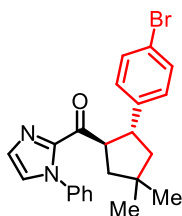
The d.r. value was determined through ^1H NMR of crude materials as >20:1; enantiomeric excess was established by HPLC analysis using a Chiralpak AD-H column, ee = 96% (HPLC: IG, 254 nm, *n*-hexane/isopropanol = 95:5, flow rate 1 mL/min, 25 °C, t_r (major) = 7.7 min, t_r (minor) = 9.2 min). $[\alpha]_D^{22} = -97.8^\circ$ (*c* 1.0, CH_2Cl_2).

^1H NMR (300 MHz, CDCl_3) δ 7.48-7.40 (m, 3H), 7.25-7.18 (m, 3H), 7.18-7.13 (m, 2H), 7.12-6.99 (m, 1H), 6.96-6.85 (m, 2H), 4.43 (q, $J = 10.5$ Hz, 1H), 3.68 (td, $J_1 = 11.7$ Hz, $J_2 = 7.5$ Hz, 1H), 2.23 (dd, $J_1 = 12.9$ Hz, $J_2 = 9.6$ Hz, 1H), 1.95 (dd, $J_1 = 12.6$ Hz, $J_2 = 7.5$ Hz, 1H), 1.74 (t, $J = 12.0$ Hz, 1H), 1.69 (dd, $J_1 = 12.9$ Hz, $J_2 = 9.6$ Hz, 1H), 1.20 (s, 3H), 1.10 (s, 3H).

^{13}C NMR (75 MHz, CDCl_3) δ 192.7, 161.3 (d, $J = 242.0$), 143.3, 139.2 (d, $J = 2.9$ Hz), 138.4, 129.6, 128.9, 128.8 (d, $J = 7.5$ Hz), 128.7, 127.0, 125.7, 114.9 (d, $J = 20.6$ Hz), 54.8, 50.3, 46.6, 46.4, 38.4, 30.7, 30.2.

IR (film): ν (cm^{-1}) 3112, 3047, 2950, 2864, 1679, 1599, 1503, 1447, 1403, 1304, 1222, 1154, 1070, 1033, 979, 893, 833, 760, 732, 692, 661, 531.

HRMS (ESI, m/z) calcd for $\text{C}_{23}\text{H}_{24}\text{FN}_2\text{O}$ $[\text{M}+\text{H}]^+$: 363.1867, found: 363.1865.



((1R,2R)-2-(4-Bromophenyl)-4,4-dimethylcyclopentyl)(1-phenyl-1H-imidazol-2-yl)methanone (43k)

According to the general procedure, the reaction of (2,2-dimethylcyclopropyl)(1-phenyl-1H-imidazol-2-yl)methanone **41a** (24.0 mg, 0.10 mmol), 1-bromo-4-vinylbenzene **42k** (45.8 mg, 2.5 equiv), Δ -RhS (3.5 mg, 4 mol%) and DIPEA (25.8 mg, 2.0 equiv) in acetone (1.0 mL, 0.1 M) under nitrogen atmosphere with blue LEDs for 26 hours, afforded 31.2 mg (74% yield) of **43k** as a white solid.

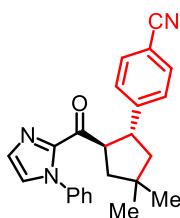
The d.r. value was determined through ^1H NMR of crude materials as >20:1; enantiomeric excess was established by HPLC analysis using a Chiralpak IG column, ee = 97% (HPLC: IG, 254 nm, *n*-hexane/isopropanol = 90:10, flow rate 1 mL/min, 25 °C, t_r (major) = 5.9 min, t_r (minor) = 6.5 min). $[\alpha]_D^{22} = -123.4^\circ$ (*c* 1.0, CH_2Cl_2).

^1H NMR (300 MHz, CDCl_3) δ 7.48-7.40 (m, 3H), 7.36-7.30 (m, 2H), 7.23-7.20 (m, 1H), 7.19-7.10 (m, 5H), 4.44 (q, $J = 9.8$ Hz, 1H), 3.67 (td, $J_1 = 11.4$ Hz, $J_2 = 7.8$ Hz, 1H), 2.24 (dd, $J_1 = 12.9$ Hz, $J_2 = 9.9$ Hz, 1H), 1.95 (dd, $J_1 = 12.3$ Hz, $J_2 = 7.5$ Hz, 1H), 1.73 (t, $J = 12.0$ Hz, 1H), 1.68 (dd, $J_1 = 13.5$ Hz, $J_2 = 9.6$ Hz, 1H), 1.20 (s, 3H), 1.10 (s, 3H).

^{13}C NMR (75 MHz, CDCl_3) δ 192.5, 143.2, 142.6, 138.4, 131.3, 129.6, 129.3, 128.9, 128.7, 127.1, 125.7, 119.7, 54.5, 50.1, 46.7, 46.4, 38.5, 30.7, 30.2.

IR (film): ν (cm^{-1}) 3121, 3046, 2947, 2925, 2859, 1680, 1491, 1451, 1405, 1369, 1303, 1074, 1035, 1006, 893, 818, 763, 693, 654, 528.

HRMS (ESI, m/z) calcd for $\text{C}_{23}\text{H}_{24}\text{BrN}_2\text{O}$ $[\text{M}+\text{H}]^+$: 423.1067, found: 423.1063.



4-((1R,2R)-4,4-Dimethyl-2-(1-phenyl-1H-imidazole-2-carbonyl)cyclopentyl)benzonitrile (**43I**)

According to the general procedure, the reaction of (2,2-dimethylcyclopropyl)(1-phenyl-1H-imidazol-2-yl)methanone **41a** (24.0 mg, 0.10 mmol), 4-vinylbenzonitrile **42I** (32.3 mg, 2.5 equiv), Δ -**RhS** (1.7 mg, 2 mol%) and DIPEA (6.5 mg, 0.5 equiv) in acetone (1.0 mL, 0.1 M) under nitrogen atmosphere with blue LEDs for 20 hours, afforded 35.9 mg (97% yield) of **43I** as a colorless oil.

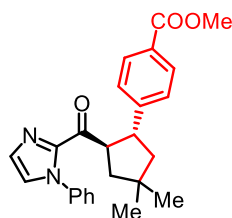
The d.r. value was determined through ^1H NMR of crude materials as >20:1; enantiomeric excess was established by HPLC analysis using a Chiralpak IG column, ee = 97% (HPLC: IG, 254 nm, *n*-hexane/isopropanol = 90:10, flow rate 1 mL/min, 25 °C, t_r (major) = 15.1 min, t_r (minor) = 21.3 min). $[\alpha]_{\text{D}}^{22} = -185.4^\circ$ (c 1.0, CH_2Cl_2).

^1H NMR (300 MHz, CDCl_3) δ 7.53-7.48 (m, 2H), 7.47-7.41 (m, 3H), 7.39-7.34 (m, 2H), 7.23-7.21 (m, 1H), 7.19-7.14 (m, 2H), 7.14-7.12 (m, 1H), 4.47 (q, $J = 9.8$ Hz, 1H), 3.76 (td, $J_1 = 11.4$ Hz, $J_2 = 7.5$ Hz, 1H), 2.27 (dd, $J_1 = 12.9$ Hz, $J_2 = 9.6$ Hz, 1H), 1.98 (dd, $J_1 = 12.6$ Hz, $J_2 = 7.5$ Hz, 1H), 1.75 (t, $J = 12.0$ Hz, 1H), 1.70 (dd, $J_1 = 12.9$ Hz, $J_2 = 9.3$ Hz, 1H), 1.21 (s, 3H), 1.11 (s, 3H).

^{13}C NMR (75 MHz, CDCl_3) δ 192.0, 149.4, 142.9, 138.2, 132.1, 129.7, 129.0, 128.8, 128.3, 127.2, 125.7, 119.0, 109.9, 54.4, 49.8, 46.8, 46.7, 38.6, 30.6, 30.0.

IR (film): ν (cm⁻¹) 3113, 3062, 2951, 2865, 2226, 1679, 1602, 1497, 1447, 1403, 1304, 1149, 1070, 1032, 895, 832, 763, 730, 692, 657, 558.

HRMS (ESI, m/z) calcd for C₂₄H₂₄N₃O [M+H]⁺: 370.1914, found: 370.1912.



Methyl 4-((1*R*,2*R*)-4,4-dimethyl-2-(1-phenyl-1*H*-imidazole-2-carbonyl)cyclopentyl)benzoate (43m)

According to the general procedure, the reaction of (2,2-dimethylcyclopropyl)(1-phenyl-1*H*-imidazol-2-yl)methanone **41a** (24.0 mg, 0.10 mmol), methyl 4-vinylbenzoate **42m** (40.6 mg, 2.5 equiv), Δ -**RhS** (1.7 mg, 2 mol%) and DIPEA (6.5 mg, 0.5 equiv) in acetone (1.0 mL, 0.1 M) under nitrogen atmosphere with blue LEDs for 20 hours, afforded 39.9 mg (99% yield) of **43m** as a white solid.

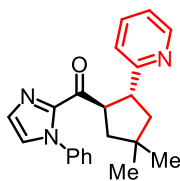
The d.r. value was determined through ¹H NMR of crude materials as >20:1; enantiomeric excess was established by HPLC analysis using a Chiralpak AD-H column, ee = 98% (HPLC: AD-H, 254 nm, *n*-hexane/isopropanol = 90:10, flow rate 1 mL/min, 25 °C, *t_r* (major) = 9.0 min, *t_r* (minor) = 12.1 min). $[\alpha]_D^{22} = -184.6^\circ$ (*c* 1.0, CH₂Cl₂).

¹H NMR (300 MHz, CDCl₃) δ 7.93-7.86 (m, 2H), 7.46-7.40 (m, 3H), 7.37-7.30 (m, 2H), 7.22-7.19 (m, 1H), 7.18-7.12 (m, 2H), 7.12-7.09 (m, 1H), 4.50 (q, *J* = 9.8 Hz, 1H), 3.86 (s, 3H), 3.76 (td, *J₁* = 11.1 Hz, *J₂* = 7.5 Hz, 1H), 2.25 (dd, *J₁* = 12.9 Hz, *J₂* = 9.6 Hz, 1H), 1.98 (dd, *J₁* = 12.9 Hz, *J₂* = 7.5 Hz, 1H), 1.79 (t, *J* = 12.0 Hz, 1H), 1.71 (dd, *J₁* = 12.9 Hz, *J₂* = 9.6 Hz, 1H), 1.21 (s, 3H), 1.11 (s, 3H).

¹³C NMR (75 MHz, CDCl₃) δ 192.4, 167.1, 149.2, 143.1, 138.3, 129.7, 129.6, 128.9, 128.7, 128.0, 127.5, 127.1, 125.7, 54.4, 51.9, 49.8, 47.1, 46.7, 38.6, 30.6, 30.1.

IR (film): ν (cm⁻¹) 3137, 2951, 2862, 1706, 1681, 1602, 1492, 1446, 1410, 1366, 1276, 1180, 1151, 1100, 1038, 1015, 984, 961, 896, 854, 788, 756, 699, 660, 531.

HRMS (ESI, m/z) calcd for C₂₅H₂₇N₂O₃ [M+H]⁺: 403.2016, found: 403.2013.



((1*R*,2*R*)-4,4-Dimethyl-2-(pyridin-2-yl)cyclopentyl)(1-phenyl-1*H*-imidazol-2-yl)methanone (43n)

According to the general procedure, the reaction of (2,2-dimethylcyclopropyl)(1-phenyl-1*H*-imidazol-2-yl)methanone **41a** (24.0 mg, 0.10 mmol), 2-vinylpyridine **42n** (26.3 mg, 2.5 equiv), Δ -**RhS** (1.7 mg, 2 mol%) and DIPEA (6.5 mg, 0.5 equiv) in acetone (1.0 mL, 0.1 M) under nitrogen atmosphere with blue LEDs for 24 hours, afforded 28.2 mg (82% yield) of **43n** as a colorless oil.

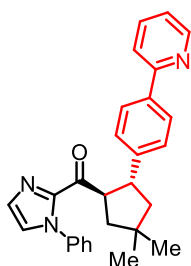
The d.r. value was determined through ^1H NMR of crude materials as >20:1; enantiomeric excess was established by HPLC analysis using a Chiralpak IG column, ee = 98% (HPLC: IG, 254 nm, *n*-hexane/isopropanol = 80:20, flow rate 1 mL/min, 25 °C, t_r (major) = 9.2 min, t_r (minor) = 11.7 min). $[\alpha]_D^{22} = -81.8^\circ$ (*c* 1.0, CH_2Cl_2).

^1H NMR (300 MHz, CDCl_3) δ 8.48 (d, $J = 4.5$ Hz, 1H), 7.50 (td, $J_1 = 7.5$ Hz, $J_2 = 1.8$ Hz, 1H), 7.46-7.40 (m, 3H), 7.29-7.23 (m, 2H), 7.22 (br s, 1H), 7.16 (d, $J = 8.1$ Hz, 1H), 7.12 (br s, 1H), 7.02 (dd, $J_1 = 7.2$ Hz, $J_2 = 5.4$ Hz, 1H), 4.66 (q, $J = 9.6$ Hz, 1H), 3.99-3.87 (m, 1H), 2.29 (dd, $J_1 = 12.9$ Hz, $J_2 = 9.9$ Hz, 1H), 2.03-1.94 (m, 2H), 1.75 (dd, $J_1 = 12.9$ Hz, $J_2 = 9.0$ Hz, 1H), 1.21 (s, 3H), 1.12 (s, 3H).

^{13}C NMR (75 MHz, CDCl_3) δ 193.1, 162.9, 149.1, 143.5, 138.6, 135.9, 129.5, 128.9, 128.5, 126.6, 125.7, 122.2, 121.0, 53.3, 48.7, 48.1, 46.3, 38.9, 30.3, 30.0.

IR (film): ν (cm^{-1}) 3060, 2950, 2864, 1679, 1591, 1497, 1442, 1404, 1305, 1148, 1072, 1034, 991, 900, 806, 757, 692, 661, 531.

HRMS (ESI, m/z) calcd for $\text{C}_{22}\text{H}_{24}\text{N}_3\text{O}$ $[\text{M}+\text{H}]^+$: 346.1914, found: 346.1911.



((1*R*,2*R*)-4,4-Dimethyl-2-(4-(pyridin-2-yl)phenyl)cyclopentyl)(1-phenyl-1*H*-imidazol-2-yl)methanone (43o)

According to the general procedure, the reaction of (2,2-dimethylcyclopropyl)(1-phenyl-1*H*-imidazol-2-yl)methanone **41a** (24.0 mg, 0.10 mmol), 2-(4-vinylphenyl)pyridine **42o** (45.4 mg, 2.5 equiv), Δ -**RhS** (1.7 mg, 2 mol%) and DIPEA (6.5 mg, 0.5 equiv) in acetone (1.0 mL, 0.1 M) under nitrogen atmosphere with blue LEDs for 20 hours, afforded 41.1 mg (98% yield) of **43o** as a colorless oil.

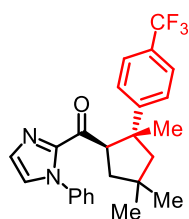
The d.r. value was determined through ^1H NMR of crude materials as >20:1; enantiomeric excess was established by HPLC analysis using a Chiralpak AD-H column, ee = 96% (HPLC: AD-H, 254 nm, *n*-hexane/isopropanol = 90:10, flow rate 1 mL/min, 40 °C, t_r (major) = 13.2 min, t_r (minor) = 15.6 min). $[\alpha]_D^{22} = -200.8^\circ$ (*c* 1.0, CH_2Cl_2).

^1H NMR (300 MHz, CDCl_3) δ 8.67-8.62 (m, 1H), 7.89-7.83 (m, 2H), 7.74-7.64 (m, 2H), 7.45-7.35 (m, 5H), 7.22-7.13 (m, 4H), 7.10-7.08 (m, 1H), 4.54 (q, $J = 9.8$ Hz, 1H), 3.77 (td, $J_1 = 11.4$ Hz, $J_2 = 7.5$ Hz, 1H), 2.26 (dd, $J_1 = 12.9$ Hz, $J_2 = 9.3$ Hz, 1H), 2.00 (dd, $J_1 = 12.6$ Hz, $J_2 = 7.5$ Hz, 1H), 1.83 (t, $J = 12.3$ Hz, 1H), 1.72 (dd, $J_1 = 12.6$ Hz, $J_2 = 9.3$ Hz, 1H), 1.23 (s, 3H), 1.13 (s, 3H).

^{13}C NMR (75 MHz, CDCl_3) δ 192.8, 157.4, 149.5, 144.6, 143.3, 138.4, 137.2, 136.6, 129.6, 128.9, 128.6, 127.9, 127.0, 126.8, 125.7, 121.7, 120.2, 54.5, 50.2, 47.1, 46.8, 38.5, 30.7, 30.2.

IR (film): ν (cm^{-1}) 3056, 2950, 2863, 1678, 1586, 1497, 1461, 1440, 1403, 1302, 1150, 1069, 1034, 982, 896, 819, 765, 731, 692, 663, 561, 507.

HRMS (ESI, m/z) calcd for $\text{C}_{28}\text{H}_{28}\text{N}_3\text{O}$ $[\text{M}+\text{H}]^+$: 422.2227, found: 422.2226.



(1-Phenyl-1*H*-imidazol-2-yl)((1*R*,2*R*)-2,4,4-trimethyl-2-(4-(trifluoromethyl)phenyl)cyclopentyl)methanone (43p**)**

According to the general procedure, the reaction of (2,2-dimethylcyclopropyl)(1-phenyl-1*H*-imidazol-2-yl)methanone **41a** (24.0 mg, 0.10 mmol), 1-(prop-1-en-2-yl)-4-(trifluoromethyl)benzene **42p** (46.6 mg, 2.5 equiv), Δ -**RhS** (3.5 mg, 4 mol%) and DIPEA (25.8 mg, 2.0 equiv) in acetone (1.0 mL, 0.1 M) under nitrogen atmosphere with blue LEDs for 26 hours, afforded 40.5 mg (95% yield) of **43p** as a colorless oil.

The d.r. value was determined through ^1H NMR of crude materials as >20:1; enantiomeric excess was established by HPLC analysis using a Chiralpak IG column, ee = >99% (HPLC: IG, 254 nm, *n*-hexane/isopropanol = 90:10, flow rate 1 mL/min, 25 °C, t_r (major) = 4.4 min, t_r (minor) = 5.4 min). $[\alpha]_D^{22} = -108.8^\circ$ (*c* 1.0, CH_2Cl_2).

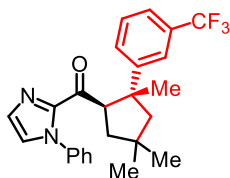
^1H NMR (300 MHz, CDCl_3) δ 7.61-7.55 (m, 2H), 7.54-7.48 (m, 2H), 7.47-7.42 (m, 3H), 7.23-7.17 (m, 2H), 7.09-7.06 (m, 2H), 4.90 (dd, $J_1 = 12.0$ Hz, $J_2 = 6.9$ Hz, 1H), 2.22-2.11 (m, 2H), 1.93-1.82 (m, 2H), 1.35 (s, 3H), 1.20 (s, 3H), 1.13 (s, 3H).

^{13}C NMR (75 MHz, CDCl_3) δ 192.4, 153.6, 143.8, 138.5, 129.3, 129.0, 128.7, 127.8 (q, $J = 29.8$ Hz), 127.0, 126.6, 125.9, 124.9 (q, $J = 3.9$ Hz), 124.4 (q, $J = 269.9$ Hz), 58.1, 54.7, 51.9, 44.4, 36.7, 31.7, 31.4, 25.5.

^{19}F NMR (282 MHz, CDCl_3) δ -62.34 (s, 3F).

IR (film): ν (cm^{-1}) 2954, 2870, 1678, 1617, 1497, 1447, 1404, 1323, 1163, 1116, 1072, 1014, 968, 910, 877, 826, 762, 691, 661, 605, 541, 524.

HRMS (ESI, m/z) calcd for $\text{C}_{25}\text{H}_{26}\text{F}_3\text{N}_2\text{O}$ $[\text{M}+\text{H}]^+$: 427.1992, found: 427.1986.



(1-Phenyl-1H-imidazol-2-yl)((1R,2R)-2,4,4-trimethyl-2-(3-(trifluoromethyl)phenyl)cyclopentyl)methanone (43q)

According to the general procedure, the reaction of (2,2-dimethylcyclopropyl)(1-phenyl-1H-imidazol-2-yl)methanone **41a** (24.0 mg, 0.10 mmol), 1-(prop-1-en-2-yl)-3-(trifluoromethyl)benzene **42q** (40.5 mg, 2.5 equiv), Δ -**RhS** (3.5 mg, 4 mol%) and DIPEA (25.8 mg, 2.0 equiv) in acetone (1.0 mL, 0.1 M) under nitrogen atmosphere with blue LEDs for 28 hours, afforded 26.7 mg (63% yield) of **43q** as a colorless oil.

The d.r. value was determined through ^1H NMR of crude materials as >20:1; enantiomeric excess was established by HPLC analysis using a Chiralpak IG column, ee = 99% (HPLC: IG, 254 nm, *n*-hexane/isopropanol = 90:10, flow rate 1 mL/min, 40 °C, t_r (major) = 4.0 min, t_r (minor) = 4.5 min). $[\alpha]_D^{22} = -159.2^\circ$ (*c* 1.0, CH_2Cl_2).

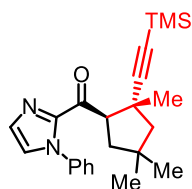
^1H NMR (300 MHz, CDCl_3) δ 7.71-7.64 (m, 2H), 7.49-7.42 (m, 3H), 7.41-7.36 (m, 2H), 7.23-7.16 (m, 2H), 7.08-7.04 (m, 2H), 4.88 (dd, $J_1 = 12.3$ Hz, $J_2 = 6.9$ Hz, 1H), 2.24-2.13 (m, 2H), 1.91-1.81 (m, 2H), 1.34 (s, 3H), 1.20 (s, 3H), 1.15 (s, 3H).

^{13}C NMR (75 MHz, CDCl_3) δ 192.4, 150.3, 143.9, 138.5, 130.1 (q, $J = 34.5$ Hz), 129.9 (q, $J = 1.0$ Hz), 129.3, 129.0, 128.7, 128.4, 127.0, 125.9, 124.4 (q, $J = 270.1$ Hz), 123.0 (q, $J = 3.8$ Hz), 122.5 (q, $J = 3.9$ Hz), 57.9, 54.9, 51.9, 44.2, 36.6, 31.8, 31.5, 25.3.

^{19}F NMR (282 MHz, CDCl_3) δ -62.37 (s, 3F).

IR (film): ν (cm^{-1}) 3067, 2954, 2870, 1678, 1596, 1496, 1443, 1404, 1326, 1161, 1120, 1074, 969, 902, 823, 799, 763, 695, 661, 541.

HRMS (ESI, m/z) calcd for $\text{C}_{25}\text{H}_{26}\text{F}_3\text{N}_2\text{O}$ $[\text{M}+\text{H}]^+$: 427.1992, found: 427.1990.



(1-Phenyl-1H-imidazol-2-yl)((1R,2R)-2,4,4-trimethyl-2-((trimethylsilyl)ethynyl)cyclopentyl)methanone (43r)

According to the general procedure, the reaction of (2,2-dimethylcyclopropyl)(1-phenyl-1H-imidazol-2-yl)methanone **41a** (24.0 mg, 0.10 mmol), trimethyl(3-methylbut-3-en-1-yn-1-yl)silane **42r** (34.6 mg, 2.5 equiv), Δ -**RhS** (3.5 mg, 4 mol%) and DIPEA (25.8 mg, 2.0 equiv) in acetone (1.0 mL, 0.1 M) under nitrogen atmosphere with blue LEDs for 28 hours, afforded 37.4 mg (98% yield) of **43r** as a colorless oil.

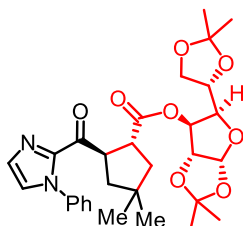
The d.r. value was determined through ^1H NMR of crude materials as >20:1; enantiomeric excess was established by HPLC analysis using a Chiralpak IG column, ee = >99% (HPLC: IG, 254 nm, *n*-hexane/isopropanol = 90:10, flow rate 1 mL/min, 25 °C, t_r (major) = 4.7 min, t_r (minor) = 5.1 min). $[\alpha]_D^{22} = -135.8^\circ$ (*c* 1.0, CH_2Cl_2).

^1H NMR (300 MHz, CDCl_3) δ 7.49-7.42 (m, 3H), 7.30-7.24 (m, 3H), 7.19-7.16 (m, 1H), 4.73 (dd, $J_1 = 11.1$ Hz, $J_2 = 7.2$ Hz, 1H), 2.04-1.90 (m, 2H), 1.75-1.64 (m, 2H), 1.19 (s, 3H), 1.13 (s, 3H), 1.07 (s, 3H), 0.07 (s, 9H).

^{13}C NMR (75 MHz, CDCl_3) δ 192.1, 144.5, 138.6, 129.5, 129.0, 128.6, 126.9, 125.9, 114.4, 84.2, 56.9, 55.3, 42.30, 42.27, 37.4, 31.2, 31.1, 24.8, 0.12.

IR (film): ν (cm^{-1}) 2955, 2868, 2160, 1679, 1497, 1445, 1406, 1309, 1248, 1049, 967, 907, 838, 759, 693, 663, 533.

HRMS (ESI, m/z) calcd for $\text{C}_{23}\text{H}_{31}\text{N}_2\text{OSi}$ $[\text{M}+\text{H}]^+$: 379.2200, found: 379.2198.



(3a*R*,5*R*,6*S*,6a*R*)-5-((*S*)-2,2-Dimethyl-1,3-dioxolan-4-yl)-2,2-dimethyltetrahydrofuro[2,3-*d*][1,3]dioxol-6-yl (1*R*,2*R*)-4,4-dimethyl-2-(1-phenyl-1*H*-imidazole-2-carbonyl)cyclopentane-1-carboxylate ((1*R*,2*R*)-43s)

According to the general procedure, the reaction of (2,2-dimethylcyclopropyl)(1-phenyl-1*H*-imidazol-2-yl)methanone **41a** (24.0 mg, 0.10 mmol), the corresponding **glucofuranose** derived alkene **42s** (39.3 mg, 1.25 equiv), Δ -**RhS** (3.5 mg, 4 mol%) and DIPEA (25.8 mg, 2.0 equiv) in acetone (1.0 mL, 0.1 M) under nitrogen atmosphere with blue LEDs for 24 hours, afforded 55.0 mg (99% yield) of (1*R*,2*R*)-**43s** as a colorless oil.

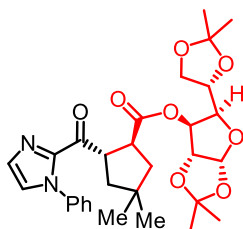
Only a single isomer was formed as determined through ^1H NMR of crude materials. $[\alpha]_{\text{D}}^{22} = -67.4^\circ$ (*c* 1.0, CH_2Cl_2).

^1H NMR (300 MHz, CDCl_3) δ 7.42-7.34 (m, 3H), 7.25-7.17 (m, 3H), 7.13-7.10 (m, 1H), 5.71 (d, $J = 3.6$ Hz, 1H), 5.16 (d, $J = 3.0$ Hz, 1H), 4.51 (q, $J = 9.3$ Hz, 1H), 4.36 (d, $J = 3.6$ Hz, 1H), 4.08 (dd, $J_1 = 7.8$ Hz, $J_2 = 3.0$ Hz, 1H), 4.02-3.94 (m, 1H), 3.88-3.82 (m, 2H), 3.46 (q, $J = 9.3$ Hz, 1H), 2.09 (dd, $J_1 = 12.6$ Hz, $J_2 = 9.6$ Hz, 1H), 1.79 (d, $J = 9.0$ Hz, 2H), 1.53 (dd, $J_1 = 12.6$ Hz, $J_2 = 9.3$ Hz, 1H), 1.42 (s, 3H), 1.30 (s, 3H), 1.21 (s, 6H), 1.04 (s, 3H), 0.94 (s, 3H).

^{13}C NMR (75 MHz, CDCl_3) δ 191.4, 173.4, 142.7, 138.4, 129.8, 129.0, 128.8, 127.2, 125.9, 112.2, 109.3, 105.1, 83.2, 80.1, 76.0, 72.3, 67.3, 50.3, 46.0, 45.0, 43.6, 39.7, 28.9, 26.8, 26.2, 25.1.

IR (film): ν (cm^{-1}) 2984, 2954, 2871, 1740, 1684, 1497, 1449, 1407, 1376, 1306, 1252, 1213, 1154, 1071, 1020, 912, 886, 848, 803, 763, 732, 694, 659, 538, 511.

HRMS (ESI, m/z) calcd for $\text{C}_{30}\text{H}_{38}\text{N}_2\text{O}_8\text{Na}$ $[\text{M}+\text{Na}]^+$: 577.2520, found: 577.2516.



(3aR,5R,6S,6aR)-5-((S)-2,2-Dimethyl-1,3-dioxolan-4-yl)-2,2-dimethyltetrahydrofuro[2,3-d][1,3]dioxol-6-yl (1S,2S)-4,4-dimethyl-2-(1-phenyl-1H-imidazole-2-carbonyl)cyclopentane-1-carboxylate ((1S,2S)-43s)

According to the general procedure, the reaction of (2,2-dimethylcyclopropyl)(1-phenyl-1H-imidazol-2-yl)methanone **41a** (24.0 mg, 0.10 mmol), the corresponding **glucofuranose** derived alkene **42s** (39.3 mg, 1.25 equiv), **4-RhS** (3.5 mg, 4 mol%) and DIPEA (25.8 mg, 2.0 equiv) in acetone (1.0 mL, 0.1 M) under nitrogen atmosphere with blue LEDs for 24 hours, afforded 54.6 mg (98% yield) of **(1S,2S)-43s** as a colorless oil.

Only a single isomer was formed as determined through ^1H NMR of crude materials (>20:1 d.r.). $[\alpha]_{\text{D}}^{22} = +28.8^\circ$ (c 1.0, CH_2Cl_2).

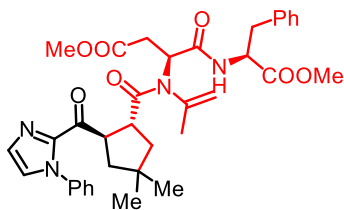
^1H NMR (300 MHz, CDCl_3) δ 7.46-7.39 (m, 3H), 7.28-7.22 (m, 3H), 7.18-7.15 (m, 1H), 5.40 (d, $J = 3.9$ Hz, 1H), 5.19 (d, $J = 2.7$ Hz, 1H), 4.53 (q, $J = 9.4$ Hz, 1H), 4.36 (d, $J = 3.6$ Hz, 1H), 4.10 (dd, $J_1 = 7.8$ Hz, $J_2 = 3.0$ Hz, 1H), 4.06-3.86 (m, 3H), 3.45 (q, $J = 9.2$ Hz, 1H), 2.08 (dd, $J_1 = 12.6$ Hz, $J_2 = 9.0$ Hz, 1H), 1.88-1.80 (m, 2H), 1.57 (dd, $J_1 = 12.6$ Hz, $J_2 = 9.9$ Hz, 1H), 1.45 (s, 3H), 1.34 (s, 3H), 1.24 (s, 3H), 1.23 (s, 3H), 1.09 (s, 3H), 1.00 (s, 3H).

^{13}C NMR (75 MHz, CDCl_3) δ 191.7, 173.2, 142.8, 138.4, 129.7, 128.9, 128.8, 127.5, 125.9, 112.1, 109.2, 105.0, 83.2, 80.0, 75.8, 72.3, 67.3, 50.0, 46.0, 45.5, 43.3, 39.6, 29.2, 26.8, 26.7, 26.2, 25.2.

IR (film): ν (cm^{-1}) 2950, 2870, 1743, 1683, 1598, 1497, 1450, 1406, 1376, 1306, 1251, 1214, 1156, 1073, 1020, 911, 848, 802, 765, 731, 694, 646, 511, 421.

HRMS (ESI, m/z) calcd for $\text{C}_{30}\text{H}_{38}\text{N}_2\text{O}_8\text{Na}$ $[\text{M}+\text{Na}]^+$: 577.2520, found: 577.2536.

The spectra of (1R,2R)-**43s** and (1S,2S)-**43s** are compared with the crude ^1H NMR of the corresponding reaction mixture catalyzed by *rac*-**RhS** which shown a 1:1 mixture of (1R,2R)-**43s** and (1S,2S)-**43s**.



Methyl (S)-3-((1*R*,2*R*)-4,4-dimethyl-2-(1-phenyl-1*H*-imidazole-2-carbonyl)-*N*-(prop-1-en-2-yl)cyclopentane-1-carboxamido)-4-(((*S*)-1-methoxy-1-oxo-3-phenylpropan-2-yl)amino)-4-oxobutanoate (43t**)**

According to the general procedure, the reaction of (2,2-dimethylcyclopropyl)(1-phenyl-1*H*-imidazol-2-yl)methanone **41a** (24.0 mg, 0.10 mmol), the corresponding **aspartame** derived alkene **42t** (50.3 mg, 1.25 equiv), Δ -**RhS** (3.5 mg, 4 mol%) and DIPEA (25.8 mg, 2.0 equiv) in acetone (1.0 mL, 0.1 M) under nitrogen atmosphere with blue LEDs for 24 hours, afforded 56.7 mg (88% yield) of **43t** as a yellow solid.

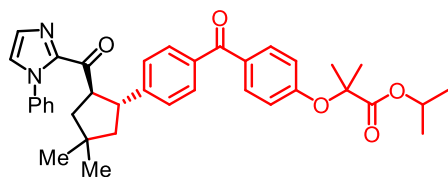
Only a single isomer was formed as determined through ^1H NMR of crude materials. $[\alpha]_{\text{D}}^{22} = -135.4^\circ$ (*c* 1.0, CH_2Cl_2).

^1H NMR (500 MHz, $(\text{CD}_3)_2\text{SO}$) δ 8.12 (d, $J = 7.6$ Hz, 1H), 7.64 (d, $J = 1.0$ Hz, 1H), 7.47-7.43 (m, 3H), 7.31-7.27 (m, 3H), 7.27-7.22 (m, 2H), 7.21-7.17 (m, 3H), 5.14 (dd, $J_1 = 8.3$ Hz, $J_2 = 6.1$ Hz, 1H), 4.92 (s, 1H), 4.52 (q, $J = 9.2$ Hz, 1H), 4.44-4.36 (m, 2H), 3.58 (s, 3H), 3.52 (s, 3H), 3.41 (q, $J = 9.1$ Hz, 1H), 2.98 (dd, $J_1 = 13.8$ Hz, $J_2 = 5.1$ Hz, 1H), 2.89 (dd, $J_1 = 13.8$ Hz, $J_2 = 9.5$ Hz, 1H), 2.82 (dd, $J_1 = 16.5$ Hz, $J_2 = 8.7$ Hz, 1H), 2.46 (dd, $J_1 = 16.3$ Hz, $J_2 = 5.8$ Hz, 1H), 2.04 (dd, $J_1 = 12.5$ Hz, $J_2 = 9.4$ Hz, 1H), 1.60-1.50 (m, 3H), 1.57 (s, 3H), 1.12 (s, 3H), 0.93 (s, 3H).

^{13}C NMR (125 MHz, $(\text{CD}_3)_2\text{SO}$) δ 191.5, 173.2, 171.7, 170.6, 169.2, 142.1, 141.7, 138.1, 137.2, 129.6, 129.0, 128.9, 128.4, 128.3, 128.1, 126.5, 125.6, 117.6, 54.9, 54.0, 51.9, 51.4, 50.9, 46.0, 45.3, 43.1, 39.3, 36.3, 33.8, 29.3, 29.0, 22.2.

IR (film): ν (cm^{-1}) 3423, 3332, 3112, 2952, 2865, 1738, 1678, 1499, 1442, 1399, 1306, 1209, 1169, 1036, 912, 845, 760, 696, 535, 508.

HRMS (ESI, m/z) calcd for $\text{C}_{36}\text{H}_{42}\text{N}_4\text{O}_7\text{Na}$ $[\text{M}+\text{Na}]^+$: 665.2946, found: 665.2947.



Isopropyl 2-(4-(4-((1*R*,2*R*)-4,4-dimethyl-2-(1-phenyl-1*H*-imidazole-2-carbonyl)cyclopentyl)benzoyl)phenoxy)-2-methylpropanoate (43u)

According to the general procedure, the reaction of (2,2-dimethylcyclopentyl)(1-phenyl-1*H*-imidazol-2-yl)methanone **41a** (24.0 mg, 0.10 mmol), the corresponding **fenofibrate** derived alkene **42u** (44.1 mg, 1.25 equiv), Δ -**RhS** (3.5 mg, 4 mol%) and DIPEA (25.8 mg, 2.0 equiv) in acetone (1.0 mL, 0.1 M) under nitrogen atmosphere with blue LEDs for 22 hours, afforded 58.8 mg (99% yield) of **43u** as a colorless oil.

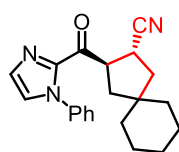
The d.r. value was determined through ^1H NMR of crude materials as >20:1; enantiomeric excess was established by HPLC analysis using a Chiralpak IG column, ee = 99% (HPLC: IG, 254 nm, *n*-hexane/isopropanol = 70:30, flow rate 1 mL/min, 40 °C, t_r (major) = 10.3 min, t_r (minor) = 13.2 min). $[\alpha]_D^{22} = -129.8^\circ$ (*c* 1.0, CH_2Cl_2).

^1H NMR (300 MHz, CDCl_3) δ 7.74-7.68 (m, 2H), 7.65-7.59 (m, 2H), 7.46-7.49 (m, 3H), 7.39-7.32 (m, 2H), 7.23-7.20 (m, 1H), 7.20-7.14 (m, 2H), 7.13-7.10 (m, 1H), 6.87-6.80 (m, 2H), 5.08 (sept, $J = 6.3$ Hz, 1H), 4.52 (q, $J = 10.5$ Hz, 1H), 3.86-3.73 (m, 1H), 2.27 (dd, $J_1 = 13.2$ Hz, $J_2 = 9.6$ Hz, 1H), 2.01 (dd, $J_1 = 12.6$ Hz, $J_2 = 7.8$ Hz, 1H), 1.81 (t, $J = 12.3$ Hz, 1H), 1.72 (dd, $J_1 = 12.9$ Hz, $J_2 = 9.6$ Hz, 1H), 1.65 (s, 6H), 1.22 (s, 3H), 1.20 (s, 3H), 1.18 (s, 3H), 1.12 (s, 3H).

^{13}C NMR (75 MHz, CDCl_3) δ 195.2, 192.4, 173.1, 159.3, 148.3, 143.1, 138.3, 136.0, 131.9, 130.9, 129.9, 129.7, 128.9, 128.7, 127.3, 127.1, 125.7, 117.1, 79.3, 69.2, 54.5, 50.0, 46.9, 46.7, 38.6, 30.6, 30.1, 25.3, 21.5.

IR (film): ν (cm^{-1}) 2949, 2866, 1730, 1680, 1651, 1599, 1499, 1449, 1406, 1282, 1247, 1175, 1146, 1101, 1033, 974, 922, 848, 817, 763, 730, 691, 636, 522.

HRMS (ESI, m/z) calcd for $\text{C}_{37}\text{H}_{41}\text{N}_2\text{O}_5$ $[\text{M}+\text{H}]^+$: 593.3010, found: 593.3008.



(2*R*,3*R*)-3-(1-Phenyl-1*H*-imidazole-2-carbonyl)spiro[4.5]decane-2-carbonitrile (43v)

According to the general procedure, the reaction of (1-phenyl-1*H*-imidazol-2-yl) (spiro[2.5]octan-1-yl)methanone **41f** (28.0 mg, 0.10 mmol), acrylonitrile **42a** (13.3 mg, 2.5 equiv), Δ -**RhS** (1.7 mg, 2 mol%) and DIPEA (6.5 mg, 0.5 equiv) in acetone (1.0 mL, 0.1 M) under nitrogen atmosphere with blue LEDs for 40 hours, afforded 19.1 mg (a colorless oil) of the major diastereoisomer and 2.5 mg of the minor diastereoisomer of **43v** (65% total yield).

The d.r. value was determined through ^1H NMR of crude materials as 7:1.

The major diastereoisomer: enantiomeric excess was established by HPLC analysis using a Chiralpak IG column, ee = 96% (HPLC: IG, 254 nm, *n*-hexane/isopropanol = 70:10, flow rate 1 mL/min, 25 °C, t_r (major) = 16.2 min, t_r (minor) = 27.0 min). $[\alpha]_D^{22} = -62.6^\circ$ (*c* 1.0, CH_2Cl_2).

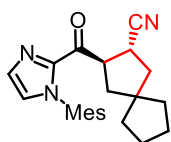
^1H NMR (300 MHz, CDCl_3) δ 7.52-7.44 (m, 3H), 7.34-7.32 (m, 1H), 7.32-7.25 (m, 2H), 7.24-7.21 (m, 1H), 4.52 (q, $J = 9.3$ Hz, 1H), 3.35 (q, $J = 9.0$ Hz, 1H), 2.34 (dd, $J_1 = 12.9$ Hz, $J_2 = 9.3$ Hz, 1H), 2.03 (dd, $J_1 = 12.9$ Hz, $J_2 = 8.7$ Hz, 1H), 1.88 (dd, $J_1 = 12.9$ Hz, $J_2 = 9.3$ Hz, 1H), 1.58-1.46 (m, 5H), 1.45-1.25 (m, 6H).

^{13}C NMR (75 MHz, CDCl_3) δ 189.4, 142.1, 138.1, 130.3, 129.03, 128.96, 127.7, 125.9, 122.1, 51.5, 43.64, 43.58, 42.8, 37.9, 27.8, 25.8, 23.35, 23.32. (Missing one ^{13}C signal)

IR (film): ν (cm^{-1}) 3113, 3062, 2924, 2852, 2239, 1682, 1596, 1496, 1447, 1403, 1339, 1307, 1149, 1066, 1033, 962, 912, 841, 762, 731, 692, 661, 532.

HRMS (ESI, m/z) calcd for $\text{C}_{21}\text{H}_{24}\text{N}_3\text{O}$ $[\text{M}+\text{H}]^+$: 334.1914, found: 334.1906.

The minor diastereoisomer: ^1H NMR (300 MHz, CDCl_3) δ 7.50-7.43 (m, 3H), 7.39-7.32 (m, 2H), 7.30-7.27 (m, 1H), 7.24-7.20 (m, 1H), 4.49-4.36 (m, 1H), 3.62-3.51 (m, 1H), 2.09-1.78 (m, 4H), 1.55-1.30 (m, 10H).



(2*R*,3*R*)-3-(1-Mesityl-1*H*-imidazole-2-carbonyl)spiro[4.4]nonane-2-carbonitrile (43w**)**

According to the general procedure, the reaction of (1-phenyl-1*H*-imidazol-2-yl) (spiro[2.4]heptan-1-yl)methanone **41g** (30.8 mg, 0.10 mmol), acrylonitrile **42a** (13.3 mg, 2.5 equiv), Δ -**RhS** (3.5 mg, 4 mol%) and DIPEA (25.8 mg, 2.0 equiv) in acetone (1.0 mL, 0.1 M) under nitrogen atmosphere with blue LEDs for 24 hours, afforded 32.9 mg of **43w** (91% yield) as a white solid.

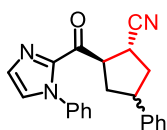
The d.r. value was determined through ^1H NMR of crude materials as >20:1; enantiomeric excess was established by HPLC analysis using a Chiralpak IG column, ee = 99% (HPLC: IG, 254 nm, *n*-hexane/isopropanol = 90:10, flow rate 1 mL/min, 40 °C, t_r (major) = 17.1 min, t_r (minor) = 14.0 min). $[\alpha]_D^{22} = -35.4^\circ$ (*c* 1.0, CH_2Cl_2).

^1H NMR (300 MHz, CDCl_3) δ 7.42-7.38 (m, 1H), 7.05-7.01 (m, 1H), 6.99 (br s, 1H), 6.95 (br s, 1H), 4.53 (q, $J = 8.9$ Hz, 1H), 3.42 (q, $J = 8.3$ Hz, 1H), 2.36 (dd, $J_1 = 12.9$ Hz, $J_2 = 9.3$ Hz, 1H), 2.34 (s, 3H), 2.03 (dd, $J_1 = 12.6$ Hz, $J_2 = 8.7$ Hz, 1H), 1.95 (dd, $J_1 = 12.6$ Hz, $J_2 = 7.8$ Hz, 1H), 1.91 (s, 3H), 1.83 (s, 3H), 1.70-1.52 (m, 7H), 1.46-1.35 (m, 2H).

^{13}C NMR (75 MHz, CDCl_3) δ 189.2, 142.1, 138.7, 134.5, 134.2, 133.7, 130.9, 129.1, 128.9, 126.3, 122.4, 51.9, 51.4, 44.4, 43.3, 38.7, 38.6, 27.8, 24.4, 24.3, 21.1, 17.3, 17.1.

IR (film): ν (cm^{-1}) 3108, 2949, 2921, 2859, 2238, 1681, 1485, 1448, 1402, 1314, 1282, 1218, 1155, 1030, 979, 912, 866, 818, 781, 737, 665, 562.

HRMS (ESI, m/z) calcd for $\text{C}_{23}\text{H}_{28}\text{N}_3\text{O}$ $[\text{M}+\text{H}]^+$: 362.2227, found: 362.2225.



(1R,2R)-4-Phenyl-2-(1-phenyl-1H-imidazole-2-carbonyl)cyclopentane-1-carbonitrile (45a)

According to the general procedure, the reaction of (1-phenyl-1H-imidazol-2-yl) (2-phenylcyclopropyl)methanone **44a** (28.8 mg, 0.10 mmol), acrylonitrile **42a** (13.3 mg, 2.5 equiv), $\Delta\text{-RhS}$ (1.7 mg, 2 mol%) and DIPEA (6.5 mg, 0.5 equiv) in acetone (1.0 mL, 0.1 M) under nitrogen atmosphere with blue LEDs for 16 hours, afforded 33.0 mg of **45a** (97% yield, a colorless oil) as a mixture of two diastereoisomers.

The d.r. value was determined through ^1H NMR of crude materials as 2.1:1; enantiomeric excess was established by HPLC analysis using a Chiralpak OD-H column, ee [major] = 97% (t_r (major) = 10.3 min, t_r (minor) = 8.0 min), ee [minor] = 99% (t_r (major) = 22.0 min, t_r (minor) = 9.9 min) (HPLC: OD-H, 254 nm, *n*-hexane/isopropanol = 70:30, flow rate 1 mL/min, 40 °C). $[\alpha]_D^{22} = -19.4^\circ$ (*c* 1.0, CH_2Cl_2).

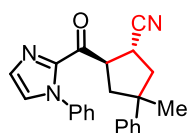
^1H NMR (500 MHz, CDCl_3) δ 7.53-7.48 (m, 3H), 7.38-7.36 (m, 1H), 7.36-7.54 (m, 4H), 7.25-7.23 (m, 1H), 7.23-7.18 (m, 3H), 4.74-4.68 (m, 0.33H, minor), 4.67-4.61 (m, 0.67H, major), 3.64-3.58 (m,

0.67H, major), 3.58-3.46 (m, 1H), 3.15-3.05 (m, 0.33H, minor), 2.93-2.85 (m, 0.67H, major), 2.64-2.56 (m, 0.33H, minor), 2.53-2.43 (m, 1H), 2.37-2.30 (m, 0.33H, minor), 2.20-2.08 (m, 1H), 1.84-1.75 (m, 0.67H, major). (Mixture of two diastereoisomers)

^{13}C NMR (125 MHz, CDCl_3) δ 189.2, 188.6, 141.8, 141.75, 141.68, 141.6, 138.00, 137.96, 130.4, 129.06, 129.05, 128.61, 128.58, 127.89, 127.87, 126.89, 126.88, 126.85, 126.80, 126.78, 125.88, 125.86, 122.5, 121.7, 52.3, 50.9, 45.3, 44.2, 40.2, 39.4, 38.6, 38.2, 28.6. (Mixture of two diastereoisomers)

IR (film): ν (cm^{-1}) 3394, 3067, 2238, 1670, 1627, 1577, 1494, 1449, 1417, 1333, 1312, 1283, 1220, 1073, 977, 911, 846, 766, 708, 681, 589, 541, 480.

HRMS (ESI, m/z) calcd for $\text{C}_{22}\text{H}_{20}\text{N}_3\text{O}$ $[\text{M}+\text{H}]^+$: 342.1601, found: 342.1600.

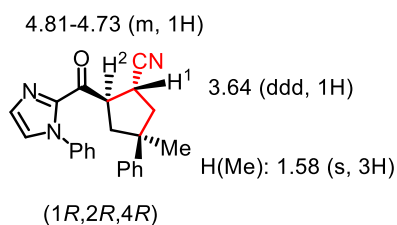


(1R,2R)-4-Methyl-4-phenyl-2-(1-phenyl-1H-imidazole-2-carbonyl)cyclopentane-1-carbonitrile (45b)

According to the general procedure, the reaction of (2-methyl-2-phenylcyclopropyl) (1-phenyl-1H-imidazol-2-yl)methanone **44b** (30.2 mg, 0.10 mmol), acrylonitrile **42a** (13.3 mg, 2.5 equiv), Δ -RhS (1.7 mg, 2 mol%) and DIPEA (6.5 mg, 0.5 equiv) in acetone (1.0 mL, 0.1 M) under nitrogen atmosphere with blue LEDs for 24 hours, afforded 29.8 mg of **45b** (84% total yield) as two separable diastereoisomers.

The d.r. value was determined through ^1H NMR of crude materials as 2.2:1.

The major diastereoisomer:



Eenantiomeric excess was established by HPLC analysis using a Chiralpak IG column, ee [major] = 95% (HPLC: IG, 254 nm, *n*-hexane/isopropanol = 80:20, flow rate 1 mL/min, 40 °C, t_r (major) = 16.2 min, t_r (minor) = 25.4 min). $[\alpha]_{\text{D}}^{22} = -86.8^\circ$ (c 1.0, CH_2Cl_2).

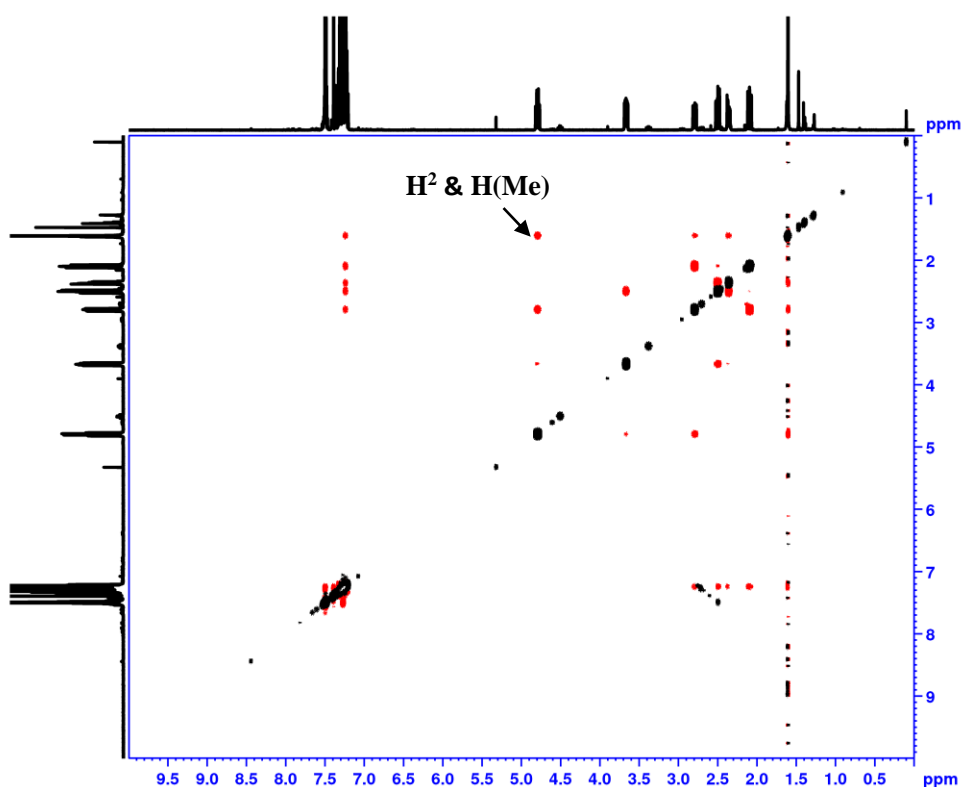
^1H NMR (500 MHz, CDCl_3) δ 7.48-7.46 (m, 3H), 7.37-7.36 (m, 1H), 7.31-7.26 (m, 2H), 7.26-7.23 (m, 3H), 7.23-7.17 (m, 3H), 4.81-4.73 (m, 1H), 3.64 (ddd, $J_1 = 12.2$ Hz, $J_2 = 7.5$ Hz, $J_3 = 4.8$ Hz, 1H), 2.77 (ddd, $J_1 = 12.6$ Hz, $J_2 = 8.2$ Hz, $J_3 = 1.6$ Hz, 1H), 2.48 (dd, $J_1 = 13.3$ Hz, $J_2 = 10.5$ Hz, 1H), 2.34 (ddd, $J_1 = 13.3$ Hz, $J_2 = 4.8$ Hz, $J_3 = 1.6$ Hz, 1H), 2.07 (dd, $J_1 = 12.5$ Hz, $J_2 = 11.0$ Hz, 1H), 1.58 (s, 3H).

^{13}C NMR (125 MHz, CDCl_3) δ 188.6, 148.2, 141.8, 138.0, 130.4, 129.0, 128.5, 127.8, 126.2, 125.8, 125.4, 123.0, 51.7, 48.4, 45.3, 43.5, 29.7, 26.9. (Missing one ^{13}C signal)

IR (film): ν (cm^{-1}) 3112, 3058, 2964, 2871, 2239, 1682, 1597, 1496, 1447, 1402, 1338, 1305, 1220, 1150, 1103, 1068, 1029, 974, 909, 834, 801, 762, 730, 695, 659, 539.

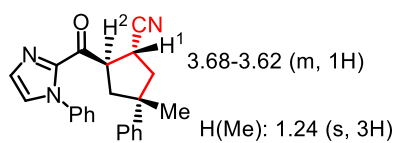
HRMS (ESI, m/z) calcd for $\text{C}_{23}\text{H}_{22}\text{N}_3\text{O}$ $[\text{M}+\text{H}]^+$: 356.1757, found: 356.1755.

NOE spectrum:



The minor diastereoisomer:

4.62-4.54 (m, 1H)



(1*R*,2*R*,4*S*)

Enantiomeric excess was established by HPLC analysis using a Chiralpak IG column, ee [minor] = 99% (HPLC: IG, 254 nm, *n*-hexane/isopropanol = 80:20, flow rate 1 mL/min, 40 °C, t_r (major) = 16.9 min, t_r (minor) = 22.9 min). $[\alpha]_D^{22} = +13.6^\circ$ (c 0.5, CH_2Cl_2).

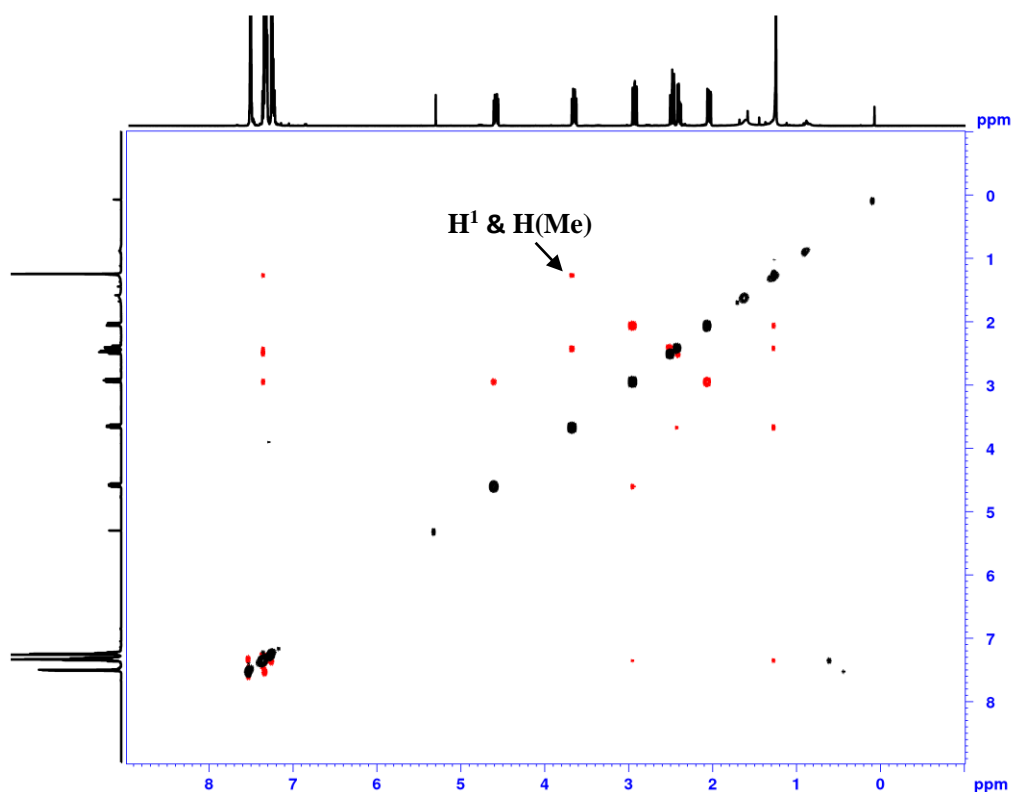
^1H NMR (500 MHz, CDCl_3) δ 7.53-7.48 (m, 3H), 7.37-7.30 (m, 7H), 7.25-7.21 (m, 2H), 4.62-4.54 (m, 1H), 3.68-3.62 (m, 1H), 2.93 (dd, $J_1 = 13.5$ Hz, $J_2 = 11.3$ Hz, 1H), 2.48 (dd, $J_1 = 12.5$ Hz, $J_2 = 10.5$ Hz, 1H), 2.40 (ddd, $J_1 = 12.5$ Hz, $J_2 = 7.7$ Hz, $J_3 = 0.8$ Hz, 1H), 2.07 (ddd, $J_1 = 13.6$ Hz, $J_2 = 7.2$ Hz, $J_3 = 1.1$ Hz, 1H), 1.24 (s, 3H).

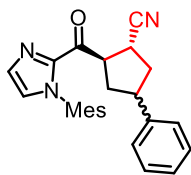
^{13}C NMR (125 MHz, CDCl_3) δ 189.0, 148.2, 141.9, 138.0, 130.4, 129.09, 129.06, 128.5, 127.8, 126.3, 125.9, 125.6, 121.6, 51.4, 47.2, 44.5, 44.1, 30.0, 27.6.

IR (film): ν (cm^{-1}) 3105, 3057, 2929, 2877, 2241, 1683, 1597, 1496, 1450, 1406, 1304, 1241, 1145, 1103, 1069, 1031, 983, 910, 839, 801, 767, 694, 544.

HRMS (ESI, m/z) calcd for $\text{C}_{23}\text{H}_{21}\text{N}_3\text{ONa}$ $[\text{M}+\text{Na}]^+$: 378.1577, found: 378.1573.

NOE spectrum:





(1*R*,2*R*)-2-(1-Mesityl-1*H*-imidazole-2-carbonyl)-4-phenylcyclopentane-1-carbonitrile (45c)

According to the general procedure, the reaction of (1-mesityl-1*H*-imidazol-2-yl) (2-phenylcyclopropyl)methanone **44c** (33.0 mg, 0.10 mmol), acrylonitrile **42a** (13.3 mg, 2.5 equiv), Δ -**RhS** (1.7 mg, 2 mol%) and DIPEA (6.5 mg, 0.5 equiv) in acetone (1.0 mL, 0.1 M) under nitrogen atmosphere with blue LEDs for 24 hours, afforded 38.0 mg of **45c** (99% yield, a yellow oil) as a mixture of two diastereoisomers.

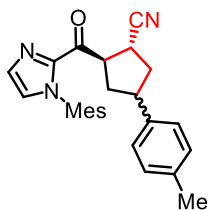
The d.r. value was determined through ^1H NMR of crude materials as 1.9:1; enantiomeric excess was established by HPLC analysis using a Chiralpak IC column, ee [major] = 99% (t_r (major) = 24.6 min, t_r (minor) = 19.5 min), ee [minor] = 99% (t_r (major) = 30.6 min, t_r (minor) = 21.6 min) (HPLC: IC, 254 nm, *n*-hexane/isopropanol = 95:5, flow rate 1 mL/min, 40 °C). $[\alpha]_D^{22} = +6.4^\circ$ (*c* 1.0, CH_2Cl_2).

^1H NMR (300 MHz, CDCl_3) δ 7.43-7.41 (m, 1H), 7.35-7.26 (m, 2H), 7.25-7.15 (m, 3H), 7.08-7.05 (m, 1H), 7.02 (br s, 1H), 6.97 (br s, 1H), 4.78-4.58 (m, 1H), 3.64-3.43 (m, 1H), 3.64-3.43 (m, 0.67H, major), 3.14-3.00 (m, 0.33H, minor), 2.95-2.83 (m, 0.67H, major), 2.65-2.54 (m, 0.33H, minor), 2.52-2.40 (m, 1H), 2.36 (s, 3H), 2.32-2.22 (m, 0.33H, minor), 2.22-2.05 (m, 1H), 1.94 (s, 3H), 1.86 (s, 1H, minor), 1.83 (s, 2H, major), 1.77-1.62 (m, 0.67H, major). (Mixture of two diastereoisomers)

^{13}C NMR (75 MHz, CDCl_3) δ 189.3, 188.6, 141.9, 141.8, 141.7, 138.8, 134.44, 134.40, 134.2, 133.70, 133.68, 131.1, 129.2, 129.0, 128.64, 128.61, 126.9, 126.85, 126.80, 126.6, 126.5, 122.4, 121.6, 52.3, 50.9, 45.4, 44.2, 40.4, 39.5, 38.8, 38.2, 28.5, 28.4, 21.1, 17.4, 17.1. (Mixture of two diastereoisomers)

IR (film): ν (cm^{-1}) 3028, 2923, 2865, 2241, 1680, 1603, 1487, 1450, 1404, 1339, 1315, 1281, 1149, 1083, 1027, 976, 909, 851, 773, 731, 698, 580, 519.

HRMS (ESI, m/z) calcd for $\text{C}_{25}\text{H}_{25}\text{N}_3\text{ONa}$ $[\text{M}+\text{Na}]^+$: 406.1890, found: 406.1887.



(1*R*,2*R*)-2-(1-Mesityl-1*H*-imidazole-2-carbonyl)-4-(*p*-tolyl)cyclopentane-1-carbonitrile (45d**)**

According to the general procedure, the reaction of (1-mesityl-1*H*-imidazol-2-yl) (2-(*p*-tolyl)cyclopropyl)methanone **44d** (34.5 mg, 0.10 mmol), acrylonitrile **42a** (13.3 mg, 2.5 equiv), Δ -**RhS** (1.7 mg, 2 mol%) and DIPEA (6.5 mg, 0.5 equiv) in acetone (1.0 mL, 0.1 M) under nitrogen atmosphere with blue LEDs for 24 hours, afforded 37.1 mg of **45d** (93% yield, a yellow oil) as a mixture of two diastereoisomers.

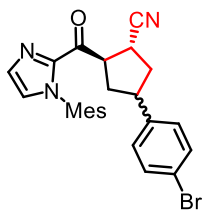
The d.r. value was determined through ^1H NMR of crude materials as 1.5:1; enantiomeric excess was established by HPLC analysis using a Chiralpak IG column, ee [major] = 98% (t_r (major) = 19.9 min, t_r (minor) = 17.8 min), ee [minor] = 99% (t_r (major) = 23.0 min, t_r (minor) = 18.7 min) (HPLC: IG, 254 nm, *n*-hexane/isopropanol = 90:10, flow rate 1 mL/min, 40 °C). $[\alpha]_D^{22} = +22.8^\circ$ (*c* 1.0, CH_2Cl_2).

^1H NMR (300 MHz, CDCl_3) δ 7.42-7.40 (m, 1H), 7.14-7.04 (m, 5H), 7.01 (br s, 1H), 6.97 (br s, 1H), 4.76-4.58 (m, 1H), 3.63-3.55 (m, 0.6H, major), 3.55-3.42 (m, 1H), 3.10-2.95 (m, 0.4H, minor), 2.92-2.80 (m, 0.6H, major), 2.62-2.51 (m, 0.4H, minor), 2.49-2.38 (m, 1H), 2.36 (s, 3H), 2.32 (s, 1.2H, minor), 2.31 (s, 1.8H, major), 2.28-2.19 (m, 0.4H, minor), 2.18-2.04 (m, 1H), 1.94 (s, 3H), 1.85 (s, 1.2H, minor), 1.82 (s, 1.8H, major), 1.75-1.60 (m, 0.6H, major). (Mixture of two diastereoisomers)

^{13}C NMR (75 MHz, CDCl_3) δ 189.3, 188.7, 142.0, 141.9, 138.80, 138.77, 138.6, 136.44, 136.40, 134.45, 134.41, 134.2, 133.7, 131.0, 129.30, 129.27, 129.2, 129.1, 128.974, 128.965, 126.8, 126.7, 126.52, 126.49, 122.5, 121.7, 52.3, 50.9, 45.0, 43.8, 40.5, 39.6, 38.8, 38.3, 28.41, 28.39, 21.1, 20.9, 17.4, 17.1. (Mixture of two diastereoisomers)

IR (film): ν (cm^{-1}) 3112, 3016, 2922, 2866, 2240, 1680, 1511, 1484, 1450, 1404, 1341, 1315, 1281, 1148, 1083, 1025, 976, 909, 851, 811, 780, 729, 672, 649, 578, 523, 443.

HRMS (ESI, m/z) calcd for $\text{C}_{26}\text{H}_{27}\text{N}_3\text{ONa}$ $[\text{M}+\text{Na}]^+$: 420.2046, found: 420.2044.



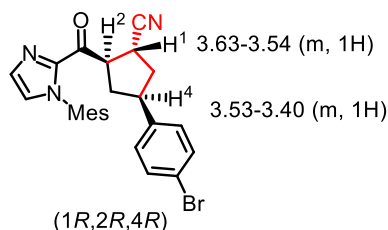
(1*R*,2*R*)-4-(4-Bromophenyl)-2-(1-mesityl-1*H*-imidazole-2-carbonyl)cyclopentane-1-carbonitrile (45e)

According to the general procedure, the reaction of (2-(4-bromophenyl)cyclopropyl) (1-mesityl-1*H*-imidazol-2-yl)methanone **44e** (40.9 mg, 0.10 mmol), acrylonitrile **42a** (13.3 mg, 2.5 equiv), Δ -**RhS** (1.7 mg, 2 mol%) and DIPEA (6.5 mg, 0.5 equiv) in acetone (1.0 mL, 0.1 M) under nitrogen atmosphere with blue LEDs for 24 hours, afforded 38.0 mg of **45e** (90% total yield) as two separable diastereoisomers.

The d.r. value was determined through ^1H NMR of crude materials as 1.3:1.

The major diastereoisomer:

4.68-4.58 (m, 1H)



Enantiomeric excess was established by HPLC analysis using a Chiralpak IG column, ee [major] = 98% (HPLC: IG, 254 nm, *n*-hexane/isopropanol = 70:30, flow rate 1 mL/min, 25 °C, t_r (major) = 16.7 min, t_r (minor) = 12.8 min). $[\alpha]_D^{22} = +25.4^\circ$ (c 1.0, CH_2Cl_2).

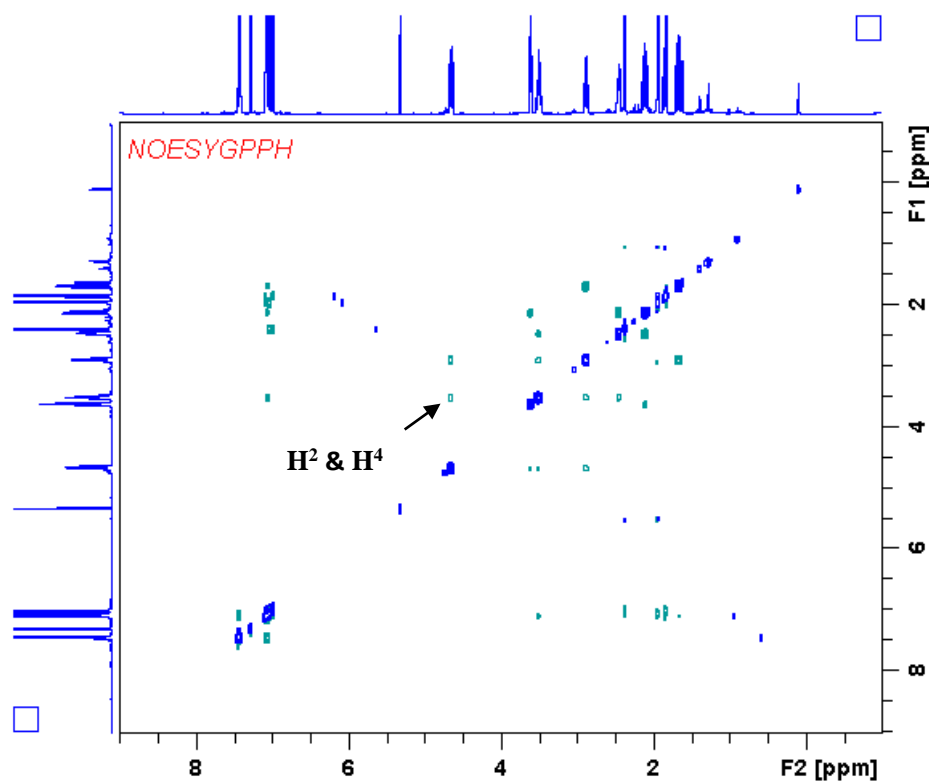
^1H NMR (300 MHz, CDCl_3) δ 7.44-7.37 (m, 3H), 7.08-7.02 (m, 3H), 7.03 (br s, 1H), 6.97 (br s, 1H), 4.68-4.58 (m, 1H), 3.63-3.54 (m, 1H), 3.53-3.40 (m, 1H), 2.92-2.80 (m, 1H), 2.48-2.38 (m, 1H), 2.36 (s, 3H), 2.15-2.02 (m, 1H), 1.92 (s, 3H), 1.82 (s, 3H), 1.72-1.58 (m, 1H).

^{13}C NMR (75 MHz, CDCl_3) δ 188.5, 141.9, 140.8, 138.9, 134.4, 134.2, 133.7, 131.7, 131.1, 129.2, 129.0, 128.6, 126.7, 122.2, 120.6, 52.1, 44.8, 40.2, 38.1, 28.6, 21.1, 17.4, 17.2.

IR (film): ν (cm^{-1}) 3114, 2923, 2863, 2241, 1680, 1487, 1451, 1403, 1340, 1314, 1282, 1149, 1078, 1034, 1011, 976, 909, 851, 819, 781, 730, 672, 650, 581, 519.

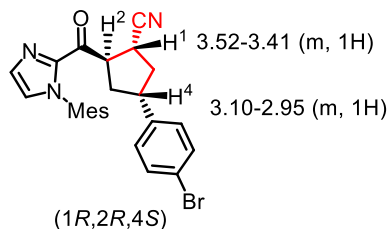
HRMS (ESI, m/z) calcd for $\text{C}_{25}\text{H}_{25}\text{BrN}_3\text{O}$ $[\text{M}+\text{H}]^+$: 462.1176, found: 462.1175.

NOE spectrum:



The minor diastereoisomer:

4.75-4.65 (m, 1H)



Enantiomeric excess was established by HPLC analysis using a Chiralpak IG column, ee [minor] = 99% (HPLC: IG, 254 nm, *n*-hexane/isopropanol = 70:30, flow rate 1 mL/min, 25 °C, t_r (major) = 18.6 min, t_r (minor) = 13.8 min). $[\alpha]_D^{22} = +74.2^\circ$ (c 1.0, CH_2Cl_2).

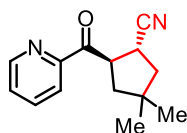
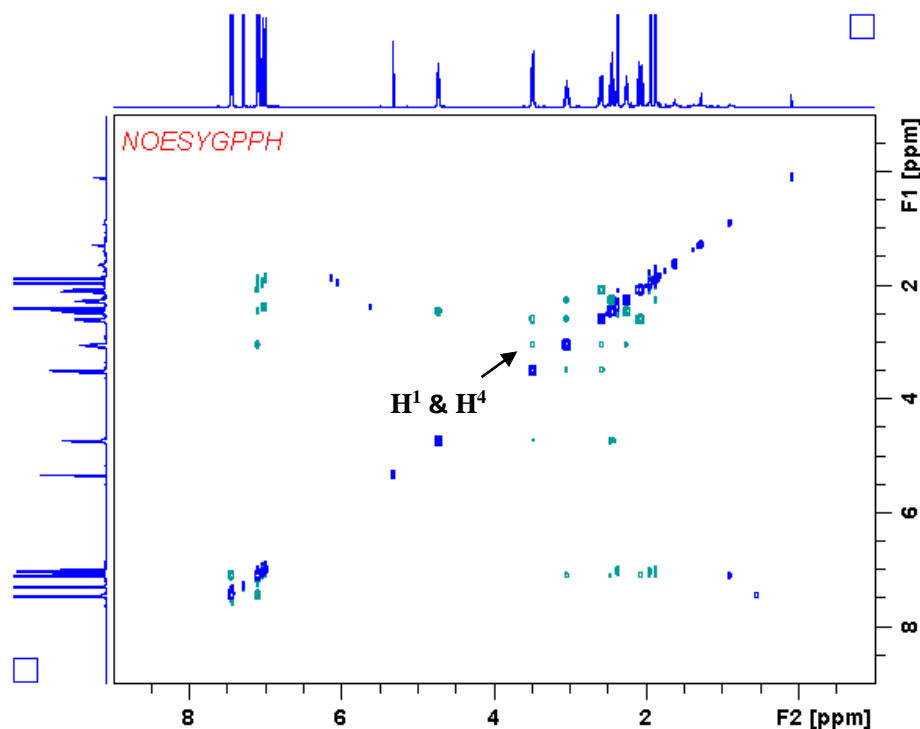
^1H NMR (300 MHz, CDCl_3) δ 7.46-7.40 (m, 3H), 7.10-7.04 (m, 3H), 7.01 (br s, 1H), 6.98 (br s, 1H), 4.75-4.65 (m, 1H), 3.52-3.41 (m, 1H), 3.10-2.95 (m, 1H), 2.62-2.51 (m, 1H), 2.50-2.37 (m, 1H), 2.36 (s, 3H), 2.29-2.18 (m, 1H), 2.12-1.98 (m, 1H), 1.92 (s, 3H), 1.85 (s, 3H).

^{13}C NMR (75 MHz, CDCl_3) δ 189.1, 141.8, 140.7, 138.9, 134.4, 134.2, 133.7, 131.8, 131.1, 129.2, 129.0, 128.6, 126.6, 121.4, 120.6, 50.8, 43.6, 39.3, 38.6, 28.5, 21.1, 17.4, 17.2.

IR (film): ν (cm^{-1}) 2916, 2858, 2240, 1676, 1486, 1448, 1403, 1320, 1279, 1145, 1075, 1011, 977, 912, 848, 818, 787, 737, 660, 585, 551, 513.

HRMS (ESI, m/z) calcd for $C_{25}H_{25}BrN_3O$ $[M+H]^+$: 462.1176, found: 462.1176.

NOE spectrum:



((1*R*,2*R*)-4,4-Dimethyl-2-picolinoylcyclopentane-1-carbonitrile (45f))

According to the general procedure, the mixture of (2,2-dimethylcyclopropyl)(pyridin-2-yl) methanone **44f** (17.5 mg, 0.10 mmol), acrylonitrile **42a** (13.3 mg, 2.5 equiv), Δ -**RhS** (3.5 mg, 4 mol%) and DIPEA (25.8 mg, 2.0 equiv) in acetone/MeCN (1:1 v/v, 1.0 mL, 0.1 M) were stirred under nitrogen atmosphere with blue LEDs for 24 hours; then, another portion of Δ -**RhS** (3.5 mg, 4 mol%) was added and the mixture was continued to stir for another 20 hours. The reaction afforded 12.4 mg (54% yield) of the major diastereoisomer of **45f** as a colorless oil.

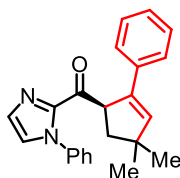
The d.r. value was determined through ^1H NMR of crude materials as 6:1, therefore the total yield is estimated as 63%. Enantiomeric excess of the major diastereoisomer was established by HPLC analysis using a Chiralpak IG column, ee = 94% (HPLC: IG, 254 nm, *n*-hexane/isopropanol = 95:5, flow rate 1 mL/min, 25 °C, t_r (major) = 19.4 min, t_r (minor) = 20.4 min). $[\alpha]_D^{22} = -106.4^\circ$ (*c* 1.0, CH_2Cl_2).

^1H NMR (500 MHz, CDCl_3) δ 8.75-8.71 (m, 1H), 8.12-8.08 (m, 1H), 7.88 (td, $J_1 = 7.7$ Hz, $J_2 = 1.8$ Hz, 1H), 7.52 (ddd, $J_1 = 7.6$ Hz, $J_2 = 4.7$ Hz, $J_3 = 1.2$ Hz, 1H), 4.76 (q, $J = 9.0$ Hz, 1H), 3.66 (q, $J = 8.5$ Hz, 1H), 2.28 (dd, $J_1 = 13.0$ Hz, $J_2 = 9.8$ Hz, 1H), 2.06 (dd, $J_1 = 12.9$ Hz, $J_2 = 8.9$ Hz, 1H), 1.96 (ddd, $J_1 = 12.9$ Hz, $J_2 = 8.2$ Hz, $J_3 = 0.5$ Hz, 1H), 1.51 (dd, $J_1 = 13.0$ Hz, $J_2 = 9.0$ Hz, 1H), 1.25 (s, 3H), 1.04 (s, 3H).

^{13}C NMR (125 MHz, CDCl_3) δ 199.9, 152.1, 149.2, 136.9, 127.5, 122.8, 122.7, 50.6, 45.5, 45.2, 40.4, 28.6, 28.4, 28.0.

IR (film): ν (cm^{-1}) 2957, 2869, 2239, 1694, 1579, 1461, 1441, 1365, 1298, 1220, 1018, 850, 797, 744, 685, 615.

HRMS (ESI, m/z) calcd for $\text{C}_{14}\text{H}_{16}\text{N}_2\text{ONa}$ $[\text{M}+\text{Na}]^+$: 251.1155, found: 251.1155.



(R)-(4,4-Dimethyl-2-phenylcyclopent-2-en-1-yl)(1-phenyl-1H-imidazol-2-yl)methanone (47a)

According to the general procedure, as shown in **Table 18**, entry 9, the reaction of (2,2-dimethylcyclopropyl)(1-phenyl-1H-imidazol-2-yl)methanone **41a** (12.0 mg, 0.05 mmol), ethynylbenzene **46a** (25.6 mg, 5.0 equiv), Δ -**RhS** (1.7 mg, 4 mol%) and Et_3N (10.1 mg, 2.0 equiv) in THF (0.5 mL, 0.1 M) under nitrogen atmosphere with blue LEDs for 24 hours, afforded 15.8 mg (92% yield, 95% NMR yield) of **47a** as a colorless oil.

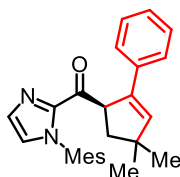
The enantiomeric excess was established by HPLC analysis using a Chiralpak OD-H column, ee = 89% (HPLC: OD-H, 254 nm, *n*-hexane/isopropanol = 98:2, flow rate 1 mL/min, 25 °C, t_r (major) = 8.9 min, t_r (minor) = 8.3 min). $[\alpha]_D^{22} = +90.6^\circ$ (*c* 1.0, CH_2Cl_2).

^1H NMR (300 MHz, CDCl_3) δ 7.36-7.29 (m, 6H), 7.25-7.12 (m, 4H), 7.10-7.04 (m, 2H), 6.09 (d, $J = 1.5$ Hz, 1H), 5.62 (ddd, $J_1 = 9.6$ Hz, $J_2 = 6.3$ Hz, $J_3 = 1.8$ Hz, 1H), 2.39 (dd, $J_1 = 12.9$ Hz, $J_2 = 9.3$ Hz, 1H), 1.96 (dd, $J_1 = 12.9$ Hz, $J_2 = 6.0$ Hz, 1H), 1.19 (s, 3H), 1.18 (s, 3H).

^{13}C NMR (75 MHz, CDCl_3) δ 193.2, 143.5, 140.5, 138.8, 138.2, 135.9, 129.7, 128.9, 128.5, 128.2, 127.1, 126.9, 126.1, 125.5, 53.4, 45.4, 44.6, 29.1, 28.9.

IR (film): ν (cm⁻¹) 3057, 3030, 2953, 2862, 1683, 1596, 1496, 1445, 1398, 1309, 1045, 906, 828, 757, 691, 554, 516.

HRMS (ESI, m/z) calcd for C₂₃H₂₃N₂O [M+H]⁺: 343.1805, found: 343.1813.



(R)-(4,4-Dimethyl-2-phenylcyclopent-2-en-1-yl)(1-mesityl-1H-imidazol-2-yl)methanone (47b)

According to the general procedure, as shown in **Table 18**, entry 16, the reaction of (2,2-dimethylcyclopropyl)(1-mesityl-1H-imidazol-2-yl)methanone **41e** (14.1 mg, 0.05 mmol), ethynylbenzene **46a** (25.6 mg, 5.0 equiv), Δ -**RhS** (1.7 mg, 4 mol%) and Et₃N (10.1 mg, 2.0 equiv) in THF (0.5 mL, 0.1 M) under nitrogen atmosphere with blue LEDs for 22 hours, afforded 18.3 mg (95% yield, 99% NMR yield) of **47b** as a colorless oil.

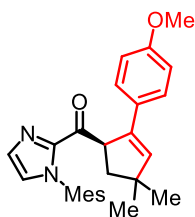
The enantiomeric excess was established by HPLC analysis using a Chiralpak OD-H column, ee = 98% (HPLC: OD-H, 254 nm, *n*-hexane/isopropanol = 98:2, flow rate 1 mL/min, 25 °C, t_r (major) = 6.1 min, t_r (minor) = 5.7 min). $[\alpha]_D^{22} = +62.8^\circ$ (*c* 1.0, CH₂Cl₂).

¹H NMR (300 MHz, CDCl₃) δ 7.44-7.42 (m, 1H), 7.32-7.27 (m, 2H), 7.19-7.07 (m, 3H), 7.01-6.98 (m, 1H), 6.88 (br s, 1H), 6.80 (br s, 1H), 6.05 (d, $J = 1.5$ Hz, 1H), 5.65 (ddd, $J_1 = 9.3$ Hz, $J_2 = 6.0$ Hz, $J_3 = 1.5$ Hz, 1H), 2.37 (dd, $J_1 = 12.9$ Hz, $J_2 = 9.6$ Hz, 1H), 2.25 (s, 3H), 1.90 (dd, $J_1 = 12.9$ Hz, $J_2 = 6.3$ Hz, 1H), 1.85 (s, 3H), 1.60 (s, 3H), 1.18 (s, 3H), 1.14 (s, 3H).

¹³C NMR (75 MHz, CDCl₃) δ 193.0, 143.3, 140.3, 138.9, 138.2, 135.8, 134.8, 134.1, 133.7, 130.3, 128.9, 128.7, 128.1, 126.8, 126.0, 52.9, 45.4, 44.8, 29.1, 28.8, 21.0, 17.2, 16.9. (Missing one ¹³C signal)

IR (film): ν (cm⁻¹) 3027, 2954, 2926, 2862, 1681, 1488, 1447, 1399, 1316, 1283, 1147, 1039, 906, 849, 761, 692, 577.

HRMS (ESI, m/z) calcd for C₂₆H₂₉N₂O [M+H]⁺: 385.2274, found: 385.2266.



(R)-(1-Mesityl-1H-imidazol-2-yl)(2-(4-methoxyphenyl)-4,4-dimethylcyclopent-2-en-1-yl)methanone (47c)

According to the general procedure, the reaction of (2,2-dimethylcyclopropyl)(1-mesityl-1H-imidazol-2-yl)methanone **41e** (28.2 mg, 0.10 mmol), 1-ethynyl-4-methoxybenzene **46b** (66.1 mg, 5.0 equiv), Δ -**RhS** (3.5 mg, 4 mol%) and Et₃N (20.2 mg, 2.0 equiv) in THF (1.0 mL, 0.1 M) under nitrogen atmosphere with blue LEDs for 24 hours, afforded 39.2 mg (95% yield) of **47c** as an oil.

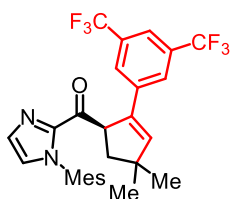
The enantiomeric excess was established by HPLC analysis using a Chiralpak OD-H column, ee = 97% (HPLC: OD-H, 254 nm, *n*-hexane/isopropanol = 95:5, flow rate 1 mL/min, 25 °C, *t_r* (major) = 8.5 min, *t_r* (minor) = 5.8 min). [α]_D²² = +36.0° (*c* 1.0, CH₂Cl₂).

¹H NMR (300 MHz, CDCl₃) δ 7.44-7.41 (m, 1H), 7.26-7.20 (m, 2H), 7.01-6.99 (m, 1H), 6.88 (br s, 1H), 6.81 (br s, 1H), 6.74-6.76 (m, 2H), 5.93 (d, *J* = 1.8 Hz, 1H), 5.60 (ddd, *J*₁ = 9.6 Hz, *J*₂ = 6.3 Hz, *J*₃ = 1.8 Hz, 1H), 3.74 (s, 3H), 2.35 (dd, *J*₁ = 12.6 Hz, *J*₂ = 9.3 Hz, 1H), 2.26 (s, 3H), 1.88 (dd, *J*₁ = 12.9 Hz, *J*₂ = 6.3 Hz, 1H), 1.85 (s, 3H), 1.62 (s, 3H), 1.16 (s, 3H), 1.12 (s, 3H).

¹³C NMR (75 MHz, CDCl₃) δ 193.1, 158.6, 143.3, 138.5, 138.2, 134.8, 134.1, 133.7, 130.3, 128.9, 128.75, 128.67, 127.2, 126.0, 113.6, 55.2, 53.0, 45.4, 44.8, 29.3, 29.0, 21.0, 17.2, 16.9. (Missing one ¹³C signal)

IR (film): ν (cm⁻¹) 2951, 2925, 2861, 1682, 1607, 1510, 1487, 1451, 1400, 1288, 1248, 1177, 1035, 906, 829, 777, 730, 582, 555, 522.

HRMS (ESI, *m/z*) calcd for C₂₇H₃₁N₂O₂ [M+H]⁺: 415.2380, found: 415.2380.



(R)-(2-(3,5-Bis(trifluoromethyl)phenyl)-4,4-dimethylcyclopent-2-en-1-yl)(1-mesityl-1H-imidazol-2-yl)methanone (47d)

According to the general procedure, the reaction of (2,2-dimethylcyclopropyl)(1-mesityl-1*H*-imidazol-2-yl)methanone **41e** (28.2 mg, 0.10 mmol), 1-ethynyl-3,5-bis(trifluoromethyl)benzene **46c** (59.5 mg, 2.5 equiv), Δ -**RhS** (3.5 mg, 4 mol%) and Et₃N (20.2 mg, 2.0 equiv) in acetone (1.0 mL, 0.1 M) under nitrogen atmosphere with blue LEDs for 24 hours, afforded 35.0 mg (67% yield) of **47d** as an oil.

The enantiomeric excess was established by HPLC analysis using a Chiralpak OD-H column, ee = 95% (HPLC: OD-H, 254 nm, *n*-hexane/isopropanol = 98:2, flow rate 1 mL/min, 25 °C, *t_r* (major) = 3.6 min, *t_r* (minor) = 4.0 min). [α]_D²² = +69.8° (*c* 1.0, CH₂Cl₂).

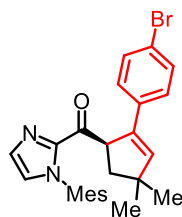
¹H NMR (300 MHz, CDCl₃) δ 7.75 (s, 2H), 7.60 (s, 1H), 7.46 (d, *J* = 1.5 Hz, 1H), 7.42 (d, *J* = 1.5 Hz, 1H), 6.89 (br s, 1H), 6.82 (br s, 1H), 6.23 (d, *J* = 1.5 Hz, 1H), 5.72 (ddd, *J*₁ = 9.6 Hz, *J*₂ = 6.3 Hz, *J*₃ = 1.8 Hz, 1H), 2.41 (dd, *J*₁ = 12.6 Hz, *J*₂ = 9.3 Hz, 1H), 2.26 (s, 3H), 1.98 (dd, *J*₁ = 12.9 Hz, *J*₂ = 6.6 Hz, 1H), 1.85 (s, 3H), 1.51 (s, 3H), 1.20 (s, 3H), 1.18 (s, 3H).

¹³C NMR (125 MHz, CDCl₃) δ 192.1, 144.2, 142.8, 138.5, 138.0, 136.8, 134.6, 133.9, 133.6, 131.4 (q, *J* = 32.8 Hz), 130.7, 129.0, 128.8, 126.5, 126.1-126.0 (m), 123.3 (q, *J* = 271.2 Hz), 120.4-120.2 (m, 1H), 52.7, 45.7, 44.5, 28.7, 28.6, 21.0, 17.2, 16.5.

¹⁹F NMR (282 MHz, CDCl₃) δ -63.00 (s, 6F).

IR (film): ν (cm⁻¹) 2958, 2930, 2866, 1681, 1451, 1385, 1275, 1172, 1130, 1035, 899, 857, 777, 735, 680, 579.

HRMS (ESI, *m/z*) calcd for C₂₈H₂₇F₆N₂O [M+H]⁺: 521.2022, found: 521.2013.



(*R*)-(2-(4-Bromophenyl)-4,4-dimethylcyclopent-2-en-1-yl)(1-mesityl-1*H*-imidazol-2-yl)methanone (47e**)**

According to the general procedure, the reaction of (2,2-dimethylcyclopropyl)(1-mesityl-1*H*-imidazol-2-yl)methanone **41e** (28.2 mg, 0.10 mmol), 1-bromo-4-ethynylbenzene **46d** (90.5 mg, 5.0 equiv), Δ -**RhS** (6.9 mg, 8 mol%) and Et₃N (20.2 mg, 2.0 equiv) in PhCl (1.0 mL, 0.1 M) under

nitrogen atmosphere with blue LEDs for 24 hours, afforded 44.8 mg (97% yield) of **47e** as a grey solid.

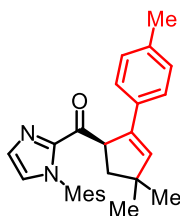
The enantiomeric excess was established by HPLC analysis using a Chiralpak OD-H column, ee = 98% (HPLC: OD-H, 254 nm, *n*-hexane/isopropanol = 98:2, flow rate 1 mL/min, 25 °C, *t_r* (major) = 7.1 min, *t_r* (minor) = 6.1 min). $[\alpha]_{\text{D}}^{22} = +12.6^{\circ}$ (*c* 1.0, CH₂Cl₂).

¹H NMR (300 MHz, CDCl₃) δ 7.44-7.41 (m, 1H), 7.32-7.25 (m, 2H), 7.20-7.13 (m, 2H), 7.03-7.00 (m, 1H), 6.89 (br s, 1H), 6.84 (br s, 1H), 6.05 (d, *J* = 1.5 Hz, 1H), 5.61 (ddd, *J₁* = 9.3 Hz, *J₂* = 6.0 Hz, *J₃* = 1.5 Hz, 1H), 2.37 (dd, *J₁* = 12.6 Hz, *J₂* = 9.3 Hz, 1H), 2.27 (s, 3H), 1.90 (dd, *J₁* = 12.9 Hz, *J₂* = 6.0 Hz, 1H), 1.85 (s, 3H), 1.63 (s, 3H), 1.18 (s, 3H), 1.13 (s, 3H).

¹³C NMR (75 MHz, CDCl₃) δ 192.7, 143.2, 141.2, 138.3, 137.9, 134.9, 134.7, 134.0, 133.7, 131.2, 130.4, 128.9, 128.8, 127.7, 126.2, 120.6, 52.9, 45.5, 44.7, 29.0, 28.7, 21.0, 17.2, 16.9.

IR (film): ν (cm⁻¹) 3030, 2953, 2926, 2862, 1681, 1485, 1448, 1399, 1319, 1281, 1147, 1071, 1042, 1010, 904, 822, 774, 734, 700, 673, 578, 552, 516, 435.

HRMS (ESI, *m/z*) calcd for C₂₆H₂₈BrN₂O [M+H]⁺: 463.1380, found: 463.1377.



(R)-(4,4-Dimethyl-2-(*p*-tolyl)cyclopent-2-en-1-yl)(1-mesityl-1*H*-imidazol-2-yl)methanone (47f**)**

According to the general procedure, the reaction of (2,2-dimethylcyclopropyl)(1-mesityl-1*H*-imidazol-2-yl)methanone **41e** (28.2 mg, 0.10 mmol), 1-ethynyl-4-methylbenzene **46e** (29.1 mg, 2.5 equiv), Δ -**RhS** (3.5 mg, 4 mol%) and Et₃N (20.2 mg, 2.0 equiv) in THF (1.0 mL, 0.1 M) under nitrogen atmosphere with blue LEDs for 28 hours, afforded 34.6 mg (87% yield) of **47f** as an oil.

The enantiomeric excess was established by HPLC analysis using a Chiralpak OD-H column, ee = 98% (HPLC: OD-H, 254 nm, *n*-hexane/isopropanol = 98:2, flow rate 1 mL/min, 25 °C, *t_r* (major) = 6.8 min, *t_r* (minor) = 5.1 min). $[\alpha]_{\text{D}}^{22} = +36.0^{\circ}$ (*c* 1.0, CH₂Cl₂).

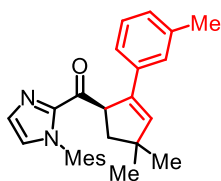
¹H NMR (300 MHz, CDCl₃) δ 7.43 (s, 1H), 7.19 (d, *J* = 8.1 Hz, 2H), 7.00 (s, 1H), 6.97 (d, *J* = 8.1 Hz, 2H), 6.88 (br s, 1H), 6.81 (br s, 1H), 6.00 (d, *J* = 1.2 Hz, 1H), 5.62 (ddd, *J₁* = 9.6 Hz, *J₂* = 6.3 Hz, *J₃* =

1.5 Hz, 1H), 2.36 (dd, $J_1 = 12.6$ Hz, $J_2 = 9.3$ Hz, 1H), 2.25 (s, 6H), 1.87 (dd, $J_1 = 12.9$ Hz, $J_2 = 6.0$ Hz, 1H), 1.85 (s, 3H), 1.62 (s, 3H), 1.17 (s, 3H), 1.13 (s, 3H).

^{13}C NMR (75 MHz, CDCl_3) δ 193.0, 143.3, 139.4, 138.6, 138.2, 136.5, 134.8, 134.1, 133.7, 133.0, 130.2, 128.9, 128.8, 128.7, 126.0, 125.9, 53.0, 45.3, 44.8, 29.2, 28.9, 21.03, 20.98, 17.2, 16.9.

IR (film): ν (cm^{-1}) 3025, 2952, 2925, 2863, 1681, 1508, 1486, 1448, 1399, 1316, 1283, 1041, 906, 848, 816, 775, 729, 578, 516.

HRMS (ESI, m/z) calcd for $\text{C}_{27}\text{H}_{31}\text{N}_2\text{O}$ $[\text{M}+\text{H}]^+$: 399.2431, found: 399.2431.



(R)-(4,4-Dimethyl-2-(*m*-tolyl)cyclopent-2-en-1-yl)(1-mesityl-1*H*-imidazol-2-yl)methanone (47g)

According to the general procedure, the reaction of (2,2-dimethylcyclopropyl)(1-mesityl-1*H*-imidazol-2-yl)methanone **41e** (28.2 mg, 0.10 mmol), 1-ethynyl-3-methylbenzene **46f** (58.1 mg, 5.0 equiv), Δ -**RhS** (3.5 mg, 4 mol%) and Et_3N (20.2 mg, 2.0 equiv) in PhCl (1.0 mL, 0.1 M) under nitrogen atmosphere with blue LEDs for 22 hours, afforded 39.0 mg (98% yield) of **47g** as an oil.

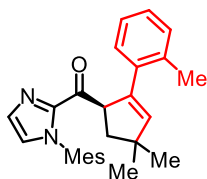
The enantiomeric excess was established by HPLC analysis using a Chiralpak OD-H column, ee = 95% (HPLC: OD-H, 254 nm, *n*-hexane/isopropanol = 99:1, flow rate 0.6 mL/min, 40 °C, t_r (major) = 8.8 min, t_r (minor) = 9.6 min). $[\alpha]_{\text{D}}^{22} = +60.0^\circ$ (c 1.0, CH_2Cl_2).

^1H NMR (300 MHz, CDCl_3) δ 7.44 (d, $J = 0.9$ Hz, 1H), 7.14 (br s, 1H), 7.13-7.07 (m, 1H), 7.04 (t, $J = 7.5$ Hz, 1H), 7.00 (d, $J = 0.6$ Hz, 1H), 6.95-6.89 (m, 1H), 6.88 (br s, 1H), 6.80 (br s, 1H), 6.04 (d, $J = 1.8$ Hz, 1H), 5.66 (ddd, $J_1 = 9.0$ Hz, $J_2 = 6.0$ Hz, $J_3 = 1.5$ Hz, 1H), 2.36 (dd, $J_1 = 12.6$ Hz, $J_2 = 9.3$ Hz, 1H), 2.26 (s, 3H), 2.21 (s, 3H), 1.90 (dd, $J_1 = 12.9$ Hz, $J_2 = 6.3$ Hz, 1H), 1.86 (s, 3H), 1.58 (s, 3H), 1.17 (s, 3H), 1.15 (s, 3H).

^{13}C NMR (75 MHz, CDCl_3) δ 193.1, 143.3, 140.1, 139.0, 138.2, 137.5, 135.7, 134.8, 134.0, 133.7, 130.3, 128.9, 128.7, 128.0, 127.6, 126.8, 126.0, 123.2, 52.9, 45.3, 44.7, 29.1, 28.9, 21.3, 21.0, 17.2, 16.8.

IR (film): ν (cm^{-1}) 3028, 2952, 2925, 2862, 1681, 1604, 1486, 1448, 1399, 1317, 1284, 1147, 1035, 910, 856, 778, 730, 695, 579, 444.

HRMS (ESI, m/z) calcd for $C_{27}H_{31}N_2O$ $[M+H]^+$: 399.2431, found: 399.2429.



(R)-(4,4-Dimethyl-2-(*o*-tolyl)cyclopent-2-en-1-yl)(1-mesityl-1*H*-imidazol-2-yl)methanone (47h)

According to the general procedure, the reaction of (2,2-dimethylcyclopropyl)(1-mesityl-1*H*-imidazol-2-yl)methanone **41e** (28.2 mg, 0.10 mmol), 1-ethynyl-2-methylbenzene **46g** (58.1 mg, 5.0 equiv), Δ -**RhS** (3.5 mg, 4 mol%) and Et_3N (20.2 mg, 2.0 equiv) in PhCl (1.0 mL, 0.1 M) under nitrogen atmosphere with blue LEDs for 22 hours, afforded 39.6 mg (99% yield) of **47h** as an oil.

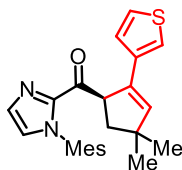
The enantiomeric excess was established by HPLC analysis using a Chiralpak IC column, ee = 99% (HPLC: IC, 254 nm, *n*-hexane/isopropanol = 99:1, flow rate 0.6 mL/min, 25 °C, t_r (major) = 12.5 min, t_r (minor) = 11.1 min). $[\alpha]_D^{22} = +90.8^\circ$ (c 1.0, CH_2Cl_2).

1H NMR (300 MHz, $CDCl_3$) δ 7.32 (d, $J = 0.9$ Hz, 1H), 7.17-7.12 (m, 1H), 7.07-6.92 (m, 3H), 6.90-6.86 (m, 2H), 6.79 (br s, 1H), 5.66 (ddd, $J_1 = J_2 = 7.8$ Hz, $J_3 = 1.8$ Hz, 1H), 5.63 (d, $J = 1.8$ Hz, 1H), 2.35 (s, 3H), 2.28 (s, 3H), 2.25 (dd, $J_1 = 12.6$ Hz, $J_2 = 8.4$ Hz, 1H), 1.97 (dd, $J_1 = 12.3$ Hz, $J_2 = 8.1$ Hz, 1H), 1.83 (s, 3H), 1.30 (s, 3H), 1.21 (s, 3H), 1.19 (s, 3H).

^{13}C NMR (75 MHz, $CDCl_3$) δ 192.9, 143.4, 143.1, 139.4, 138.1, 136.5, 135.9, 134.8, 134.1, 133.7, 130.1, 128.8, 128.7, 128.6, 126.5, 125.9, 125.1, 55.0, 45.6, 44.4, 29.0, 28.5, 21.0, 20.8, 17.2, 16.4.
(Missing one ^{13}C signal)

IR (film): ν (cm^{-1}) 3020, 2953, 2925, 2862, 1680, 1486, 1450, 1400, 1318, 1282, 1147, 1043, 907, 847, 759, 728, 673, 579, 455.

HRMS (ESI, m/z) calcd for $C_{27}H_{31}N_2O$ $[M+H]^+$: 399.2431, found: 399.2431.



(R)-(4,4-Dimethyl-2-(thiophen-3-yl)cyclopent-2-en-1-yl)(1-mesityl-1*H*-imidazol-2-yl)methanone (47i)

According to the general procedure, the reaction of (2,2-dimethylcyclopropyl)(1-mesityl-1*H*-imidazol-2-yl)methanone **41e** (28.2 mg, 0.10 mmol), 3-ethynylthiophene **46h** (54.1 mg, 5.0 equiv), Δ -**RhS** (3.5 mg, 4 mol%) and Et₃N (20.2 mg, 2.0 equiv) in PhCl (1.0 mL, 0.1 M) under nitrogen atmosphere with blue LEDs for 24 hours, afforded 33.8 mg (87% yield) of **47i** as an oil.

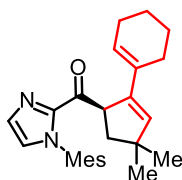
The enantiomeric excess was established by HPLC analysis using a Chiralpak IG column, ee = 97% (HPLC: IG, 254 nm, *n*-hexane/isopropanol = 90:10, flow rate 1 mL/min, 25 °C, *t_r* (major) = 5.3 min, *t_r* (minor) = 5.7 min). [α]_D²² = +34.6° (*c* 1.0, CH₂Cl₂).

¹H NMR (300 MHz, CDCl₃) δ 7.44-7.42 (m, 1H), 7.15-7.10 (m, 2H), 7.03-7.01 (m, 1H), 6.99-6.95 (m, 1H), 6.90 (br s, 1H), 6.84 (br s, 1H), 5.93 (d, *J* = 1.5 Hz, 1H), 5.57 (ddd, *J*₁ = 9.9 Hz, *J*₂ = 5.7 Hz, *J*₃ = 1.5 Hz, 1H), 2.31 (dd, *J*₁ = 13.2 Hz, *J*₂ = 9.6 Hz, 1H), 2.27 (s, 3H), 1.90 (dd, *J*₁ = 12.9 Hz, *J*₂ = 5.7 Hz, 1H), 1.86 (s, 3H), 1.66 (s, 3H), 1.16 (s, 3H), 1.15 (s, 3H).

¹³C NMR (75 MHz, CDCl₃) δ 193.2, 143.4, 139.6, 138.2, 137.8, 134.8, 134.1, 134.0, 133.7, 130.3, 128.9, 128.8, 126.3, 126.2, 125.1, 120.5, 53.5, 45.5, 44.5, 29.4, 28.9, 21.0, 17.2, 17.0.

IR (film): ν (cm⁻¹) 3028, 2952, 2863, 1680, 1485, 1448, 1398, 1315, 1281, 1147, 1039, 913, 889, 858, 773, 730, 677, 640, 577.

HRMS (ESI, *m/z*) calcd for C₂₄H₂₇N₂OS [M+H]⁺: 391.1839, found: 391.1838.



(*R*)-(2-(Cyclohex-1-en-1-yl)-4,4-dimethylcyclopent-2-en-1-yl)(1-mesityl-1*H*-imidazol-2-yl)methanone (47j**)**

According to the general procedure, the reaction of (2,2-dimethylcyclopropyl)(1-mesityl-1*H*-imidazol-2-yl)methanone **41e** (28.2 mg, 0.10 mmol), 1-ethynylcyclohex-1-ene **46i** (53.1 mg, 5.0 equiv), Δ -**RhS** (3.5 mg, 4 mol%) and Et₃N (20.2 mg, 2.0 equiv) in PhCl (1.0 mL, 0.1 M) under nitrogen atmosphere with blue LEDs for 24 hours, afforded 36.5 mg (94% yield) of **47j** as an oil.

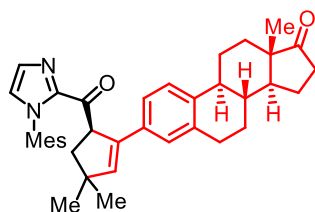
The enantiomeric excess was established by HPLC analysis using a Chiralpak OD-H column, ee = 97% (HPLC: OD-H, 254 nm, *n*-hexane/isopropanol = 98:2, flow rate 1 mL/min, 25 °C, *t_r* (major) = 4.3 min, *t_r* (minor) = 4.9 min). [α]_D²² = +126.4° (*c* 1.0, CH₂Cl₂).

^1H NMR (300 MHz, CDCl_3) δ 7.28 (d, $J = 0.9$ Hz, 1H), 6.99 (d, $J = 0.9$ Hz, 1H), 6.90 (br s, 2H), 5.60 (s, 1H), 5.47-5.41 (m, 1H), 5.30 (ddd, $J_1 = 8.7$ Hz, $J_2 = 4.5$ Hz, $J_3 = 0.9$ Hz, 1H), 2.30 (s, 3H), 2.23 (dd, $J_1 = 12.9$ Hz, $J_2 = 10.2$ Hz, 1H), 2.19-2.11 (m, 2H), 2.08-1.85 (m, 2H), 1.86 (s, 3H), 1.83 (s, 3H), 1.73 (dd, $J_1 = 13.2$ Hz, $J_2 = 4.8$ Hz, 1H), 1.66-1.55 (m, 2H), 1.54-1.44 (m, 2H), 1.09 (s, 3H), 1.04 (s, 3H).

^{13}C NMR (75 MHz, CDCl_3) δ 193.5, 143.2, 140.5, 138.2, 137.7, 135.1, 134.0, 133.8, 132.6, 130.2, 128.9, 128.8, 125.8, 125.0, 52.2, 45.2, 44.4, 29.8, 28.8, 26.1, 25.6, 22.6, 22.2, 21.0, 17.2, 17.1.

IR (film): ν (cm^{-1}) 3033, 2926, 2862, 1681, 1486, 1446, 1399, 1316, 1282, 1144, 1039, 899, 855, 805, 772, 729, 576.

HRMS (ESI, m/z) calcd for $\text{C}_{26}\text{H}_{33}\text{N}_2\text{O}$ $[\text{M}+\text{H}]^+$: 389.2587, found: 389.2587.



(8R,9S,13S,14S)-3-((R)-5-(1-Mesityl-1H-imidazole-2-carbonyl)-3,3-dimethylcyclopent-1-en-1-yl)-13-methyl-6,7,8,9,11,12,13,14,15,16-decahydro-17H-cyclopenta[*a*]phenanthren-17-one (47k)

According to the general procedure, the reaction of (2,2-dimethylcyclopropyl)(1-mesityl-1H-imidazol-2-yl)methanone **41e** (28.2 mg, 0.10 mmol), the corresponding **estrone** derived alkyne **46j** (34.8 mg, 1.25 equiv), Δ -**RhS** (6.9 mg, 8 mol%) and Et_3N (20.2 mg, 2.0 equiv) in PhCl (1.0 mL, 0.1 M) under nitrogen atmosphere with blue LEDs for 24 hours, afforded 41.8 mg (75% yield) of **47k** as a white solid.

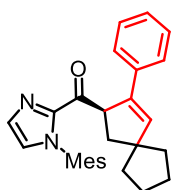
The diastereoselectivity was established by HPLC analysis using a Chiralpak IG column, d.e. = 96% (HPLC: IG, 254 nm, *n*-hexane/isopropanol = 90:10, flow rate 1 mL/min, 40 °C, t_r (major) = 18.7 min, t_r (minor) = 16.3 min). $[\alpha]_{\text{D}}^{22} = +28.6^\circ$ (c 1.0, CH_2Cl_2).

^1H NMR (300 MHz, CDCl_3) δ 7.44 (d, $J = 0.6$ Hz, 1H), 7.09-7.01 (m, 3H), 7.00 (d, $J = 0.6$ Hz, 1H), 6.88 (br s, 1H), 6.81 (br s, 1H), 6.00 (d, $J = 1.2$ Hz, 1H), 5.63 (ddd, $J_1 = 8.7$ Hz, $J_2 = 6.3$ Hz, $J_3 = 1.2$ Hz, 1H), 2.90-2.74 (m, 1H), 2.73-2.62 (m, 1H), 2.49 (dd, $J_1 = 18.6$ Hz, $J_2 = 8.7$ Hz, 1H), 2.40-2.30 (m, 2H), 2.26 (s, 3H), 2.24-1.86 (m, 5H), 1.85 (s, 3H), 1.70-1.28 (m, 7H), 1.59 (s, 3H), 1.16 (s, 3H), 1.13 (s, 3H), 0.89 (s, 3H).

^{13}C NMR (75 MHz, CDCl_3) δ 193.1, 143.3, 139.7, 138.7, 138.4, 138.2, 135.9, 134.8, 133.9, 133.8, 133.3, 130.2, 128.9, 128.8, 126.6, 126.0, 125.1, 123.6, 52.9, 50.5, 47.9, 45.3, 44.8, 44.3, 38.2, 35.8, 31.6, 29.7, 29.3, 29.0, 28.8, 26.5, 25.7, 21.5, 21.0, 17.2, 16.8, 13.8.

IR (film): ν (cm^{-1}) 2925, 2861, 1736, 1682, 1491, 1450, 1401, 1318, 1285, 1256, 1148, 1086, 1043, 910, 854, 825, 774, 728, 675, 646, 579, 433.

HRMS (ESI, m/z) calcd for $\text{C}_{38}\text{H}_{45}\text{N}_2\text{O}_2$ $[\text{M}+\text{H}]^+$: 561.3476, found: 561.3475.



(R)-(1-Mesityl-1H-imidazol-2-yl)(3-phenylspiro[4.4]non-3-en-2-yl)methanone (47I)

According to the general procedure, the reaction of (1-mesityl-1H-imidazol-2-yl)(spiro[2.4]heptan-1-yl)methanone **41g** (30.8 mg, 0.10 mmol), ethynylbenzene **46a** (51.1 mg, 5.0 equiv), Δ -RhS (3.5 mg, 4 mol%) and Et_3N (20.2 mg, 2.0 equiv) in PhCl (1.0 mL, 0.1 M) under nitrogen atmosphere with blue LEDs for 24 hours, afforded 37.9 mg (92% yield) of **47I** as an oil.

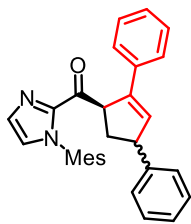
The enantiomeric excess was established by HPLC analysis using a Chiralpak OD-H column, ee = 98% (HPLC: OD-H, 254 nm, *n*-hexane/isopropanol = 98:2, flow rate 1 mL/min, 25 °C, t_r (major) = 7.8 min, t_r (minor) = 6.1 min). $[\alpha]_D^{22} = +182.2^\circ$ (c 1.0, CH_2Cl_2).

^1H NMR (300 MHz, CDCl_3) δ 7.43 (d, J = 1.2 Hz, 1H), 7.34-7.27 (m, 2H), 7.21-7.06 (m, 3H), 7.00 (d, J = 0.9 Hz, 1H), 6.88 (br s, 1H), 6.80 (br s, 1H), 6.14 (d, J = 1.5 Hz, 1H), 5.61 (ddd, J_1 = 9.6 Hz, J_2 = 5.7 Hz, J_3 = 1.5 Hz, 1H), 2.44 (dd, J_1 = 12.9 Hz, J_2 = 9.6 Hz, 1H), 2.26 (s, 3H), 1.94 (dd, J_1 = 12.9 Hz, J_2 = 5.7 Hz, 1H), 1.86 (s, 3H), 1.73-1.60 (m, 7H), 1.61 (s, 3H), 1.57-1.44 (m, 1H).

^{13}C NMR (75 MHz, CDCl_3) δ 192.9, 143.3, 139.2, 138.6, 138.2, 135.8, 134.8, 134.0, 133.7, 130.3, 128.9, 128.7, 128.1, 126.8, 126.00, 125.96, 56.7, 52.7, 43.8, 39.7, 39.5, 24.5, 24.4, 21.0, 17.2, 16.9.

IR (film): ν (cm^{-1}) 3027, 2947, 2861, 1681, 1488, 1446, 1399, 1316, 1283, 1146, 1036, 908, 850, 764, 730, 692, 646, 559.

HRMS (ESI, m/z) calcd for $\text{C}_{28}\text{H}_{31}\text{N}_2\text{O}$ $[\text{M}+\text{H}]^+$: 411.2431, found: 411.2429.

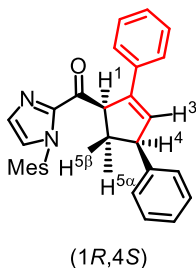


(R)-(2,4-Diphenylcyclopent-2-en-1-yl)(1-mesityl-1H-imidazol-2-yl)methanone (47m)

According to the general procedure, the reaction of (1-mesityl-1H-imidazol-2-yl)(2-phenylcyclopropyl)methanone **44c** (33.0 mg, 0.10 mmol), ethynylbenzene **46a** (51.1 mg, 5.0 equiv), Δ -RhS (6.9 mg, 8 mol%) and Et₃N (20.2 mg, 2.0 equiv) in PhCl (1.0 mL, 0.1 M) under nitrogen atmosphere with blue LEDs for 24 hours, afforded 27.1 mg of **47m** (63% total yield) as two separable diastereoisomers.

The d.r. value was determined through ¹H NMR of crude materials as 1.7:1.

The major diastereoisomer:



Enantiomeric excess was established by HPLC analysis using a Chiralpak IG column, ee [major] = 94% (HPLC: IG, 254 nm, *n*-hexane/isopropanol = 98:2, flow rate 1 mL/min, 40 °C, *t_r* (major) = 18.5 min, *t_r* (minor) = 15.0 min). [α]_D²² = +109.4° (*c* 1.0, CH₂Cl₂).

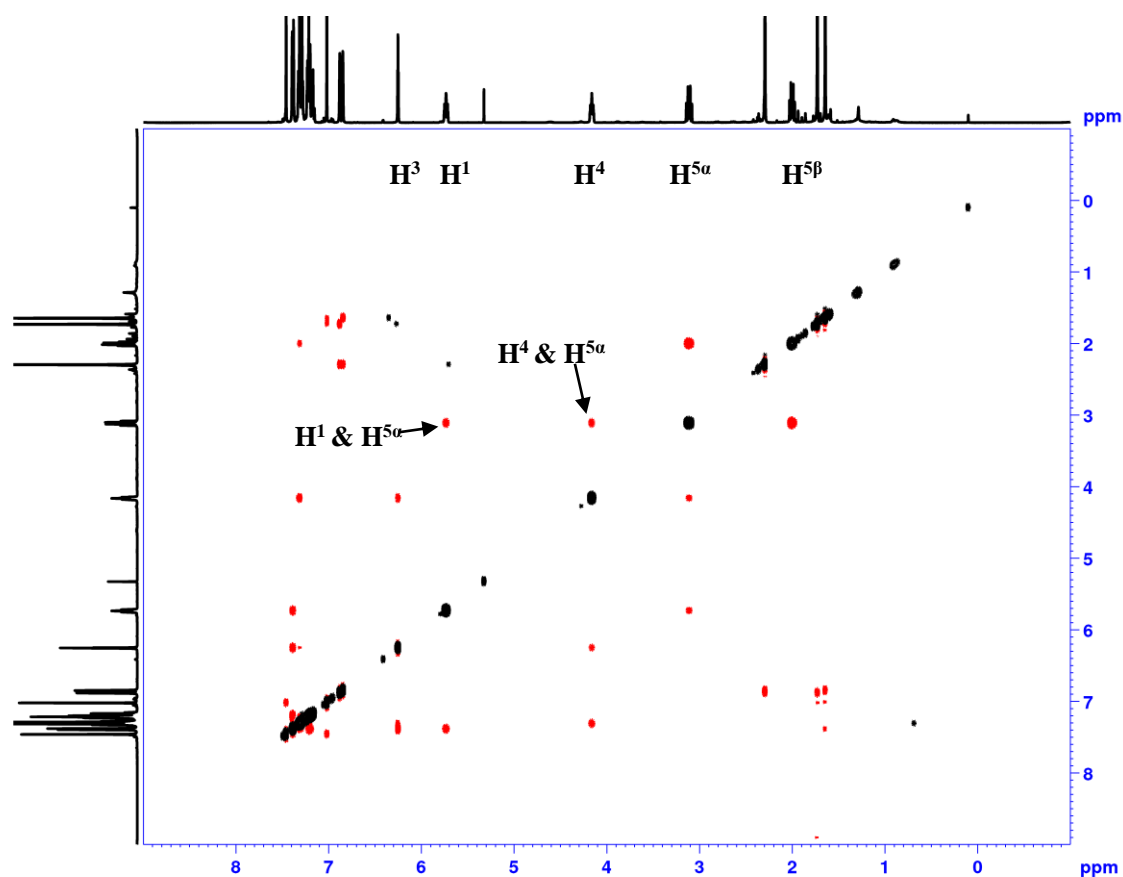
¹H NMR (500 MHz, CDCl₃) δ 7.44-7.42 (m, 1H), 7.38-7.34 (m, 2H), 7.31-7.24 (m, 4H), 7.22-7.17 (m, 3H), 7.16-7.12 (m, 1H), 7.00-6.99 (m, 1H), 6.85 (br s, 1H), 6.82 (br s, 1H), 6.23 (t, *J* = 2.1 Hz, 1H), 5.71 (tt, *J₁* = 8.3 Hz, *J₂* = 2.2 Hz, 1H), 4.14 (tt, *J₁* = 8.0 Hz, *J₂* = 2.3 Hz, 1H), 3.09 (dt, *J₁* = 13.1 Hz, *J₂* = 6.5 Hz, 1H), 2.27 (s, 3H), 1.98 (dt, *J₁* = 13.1 Hz, *J₂* = 6.5 Hz, 1H), 1.70 (s, 3H), 1.62 (s, 3H).

¹³C NMR (125 MHz, CDCl₃) δ 192.6, 145.3, 143.6, 143.2, 138.3, 135.7, 134.7, 134.0, 133.8, 133.2, 130.4, 128.9, 128.8, 128.4, 128.2, 127.9, 127.2, 126.4, 126.3, 126.2, 53.1, 51.1, 40.3, 21.1, 17.2, 17.0.

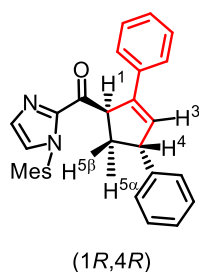
IR (film): ν (cm⁻¹) 3130, 3023, 2924, 2848, 1679, 1602, 1489, 1447, 1398, 1321, 1286, 1147, 1056, 1024, 984, 912, 855, 830, 783, 757, 699, 639, 583, 549, 506, 428.

HRMS (ESI, *m/z*) calcd for C₃₀H₂₉N₂O [M+H]⁺: 433.2274, found: 433.2274.

NOE spectrum:



The minor diastereoisomer:



Enantiomeric excess was established by HPLC analysis using a Chiralpak IG column, ee [minor] = 91% (HPLC: IG, 254 nm, *n*-hexane/isopropanol = 90:10, flow rate 1 mL/min, 40 °C, t_r (major) = 6.7 min, t_r (minor) = 11.0 min). $[\alpha]_D^{22} = +92.6^\circ$ (c 1.0, CH₂Cl₂).

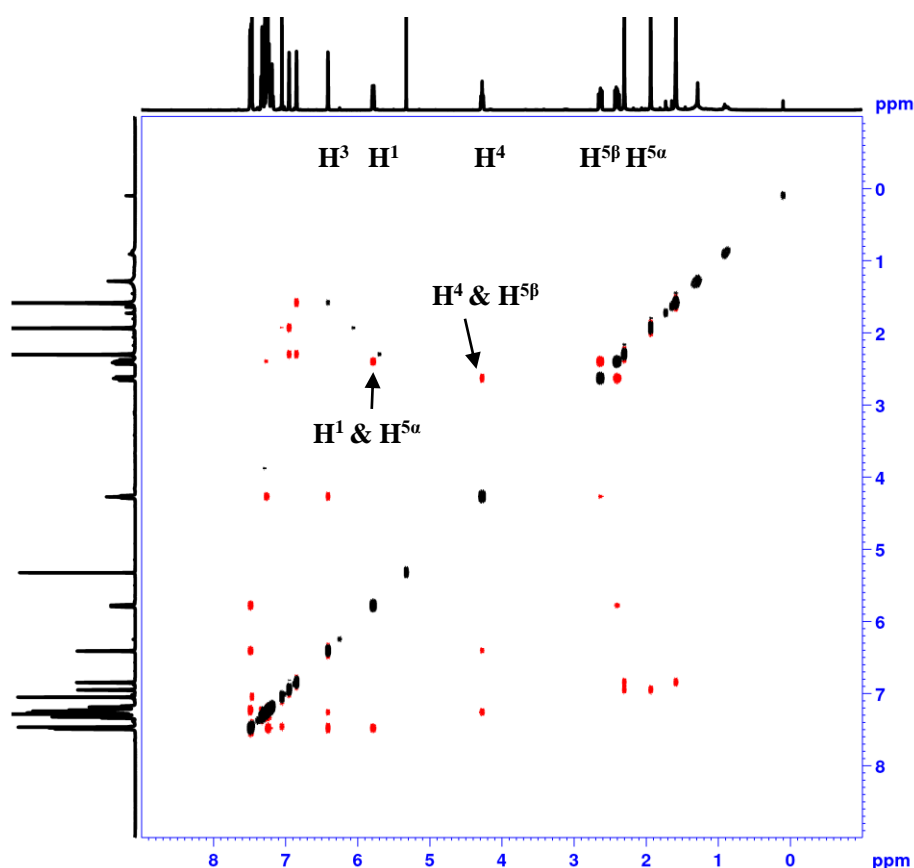
¹H NMR (500 MHz, CDCl₃) δ 7.50-7.46 (m, 3H), 7.35-7.30 (m, 2H), 7.27-7.22 (m, 5H), 7.21-7.16 (m, 1H), 7.06-7.04 (m, 1H), 6.95 (br s, 1H), 6.85 (br s, 1H), 6.41 (dd, $J_1 = 2.2$ Hz, $J_2 = 1.2$ Hz, 1H), 5.81-5.76 (m, 1H), 4.27 (tt, $J_1 = 8.0$ Hz, $J_2 = 2.1$ Hz, 1H), 2.63 (ttt, $J_1 = 13.3$ Hz, $J_2 = 8.3$ Hz, $J_3 = 2.9$ Hz, 1H), 2.44-2.36 (m, 1H), 2.30 (s, 3H), 1.93 (s, 3H), 1.58 (s, 3H).

^{13}C NMR (125 MHz, CDCl_3) δ 192.9, 145.3, 143.0, 142.8, 138.4, 134.9, 134.7, 134.0, 133.8, 133.4, 130.5, 129.0, 128.8, 128.6, 128.3, 127.5, 127.4, 126.4, 126.32, 126.26, 53.0, 51.1, 40.3, 21.1, 17.4, 16.8.

IR (film): ν (cm^{-1}) 3055, 3026, 2924, 2859, 1679, 1601, 1489, 1447, 1398, 1316, 1282, 1149, 1079, 1034, 977, 908, 855, 784, 752, 695, 584, 558, 529.

HRMS (ESI, m/z) calcd for $\text{C}_{30}\text{H}_{29}\text{N}_2\text{O}$ $[\text{M}+\text{H}]^+$: 433.2274, found: 433.2274.

NOE spectrum:



5.6.4 Quantum Yield Measurement Using Powermeter as the Detector

The quantum yield of reaction $41\text{a} + 42\text{a} \rightarrow 43\text{a}$ was measured according to the method initially developed by the Riedle group.⁴ Accordingly, a 400 nm LED was employed as light source. A Powermeter was used as detector. The measurement was accomplished in a dark room with a 1.1 W red LEDs.

Step 1: The radiant power of light transmitted by the cuvette with a blank solution was measured as $P_{\text{blank}} = 34.37 \text{ mW}$.

Step 2: The reaction mixture of **41a** (48.0 mg, 0.20 mmol), **42a** (26.6 mg, 2.5 equiv), *rac*-**RhS** (3.5 mg, 2 mol%) and DIPEA (13.0 mg, 0.5 equiv) in acetone (2.0 mL, 0.1 M) was filled into a fluorescence cuvette with a stirring bar and septum and degassed by bubbling with nitrogen (10 min). Then, the cuvette was put into the setups and illuminated with the 400 nm LED. The transmitted radiant power $P_{\text{sample}} = 1.04 \text{ mW}$ was noted. The transmitted radiant power was monitored during the irradiation and remained constant.

Step 3: After illumination for 2 hours ($t = 2 \times 3600 \text{ s}$), the amount of the formed **43a** was determined as $7.881 \times 10^{-5} \text{ mol}$ (n_{product}) by ^1H NMR.

Step 4: The overall quantum yield can be calculated as following:

$$\begin{aligned} \text{Quantum Yield} &= \frac{N_{\text{product}}}{N_{\text{photon}}} = \frac{N_A \times n_{\text{product}}}{\frac{P_{\text{absorbed}} \times t}{\frac{h \times c}{\lambda}}} = \frac{h \times c \times N_A \times n_{\text{product}}}{(P_{\text{blank}} - P_{\text{sample}}) \times t \times \lambda} \\ &= \frac{6.626 \times 10^{-34} \text{ Js} \times 2.998 \times 10^8 \text{ ms}^{-1} \times 6.022 \times 10^{23} \text{ mol}^{-1} \times 7.881 \times 10^{-5} \text{ mol}}{(34.37 - 1.04) \times 10^{-3} \text{ Js}^{-1} \times 2 \times 3600 \text{ s} \times 400 \times 10^{-9} \text{ m}} = 0.098 \end{aligned}$$

where N_{product} is the number of product **43a** formed; N_{photon} is the number of photons absorbed; N_A is Avogadro's constant; n_{product} is the molar amount of product **43a** formed; P_{absorbed} is the radiant power absorbed; t is the irradiation time; h is the Planck's constant; c is the speed of light; λ is the wavelength of light source, P_{blank} is the radiant power transmitted by the cuvette with a blank solution; P_{sample} is the radiant power transmitted by the cuvette with reaction mixture.

Steps 1-4 were repeated leading to the following result:

$$\begin{aligned} \text{Quantum Yield of second exp.} &= \frac{N_{\text{product}}}{N_{\text{photon}}} = \frac{N_A \times n_{\text{product}}}{\frac{P_{\text{absorbed}} \times t}{\frac{h \times c}{\lambda}}} = \frac{h \times c \times N_A \times n_{\text{product}}}{(P_{\text{blank}} - P_{\text{sample}}) \times t \times \lambda} \\ &= \frac{6.626 \times 10^{-34} \text{ Js} \times 2.998 \times 10^8 \text{ ms}^{-1} \times 6.022 \times 10^{23} \text{ mol}^{-1} \times 9.773 \times 10^{-5} \text{ mol}}{(34.07 - 1.21) \times 10^{-3} \text{ Js}^{-1} \times 2 \times 3600 \text{ s} \times 400 \times 10^{-9} \text{ m}} = 0.124 \end{aligned}$$

Therefore, the average quantum yield for the reaction **41a** + **42a** \rightarrow **43a** was determined as 0.11.

5.6.5 Single-Crystal X-Ray Diffraction Studies

Single crystals of **43k** suitable for X-ray diffraction were obtained by slow diffusion from of a solution of **43k** (30 mg) in Et₂O (0.5 mL) layered with *n*-hexane (1.0 mL) at room temperature for several days in a NMR tube.

Data was collected with an STOE STADIVARI diffractometer equipped with CuK α radiation, a graded multilayer mirror monochromator ($\lambda = 1.54186$ Å) and a DECTRIS PILATUS 300K detector using an oil-coated shock-cooled crystal at 230(2) K. Absorption effects were corrected semi-empirical using multiscanned reflexions (X-Area LANA 1.68.2.0 (STOE, 2016)). Cell constants were refined using 20587 of observed reflections of the data collection. The structure was solved by direct methods by using the program XT V2014/1 (Bruker AXS Inc., 2014) and refined by full matrix least squares procedures on F² using SHELXL-2017/1 (Sheldrick, 2017). The non-hydrogen atoms have been refined anisotropically, carbon bonded hydrogen atoms were included at calculated positions and refined using the ‘riding model’ with isotropic temperature factors at 1.2 times (for CH₃ groups 1.5 times) that of the preceding carbon atom. CH₃ groups were allowed to rotate about the bond to their next atom to fit the electron density. Nitrogen or oxygen bonded hydrogen atoms were located and allowed to refine isotropically.

Relative and absolute configuration of compound **43k** was determined (**Figure 129**).

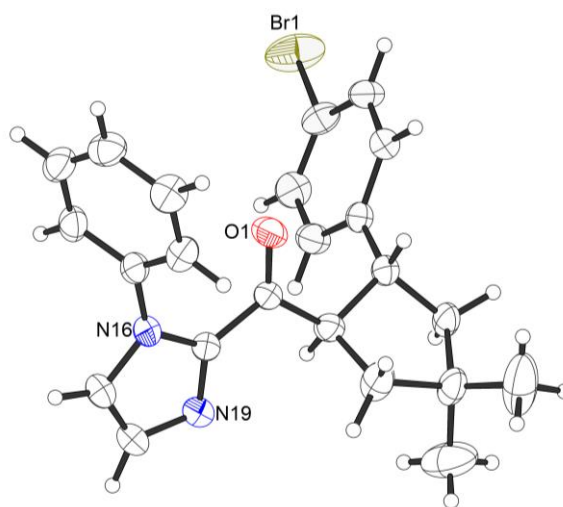


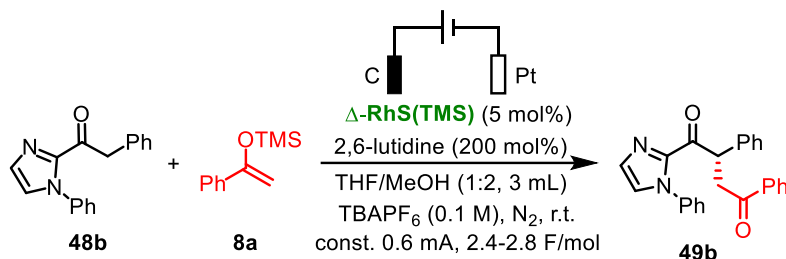
Figure 129. Crystal structure of compound **43k**.

Table 32. Crystal data and structure refinement for **43k**.

Crystal data		
CCDC number	1815472	
Identification code	hxqJ27_230k	
Habitus, color	needle, colorless	
Crystal size	0.35 x 0.05 x 0.03 mm ³	
Crystal system	Orthorhombic	
Space group	P2 ₁ 2 ₁ 2 ₁	Z = 4
Unit cell dimensions	a = 6.37310(10) Å	α = 90 °
	b = 9.9779(2) Å	β = 90 °
	c = 32.3962(9) Å	γ = 90 °
Volume	2060.08(8) Å ³	
Cell determination	20587 peaks with Theta 2.7 to 72.5 °	
Empirical formula	C ₂₃ H ₂₃ Br N ₂ O	
Moiety formula	C ₂₃ H ₂₃ Br N ₂ O	
Formula weight	423.34	
Density (calculated)	1.365 Mg/m ³	
Absorption coefficient	2.822 mm ⁻¹	
F(000)	872	
Data collection:		
Diffractometer type	STOE STADIVARI	
Wavelength	1.54186 Å	
Temperature	230(2) K	
Theta range for data collection	2.728 to 72.236 °	
Index ranges	-7<=h<=6, -10<=k<=12, -38<=l<=39	
Data collection software	X-Area Pilatus3_SV 1.31.127.0 (STOE, 2016)	
Cell refinement software	X-Area Recipe 1.33.0.0 (STOE, 2015)	
Data reduction software	X-Area Integrate 1.71.0.0 (STOE, 2016)	
	X-Area LANA 1.68.2.0 (STOE, 2016)	
Solution and refinement:		
Reflections collected	20724	
Independent reflections	4008 [R(int) = 0.0274]	
Completeness to theta = 67.686 °	99.9 %	
Observed reflections	3727[I > 2σ(I)]	
Reflections used for refinement	4008	
Absorption correction	Semi-empirical from equivalents	
Max. and min. transmission	1.0000 and 0.4568	
Flack parameter (absolute struct.)	-0.026(6)	
Largest diff. peak and hole	0.232 and -0.412 e.Å ⁻³	
Solution	intrinsic phases	
Refinement	Full-matrix least-squares on F ²	
Treatment of hydrogen atoms	Calculated positions, constr. ref.	
Programs used	XT V2014/1 (Bruker AXS Inc., 2014)	
	SHELXL-2017/1 (Sheldrick, 2017)	
	DIAMOND (Crystal Impact)	
	ShelXle (Hübschle, Sheldrick, Dittrich, 2011)	
Data / restraints / parameters	4008 / 72 / 294	
Goodness-of-fit on F ²	1.068	
R index (all data)	wR2 = 0.0620	
R index conventional [I>2sigma(I)]	R1 = 0.0245	

5.7 Asymmetric Electrosynthesis

5.7.1 General Procedure



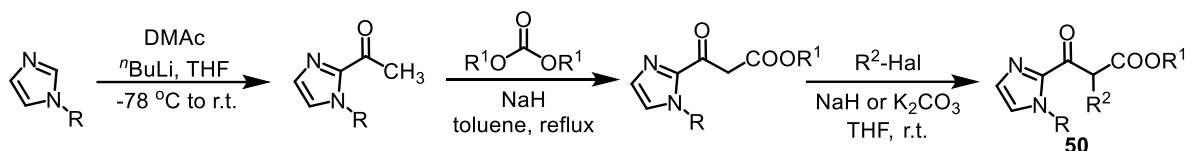
Exemplary, to a 5 mL ElectraSyn vial with a stirring bar, Δ -Rh(TMS) (4.5 mg, 0.005 mmol), 2-acyl imidazole **48b** (26.2 mg, 0.10 mmol), TBAPF₆ (116.2 mg, 0.30 mmol), THF (1.0 mL), MeOH (2.0 mL), 2,6-lutidine (21.4 mg, 0.20 mmol) and silyl enol ether **8a** (115.4 mg, 0.60 mmol) were added in sequence. The screw thread area of the vial was covered with a piece of Parafilm and screwed to finger-tight with the ElectraSyn vial cap that equipped with a graphite electrode (anode) and a Pt electrode (cathode). Then, the mixture was purged with nitrogen gas for 3–5 min by a nitrogen balloon. The undivided cell was adapted to the ElectraSyn 2.0 vial holder and electrolyzed under a constant current of 0.6 mA. After consumption of 2.4 F/mol of current (~11 hours for 0.1 mmol substrate), the reaction medium was transferred to a 25 mL round-bottom flask and purified by flash chromatography on silica gel (*n*-hexane/EtOAc) to afford the product **49b**. The enantiomeric excess was determined by HPLC analysis on a chiral stationary phase. Racemic samples were obtained by carrying out the reactions with *rac*-RhS(TMS).

One-pot procedure: Exemplary, in a 5 mL ElectraSyn vial with a stirring bar, to the solution of acetophenone **8a'** (72.0 mg, 0.60 mmol) and 2,6-lutidine (74.9 mg, 0.70 mmol) in anhydrous THF (1.0 mL), TMSOTf (111.1 mg, 0.5 mmol) was added dropwise at 0 °C. After stirring at the same temperature for 0.5 hour, MeOH (2.0 mL), TBAPF₆ (116.2 mg, 0.30 mmol), Δ -Rh(TMS) (4.5 mg, 0.005 mmol), and 2-acyl imidazole **48b** (26.2 mg, 0.10 mmol) were added in sequence. Following the typical procedure, the mixture was electrolyzed at a constant current of 0.6 mA with the consumption of 2.4 F/mol of electricity, to give product **49b** in 56% yield (21.2 mg) with 95% ee.

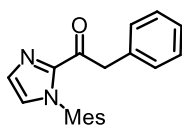
Note: The synthesis, characterization and crystal structure of Rh(TMS) are presented in Jiahui Lin's M. Sc. thesis.

5.7.2 Synthesis of Substrates

Acyl imidazoles **48** were prepared via the well-established Weinreb ketone synthesis.⁵ Silyl enol ethers **8** used were prepared according to well-developed methods¹⁵ and subjected to the reaction after simple extraction without further distillation. Racemic imidazoles **50** were synthesized according to the following route.



The data of new starting materials are shown below.

**1-(1-Mesityl-1H-imidazol-2-yl)-2-phenylethan-1-one (48a)**

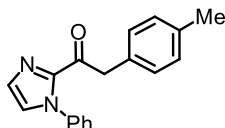
A white solid.

¹H NMR (300 MHz, CDCl₃) δ 7.40-7.38 (m, 1H), 7.31-7.15 (m, 5H), 7.01-6.98 (m, 1H), 6.90 (br s, 2H), 4.42 (s, 2H), 2.29 (s, 3H), 1.78 (s, 6H).

¹³C NMR (125 MHz, CDCl₃) δ 188.4, 143.0, 138.4, 134.6, 134.4, 134.0, 130.3, 129.8, 128.9, 128.4, 126.7, 126.0, 45.4, 21.0, 17.1.

IR (film): ν (cm⁻¹) 3133, 2915, 1667, 1601, 1488, 1449, 1396, 1324, 1284, 1184, 1141, 1095, 1045, 976, 936, 911, 853, 801, 768, 733, 694, 625, 576, 518, 462, 438, 402.

HRMS (ESI, *m/z*) calcd for C₂₀H₂₀N₂ONa [M+Na]⁺: 327.1468, found: 327.1466.

**1-(1-Phenyl-1H-imidazol-2-yl)-2-(p-tolyl)ethan-1-one (48g)**

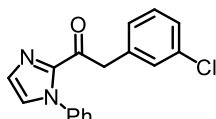
A white solid.

¹H NMR (300 MHz, CDCl₃) δ 7.45-7.39 (m, 3H), 7.34-7.32 (m, 1H), 7.27-7.18 (m, 5H), 7.15-7.08 (m, 2H), 4.42 (s, 2H), 2.32 (s, 3H).

^{13}C NMR (75 MHz, CDCl_3) δ 188.7, 142.8, 138.3, 136.3, 131.2, 129.8, 129.7, 129.1, 128.9, 128.6, 127.3, 125.8, 45.2, 21.0.

IR (film): ν (cm^{-1}) 3055, 2899, 1686, 1593, 1490, 1447, 1398, 1306, 1209, 1139, 1092, 1028, 960, 910, 852, 815, 763, 729, 689, 565, 504, 474, 404.

HRMS (ESI, m/z) calcd for $\text{C}_{18}\text{H}_{16}\text{N}_2\text{ONa}$ $[\text{M}+\text{Na}]^+$: 299.1155, found: 299.1153.



2-(3-Chlorophenyl)-1-(1-phenyl-1H-imidazol-2-yl)ethan-1-one (48i)

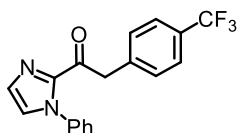
A white solid.

^1H NMR (300 MHz, CDCl_3) δ 7.47-7.40 (m, 3H), 7.34-7.31 (m, 2H), 7.28-7.17 (m, 6H), 4.44 (s, 2H).

^{13}C NMR (75 MHz, CDCl_3) δ 187.7, 142.6, 138.2, 136.3, 134.2, 130.1, 129.8, 129.6, 129.0, 128.8, 128.2, 127.7, 127.0, 125.9, 45.1.

IR (film): ν (cm^{-1}) 3115, 1679, 1592, 1489, 1449, 1392, 1344, 1309, 1213, 1172, 1143, 1085, 1028, 960, 909, 764, 687, 591, 535, 502, 444, 411.

HRMS (ESI, m/z) calcd for $\text{C}_{17}\text{H}_{13}\text{ClN}_2\text{ONa}$ $[\text{M}+\text{Na}]^+$: 319.0609, found: 319.0606.



1-(1-Phenyl-1H-imidazol-2-yl)-2-(4-(trifluoromethyl)phenyl)ethan-1-one (48l)

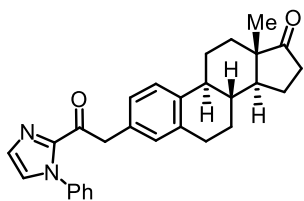
A white solid.

^1H NMR (300 MHz, CDCl_3) δ 7.59-7.52 (m, 2H), 7.48-7.41 (m, 5H), 7.36-7.33 (m, 1H), 7.29-7.21 (m, 3H), 4.53 (s, 2H).

^{13}C NMR (75 MHz, CDCl_3) δ 187.5, 142.5, 138.5, 138.1, 130.3, 130.0, 129.1 (q, $J = 31.8$ Hz), 129.0, 128.8, 127.7, 125.8, 125.3 (q, $J = 4.0$ Hz), 124.2 (q, $J = 269.7$ Hz), 45.3.

IR (film): ν (cm^{-1}) 3062, 2921, 1690, 1600, 1496, 1449, 1400, 1320, 1152, 1101, 1063, 1018, 959, 913, 866, 819, 766, 692, 638, 591, 532.

HRMS (ESI, m/z) calcd for $\text{C}_{18}\text{H}_{13}\text{F}_3\text{N}_2\text{ONa}$ $[\text{M}+\text{Na}]^+$: 353.0872, found: 353.0869.



(8*R*,9*S*,13*S*,14*S*)-13-Methyl-3-(2-oxo-2-(1-phenyl-1*H*-imidazol-2-yl)ethyl)-6,7,8,9,11,12,13,14,15,16-decahydro-17*H*-cyclopenta[*a*]phenanthren-17-one (48o)

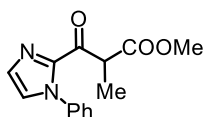
A white solid.

^1H NMR (300 MHz, CDCl_3) δ 7.43-7.38 (m, 3H), 7.33-7.30 (m, 1H), 7.27-7.20 (m, 3H), 7.20-7.18 (m, 1H), 7.09 (dd, $J_1 = 8.1$ Hz, $J_2 = 1.8$ Hz, 1H), 7.03 (br s, 1H), 4.40 (s, 2H), 2.92-2.84 (m, 2H), 2.49 (dd, $J_1 = 17.7$ Hz, $J_2 = 7.8$ Hz, 1H), 2.45-1.90 (m, 6H), 1.70-1.30 (m, 6H), 0.89 (s, 3H).

^{13}C NMR (75 MHz, CDCl_3) δ 188.7, 142.8, 138.32, 138.25, 136.5, 131.7, 130.5, 129.7, 128.9, 128.7, 127.41, 127.35, 125.9, 125.4, 50.5, 48.0, 45.0, 44.3, 38.1, 35.8, 31.6, 29.3, 26.5, 25.6, 21.6, 13.8. (^{13}C signal of carbonyl in estrone motif (expected at ~ 220 ppm) is beyond the range of the measurement)

IR (film): ν (cm^{-1}) 2924, 2860, 1734, 1684, 1597, 1496, 1447, 1398, 1340, 1307, 1257, 1147, 1080, 1047, 1010, 969, 910, 763, 728, 692, 647, 554, 519, 439.

HRMS (ESI, m/z) calcd for $\text{C}_{29}\text{H}_{30}\text{N}_2\text{O}_2\text{Na}$ $[\text{M}+\text{Na}]^+$: 461.2199, found: 461.2196.



Methyl 2-methyl-3-oxo-3-(1-phenyl-1*H*-imidazol-2-yl)propanoate (50a)

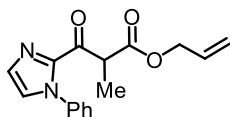
A colorless oil. Racemic.

^1H NMR (300 MHz, CDCl_3) δ 7.49-7.42 (m, 3H), 7.33-7.27 (m, 3H), 7.22-7.19 (m, 1H), 4.78 (q, $J = 7.5$ Hz, 1H), 3.71 (s, 3H), 1.44 (d, $J = 7.2$ Hz, 3H).

^{13}C NMR (75 MHz, CDCl_3) δ 186.7, 171.7, 142.2, 138.0, 130.0, 129.0, 128.8, 127.4, 125.7, 52.3, 48.3, 13.1.

IR (film): ν (cm^{-1}) 3113, 2992, 2948, 1736, 1687, 1596, 1497, 1447, 1400, 1311, 1203, 1173, 1083, 1028, 973, 940, 909, 858, 762, 691, 551, 515.

HRMS (ESI, m/z) calcd for $\text{C}_{14}\text{H}_{14}\text{N}_2\text{O}_3\text{Na}$ $[\text{M}+\text{Na}]^+$: 281.0897, found: 281.0895.



Allyl 2-methyl-3-oxo-3-(1-phenyl-1H-imidazol-2-yl)propanoate (50b)

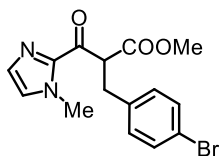
A colorless oil. Racemic.

^1H NMR (300 MHz, CDCl_3) δ 7.48-7.42 (m, 3H), 7.34-7.27 (m, 3H), 7.22-7.19 (m, 1H), 5.93-5.78 (m, 1H), 5.30-5.15 (m, 2H), 4.80 (q, $J = 7.2$ Hz, 1H), 4.64-4.57 (m, 2H), 1.45 (d, $J = 6.9$ Hz, 3H).

^{13}C NMR (75 MHz, CDCl_3) δ 186.7, 170.9, 142.3, 138.0, 131.9, 130.0, 129.0, 128.8, 127.3, 125.7, 118.1, 65.6, 48.4, 13.0.

IR (film): ν (cm^{-1}) 3113, 2988, 2940, 1735, 1688, 1650, 1596, 1497, 1449, 1401, 1310, 1214, 1177, 1081, 1024, 1005, 939, 908, 761, 691, 549, 514.

HRMS (ESI, m/z) calcd for $\text{C}_{16}\text{H}_{16}\text{N}_2\text{O}_3\text{Na}$ $[\text{M}+\text{Na}]^+$: 307.1053, found: 307.1051.



Methyl 2-(4-bromobenzyl)-3-(1-methyl-1H-imidazol-2-yl)-3-oxopropanoate (50c)

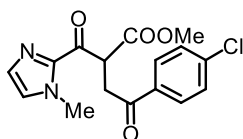
A white solid. Racemic.

^1H NMR (300 MHz, CDCl_3) δ 7.38-7.33 (m, 2H), 7.18-7.12 (m, 3H), 7.03 (br s, 1H), 5.08 (t, $J = 7.4$ Hz, 1H), 3.96 (s, 3H), 3.66 (s, 3H), 3.29 (dd, $J_1 = 14.1$ Hz, $J_2 = 7.5$ Hz, 1H), 3.22 (dd, $J_1 = 14.1$ Hz, $J_2 = 7.8$ Hz, 1H).

^{13}C NMR (75 MHz, CDCl_3) δ 186.3, 170.1, 142.3, 137.5, 131.4, 130.8, 129.9, 127.7, 120.4, 55.1, 52.4, 36.1, 33.9.

IR (film): ν (cm^{-1}) 3108, 2951, 1721, 1680, 1581, 1479, 1442, 1401, 1331, 1279, 1234, 1196, 1161, 1099, 1068, 1011, 936, 904, 869, 820, 784, 744, 717, 687, 638, 613, 579, 530.

HRMS (ESI, m/z) calcd for $\text{C}_{15}\text{H}_{15}\text{BrN}_2\text{O}_3\text{Na}$ $[\text{M}+\text{Na}]^+$: 373.0158, found: 373.0156.



Methyl 4-(4-chlorophenyl)-2-(1-methyl-1H-imidazole-2-carbonyl)-4-oxobutanoate (50d)

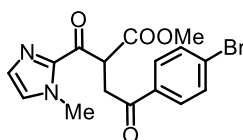
A white solid. Racemic.

^1H NMR (300 MHz, CDCl_3) δ 7.95-7.88 (m, 2H), 7.46-7.40 (m, 2H), 7.23-7.20 (m, 1H), 7.07 (br s, 1H), 5.40 (dd, $J_1 = 8.4$ Hz, $J_2 = 5.7$ Hz, 1H), 4.00 (s, 3H), 3.81 (dd, $J_1 = 17.7$ Hz, $J_2 = 8.1$ Hz, 1H), 3.73 (s, 3H), 3.63 (dd, $J_1 = 17.7$ Hz, $J_2 = 5.7$ Hz, 1H).

^{13}C NMR (75 MHz, CDCl_3) δ 195.4, 186.4, 170.4, 142.3, 139.8, 134.5, 130.0, 129.6, 128.9, 127.5, 52.7, 49.2, 38.0, 36.1.

IR (film): ν (cm^{-1}) 3135, 2958, 1738, 1674, 1587, 1469, 1441, 1406, 1364, 1319, 1268, 1242, 1167, 1087, 991, 950, 908, 823, 788, 689, 648, 607, 529, 490, 458, 403.

HRMS (ESI, m/z) calcd for $\text{C}_{16}\text{H}_{15}\text{ClN}_2\text{O}_4\text{Na}$ $[\text{M}+\text{Na}]^+$: 357.0613, found: 357.0610.



Methyl 4-(4-bromophenyl)-2-(1-methyl-1H-imidazole-2-carbonyl)-4-oxobutanoate (50e)

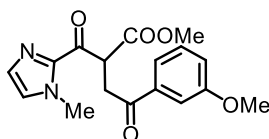
A white solid. Racemic.

^1H NMR (300 MHz, CDCl_3) δ 7.87-7.80 (m, 2H), 7.63-7.56 (m, 2H), 7.21 (br s, 1H), 7.06 (br s, 1H), 5.39 (dd, $J_1 = 8.4$ Hz, $J_2 = 5.7$ Hz, 1H), 3.99 (s, 3H), 3.79 (dd, $J_1 = 18.3$ Hz, $J_2 = 8.4$ Hz, 1H), 3.72 (s, 3H), 3.63 (dd, $J_1 = 17.7$ Hz, $J_2 = 5.7$ Hz, 1H).

^{13}C NMR (75 MHz, CDCl_3) δ 195.6, 186.4, 170.4, 142.3, 134.5, 131.9, 130.0, 129.7, 128.6, 127.5, 52.7, 49.2, 38.0, 36.0.

IR (film): ν (cm^{-1}) 3137, 2956, 1735, 1674, 1580, 1476, 1405, 1363, 1319, 1266, 1167, 1093, 1067, 991, 949, 908, 821, 785, 756, 685, 648, 613, 531, 495, 450, 408.

HRMS (ESI, m/z) calcd for $\text{C}_{16}\text{H}_{15}\text{BrN}_2\text{O}_4\text{Na}$ $[\text{M}+\text{Na}]^+$: 401.0107, found: 401.0105.



Methyl 4-(3-methoxyphenyl)-2-(1-methyl-1H-imidazole-2-carbonyl)-4-oxobutanoate (50f)

A colorless oil. Racemic.

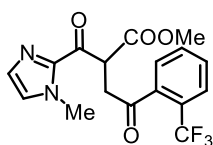
^1H NMR (300 MHz, CDCl_3) δ 7.58 (d, $J = 7.5$ Hz, 1H), 7.51-7.46 (m, 1H), 7.36 (t, $J = 9.3$ Hz, 1H),

7.21 (br s, 1H), 7.14-7.08 (m, 1H), 7.06 (br s, 1H), 5.41 (dd, $J_1 = 8.4$ Hz, $J_2 = 5.4$ Hz, 1H), 4.00 (s, 3H), 3.85 (dd, $J_1 = 17.7$ Hz, $J_2 = 8.7$ Hz, 1H), 3.83 (s, 3H), 3.73 (s, 3H), 3.66 (dd, $J_1 = 18.3$ Hz, $J_2 = 5.7$ Hz, 1H).

^{13}C NMR (75 MHz, CDCl_3) δ 196.4, 186.6, 170.5, 159.8, 142.4, 137.5, 129.9, 129.6, 127.4, 120.9, 120.1, 112.2, 55.4, 52.6, 49.2, 38.2, 36.0.

IR (film): ν (cm^{-1}) 3111, 2954, 2839, 1736, 1676, 1589, 1459, 1402, 1359, 1326, 1260, 1158, 1086, 1012, 956, 905, 867, 782, 739, 685, 611, 571, 500.

HRMS (ESI, m/z) calcd for $\text{C}_{17}\text{H}_{18}\text{N}_2\text{O}_5\text{Na}$ $[\text{M}+\text{Na}]^+$: 353.1108, found: 353.1106.



Methyl 2-(1-methyl-1H-imidazole-2-carbonyl)-4-oxo-4-(2-(trifluoromethyl)phenyl)butanoate (50g)

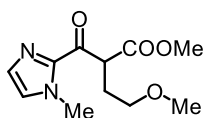
A white solid. Racemic.

^1H NMR (300 MHz, CDCl_3) δ 7.74-7.54 (m, 4H), 7.22 (br s, 1H), 7.06 (br s, 1H), 5.38 (dd, $J_1 = 8.4$ Hz, $J_2 = 6.3$ Hz, 1H), 4.00 (s, 3H), 3.73 (s, 3H), 3.67 (dd, $J_1 = 18.6$ Hz, $J_2 = 8.4$ Hz, 1H), 3.49 (dd, $J_1 = 18.3$ Hz, $J_2 = 6.0$ Hz, 1H).

^{13}C NMR (125 MHz, CDCl_3) δ 200.4, 185.9, 170.2, 142.2, 139.3 (q, $J = 1.7$ Hz), 131.8, 130.3, 130.0, 127.6, 127.5, 127.1 (q, $J = 32.3$ Hz), 126.6 (q, $J = 5.1$ Hz), 123.4 (q, $J = 272.1$ Hz), 52.7, 49.6, 41.8, 36.0.

IR (film): ν (cm^{-1}) 3031, 2955, 2917, 1736, 1706, 1674, 1402, 1308, 1279, 1162, 1135, 1064, 1030, 994, 946, 906, 774, 660, 564.

HRMS (ESI, m/z) calcd for $\text{C}_{17}\text{H}_{15}\text{F}_3\text{N}_2\text{O}_4\text{Na}$ $[\text{M}+\text{Na}]^+$: 391.0876, found: 391.0872.



Methyl 4-methoxy-2-(1-methyl-1H-imidazole-2-carbonyl)butanoate (50h)

A colorless oil. Racemic.

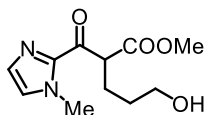
^1H NMR (300 MHz, CDCl_3) δ 7.19-7.16 (m, 1H), 7.04 (br s, 1H), 4.87 (t, $J = 7.1$ Hz, 1H), 4.00 (s, 3H),

3.70 (s, 3H), 3.50-3.40 (m, 2H), 3.23 (s, 3H), 2.37-2.16 (m, 2H).

^{13}C NMR (75 MHz, CDCl_3) δ 187.4, 170.8, 142.6, 129.6, 127.4, 70.2, 58.4, 52.4, 51.1, 36.0, 28.9.

IR (film): ν (cm^{-1}) 3113, 2951, 2874, 2819, 1737, 1676, 1510, 1438, 1402, 1331, 1287, 1245, 1196, 1163, 1115, 1087, 978, 912, 846, 780, 693, 610, 524.

HRMS (ESI, m/z) calcd for $\text{C}_{11}\text{H}_{16}\text{N}_2\text{O}_4\text{Na}$ $[\text{M}+\text{Na}]^+$: 263.1002, found: 263.1001.



Methyl 5-hydroxy-2-(1-methyl-1H-imidazole-2-carbonyl)pentanoate (50i)

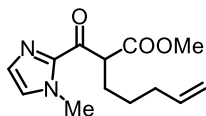
A colorless oil. Racemic.

^1H NMR (300 MHz, CDCl_3) δ 7.17 (br s, 1H), 7.06 (br s, 1H), 4.81 (t, $J = 6.9$ Hz, 1H), 4.01 (s, 3H), 3.77-3.65 (m, 2H), 3.72 (s, 3H), 2.64 (br s, 1H), 2.22-2.00 (m, 2H), 1.80-1.52 (m, 2H).

^{13}C NMR (75 MHz, CDCl_3) δ 187.7, 170.7, 142.2, 129.7, 127.6, 61.8, 53.1, 52.3, 36.2, 30.1, 25.3.

IR (film): ν (cm^{-1}) 3383, 2955, 2880, 1733, 1674, 1401, 1281, 1236, 1202, 1159, 1059, 1003, 957, 913, 778, 691.

HRMS (ESI, m/z) calcd for $\text{C}_{11}\text{H}_{16}\text{N}_2\text{O}_4\text{Na}$ $[\text{M}+\text{Na}]^+$: 263.1002, found: 263.1000.



Methyl 2-(1-methyl-1H-imidazole-2-carbonyl)hept-6-enoate (50j)

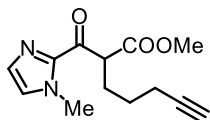
A colorless oil. Racemic.

^1H NMR (300 MHz, CDCl_3) δ 7.17 (br s, 1H), 7.05 (br s, 1H), 5.86-5.70 (m, 1H), 5.05-4.90 (m, 2H), 4.74 (t, $J = 7.4$ Hz, 1H), 4.01 (s, 3H), 3.69 (s, 3H), 2.14-2.04 (m, 2H), 2.04-1.94 (m, 2H), 1.55-1.38 (m, 2H).

^{13}C NMR (75 MHz, CDCl_3) δ 187.6, 170.9, 142.6, 138.2, 129.7, 127.6, 114.9, 53.6, 52.3, 36.1, 33.5, 28.3, 26.8.

IR (film): ν (cm^{-1}) 3113, 2949, 2858, 1737, 1675, 1440, 1402, 1336, 1283, 1235, 1202, 1160, 990, 961, 912, 872, 774, 692.

HRMS (ESI, m/z) calcd for $\text{C}_{13}\text{H}_{18}\text{N}_2\text{O}_3\text{Na}$ $[\text{M}+\text{Na}]^+$: 273.1210, found: 273.1208.


Methyl 2-(1-methyl-1*H*-imidazole-2-carbonyl)hept-6-ynoate (50k)

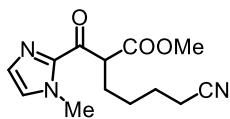
A colorless oil. Racemic.

^1H NMR (300 MHz, CDCl_3) δ 7.18-7.15 (m, 1H), 7.05 (br s, 1H), 4.75 (t, $J = 7.4$ Hz, 1H), 4.01 (s, 3H), 3.69 (s, 3H), 2.23 (td, $J_1 = 6.9$ Hz, $J_2 = 2.7$ Hz, 2H), 2.09 (q, $J = 7.5$ Hz, 2H), 1.93 (t, $J = 2.7$ Hz, 1H), 1.68-1.50 (m, 2H).

^{13}C NMR (75 MHz, CDCl_3) δ 187.3, 170.7, 142.5, 129.8, 127.6, 83.7, 68.7, 53.2, 52.3, 36.1, 27.9, 26.3, 18.3.

IR (film): ν (cm^{-1}) 3288, 2952, 1735, 1674, 1440, 1402, 1335, 1283, 1201, 1155, 1086, 994, 961, 913, 873, 777, 637, 512.

HRMS (ESI, m/z) calcd for $\text{C}_{13}\text{H}_{16}\text{N}_2\text{O}_3\text{Na}$ $[\text{M}+\text{Na}]^+$: 271.1053, found: 271.1051.


Methyl 6-cyano-2-(1-methyl-1*H*-imidazole-2-carbonyl)hexanoate (50l)

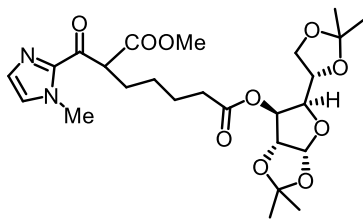
A colorless oil. Racemic.

^1H NMR (300 MHz, CDCl_3) δ 7.19-7.16 (m, 1H), 7.07 (br s, 1H), 4.75 (t, $J = 7.8$ Hz, 1H), 4.01 (s, 3H), 3.70 (s, 3H), 2.34 (t, $J = 7.2$ Hz, 2H), 2.01 (q, $J = 7.5$ Hz, 2H), 1.79-1.65 (m, 2H), 1.60-1.44 (m, 2H).

^{13}C NMR (75 MHz, CDCl_3) δ 187.2, 170.6, 142.4, 129.8, 127.8, 119.4, 53.2, 52.4, 36.1, 27.8, 26.5, 25.1, 16.9.

IR (film): ν (cm^{-1}) 2950, 2278, 1736, 1674, 1458, 1402, 1263, 1200, 1155, 1085, 1002, 957, 909, 845, 782, 692.

HRMS (ESI, m/z) calcd for $\text{C}_{13}\text{H}_{17}\text{N}_3\text{O}_3\text{Na}$ $[\text{M}+\text{Na}]^+$: 286.1162, found: 286.1160.



7-((3aR,5R,6S,6aR)-5-((S)-2,2-Dimethyl-1,3-dioxolan-4-yl)-2,2-dimethyltetrahydrofuro[2,3-d][1,3]dioxol-6-yl) 1-methyl 2-(1-methyl-1H-imidazole-2-carbonyl)heptanedioate (50m)

A colorless oil. Mixture of two diastereoisomers.

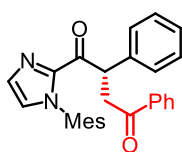
^1H NMR (300 MHz, CDCl_3) δ 7.17-7.15 (m, 1H), 7.05 (br s, 1H), 5.88-5.84 (m, 1H), 5.25-5.22 (m, 1H), 4.72 (t, $J = 7.1$ Hz, 1H), 4.47 (d, $J = 3.6$ Hz, 1H), 4.22-4.12 (m, 2H), 4.10-4.03 (m, 1H), 4.02-3.96 (m, 1H), 4.01 (s, 3H), 3.68 (s, 3H), 2.34 (t, $J = 7.5$ Hz, 2H), 1.98 (q, $J = 7.8$ Hz, 2H), 1.72-1.61 (m, 2H), 1.51 (s, 3H), 1.48-1.35 (m, 2H), 1.39 (s, 3H), 1.30 (s, 6H).

^{13}C NMR (75 MHz, CDCl_3) δ 187.4, 172.0, 170.7, 142.5, 142.4, 129.7, 127.6, 112.2, 109.3, 105.1, 83.4, 79.9, 75.9, 72.4, 67.2, 53.4, 52.3, 36.1, 33.8, 28.3, 26.9, 26.8, 26.7, 26.2, 25.2, 24.59, 24.57.

IR (film): ν (cm^{-1}) 2987, 2944, 2869, 1739, 1677, 1458, 1405, 1376, 1211, 1154, 1071, 1017, 952, 910, 884, 846, 782, 735, 512.

HRMS (ESI, m/z) calcd for $\text{C}_{25}\text{H}_{36}\text{N}_2\text{O}_{10}\text{Na}$ $[\text{M}+\text{Na}]^+$: 547.2262, found: 547.2260.

5.7.3 Experimental and Characterization Data of Novel Products



(S)-1-(1-Mesityl-1H-imidazol-2-yl)-2,4-diphenylbutane-1,4-dione (49a)

According to the general procedure, electrolysis of the reaction mixture of 1-(1-mesityl-1H-imidazol-2-yl)-2-phenylethan-1-one **48a** (30.4 mg, 0.10 mmol) and trimethyl((1-phenylvinyl)oxy)silane **8a** (115.4 mg, 6.0 equiv) afforded 21.3 mg (50% yield) of **49a** as a colorless oil after electricity consumption of 2.2 F/mol.

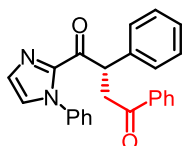
Enantiomeric excess was established by HPLC analysis using a Chiralpak IG column, ee = 99.6% (HPLC: IG, 254 nm, *n*-hexane/isopropanol = 70:30, flow rate 1 mL/min, 40 °C, t_r (major) = 16.6 min, t_r (minor) = 9.5 min). $[\alpha]_{\text{D}}^{22} = +153.8^\circ$ (*c* 1.0, CH_2Cl_2).

^1H NMR (300 MHz, CD_2Cl_2) δ 7.95-7.88 (m, 2H), 7.60-7.51 (m, 1H), 7.49-7.35 (m, 5H), 7.33-7.18 (m, 3H), 6.97 (br s, 1H), 6.94 (br s, 1H), 6.89 (br s, 1H), 5.68 (dd, $J_1 = 11.1$ Hz, $J_2 = 3.6$ Hz, 1H), 3.99 (dd, $J_1 = 18.0$ Hz, $J_2 = 10.8$ Hz, 1H), 3.32 (dd, $J_1 = 18.3$ Hz, $J_2 = 3.9$ Hz, 1H), 2.31 (s, 3H), 1.94 (s, 3H), 1.53 (s, 3H).

^{13}C NMR (75 MHz, CD_2Cl_2) δ 198.1, 189.9, 143.2, 139.1, 138.7, 137.0, 135.4, 135.2, 134.5, 133.4, 130.8, 129.1, 129.0, 128.93, 128.89, 128.3, 127.5, 126.2, 48.6, 43.1, 21.1, 17.4, 16.9. (Missing one ^{13}C signal because the resolution of NMR spectrometer is not enough.)

IR (film): ν (cm^{-1}) 3059, 3029, 2918, 2859, 1679, 1598, 1488, 1449, 1403, 1361, 1326, 1283, 1247, 1203, 1149, 1084, 1013, 989, 959, 933, 907, 849, 736, 693, 561, 522.

HRMS (ESI, m/z) calcd for $\text{C}_{28}\text{H}_{26}\text{N}_2\text{O}_2\text{Na}$ $[\text{M}+\text{Na}]^+$: 445.1886, found: 445.1882.



(S)-2,4-Diphenyl-1-(1-phenyl-1H-imidazol-2-yl)butane-1,4-dione (49b)

According to the general procedure, electrolysis of the reaction mixture of 2-phenyl-1-(1-phenyl-1H-imidazol-2-yl)ethan-1-one **48b** (26.2 mg, 0.10 mmol) and trimethyl((1-phenylvinyl)oxy)silane **8a** (115.4 mg, 6.0 equiv) afforded 30.1 mg (79% yield) of **49b** as a yellow solid after electricity consumption of 2.4 F/mol.

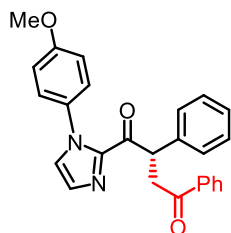
Enantiomeric excess was established by HPLC analysis using a Chiralpak IG column, ee = 97% (HPLC: IG, 254 nm, *n*-hexane/isopropanol = 60:40, flow rate 1 mL/min, 40 °C, t_r (major) = 19.3 min, t_r (minor) = 13.9 min). $[\alpha]_D^{22} = +218.4^\circ$ (c 1.0, CH_2Cl_2).

^1H NMR (300 MHz, CD_2Cl_2) δ 7.98-7.92 (m, 2H), 7.61-7.52 (m, 1H), 7.49-7.39 (m, 7H), 7.38-7.30 (m, 2H), 7.29-7.20 (m, 4H), 7.20-7.17 (m, 1H), 5.69 (dd, $J_1 = 11.1$ Hz, $J_2 = 3.6$ Hz, 1H), 4.03 (dd, $J_1 = 18.0$ Hz, $J_2 = 11.1$ Hz, 1H), 3.37 (dd, $J_1 = 18.3$ Hz, $J_2 = 3.6$ Hz, 1H).

^{13}C NMR (75 MHz, CD_2Cl_2) δ 198.2, 189.9, 143.1, 138.99, 138.96, 136.9, 133.5, 130.1, 129.20, 129.15, 129.1, 128.9, 128.8, 128.4, 127.6, 127.5, 126.1, 48.9, 43.4.

IR (film): ν (cm^{-1}) 3060, 2910, 1678, 1592, 1495, 1448, 1401, 1360, 1307, 1247, 1204, 1149, 1098, 1074, 1023, 992, 939, 907, 867, 755, 691, 587, 522, 435.

HRMS (ESI, m/z) calcd for $\text{C}_{25}\text{H}_{20}\text{N}_2\text{O}_2\text{Na}$ $[\text{M}+\text{Na}]^+$: 403.1417, found: 403.1415.



(S)-1-(1-(4-Methoxyphenyl)-1H-imidazol-2-yl)-2,4-diphenylbutane-1,4-dione (49c)

According to the general procedure, electrolysis of the reaction mixture of 1-(1-(4-methoxyphenyl)-1H-imidazol-2-yl)-2-phenylethan-1-one **48c** (29.2 mg, 0.10 mmol) and trimethyl((1-phenylvinyl)oxy)silane **8a** (115.4 mg, 6.0 equiv) afforded 22.5 mg (55% yield) of **49c** as a white solid after electricity consumption of 2.4 F/mol.

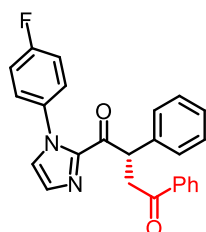
Enantiomeric excess was established by HPLC analysis using a Chiralpak OD-H column, ee = 96% (HPLC: OD-H, 254 nm, *n*-hexane/isopropanol = 80:20, flow rate 1 mL/min, 40 °C, *t_r* (major) = 12.4 min, *t_r* (minor) = 10.8 min). $[\alpha]_D^{22} = +237.8^\circ$ (*c* 1.0, CH₂Cl₂).

¹H NMR (500 MHz, CD₂Cl₂) δ 7.96-7.92 (m, 2H), 7.59-7.55 (m, 1H), 7.48-7.41 (m, 4H), 7.36-7.30 (m, 2H), 7.27-7.22 (m, 2H), 7.15-7.11 (m, 3H), 6.93-6.88 (m, 2H), 5.66 (dd, *J₁* = 11.0 Hz, *J₂* = 4.0 Hz, 1H), 4.02 (dd, *J₁* = 18.0 Hz, *J₂* = 11.0 Hz, 1H), 3.82 (s, 3H), 3.35 (dd, *J₁* = 18.0 Hz, *J₂* = 3.5 Hz, 1H).

¹³C NMR (125 MHz, CD₂Cl₂) δ 198.2, 189.8, 159.9, 143.1, 138.9, 136.8, 133.5, 131.7, 129.8, 129.1, 129.0, 128.9, 128.3, 127.8, 127.5, 127.1, 114.1, 55.8, 48.7, 43.4.

IR (film): ν (cm⁻¹) 3060, 2911, 2839, 1678, 1592, 1513, 1450, 1400, 1360, 1332, 1297, 1246, 1207, 1176, 1149, 1103, 1076, 1030, 998, 940, 907, 834, 735, 693, 623, 523, 402.

HRMS (ESI, *m/z*) calcd for C₂₆H₂₂N₂O₃Na [M+Na]⁺: 433.1523, found: 433.1519.



(S)-1-(1-(4-Fluorophenyl)-1H-imidazol-2-yl)-2,4-diphenylbutane-1,4-dione (49d)

According to the general procedure, electrolysis of the reaction mixture of 1-(1-(4-fluorophenyl)-1H-imidazol-2-yl)-2-phenylethan-1-one **48d** (28.0 mg, 0.10 mmol) and trimethyl((1-phenylvinyl)oxy)silane **8a** (115.4 mg, 6.0 equiv) afforded 20.8 mg (52% yield) of **49d** as a white solid after electricity consumption of 2.2 F/mol.

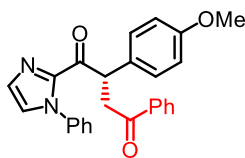
Enantiomeric excess was established by HPLC analysis using a Chiralpak IG column, ee = 96% (HPLC: IG, 254 nm, *n*-hexane/isopropanol = 20:80, flow rate 1 mL/min, 40 °C, *t_r* (major) = 10.5 min, *t_r* (minor) = 9.4 min). $[\alpha]_{\text{D}}^{22} = +130.8^{\circ}$ (*c* 1.0, CH₂Cl₂).

¹H NMR (300 MHz, CD₂Cl₂) δ 7.98-7.92 (m, 2H), 7.61-7.53 (m, 1H), 7.50-7.42 (m, 4H), 7.37-7.30 (m, 2H), 7.29-7.19 (m, 4H), 7.18-7.16 (m, 1H), 7.15-7.06 (m, 2H), 5.67 (dd, *J*₁ = 11.1 Hz, *J*₂ = 3.6 Hz, 1H), 4.03 (dd, *J*₁ = 18.0 Hz, *J*₂ = 11.1 Hz, 1H), 3.38 (dd, *J*₁ = 18.3 Hz, *J*₂ = 3.6 Hz, 1H).

¹³C NMR (75 MHz, CD₂Cl₂) δ 198.3, 190.1, 162.7 (d, *J* = 246.1), 143.2, 138.9, 136.9, 135.0 (d, *J* = 3.2 Hz), 133.6, 130.2, 129.2, 129.1, 129.0, 128.4, 128.0 (d, *J* = 8.7 Hz), 127.63, 127.57, 116.4 (d, *J* = 23.0 Hz), 48.8, 43.5.

IR (film): ν (cm⁻¹) 3062, 2910, 1678, 1598, 1508, 1449, 1402, 1360, 1323, 1220, 1152, 1095, 1020, 989, 940, 907, 840, 814, 735, 693, 621, 531.

HRMS (ESI, *m/z*) calcd for C₂₅H₁₉FN₂O₂Na [M+Na]⁺: 421.1323, found: 421.1320.



(S)-2-(4-Methoxyphenyl)-4-phenyl-1-(1-phenyl-1H-imidazol-2-yl)butane-1,4-dione (49f)

According to the general procedure, electrolysis of the reaction mixture of 2-(4-methoxyphenyl)-1-(1-phenyl-1H-imidazol-2-yl)ethan-1-one **48f** (29.2 mg, 0.10 mmol) and trimethyl((1-phenylvinyl)oxy)silane **8a** (115.4 mg, 6.0 equiv) afforded 28.0 mg (68% yield) of **49f** as a yellow oil after electricity consumption of 2.4 F/mol.

Enantiomeric excess was established by HPLC analysis using a Chiralpak IG column, ee = 97% (HPLC: IG, 254 nm, *n*-hexane/isopropanol = 20:80, flow rate 1 mL/min, 40 °C, *t_r* (major) = 19.8 min, *t_r* (minor) = 15.0 min). $[\alpha]_{\text{D}}^{22} = +268.2^{\circ}$ (*c* 1.0, CH₂Cl₂).

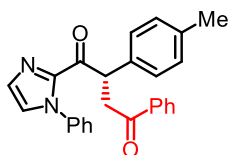
¹H NMR (300 MHz, CD₂Cl₂) δ 7.97-7.91 (m, 2H), 7.60-7.52 (m, 1H), 7.49-7.34 (m, 7H), 7.29-7.26 (m, 1H), 7.24-7.16 (m, 3H), 6.90-6.84 (m, 2H), 5.62 (dd, *J*₁ = 10.8 Hz, *J*₂ = 3.9 Hz, 1H), 3.99 (dd, *J*₁ = 18.0 Hz, *J*₂ = 10.8 Hz, 1H), 3.77 (s, 3H), 3.33 (dd, *J*₁ = 18.0 Hz, *J*₂ = 3.9 Hz, 1H).

¹³C NMR (75 MHz, CD₂Cl₂) δ 198.4, 190.1, 159.3, 143.2, 139.0, 137.0, 133.5, 130.7, 130.1, 130.0, 129.2, 128.9, 128.8, 128.4, 127.4, 126.1, 114.5, 55.6, 48.0, 43.3.

IR (film): ν (cm⁻¹) 3060, 2907, 2837, 1678, 1601, 1504, 1447, 1401, 1356, 1305, 1248, 1204, 1178,

1149, 1106, 1076, 1027, 992, 940, 907, 874, 834, 763, 734, 690, 655, 574, 535, 422.

HRMS (ESI, m/z) calcd for $C_{26}H_{22}N_2O_3Na$ $[M+H]^+$: 433.1523, found: 433.1519.



(S)-4-Phenyl-1-(1-phenyl-1H-imidazol-2-yl)-2-(p-tolyl)butane-1,4-dione (49g)

According to the general procedure, electrolysis of the reaction mixture of 1-(1-phenyl-1H-imidazol-2-yl)-2-(p-tolyl)ethan **48g** (27.6 mg, 0.10 mmol) and trimethyl((1-phenylvinyl)oxy)silane **8a** (115.4 mg, 6.0 equiv) afforded 34.6 mg (88% yield) of **49g** as a yellow solid after electricity consumption of 2.4 F/mol.

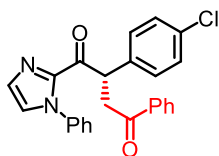
Enantiomeric excess was established by HPLC analysis using a Chiralpak IG column, ee = 97% (HPLC: IG, 254 nm, *n*-hexane/isopropanol = 30:70, flow rate 1 mL/min, 40 °C, t_r (major) = 16.2 min, t_r (minor) = 12.8 min). $[\alpha]_D^{22} = +238.0^\circ$ (c 1.0, CH_2Cl_2).

1H NMR (300 MHz, CD_2Cl_2) δ 7.97-7.91 (m, 2H), 7.60-7.52 (m, 1H), 7.50-7.40 (m, 5H), 7.37-7.30 (m, 2H), 7.24-7.27 (m, 1H), 7.25-7.20 (m, 2H), 7.19-7.12 (m, 3H), 5.64 (dd, $J_1 = 10.5$ Hz, $J_2 = 3.3$ Hz, 1H), 4.01 (dd, $J_1 = 18.0$ Hz, $J_2 = 10.8$ Hz, 1H), 3.34 (dd, $J_1 = 17.7$ Hz, $J_2 = 3.3$ Hz, 1H), 2.32 (s, 3H).

^{13}C NMR (75 MHz, CD_2Cl_2) δ 198.3, 190.0, 143.1, 139.0, 137.4, 137.0, 135.8, 133.5, 130.3, 130.0, 129.8, 129.2, 128.9, 128.8, 128.4, 127.5, 126.1, 48.5, 43.4, 21.1.

IR (film): ν (cm^{-1}) 3062, 2914, 1718, 1676, 1592, 1498, 1449, 1406, 1352, 1320, 1295, 1247, 1193, 1176, 1146, 1108, 1077, 1021, 992, 943, 908, 827, 767, 689, 655, 570, 534, 494.

HRMS (ESI, m/z) calcd for $C_{26}H_{22}N_2O_2Na$ $[M+Na]^+$: 417.1573, found: 417.1571.



(S)-2-(4-Chlorophenyl)-4-phenyl-1-(1-phenyl-1H-imidazol-2-yl)butane-1,4-dione (49h)

According to the general procedure, electrolysis of the reaction mixture of 2-(4-chlorophenyl)-1-(1-phenyl-1H-imidazol-2-yl)ethan-1-one **48h** (29.7 mg, 0.10 mmol) and trimethyl((1-phenylvinyl)oxy)silane **8a** (115.4 mg, 6.0 equiv) afforded 28.5 mg (67% yield) of **49h** as a yellow solid after

Enantiomeric excess was established by HPLC analysis using a Chiralpak IG column, ee = 95% (HPLC: IG, 254 nm, *n*-hexane/isopropanol = 30:70, flow rate 1 mL/min, 40 °C, t_r (major) = 15.0 min, t_r (minor) = 10.8 min). [α]_D²² = +229.8° (*c* 1.0, CH₂Cl₂).

¹³C NMR (75 MHz, CD₂Cl₂) δ 198.0, 189.5, 142.9, 138.9, 137.5, 136.8, 133.6, 133.4, 130.6, 130.2, 129.24, 129.21, 129.0, 128.9, 128.4, 127.7, 126.1, 48.2, 43.2.

HRMS (ESI, m/z) calcd for $C_{25}H_{19}ClN_2O_2Na$ $[M+Na]^+$: 437.1027, found: 437.1023.



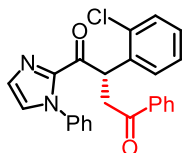
Enantiomeric excess was established by HPLC analysis using a Chiralpak IG column, ee = 96% (HPLC: IG, 254 nm, *n*-hexane/isopropanol = 20:80, flow rate 1 mL/min, 40 °C, t_r (major) = 14.9 min, t_r (minor) = 12.0 min). [α]_D²² = +172.8° (*c* 1.0, CH₂Cl₂).

¹³C NMR (75 MHz, CD₂Cl₂) δ 197.9, 189.3, 143.0, 141.1, 138.9, 136.8, 134.7, 133.6, 130.4, 130.2, 129.2, 129.1, 129.0, 128.9, 128.4, 127.8, 127.7, 127.5, 126.1, 48.4, 43.2.

403

1023, 992, 940, 906, 763, 732, 689, 662, 601, 559, 527, 507.

HRMS (ESI, m/z) calcd for $C_{25}H_{19}ClN_2O_2Na$ $[M+Na]^+$: 437.1027, found: 437.1023.



(S)-2-(2-Chlorophenyl)-4-phenyl-1-(1-phenyl-1H-imidazol-2-yl)butane-1,4-dione (49j)

According to the general procedure, electrolysis of the reaction mixture of 2-(2-chlorophenyl)-1-(1-phenyl-1H-imidazol-2-yl)ethan-1-one **48j** (29.7 mg, 0.10 mmol) and trimethyl((1-phenylvinyl)oxy)silane **8a** (115.4 mg, 6.0 equiv) afforded 31.4 mg (76% yield) of **49j** as a yellow solid after electricity consumption of 2.2 F/mol.

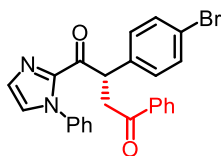
Enantiomeric excess was established by HPLC analysis using a Chiralpak IG column, ee = 94% (HPLC: IG, 254 nm, *n*-hexane/isopropanol = 30:70, flow rate 1 mL/min, 40 °C, t_r (major) = 12.7 min, t_r (minor) = 10.2 min). $[\alpha]_D^{22} = +283.2^\circ$ (c 1.0, CH_2Cl_2).

1H NMR (300 MHz, CD_2Cl_2) δ 7.97-7.90 (m, 2H), 7.61-7.52 (m, 1H), 7.50-7.41 (m, 6H), 7.33-7.26 (m, 2H), 7.25-7.17 (m, 5H), 6.06 (dd, $J_1 = 10.8$ Hz, $J_2 = 3.3$ Hz, 1H), 3.86 (dd, $J_1 = 18.3$ Hz, $J_2 = 11.1$ Hz, 1H), 3.31 (dd, $J_1 = 18.0$ Hz, $J_2 = 3.3$ Hz, 1H).

^{13}C NMR (75 MHz, CD_2Cl_2) δ 197.8, 189.5, 143.1, 138.9, 137.2, 136.8, 134.3, 133.6, 130.6, 130.3, 129.3, 129.1, 128.94, 128.92, 128.8, 128.4, 127.7, 127.5, 126.2, 45.8, 42.1.

IR (film): ν (cm^{-1}) 3060, 2909, 1679, 1592, 1497, 1445, 1401, 1353, 1304, 1244, 1205, 1150, 1097, 1078, 1039, 1011, 990, 938, 906, 845, 754, 690, 540, 485.

HRMS (ESI, m/z) calcd for $C_{25}H_{19}ClN_2O_2Na$ $[M+Na]^+$: 437.1027, found: 437.1024.



(S)-2-(4-Bromophenyl)-4-phenyl-1-(1-phenyl-1H-imidazol-2-yl)butane-1,4-dione (49k)

According to the general procedure, electrolysis of the reaction mixture of 2-(4-bromophenyl)-1-(1-phenyl-1H-imidazol-2-yl)ethan-1-one **48k** (34.1 mg, 0.10 mmol) and trimethyl((1-phenylvinyl)oxy)silane **8a** (115.4 mg, 6.0 equiv) afforded 38.2 mg (83% yield) of **49k** as a yellow solid after

electricity consumption of 2.2 F/mol.

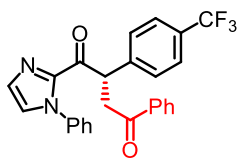
Enantiomeric excess was established by HPLC analysis using a Chiralpak IG column, ee = 97% (HPLC: IG, 254 nm, *n*-hexane/isopropanol = 30:70, flow rate 1 mL/min, 40 °C, t_r (major) = 16.9 min, t_r (minor) = 11.5 min). $[\alpha]_D^{22} = +194.6^\circ$ (*c* 1.0, CH₂Cl₂).

¹H NMR (250 MHz, CD₂Cl₂) δ 7.97-7.90 (m, 2H), 7.60-7.52 (m, 1H), 7.52-7.31 (m, 9H), 7.31-7.16 (m, 4H), 5.66 (dd, $J_1 = 10.6$ Hz, $J_2 = 3.4$ Hz, 1H), 3.99 (dd, $J_1 = 18.0$ Hz, $J_2 = 10.9$ Hz, 1H), 3.36 (dd, $J_1 = 17.9$ Hz, $J_2 = 3.4$ Hz, 1H).

¹³C NMR (75 MHz, CD₂Cl₂) δ 198.0, 189.4, 142.9, 138.9, 138.1, 136.8, 133.6, 132.2, 130.9, 130.2, 129.2, 129.0, 128.9, 128.4, 127.7, 126.1, 121.5, 48.2, 43.1.

IR (film): ν (cm⁻¹) 3063, 2922, 2854, 1675, 1592, 1486, 1449, 1406, 1353, 1315, 1247, 1202, 1073, 1005, 943, 909, 832, 770, 720, 685, 558, 528.

HRMS (ESI, *m/z*) calcd for C₂₅H₁₉BrN₂O₂Na [M+Na]⁺: 481.0522, found: 481.0518.



(S)-4-Phenyl-1-(1-phenyl-1H-imidazol-2-yl)-2-(4-(trifluoromethyl)phenyl)butane-1,4-dione (49I)

According to the general procedure, electrolysis of the reaction mixture of 1-(1-phenyl-1H-imidazol-2-yl)-2-(4-(trifluoromethyl)phenyl)ethan-1-one **48I** (33.0 mg, 0.10 mmol) and trimethyl((1-phenylvinyl)oxy)silane **8a** (115.4 mg, 6.0 equiv) afforded 39.0 mg (87% yield) of **49I** as a yellow solid after electricity consumption of 2.2 F/mol.

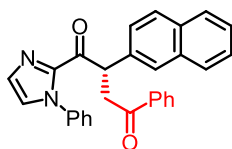
Enantiomeric excess was established by HPLC analysis using a Chiralpak IG column, ee = 95% (HPLC: IG, 254 nm, *n*-hexane/isopropanol = 30:70, flow rate 1 mL/min, 40 °C, t_r (major) = 11.2 min, t_r (minor) = 7.0 min). $[\alpha]_D^{22} = +193.6^\circ$ (*c* 1.0, CH₂Cl₂).

¹H NMR (500 MHz, CD₂Cl₂) δ 7.97-7.93 (m, 2H), 7.65-7.55 (m, 5H), 7.51-7.40 (m, 5H), 7.30 (d, $J = 1.0$ Hz, 1H), 7.26-7.22 (m, 2H), 7.21 (d, $J = 1.0$ Hz, 1H), 5.79 (dd, $J_1 = 11.0$ Hz, $J_2 = 4.0$ Hz, 1H), 4.04 (dd, $J_1 = 18.0$ Hz, $J_2 = 10.5$ Hz, 1H), 3.40 (dd, $J_1 = 18.0$ Hz, $J_2 = 4.0$ Hz, 1H).

¹³C NMR (125 MHz, CD₂Cl₂) δ 197.7, 189.1, 143.2, 142.7, 138.7, 136.6, 133.7, 130.2, 129.52, 129.50 (q, $J = 32.0$ Hz), 129.2, 128.94, 128.90, 128.3, 127.8, 126.1, 125.9 (q, $J = 3.9$ Hz), 124.6 (q, $J = 270.3$ Hz), 48.6, 43.1.

IR (film): ν (cm⁻¹) 2919, 2853, 1679, 1593, 1496, 1449, 1407, 1321, 1250, 1159, 1112, 1066, 1013, 992, 944, 910, 845, 766, 688, 605, 557, 527.

HRMS (ESI, m/z) calcd for C₂₆H₁₉F₃N₂O₂Na [M+Na]⁺: 471.1291, found: 471.1288.



(S)-2-(Naphthalen-2-yl)-4-phenyl-1-(1-phenyl-1H-imidazol-2-yl)butane-1,4-dione (49m)

According to the general procedure, electrolysis of the reaction mixture of 2-(naphthalen-2-yl)-1-(1-phenyl-1H-imidazol-2-yl)ethan-1-one **48m** (33.0 mg, 0.10 mmol) and trimethyl((1-phenylvinyl)oxy)silane **8a** (115.4 mg, 6.0 equiv) afforded 27.1 mg (63% yield) of **49m** as a yellow solid after electricity consumption of 2.4 F/mol.

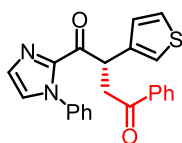
Enantiomeric excess was established by HPLC analysis using a Chiralpak IG column, ee = 96% (HPLC: IG, 254 nm, *n*-hexane/isopropanol = 30:70, flow rate 1 mL/min, 40 °C, t_r (major) = 23.5 min, t_r (minor) = 16.2 min). $[\alpha]_D^{22} = +286.8^\circ$ (*c* 1.0, CH₂Cl₂).

¹H NMR (300 MHz, CD₂Cl₂) δ 8.00-7.94 (m, 2H), 7.91 (br s, 1H), 7.87-7.80 (m, 3H), 7.62 (dd, $J_1 = 8.4$ Hz, $J_2 = 1.5$ Hz, 1H), 7.58-7.51 (m, 1H), 7.51-7.38 (m, 7H), 7.29 (d, $J = 0.9$ Hz, 1H), 7.25-7.19 (m, 2H), 7.17 (d, $J = 0.9$ Hz, 1H), 5.86 (dd, $J_1 = 11.1$ Hz, $J_2 = 3.9$ Hz, 1H), 4.14 (dd, $J_1 = 18.3$ Hz, $J_2 = 10.8$ Hz, 1H), 3.46 (dd, $J_1 = 18.3$ Hz, $J_2 = 3.9$ Hz, 1H).

¹³C NMR (75 MHz, CD₂Cl₂) δ 198.2, 189.7, 143.1, 139.0, 136.9, 136.4, 134.0, 133.6, 133.0, 130.1, 129.2, 129.0, 128.847, 128.753, 128.4, 128.1, 127.9, 127.8, 127.6, 127.2, 126.6, 126.3, 126.2, 49.0, 43.4.

IR (film): ν (cm⁻¹) 3056, 2908, 1678, 1593, 1497, 1447, 1402, 1349, 1310, 1264, 1211, 1149, 1097, 1075, 992, 939, 906, 858, 820, 759, 735, 690, 654, 567, 534, 478.

HRMS (ESI, m/z) calcd for C₂₉H₂₂N₂O₂Na [M+Na]⁺: 453.1573, found: 453.1570.



(S)-4-Phenyl-1-(1-phenyl-1H-imidazol-2-yl)-2-(thiophen-3-yl)butane-1,4-dione (49n)

According to the general procedure, electrolysis of the reaction mixture of 1-(1-phenyl-1*H*-imidazol-2-yl)-2-(thiophen-3-yl)ethan-1-one **48n** (26.8 mg, 0.10 mmol) and trimethyl((1-phenylvinyl)oxy)silane **8a** (115.4 mg, 6.0 equiv) afforded 16.2 mg (42% yield) of **49n** as a yellow solid after electricity consumption of 2.2 F/mol.

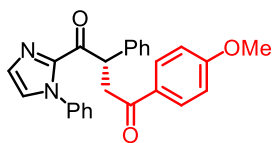
Enantiomeric excess was established by HPLC analysis using a Chiralpak IG column, ee = 98% (HPLC: IG, 254 nm, *n*-hexane/isopropanol = 30:70, flow rate 1 mL/min, 40 °C, *t_r* (major) = 13.2 min, *t_r* (minor) = 10.5 min). $[\alpha]_{\text{D}}^{22} = +162.6^\circ$ (*c* 1.0, CH₂Cl₂).

¹H NMR (300 MHz, CD₂Cl₂) δ 7.98-7.92 (m, 2H), 7.62-7.53 (m, 1H), 7.50-7.38 (m, 5H), 7.33-7.20 (m, 6H), 7.17 (dd, *J*₁ = 4.8 Hz, *J*₂ = 1.2 Hz, 1H), 5.81 (dd, *J*₁ = 11.1 Hz, *J*₂ = 3.6 Hz, 1H), 4.02 (dd, *J*₁ = 18.3 Hz, *J*₂ = 11.1 Hz, 1H), 3.41 (dd, *J*₁ = 18.3 Hz, *J*₂ = 3.9 Hz, 1H).

¹³C NMR (75 MHz, CD₂Cl₂) δ 198.2, 189.5, 143.1, 138.99, 138.97, 136.9, 133.6, 130.1, 129.2, 129.0, 128.8, 128.4, 128.2, 127.6, 126.2, 126.1, 123.0, 44.2, 42.9.

IR (film): ν (cm⁻¹) 3105, 3061, 2912, 1678, 1592, 1495, 1446, 1402, 1353, 1309, 1252, 1217, 1147, 1076, 991, 939, 907, 848, 810, 761, 733, 690, 654, 540, 510, 408.

HRMS (ESI, *m/z*) calcd for C₂₃H₁₈N₂O₂SNa [M+Na]⁺: 409.0981, found: 409.0978.



(S)-4-(4-Methoxyphenyl)-2-phenyl-1-(1-phenyl-1*H*-imidazol-2-yl)butane-1,4-dione (49o)

According to the general procedure, electrolysis of the reaction mixture of 2-phenyl-1-(1-phenyl-1*H*-imidazol-2-yl)ethan-1-one **48b** (26.2 mg, 0.10 mmol) and ((1-(4-methoxyphenyl)vinyl)oxy)trimethylsilane **8b** (133.4 mg, 6.0 equiv) afforded 37.3 mg (91% yield) of **49o** as a yellow oil after electricity consumption of 2.2 F/mol.

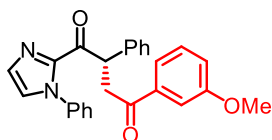
Enantiomeric excess was established by HPLC analysis using a Chiralpak IG column, ee = 94% (HPLC: IG, 254 nm, *n*-hexane/isopropanol = 20:80, flow rate 1 mL/min, 40 °C, *t_r* (major) = 24.9 min, *t_r* (minor) = 19.7 min). $[\alpha]_{\text{D}}^{22} = +168.2^\circ$ (*c* 1.0, CH₂Cl₂).

¹H NMR (300 MHz, CD₂Cl₂) δ 7.97-7.90 (m, 2H), 7.49-7.39 (m, 5H), 7.38-7.30 (m, 2H), 7.29-7.20 (m, 4H), 7.20-7.17 (m, 1H), 6.97-6.89 (m, 2H), 5.66 (dd, *J*₁ = 11.1 Hz, *J*₂ = 3.9 Hz, 1H), 3.98 (dd, *J*₁ = 17.7 Hz, *J*₂ = 10.8 Hz, 1H), 3.85 (s, 3H), 3.32 (dd, *J*₁ = 18.3 Hz, *J*₂ = 3.9 Hz, 1H).

^{13}C NMR (75 MHz, CD_2Cl_2) δ 196.6, 190.0, 164.0, 143.2, 139.1, 139.0, 130.6, 130.047, 129.979, 129.2, 129.12, 129.07, 128.8, 127.54, 127.49, 126.1, 114.1, 55.9, 48.9, 43.2.

IR (film): ν (cm^{-1}) 3060, 2908, 2841, 1673, 1598, 1499, 1449, 1402, 1360, 1310, 1250, 1212, 1169, 1105, 1075, 1023, 988, 939, 908, 836, 761, 734, 694, 588, 525.

HRMS (ESI, m/z) calcd for $\text{C}_{26}\text{H}_{22}\text{N}_2\text{O}_3\text{Na}$ $[\text{M}+\text{Na}]^+$: 433.1523, found: 433.1518.



(S)-4-(3-Methoxyphenyl)-2-phenyl-1-(1-phenyl-1*H*-imidazol-2-yl)butane-1,4-dione (49p)

According to the general procedure, electrolysis of the reaction mixture of 2-phenyl-1-(1-phenyl-1*H*-imidazol-2-yl)ethan-1-one **48b** (26.2 mg, 0.10 mmol) and ((1-(3-methoxyphenyl)vinyl)oxy)trimethylsilane **8c** (133.4 mg, 6.0 equiv) afforded 31.4 mg (76% yield) of **49p** as a yellow oil after electricity consumption of 2.4 F/mol.

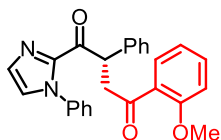
Enantiomeric excess was established by HPLC analysis using a Chiralpak IG column, ee = 97% (HPLC: IG, 254 nm, *n*-hexane/isopropanol = 20:80, flow rate 1 mL/min, 40 °C, t_r (major) = 19.1 min, t_r (minor) = 12.3 min). $[\alpha]_D^{22} = +181.8^\circ$ (c 1.0, CH_2Cl_2).

^1H NMR (300 MHz, CD_2Cl_2) δ 7.57-7.52 (m, 1H), 7.49-7.40 (m, 6H), 7.40-7.30 (m, 3H), 7.29-7.20 (m, 4H), 7.20-7.17 (m, 1H), 7.11 (ddd, $J_1 = 8.4$ Hz, $J_2 = 2.7$ Hz, $J_3 = 1.2$ Hz, 1H), 5.69 (dd, $J_1 = 10.8$ Hz, $J_2 = 3.6$ Hz, 1H), 4.01 (dd, $J_1 = 18.3$ Hz, $J_2 = 11.1$ Hz, 1H), 3.83 (s, 3H), 3.36 (dd, $J_1 = 18.0$ Hz, $J_2 = 3.6$ Hz, 1H).

^{13}C NMR (75 MHz, CD_2Cl_2) δ 198.0, 189.9, 160.3, 143.1, 139.0, 138.9, 138.3, 130.1, 130.0, 129.2, 129.146, 129.070, 128.8, 127.6, 127.5, 126.1, 121.0, 119.8, 112.8, 55.8, 48.9, 43.5.

IR (film): ν (cm^{-1}) 3060, 2913, 2839, 1679, 1590, 1492, 1449, 1402, 1311, 1259, 1166, 1077, 1023, 940, 908, 850, 761, 736, 692, 585, 531.

HRMS (ESI, m/z) calcd for $\text{C}_{26}\text{H}_{22}\text{N}_2\text{O}_3\text{Na}$ $[\text{M}+\text{Na}]^+$: 433.1523, found: 433.1519.



(S)-4-(2-Methoxyphenyl)-2-phenyl-1-(1-phenyl-1*H*-imidazol-2-yl)butane-1,4-dione (49q)

According to the general procedure, electrolysis of the reaction mixture of 2-phenyl-1-(1-phenyl-1*H*-imidazol-2-yl)ethan-1-one **48b** (26.2 mg, 0.10 mmol) and ((1-(2-methoxyphenyl)vinyl)oxy)trimethylsilane **8d** (133.4 mg, 6.0 equiv) afforded 32.8 mg (80% yield) of **49q** as a yellow solid after electricity consumption of 2.2 F/mol.

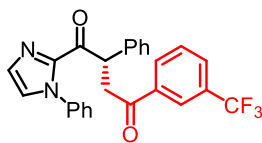
Enantiomeric excess was established by HPLC analysis using a Chiralpak IG column, ee = 94% (HPLC: IG, 254 nm, *n*-hexane/isopropanol = 30:70, flow rate 1 mL/min, 40 °C, t_r (major) = 17.4 min, t_r (minor) = 12.1 min). $[\alpha]_D^{22} = +134.4^\circ$ (*c* 1.0, CH₂Cl₂).

¹H NMR (300 MHz, CD₂Cl₂) δ 7.68 (dd, $J_1 = 7.8$ Hz, $J_2 = 1.8$ Hz, 1H), 7.52-7.40 (m, 6H), 7.37-7.28 (m, 2H), 7.28-7.20 (m, 4H), 7.20-7.17 (m, 1H), 7.02-6.94 (m, 2H), 5.64 (dd, $J_1 = 11.1$ Hz, $J_2 = 3.9$ Hz, 1H), 4.01 (dd, $J_1 = 18.6$ Hz, $J_2 = 11.1$ Hz, 1H), 3.86 (s, 3H), 3.43 (dd, $J_1 = 18.6$ Hz, $J_2 = 3.6$ Hz, 1H).

¹³C NMR (75 MHz, CD₂Cl₂) δ 199.9, 190.3, 159.5, 143.3, 139.3, 139.1, 134.1, 130.7, 130.0, 129.2, 129.1, 129.0, 128.7, 127.8, 127.4, 126.1, 120.8, 112.1, 55.9, 49.2, 48.7. (Missing one ¹³C signal because the resolution of NMR spectrometer is not enough.)

IR (film): ν (cm⁻¹) 3131, 3059, 2961, 2840, 1668, 1592, 1487, 1454, 1402, 1348, 1306, 1281, 1240, 1186, 1156, 1109, 1061, 1013, 991, 938, 909, 880, 845, 808, 755, 694, 665, 578, 539, 505.

HRMS (ESI, *m/z*) calcd for C₂₆H₂₂N₂O₃Na [M+Na]⁺: 433.1523, found: 433.1519.



(S)-2-Phenyl-1-(1-phenyl-1*H*-imidazol-2-yl)-4-(3-(trifluoromethyl)phenyl)butane-1,4-dione (49r)

According to the general procedure, electrolysis of the reaction mixture of 2-phenyl-1-(1-phenyl-1*H*-imidazol-2-yl)ethan-1-one **48b** (26.2 mg, 0.10 mmol) and trimethyl((1-(3-(trifluoromethyl)phenyl)vinyl)oxy)silane **8e** (156.2 mg, 6.0 equiv) afforded 21.2 mg (47% yield) of **49r** as a yellow oil after electricity consumption of 2.2 F/mol.

Enantiomeric excess was established by HPLC analysis using a Chiralpak IG column, ee = 98%

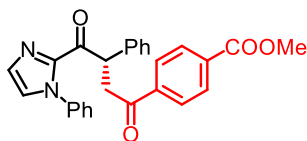
(HPLC: IG, 254 nm, *n*-hexane/isopropanol = 30:70, flow rate 1 mL/min, 40 °C, *t_r* (major) = 9.6 min, *t_r* (minor) = 6.8 min). $[\alpha]_{\text{D}}^{22} = +152.8^{\circ}$ (*c* 1.0, CH₂Cl₂).

¹H NMR (500 MHz, CD₂Cl₂) δ 8.20 (s, 1H), 8.14 (d, *J* = 7.9 Hz, 1H), 7.82 (d, *J* = 7.8 Hz, 1H), 7.61 (t, *J* = 7.8 Hz, 1H), 7.47-7.40 (m, 5H), 7.37-7.32 (m, 2H), 7.29-7.24 (m, 2H), 7.23-7.18 (m, 3H), 5.70 (dd, *J₁* = 10.9 Hz, *J₂* = 3.5 Hz, 1H), 4.04 (dd, *J₁* = 18.2 Hz, *J₂* = 11.0 Hz, 1H), 3.36 (dd, *J₁* = 18.2 Hz, *J₂* = 3.7 Hz, 1H).

¹³C NMR (125 MHz, CD₂Cl₂) δ 197.0, 189.5, 142.9, 138.8, 138.6, 137.3, 131.7, 131.2 (q, *J* = 32.4 Hz), 130.1, 129.9 (q, *J* = 3.7 Hz), 129.7, 129.2, 129.0, 128.8, 127.7, 127.6, 126.0, 125.2 (q, *J* = 2.4 Hz), 124.2 (q, *J* = 270.7 Hz), 48.7, 43.4. (Missing one ¹³C signal because the resolution of NMR spectrometer is not enough.)

IR (film): ν (cm⁻¹) 3062, 2908, 1683, 1605, 1496, 1446, 1403, 1365, 1323, 1241, 1168, 1125, 1071, 1026, 940, 905, 809, 761, 737, 691, 585, 529, 407.

HRMS (ESI, *m/z*) calcd for C₂₆H₁₉F₃N₂O₂Na [M+Na]⁺: 471.1291, found: 471.1287.



Methyl (*S*)-4-(4-oxo-3-phenyl-4-(1-phenyl-1*H*-imidazol-2-yl)butanoyl)benzoate (**49s**)

According to the general procedure, electrolysis of the reaction mixture of 2-phenyl-1-(1-phenyl-1*H*-imidazol-2-yl)ethan-1-one **48b** (26.2 mg, 0.10 mmol) and ethyl 4-(1-((trimethylsilyl)oxy)vinyl)benzoate **8f** (150.2 mg, 6.0 equiv) afforded 32.1 mg (73% yield) of **49s** as a yellow solid after electricity consumption of 2.2 F/mol.

Enantiomeric excess was established by HPLC analysis using a Chiralpak IG column, ee = 98% (HPLC: IG, 254 nm, *n*-hexane/isopropanol = 20:80, flow rate 1 mL/min, 40 °C, *t_r* (major) = 24.6 min, *t_r* (minor) = 16.9 min). $[\alpha]_{\text{D}}^{22} = +174.8^{\circ}$ (*c* 1.0, CH₂Cl₂).

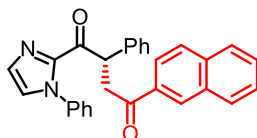
¹H NMR (300 MHz, CD₂Cl₂) δ 8.09 (d, *J* = 8.4 Hz, 2H), 7.99 (d, *J* = 8.7 Hz, 2H), 7.48-7.40 (m, 5H), 7.38-7.31 (m, 2H), 7.30-7.17 (m, 5H), 5.69 (dd, *J₁* = 10.8 Hz, *J₂* = 3.6 Hz, 1H), 4.04 (dd, *J₁* = 18.6 Hz, *J₂* = 11.1 Hz, 1H), 3.91 (s, 3H), 3.37 (dd, *J₁* = 18.3 Hz, *J₂* = 3.9 Hz, 1H).

¹³C NMR (75 MHz, CD₂Cl₂) δ 197.9, 189.7, 166.4, 143.0, 140.0, 138.9, 138.7, 134.5, 130.1, 130.0, 129.2, 129.0, 128.8, 128.4, 127.7, 127.6, 126.1, 52.7, 48.8, 43.6. (Missing one ¹³C signal because the

resolution of NMR spectrometer is not enough.)

IR (film): ν (cm⁻¹) 3059, 2952, 1722, 1681, 1597, 1496, 1444, 1402, 1362, 1276, 1195, 1150, 1107, 991, 939, 909, 858, 760, 733, 693, 530.

HRMS (ESI, m/z) calcd for C₂₇H₂₂N₂O₄Na [M+Na]⁺: 461.1472, found: 461.1467.



(S)-4-(Naphthalen-2-yl)-2-phenyl-1-(1-phenyl-1H-imidazol-2-yl)butane-1,4-dione (49t)

According to the general procedure, electrolysis of the reaction mixture of 2-phenyl-1-(1-phenyl-1H-imidazol-2-yl)ethan-1-one **48b** (26.2 mg, 0.10 mmol) and trimethyl((1-(naphthalen-2-yl)vinyl)oxy)silane **8g** (145.4 mg, 6.0 equiv) afforded 30.9 mg (72% yield) of **49t** as a yellow solid after electricity consumption of 2.2 F/mol.

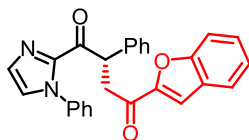
Enantiomeric excess was established by HPLC analysis using a Chiralpak IG column, ee = 96% (HPLC: IG, 254 nm, *n*-hexane/isopropanol = 30:70, flow rate 1 mL/min, 40 °C, t_r (major) = 25.8 min, t_r (minor) = 15.8 min). $[\alpha]_D^{22} = +218.4^\circ$ (*c* 1.0, CH₂Cl₂).

¹H NMR (300 MHz, CD₂Cl₂) δ 8.51 (s, 1H), 8.00 (dd, $J_1 = 8.4$ Hz, $J_2 = 1.5$ Hz, 1H), 7.96 (d, $J = 7.8$ Hz, 1H), 7.93-7.86 (m, 2H), 7.65-7.48 (m, 4H), 7.46-7.33 (m, 5H), 7.32-7.22 (m, 4H), 7.21-7.18 (m, 1H), 5.75 (dd, $J_1 = 10.8$ Hz, $J_2 = 3.3$ Hz, 1H), 4.17 (dd, $J_1 = 18.0$ Hz, $J_2 = 11.1$ Hz, 1H), 3.51 (dd, $J_1 = 18.0$ Hz, $J_2 = 3.6$ Hz, 1H).

¹³C NMR (75 MHz, CD₂Cl₂) δ 198.1, 189.9, 143.2, 139.03, 139.00, 136.0, 134.2, 132.9, 130.2, 130.1, 129.9, 129.20, 129.18, 129.1, 128.9, 128.8, 128.7, 128.1, 127.62, 127.56, 127.2, 126.1, 124.1, 49.0, 43.5.

IR (film): ν (cm⁻¹) 3058, 2908, 1675, 1628, 1594, 1495, 1447, 1401, 1363, 1309, 1265, 1217, 1178, 1124, 1076, 1025, 940, 905, 860, 822, 734, 694, 587, 529, 475.

HRMS (ESI, m/z) calcd for C₂₉H₂₂N₂O₂Na [M+Na]⁺: 453.1573, found: 453.1570.



(S)-4-(Benzofuran-2-yl)-2-phenyl-1-(1-phenyl-1*H*-imidazol-2-yl)butane-1,4-dione (49u)

According to the general procedure, electrolysis of the reaction mixture of 2-phenyl-1-(1-phenyl-1*H*-imidazol-2-yl)ethan-1-one **48b** (26.2 mg, 0.10 mmol) and ((1-(benzofuran-2-yl)vinyl)oxy)trimethylsilane **8h** (139.4 mg, 6.0 equiv) afforded 32.5 mg (77% yield) of **49u** as a yellow oil after electricity consumption of 2.4 F/mol.

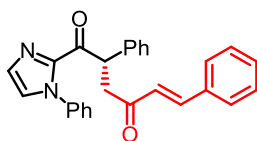
Enantiomeric excess was established by HPLC analysis using a Chiralpak IG column, ee = 99% (HPLC: IG, 254 nm, *n*-hexane/isopropanol = 30:70, flow rate 1 mL/min, 40 °C, *t_r* (major) = 26.7 min, *t_r* (minor) = 17.6 min). $[\alpha]_D^{22} = +169.4^\circ$ (*c* 1.0, CH₂Cl₂).

¹H NMR (300 MHz, CDCl₃) δ 7.59 (d, *J* = 7.8 Hz, 1H), 7.48-7.36 (m, 5H), 7.36-7.30 (m, 3H), 7.29-7.12 (m, 7H), 7.07-7.04 (m, 1H), 5.69 (dd, *J₁* = 10.8 Hz, *J₂* = 4.2 Hz, 1H), 3.95 (dd, *J₁* = 18.0 Hz, *J₂* = 10.8 Hz, 1H), 3.33 (dd, *J₁* = 18.0 Hz, *J₂* = 4.2 Hz, 1H).

¹³C NMR (75 MHz, CDCl₃) δ 189.3, 188.9, 155.6, 152.2, 142.6, 138.4, 138.1, 130.0, 128.9, 128.8, 128.7, 128.6, 128.1, 127.3, 127.00, 126.97, 125.7, 123.8, 123.2, 112.7, 112.4, 48.0, 43.0.

IR (film): ν (cm⁻¹) 3060, 2913, 1676, 1594, 1555, 1495, 1448, 1400, 1369, 1337, 1308, 1265, 1192, 1140, 1103, 1075, 1018, 935, 909, 874, 833, 735, 694, 537, 499.

HRMS (ESI, *m/z*) calcd for C₂₇H₂₀N₂O₃Na [M+Na]⁺: 443.1366, found: 443.1362.



(S,E)-2,6-Diphenyl-1-(1-phenyl-1*H*-imidazol-2-yl)hex-5-ene-1,4-dione (49v)

According to the general procedure, electrolysis of the reaction mixture of 2-phenyl-1-(1-phenyl-1*H*-imidazol-2-yl)ethan-1-one **48b** (26.2 mg, 0.10 mmol) and (*E*)-trimethyl((4-phenylbuta-1,3-dien-2-yl)oxy)silane **8i** (131.0 mg, 6.0 equiv) afforded 31.2 mg (77% yield) of **49v** as a yellow oil after electricity consumption of 2.4 F/mol.

Enantiomeric excess was established by HPLC analysis using a Chiralpak IG column, ee = 96% (HPLC: IG, 254 nm, *n*-hexane/isopropanol = 30:70, flow rate 1 mL/min, 40 °C, *t_r* (major) = 19.4 min,

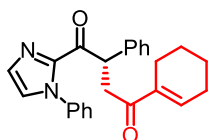
t_r (minor) = 14.0 min). $[\alpha]_D^{22} = +271.8^\circ$ (c 1.0, CH_2Cl_2).

^1H NMR (500 MHz, CD_2Cl_2) δ 7.58-7.52 (m, 3H), 7.45-7.41 (m, 5H), 7.41-7.37 (m, 3H), 7.35-7.32 (m, 2H), 7.27-7.20 (m, 4H), 7.18 (d, $J = 1.1$ Hz, 1H), 6.72 (d, $J = 16.3$ Hz, 1H), 5.59 (dd, $J_1 = 10.9$ Hz, $J_2 = 3.9$ Hz, 1H), 3.72 (dd, $J_1 = 17.9$ Hz, $J_2 = 10.9$ Hz, 1H), 3.08 (dd, $J_1 = 17.9$ Hz, $J_2 = 4.0$ Hz, 1H).

^{13}C NMR (125 MHz, CDCl_3) δ 198.1, 189.8, 143.1, 143.0, 138.9, 134.9, 130.8, 130.0, 129.24, 129.15, 129.1, 128.9, 128.8, 128.6, 127.5, 126.2, 126.0, 48.7, 44.9. (Missing two ^{13}C signal because the resolution of NMR spectrometer is not enough)

IR (film): ν (cm^{-1}) 3058, 2904, 1681, 1606, 1495, 1448, 1401, 1363, 1308, 1260, 1174, 1103, 1064, 1026, 976, 939, 909, 843, 735, 693, 585, 529.

HRMS (ESI, m/z) calcd for $\text{C}_{27}\text{H}_{22}\text{N}_2\text{O}_2\text{Na}$ $[\text{M}+\text{Na}]^+$: 429.1573, found: 429.1570.



(S)-4-(Cyclohex-1-en-1-yl)-2-phenyl-1-(1-phenyl-1H-imidazol-2-yl)butane-1,4-dione (49w)

According to the general procedure, electrolysis of the reaction mixture of 2-phenyl-1-(1-phenyl-1H-imidazol-2-yl)ethan-1-one **48b** (26.2 mg, 0.10 mmol) and ((1-(cyclohex-1-en-1-yl)vinyl)oxy)trimethylsilane **8j** (117.8 mg, 6.0 equiv) afforded 31.6 mg (82% yield) of **49w** as a yellow oil after electricity consumption of 2.0 F/mol.

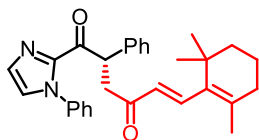
Enantiomeric excess was established by HPLC analysis using a Chiralpak IG column, ee = 95% (HPLC: IG, 254 nm, n -hexane/isopropanol = 50:50, flow rate 1 mL/min, 40 °C, t_r (major) = 14.5 min, t_r (minor) = 10.9 min). $[\alpha]_D^{22} = +232.6^\circ$ (c 1.0, CH_2Cl_2).

^1H NMR (300 MHz, CD_2Cl_2) δ 7.46-7.37 (m, 5H), 7.35-7.27 (m, 2H), 7.26-7.18 (m, 4H), 7.17-7.14 (m, 1H), 6.96-6.90 (m, 1H), 5.52 (dd, $J_1 = 11.1$ Hz, $J_2 = 3.6$ Hz, 1H), 3.68 (dd, $J_1 = 17.7$ Hz, $J_2 = 11.1$ Hz, 1H), 3.04 (dd, $J_1 = 17.7$ Hz, $J_2 = 3.9$ Hz, 1H), 2.28-2.12 (m, 4H), 1.68-1.53 (m, 4H).

^{13}C NMR (75 MHz, CD_2Cl_2) δ 199.0, 190.2, 143.2, 140.7, 139.2, 139.1, 139.0, 130.0, 129.2, 129.04, 129.02, 128.8, 127.43, 127.38, 126.1, 48.8, 42.2, 26.4, 23.4, 22.3, 21.9.

IR (film): ν (cm^{-1}) 3058, 2930, 2861, 1682, 1660, 1596, 1495, 1447, 1401, 1309, 1266, 1240, 1188, 1146, 1076, 1023, 992, 942, 907, 843, 760, 734, 695, 586, 525.

HRMS (ESI, m/z) calcd for $\text{C}_{25}\text{H}_{24}\text{N}_2\text{O}_2\text{Na}$ $[\text{M}+\text{Na}]^+$: 407.1730, found: 407.1727.



(*S,E*)-2-Phenyl-1-(1-phenyl-1*H*-imidazol-2-yl)-6-(2,6,6-trimethylcyclohex-1-en-1-yl)hex-5-ene-1,4-dione (49x)

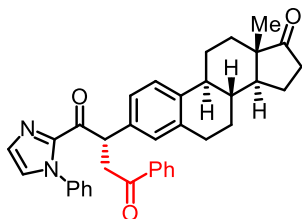
According to the general procedure, electrolysis of the reaction mixture of 2-phenyl-1-(1-phenyl-1*H*-imidazol-2-yl)ethan-1-one **48b** (26.2 mg, 0.10 mmol) and (*E*)-trimethyl((4-(2,6,6-trimethylcyclohex-1-en-1-yl)buta-1,3-dien-2-yl)oxy)silane **8k** (158.7 mg, 6.0 equiv) afforded 37.0 mg (82% yield) of **49x** as a yellow oil after electricity consumption of 2.2 F/mol. Enantiomeric excess was established by HPLC analysis using a Chiralpak IG column, ee = 97% (HPLC: IG, 254 nm, *n*-hexane/isopropanol = 50:50, flow rate 1 mL/min, 40 °C, *t_r* (major) = 8.9 min, *t_r* (minor) = 7.4 min). $[\alpha]_D^{22} = +167.6^\circ$ (*c* 1.0, CH₂Cl₂).

¹H NMR (300 MHz, CD₂Cl₂) δ 7.48-7.38 (m, 5H), 7.36-7.19 (m, 7H), 7.18-7.15 (m, 1H), 6.10 (d, *J* = 16.5 Hz, 1H), 5.55 (dd, *J₁* = 11.1 Hz, *J₂* = 3.9 Hz, 1H), 3.61 (dd, *J₁* = 18.0 Hz, *J₂* = 10.8 Hz, 1H), 3.01 (dd, *J₁* = 17.7 Hz, *J₂* = 4.2 Hz, 1H), 2.07 (t, *J* = 6.0 Hz, 2H), 1.74 (s, 3H), 1.68-1.55 (m, 2H), 1.52-1.44 (m, 2H), 1.05 (s, 6H).

¹³C NMR (75 MHz, CD₂Cl₂) δ 198.2, 189.9, 143.2, 142.8, 139.1, 139.0, 136.7, 136.3, 130.5, 130.0, 129.2, 129.07, 129.03, 128.8, 127.5, 126.1, 48.8, 44.8, 40.2, 34.4, 33.9, 28.9, 21.9, 19.3. (Missing one ¹³C signal because the resolution of NMR spectrometer is not enough.)

IR (film): ν (cm⁻¹) 2929, 2863, 1682, 1593, 1496, 1449, 1402, 1363, 1309, 1260, 1174, 1148, 1100, 1062, 1027, 977, 940, 909, 843, 761, 734, 694, 532.

HRMS (ESI, *m/z*) calcd for C₃₀H₃₂N₂O₂Na [M+Na]⁺: 475.2356, found: 475.2351.



(*S*)-2-((8*R*,9*S*,13*S*,14*S*)-13-Methyl-17-oxo-7,8,9,11,12,13,14,15,16,17-decahydro-6*H*-cyclopenta[*a*]phenanthren-3-yl)-4-phenyl-1-(1-phenyl-1*H*-imidazol-2-yl)butane-1,4-dione (49y)

According to the general procedure, electrolysis of the reaction mixture of estrone derived acyl

imidazole **48o** (43.9 mg, 0.10 mmol) and trimethyl((1-phenylvinyl)oxy)silane **8a** (115.4 mg, 6.0 equiv) afforded 26.7 mg (48% yield) of **49y** as a white solid after electricity consumption of 2.4 F/mol.

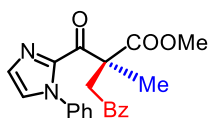
Diastereoselectivity was determined by ^1H NMR analysis of the crude mixture as $> 20:1$. $[\alpha]_{\text{D}}^{22} = +213.0^\circ$ (c 1.0, CH_2Cl_2).

^1H NMR (500 MHz, CD_2Cl_2) δ 7.96-7.91 (m, 2H), 7.59-7.53 (m, 1H), 7.48-7.40 (m, 5H), 7.29-7.16 (m, 6H), 7.14 (br s, 1H), 5.58 (dd, $J_1 = 11.0$ Hz, $J_2 = 3.5$ Hz, 1H), 3.98 (dd, $J_1 = 18.2$ Hz, $J_2 = 11.0$ Hz, 1H), 3.31 (dd, $J_1 = 18.1$ Hz, $J_2 = 3.6$ Hz, 1H), 2.95-2.85 (m, 2H), 2.46 (dd, $J_1 = 19.9$ Hz, $J_2 = 9.4$ Hz, 1H), 2.43-2.36 (m, 1H), 2.32-2.24 (m, 1H), 2.14-1.98 (m, 3H), 1.93-1.86 (m, 1H), 1.65-1.36 (m, 6H), 0.88 (s, 3H).

^{13}C NMR (125 MHz, CD_2Cl_2) δ 220.6, 198.2, 189.9, 143.1, 139.4, 138.9, 137.6, 136.8, 136.1, 133.5, 130.0, 129.3, 129.1, 128.9, 128.8, 128.3, 127.5, 126.3, 126.2, 126.1, 50.8, 48.3, 48.2, 44.7, 43.6, 38.4, 36.1, 32.0, 29.8, 26.8, 26.1, 21.8, 14.0.

IR (film): ν (cm^{-1}) 3059, 2925, 2861, 1734, 1680, 1595, 1496, 1447, 1402, 1349, 1308, 1257, 1209, 1148, 1080, 1044, 1008, 941, 906, 821, 764, 732, 692, 560, 514.

HRMS (ESI, m/z) calcd for $\text{C}_{37}\text{H}_{36}\text{N}_2\text{O}_3\text{Na}$ $[\text{M}+\text{Na}]^+$: 579.2618, found: 579.2612.



Methyl (S)-2-methyl-4-oxo-4-phenyl-2-(1-phenyl-1H-imidazole-2-carbonyl)butanoate (**51a**)

According to the general procedure, electrolysis of the reaction mixture of methyl 2-methyl-3-oxo-3-(1-phenyl-1H-imidazol-2-yl)propanoate **50a** (25.8 mg, 0.10 mmol) and trimethyl((1-phenylvinyl)oxy)silane **8a** (115.4 mg, 6.0 equiv) afforded 31.2 mg (83% yield) of **51a** as a yellow solid after electricity consumption of 2.2 F/mol.

Enantiomeric excess was established by HPLC analysis using a Chiralpak IC column, ee = 96% (HPLC: IC, 254 nm, n -hexane/isopropanol = 70:30, flow rate 1 mL/min, 40 $^\circ\text{C}$, t_{r} (major) = 7.9 min, t_{r} (minor) = 10.2 min). $[\alpha]_{\text{D}}^{22} = -5.0^\circ$ (c 1.0, CH_2Cl_2).

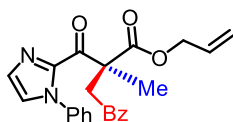
^1H NMR (300 MHz, CD_2Cl_2) δ 8.00-7.94 (m, 2H), 7.62-7.41 (m, 8H), 7.14-7.11 (m, 2H), 4.56 (d, $J = 18.3$ Hz, 1H), 3.93 (d, $J = 18.3$ Hz, 1H), 3.67 (s, 3H), 1.53 (s, 3H).

^{13}C NMR (75 MHz, CD_2Cl_2) δ 198.2, 186.6, 173.5, 141.8, 139.0, 137.3, 133.7, 129.3, 129.0, 128.8, 128.5, 126.6, 126.0, 55.5, 52.8, 46.3, 21.0. (Missing one ^{13}C signal because the resolution of NMR

spectrometer is not enough.)

IR (film): ν (cm⁻¹) 3060, 2946, 2917, 1737, 1686, 1591, 1448, 1405, 1351, 1228, 1180, 1095, 1029, 955, 897, 855, 753, 689, 580, 539.

HRMS (ESI, m/z) calcd for C₂₂H₂₀N₂O₄Na [M+Na]⁺: 399.1315, found: 399.1311.



Allyl (*S*)-2-methyl-4-oxo-4-phenyl-2-(1-phenyl-1*H*-imidazole-2-carbonyl)butanoate (51b**)**

According to the general procedure, electrolysis of the reaction mixture of allyl 2-methyl-3-oxo-3-(1-phenyl-1*H*-imidazol-2-yl)propanoate **50b** (28.4 mg, 0.10 mmol) and trimethyl((1-phenylvinyl)oxy)silane **8a** (115.4 mg, 6.0 equiv) afforded 30.2 mg (75% yield) of **51b** as a yellow oil after electricity consumption of 2.4 F/mol.

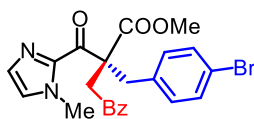
Enantiomeric excess was established by HPLC analysis using a Chiralpak IC column, ee = 95% (HPLC: IC, 254 nm, *n*-hexane/isopropanol = 80:20, flow rate 1 mL/min, 40 °C, t_r (major) = 9.0 min, t_r (minor) = 13.1 min). $[\alpha]_D^{22} = -10.4^\circ$ (c 1.0, CH₂Cl₂).

¹H NMR (300 MHz, CD₂Cl₂) δ 8.00-7.94 (m, 2H), 7.62-7.40 (m, 8H), 7.14-7.11 (m, 2H), 5.90-5.74 (m, 1H), 5.26-5.12 (m, 2H), 4.64-4.55 (m, 3H), 3.94 (d, J = 18.0 Hz, 1H), 1.55 (s, 3H).

¹³C NMR (75 MHz, CD₂Cl₂) δ 198.2, 186.5, 172.7, 141.8, 139.0, 137.3, 133.7, 132.5, 129.30, 129.27, 129.0, 128.8, 128.5, 126.6, 126.1, 118.0, 66.2, 55.6, 46.3, 21.1.

IR (film): ν (cm⁻¹) 3063, 2928, 1736, 1688, 1593, 1497, 1449, 1401, 1350, 1302, 1225, 1181, 1101, 960, 901, 852, 757, 690, 580, 535.

HRMS (ESI, m/z) calcd for C₂₄H₂₂N₂O₄Na [M+Na]⁺: 425.1472, found: 425.1469.



Methyl (*S*)-2-(4-bromobenzyl)-2-(1-methyl-1*H*-imidazole-2-carbonyl)-4-oxo-4-phenylbutanoate (51c**)**

According to the general procedure, electrolysis of the reaction mixture of methyl 2-(4-bromobenzyl)-3-(1-methyl-1*H*-imidazol-2-yl)-3-oxopropanoate **50c** (36.8 mg, 0.10 mmol) and

trimethyl((1-phenylvinyl)oxy)silane **8a** (115.4 mg, 6.0 equiv), *catalyzed by Δ -RhS* (4.3 mg, 5 mol%), afforded 39.6 mg (84% yield) of **51c** as a white solid after electricity consumption of 2.2 F/mol.

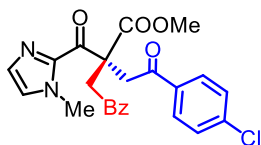
Enantiomeric excess was established by HPLC analysis using a Chiralpak IC column, ee = 93% (HPLC: IC, 254 nm, *n*-hexane/isopropanol = 70:30, flow rate 1 mL/min, 40 °C, t_r (major) = 12.6 min, t_r (minor) = 10.4 min). $[\alpha]_D^{22} = -165.8^\circ$ (*c* 1.0, CH₂Cl₂).

¹H NMR (300 MHz, CD₂Cl₂) δ 7.86-7.80 (m, 2H), 7.60-7.52 (m, 1H), 7.46-7.38 (m, 2H), 7.36-7.30 (m, 2H), 7.02-6.95 (m, 2H), 6.86-6.80 (m, 2H), 4.36 (d, *J* = 18.6 Hz, 1H), 3.95 (s, 3H), 3.69 (d, *J* = 18.6 Hz, 1H), 3.63 (s, 3H), 3.49 (d, *J* = 14.1 Hz, 1H), 3.40 (d, *J* = 13.8 Hz, 1H).

¹³C NMR (75 MHz, CD₂Cl₂) δ 198.3, 186.9, 171.5, 142.0, 137.0, 136.3, 133.8, 132.4, 131.7, 128.9, 128.8, 128.4, 126.8, 121.2, 60.2, 52.7, 42.4, 38.0, 36.2.

IR (film): ν (cm⁻¹) 3058, 2952, 2923, 1736, 1683, 1483, 1443, 1399, 1357, 1216, 1180, 1076, 1044, 1006, 941, 906, 848, 739, 690, 542, 509.

HRMS (ESI, *m/z*) calcd for C₂₃H₂₁BrN₂O₄Na [M+Na]⁺: 491.0577, found: 491.0573.



Methyl (R)-4-(4-chlorophenyl)-2-(1-methyl-1H-imidazole-2-carbonyl)-4-oxo-2-(2-oxo-2-phenylethyl)butanoate (51d)

According to the general procedure, electrolysis of the reaction mixture of 4-(4-chlorophenyl)-2-(1-methyl-1H-imidazole-2-carbonyl)-4-oxobutanoate **50d** (33.5 mg, 0.10 mmol) and trimethyl((1-phenylvinyl)oxy)silane **8a** (115.4 mg, 6.0 equiv), *catalyzed by Δ -RhS* (4.3 mg, 5 mol%), afforded 41.2 mg (91% yield) of **51d** as a yellow solid after electricity consumption of 2.4 F/mol. The reaction *catalyzed by Δ -RhS(TMS)* (4.5 mg, 5 mol%) formed **51d** in 46% with 87% ee.

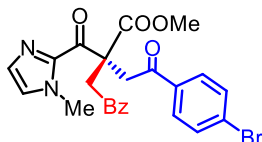
Enantiomeric excess was established by HPLC analysis using a Chiralpak IC column, ee = 96% (HPLC: IC, 254 nm, *n*-hexane/isopropanol = 60:40, flow rate 1 mL/min, 40 °C, t_r (major) = 14.2 min, t_r (minor) = 17.1 min). $[\alpha]_D^{22} = +4.0^\circ$ (*c* 1.0, CH₂Cl₂).

¹H NMR (300 MHz, CD₂Cl₂) δ 7.96-7.85 (m, 4H), 7.60-7.42 (m, 1H), 7.49-7.39 (m, 4H), 7.01-6.97 (m, 2H), 4.47 (d, *J* = 18.3 Hz, 1H), 4.42 (d, *J* = 17.7 Hz, 1H), 4.11 (d, *J* = 18.0 Hz, 1H), 4.10 (d, *J* = 18.0 Hz, 1H), 3.99 (s, 3H), 3.64 (s, 3H).

^{13}C NMR (75 MHz, CD_2Cl_2) δ 198.2, 197.2, 187.3, 171.4, 142.0, 139.9, 137.2, 135.7, 133.7, 130.0, 129.2, 128.9, 128.6, 128.5, 126.8, 59.1, 52.9, 43.3, 43.2, 36.5.

IR (film): ν (cm^{-1}) 2920, 2853, 1739, 1684, 1591, 1456, 1378, 1283, 1215, 1091, 1001, 908, 815, 757, 716, 529.

HRMS (ESI, m/z) calcd for $\text{C}_{24}\text{H}_{21}\text{ClN}_2\text{O}_5\text{Na}$ $[\text{M}+\text{Na}]^+$: 475.1031, found: 475.1025.



Methyl (R)-4-(4-bromophenyl)-2-(1-methyl-1H-imidazole-2-carbonyl)-4-oxo-2-(2-oxo-2-phenylethyl)butanoate (51e)

According to the general procedure, electrolysis of the reaction mixture of methyl 4-(4-bromophenyl)-2-(1-methyl-1H-imidazole-2-carbonyl)-4-oxobutanoate **50e** (37.9 mg, 0.10 mmol) and trimethyl((1-phenylvinyl)oxy)silane **8a** (115.4 mg, 6.0 equiv), *catalyzed by A-RhS (4.3 mg, 5 mol%)*, afforded 34.9 mg (70% yield) of **51e** as a white solid after electricity consumption of 2.4 F/mol.

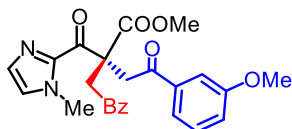
Enantiomeric excess was established by HPLC analysis using a Chiralpak IC column, ee = 93% (HPLC: IC, 254 nm, *n*-hexane/isopropanol = 50:50, flow rate 1 mL/min, 40 °C, t_r (major) = 12.3 min, t_r (minor) = 14.6 min). $[\alpha]_D^{22} = +3.0^\circ$ (*c* 1.0, CH_2Cl_2).

^1H NMR (300 MHz, CD_2Cl_2) δ 7.95-7.89 (m, 2H), 7.83-7.77 (m, 2H), 7.62-7.53 (m, 3H), 7.48-7.40 (m, 2H), 7.01-6.97 (m, 2H), 4.46 (d, $J = 18.0$ Hz, 1H), 4.41 (d, $J = 17.7$ Hz, 1H), 4.11 (d, $J = 18.0$ Hz, 1H), 4.09 (d, $J = 18.0$ Hz, 1H), 3.99 (s, 3H), 3.64 (s, 3H).

^{13}C NMR (75 MHz, CD_2Cl_2) δ 198.2, 197.5, 187.3, 171.4, 142.0, 137.2, 136.1, 133.7, 132.2, 130.1, 128.9, 128.6, 128.5, 126.8, 59.1, 52.9, 43.3, 43.2, 36.5. (Missing one ^{13}C signal because the resolution of NMR spectrometer is not enough.)

IR (film): ν (cm^{-1}) 2953, 2921, 2851, 1739, 1679, 1584, 1443, 1397, 1352, 1214, 1182, 1072, 998, 967, 942, 907, 813, 757, 734, 690, 599, 561, 530.

HRMS (ESI, m/z) calcd for $\text{C}_{24}\text{H}_{21}\text{BrN}_2\text{O}_5\text{Na}$ $[\text{M}+\text{Na}]^+$: 519.0526, found: 519.0521.



Methyl (R)-4-(3-methoxyphenyl)-2-(1-methyl-1H-imidazole-2-carbonyl)-4-oxo-2-(2-oxo-2-phenylethyl)butanoate (51f)

According to the general procedure, electrolysis of the reaction mixture of methyl 4-(3-methoxyphenyl)-2-(1-methyl-1H-imidazole-2-carbonyl)-4-oxobutanoate **50f** (33.0 mg, 0.10 mmol) and trimethyl((1-phenylvinyl)oxy)silane **8a** (115.4 mg, 6.0 equiv), *catalyzed by Δ -RhS (4.3 mg, 5 mol%)*, afforded 36.5 mg (81% yield) of **51f** as a white solid after electricity consumption of 2.2 F/mol.

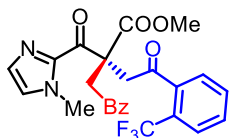
Enantiomeric excess was established by HPLC analysis using a Chiralpak IC column, ee = 95% (HPLC: IC, 254 nm, *n*-hexane/isopropanol = 50:50, flow rate 1 mL/min, 40 °C, t_r (major) = 15.1 min, t_r (minor) = 13.3 min). $[\alpha]_D^{22} = -55.0^\circ$ (*c* 1.0, CH₂Cl₂).

¹H NMR (300 MHz, CD₂Cl₂) δ 7.96-7.89 (m, 2H), 7.60-7.50 (m, 2H), 7.49-7.40 (m, 3H), 7.35 (t, *J* = 8.0 Hz, 1H), 7.09 (ddd, *J*₁ = 8.1 Hz, *J*₂ = 2.4 Hz, *J*₃ = 0.9 Hz, 8.1 Hz, 1H), 7.01-6.97 (m, 2H), 4.45 (d, *J* = 18.0 Hz, 1H), 4.44 (d, *J* = 18.0 Hz, 1H), 4.12 (d, *J* = 17.7 Hz, 1H), 4.11 (d, *J* = 18.0 Hz, 1H), 4.00 (s, 3H), 3.82 (s, 3H), 3.65 (s, 3H).

¹³C NMR (75 MHz, CD₂Cl₂) δ 198.3, 198.1, 187.4, 171.5, 160.3, 142.1, 138.6, 137.2, 133.6, 129.9, 128.9, 128.6, 128.5, 126.8, 121.1, 119.9, 112.8, 59.1, 55.8, 52.8, 43.5, 43.3, 36.5.

IR (film): ν (cm⁻¹) 3063, 3003, 2951, 2839, 1739, 1678, 1589, 1438, 1399, 1350, 1258, 1210, 1084, 1043, 1003, 969, 943, 907, 782, 734, 689, 594, 563, 531.

HRMS (ESI, *m/z*) calcd for C₂₅H₂₄N₂O₆Na [M+Na]⁺: 471.1527, found: 471.1523.



Methyl (R)-2-(1-methyl-1H-imidazole-2-carbonyl)-4-oxo-2-(2-(trifluoromethyl)phenyl)ethyl-4-phenylbutanoate (51g)

According to the general procedure, electrolysis of the reaction mixture of methyl 2-(1-methyl-1H-imidazole-2-carbonyl)-4-oxo-4-(2-(trifluoromethyl)phenyl)butanoate **50g** (36.8 mg,

0.10 mmol) and trimethyl((1-phenylvinyl)oxy)silane **8a** (115.4 mg, 6.0 equiv), *catalyzed by Δ -RhS* (4.3 mg, 5 mol%), afforded 38.4 mg (79% yield) of **51g** as a white solid after electricity consumption of 2.2 F/mol.

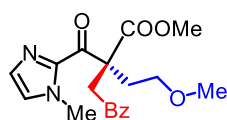
Enantiomeric excess was established by HPLC analysis using a Chiralpak IC column, ee = 93% (HPLC: IC, 254 nm, *n*-hexane/isopropanol = 70:30, flow rate 1 mL/min, 40 °C, t_r (major) = 12.6 min, t_r (minor) = 9.7 min). $[\alpha]_D^{22} = -12.2^\circ$ (*c* 1.0, CH₂Cl₂).

¹H NMR (300 MHz, CD₂Cl₂) δ 7.98-7.92 (m, 2H), 7.70-7.53 (m, 5H), 7.52-7.43 (m, 2H), 7.06-7.03 (m, 1H), 7.03-7.01 (m, 1H), 4.444 (d, *J* = 18.9 Hz, 1H), 4.436 (d, *J* = 17.7 Hz, 1H), 4.18 (d, *J* = 18.0 Hz, 1H), 4.06 (d, *J* = 19.2 Hz, 1H), 3.99 (s, 3H), 3.68 (s, 3H).

¹³C NMR (75 MHz, CD₂Cl₂) δ 202.0, 198.2, 187.0, 171.2, 142.0, 139.8 (q, *J* = 2.1 Hz), 137.2, 133.7, 132.3, 130.7, 129.0, 128.7, 128.5, 128.1, 127.1 (q, *J* = 31.5 Hz), 127.0 (q, *J* = 5.1 Hz), 126.9, 124.0 (q, *J* = 272.0 Hz), 58.9, 52.9, 47.9, 43.0, 36.5.

IR (film): ν (cm⁻¹) 2954, 2923, 1740, 1679, 1589, 1445, 1399, 1351, 1312, 1275, 1215, 1168, 1129, 1066, 1038, 966, 941, 763, 692, 649, 598, 563, 409.

HRMS (ESI, *m/z*) calcd for C₂₅H₂₁F₃N₂O₅Na [M+Na]⁺: 509.1295, found: 509.1292.



Methyl (S)-2-(2-methoxyethyl)-2-(1-methyl-1H-imidazole-2-carbonyl)-4-oxo-4-phenylbutanoate (51h)

According to the general procedure, electrolysis of the reaction mixture of methyl 4-methoxy-2-(1-methyl-1H-imidazole-2-carbonyl)butanoate **50h** (24.0 mg, 0.10 mmol) and trimethyl((1-phenylvinyl)oxy)silane **8a** (115.4 mg, 6.0 equiv) afforded 26.8 mg (75% yield) of **51h** as a colorless oil after electricity consumption of 2.2 F/mol.

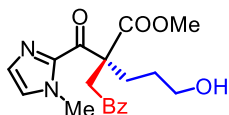
Enantiomeric excess was established by HPLC analysis using a Chiralpak OD-H column, ee = 96% (HPLC: OD-H, 254 nm, *n*-hexane/isopropanol = 85:15, flow rate 1 mL/min, 40 °C, t_r (major) = 9.4 min, t_r (minor) = 8.8 min). $[\alpha]_D^{22} = -78.8^\circ$ (*c* 1.0, CH₂Cl₂).

¹H NMR (300 MHz, CD₂Cl₂) δ 7.93-7.86 (m, 2H), 7.58-7.50 (m, 1H), 7.47-7.38 (m, 2H), 6.99-6.96 (m, 1H), 6.96-6.94 (m, 1H), 4.43 (d, *J* = 18.0 Hz, 1H), 4.08 (d, *J* = 18.0 Hz, 1H), 3.96 (s, 3H), 3.63 (s, 3H), 3.44 (t, *J* = 5.7 Hz, 2H), 3.06 (s, 3H), 2.37 (t, *J* = 5.7 Hz, 2H).

^{13}C NMR (75 MHz, CD_2Cl_2) δ 198.1, 187.8, 172.4, 142.3, 137.3, 133.4, 128.8, 128.5, 128.4, 126.4, 69.1, 58.4, 57.8, 52.7, 43.9, 36.1, 33.3.

IR (film): ν (cm^{-1}) 2925, 2872, 2811, 1736, 1683, 1591, 1443, 1399, 1356, 1290, 1217, 1188, 1111, 1001, 972, 907, 820, 757, 691, 571.

HRMS (ESI, m/z) calcd for $\text{C}_{19}\text{H}_{22}\text{N}_2\text{O}_5\text{Na}$ $[\text{M}+\text{Na}]^+$: 381.1421, found: 381.1419.



Methyl (S)-5-hydroxy-2-(1-methyl-1H-imidazole-2-carbonyl)-2-(2-oxo-2-phenylethyl) pentanoate (51i)

According to the general procedure, electrolysis of the reaction mixture of methyl 5-hydroxy-2-(1-methyl-1H-imidazole-2-carbonyl)pentanoate **50i** (24.0 mg, 0.10 mmol) and trimethyl((1-phenylvinyl)oxy)silane **8a** (115.4 mg, 6.0 equiv), catalyzed by Δ -RhS (4.3 mg, 5 mol%), afforded 24.7 mg (69% yield) of **51i** as a colorless oil after electricity consumption of 2.2 F/mol.

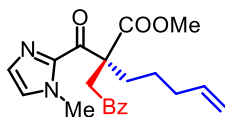
Enantiomeric excess was established by HPLC analysis using a Chiralpak OD-H column, ee = 96% (HPLC: OD-H, 254 nm, *n*-hexane/isopropanol = 70:30, flow rate 1 mL/min, 40 °C, t_r (major) = 6.3 min, t_r (minor) = 7.3 min). $[\alpha]_D^{22} = -22.8^\circ$ (c 1.0, CH_2Cl_2).

^1H NMR (500 MHz, CD_2Cl_2) δ 7.90-7.85 (m, 2H), 7.58-7.53 (m, 1H), 7.46-7.40 (m, 2H), 6.99-6.98 (m, 1H), 6.97-6.95 (m, 1H), 4.40 (d, J = 18.0 Hz, 1H), 3.94 (d, J = 18.0 Hz, 1H), 3.93 (s, 3H), 3.63 (s, 3H), 3.56 (t, J = 6.3 Hz, 2H), 2.26-2.07 (m, 2H), 1.61 (br s, 1H), 1.58-1.42 (m, 2H).

^{13}C NMR (125 MHz, CD_2Cl_2) δ 198.1, 187.9, 172.4, 142.1, 137.1, 133.6, 128.9, 128.6, 128.3, 126.5, 62.9, 58.9, 52.6, 43.1, 36.2, 29.5, 28.1.

IR (film): ν (cm^{-1}) 3523, 2926, 2865, 1733, 1682, 1592, 1446, 1398, 1356, 1220, 1183, 1091, 1053, 1005, 942, 905, 757, 691, 565.

HRMS (ESI, m/z) calcd for $\text{C}_{19}\text{H}_{22}\text{N}_2\text{O}_5\text{Na}$ $[\text{M}+\text{Na}]^+$: 381.1421, found: 381.1419.



Methyl (S)-2-(1-methyl-1H-imidazole-2-carbonyl)-2-(2-oxo-2-phenylethyl)hept-6-enoate (51j)

According to the general procedure, electrolysis of the reaction mixture of methyl

2-(1-methyl-1*H*-imidazole-2-carbonyl)hept-6-enoate **50j** (25.0 mg, 0.10 mmol) and trimethyl((1-phenylvinyl)oxy)silane **8a** (115.4 mg, 6.0 equiv), catalyzed by Δ -RhS (4.3 mg, 5 mol%), afforded 20.3 mg (55% yield) of **51j** as a colorless oil after electricity consumption of 2.4 F/mol.

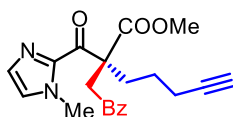
Enantiomeric excess was established by HPLC analysis using a Chiralpak IC column, ee = 94% (HPLC: IC, 254 nm, *n*-hexane/isopropanol = 85:15, flow rate 1 mL/min, 40 °C, t_r (major) = 11.9 min, t_r (minor) = 11.2 min). $[\alpha]_D^{22} = -23.4^\circ$ (*c* 1.0, CH₂Cl₂).

¹H NMR (300 MHz, CD₂Cl₂) δ 7.91-7.85 (m, 2H), 7.59-7.51 (m, 1H), 7.46-7.39 (m, 2H), 6.99-6.97 (m, 1H), 6.96-6.94 (m, 1H), 5.82-5.65 (m, 1H), 5.01-4.87 (m, 2H), 4.40 (d, *J* = 18.0 Hz, 1H), 3.945 (d, *J* = 18.0 Hz, 1H), 3.941 (s, 3H), 3.63 (s, 3H), 2.21-1.98 (m, 4H), 1.46-1.18 (m, 2H).

¹³C NMR (75 MHz, CD₂Cl₂) δ 198.2, 188.0, 172.4, 142.3, 138.7, 137.3, 135.6, 128.9, 128.6, 128.4, 126.5, 114.9, 59.2, 52.6, 43.1, 36.2, 34.2, 32.6, 24.2.

IR (film): ν (cm⁻¹) 3069, 2950, 2925, 2856, 1736, 1683, 1591, 1444, 1400, 1355, 1291, 1220, 1085, 996, 907, 758, 691, 565, 400.

HRMS (ESI, *m/z*) calcd for C₂₁H₂₄N₂O₄Na [M+Na]⁺: 391.1628, found: 391.1622.



Methyl (*S*)-2-(1-methyl-1*H*-imidazole-2-carbonyl)-2-(2-oxo-2-phenylethyl)hept-6-ynoate (**51k**)

According to the general procedure, electrolysis of the reaction mixture of methyl 2-(1-methyl-1*H*-imidazole-2-carbonyl)hept-6-ynoate **50k** (24.8 mg, 0.10 mmol) and trimethyl((1-phenylvinyl)oxy)silane **8a** (115.4 mg, 6.0 equiv) afforded 25.1 mg (69% yield) of **51k** as a colorless oil after electricity consumption of 2.2 F/mol.

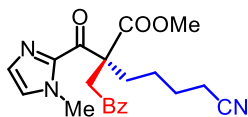
Enantiomeric excess was established by HPLC analysis using a Chiralpak IG column, ee = 90% (HPLC: IG, 254 nm, *n*-hexane/isopropanol = 90:10, flow rate 1 mL/min, 40 °C, t_r (major) = 34.9 min, t_r (minor) = 33.1 min). $[\alpha]_D^{22} = -37.8^\circ$ (*c* 1.0, CH₂Cl₂).

¹H NMR (300 MHz, CD₂Cl₂) δ 7.92-7.87 (m, 2H), 7.59-7.52 (m, 1H), 7.47-7.39 (m, 2H), 7.00-6.97 (m, 1H), 6.97-6.94 (m, 1H), 4.43 (d, *J* = 18.0 Hz, 1H), 3.95 (s, 3H), 3.93 (d, *J* = 18.0 Hz, 1H), 3.64 (s, 3H), 2.31-2.07 (m, 4H), 1.92 (t, *J* = 5.4 Hz, 1H), 1.60-1.35 (m, 2H).

¹³C NMR (75 MHz, CD₂Cl₂) δ 198.1, 187.7, 172.3, 142.2, 137.3, 133.6, 128.9, 128.6, 128.4, 126.5, 84.1, 68.7, 59.0, 52.7, 43.2, 36.2, 32.4, 24.2, 19.0.

IR (film): ν (cm⁻¹) 3289, 2950, 1735, 1683, 1591, 1445, 1399, 1355, 1293, 1218, 1179, 1085, 998, 937, 905, 758, 690, 640, 566, 523, 481.

HRMS (ESI, m/z) calcd for C₂₁H₂₂N₂O₄Na [M+Na]⁺: 389.1472, found: 389.1469.



Methyl (S)-6-cyano-2-(1-methyl-1H-imidazole-2-carbonyl)-2-(2-oxo-2-phenylethyl)hexanoate (51I)

According to the general procedure, electrolysis of the reaction mixture of methyl 6-cyano-2-(1-methyl-1H-imidazole-2-carbonyl)hexanoate **50I** (26.3 mg, 0.10 mmol) and trimethyl((1-phenylvinyl)oxy)silane **8a** (115.4 mg, 6.0 equiv), catalyzed by *Δ-RhS* (4.3 mg, 5 mol%), afforded 21.0 mg (55% yield) of **51I** as a colorless oil after electricity consumption of 2.2 F/mol.

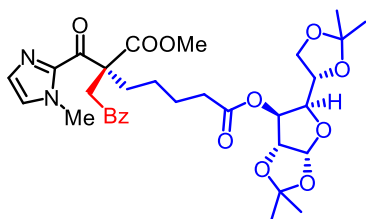
Enantiomeric excess was established by HPLC analysis using a Chiralpak OD-H column, ee = 91% (HPLC: OD-H, 254 nm, *n*-hexane/isopropanol = 80:20, flow rate 1 mL/min, 40 °C, t_r (major) = 14.8 min, t_r (minor) = 19.6 min). $[\alpha]_D^{22} = -59.2^\circ$ (c 1.0, CH₂Cl₂).

¹H NMR (300 MHz, CD₂Cl₂) δ 7.92-7.85 (m, 2H), 7.61-7.52 (m, 1H), 7.47-7.39 (m, 2H), 7.01-6.98 (m, 1H), 6.98-6.95 (m, 1H), 4.42 (d, J = 18.0 Hz, 1H), 3.93 (s, 3H), 3.92 (d, J = 17.7 Hz, 1H), 3.64 (s, 3H), 2.31 (t, J = 7.4 Hz, 2H), 2.25-2.03 (m, 2H), 1.70-1.56 (m, 2H), 1.51-1.25 (m, 2H).

¹³C NMR (75 MHz, CD₂Cl₂) δ 198.1, 187.7, 172.3, 142.1, 137.2, 133.7, 128.9, 128.7, 128.4, 126.7, 119.9, 59.1, 52.7, 43.1, 36.2, 32.3, 26.0, 24.0, 17.2.

IR (film): ν (cm⁻¹) 2950, 2870, 2246, 1736, 1683, 1591, 1450, 1400, 1356, 1286, 1220, 1174, 1091, 1044, 1001, 944, 906, 852, 759, 692, 567.

HRMS (ESI, m/z) calcd for C₂₁H₂₃N₃O₄Na [M+Na]⁺: 404.1581, found: 404.1578.



7-((3aR,5R,6S,6aR)-5-((S)-2,2-Dimethyl-1,3-dioxolan-4-yl)-2,2-dimethyltetrahydrofuro[2,3-d][1,3]dioxol-6-yl)-1-methyl (S)-2-(1-methyl-1H-imidazole-2-carbonyl)-2-(2-oxo-2-phenylethyl)hexanoate

heptanedioate (51m)

According to the general procedure, electrolysis of the reaction mixture of glucofuranose derived acyl imidazole **50m** (52.5 mg, 0.10 mmol) and trimethyl((1-phenylvinyl)oxy)silane **8a** (115.4 mg, 6.0 equiv), *catalyzed by Δ -RhS (4.3 mg, 5 mol%)*, afforded 38.7 mg (60% yield) of **51m** as a yellow solid after electricity consumption of 2.0 F/mol.

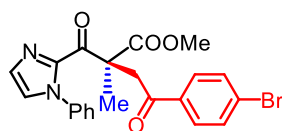
Diastereoselectivity was determined by HPLC analysis using a Chiralpak IC column, de = 94% (HPLC: IC, 254 nm, *n*-hexane/isopropanol = 85:15, flow rate 1 mL/min, 40 °C, t_r (major) = 39.2 min, t_r (minor) = 34.7 min). $[\alpha]_D^{22} = -32.8^\circ$ (*c* 1.0, CH₂Cl₂).

¹H NMR (500 MHz, CD₂Cl₂) δ 7.90-7.85 (m, 2H), 7.58-7.53 (m, 1H), 7.46-7.40 (m, 2H), 6.99-6.98 (m, 1H), 6.97-6.95 (m, 1H), 5.86 (d, *J* = 3.7 Hz, 1H), 5.14 (d, *J* = 2.7 Hz, 1H), 4.45 (d, *J* = 3.8 Hz, 1H), 4.39 (d, *J* = 18.0 Hz, 1H), 4.22-4.14 (m, 2H), 4.05-4.01 (m, 1H), 3.98-3.93 (m, 1H), 3.93 (s, 3H), 3.91 (d, *J* = 18.0 Hz, 1H), 3.62 (s, 3H), 2.30 (t, *J* = 7.6 Hz, 2H), 2.19-2.00 (m, 2H), 1.64-1.56 (m, 2H), 1.49 (s, 3H), 1.37 (s, 3H), 1.35-1.20 (m, 2H), 1.29 (s, 3H), 1.28 (s, 3H).

¹³C NMR (125 MHz, CD₂Cl₂) δ 198.1, 187.8, 172.4, 172.3, 142.0, 137.1, 133.6, 128.9, 128.6, 128.3, 126.5, 112.4, 109.4, 105.5, 83.7, 80.0, 76.2, 72.8, 67.2, 59.0, 52.6, 43.0, 36.2, 34.1, 32.5, 26.79, 26.77, 26.3, 25.30, 25.27, 24.3.

IR (film): ν (cm⁻¹) 2987, 2942, 2871, 1739, 1685, 1596, 1509, 1453, 1401, 1377, 1214, 1157, 1071, 1018, 945, 903, 846, 759, 734, 692, 565, 512.

HRMS (ESI, *m/z*) calcd for C₃₃H₄₂N₂O₁₁Na [M+Na]⁺: 665.2681, found: 665.2679.

**Methyl (S)-4-(4-bromophenyl)-2-methyl-4-oxo-2-(1-phenyl-1H-imidazole-2-carbonyl) butanoate (51n)**

According to the general procedure, electrolysis of the reaction mixture of methyl 2-methyl-3-oxo-3-(1-phenyl-1H-imidazol-2-yl)propanoate **50a** (25.8 mg, 0.10 mmol) and ((1-(4-bromophenyl)vinyl)oxy)trimethylsilane **8l** (162.7 mg, 6.0 equiv) afforded 37.2 mg (82% yield) of **51n** as a yellow solid after electricity consumption of 2.4 F/mol.

Enantiomeric excess was established by HPLC analysis using a Chiralpak IC column, ee = 97%

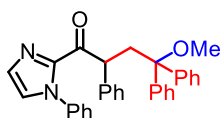
(HPLC: OD-H, 254 nm, *n*-hexane/isopropanol = 90:10, flow rate 1 mL/min, 40 °C, t_r (major) = 12.2 min, t_r (minor) = 14.0 min). $[\alpha]_D^{22} = -42.6^\circ$ (c 1.0, CH_2Cl_2).

^1H NMR (500 MHz, CD_2Cl_2) δ 7.86-7.82 (m, 2H), 7.64-7.59 (m, 2H), 7.54-7.45 (m, 3H), 7.44-7.39 (m, 2H), 7.15-7.11 (m, 2H), 4.51 (d, J = 18.2 Hz, 1H), 3.88 (d, J = 18.2 Hz, 1H), 3.66 (s, 3H), 1.52 (s, 3H).

^{13}C NMR (125 MHz, CD_2Cl_2) δ 197.2, 186.3, 173.4, 141.5, 138.8, 135.9, 132.2, 130.0, 129.30, 129.26, 128.8, 128.7, 126.6, 125.9, 55.4, 52.8, 46.2, 21.0.

IR (film): ν (cm^{-1}) 2922, 2851, 1736, 1690, 1583, 1495, 1449, 1398, 1347, 1300, 1232, 1180, 1101, 1070, 1028, 1002, 958, 903, 855, 813, 760, 691, 527, 453.

HRMS (ESI, m/z) calcd for $\text{C}_{22}\text{H}_{19}\text{BrN}_2\text{O}_4\text{Na}$ $[\text{M}+\text{Na}]^+$: 479.0403, found: 479.0394.



4-Methoxy-2,4,4-triphenyl-1-(1-phenyl-1H-imidazol-2-yl)butan-1-one (**58**)

According to the general procedure, the reaction of **48b** with 6.0 equiv 1,1-diphenyl ethylene in the absence of **8a** furnished a three-component product **58** in 51% yield with 99% ee. Enantiomeric excess was established by HPLC analysis using a Chiralpak IG column, ee = 99% (HPLC: IG, 254 nm, *n*-hexane/isopropanol = 95:5, flow rate 1 mL/min, 40 °C, t_r (major) = 6.4 min, t_r (minor) = 7.6 min). $[\alpha]_D^{22} = +157.8^\circ$ (c 1.0, CH_2Cl_2).

^1H NMR (300 MHz, CD_2Cl_2) δ 7.42-7.21 (m, 14H), 7.20-7.09 (m, 5H), 7.05-7.03 (m, 1H), 7.02-6.96 (m, 2H), 5.31 (dd, J_1 = 9.3 Hz, J_2 = 1.5 Hz, 1H), 3.59 (dd, J_1 = 14.4 Hz, J_2 = 9.3 Hz, 1H), 2.91 (s, 3H), 2.57 (dd, J_1 = 14.4 Hz, J_2 = 1.5 Hz, 1H).

^{13}C NMR (75 MHz, CD_2Cl_2) δ 188.8, 145.3, 144.7, 142.5, 141.1, 138.6, 129.3, 128.6, 128.5, 128.3, 127.9, 127.5, 127.4, 127.2, 127.1, 126.8, 126.6, 126.0, 82.4, 50.4, 47.3, 38.2.

IR (film): ν (cm^{-1}) 3058, 2928, 1683, 1596, 1493, 1446, 1399, 1311, 1261, 1152, 1073, 1030, 956, 908, 859, 758, 696, 618, 582, 531.

HRMS (ESI, m/z) calcd for $\text{C}_{32}\text{H}_{28}\text{N}_2\text{O}_2\text{Na}$ $[\text{M}+\text{Na}]^+$: 495.2043, found: 495.2037.

5.7.4 Single-Crystal X-Ray Diffraction Studies

Single crystals of **49k** suitable for X-ray diffraction were obtained by slow diffusion of a solution

of **49k** (30 mg) in CH₂Cl₂ (0.5 mL) layered with *n*-hexane (1.0 mL) at room temperature for several days in a NMR tube.

Single crystals of **51n** suitable for X-ray diffraction were obtained by slow diffusion of a solution of **51n** (30 mg) in CH₂Cl₂ (0.5 mL) layered with *n*-hexane (1.0 mL) at –20 °C for several days in a NMR tube.

Single crystals of **Rh-enolate2** suitable for X-ray diffraction were obtained by slow diffusion of a solution of **Rh-enolate2** (20 mg) in CH₂Cl₂ (0.5 mL) layered with Et₂O (1.0 mL) at room temperature for several days in a NMR tube.

Data was collected with an STOE STADIVARI diffractometer equipped with CuK_α radiation, a graded multilayer mirror monochromator ($\lambda = 1.54186$ Å) and a DECTRIS PILATUS 300K detector using an oil-coated shock-cooled crystal at 100(2) K. The absolute configurations of compounds **49k** and **51n** could be determined (**Figure 130**). The structures of **Rh-enolate2** are shown in **Figure 104a**.

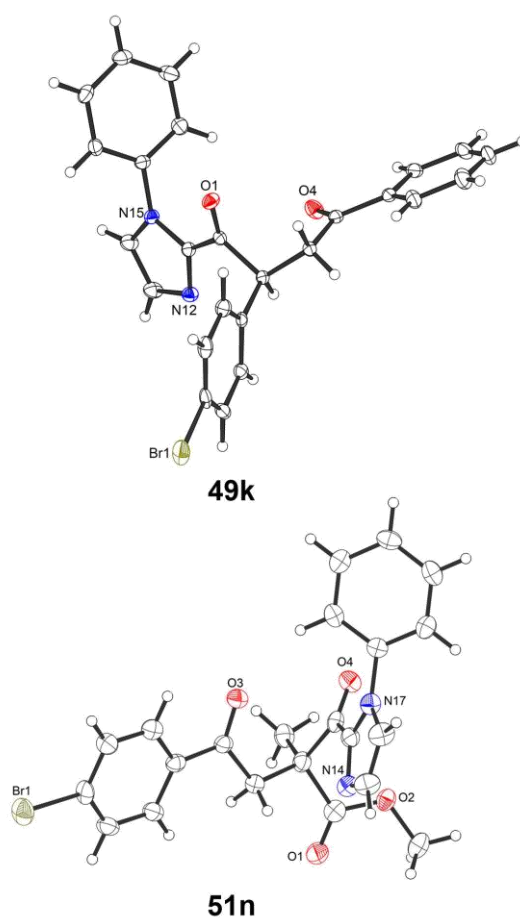


Figure 130. Crystal structures of compounds **49k**, and **51n**.

Table 33. Crystal data and structure refinement for **Rh-enolate2**.

Crystal data

CCDC number	1866728	
Identification code	hxqM39_5	
Habitus, color	needle, pale yellow	
Crystal size	0.23 x 0.04 x 0.04 mm ³	
Crystal system	Triclinic	
Space group	P-1	Z = 4
Unit cell dimensions	a = 11.8377(5) Å	α = 81.120(3) °
	b = 19.7310(7) Å	β = 81.221(3) °
	c = 19.8024(8) Å	γ = 78.747(3) °
Volume	4446.0(3) Å ³	
Cell determination	28713 peaks with Theta 3.8 to 75.5 °	
Empirical formula	C ₄₉ H ₄₅ N ₄ O Rh S ₂ S _{i2}	
Moiety formula	C ₄₉ H ₄₅ N ₄ O Rh S ₂ S _{i2}	
Formula weight	929.10	
Density (calculated)	1.388 Mg/m ³	
Absorption coefficient	4.823 mm ⁻¹	
F(000)	1920	

Data collection:

Diffractometer type	STOE STADIVARI
Wavelength	1.54186 Å
Temperature	100(2) K
Theta range for data collection	3.023 to 75.866 °
Index ranges	-10 ≤ h ≤ 14, -24 ≤ k ≤ 24, -24 ≤ l ≤ 24
Data collection software	X-Area Pilatus3_SV 1.31.127.0 (STOE, 2016)
Cell refinement software	X-Area Recipe 1.33.0.0 (STOE, 2015)
Data reduction software	X-Area Integrate 1.71.0.0 (STOE, 2016)
	X-Area LANA 1.68.2.0 (STOE, 2016)

Solution and refinement:

Reflections collected	87185
Independent reflections	28982 [R(int) = 0.0895]
Completeness to theta = 67.686 °	92.3 %
Observed reflections	15724 [I > 2σ(I)]
Reflections used for refinement	28982
Absorption correction	Semi-empirical from equivalents
Max. and min. transmission	0.87 and 0.38
Largest diff. peak and hole	1.331 and -1.224 e.Å ⁻³
Solution	intrinsic phases
Refinement	Full-matrix least-squares on F ²
Treatment of hydrogen atoms	Calculated positions, constr. ref.
Programs used	XT V2014/1 (Bruker AXS Inc., 2014) SHELXL-2018/3 (Sheldrick, 2018) DIAMOND (Crystal Impact) ShelXle (Hübschle, Sheldrick, Dittrich, 2011)
Data / restraints / parameters	28982 / 1302 / 1076
Goodness-of-fit on F ²	0.928
R index (all data)	wR2 = 0.1938
R index conventional [I > 2σ(I)]	R1 = 0.0726

Table 34. Crystal data and structure refinement for **49k**.

Crystal data

CCDC number	1866727
Identification code	hxqL160R
Habitus, color	nugget, colorless
Crystal size	0.49 x 0.36 x 0.21 mm ³
Crystal system	Orthorhombic
Space group	P2 ₁ 2 ₁ 2 ₁
Unit cell dimensions	$a = 12.1520(2) \text{ \AA}$ $b = 12.7735(3) \text{ \AA}$ $c = 13.4315(2) \text{ \AA}$
	$Z = 4$ $\alpha = 90^\circ$ $\beta = 90^\circ$ $\gamma = 90^\circ$
Volume	2084.89(7) Å ³
Cell determination	35530 peaks with Theta 3.3 to 76.2 °
Empirical formula	C ₂₅ H ₁₉ Br N ₂ O ₂
Moiety formula	C ₂₅ H ₁₉ Br N ₂ O ₂
Formula weight	459.33
Density (calculated)	1.463 Mg/m ³
Absorption coefficient	2.881 mm ⁻¹
F(000)	936

Data collection:

Diffraction type	STOE STADIVARI
Wavelength	1.54186 Å
Temperature	100(2) K
Theta range for data collection	4.908 to 75.603 °
Index ranges	-15 ≤ h ≤ 12, -13 ≤ k ≤ 15, -15 ≤ l ≤ 16
Data collection software	X-Area Pilatus3_SV 1.31.127.0 (STOE, 2016)
Cell refinement software	X-Area Recipe 1.33.0.0 (STOE, 2015)
Data reduction software	X-Area Integrate 1.71.0.0 (STOE, 2016) X-Area LANA 1.68.2.0 (STOE, 2016)

Solution and refinement:

Reflections collected	20804
Independent reflections	4273 [R(int) = 0.0193]
Completeness to theta = 67.686 °	99.9 %
Observed reflections	4266 [I > 2σ(I)]
Reflections used for refinement	4273
Absorption correction	Semi-empirical from equivalents
Max. and min. transmission	0.5407 and 0.2622
Flack parameter (absolute struct.)	-0.016(4)
Largest diff. peak and hole	0.302 and -0.757 e.Å ⁻³
Solution	intrinsic phases
Refinement	Full-matrix least-squares on F ²
Treatment of hydrogen atoms	Calculated positions, constr. ref.
Programs used	XT V2014/1 (Bruker AXS Inc., 2014) SHELXL-2018/3 (Sheldrick, 2018) DIAMOND (Crystal Impact) ShelXle (Hübschle, Sheldrick, Dittrich, 2011)
Data / restraints / parameters	4273 / 0 / 271
Goodness-of-fit on F ²	1.104
R index (all data)	wR2 = 0.0590
R index conventional [I > 2σ(I)]	R1 = 0.0228

Table 35. Crystal data and structure refinement for **51n**.

Crystal data		
CCDC number	1868792	
Identification code	hxqM124	
Habitus, color	needle, colorless	
Crystal size	0.24 x 0.03 x 0.02 mm ³	
Crystal system	Orthorhombic	
Space group	P2 ₁ 2 ₁ 2 ₁	Z = 4
Unit cell dimensions	a = 7.0991(3) Å	α = 90 °
	b = 14.6639(9) Å	β = 90 °
	c = 19.2121(9) Å	γ = 90 °
Volume	1999.99(18) Å ³	
Cell determination	20187 peaks with Theta 3.8 to 75.4 °	
Empirical formula	C ₂₂ H ₁₉ Br N ₂ O ₄	
Moiety formula	C ₂₂ H ₁₉ Br N ₂ O ₄	
Formula weight	455.30	
Density (calculated)	1.512 Mg/m ³	
Absorption coefficient	3.070 mm ⁻³	
F(000)	928	
Data collection:		
Diffraction type	STOE STADIVARI	
Wavelength	1.54186 Å	
Temperature	100(2) K	
Theta range for data collection	3.792 to 75.320 °	
Index ranges	-8<=h<=8, -16<=k<=18, -13<=l<=23	
Data collection software	X-Area Pilatus3_SV 1.31.127.0 (STOE, 2016)	
Cell refinement software	X-Area Recipe 1.33.0.0 (STOE, 2015)	
Data reduction software	X-Area Integrate 1.71.0.0 (STOE, 2016)	
	X-Area LANA 1.68.2.0 (STOE, 2016)	
Solution and refinement:		
Reflections collected	18971	
Independent reflections	4044 [R(int) = 0.0506]	
Completeness to theta = 67.686 °	99.6 %	
Observed reflections	3407[I > 2σ(I)]	
Reflections used for refinement	4044	
Absorption correction	Semi-empirical from equivalents	
Max. and min. transmission	0.6496 and 0.1848	
Flack parameter (absolute struct.)	-0.032(12)	
Largest diff. peak and hole	0.545 and -0.312 e.Å ⁻³	
Solution	intrinsic phases	
Refinement	Full-matrix least-squares on F ²	
Treatment of hydrogen atoms	Calculated positions, constr. ref.	
Programs used	XT V2014/1 (Bruker AXS Inc., 2014)	
	SHELXL-2018/3 (Sheldrick, 2018)	
	DIAMOND (Crystal Impact)	
	ShelXle (Hübschle, Sheldrick, Dittrich, 2011)	
Data / restraints / parameters	4044 / 0 / 264	
Goodness-of-fit on F ²	1.006	
R index (all data)	wR2 = 0.0994	
R index conventional [I>2sigma(I)]	R1 = 0.0402	

References

1. J. Ma, X. Zhang, X. Huang, S. Luo, E. Meggers, *Nat. Protoc.* **2018**, *13*, 605-632.
2. M. Yan, Y. Kawamata, P. S. Baran, *Angew. Chem. Int. Ed.* **2017**, *57*, 4149-4155.
3. M. A. Cismesia, T. P. Yoon, *Chem. Sci.* **2015**, *6*, 5426-5434.
4. U. Megerle, R. Lechner, B. König, E. Riedle, *Photochem. Photobiol. Sci.* **2010**, *9*, 1400-1406.
5. C. Wang, Y. Zheng, H. Huo, P. Röse, L. Zhang, K. Harms, G. Hilt, E. Meggers, *Chem. Eur. J.* **2015**, *21*, 7355-7359.
6. a) L.-M. Jin, X. Xu, H. Lu, X. Cui, L. Wojtas, X. P. Zhang, *Angew. Chem. Int. Ed.* **2013**, *52*, 5309-5313; b) J. Ryu, K. Shin, S. H. Park, J. Y. Kim, S. Chang, *Angew. Chem. Int. Ed.* **2012**, *51*, 9904-9908; c) S. V. Chapyshev, *Chem. Heterocycl. Compd.* **2001**, *37*, 968-975; d) W. Zhao, H. Li, J. Zhang, S. Cao, *Chin. J. Chem.* **2011**, *29*, 2763-2768.
7. a) T. Toma, J. Shimokawa, T. Fukuyama, *Org. Lett.* **2007**, *9*, 3195-3197; b) Å. Kaupang, T. Bonge-Hansen, *Beilstein J. Org. Chem.* **2013**, *9*, 1407-1413.
8. a) H. Huo, K. Harms, E. Meggers, *J. Am. Chem. Soc.* **2016**, *138*, 6936-6939; b) Y.-C. Chung, D. Janmanchi, H.-L. Wu, *Org. Lett.* **2012**, *14*, 2766-2769.
9. a) C. Wang, L.-A. Chen, H. Huo, X. Shen, K. Harms, L. Gong, E. Meggers, *Chem. Sci.* **2015**, *6*, 1094-1100; b) J. Ma, X. Shen, K. Harms, E. Meggers, *Dalton Trans.* **2016**, *45*, 8320-8323.
10. a) A. L. Fuentes de Arriba, F. Urbitsch, D. J. Dixon, *Chem. Commun.* **2016**, *52*, 14434-14437; b) J. Zhang, Y. Li, F. Zhang, C. Hu, Y. Chen, *Angew. Chem. Int. Ed.* **2016**, *55*, 1872-1875; c) M. P. Sibi, K. Itoh, *J. Am. Chem. Soc.* **2007**, *129*, 8064-8065; d) H. T. Abdel-Mohsen, J. Conrad, U. Beifuss, *Green Chem.* **2012**, *14*, 2686-2690.
11. a) T. W. Liwosz, S. R. Chemler, S. R. *Chem. Eur. J.* **2013**, *19*, 12771-12777; b) Y. Yasu, T. Koike, M. Akita, *Org. Lett.* **2013**, *15*, 2136-2139; c) J. B. Metternich, R. Gilmour, *J. Am. Chem. Soc.* **2015**, *137*, 11254-11257.
12. a) Boehringer Ingelheim Pharma, K. G., Ed. 2003. Patent number: US2003/162788; b) Z. Liu, P. Liao, X. Bi, *Org. Lett.* **2014**, *16*, 3668-3671; c) L. Xiang, Y. Niu, X. Pang, X. Yang, R. Yan, *Chem. Commun.* **2015**, *51*, 6598-6600; d) Z. Liu, J. Liu, L. Zhang, P. Liao, J. Song, X. Bi, *Angew. Chem. Int. Ed.* **2014**, *53*, 5305-5309.
13. a) D. Uraguchi, K. Yamada, T. Ooi, *Angew. Chem, Int. Ed.* **2015**, *54*, 9954-9957; b) T.

- Burgemeister, G. Dannhardt, M. Mach-Bindl, *Arch. Pharm.* **1988**, 321, 521-525.
- 14 a) C. L. Ladd, D. Sustac Roman, A. B. Charette, *Org. Lett.* **2013**, 15, 1350-1353; b) P. Brückner, D. Koch, U. Voigtmann, S. Blechert, *Synth. Commun.* **2007**, 37, 2757-2769; c) E. Alacid, C. Nájera, *J. Org. Chem.* **2009**, 74, 8191-8195.
- 15 J. Miguñez, V. R. Batchu, A. Boto, *J. Org. Chem.* **2012**, 77, 7652-7658.

Chapter 6. Appendices

6.1 List of Figures

Figure 1.	Visible light and electricity driven chemistry providing new opportunities for asymmetric catalysis.....	2
Figure 2.	Enthalpy diagrams of a thermal, a photo-activated, and an electricity-driven reaction.	3
Figure 3.	Merging photoredox and enamine catalysis for α -functionalization of aldehydes reported by MacMillan. Radical chain mechanism revised by Yoon.	5
Figure 4.	Selected other strategies for asymmetric photoredox α -functionalization of aldehydes.....	6
Figure 5.	Enantioselective α -alkylation of aldehydes with olefins via triple catalytic activation.	8
Figure 6.	Reductive generations of α -carbonyl carbon-centered radicals and their asymmetric transformations.	10
Figure 7.	Enantioselective conjugate addition of α -amino radicals.	11
Figure 8.	Other strategies for enantioselective radical conjugate additions.	12
Figure 9.	Dual photoredox/acid catalysis enabled enantioselective radical additions.....	14
Figure 10.	Ooi's work on synergistic catalysis of photoredox catalyst and chiral arylaminophosphonium barfate for a photoinduced asymmetric radical-radical cross coupling.	15
Figure 11.	Melchiorre's work on stereocontrolled β -alkylation of enals enabled by direct photoexcitation of iminium ion and radical-radical recombination.....	16
Figure 12.	Dual photoredox/nickel catalysis.	18
Figure 13.	Photoinduced asymmetric copper catalysis.	20
Figure 14.	Yoon's reports on dual photoredox/chiral Lewis acid catalysis enabled asymmetric photocycloadditions which involve SET processes.	22
Figure 15.	Asymmetric [2+2] photocycloadditions enabled by chromophore activation and direct excitation.....	24
Figure 16.	Asymmetric [2+2] photocycloadditions enabled by H-bonding catalysis through intramolecular energy transfer (EnT).....	25
Figure 17.	Enantioselective [2+2] photocycloadditions via triplet chromophore activation.....	26
Figure 18.	Xiao's work on enantioselective hydroxylation catalyzed by a bifunctional photocatalyst.	28
Figure 19.	Strategies for catalytic asymmetric organic electrosynthesis (taking anodic oxidations as examples).....	29
Figure 20.	Separating asymmetric enamine catalysis from anodic oxidation.	30
Figure 21.	Selected examples of asymmetric catalysis with direct electrochemical generation of active catalyst.	32
Figure 22.	Generation of chiral catalyst through indirect electrolysis with a redox mediator.....	34
Figure 23.	Enamine formation facilitated anodic oxidation, as reported by Jang.	35
Figure 24.	Overview of the chiral-at-metal Lewis acid catalysts developed by Meggers.	37
Figure 25.	Enantioselective α -functionalization of carbonyls by a single chiral-at-metal catalyst. ..	39
Figure 26.	Enantioselective radical conjugate addition by dual chiral-at-Rh/photoredox catalysis..	40

Figure 27.	Enantioselective radical-radical recombination catalyzed by chiral-at-metal complexes.	42
Figure 28.	Diverse reactive intermediates based on the chiral-at-metal complexes.....	50
Figure 29.	Previous reports and this design for visible-light-induced enantioselective α -amination.	54
Figure 30.	Removal of the imidazolyl group of compound 5ba	59
Figure 31.	Substrate scope of the enantioselective α -amination with aryl azides.	61
Figure 32.	Selective ^1H - $\{^{19}\text{F}\}$ decoupling NMR experiments of compound 3bh	61
Figure 33.	Substrate scope of the enantioselective α -alkylation with diazo compounds.	62
Figure 34.	Limitations of the present asymmetric α -functionalization.....	63
Figure 35.	Synthesis and X-ray diffraction structure of the key Rh-enolate1 intermediate.	63
Figure 36.	Control experiments supporting a radical mechanism involved in dual-catalytic system.	65
Figure 37.	EPR experiments that demonstrate the involvement of the carbon centered radical derived from EDA.	66
Figure 38.	UV/Vis absorption spectra of [Ru] and Rh-enolate1 and luminescence emission spectrum of [Ru].....	67
Figure 39.	Stern-Volmer quenching experiments with photoexcited [Ru(bpy) ₃](PF ₆) ₂	68
Figure 40.	Quenching effect of Rh-enolate1 on the solution of [Ru] excited by light with different wavelengths.	68
Figure 41.	Cyclic voltammograms of RhS , Rh-enolate1 , 2a , 4a and quenching mechanism for photoexcited [Ru]..	69
Figure 42.	Proposed mechanism of dual-catalyst enabled α -functionalization.	70
Figure 43.	Steric model for the reaction and geometries of Λ - Rh-enolate1 and transition states.	71
Figure 44.	A radical addition to carbene mechanism proposed by Gryko <i>et al.</i>	74
Figure 45.	Reaction design to expand the reactivity of the Meggers catalysts by trapping the β -enolate radical.	77
Figure 46.	Previous reports on visible-light-activated asymmetric transformations with allylic C(sp ²) radical intermediates.	78
Figure 47.	Initial attempts to trap the rhodium bound β -enolate radical intermediates.	80
Figure 48.	Reactions with different pyrazoles and an alkenyl sulfone.	85
Figure 49.	Transformations of the β -functionalized products.	85
Figure 50.	Robustness screening in the presence of additives.	86
Figure 51.	Proposed reaction mechanism of the β -functionalization.	87
Figure 52.	Preparation and identification of the key RhO-Pz intermediate..	88
Figure 53.	UV/Vis absorption and luminescence spectra measured for the β -functionalization reation.	89
Figure 54.	CV spectra of compounds 18a , RhO-Pz , and HE-1	90
Figure 55.	Stern-Volmer plots of the quenching on HE-1	91
Figure 56.	Stern-Volmer plots of the quenching experiments by 18a	91
Figure 57.	EPR experiments on the β -functionalization reaction with the addition of DMPO (X band, r.t.).....	92
Figure 58.	Analysis of the dimerization cyclobutane side product.....	98
Figure 59.	Previous strategies for stereocontrolled reactions from electronically excited states.	99
Figure 60.	Scope of the [2+2] photocycloaddition with respect to α,β -unsaturated carbonyl compounds.....	102

Figure 61.	Scope of the [2+2] photocycloaddition with respect to alkenes..	103
Figure 62.	Auxiliary enabled [2+2] photocycloaddition with aliphatic (internal) alkenes.....	104
Figure 63.	Limitations of the scope of the [2+2] photocycloaddition.....	105
Figure 64.	¹ H NMR experiments (300 M, CD ₂ Cl ₂) demonstrating the fast generation of RhS-Im complex.....	106
Figure 65.	Two key rhodium/substrate complexes synthesized for mechanistic studies of the [2+2] photocycloaddition.	106
Figure 66.	UV/Vis absorption spectra measured in the [2+2] photocycloaddition.	107
Figure 67.	Cyclic voltammetry disapproving of a redox mechanism for the [2+2] photocycloaddition..	108
Figure 68.	Control experiments supporting a triplet mechanism for the [2+2] photocycloaddition.	109
Figure 69.	Experiments probing the formation of singlet oxygen in the presence of dioxygen.	110
Figure 70.	Effect of O ₂ on the [2+2] photocycloaddition.....	112
Figure 71.	Calculated spin density distribution and triplet energy of the excited 26a and RhS-Im .	113
Figure 72.	Proposed mechanism of the [2+2] photocycloaddition.....	114
Figure 73.	Chemistry of the photochemically excited states and effort to access new structural motifs by interference with the excited rhodium/substrate complex.	118
Figure 74.	New chemistry of photochemically excited state and new access to chiral <i>N</i> -heterocycles provided by exploring unprecedented reactivity of vinyl azides.	119
Figure 75.	Proposed mechanism of the [2+3] photocycloaddition.....	124
Figure 76.	Synthesis and a crystal structure of the key rhodium/substrate intermediate RhS-PPz .	124
Figure 77.	UV/Vis absorption spectra obtained in the study of the [2+3] photocycloaddition.	125
Figure 78.	Control experiment with 2 <i>H</i> -azirine and quantum yield measurement.	126
Figure 79.	Calculated energy profiles for ligand exchanges with RhS and IrS	126
Figure 80.	Calculated spin distribution and energy of the excited triplet states of 30f , RhS-PPz , and IrS-PPz	127
Figure 81.	Hypothesis to explain the factors that affect the outcome of the [2+3] photocycloaddition.	128
Figure 82.	Substrate scope of the [2+3] photocycloaddition with respect to <i>N</i> -acyl pyrazole.....	129
Figure 83.	Substrate scope of the [2+3] photocycloaddition with respect to vinyl azide.....	130
Figure 84.	Scope limitations of the present [2+3] photocycloaddition.	130
Figure 85.	Synthetic applications of the [2+3] photocycloaddition.	131
Figure 86.	Simple reaction set-up for large-scale [2+3] photocycloaddition.....	131
Figure 87.	Strategies to broaden the scope of photocycloadditions from α,β -unsaturated carbonyls to acceptor-substituted cyclopropanes.	136
Figure 88.	Changes of the photophysical and redox properties of cyclopropyl ketone 41a upon RhS coordination.	138
Figure 89.	Effort to improve the diastereoselectivity of 45a by catalyst modification.	140
Figure 90.	Effort to extend the scope of the [3+2] photocycloaddition to synthetically useful substrates with <i>N</i> -pyrazole as auxiliary.	141
Figure 91.	Substrate scope of the [3+2] photocycloaddition with respect to alkenes.	144
Figure 92.	Substrate scope of the [3+2] photocycloaddition with respect to acceptor-substituted cyclopropanes.	145
Figure 93.	Limitations of the [3+2] photocycloaddition of cyclopropanes with alkenes.....	146

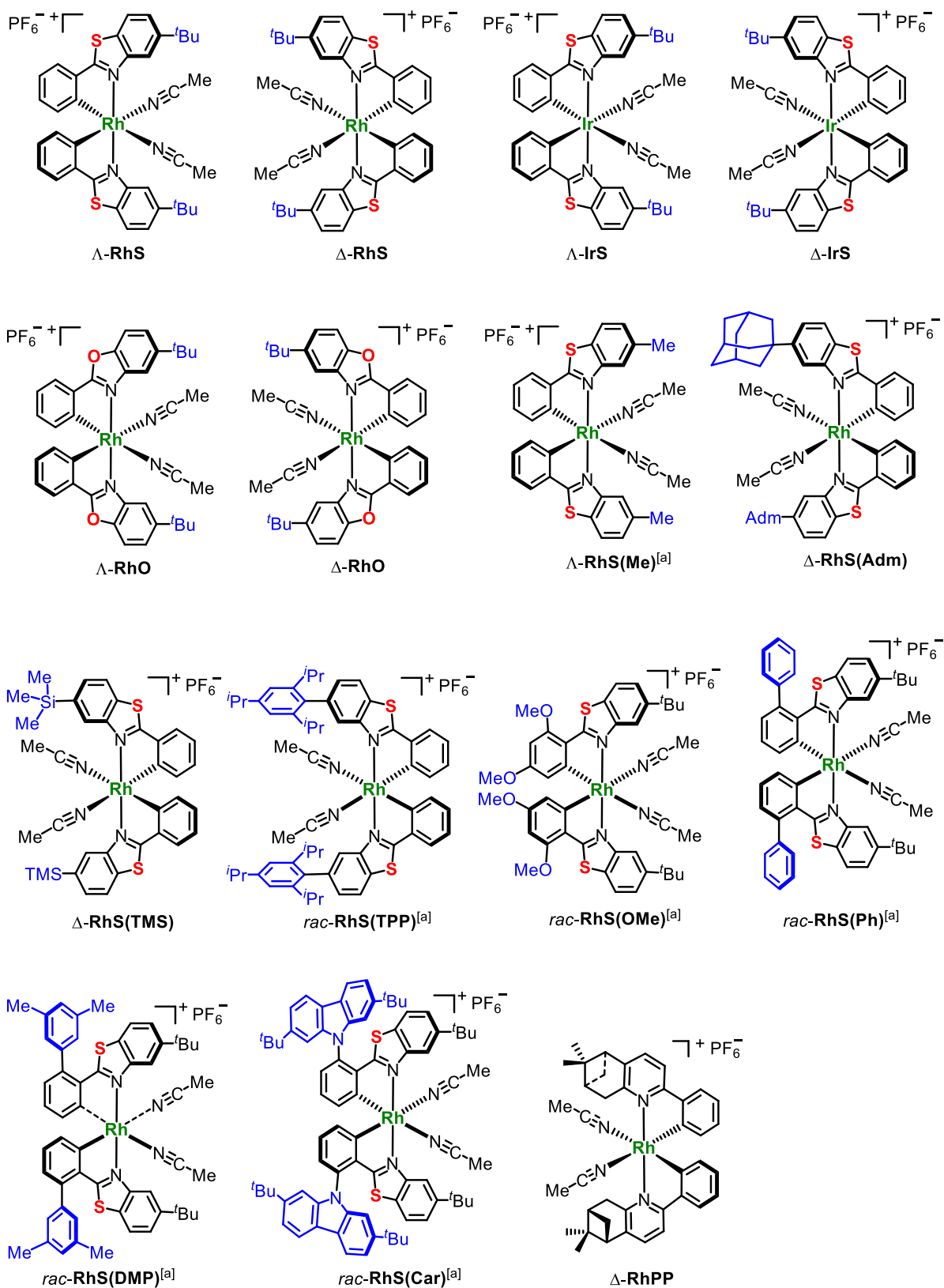
Figure 94.	Substrate scope of the [3+2] photocycloaddition with respect to alkynes.....	146
Figure 95.	Proposed mechanism of the [3+2] photocycloadditions and quantum yield determination.	147
Figure 96.	Cyclic voltammogram of DIPEA.....	148
Figure 97.	Competitive coordination of 41a and 43a to RhS as demonstrated by ¹ H NMR experiments.....	150
Figure 98.	Rational design leading to an electricity driven asymmetric Lewis acid catalysis for highly selective cross coupling of enolates.....	155
Figure 99.	Two highly asymmetric electrochemical transformations that separate the asymmetric catalysis from electrochemical oxidation.....	156
Figure 100.	Substrate scope of the electrosynthesis with the generation of tertiary carbon stereocenters.	161
Figure 101.	Substrate scope of the electrosynthesis with the generation of all-carbon quaternary centers.....	162
Figure 102.	Limitations of the present electrosynthesis.....	163
Figure 103.	Comparisons of different synthetic methodologies and scope for synthetic applications of the electrosynthesis.....	165
Figure 104.	Mechanistic studies on the present electrosynthesis.....	166
Figure 105.	Proposed catalytic cycle for the present electrosynthesis.....	167
Figure 106.	Electricity driven chiral Lewis acid catalyzed α -oxygenation with TEMPO.....	168
Figure 107.	Electricity driven chiral Lewis acid catalyzed C-S formation.....	169
Figure 108.	Electricity driven chiral Lewis acid catalyzed α -amination with 10 <i>H</i> -phenothiazine..	170
Figure 109.	Electricity driven chiral Lewis acid catalyzed three-component reaction.....	171
Figure 110.	Electricity driven chiral Lewis acid catalyzed oxidative [2+2] photocycloaddition....	172
Figure 111.	Electricity driven oxidative cyclization.....	173
Figure 112.	Overview of the discoveries of this thesis: visible light or electricity driven asymmetric chiral-at-rhodium catalysis for various novel transformations.....	177
Figure 113.	Summary of α -amination/alkylation with dual-catalyst.....	178
Figure 114.	Summary of a single RhO enabled two distinct processes.....	179
Figure 115.	Summary of a single RhS enabled [2+2] and [2+3] photocycloadditions via direct visible-light-excitation and direct bond formation on electronically excited state.....	180
Figure 116.	Summary of a single RhS enabled [3+2] photocycloaddition.....	182
Figure 117.	Summary of the electricity driven asymmetric chiral-at-rhodium catalysis.....	183
Figure 118.	Emission spectrum of the 21 W CFL lamp.....	190
Figure 119.	Emission spectrum of the 23 W blue LEDs lamp.....	190
Figure 120.	CD spectrum of Λ - RhS(Me)	228
Figure 121.	Crystal structure of 50a	229
Figure 122.	Modified resolution method for the synthesis of enantiopure RhO	233
Figure 123.	Crystal structures of compounds 21d and 25	260
Figure 124.	Crystal structure of compound 28e	290
Figure 125.	Crystal structure of compound 28p'	290
Figure 126.	NOESY spectrum of compound 37	332
Figure 127.	NOESY spectrum of compound 39	333
Figure 128.	Crystal structure of compound 32k	334

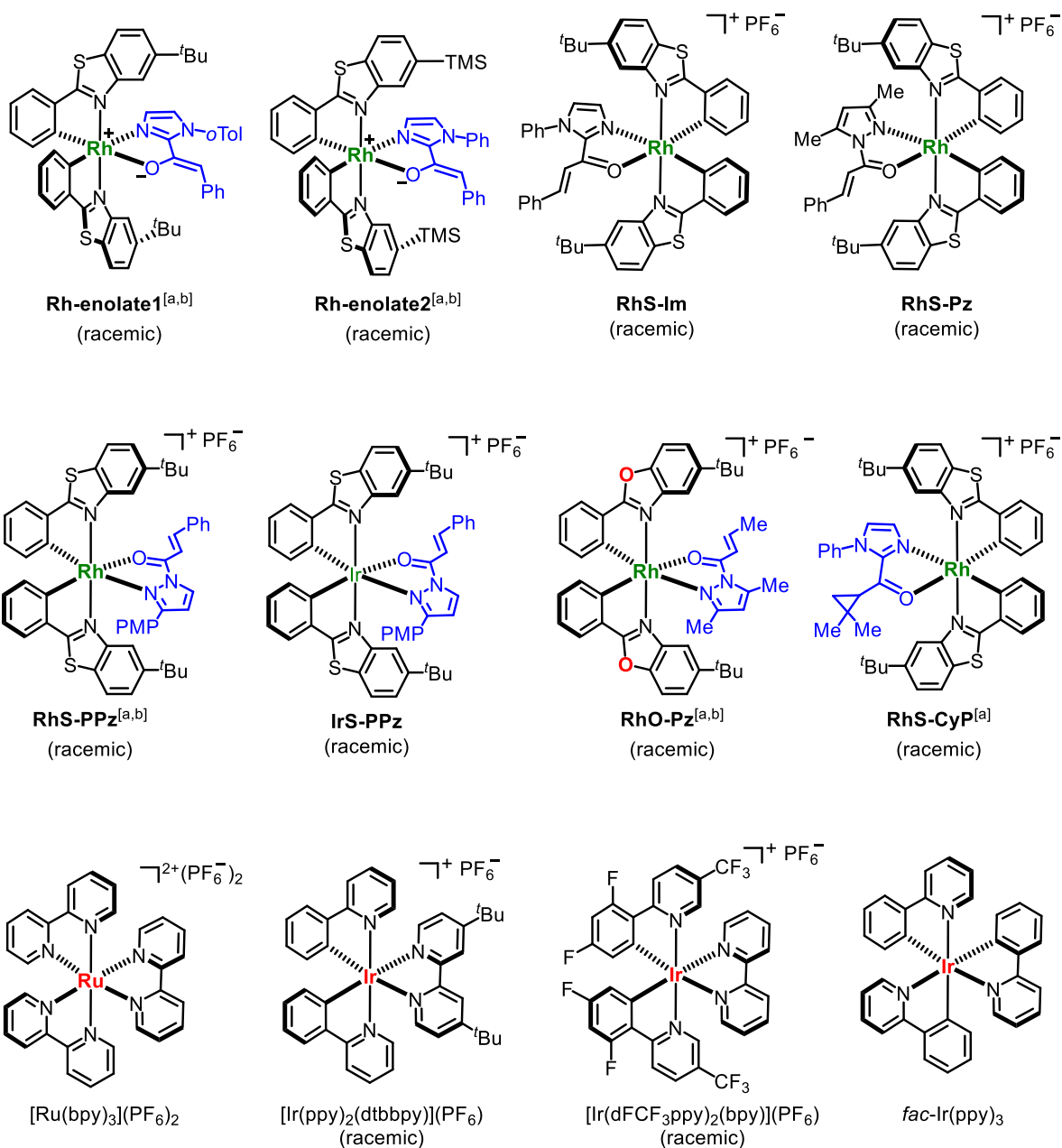
Figure 129. Crystal structure of compound 43k	387
Figure 130. Crystal structures of compounds 49k and 51n	426

6.2 List of Tables

Table 1. The development of dual-catalyst system for α -amination.	55
Table 2. Solvent effect on α -amination.	56
Table 3. Effect of water and solvent ratio on α -amination.	57
Table 4. Base effect on α -amination.	57
Table 5. Asymmetric α -alkylation with EDA.	59
Table 6. Catalytic behavior of Rh-enolate1	64
Table 7. Effect of imidazole <i>N</i> -substituents and steric groups on catalyst.	72
Table 8. Effect of Lewis acid catalyst and Hantzsch ester on the β -functionalization.	82
Table 9. Effect of solvent and light source on the β -functionalization.	83
Table 10. Substrate scope of the β -functionalization with respect to allyl sulfones.	84
Table 11. Initial experiments leading to a single chiral-at-rhodium catalyst system.	100
Table 12. Robustness of the [2+2] photocycloaddition.	101
Table 13. Effect of sensitizers on the [2+2] photocycloaddition.	108
Table 14. [2+3] Photocycloaddition with an α,β -unsaturated 2-acyl imidazole	120
Table 15. [2+3] Photocycloaddition with an α,β -unsaturated <i>N</i> -acyl pyrazole.	121
Table 16. Effect of auxiliary and solvent on the [2+3] photocycloaddition.	122
Table 17. [3+2] Photocycloaddition of a simple cyclopropane with acrylonitrile.	139
Table 18. Conditions optimization for [3+2] photocycloaddition with alkyne.	142
Table 19. <i>Cis</i> - to <i>trans</i> -isomerization of aryl cyclopropane 44b	149
Table 20. Initial experiments for electricity driven enolates cross coupling.	159
Table 21. Optimizations of the electricity driven asymmetric enolates cross coupling.	160
Table 22. Crystal data and structure refinement for Rh-enolate1	230
Table 23. Crystal data and structure refinement for 50a	231
Table 24. Crystal data and structure refinement for RhO-Pz	261
Table 25. Crystal data and structure refinement for 21d	262
Table 26. Crystal data and structure refinement for 25	263
Table 27. Crystal data and structure refinement for 28e	291
Table 28. Crystal data and structure refinement for 28p'	292
Table 29. NOESY cross peaks and molecular structure of compound 37	331
Table 30. Crystal data and structure refinement for RhS-PPz	335
Table 31. Crystal data and structure refinement for 32k	336
Table 32. Crystal data and structure refinement for 43k	388
Table 33. Crystal data and structure refinement for Rh-enolate2	427
Table 34. Crystal data and structure refinement for 49k	428
Table 35. Crystal data and structure refinement for 51n	429

6.3 List of Organometallic Complexes

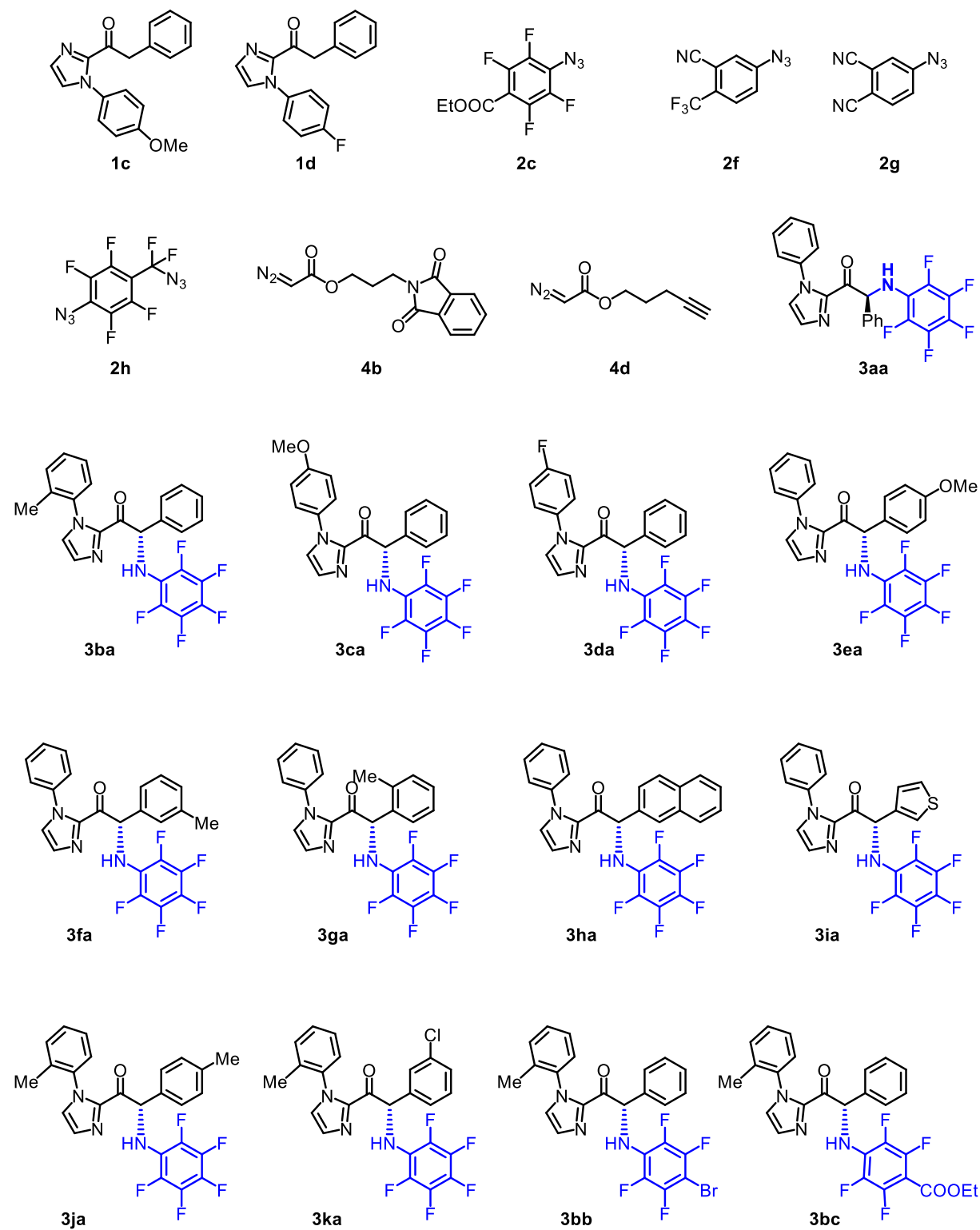


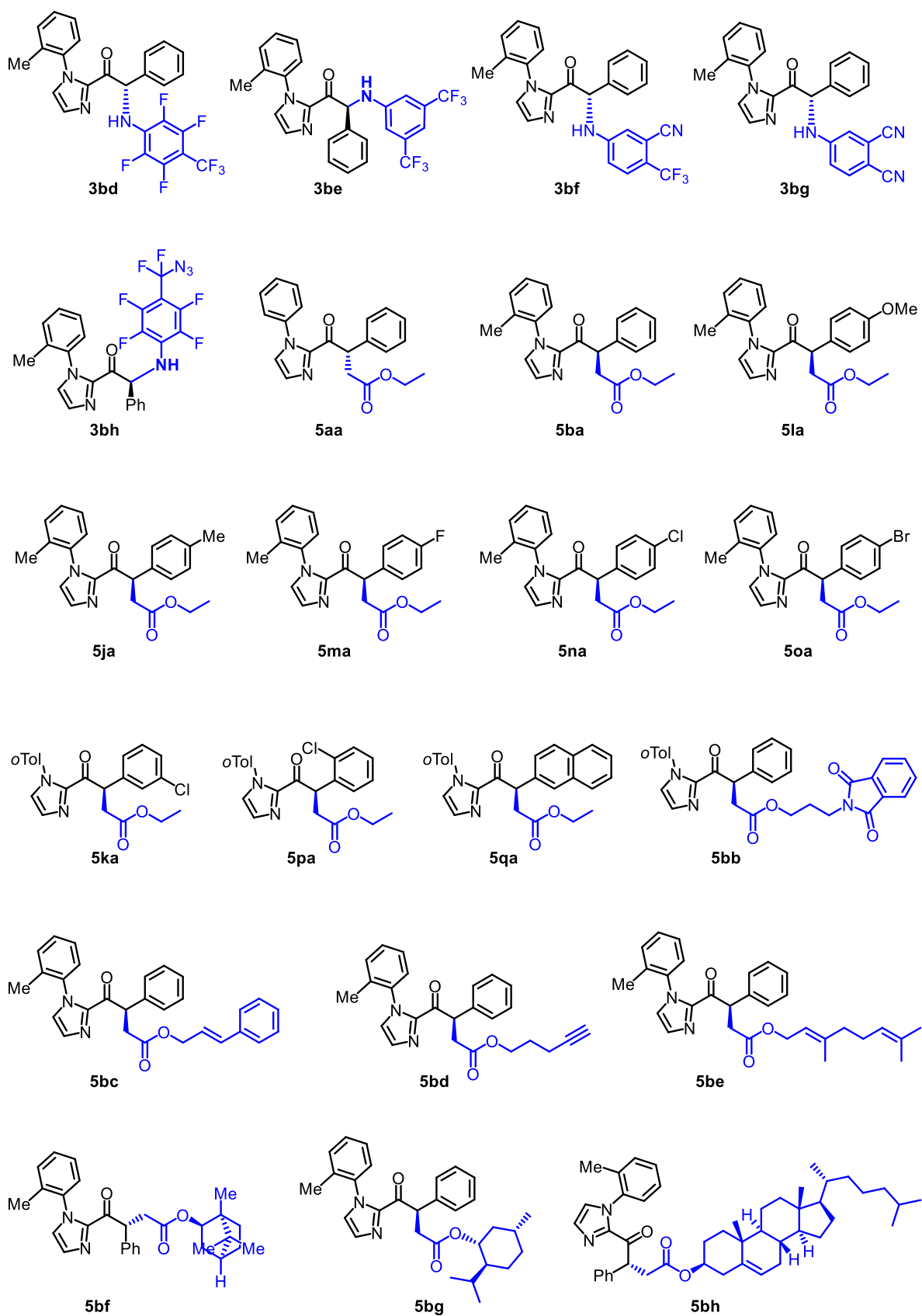


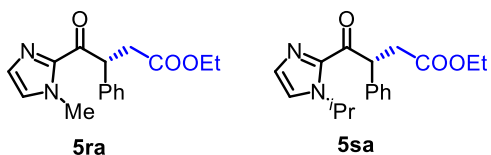
[a] Firstly synthesized by the author of this thesis; [b] Characterized by Single-Crystal X-Ray Diffraction Study.

6.4 List of Novel Organic Compounds

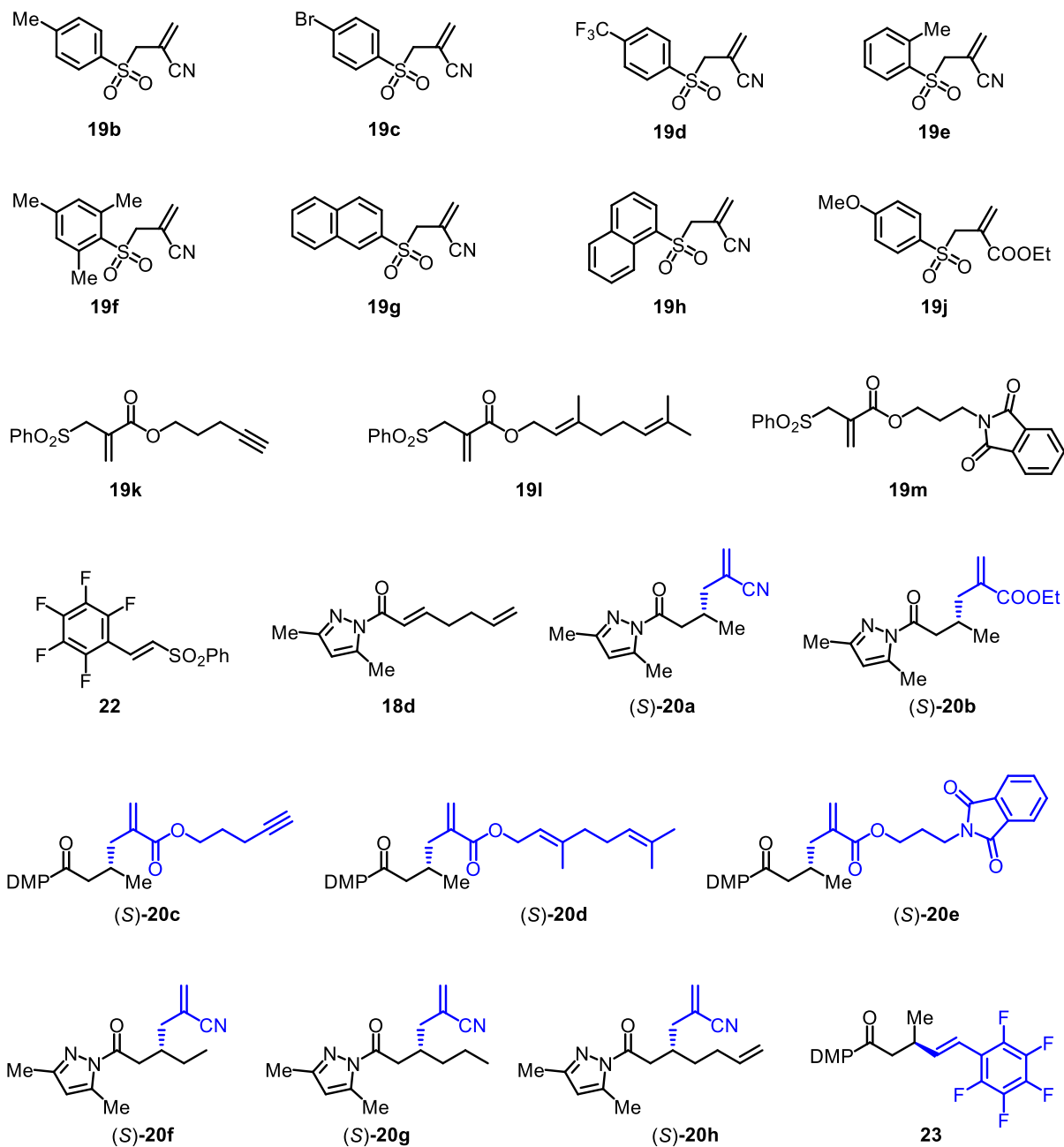
1) Chapter 3.1 and the corresponding experimental part chapter 5.2

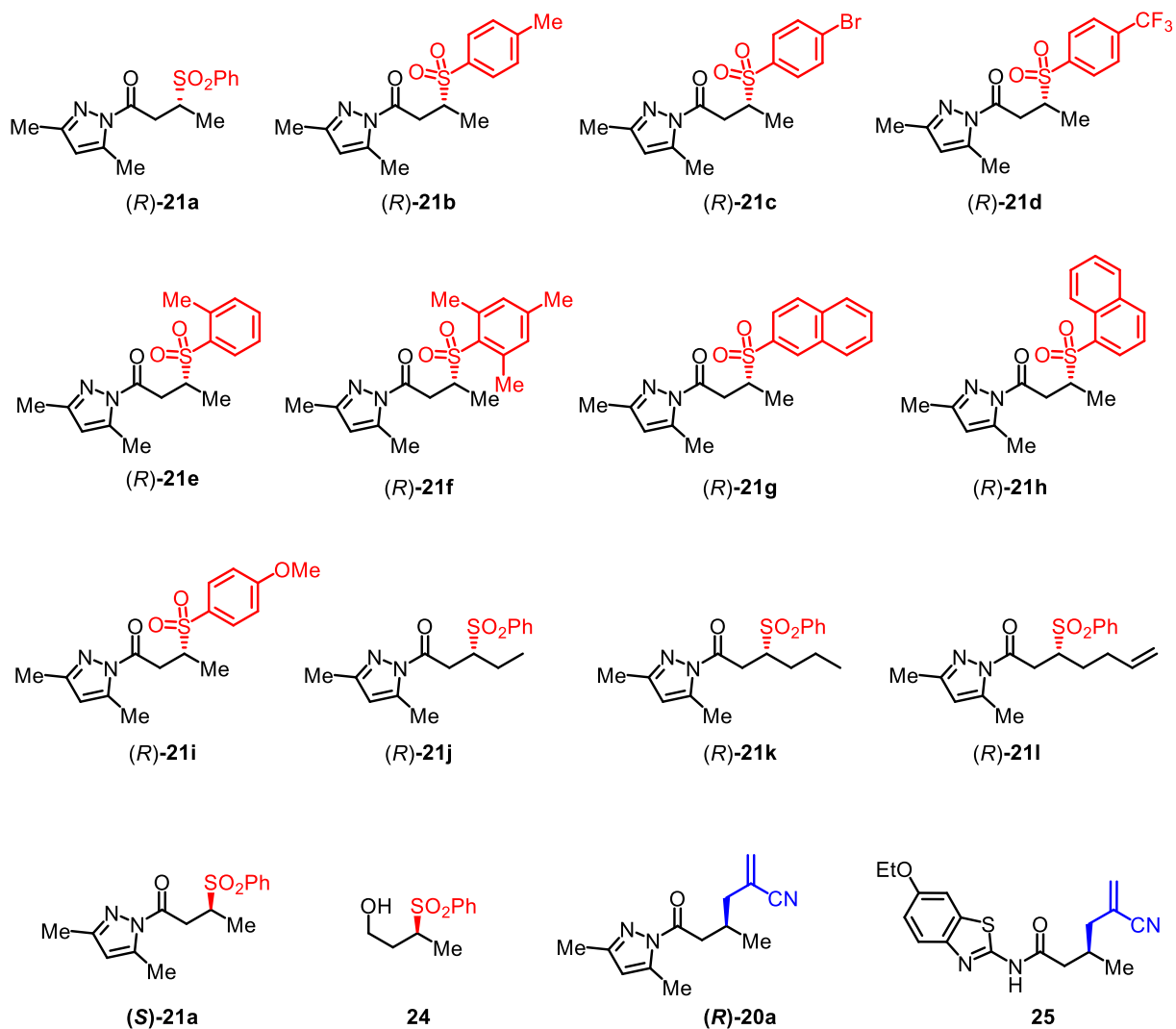




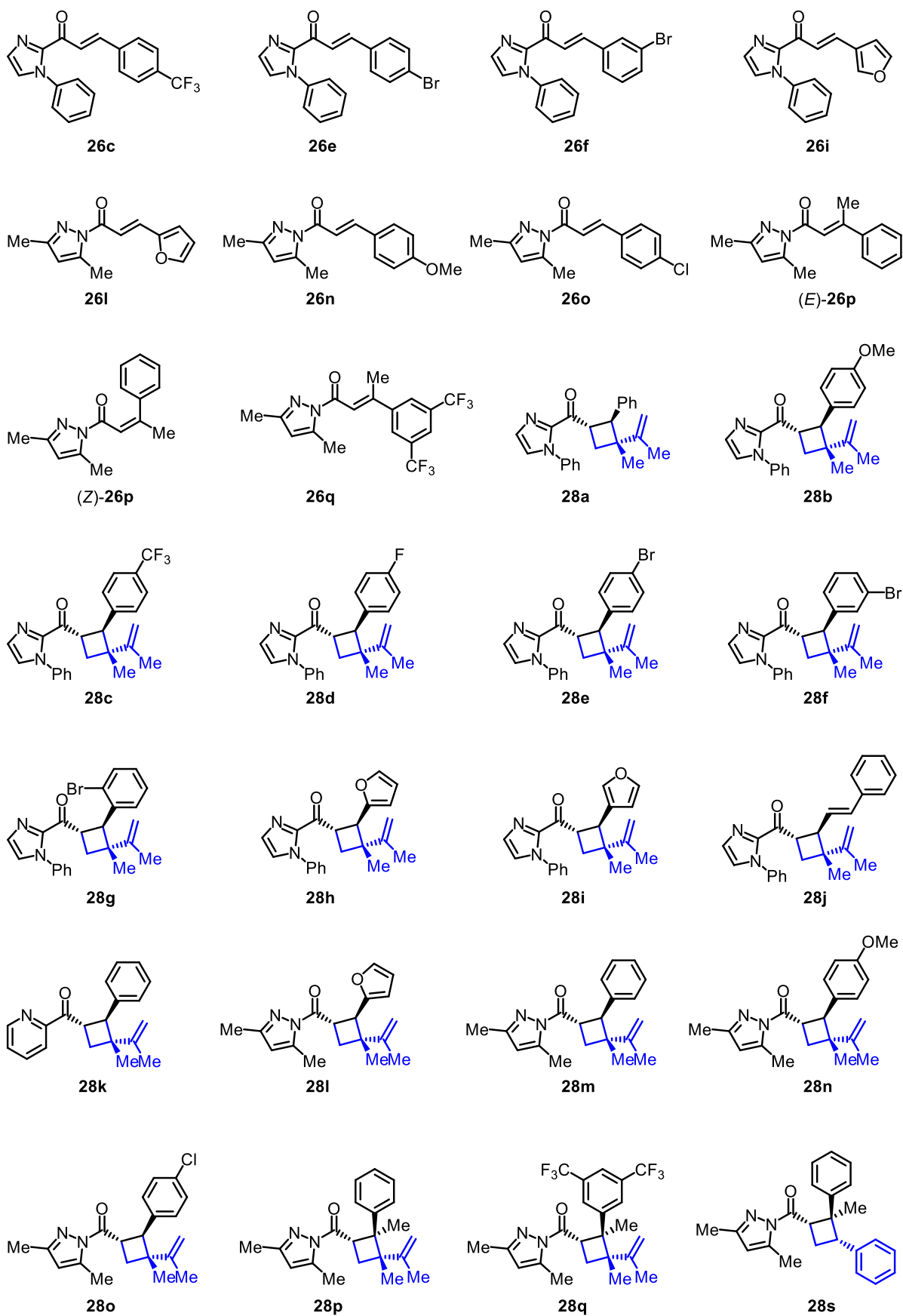


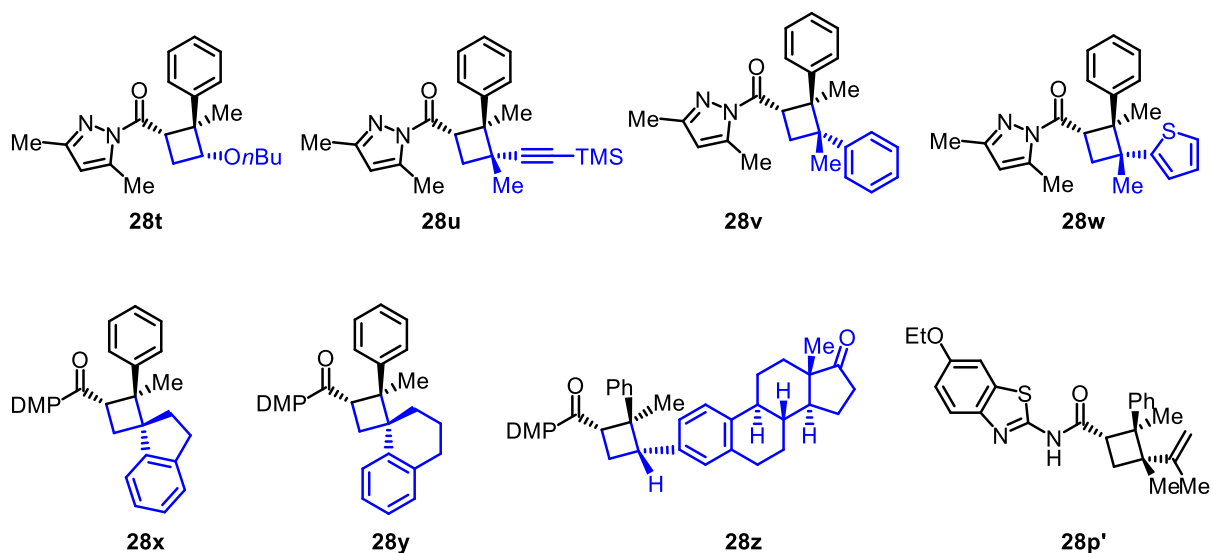
2) Chapter 3.2 and the corresponding experimental part chapter 5.3



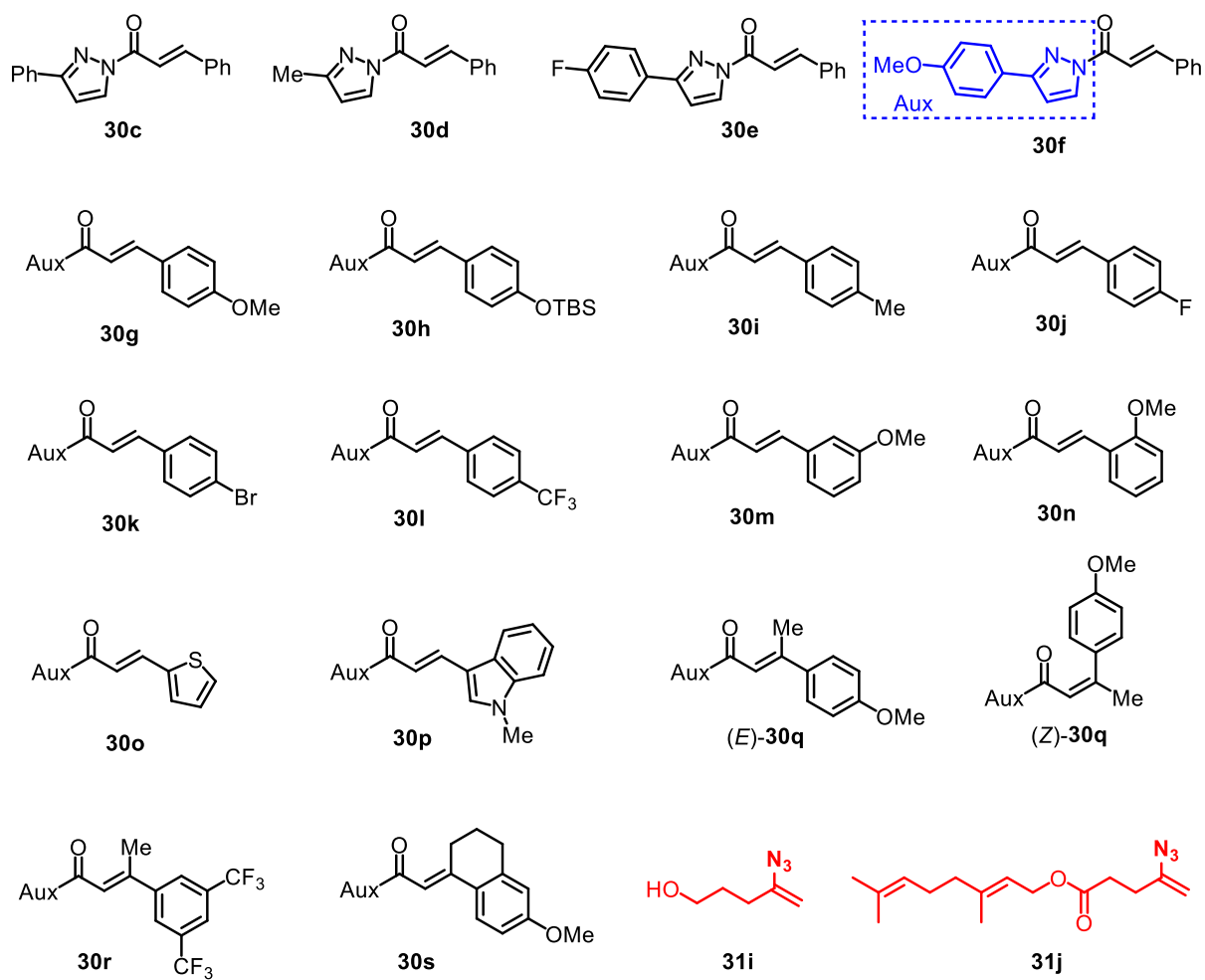


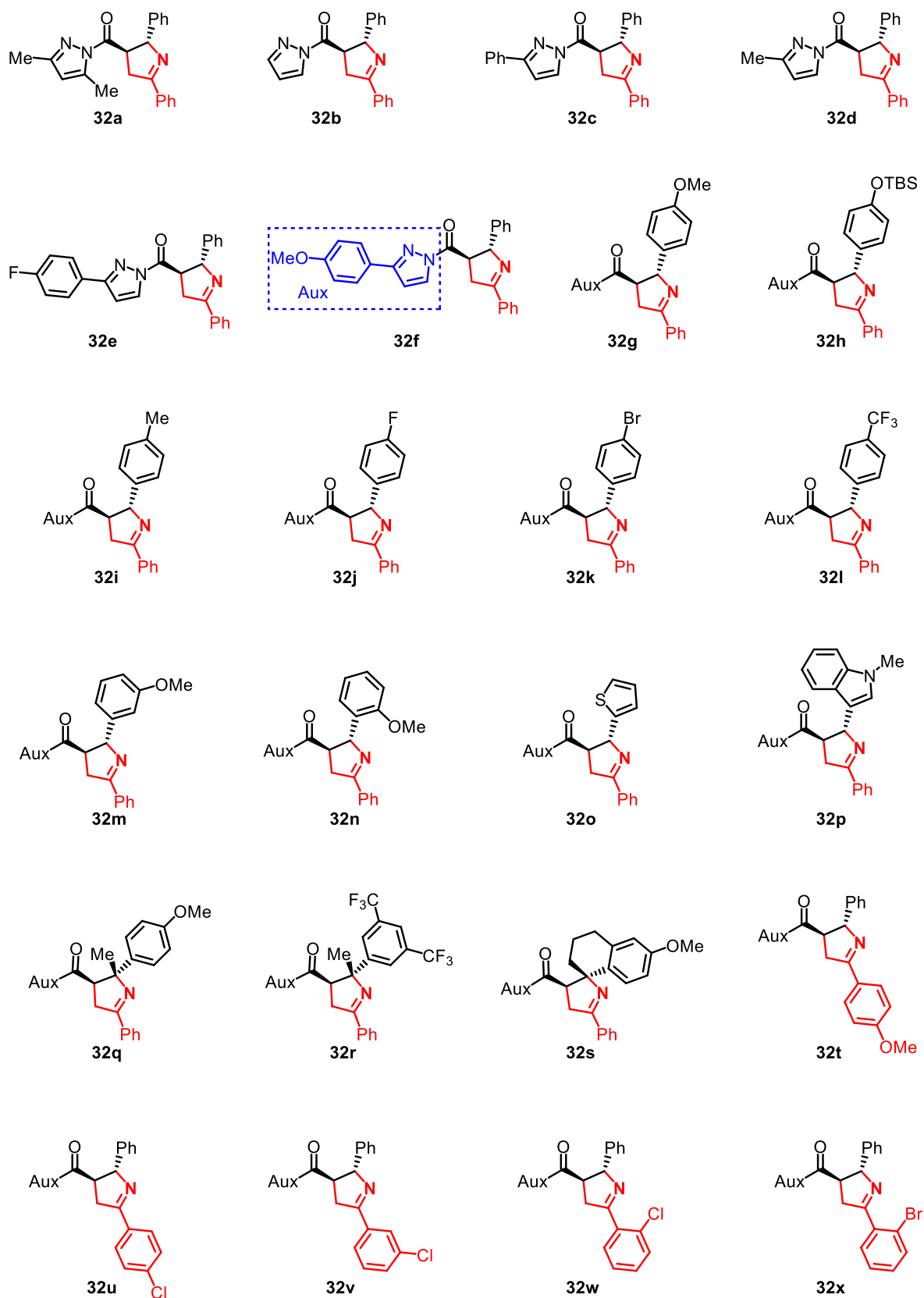
3) Chapter 3.3 and the corresponding experimental part chapter 5.4

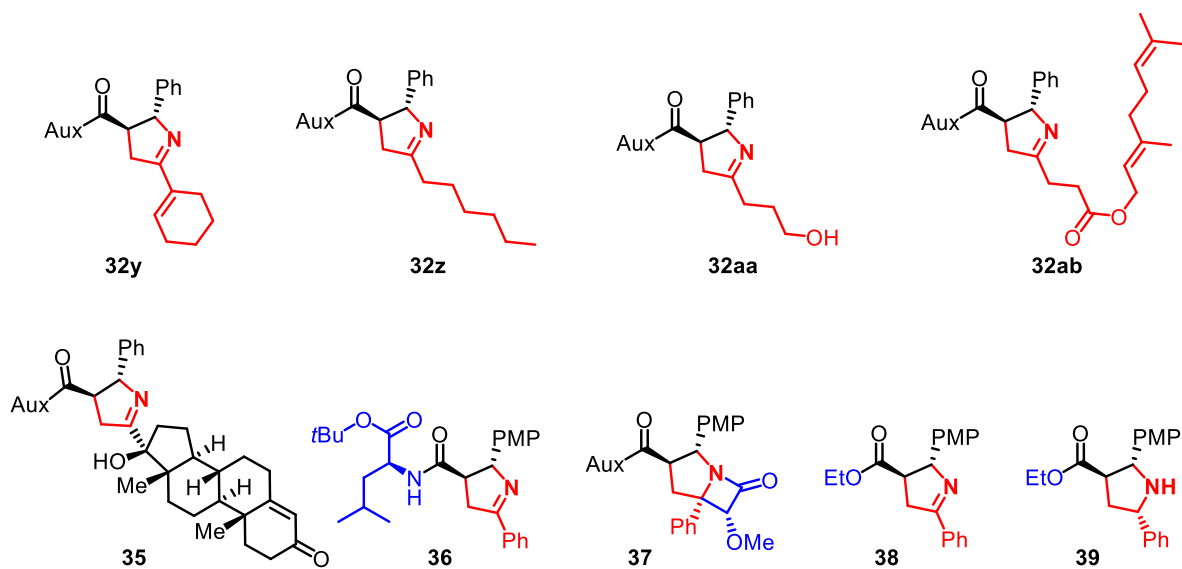




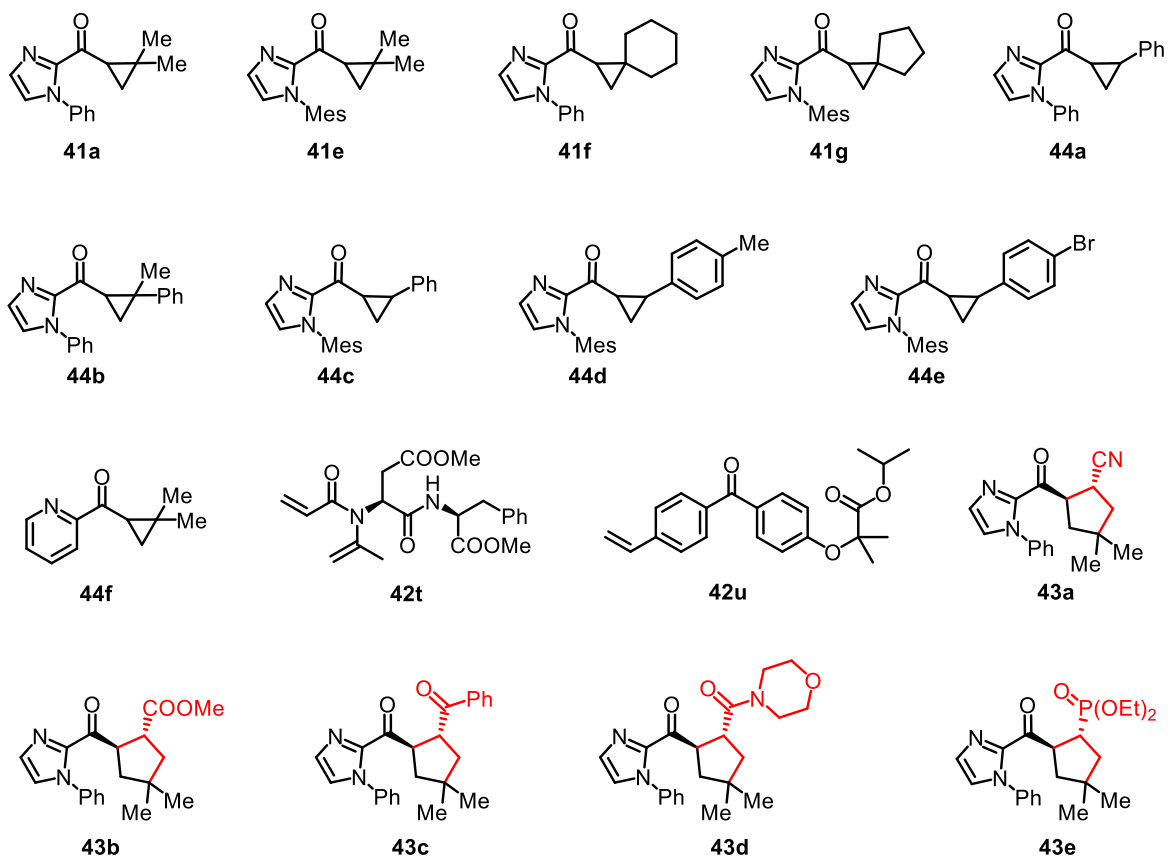
4) Chapter 3.4 and the corresponding experimental part chapter 5.5

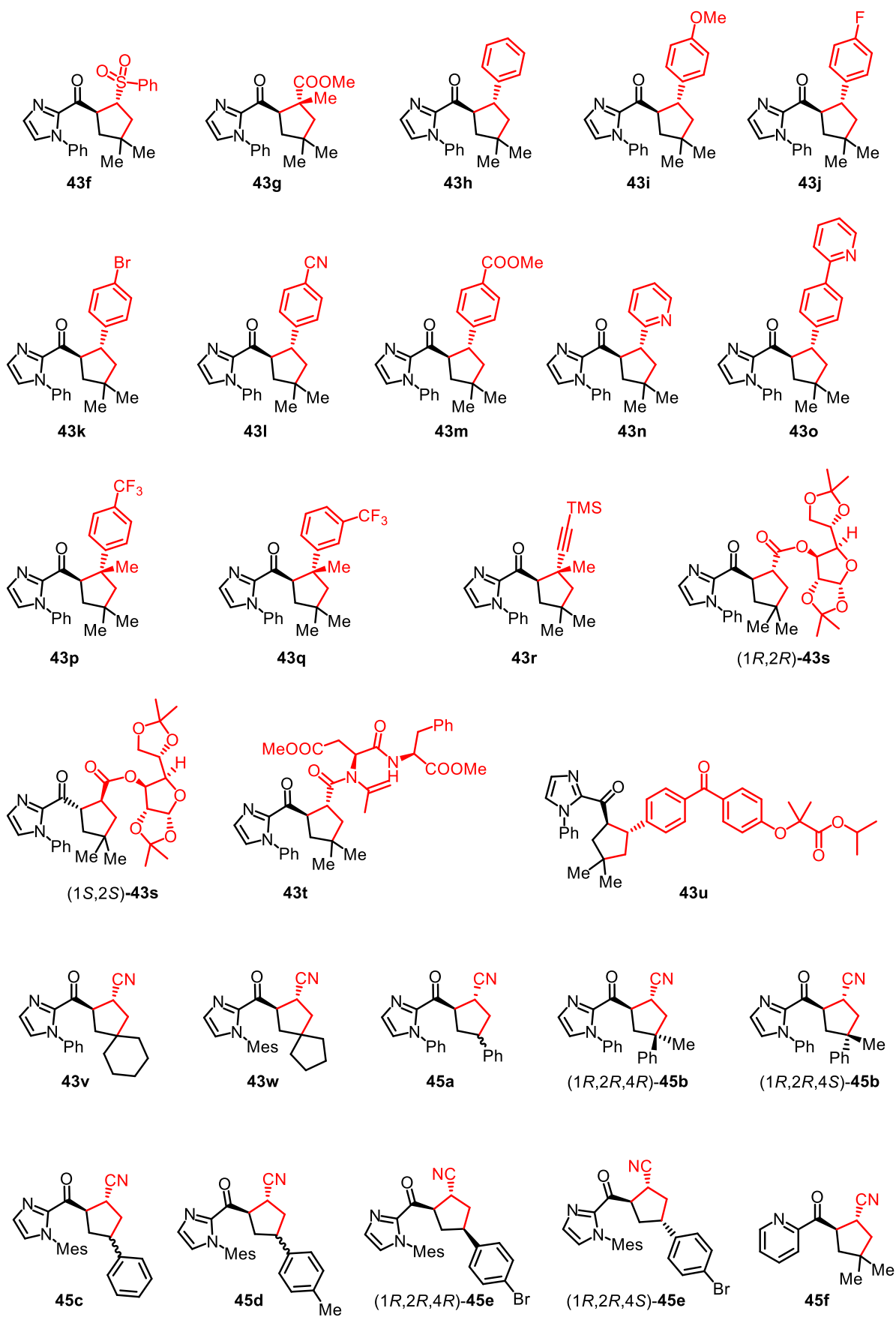


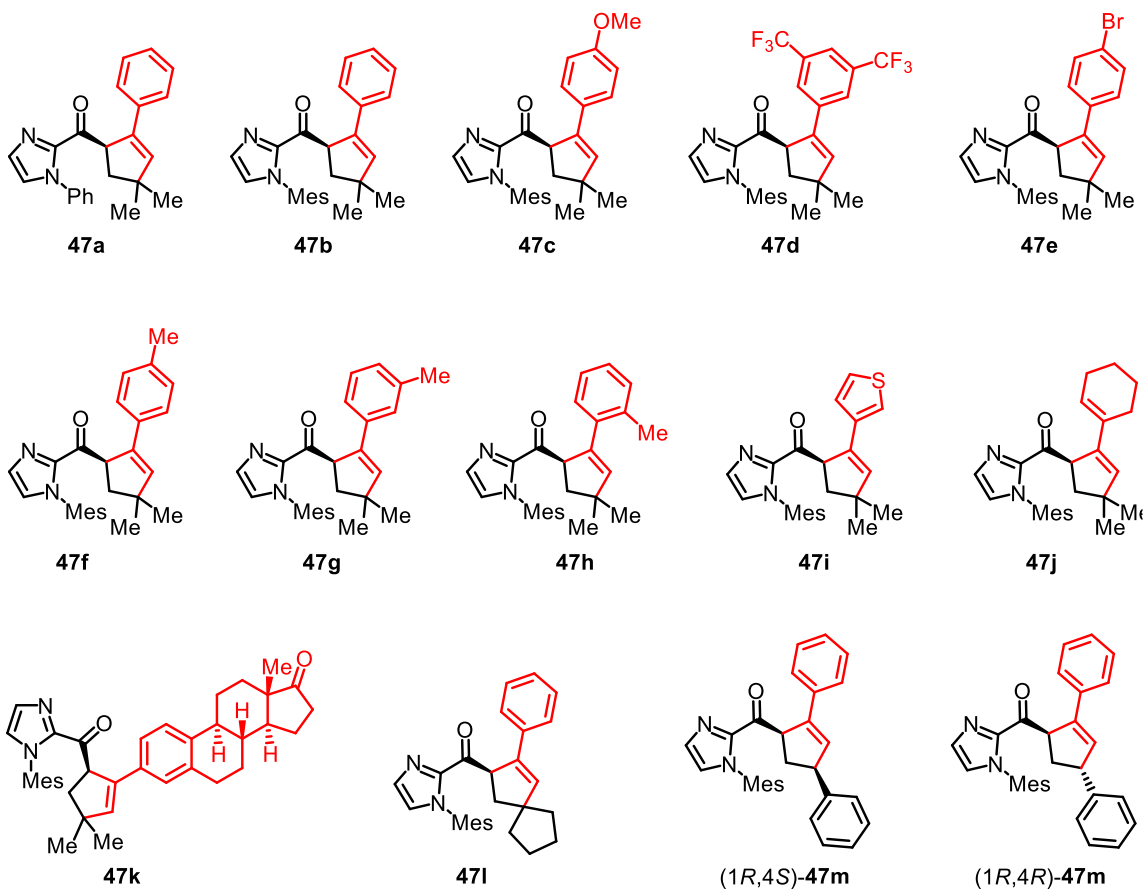




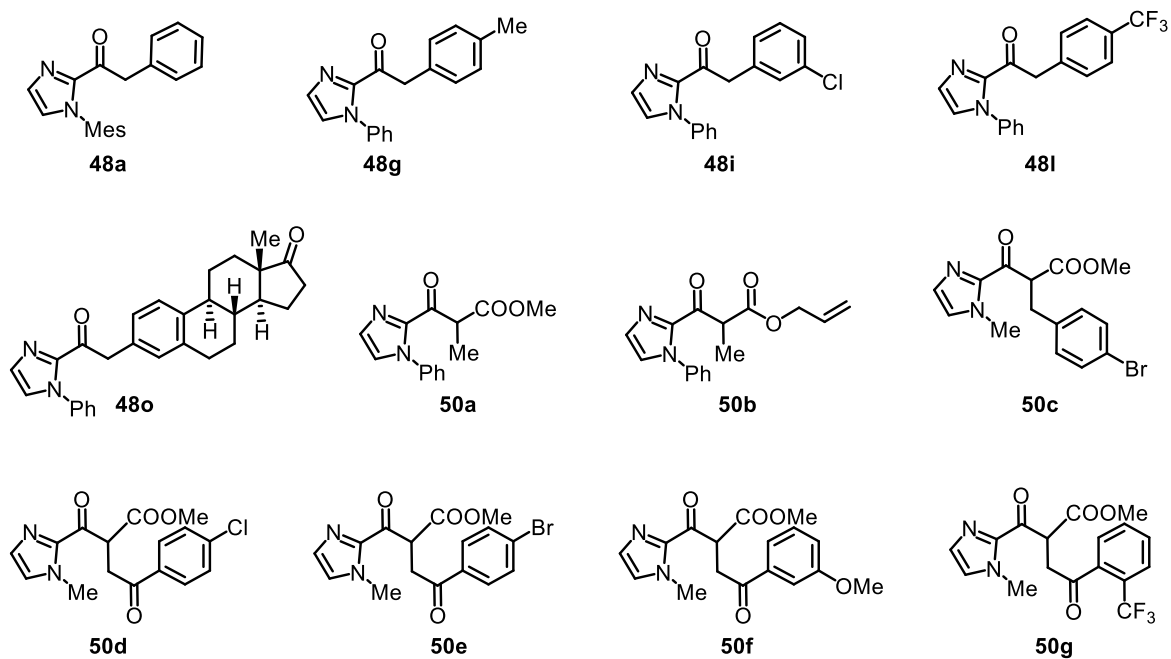
5) Chapter 3.5 and the corresponding experimental part chapter 5.6

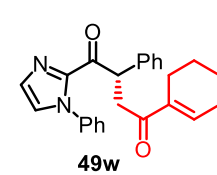
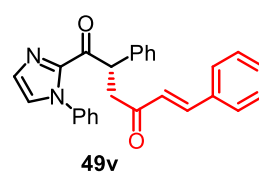
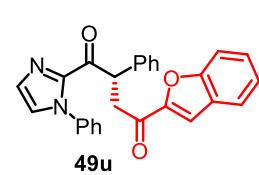
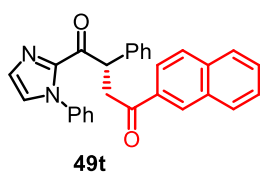
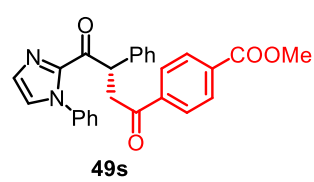
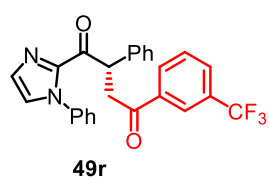
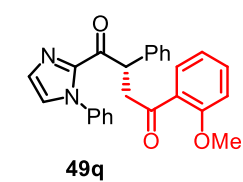
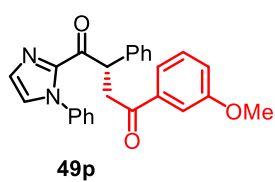
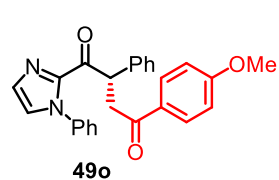
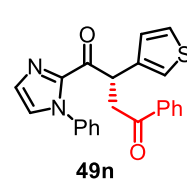
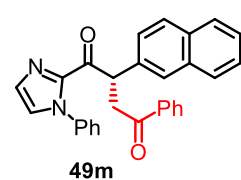
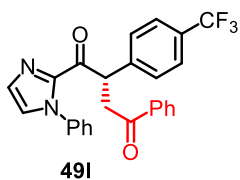
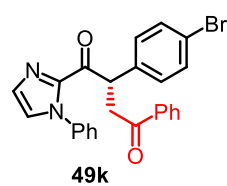
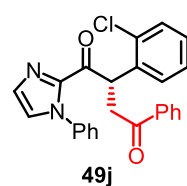
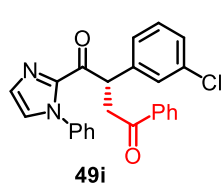
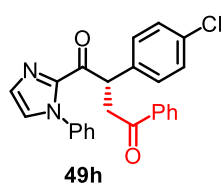
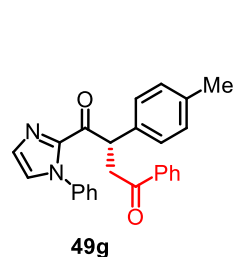
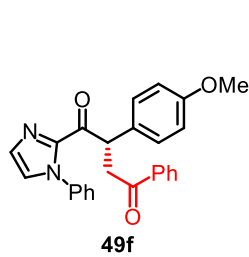
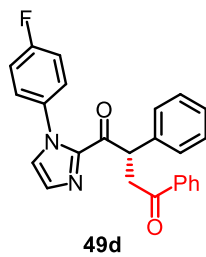
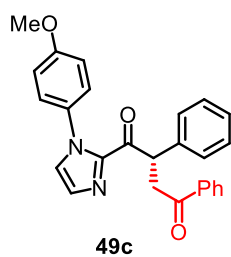
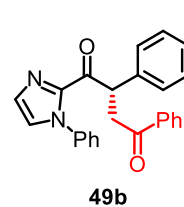
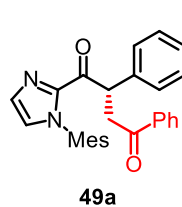
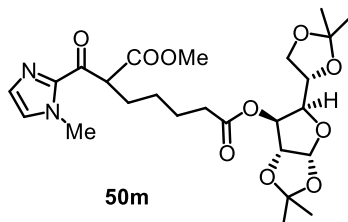
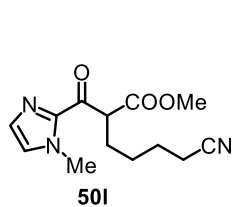
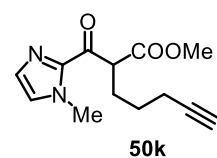
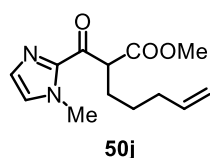
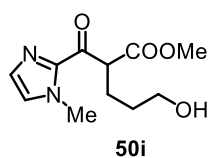
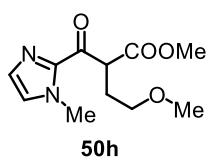


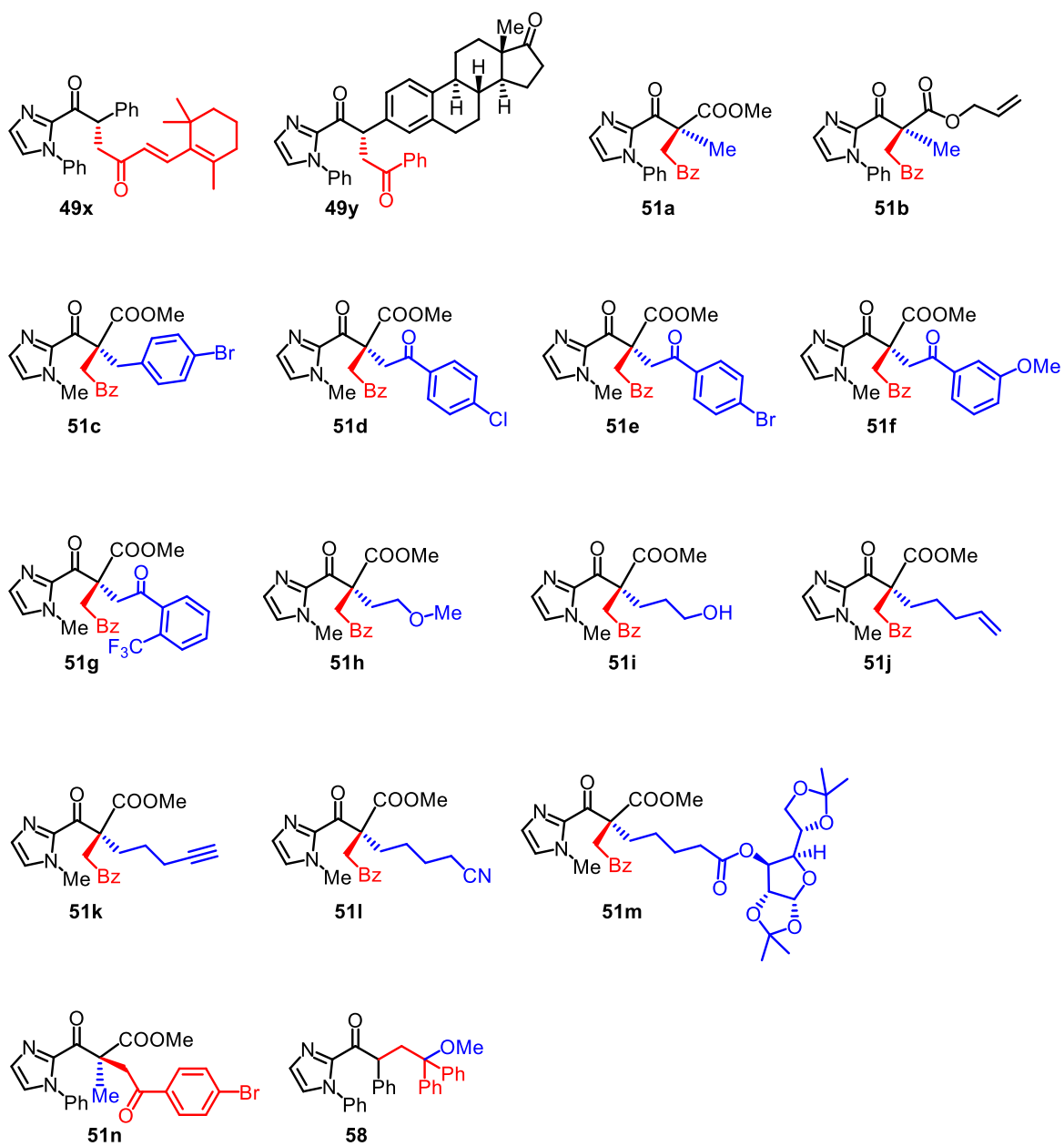




6) Chapter 3.6 and the corresponding experimental part chapter 5.7







Statement

gemäß § 10, Abs. 1 der Promotionsordnung der mathematisch-naturwissenschaftlichen Fachbereiche und des Medizinischen Fachbereichs für seine mathematisch-naturwissenschaftlichen Fächer der Philipps-Universität Marburg vom 15.07.2009

Ich erkläre, dass eine Promotion noch an keiner anderen Hochschule als der Philipps-Universität Marburg, Fachbereich Chemie, versucht wurde und versichere, dass ich meine vorgelegte Dissertation

Asymmetric Chiral-at-Rhodium Catalysis Driven by Visible Light or Electricity

selbst und ohne fremde Hilfe verfasst, nicht andere als die in ihr angegebenen Quellen oder Hilfsmittel benutzt, alle vollständig oder sinngemäß übernommenen Zitate als solche gekennzeichnet sowie die Dissertation in der vorliegenden oder ähnlichen Form noch bei keiner anderen in- oder ausländischen Hochschule anlässlich eines Promotionsgesuchs oder zu anderen Prüfungszwecken eingereicht habe.

Xiaoqiang Huang

Marburg, den Dec. 3rd, 2018

Curriculum Vitae

Xiaoqiang Huang

Male, born September 24, 1991 in Fujian, P. R. China

Email: huangx513@gmail.com

Education

- | | |
|-----------------|--|
| 09/2015–present | Ph.D. Organic Chemistry, Philipps-Universität Marburg, Germany
Supervisor: Prof. Eric Meggers |
| 2013/09–2015/07 | M.Sc. Medicinal Chemistry, Peking University, China
Supervisor: Prof. Ning Jiao |
| 2009/09–2013/07 | B.Sc. Pharmacy, Peking University, China |

Research Experiences

Ph.D. thesis: Asymmetric Chiral-at-Rhodium Catalysis Driven by Visible Light or Electricity

Publications:

1. **X. Huang**, E. Meggers, *Acc. Chem. Res.* **2019**, 52, in revision.
2. **X. Huang**, Q. Zhang, J. Lin, K. Harms, E. Meggers, *Nat. Catal.* **2019**, 2, 34-40.
3. **X. Huang**, J. Lin, T. Shen, K. Harms, M. Marchini, P. Ceroni, E. Meggers, *Angew. Chem. Int. Ed.* **2018**, 57, 5454-5458.
4. **X. Huang**, X. Li, X. Xie, K. Harms, R. Riedel, E. Meggers, *Nat. Commun.* **2017**, 8, 2245.
5. **X. Huang**,[‡] S. Luo,[‡] O. Burghaus, R. D. Webster, K. Harms, E. Meggers, *Chem. Sci.* **2017**, 8, 7126-7131. (‡ Equal contribution)
6. **X. Huang**, T. R. Quinn, K. Harms, R. D. Webster, L. Zhang, O. Wiest, E. Meggers, *J. Am. Chem. Soc.* **2017**, 139, 9120-9123.
7. **X. Huang**, R. D. Webster, K. Harms, E. Meggers, *J. Am. Chem. Soc.* **2016**, 138, 12636-12642.
8. H. Huo,[‡] **X. Huang**,[‡] X. Shen, K. Harms, E. Meggers, *Synlett* **2016**, 27, 749-753. (‡ Equal contribution)
9. F. F. de Assis, **X. Huang**, M. Akiyama, R. A. Pilli, E. Meggers, *J. Org. Chem.* **2018**, 83, 10922-10932.
10. J. Ma, X. Zhang, **X. Huang**, S. Luo, E. Meggers, *Nat. Protoc.* **2018**, 13, 605-632.
11. X. Zhang, J. Qin, **X. Huang**, E. Meggers, *Eur. J. Org. Chem.* **2018**, 2018, 571-577.

12. X. Zhang, J. Qin, **X. Huang**, E. Meggers, *Org. Chem. Front.* **2018**, *5*, 166-170.
13. J. Ma, A. R. Rosales, **X. Huang**, K. Harms, R. Riedel, O. Wiest, E. Meggers, *J. Am. Chem. Soc.* **2017**, *139*, 17245-17248.
14. S. Chen, **X. Huang**, E. Meggers, K. N. Houk, *J. Am. Chem. Soc.* **2017**, *139*, 17902-17907.

M.Sc. thesis: The Oxygenation and Nitrogenation Reactions of Alkynes, Ketones and Imines

Publications:

1. **X. Huang**, X. Li, M. Zou, S. Song, C. Tang, Y. Yuan, N. Jiao, *J. Am. Chem. Soc.* **2014**, *136*, 14858-14865.
2. F. Chen,[‡] **X. Huang**,[‡] X. Li,[‡] T. Shen, M. Zou, N. Jiao, *Angew. Chem. Int. Ed.* **2014**, *53*, 10495-10499. ([‡] Equal contribution)
3. **X. Huang**, X. Li, N. Jiao, *Chem. Sci.* **2015**, *6*, 6355-6360.
4. **X. Huang**, X. Li, M. Zou, J. Pan, N. Jiao, *Org. Chem. Front.* **2015**, *2*, 354-359.
5. **X. Huang**, N. Jiao, *Org. Biomol. Chem.* **2014**, *12*, 4324-4328.
6. J. Liu, X. Qiu, **X. Huang**, X. Luo, C. Zhang, J. Wei, J. Pan, Y. Liang, Y. Zhu, Q. Qin, S. Song, N. Jiao, *Nat. Chem.* **2019**, *11*, 71-77.
7. Y. Zhu, X. Li, X. Wang, **X. Huang**, T. Shen, Y. Zhang, X. Sun, M. Zou, S. Song, N. Jiao, *Org. Lett.* **2015**, *17*, 4702-4705.
8. S. Song, **X. Huang**, Y.-F. Liang, C. Tang, X. Li, N. Jiao, *Green Chem.* **2015**, *17*, 2727-2731.
9. T. Shen, **X. Huang**, Y.-F. Liang, N. Jiao, *Org. Lett.* **2015**, *17*, 6186-6189.
10. Y.-F. Liang, K. Wu, S. Song, X. Li, **X. Huang**, N. Jiao, *Org. Lett.* **2015**, *17*, 876-879.
11. Z. Li, **X. Huang**, F. Chen, C. Zhang, X. Wang, N. Jiao, *Org. Lett.* **2015**, *17*, 584-587.
12. F. Chen, **X. Huang**, Y. Cui, N. Jiao, *Chem. Eur. J.* **2013**, *19*, 11199-11202.